

**The Development of  
Zonal Centrifuges**

INCORPORATED

**MONOGRAPH 21**



LIBRARY  
AUG 21 1970  
NATIONAL INSTITUTES OF HEALTH



JUNE 1966

Anderson, Norman G

# **The Development of Zonal Centrifuges and Ancillary Systems for Tissue Fractionation and Analysis**

U.S. DEPARTMENT OF HEALTH, EDUCATION, AND WELFARE  
PUBLIC HEALTH SERVICE  
NATIONAL CANCER INSTITUTE, BETHESDA, MARYLAND

# NATIONAL CANCER INSTITUTE MONOGRAPHS

KENNETH M. ENDICOTT, *Director, National Cancer Institute*

The proceedings of conferences and symposia dealing with cancer or closely related research fields and series of papers on specific subjects of importance to cancer research are presented in these monographs. Send an original, 1 carbon copy, and 2 sets of illustrations (1 mounted) to the Scientific Editor, National Cancer Institute, Bethesda, Maryland 20014. If there is a Conference Editor, manuscripts should be submitted to him.

*Text:* Double space all material. Block title and byline on right half of page. Official title or academic degree is optional. Align first word of text with first word of title. In typing, do *not* split a paragraph from one page to another—even if a large amount of blank space is left at the end of the last full paragraph on a page. Type tables on separate pages immediately after their description in text. Insert footnotes as separate paragraphs immediately after they are mentioned. Follow *Webster's International Dictionary* in matters of spelling, capitalization, punctuation, and hyphenation. Follow *Chemical Abstracts* for chemical terms.

*References:* Double space and number in order of citation in both text and reference page. Give author, title, journal, volume, first and last page numbers, and year. For book references, give chapter titles when referred to, and name and location of publisher.

*Illustrations:* Refer to graphs, charts, and line drawings as text-figures and number consecutively throughout text. Type legends in text immediately after paragraph in which text-figures are described. Make lettering of art uniform and large enough to be legible if reduced. Original drawings in black India ink or glossy prints are acceptable. Orient horizontally instead of vertically.

Photographs are printed at the end of each article. Refer to them as figures and number consecutively throughout text. Trim each photograph to show only important area. Maximum size of page for photographs is  $5\frac{1}{4} \times 6$  inches. Mount and number one set on white cardboard, with as many figures to a page as possible. Reproduction is best when prints are from negatives of evenly illuminated subject in which details are sharp.

## BOARD OF EDITORS

HOWARD B. ANDERVONT, *Scientific Editor*

JOHN C. BAILAR III,  
*Associate Editor*

GREGORY T. O'CONOR,  
*Associate Editor*

LAURENCE R. DRAPER,  
*Associate Editor*

SHERMAN M. WEISSMAN,  
*Associate Editor*

JACQUELINE J. K. WHANG, *Associate Editor*

## EDITORIAL STAFF

DORIS M. CHANEY, *Managing Editor*

VIVIAN J. HESTON,  
*Assistant Managing Editor*

MARIE K. MURPHY,  
*Monograph Editor*

*Assistant Editors:* MERCEDES B. LA CHARITY, ALICE McA. LEE, and  
JOAN O'BRIEN

THE DEVELOPMENT OF ZONAL CENTRIFUGES  
AND  
ANCILLARY SYSTEMS FOR TISSUE FRACTIONATION  
AND ANALYSIS

Research performed under the Joint National Institutes of Health-Atomic Energy Commission Zonal Centrifuge Development Program, supported by the U.S. Atomic Energy Commission, the National Cancer Institute, and the National Institute of Allergy and Infectious Diseases

Edited by  
Norman G. Anderson, Ph.D.  
Biology Division  
Oak Ridge National Laboratory  
Oak Ridge, Tennessee



## TABLE OF CONTENTS

	Page
Foreword	
Glenn T. Seaborg.....	ix
Introduction	
Norman G. Anderson.....	1
<b>Development of Zonal Centrifuges</b>	
An Introduction to Particle Separations in Zonal Centrifuges	
Norman G. Anderson.....	9
Theory of Centrifugation: Miscellaneous Studies	
A. S. Berman.....	41
The Design of Zonal Centrifuges	
H. P. Barringer.....	77
The Development of Low-Speed "A" Series Zonal Rotors	
N. G. Anderson, H. P. Barringer, N. Cho, C. E. Nunley, E. F. Babelay, R. E. Canning, and C. T. Rankin, Jr.....	113
The Design and Operation of the B-IV Zonal Centrifuge System	
N. G. Anderson, H. P. Barringer, E. F. Babelay, C. E. Nunley, M. J. Bartkus, W. D. Fisher, and C. T. Rankin, Jr.....	137
Zonal Rotors with Removable Seals: Rotors B-X and B-XI	
H. P. Barringer, N. G. Anderson, C. E. Nunley, K. T. Ziehlke, and W. S. Dritt.....	165
Digital Computation of Sedimentation Coefficients in Zonal Centrifuges	
Barbara S. Bishop.....	175
<b>Continuous-Flow Centrifuges</b>	
Design of the B-V Continuous-Flow Centrifuge System	
H. P. Barringer, N. G. Anderson, and C. E. Nunley.....	191
Continuous-Flow Centrifugation Combined With Isopycnic Banding: Rotors B-VIII and B-IX	
N. G. Anderson, H. P. Barringer, J. W. Amburgey, Jr., G. B. Cline, C. E. Nunley, and A. S. Berman.....	199
<b>Studies on Gradient Materials</b>	
Calculation of Density and Viscosity of Sucrose Solutions as a Function of Concentration and Temperature	
E. J. Barber.....	219
Preparation and Recovery of Cesium Compounds for Density Gradient Solutions	
R. R. Wright, W. S. Pappas, J. A. Carter, and C. W. Weber.....	241

## Subcellular Particle Separation by Zonal Centrifugation

	Page
✓ Separation of Subcellular Components and Viruses by Combined Rate- and Isopycnic-Zonal Centrifugation N. G. Anderson, W. W. Harris, A. A. Barber, C. T. Rankin, JR., and E. L. Candler.....	253
Isolation of Native Glycogen by Combined Rate-Zonal and Isopycnic Centrifugation Albert A. Barber, Warren W. Harris, and Norman G. Anderson.....	285
Isolation of Paramylon from <i>Euglena Gracilis</i> Var <i>Bacillarus</i> SML-1 by Combined Rate-Zonal and Isopycnic-Zonal Centrifugation Albert A. Barber, Theodore W. Bartlett, and Blaine H. Levedahl.....	303
The Isolation of Oral Structures From <i>Tetrahymena pyriformis</i> by Low-Speed Zonal Centrifugation G. L. Whitson, G. M. Padilla, R. E. Canning, I. L. Cameron, N. G. Anderson, and L. H. Elrod.....	317
Resolution of the Components in the Microsomal Fraction of Liver in the B-IV Zonal Centrifuge A. A. El-Aaser, E. Reid, E. Klucis, P. Alexander, J. T. Lett, and Jacqueline Smith.....	323
Lipid Peroxidation in Rat Tissue Particulates Separated by Zonal Centrifugation Albert A. Barber, C. T. Rankin, JR., and N. G. Anderson.....	333
Extraction of Contractile Proteins From Myofibrils Prepared by Rate-Zonal Centrifugation Mary Lee S. Barber and Robert E. Canning.....	345
Polysomes from <i>Tetrahymena</i> Following Pyrimidine Deprivation and Replacement I. L. Cameron, G. B. Cline, G. M. Padilla, O. L. Miller, JR., and P. A. Van Dreal.....	361

## Virus Isolation by Centrifugal Methods

An Evaluation of the B-V (Continuous-Flow) and B-IV (Density Gradient) Rotors by Use of Live Polio Virus C. B. Reimer, T. E. Newlin, M. L. Havens, R. S. Baker, N. G. Anderson, G. B. Cline, H. P. Barringer, and C. E. Nunley.....	375
Unusual Particles in Human Plasma From Leukemia and Lymphosarcoma W. W. Harris, N. G. Anderson, T. W. Bartlett, Elizabeth L. Rutenberg, L. L. McCauley, and R. M. Kniseley.....	389

## Molecular Separations in Zonal Centrifuges

Use of the Zonal Ultracentrifuge to Separate Components of Ribosomal RNA J. R. B. Hastings, J. H. Parish, K. S. Kirby, and E. Klucis.....	397
Isolation and Characterization of Rat Macroglobulin W. D. Fisher and R. E. Canning.....	403

## Ancillary Studies

	Page
Centrifugal Freezing. I. A System for Rapid Freezing of Aqueous Cell Suspensions N. G. Anderson, John G. Green, and Peter Mazur.....	415
High-Pressure Column Chromatography. I. Design of Apparatus and Separation of Bases, Nucleosides, and Nucleotides J. G. Green, C. E. Nunley, and N. G. Anderson.....	431
Separation of Acid-Soluble Nucleotides From Yeast With the Nucleotide Analyzer Ivan L. Cameron and William D. Fisher .....	441
Automated Carbohydrate Analyzer: Experimental Prototype John G. Green.....	447
A Flame Ionization Analyzer for the Continuous, Rapid Determination of Carbon in Liquid Streams or Solid Samples R. H. Stevens.....	469
Problems in Biocontainment N. Cho, H. P. Barringer, J. W. Amburgey, G. B. Cline, N. G. Anderson, L. L. McCauley, R. H. Stevens, and W. M. Swartout.....	485



## FOREWORD

THE PAPERS appearing in this volume might appropriately be judged separately on their intrinsic merits, and I am confident that in this respect they will receive deserved attention. Taken as a group their significance may add up to even more than the sum of the individual presentations.

The material presented is broadly interdisciplinary, cutting across many avenues of technology and several scientific domains, and embracing theoretical considerations, experimental design, specific techniques, and the evolution of equipment. It is particularly interesting to note the use of one of our large National Laboratories to attack a basic problem in biology.

The problem in this case—the separation of subcellular particles—is in many ways parallel to other difficult separation problems undertaken at the Atomic Energy Commission facilities in Oak Ridge, Tennessee. These include large-scale isotope and chemical separations, and more recently the preparation and isolation of transuranium elements, and the separation of salt from sea water. The approach to a solution of the problem is based on a unique Oak Ridge invention—the zonal centrifuge.

The potential capability of this equipment to offer a spectrum of separated particles in sufficient quantity for analysis by conventional biochemical techniques is already an impressive achievement. The distribution of enzymes, metabolites, protein, nucleic acids, polysaccharides, drugs, pesticides, or simply mass, among the fractions of a cell, may now be determined.

The possibility that zonal centrifugation opens up in the detection and isolation of trace amounts of virus which may be present in tumors is a most interesting avenue for future research. In model experiments reported in this volume, it has been possible to add trace amounts of virus to normal tissues and then recover them in a high state of purity. The implications of this are apparent for the preparation of virus vaccines for human use.

It is appropriate to note that the systematic research underlying the present reports is supported by the Joint National Institutes of Health-Atomic Energy Commission Zonal Centrifuge Development Program initiated in the fall of 1962. The program has involved collaborative efforts by investigators of the National Cancer Institute and the National Institute of Allergy and Infectious Diseases, representatives from industry, and consultants from other segments of the scientific community. The centrifuge development work has been done by the Technical Division of the Oak Ridge Gaseous Diffusion Plant, and biological studies by the Biology Division of the Oak Ridge National Laboratory, both of which are operated for the Atomic Energy Commission by the Union Carbide Corporation.

The ultracentrifuge system has passed, in a surprisingly short time, from an exploratory phase to a series of different designs, two of which are now available commercially to other research laboratories. It is probable that its greatest application may come in the solution of problems not yet envisioned.

I can relate my own experience in seeking new elements, using interdisciplinary resources, and enormous scaling-up of existing laboratory processes to the program objectives. I will be watching with particular interest the applications of similar approaches to the challenges confronting those whose reports appear in this volume. These reports are significant; future compilations from this team may be even more so.

GLENN T. SEABORG, *Chairman*  
U.S. Atomic Energy Commission

## Introduction <sup>1</sup>

**NORMAN G. ANDERSON**, *Biology Division, Oak Ridge National Laboratory,<sup>2</sup> and Biophysical Separations Laboratory, Oak Ridge Gaseous Diffusion Plant,<sup>2</sup> Oak Ridge, Tennessee*

The practical counsel to be derived from Pythagoras is to measure, and thus to express quality in terms of numerically determined quantity. But the biological sciences, then and till our own time, have been overwhelmingly classificatory. . . . If only the schoolmen had measured instead of classifying, how much they might have learnt.

—Alfred North Whitehead

CLASSIFICATION AND DESCRIPTION in the biological sciences have proceeded from taxonomic and morphologic studies on whole animals and plants to the study of successively smaller parts of living systems, culminating in the visualization and description of individual protein and nucleic acid molecules. Biochemical studies, beginning with the isolation and identification of urea, sugars, amino acids, and lipids, have proceeded to the analysis of larger and more complex molecules leading, within the last decade, to the nearly complete analytical description of certain protein and nucleic acid molecules. Thus are joined classical chemistry and classical biology, and the approaches of each discipline will now pervade the other. Modern crystallography allows many small molecules and some large ones to be visualized as biologists would like to see them. At the same time, larger multimolecular structures such as chloroplasts, ribosomes, mitochondria, and chromosomes are beginning to occupy the attention of the chemist. As a result a conceptual continuum is emerging that extends from the atoms of nuclear physics to the living animal of the behaviorist.

The advances that have made this juncture possible depend in a very real way on the development of techniques, and molecular biology, more than any previous branch of biological science, has been critically dependent on instrumentation. If separation and analysis are to proceed

---

<sup>1</sup> This research performed under The Joint National Institutes of Health-Atomic Energy Commission Zonal Centrifuge Development Program which is supported by the National Cancer Institute, the National Institute of Allergy and Infectious Diseases, and the U.S. Atomic Energy Commission.

<sup>2</sup> Operated for the U.S. Atomic Energy Commission by the Nuclear Division of Union Carbide Corporation.

to even higher orders of complexity, certain new basic tools must be developed. The ordered fabric of protein and nucleic acid molecules found in living cells cannot, in most cases, be unravelled by the same techniques as those used for the separation and analysis of low molecular weight substances. A case in point is protein synthesis. The initial studies on the incorporation of amino acids into the proteins of whole cells were followed by others on the localization of synthetic activity in isolated cell fractions. "Microsomes" were implicated in protein synthesis, and further fractionation suggested that ribosomal particles were the synthetic units. By use of gentler methods for breaking cells and with centrifugal separation systems having improved resolution, it was found that the active particle is a complex structure (the polysome) composed of a long ribonucleic acid molecule to which variable numbers of ribosomes are attached. The mode of attachment of the polysome to membrane surfaces now occupies the attention of a number of investigators in this field, and methods are required for isolating portions of the membrane where attachment occurs. Thus the pursuit of a biochemical problem has led to the isolation of structures of increasing complexity and increased sensitivity to the physical and chemical procedures employed.

Except for storage materials, most cell structures appear to be composed basically either of filaments or membranes. The analysis of the organization of two-dimensional structures is more difficult than the analysis of sequence in linear systems. However, as first discussed by Tiselius (1), "every fragment derived from (an) original structure and containing more than one structure element offers a piece of information about that structure if we know the size and the composition (not necessarily the structure) of the fragment." The preparation, separation, and analysis of small fragments of cell structures, therefore, may offer a key to the patterns that underlie the complex behavior of the intact organelle.

We require not only high-resolution techniques for separating the microscopically identifiable formed elements of cells, but also methods for separating their fragments which are applicable to particles as small as the smallest unit of interest—in this case, individual protein molecules. Since the initial step in certain studies involves the separation of a distinct cell type from a population of cells, our requirements may be broadened to include separation methods that cover the entire range of particle sizes extending from whole cells to proteins. Initially, zonal centrifuge systems have been and are being developed for this purpose, as is evident from the contents of this Monograph. However, additional methods are being explored concurrently, since no one separation technique will be applicable to all fractionation problems we must eventually consider.

Two fractionation problems were sufficiently urgent to catalyze zonal centrifuge development: 1) the search for trace amounts of virus in pathological tissue samples, including neoplasms, and 2) the preparation of vaccines that contain only virus particles, specific cell antigens, or viral subunits. The former interest led to support from the National Cancer Institute, and the latter to a program of virus isolation sponsored

by the National Institute of Allergy and Infectious Diseases. Emphasis on virus isolation, however, does not diminish either our interest in, or the application of the systems to, the isolation of other subcellular particles. The fractionation of particle populations with heterogeneous physical properties can best be done—and can only be done with confidence—after it has been demonstrated that polydispersity, when observed, is real and not due to an inherently low resolution of the isolation system.

If our ultimate interest is in the quantitative visualization of the cell as a spectrum of separated particles, it is evident that the separation of macromolecular species is only half the story. The low molecular weight substances found in cells, including amino acids, nucleotides, sugars, lipids, and numerous metabolic intermediates also should be quantitated with automated analytical systems, only a few of which have been developed at this writing. Two such systems, a carbohydrate analyzer and a high-pressure nucleotide analyzer, are described in this Monograph.

Conceptually, an effort to fractionate a system as complex as the cell is an extension of the simple principle that a complex structure is to be understood in terms of its parts. In addition, it should be noted that the basic philosophy of the analysis of complex mixtures has undergone a revolution in the last two decades. In place of a battery of presumably specific analytical procedures, one for each component to be tested, emphasis now is on high-resolution separation techniques, with the results of the separation monitored by a sensor which is sensitive to mass, radioactivity, color, or a chemical group. The U.S. Atomic Energy Commission's Oak Ridge installation was originally organized to achieve certain difficult separations on a large scale. These include the separation of the isotopes of uranium by the electromagnetic process, by gaseous diffusion, and by other methods; the separation of plutonium from fission products and the fractionation of the fission products themselves; the isolation of radioisotopes in pure form for experimental and therapeutic use; the separation of experimental quantities of all the major stable isotopes of all the naturally occurring elements of the atomic table; and, most recently, the construction of facilities for producing and purifying quantities of the transuranium elements. The zonal centrifuge development program is therefore an extension of a large existing program into biological areas.

There are a number of reasons why systems for the separation and analysis of all the separable constituents of cells should be pushed to the limits of available theory and technology. One is that detailed information on the structure and composition of cells and on changes occurring from injury, disease, or during the cell cycle would throw into bold relief our need (and hopefully provide information) for an adequate theory or model of the cell into which available data may be fitted. Additional reasons related to basic biochemical or clinical studies are not difficult to enumerate. However, the most valid and compelling reason for creating new methods for probing living cells still remains our simple curiosity.

This Monograph marks the completion of the joint NIH-AEC Zonal Centrifuge Development Program. The program has served as a pilot study for a broader effort concerned with instrumental approaches to Molecular Anatomy (the Man Program), which will be continued as a joint NIH-AEC effort.

In the pursuit of the studies reported in this volume, assistance and counsel have been generously given by many individuals. It is a pleasure to record the support and encouragement of Drs. C. E. Larson, A. M. Weinberg, J. A. Swartout, A. Hollaender, J. L. Liverman, and C. S. Shoup at Oak Ridge; Drs. C. L. Dunham and J. S. Kirby-Smith of the Atomic Energy Commission; Drs. Gordon Zubrod, W. Ray Bryan, P. Kotin, and Robert Stevenson of the National Cancer Institute; and Drs. Robert Huebner, R. M. Chanock, M. Mufson, and Helen Coates of the National Institute of Allergy and Infectious Diseases. Without their assistance and cooperation, the complex problem of organizing an interagency program could not have been solved.

The enthusiastic, competent, and original contributions of members of the Technical Division of the Oak Ridge Gaseous Diffusion Plant have been important to the centrifuge program. This group, under Paul Huber, included P. R. Vanstrum, E. F. Babelay, H. P. Barringer, A. S. Berman, E. C. Evans, N. Cho, W. J. Wilcox, Jr., E. J. Barber, J. G. Green, C. E. Nunley, D. A. Waters, J. W. Amburgey, Jr., and L. L. McCauley. Special assistance in electron microscopy under W. W. Harris has been provided by T. W. Bartlett and F. L. Ball. The development of new instrumentation is due to the efforts of H. D. Culpepper, R. H. Stevens, G. R. Jamieson, G. M. Lindner, and M. J. Bartkus. Computer studies and programming were carried out by Barbara Bishop, Dr. K. O. Bowman, Elizabeth L. Rutenberg, and E. F. Martin, Jr., and metallurgical studies by W. S. Dritt, K. T. Ziehlke, and C. E. Weaver. Work on the chemistry of gradient materials was done by C. W. Weber, R. R. Wright, W. S. Pappas, and J. A. Carter. We cannot fully record our indebtedness to all the many additional staff members who have assisted in the solution of technical, supply, legal, design, and fabrication problems.

In the Biology Division of the Oak Ridge National Laboratory the research programs of Drs. W. D. Fisher, G. M. Padilla, I. L. Cameron, Peter Mazur, G. L. Whitson, and G. B. Cline have contributed directly to the experimental evaluation of new rotor systems. In addition, Drs. A. A. Barber and M. L. Barber (University of California, Los Angeles), Dr. Charles Burger (Upstate Medical Center, New York), Dr. Carl Price (Rutgers University), Dr. Herbert Schuel (Oakland University, Michigan), Dr. Charles Reimer (Eli Lilly Research Laboratories), Drs. Jacob Holper and John Garin (Abbott Laboratories), and Mr. Irving Toplin (Charles Pfizer and Company) have contributed in many important ways to the development of the program.

The difficult task of operating new experimental systems has been performed by R. E. Canning, C. T. Rankin, Jr., E. L. Candler, Jr., Tom Grizzard and Hunter Elrod. Without their skillful assistance

many of the difficult experimental problems would not have been solved. The existence of this volume is largely due to the editorial assistance of Domenic Fuccillo and to the assistance of Mrs. Margie Harding in manuscript preparation.

Finally, I would like to thank Dr. Jesse Beams of the University of Virginia and Dr. Rodes Trautman, Plum Island Animal Disease Laboratory, U.S. Department of Agriculture, Greenport, Long Island, New York, for their advice and encouragement during the entire course of this program and for reviewing the manuscripts which comprise this Monograph.

## REFERENCES

- (1) TISELIUS, A.: Some general relations between the composition of fragments and the structure from which they originate. I. Random fragmentation. *Arkiv för Kemi* 15: 171-180, 1959.



## **Development of Zonal Centrifuges**



# An Introduction to Particle Separations in Zonal Centrifuges<sup>1</sup>

NORMAN G. ANDERSON, *Biology Division, Oak Ridge National Laboratory,<sup>2</sup> and the Biophysical Separations Laboratory, Oak Ridge Gaseous Diffusion Plant,<sup>2</sup> Oak Ridge, Tennessee*

## SUMMARY

Zonal centrifugation, based either on sedimentation rate or on isopycnic banding in liquid density gradients, is useful for high-resolution separation of subcellular particles. However, the amount of material which may be separated is extremely limited when conventional centrifuges are employed. To increase the capacity and, in certain instances, the resolution of the method, the possibility of employing large-volume hollow rotors has been explored.

These are either loaded and unloaded while spinning or are designed to allow the density gradient in the rotor to reorient from a rest position to spin orientation and back with minimal shear and disturbance. The principles of operation and construction of low-speed A series and intermediate-speed B series zonal rotors are reviewed.—*Nat Cancer Inst Monogr* 21: 9-39 1966.

FOR THE EXPLORATION of cell substructure, high-resolution preparative and analytical centrifugal separations systems are required which cover the size range from whole cells to protein molecules. This is roughly the range of particle sizes that may be resolved in the electron microscope. The Svedberg analytical ultracentrifuge (1) is admirably suited for determining the sedimentation rates of particles of viral dimensions and less, down to and including small protein molecules, and for measuring buoyant densities of proteins and all larger particles for which suitable suspending media are available. Analytical centrifuges for determining the sedimentation rates of particles much larger than viruses and preparative zonal centrifuges for physically separating quantities of particles over the entire size range of interest were not available prior to the inception of the work described here. One of the principal purposes of the Joint National Institutes of Health-Atomic Energy Commission Zonal Centrifuge Development Program is to develop the centrifuges and ancillary instrumentation necessary to fill these gaps. The instru-

---

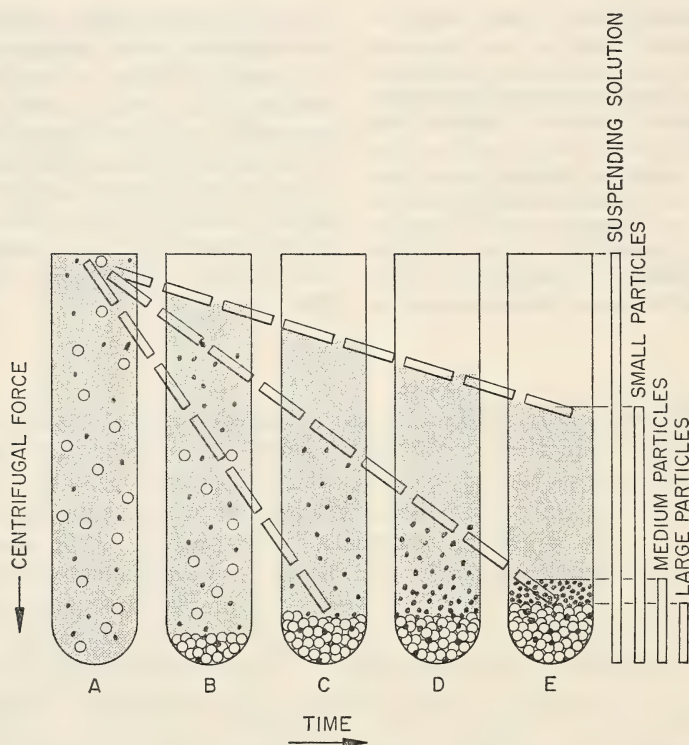
<sup>1</sup> This research performed under the Joint National Institutes of Health-Atomic Energy Commission Zonal Centrifuge Development Program which is supported by the National Cancer Institute, the National Institute of Allergy and Infectious Diseases, and the U.S. Atomic Energy Commission.

<sup>2</sup> Operated for the U.S. Atomic Energy Commission by the Nuclear Division of Union Carbide Corporation.

ments developed under this program are also useful, under certain conditions, for separations in the low-molecular-weight range where centrifugal separations have not been previously employed.

## DIFFERENTIAL CENTRIFUGATION

The centrifuge has had a long and successful history as a means for isolating particles of biological interest. Most tissue separations have been made by so-called differential centrifugation, in which centrifuge tubes are filled with a homogeneous particle preparation at the outset. Particle sedimentation in a centrifugal field in such a tube is shown diagrammatically in text-figure 1.



TEXT-FIGURE 1.—Sedimentation of a particulate suspension in a centrifugal field. Initially all particles are uniformly distributed through the centrifuge tube (A). As centrifugation proceeds (B) all particles present sediment at their respective sedimentation rates, resulting first in the total sedimentation of the largest particle species (C). The degree of cross contamination in the pellet between two species of particles at the moment when one species has sedimented completely is approximately proportional to the ratio of sedimentation rates. Further centrifugation (D) results in complete sedimentation of the intermediate-sized particles (E). The distribution of particles in tube E is shown in the bar graph at the right.

Since a few particles of every size, including the smallest ones, are present at the bottom before centrifugation starts, it is evident that a pure pellet of the largest particles present cannot be obtained in one centrifugation. In addition, as shown in text-figure 1B through 1E, some of the small particles sediment during the complete sedimentation of larger particles. The intermediate particulate species is likewise contaminated by the smallest sedimenting units. The result is that only a fraction of the most slowly sedimenting species is obtained in a pure form in one centrifugation. Some redistribution according to particle density may occur in the pellet, however. If a very small particle is denser than a large one, this may increase the contamination as the small particles move slowly between the previously sedimented larger, but lighter, particles.

In differential centrifugation the supernatant (entire fluid volume over the pellet) would be removed after a certain period of centrifugation, for example, at tube C of text-figure 1. Repeated resuspension and resedimentation of the first pellet will yield a reasonably pure preparation of the large particles. All supernatants are then combined and centrifuged long enough to sediment the intermediate-sized particles completely. The second pellet is then cyclically purified as was the first. The reason that this method, with its apparent low resolution, has worked so well is that it has been most often applied to the separation of particles whose sedimentation coefficients differ by orders of magnitude. It has been least successful in those instances where very small differences in sedimentation rate exist, as, for example, in the separation of certain large lipid-containing viruses from small cytoplasmic fragments having very nearly the same properties.

In the analytical ultracentrifuge, particles sediment as shown in text-figure 1, but in a special sector-shaped cell with transparent windows. With suitable optical or combined optical and electronic techniques, the moving particle boundaries can be visualized either as a series of steps in a concentration versus radius plot, or as a series of peaks when the first derivative of the concentration versus rotor radius curve is plotted. The problem considered here is the development of centrifuges that would physically separate quantities of particles into fractions identical to those visualized as peaks during analytical centrifugation, *i.e.*, to devise a true preparative counterpart of the analytical ultracentrifuge.

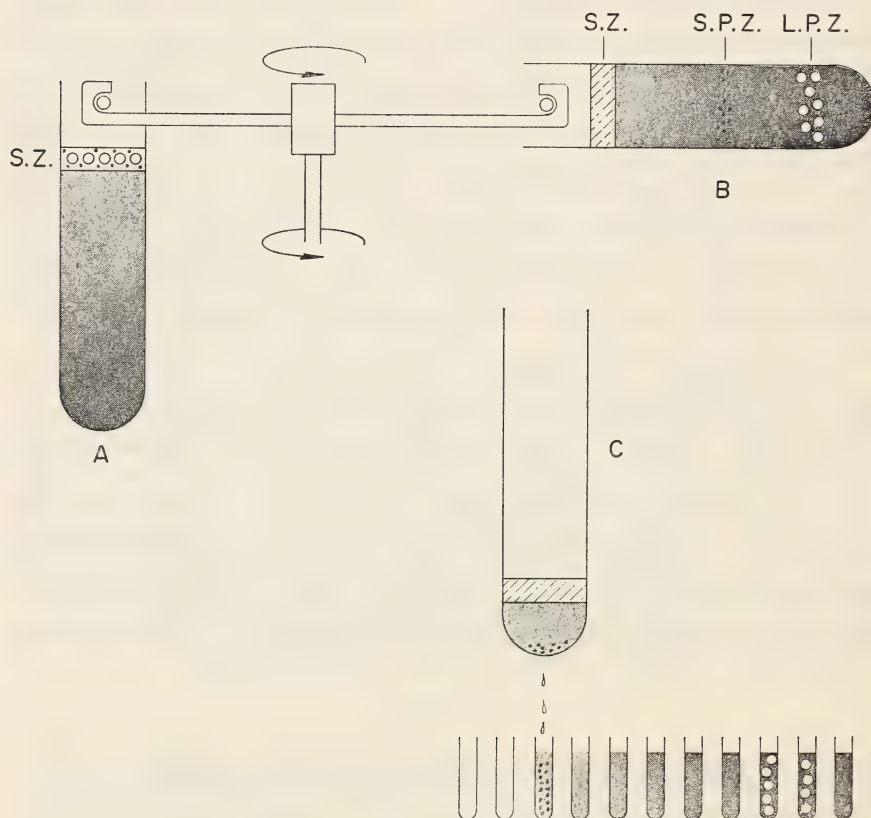
## PRINCIPLES OF ZONAL CENTRIFUGATION

To achieve separations of higher resolution, two types of centrifugation have been developed. In the first, particles are separated into discrete zones on the basis of differences in sedimentation rate (rate-zonal centrifugation), and in the second, separation is based solely on differences in buoyant or banding density (isopycnic-zonal centrifugation).

### Rate-Zonal Centrifugation

If the mixture to be separated could be confined initially to a narrow zone at the top of a centrifuge tube, the sedimenting particles might be expected to separate into discrete zones according to their sedimentation rates. The difficulty observed experimentally is that convective disturbances will occur unless we contrive to always have every level of the liquid, whether it contains particles or not, lighter than the liquid immediately underneath it, *i.e.*, to sediment the particles through a liquid density gradient as shown in text-figure 2.

This technique, originated by Brakke (2-4), has been termed rate-zonal centrifugation, or more conveniently *s*-zonal centrifugation, since it depends on the particle sedimentation rate, *s*. In this technique, a centrifuge tube is prepared which contains a continuous liquid density gradient, formed either by diffusion between initially discontinuous layers



TEXT-FIGURE 2.—Rate-zonal centrifugation in a swinging-bucket rotor. The gradient and sample layer are introduced at rest (A). The tubes are accelerated to a horizontal position (B) and centrifuged until the desired separation is effected. The rotor is decelerated to rest, at which time the gradient and the separated zones (sample zone, S.Z., small particle zone, S.P.Z., and large particle zone, L.P.Z.) are recovered (C), usually through a small hole punctured in the bottom of the tube.

or by a gradient-mixing device. At rest, a thin zone of the suspension to be fractionated is layered on top of the gradient. If particles lighter than any portion of the gradient are to be separated, then the sample is placed at the bottom of the gradient. Since the latter method depends on the rate of flotation, it may be termed  $s_r$ -zonal centrifugation.

The centrifuge tube is accelerated slowly so that the transition from rest to a horizontal position occurs without disturbing the gradient or the sample layer (5). After the required separation has been made, the tubes are decelerated to rest and the gradient is recovered as a series of discrete fractions. This method has been extensively used for the separation of small amounts of nucleic acids, RNA-DNA hybrids, ribosomes, ribosomal subunits, polysomes, and other cell components. The amount of material that may be separated with available high-speed swinging-bucket centrifuges is very small; for the SW 39 rotor the gradient is 4 ml per tube (3 tubes per rotor), and the sample layer is only a fraction of a milliliter. Because of the small starting sample, this method is primarily an analytical one. Its success has resulted from the high sensitivity of both the monitoring devices employed for scanning the collected fractions and of biological assays. For example, nucleic acids can be detected in very small amounts because of their very high ultraviolet absorbance. Generally, insufficient material is collected for chemical analysis by conventional methods, or for use as the starting material in further fractionation studies.

Rate-zonal centrifugation should be clearly distinguished from analytical ultracentrifugation as it is conventionally done with homogeneous, dilute aqueous solutions. In the latter method, the physical properties of the particle and the suspending medium through which it passes do not change appreciably during sedimentation. Calculation of the sedimentation rate may be made without knowing or assuming values for particle density. In rate-zonal centrifugation the sedimenting particle moves through a medium of increasing density, viscosity, and (in most gradients) osmotic pressure. If the particle behaves as a small osmometer, the dimensions and the effective density change during sedimentation. In addition, gradient solutes may be bound to the particle.

If the osmotic properties and permeability are sufficiently well understood, the sedimentation coefficient can be calculated from the position of the particle after centrifugation (6-8). For most viruses and many proteins it may be assumed, as a first approximation, that only minor changes in osmotic volume or density occur in sucrose gradients. For mitochondria and other semipermeable structures, changes in the physical properties during sedimentation must be considered.

Previous work on centrifugation through gradients by use of swinging-bucket centrifuge rotors has been extensively reviewed (4-6, 9). While excellent separations have been made in density gradients set up in tubes, the method has had certain disadvantages. For example, considerable time is required to set up the gradients; care must be taken to avoid disturbances during acceleration and deceleration and the gradient must

be recovered with the tubes at rest. Especially in high-speed rotors, the capacity of the centrifuge tube is severely limited. Wall effects may produce clumping, premature sedimentation of particles, and convective disturbances. Because of the limitation on the amount of material which may be separated, the techniques for *s*-zonal separations have not been widely used for the isolation of large particles such as whole cells, nuclei, and mitochondria.

Rate and isopycnic separations of high-molecular-weight DNA present a special problem because, as first pointed out in 1953 (10), this material is broken by shearing. In addition, the sample layer should be sufficiently dilute to allow each molecule a free sphere of rotation. Without high-capacity zonal centrifuges, it is difficult to isolate for chemical analysis sufficient mammalian DNA with a very narrow sedimentation coefficient range by the rate-zonal method. Large-capacity systems are also required for the isolation of analyzable quantities of minor DNA satellite bands.

Theoretical studies on zone capacity (11, 12) in rate-zonal centrifugation have been made. In practice the amount of material which may be supported in a zone has been reported to be smaller than predicted (4). Difficulty in maintaining adequate temperature control may account for this in part.

The shape of a density gradient may be considered to be convex when the rate of increase in density decreases with radius in the centrifuge, and concave when the rate increases with radius. A linear gradient changes in density linearly with radius. (In a sector-shaped centrifuge compartment, the plot of density with radius is not the same as a plot of density vs. volume.) The following factors favor the use of convex gradients:

1. The capacity of a gradient increases as the difference between the particle and solvent density decreases. If the capacity of a gradient is to be the same along its length—a desirable situation when a single virus species is being purified—then  $dc/dr$  should decrease as  $\rho' - \rho$  decreases (where  $dc/dr$  refers to the rate of change in concentration of the gradient solute  $c$  with radius  $r$ , and  $\rho'$  and  $\rho$  are the densities of the particle and the solution, respectively).

2. In a multicomponent system a series of zones will leave the starting zone with little separation between them, but these will become more widely distributed during centrifugation. The greatest gradient capacity is therefore required through, and just below, the sample zone, and the gradient should be steep and convex in this region. However, if the gradient rises too steeply just under the sample layer, particles may be concentrated into an excessively narrow zone before starting through the less steep portion of the gradient.

3. In sector-shaped compartments radial dilution and diffusion combine to decrease the particle concentration (but not the total particle mass), in a sedimenting zone composed of homogeneous particles. As the concentration diminishes, the gradient slope required to maintain stability also decreases. This effect again favors a convex gradient.

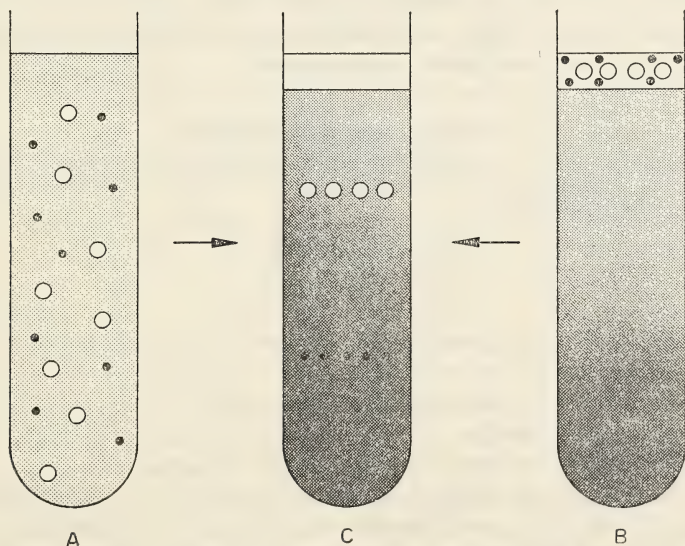
Concave gradients may be employed when it is desirable to band a rapidly sedimenting or dense particle at its isopycnic point while allowing a slowly sedimenting component to sediment through a shallow gradient. Complex gradients have been used for cell component isolation in the present volume. Some of the larger components are banded isopycnically while others are separated on the basis of sedimentation rate.

### Isopycnic-Zonal Centrifugation

If sedimentation of particles is continued until they reach a portion of the gradient where the gradient density ( $\rho_s$ ) and the buoyant density of the particles ( $\rho_B$ ) are equal, no further sedimentation will occur and the particles may be considered to be at equilibrium (text-fig. 3).

This method, termed isopycnic-zonal or  $\rho_B$ -zonal centrifugation (where  $\rho_B$  indicates buoyant density), may be used to separate particles differing in buoyant density without regard to particle size (5, 13), except as particle size contributes to diffusivity. The initial position of the particles to be banded is usually unimportant, *i.e.*, they may be uniformly distributed through the tube or they may be introduced as a discrete zone.

Isopycnic-zonal centrifugation was originally used by E. N. Harvey (14) and E. B. Harvey (15) to stratify *in situ* the subcellular particulates of sea urchin eggs and to separate the eggs into light and heavy halves. Linderström-Lang (16) used density gradient columns of water-saturated organic liquids at rest to measure the densities of droplets of aqueous



TEXT-FIGURE 3.—Isopycnic-zonal centrifugation. The particles to be banded at first may be uniformly distributed in a homogeneous suspending medium (A) and then separated on the basis of buoyant density as a gradient is formed in the centrifugal field (C), or the particles may be layered over a preformed gradient (B) and centrifuged to equilibrium (C).

solutions. The separation of powders of dried cells and tissues into nuclear and cytoplasmic fractions in nonaqueous density gradients was introduced by Behrens (17, 18) and used by Mirsky and co-workers (19-21) to determine the partition of enzymes and soluble components between the nucleus and cytoplasm of a variety of tissues. More recently, Meselson, Stahl, and Vinograd (13) extended  $\rho_B$ -zonal centrifugation to the molecular level with their classical studies on zonal separations of DNA in cesium chloride gradients. The studies that have extended this method to the separation of small amounts of DNA, RNA, DNA-RNA hybrids, viruses, ribosomes, ribosomal subunits, polysomes, and other cell components are now too numerous to be reviewed here. As with rate separations in swinging buckets, the amount of material that may be separated has been severely limited.

The density at which a particle will band isopycnically ( $\rho_B$ ) is a function of its density in the medium employed and is altered when the particle is permeable to the solutes used, or when the solutes are bound to the particle. For these reasons, the buoyant density of particles of biological interest is often a function of the suspending medium. Further, the buoyant density measured will usually not be the same as the density value (reciprocal of the partial specific volume) used in rate sedimentation studies.

Interestingly, changes in particle density by specific binding create new separation possibilities. For example, if a reagent specific for a given binding site is heavier or lighter than the particle containing the binding site, it should change the banding density. The effect of stains used to distinguish DNA and RNA, sulfhydryl reagents, and ferritin-conjugated antisera should be investigated in this regard.

#### *Combined $s$ - $\rho_B$ zonal methods*

The sedimentation rate of a spherical particle in a centrifuge is given by the familiar equation:

$$s = \frac{2a^2(\rho' - \rho)}{9\eta} \quad [1]$$

where  $s$  = sedimentation rate in cm/sec per unit centrifugal field

$a$  = particle radius in cm

$\rho'$  = density of a solvated particle in g/cm<sup>3</sup>

$\rho$  = solution density

$\eta$  = viscosity of the suspending medium in poises

The rate is therefore dependent on the square of the particle radius (assuming it is a sphere) and the difference between the solvated density of the particle and the density of the suspending fluid. The sedimentation rate is also sensitive to particle shape. However, particles having quite different densities and radii may have the same sedimentation rate provided the product of  $a^2$  and  $(\rho' - \rho)$  is the same for all of them.

For this reason, we would like to separate particles on the basis of their

effective size and their density separately. Since the sedimentation rate is a function of both, it is evident that the two parameters can only be effectively separated by a two-step procedure using *s*-zonal centrifugation for one and  $\rho_B$ -zonal centrifugation for the other (22). The choice of the order of the separation depends on several considerations and is considered in detail in a subsequent paper in this volume (22). The method is useful for studying enzyme activities in microsomal subfractions (22a and 22b) and for the isolation of native glycogen (23).

To maximize the particle radius dependence of the rate separations in practice, the difference in density between the particle of interest and the solvent should be maximized, and the separations should be carried out in gradients having the lowest density practicable. This is evidenced from the fact that the effect of radius *a* on sedimentation approaches zero as the term  $(\rho_B - \rho_s)$ , where  $\rho_B$  is the buoyant density of the particle and  $\rho_s$ , the density of the gradient, approaches zero (*i.e.*, particles of any radius may band at the same density). These considerations suggest that the maximal separation for scanning purposes may be obtained first by separation of subcellular particles on the basis of sedimentation rate in a zonal centrifuge and then by separation of the collected fractions on the basis of density alone. Of interest here is the question: Will such separations yield relatively pure subcellular particles? The range of sedimentation rates of subcellular particles (including proteins) is approximately  $10^6$  Svedberg units, while the banding densities vary from approximately 1 to 2. If the sedimentation coefficients of sedimentable particles are plotted against particle buoyant density in a given medium (such as CsCl) to give a so-called "*s*- $\rho$ " plot, it is evident that many known particulates would be widely separated (22). For example, microsomes and glycogen span nearly the same range of sedimentation coefficients, but differ greatly in buoyant density, and band at approximately 1.18 and 1.62, respectively (23). Conversely, mitochondria and microsomes have nearly the same buoyant density but differ very much in sedimentation rate.

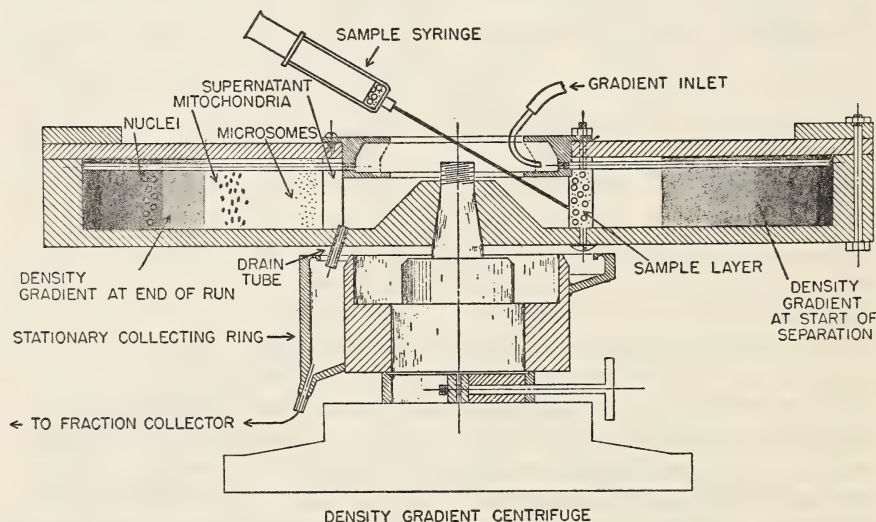
If the necessary centrifuge systems for making high-resolution *s*- $\rho$  separations can be built, the possibility exists that minor cell constituents may be found which have sedimentation rates and banding densities unlike those of known components. In addition, it may be possible to isolate trace amounts of virus from cell homogenates. If this is feasible, the problem of analyzing the virus-like particles that have been occasionally described in electron micrographs of human tumors can be considered. The experimental possibilities that would be opened up by the development of techniques for high-resolution *s*- $\rho$  separations are many and are discussed in detail in subsequent papers in this monograph (22, 23). Briefly, the problem is to develop separation techniques that would parallel the electron microscope in the range of particle sizes to be separated, and that would be sensitive to two of the several elements of morphology on which visual characterization depends, namely, size (to a lesser degree shape) and density. The development of zonal centrifuges has been the first step in the exploration of *s*- $\rho_B$  separation systems.

## DEVELOPMENT OF ZONAL CENTRIFUGES

Ideally, one would wish to achieve simultaneously in one rotor system the following: 1) ideal sedimentation and maximum resolution in sector-shaped compartments, 2) rapid gradient formation in the rotor with minimal stirring or convection, 3) sharp starting or sample zones, 4) high rotational speed, 5) large capacity, and 6) rapid recovery of the gradient after centrifugation without loss of resolution. A number of rotors in the A and B series have been designed to fulfill these requirements.

Initially, a swinging-bucket system (A-I) was used to demonstrate that high resolution could be obtained (fig. 1) with glass tubes of modified sector shape (24, 25). Because density gradients are greatly stabilized in a centrifugal field, the A-II rotor system was developed in which the density gradient was introduced into the centrifuge tubes through a central distributor cup (fig. 2) while the centrifuge was running (26). In the A-II system, however, the gradients had to be recovered from the tubes at rest.

The possibility that centrifuge tubes could be eliminated entirely was explored by using a hollow centrifuge head filled and emptied *during* rotation. The first rotor of this type (27, 28) was the A-III and is shown in text-figure 4 and figure 3. The gradient was introduced to the edge of the rotor, light end of the gradient first, through radially oriented tubes attached to an annular groove near the rotor center. After the gradient was in position, the sample was introduced manually to its inner



TEXT-FIGURE 4.—Schematic drawing of operation of zonal rotor A-III. The density gradient flows into the spinning rotor through the center annular ring, and thence through small tubes to the rotor edge. The sample layer is then manually layered on the central (*light*) edge of the gradient. After separation of the particles, the gradient is recovered by displacement toward the center drain tube using a dense sucrose solution introduced to the rotor edge.

surface. After particle separation had occurred (text-fig. 4) the gradient was displaced toward the center by allowing a very dense fluid to flow to the rotor edge. The gradient was collected as a stream flowing out the exit tubes in the bottom of the rotor near the axis of rotation. This relatively crude rotor demonstrated the feasibility of the zonal centrifuge. A more refined rotor (A-IV, fig. 4), demonstrated that gradients could be introduced into and recovered from rotors operating at speeds up to 18,000 rpm. Additional "A"-series rotors have been designed and tested (29, 30) and have culminated in A-XII, which is now commercially available.<sup>3</sup>

Based on early studies with the A-III and IV rotors, construction of an intermediate-speed zonal rotor was proposed, and two experimental models were built on subcontract by the Spinco Division of Beckman Instruments, Inc. Rotor B-I, constructed under this contract, was extremely unstable for reasons not understood at that time. It now appears to have had the wrong ratio of moments of inertia (31). Rotor B-II (fig. 5), tested extensively under the present Joint National Institutes of Health-Atomic Energy Commission Zonal Centrifuge Development Program, has produced excellent separations (32-35) but as originally built did not reach the maximum design speed for reasons that are discussed by Barringer (31).

The rotational stability problems were solved in the design of the B-IV rotor<sup>4</sup> (36, 37), and the basic principles of zonal centrifuge operation may be best illustrated by considering this rotor in some detail.

The rotor is filled during rotation at a low speed, as shown diagrammatically in figure 6B. The light end of the gradient is pumped to the rotor wall first, followed by denser fluid, which displaces the lighter fluid end of the gradient toward the rotor core. When the gradient is in the rotor, additional dense fluid, termed the "underlay" is pumped in until the light end of the gradient begins to flow out the center line. At this point the sample layer is introduced through the center line (fig. 6C), reversing the direction of fluid flow through the rotor and causing part of the underlay to flow back out through the edge line. To push the sample layer further into the rotor chamber clear of the core, additional light fluid (the overlay) is pumped in as is shown in figure 6D. The connection to the rotor edge is then closed, and the center line attached to a reservoir of water to allow a small volume of fluid to flow into the rotor during acceleration to compensate for rotor expansion. The rotor is then accelerated to a speed sufficient to effect the desired particle separation (fig. 6E).

After deceleration to low speed, the gradient is displaced by a dense solution toward the core and out through the center line (fig. 6F). The gradient flows through an ultraviolet absorbance monitor and into a fraction collector. Part of the gradient may be pumped through auto-

<sup>3</sup> The A-XII rotor is available from International Equipment Company, Needham Heights, Mass.

<sup>4</sup> The B-IV zonal ultracentrifuge is available from the Spinco Division of Beckman Instruments, Palo Alto, Calif.

mated systems to assay for enzyme or total protein activity (fig. 6). A radioactivity analyzer can also be used in this system. The operation of the "A" series, dynamically loaded (*i.e.*, loaded and unloaded during rotation) rotors (A-V, VI, IX, and XII) is similar in principle to that of the B-IV rotor described.

It is evident that the sample layer may also be introduced first to the rotor edge and then be picked off the rotor wall by the inflowing gradient. This method has two disadvantages: It allows some particles to sediment to the rotor wall at once, and it increases mixing by both diffusion and laminar flow as the gradient streams in under the sample layer, which is initially spread over the entire inner wall of the rotor.

It is also evident that the gradient may be backed into a compartment containing a dense fluid, which is withdrawn through the outer edge line. The gradient may also be recovered in the reverse direction, that is, through the connection to the outer edge. Of these methods, the one used in the continuously rotating zonal rotors described in the present report is believed to give the highest resolution.

The design of the core, considered in greater detail in a subsequent paper (37), is critical for high resolution separations. In a dynamically loaded rotor it serves to divide the rotor volume into sector-shaped compartments, to connect the center and edge of each compartment with the seal lines, and to guide the sample in and the gradient out of the rotor with minimal mixing and loss of resolution.

### ROTORS WITH REMOVABLE SEALS

As previously suggested (32) the seal system of a dynamically loaded rotor may be removed during high-speed operation, making a bearing on the end of the rotor to which the seal is attached unnecessary if the rotor is self-balancing. The problems associated with the construction and operation of such rotors have been largely solved with the development of rotors B-X and B-XI (38). It is probable that zonal centrifuges based on this design will find very wide application in biochemical and virological studies. They are not, however, adaptable to continuous flow operation in their present form.

### REORIENTING GRADIENT ROTORS

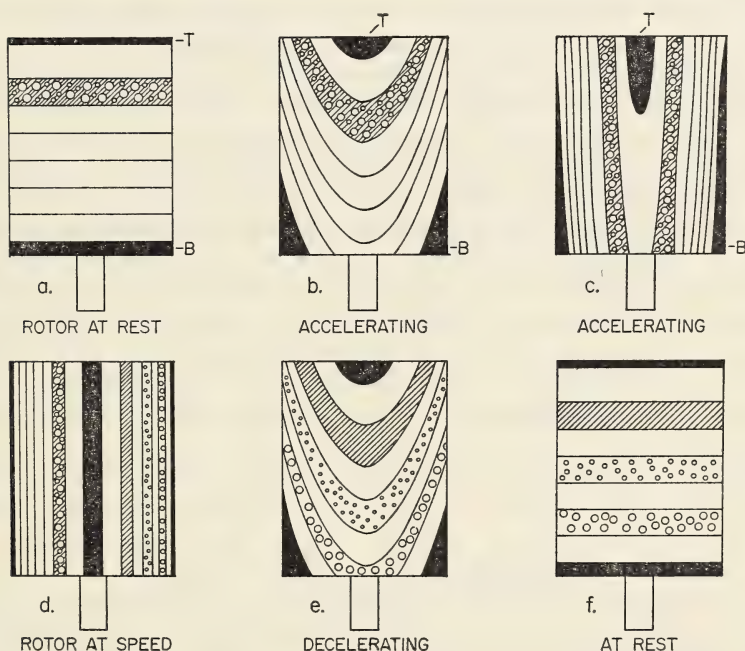
Dynamically loaded zonal rotors have been shown in practice to give very high resolution separations (23, 33). It is unlikely, however, that suitable rotating seals can be built which would operate in a satisfactory manner in the range of 100,000 rpm and faster. We have therefore examined two alternate possibilities (*a*) gradient reorientation in the rotor during acceleration and again during deceleration so that gradients may be set up and recovered at rest (39), and (*b*) removable-seal rotors in which the seals are attached to the rotor only during filling and emptying

of the rotor at low speed. The possibility of building reorienting-gradient rotors arises from the following considerations.

The shearing forces occurring in a liquid confined in a closed cylinder during the transition from rest to a stable orientation in a high centrifugal force field may be considered qualitatively by examining text-figure 5. The horizontal lines indicate levels, or surfaces, of equal density in a continuous density gradient.

During acceleration, each isodense surface becomes part of a paraboloid of revolution. At a given rotational speed, all isodensity curves are identical, being merely transposed vertically. Acceleration results in a series of configurations shown diagrammatically in text-figures 5b and 5c. At high speed, where the ratio between the centrifugal force and the acceleration due to gravity in a downward direction is very high, the isodensity surfaces will be nearly vertical (text-fig. 5d).

Deformations occurring at the various levels may be best understood by describing the changes occurring in layers originally at the top, middle,



TEXT-FIGURE 5.—Schematic diagram of reograd rotor system. (a) Rotor is filled at rest with density gradient and sample layer. To indicate extremes of zone deformation, a thin upper layer, *T*, and bottom layer, *B*, are also indicated. (b) During acceleration, each zone forms a paraboloid of revolution about the axis. Note *T* and *B*. (c) Near operating speed, the zones approach a vertical orientation. (d) At a sufficiently high speed, the zones become nearly vertical. Separation of particle zones is shown at *right*. (e) During deceleration, zones again form paraboloids of revolution. (f) At rest, various zones may be recovered by draining rotor contents out the bottom, or displacing the gradient out through the top. Reprinted from Anderson *et al.* (39).

and bottom of the rotor. The fluid originally against the upper rotor cap becomes squeezed into a small paraboloid of revolution during acceleration (text-fig. 5b) and then occupies the center of the rotor at high speed (text-fig. 5d). A zone in the middle of the rotor (5a) at rest increases in area during acceleration, and then decreases in area slightly as an approximately vertical position is approached. The zone at the very bottom of the rotor at rest (text-fig. 5a) decreases markedly in surface area during acceleration (text-fig. 5b), but covers the entire surface of the rotor wall at high speed (text-fig. 5d). The greatest area changes, therefore, occur in those zones near the top and bottom when at rest but near the center and the edge at high speed.

The reoriented gradient, before the particles have sedimented appreciably, is shown at the left (text-fig. 5d), and after sedimentation at the right. The distribution during deceleration is shown in text-figure 5e, with the distribution at rest shown in text-figure 5f. The separated zones are recovered by draining the gradient out of the bottom of the rotor, or by displacing it out the top.

A mathematical analysis of the areas of isodensity surfaces (40) shows that shearing in the center of the gradient in a sector-compartmented rotor is not excessive. While increases and decreases in area occur, the difference in rate of increase or decrease in the areas of adjacent zones is rather small. By placing a dense "cushion" or underlay in the bottom, and an overlay of light fluid above the sample layer at the top, the sample layer and density gradient may be restricted to that part of the rotor where least shearing occurs. As the fluid layers change position during acceleration and deceleration, their tangential velocity will change, since the velocity at any point in the rotor is a function of both the rotational speed and the radius of the point. Fluid in the upper layer, originally near the edge of the rotor, decreases in tangential velocity relative to previously underlying fluid during acceleration, for example. Vertical septa, therefore, are considered necessary to prevent swirling during reorientation of the gradient.

High-speed reorienting-gradient zonal rotors are still in a very experimental stage although rotors with a capacity of 100 ml have been successfully tested to 141,000 rpm ( $310,000 \times g$  at  $R_{\max}$ ), and a 10 ml rotor with a design speed of 400,000 rpm ( $1.2 \text{ million} \times g$ ) is under development. The details of this work will be included in future publications. These rotors are useful for both rate-zonal and isopycnic-zonal centrifugation.

Extensive experimental studies will be required to determine whether the removable-seal design or the reorienting gradient configuration will give the best resolution with high-speed rotors designed expressly for protein or nucleic acid separations.

## CONTINUOUS-FLOW CENTRIFUGATION

In the centrifuge systems described thus far it has been assumed that the starting sample contains a high concentration of particles. In many

instances this is not the case, and some preliminary method for concentrating particles must be employed. This is especially true of culture fluids of animal viruses where multiliter volumes may contain only a few milligrams of viral particles.

While continuous-flow centrifugation has been widely used industrially and for a few laboratory separations such as the recovery of bacteria from multiliter cultures, the full capabilities of the method do not appear to have been realized. In an ideal continuous-flow centrifuge it is evident that initial separations should be as good as those observed in a single sedimentation in differential centrifugation. The problem is to develop rotor systems that will function efficiently over a very wide range of particle sizes, and which, in addition, will not form aerosols of the sample material during its passage through the rotor. Of immediate concern in the present program is the development of contained high-speed continuous flow centrifuges that can be used to recover pathogenic virus particles from large volumes of culture fluid.

In addition, a continuous-flow centrifuge is needed where the particles removed from the fluid stream are not compacted, but are allowed to sediment into a gradient imprisoned in the rotor chambers (33). This would allow buoyant density to be used as an additional separation parameter and would also enable the experimenter to make repeated separations without disassembling the rotor.

The B-V rotor system (41) has been developed for high-speed continuous flow separation of particles which can be pelleted, while the B-VIII and B-IX rotors (42) have been successfully developed for continuous-flow centrifugation combined with isopycnic banding.

These rotor systems allow particulate material to be isolated from rather large volumes of vaccines. The distribution of mass through a density gradient may then be determined during approach to equilibrium (rate-zonal centrifugation) or at equilibrium (isopycnic-zonal centrifugation) in the B-IV rotor. The importance of characterizing of the particulate material in vaccines for human use and of attempts to prepare vaccines containing only those antigens required for protection has been previously stressed (33).

## OTHER GRADIENT SEPARATIONS

The centrifuge systems described in this volume make possible a number of separations in addition to those already described. These will be discussed in greater detail elsewhere and are merely listed here. These include:

### 1. *Particle immobilization during chemical dissection*

Bacterial cells, or subcellular particles, may be banded isopycnically in a gradient containing detergents, enzymes, solubilizing agents either uniformly distributed through the gradient, at the particle banding level, or in an overlay from which they sediment or diffuse into the particle band. As the particles disrupt, DNA or other material may be released and

separated in the gradient on the basis of sedimentation rate or banding density.

*2. Particle dissection by sedimentation through reagents immobilized in a density gradient*

The sequential removal of globulins and histones by sedimentation of nuclei through a gradient of increasing ionic strength and acidity is an example of sequential gradient particle dissection.

*3. Gradient resolubilization*

In an alcohol-water gradient an alcohol-precipitated protein will sediment until it reaches a level where it can dissolve. If the centrifugal field is not too high, it will remain at the level where it dissolves. This method is applicable to many proteins and to RNA-DNA separations (Anderson, 1956, unpublished). In addition, the method can be used to concentrate small amounts of protein, nucleic acid, or virus from large volumes of fluid with the B-IX rotor. The precipitating agent is added before the fluid is run through the rotor. During centrifugation the precipitate sediments into the immobilized gradient in the rotor and either dissolves or bands isopycnically. This method is also applicable to low-molecular-weight materials.

*4. Precipitation in a gradient followed by isopycnic banding*

Water-insoluble organic substances in a water-miscible organic solvent may be layered over a suitable aqueous density gradient in which either crystalline or amorphous particles of the organic solids will band. With proper choice of solvents, all levels of the gradient and sample layer can be made denser than water, which is layered over the sample. As water diffuses into the sample layer, precipitation occurs and particles move out through the gradient to their isopycnic level. Similar systems using water-soluble materials layered over gradients prepared from dense water miscible organic solvents have also been explored. These concepts extend the usefulness of zonal centrifuges into the field of small molecules.

## ANCILLARY STUDIES

Although the central problem in this program has been the development of high-resolution centrifuge systems, other preparative and analytical methods have been explored. An automated analytical system for bases, nucleosides, and nucleotides previously developed (43) has been extensively modified for high pressure studies on columns of very small bore (44). A prototype of a complete system for the analysis of mixtures of sugars has been completed and tested (45). The final design work on a model suitable for general laboratory use is now under way (46). In addition, new methods for countercurrent separations are being devised (47). To monitor the effluent from lipid separation columns, a flame ionization analyzer

using a fine wire to transport samples into a hydrogen flame has been explored (48).

## SEPARATION OF SUBCELLULAR PARTICLES IN ZONAL CENTRIFUGES

The studies recorded in this volume were begun by experimental biologists interested in fractionating real cells. It soon became evident that certain basic problems concerned with the physical chemistry of subcellular particles should be considered along with purely empirical approaches. The following discussion poses some of the problems that have emerged. The view taken here, admittedly the result of personal bias and limitations, is that in nearly all instances we must attempt to measure each parameter of a subcellular particle directly by methods that are, if possible, independent of other measurements.

The reasons for this approach can be made clear by considering systematically the relationships between the models that may be considered mathematically and the real objects that we wish to separate. The following paragraphs describe a series of cases and indicate some of the problems associated with the zonal centrifugation of each type of particle. The viewpoint is that of a physiologist rather than of a physical chemist.

- Case I.* Particles that are ideal, smooth, round, uncharged, unhydrated, and impermeable.
- Case II.* Polymeric molecules that are hydrated, charged, and may not be round or smooth, such as proteins or nucleic acid molecules, but are often homogeneous with respect to molecular weight.
- Case III.* Particles composed of aggregates of polymeric molecules; these occur in a range of sizes and may show marked changes in frictional ratio with size but do not exhibit osmotic behavior.
- Case IV.* Vesicles that exhibit osmotic behavior.
- Case V.* Vesicles that exhibit osmotic behavior and also size or volume changes in response to physiological variables.
- Case VI.* Particles that are hydrated, exhibit large volume changes in response to physiological variables, but do not show osmotic behavior.

In *Case I* (see text-fig. 6) all the classical equations of centrifugation apply.<sup>5</sup> The diameter,  $2a$ , corresponds to the hydrodynamic diameter (distance between shearing planes on opposite sides of the molecule), the particle does not absorb water, and the solvated layer is negligible. The physical properties of the suspending medium or density gradient do not in any way affect the physical properties of the particle. The forces acting on a particle are buoyant ( $F_b$ ), centrifugal ( $F_c$ ), and frictional ( $F_f$ ) forces. These may be defined as

$$F_b = -v\rho\omega^2r \quad [2]$$

$$F_c = m\omega^2r \quad [3]$$

$$F_f = -6\pi\eta a\omega^2rs \quad [4]$$

<sup>5</sup> The author is indebted to Dr. Rodos Trautman for invaluable assistance in the development of this section.

where

- $v$  = volume of particle in ml
- $\rho$  = density of the solution (g/ml)
- $\omega$  = angular velocity in radians per second
- $r$  = distance from axis of rotation to the particle
- $m$  = anhydrous mass of particle
- $\eta$  = viscosity of the solution
- $a$  = particle radius
- $s$  = sedimentation coefficient
- $f/f_o$  = friction factor
- $\omega^2rs$  = velocity of the particle (cm/sec)
- $h$  = particle solvation
- $d$  = density (g/ml) of solvated layer

The net force per particle is zero ( $F_b + F_c + F_f = 0$ ) once particles have been accelerated to their average velocity during a sedimentation velocity experiment; hence

$$s = \frac{4a^2(\rho^d - \rho)}{18\eta(f/f_o)} \quad [5]$$

where  $\rho^d$  is the density (g/ml) of the anhydrous particle.

*Case II.* Proteins and nucleic acids in solution are hydrated. If the particle solvation is  $h$  (ml) of density  $d$  (g/ml) the solvated particle density  $\rho'$  (g/ml) is

$$\rho' = \frac{m + hd}{v + h} \quad [6]$$

The radius  $a$  (cm) of an equivalent sphere having a volume equal to the volume of the solvated particle is

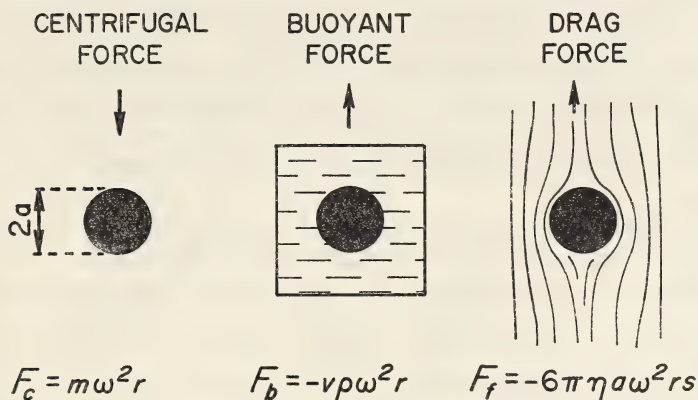
$$4/3\pi a^3 = v + h \quad [7]$$

As shown in text-figure 6, *Case II*, the forces acting on the solvated particle are the centrifugal force,  $F_c = (m + hd)\omega^2r$ , the buoyant force,  $F_b = -(v + h)\rho\omega^2r$ , and the friction force,  $F_f = -6\pi a(f/f_o)\omega^2rs$ .

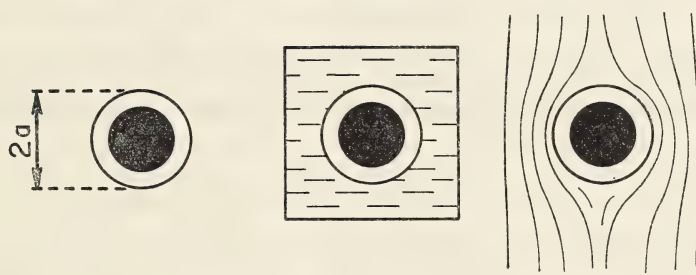
In a density gradient the behavior of these particles will differ from that for *Case I* to the extent that the amount of bound gradient constituents varies during sedimentation, and to the degree that the hydrodynamic radius changes during movement through the gradient.

*Case III.* The best example of *Case III* is liver glycogen. It is composed of small, apparently oval, and homogeneous subunits ( $\gamma$  particles) that are quite dense (23). These appear to exhibit quite normal sedimentation properties. Clusters of  $\gamma$  particles are assembled into  $\beta$  particles, which sediment more slowly than measurements of their greatest diameter predict. The  $\beta$  particles are assembled into still larger  $\alpha$  clusters, which sediment more slowly than predicted. Isopycnic banding density is very nearly the same for all sizes, and no evidence for

## CASE I



## CASE II



TEXT-FIGURE 6.—Diagrammatic representation of forces acting on an anhydrous particle (*Case I*) and a hydrated particle (*Case II*) in a centrifugal field. Arrows indicate the direction of centrifugal force ( $F_c$ ), buoyant force ( $F_b$ ), and drag force ( $F_f$ ). See text for definitions of terms used.

osmotic behavior has been observed. With this particle,  $F_c$  and  $F_b$  are probably the same as for *Case I*; however, the friction force,  $F_f$ , varies in a peculiar way with the maximal radius, and a different frictional ratio ( $f/f_0$ ) must be used with different-sized particles.

*Case IV.* Vesicles that exhibit pure osmotic behavior and remain perfectly spherical while changing volume in a gradient have not as yet been described. All real particles tend to (a) have a nonosmotic volume, (b) become nonspherical when excessively shrunken, and (c) take time to reach equilibrium during migration through the gradient, the time being dependent on the permeability to water of the surface membrane of the

particle. The application of the available physical data on mitochondria to the calculation of the sedimentation rates in sucrose gradients has been described (6). It is assumed that all particles behave in the same manner, and that the calculations correctly describe the particle diameter and density at every level in the density gradient. Until these values can be determined by independent methods they must be treated with caution since the sedimentation equations describe individual particles, whereas permeability and osmotic studies are done on large numbers of particles and give no indication of particle heterogeneity with regard to physical properties.

*Case V.* Experimentally, mitochondria exhibit osmotic volume changes and volume changes in response to experimental physiological variables. Thus, in isosmotic solutions, removal or addition of adenosine triphosphate, thyroxin, and a variety of other substances causes mitochondria to change markedly in volume (49). It cannot be assumed that the physiological mechanisms involved in these apparently nonosmotic volume changes are unchanged during sedimentation through a density gradient. Before the sedimentation of such particles can be adequately studied it will be necessary to measure particle sedimentation rate and diameter *continuously* during sedimentation through a gradient. Centrifuge systems specifically designed for such studies are in the design stage.

*Case VI.* Nuclei obtained from rat liver are hydrated, exhibit large volume changes in response to certain physiological variables, and do not show osmotic behavior. The volume in solution is largely a reflection of the number and type of ions present (50). In distilled water, nuclei swell greatly and ultimately dissolve. Low concentrations of calcium chloride (0.01 M) cause the nuclei to shrink below the intracellular volume. Further increases in the concentration of this salt produce swelling again. If nuclei are taken from very hypotonic (0.01 M)  $\text{CaCl}_2$  into hypertonic (0.88 M) ion-free sucrose, marked swelling is observed. Liver nuclei are permeable to relatively large molecules (51) and behave as an open anionic gelwork.

Since nuclei bind divalent cations much as negatively charged ion exchange resin beads do, a distinction must be made between the total amount of a given ion present in a nuclear suspension, and the concentration present in solution after equilibrium between free and bound cations has been reached. Thus, if a concentrated tissue homogenate is made 0.05 M with respect to calcium, relatively little change in nuclear volume or nuclear internal structure may be seen. If this homogenate is layered over a sucrose gradient containing 0.005 M  $\text{CaCl}_2$ , the nuclei sedimenting through the gradient will soon sweep through a sufficient volume of solution to come into equilibrium with a 0.005 M  $\text{CaCl}_2$  solution, will shrink, and become granular. In many instances sucrose solutions, especially if prepared with tap water, may contain enough salt to prevent nuclei from swelling excessively. Nuclei appear to be in equilibrium with some cytoplasmic proteins (52) and may gradually lose these during zonal purification. The point is that the physical properties of nuclei cannot be

assumed to be constant when sedimented out of a tissue brei and through a gradient.

Evaluation of the sedimentation rate of nuclei or other subcellular particles from two-position measurements (the starting position in the rotor and the position when unloading is begun) must be considered as crude approximations until (a) the diameter and density of the particles have been measured independently at a number of levels in the gradient, (b) the position of a given particle species has been measured continuously during centrifugation, and (c) the variation of sedimentation rate with gradient position has been determined.

That at least some part of the nuclear structure is sensitive to osmotic pressure is suggested from the observation that nuclei isolated in isotonic sucrose-dextran gradients retain their capacity for protein synthesis (53) while those isolated in conventional sucrose gradients do not.

The proof that a mathematical model of a subcellular particle actually applies to the particle must be determined experimentally. For this reason, the computer program developed for use with the B-IV zonal ultracentrifuge applies rigorously only to *Case I*, and the equivalent sedimentation coefficients,  $S^*$ , determined in Svedberg units, when used in connection with real particles, are for comparative purposes only. It is quite evident that the development of computer programs that can be shown to apply directly to each species of subcellular particle will require further work. The program applies to particles in *Case II* if the water of hydration equilibrates rapidly with the gradient medium and if the particles therefore *change* their solvated density during zonal centrifugation

## DISCUSSION

As an introduction to particle separation in zonal centrifuges, certain basic problems and some of the rotor systems developed to solve these problems have been presented. Broadly stated, the aim has been to develop high-resolution methods for separating cells and sedimentable subcellular particles in quantities sufficient for chemical analysis or for further fractionation studies. Initially, low-speed, test centrifuge systems (early A series) were used to explore the concept of dynamically loaded and unloaded zonal rotors. These were useful for "proof-of-principle" purposes but suffered from a number of operational defects. As the feasibility of this approach was demonstrated, more refined rotor systems were developed.

It appeared unlikely that one rotor system could be built which would give optimal separations over the entire particle size range of interest. Therefore four classes of rotors have been explored: Series A for particles in the size range visible in the light microscope, Series B for particles as small as plasma macroglobulins, Series C for rate separations of small proteins and large-scale nucleic acid and protein-banding studies, and Series D for exploratory studies in very high centrifugal fields. Details of the development and experimental application of some of the rotors

in the A and B series are presented in subsequent papers in this monograph. The presentations are limited to results obtained with rotors driven by conventional, and widely used, centrifuge drives. To make the techniques developed more generally available, drawings and detailed information on construction and operation have been released to the public by the Atomic Energy Commission, and two of the centrifuges described here are now commercially available as a result of this policy.

Much of the experimental work done under this program has been recorded in semiannual reports (54-57).<sup>6</sup>

## REFERENCES

- (1) SVEDBERG, T., and PEDERSON, K. O.: The Ultracentrifuge. Oxford, The Clarendon Press, 1940.
- (2) BRAKKE, M. K.: Density gradient centrifugation: A new separation technique. *J Amer Chem Soc* 73: 1847-1848, 1951.
- (3) ———: Zonal separations by density-gradient centrifugation. *Arch Biochem* 45: 275-290, 1953.
- (4) ———: Density gradient centrifugation and its application to plant viruses. *Advance Virus Res* 7: 193-224, 1960.
- (5) ANDERSON, N. G.: Techniques for the mass isolation of cellular components. In *Physical Techniques in Biological Research*, vol III. Cells and Tissues (Oster, G., and Polister, A. W., eds.). New York, Academic Press Inc., 1956, pp 299-352.
- (6) DE DUVE, C., BERTHET, J., and BEAUFAY, H.: Gradient centrifugation of cell particles. Theory and applications. *Progr Biophys* 9: 325-369, 1959.
- (7) THOMSON, J. F., and MIKUTA, E. T.: Enzymatic activity of cytoplasmic particulates of rat liver isolated by gradient centrifugation. *Arch Biochem* 51: 487-498, 1954.
- (8) MARTIN, R. G., and AMES, B. N.: A method for determining the sedimentation behavior of enzymes: Application to protein mixtures. *J Biol Chem* 236: 1372-1379, 1961.
- (9) ALLFREY, V.: The isolation of subcellular components. In *The Cell* (Brachet, J., and Mirsky, A. E., eds.). New York, Academic Press Inc., 1959, vol I, pp 193-290.
- (10) ANDERSON, N. G.: Degree of polymerization of deoxyribonucleic acid. *Nature (London)* 172: 807-808, 1953.
- (11) SVENSSON, H., HAGDAHL, L., and LERNER, K. D.: Zonal electrophoresis in a density gradient. Stability conditions and separation of serum proteins. *Sci Tools* 4: 1-10, 1957.
- (12) BERMAN, A. S.: Theory of centrifugation: Miscellaneous studies. *Nat Cancer Inst Monogr* 21: 41-76, 1966.
- (13) MESELSOHN, M., STAHL, F. W., and VINOGRAD, J.: Equilibrium sedimentation of macromolecules in density gradients. *Proc Nat Acad Sci USA* 43: 581-588, 1957.
- (14) HARVEY, E. N.: The tension at the surface of marine eggs, especially those of the sea urchin, *Arbacia*. *Biol Bull* 61: 273-279, 1931.
- (15) HARVEY, E. B.: The development of half and quarter eggs of *Arbacia punctulata* and of strongly centrifuged whole eggs. *Biol Bull* 62: 155-167, 1932.
- (16) LINDERSTRÖM-LANG, K.: Dilatometric ultra-micro-estimation of peptidase activity. *Nature (London)* 139: 713-714, 1937.

<sup>6</sup> Available from the Clearinghouse, National Bureau of Standards, U.S. Department of Commerce, Springfield, Va. 22151.

- (17) BEHRENS, M.: Zell-und Gewebetrennung. In *Handbuch der biologischen Arbeitsmethoden* (Abderhalden, E. ed.). Berlin, Urban and Schwarzenberg, 1938, vol V, part 10, II, pp 1363-1392.
- (18) ———: Über die Verteilung der Lipase und Arginase zwischen Zellkern und Protoplasma der Leber. *Z Physiol Chem* 258: 27-32, 1939.
- (19) STERN, H., and MIRSKY, A. E.: Soluble enzymes of nuclei isolated in sucrose and non-aqueous media; a comparative study. *J Gen Physiol* 37: 177-187, 1953.
- (20) OSAWA, S., ALLFREY, V. G., and MIRSKY, A. E.: Mononucleotides of the cell nucleus. *J Gen Physiol* 40: 491-513, 1957.
- (21) NAORA, H., NAORA, H., MIRSKY, A. E., and ALLFREY, V. G.: Magnesium and calcium in isolated cell nuclei. *J Gen Physiol* 44: 713-742, 1961.
- (22) ANDERSON, N. G., HARRIS, W. W., BARBER, A. A., RANKIN, C. T., JR., and E. L. CANDLER: Separation of subcellular components and viruses by combined rate-zonal and isopycnic-zonal centrifugation. *Nat Cancer Inst Monogr* 21: 253-283, 1966.
- (22a) BARBER, A. A., RANKIN, C. T., JR., and ANDERSON, N. G.: Lipid peroxidation in rat tissue particulates separated by zonal centrifugation. *Nat Cancer Inst Monogr* 21: 333-344, 1966.
- (22b) EL-AASER, A. A., REID, E., KLUCIS, E., ALEXANDER, P., LETT, J. T., and SMITH, J.: Resolution of the components in the microsomal fraction of liver in the B-IV zonal centrifuge. *Nat Cancer Inst Monogr* 21: 323-332, 1966.
- (23) BARBER, A. A., HARRIS, W. W., and ANDERSON, N. G.: Isolation of native glycogen by combined rate-zonal and isopycnic centrifugation. *Nat Cancer Inst Monogr* 21: 285-302, 1966.
- (24) ANDERSON, N. G.: Brei fractionation. *Science* 121: 775-776, 1955.
- (25) ———: Studies on isolated cell components. VIII. High resolution gradient differential centrifugation. *Exp Cell Res* 9: 446-459, 1955.
- (26) ALBRIGHT, J. F., and ANDERSON, N. G.: A method for rapid fractionation of particulate systems by gradient differential centrifugation. *Exp Cell Res* 15: 271-281, 1958.
- (27) ANDERSON, N. G.: Horizontal tubeless centrifuge head. In *Biol Div Semiann Progr Rept*, Aug 15, 1955, ORNL-1953, p 117.
- (28) ———: New fractionation methods for isolating cellular proteins. *Bull Amer Phys Soc* 1 (Ser II): 267-268, 1956.
- (29) CANNING, R. E., and ANDERSON, N. G.: Separation of subcellular fractions with a new zonal rotor. *Amer Zool* 4: 310, 1964.
- (30) ANDERSON, N. G., BARRINGER, H. P., CHO, N., NUNLEY, C. E., BABELAY, E. F., CANNING, R. E., and RANKIN, C. T., JR.: The development of low-speed "A" series zonal rotors. *Nat Cancer Inst Monogr* 21: 113-136, 1966.
- (31) BARRINGER, H. P.: The design of zonal centrifuges. *Nat Cancer Inst Monogr* 21: 77-111, 1966.
- (32) ANDERSON, N. G.: The zonal ultracentrifuge. A new instrument for fractionating mixtures of particles. *J Phys Chem* 66: 1984-1989, 1962.
- (33) ———: Virus isolation in the zonal ultracentrifuge. *Nature (London)* 199: 1166-1168, 1963.
- (34) SCHUEL, H., and ANDERSON, N. G.: Studies on isolated cell components. XVI. The distribution of acid phenyl phosphatase activities in rat liver brei fractionated in the zonal ultracentrifuge. *J Cell Biol* 21: 309-323, 1964.
- (35) SCHUEL, H., TIPTON, S. R., and ANDERSON, N. G.: Studies on isolated cell components. XVII. The distribution of cytochrome oxidase activity in rat liver brei fractionated in the zonal ultracentrifuge. *J Cell Biol* 22: 317-326, 1964.
- (36) ANDERSON, N. G., BARRINGER, H. P., BABELAY, E. F., and FISHER, W. D.: The B-IV zonal ultracentrifuge. *Life Sci* 3: 667-671, 1964.
- (37) ANDERSON, N. G., BARRINGER, H. P., BABELAY, E. F., NUNLEY, C. E., BARTEKUS, M. J., FISHER, W. D., and RANKIN, C. T., JR.: The design and operation of the B-IV zonal centrifuge system. *Nat Cancer Inst Monogr* 21: 137-164, 1966.

- (38) BARRINGER, H. P., ANDERSON, N. G., NUNLEY, C. E., ZIEHLKE, K. T., and DRITT, W. S.: Zonal rotors with removable seals: Rotons B-X and B XI. *Nat Cancer Inst Monogr* 21: 165-174, 1966.
- (39) ANDERSON, N. G., PRICE, C. A., FISHER, W. D., CANNING, R. E., and BURGER, C. L.: Analytical techniques for cell fractions. IV. Reorienting gradient rotor for zonal centrifugation. *Anal Biochem* 7: 1-9, 1964.
- (40) FISHER, W. D.: The theory of reorienting gradient rotors. In preparation.
- (41) BARRINGER, H. P., ANDERSON, N. G., and NUNLEY, C. E.: Design of the B-V continuous-flow centrifuge system. *Nat Cancer Inst Monogr* 21: 191-198, 1966.
- (42) ANDERSON, N. G., BARRINGER, H. P., AMBURGEY, J. W., JR., CLINE, G. B., NUNLEY, C. E., and BERMAN, A. S.: Continuous-flow centrifugation combined with isopycnic banding: Rotors B-VIII and B-IX. *Nat Cancer Inst Monogr* 21: 199-216, 1966.
- (43) ANDERSON, N. G., GREEN, J. G., BARBER, M. L., and LADD, SISTER F. C.: Analytical techniques for cell fractions. III. Nucleotides and related compounds. *Anal Biochem* 6: 153-169, 1963.
- (44) GREEN, J. G., NUNLEY, C. E., and ANDERSON, N. G.: High-pressure column chromatography. I. Design of apparatus and separation of bases, nucleosides, and nucleotides. *Nat Cancer Inst Monogr* 21: 431-440, 1966.
- (45) GREEN, J. G., and ANDERSON, N. G.: Prototype automatic carbohydrate analyzer. *Fed Proc* 24: 606, 1965.
- (46) GREEN, J. G.: Automated carbohydrate analyzer: Experimental prototype. *Nat Cancer Inst Monogr* 21: 447-467, 1966.
- (47) ANDERSON, N. G., and STEVENS, R. H.: Countercurrent distribution cell with centrifugal phase separation. In preparation.
- (48) STEVENS, R. H.: A flame ionization analyzer for the continuous, rapid determination of carbon in liquid streams or solid samples. *Nat Cancer Inst Monogr* 21: 469-483, 1966.
- (49) LEHNINGER, A. L.: Water uptake and extrusion by mitochondria in relation to oxidative phosphorylation. *Physiol Rev* 42: 467-517, 1962.
- (50) ANDERSON, N. G., and WILBUR, K. M.: Studies on isolated cell components. IV. The effect of various solutions on the isolated rat liver nucleus. *J Gen Physiol* 35: 781-796, 1952.
- (51) ANDERSON, N. G.: On the nuclear envelope. *Science* 117: 517-521, 1953.
- (52) SWANSON, H. D.: A study of the relation of cytoplasmic proteins to nuclear size and its implication for embryonic differentiation. Ph.D. thesis in partial fulfillment of the requirements for the degree of Doctor of Philosophy, University of Tennessee, 1960.
- (53) FISHER, W. D., and CLINE, G. B.: A density gradient for the isolation of metabolically active thymus nuclei. *Biochem Biophys Acta* 68: 640-642, 1963.
- (54) ANDERSON, N. G.: The Joint National Institutes of Health-Atomic Energy Commission Zonal Centrifuge Development Program, Semiannual Report, USAEC Report ORNL-3415 (Special), Oak Ridge National Laboratory, July 1-December 31, 1962.
- (55) ———: The Joint National Institutes of Health-Atomic Energy Commission Zonal Centrifuge Development Program, Semiannual Report, USAEC Report ORNL-3502 (Special), Oak Ridge National Laboratory, January 1-June 30, 1963.
- (56) ———: The Joint National Institutes of Health-Atomic Energy Commission Zonal Centrifuge Development Program, Semiannual Report, USAEC Report ORNL-3656 (Special), Oak Ridge National Laboratory, July 1-December 31, 1963.
- (57) ———: The Joint National Institutes of Health-Atomic Energy Commission Zonal Centrifuge Development Program, Semiannual Report, USAEC Report ORNL-3752 (Special), Oak Ridge National Laboratory, January 1-June 30, 1964.

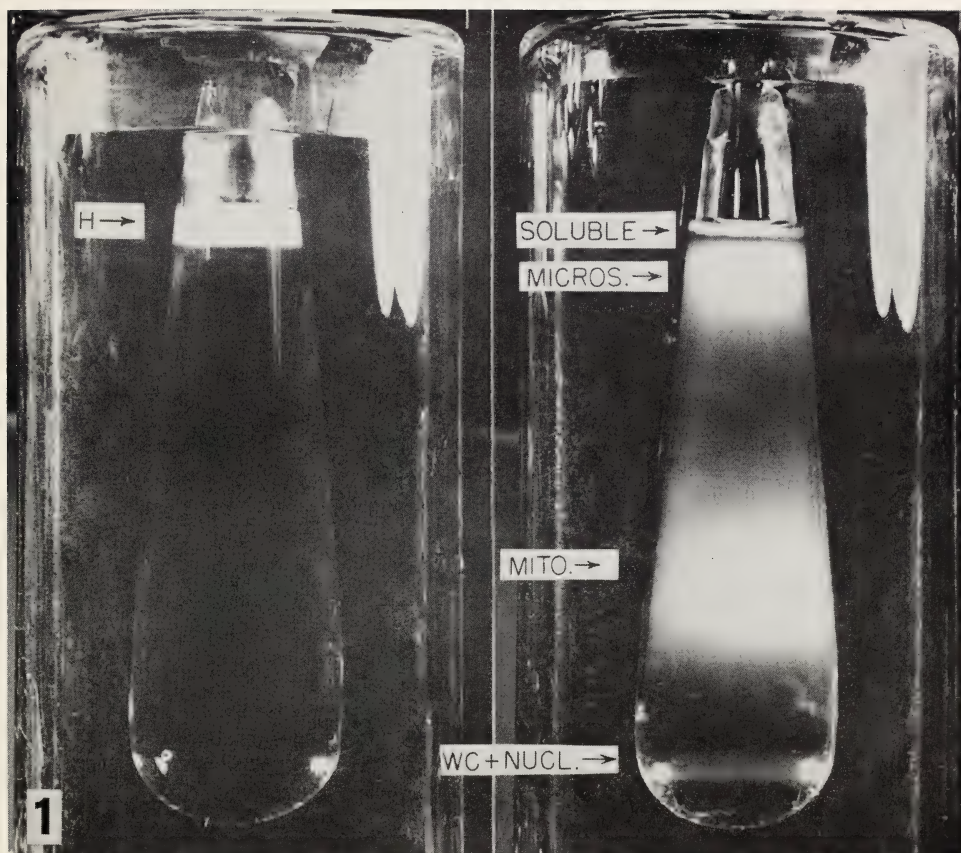


FIGURE 1.—Fractionation of rat liver subcellular particulates in a sucrose density gradient using pyrex tubes of modified sector shape. In tube on *left*, homogenate or brei has been layered over gradient at rest. On *right*, tube is shown after prolonged centrifugation. Whole cells and nuclei are banded near the *bottom* of the gradient, mitochondria in the *middle*, and microsomes near the *top*. A small zone of cleared soluble material is visible at the very *top*. The gradient volume was 65 ml; the sample volume, 2 ml; and the centrifugation time, 18 hours at 3000 rpm. Reprinted from *Science* by permission (24).

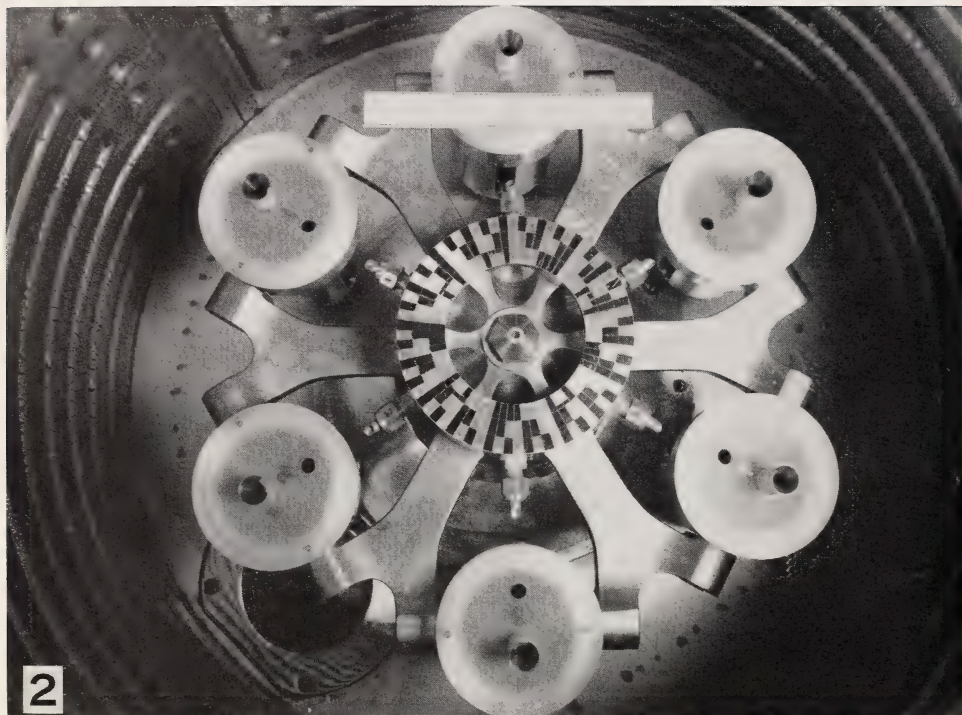


FIGURE 2.—Zonal centrifuge system A-II. During rotation the flared tubes, on the top of each centrifuge cup, tip over and make contact with the center distributing vessel. As fluid is introduced into the distributing vessel during rotation, it is proportioned to the bottom of each centrifuge cup. In this manner, identical density gradients are set up in all tubes at one time. Modified from Albright and Anderson (26).

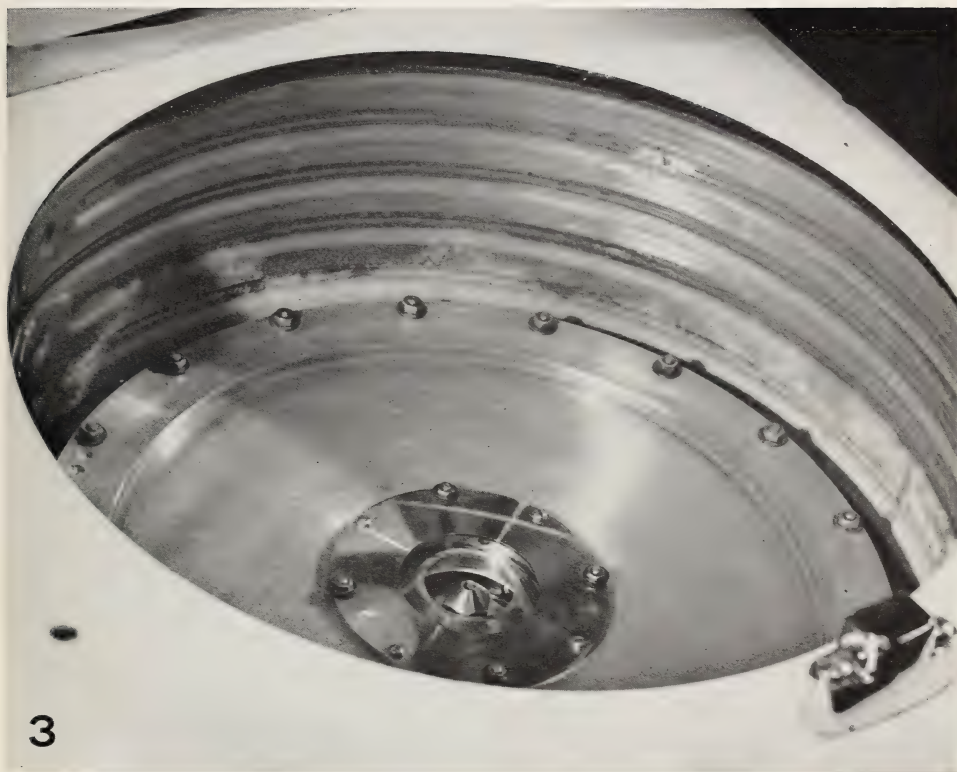


FIGURE 3.—Zonal rotor A-III mounted in International PR-2 refrigerated centrifuge.



FIGURE 4.—Zonal rotor A-IV. Rotor used to demonstrate gradient introduction and recovery from rotor at speeds up to 18,000 rpm. Used in Spinco Model K centrifuge.

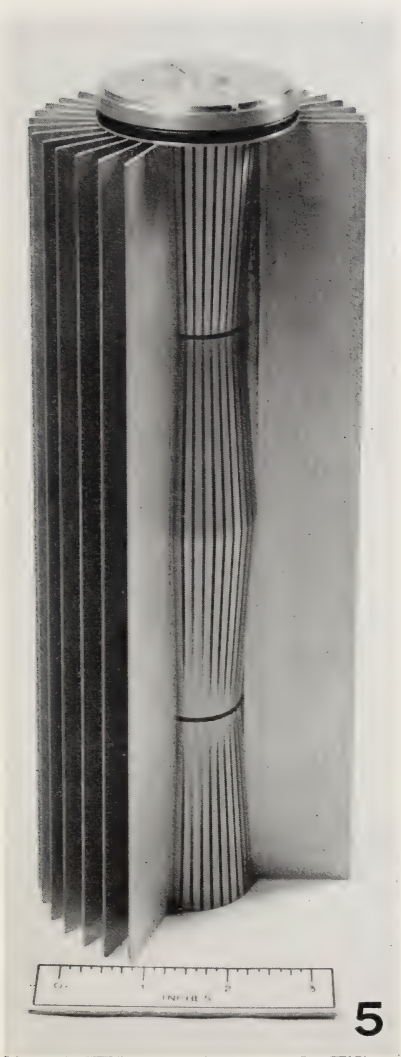
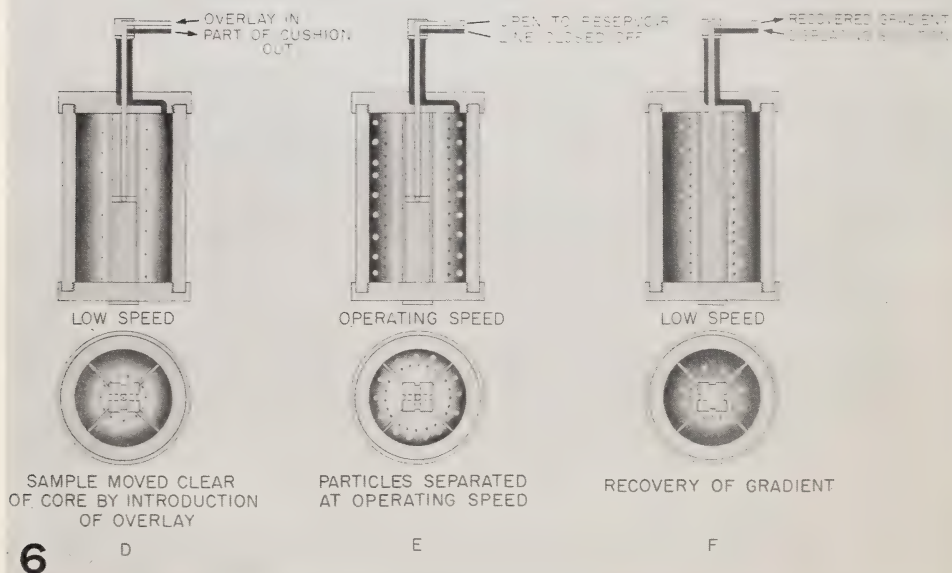
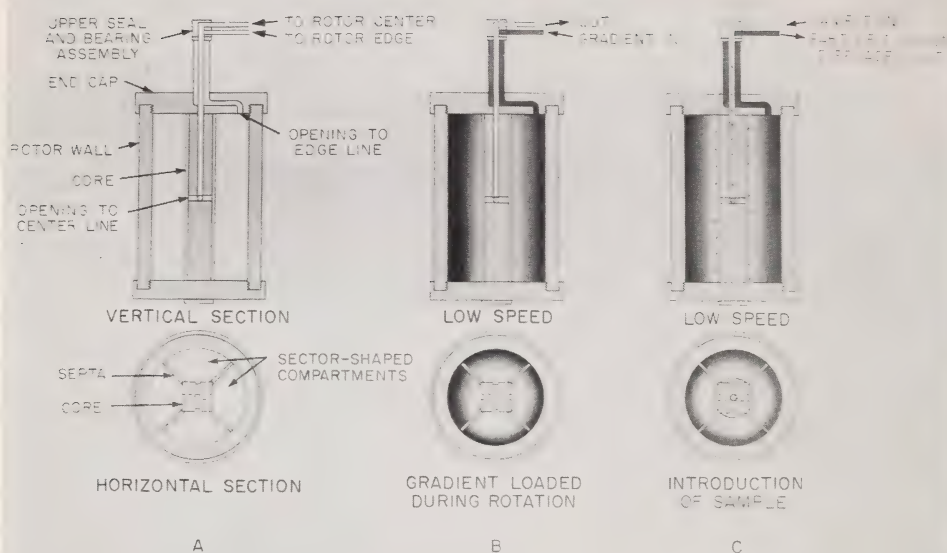


FIGURE 5.—Partially assembled core of B-II zonal centrifuge rotor.



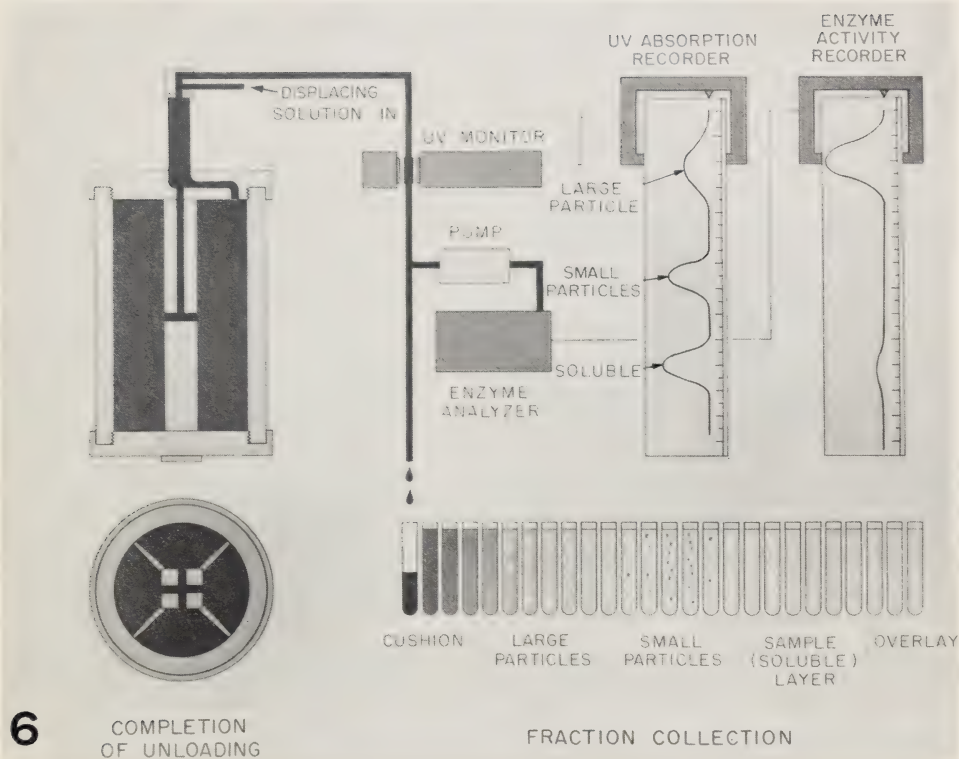


FIGURE 6.—Diagrammatic presentation of operation of the B-IV zonal centrifuge. (A) Schematic diagram of zonal centrifuge rotor. Rotation is about the vertical (*long*) axis. Rotor is shown at each stage in both side (*upper*) and cross (*lower*) section. See text for description of operation.



## Theory of Centrifugation: Miscellaneous Studies<sup>1</sup>

A. S. BERMAN, *Technical Division, Oak Ridge Gaseous Diffusion Plant,<sup>2</sup> Oak Ridge, Tennessee*

### SUMMARY

Several theoretical problems of interest in the biological centrifuge program at Oak Ridge have been investigated. These include: 1) a study to provide estimates of the Coriolis forces and transient times depending on particle, medium, and centrifuge properties, 2) an analysis of the efficiencies of batch,

semibatch, and continuous centrifugation procedures, and 3) a study of various aspects of the band capacity problem in zonal centrifugation. Where possible, specific examples have been given to illustrate and clarify the results of the theoretical work.—*Nat Cancer Inst Monogr* 21: 41-76, 1966.

THE BASIC THEORY of sedimentation in a centrifugal field has been the subject of many studies since the classic work reported by Svedberg and Pederseon (1) in 1940. Many of the subsequent significant developments have been described recently in an excellent monograph by Hiroshi Fujita (2).

The present paper describes several applications of sedimentation theory, appropriately modified where required, to problems of interest in the zonal centrifuge program at Oak Ridge.

The first part of the paper examines the conditions under which Coriolis forces and transient times become important in sedimentation problems. This is followed by an analysis of various schemes for centrifugation in a constant density medium and includes a comparison of the efficiencies of batch, semibatch, and continuous centrifugation. Finally, zonal centrifugation is discussed with emphasis on the stability of a migrating band in a density gradient.

### CORIOLIS FORCES AND TRANSIENT TIMES

Most of the work presented in this paper demands a knowledge of an appropriate sedimentation equation. In biological systems, a multitude

<sup>1</sup> This research performed under the Joint National Institutes of Health-Atomic Energy Commission Zonal Centrifuge Development Program which is supported by the National Cancer Institute, the National Institute of Allergy and Infectious Diseases, and the U.S. Atomic Energy Commission.

<sup>2</sup> Operated for the U.S. Atomic Energy Commission by the Nuclear Division of Union Carbide Corporation.

of factors can complicate the sedimentation process and virtually defy analysis because of our inherent ignorance of the detailed behavior of such systems. Since the problems treated in this paper are general, rather than specifically related to any one biological system, the sedimentation equation is, in most cases, a simple one.

For completeness, we include here a "hydrodynamic derivation" of the sedimentation equation. This derivation will provide estimates of the conditions under which Coriolis forces and transient times become important in computing sedimentation velocities and times.

### Derivation of Sedimentation Equation

Consider a coordinate system rotating with constant angular velocity  $\omega$  relative to some fixed frame of reference. Let  $\mathbf{P}$  be the position vector of a particle of mass  $m$ , in the rotating coordinate system. The equation of motion of the particle is then

$$m \frac{d^2 \mathbf{P}}{dt^2} = \mathbf{F} \quad [1]$$

where  $\mathbf{F}$  is the sum of the force acting on the particle and  $(d^2 \mathbf{P}/dt^2)$  is the acceleration of the particle relative to the space-fixed axes. The differential operator  $(d/dt)$ , representing changes relative to space-fixed axes, can be written in terms of a differential operator  $(\partial/\partial t)$ , which represents changes relative to the rotating coordinate system as follows.

$$\frac{d( )}{dt} = \frac{\partial}{\partial t} + \omega \times ( ) \quad [2]$$

Applying this operator twice to the position vector  $\mathbf{P}$  and recalling that  $\omega$  is independent of time, one obtains from equation 1

$$m \left[ \frac{\partial \mathbf{v}}{\partial t} + 2\omega \times \mathbf{v} + \omega \times (\omega \times \mathbf{P}) \right] = \mathbf{F} \quad [3]$$

where  $\mathbf{v} = (\partial \mathbf{P}/\partial t)$  and is the particle velocity measured relative to the rotating axes.

The force  $\mathbf{F}$  consists of two parts— $\mathbf{F}_1$  from the drag on the particle (Stokes' resistance) and  $\mathbf{F}_2$  from the buoyancy of the particle. For simplicity we will use the drag force as given by Stokes' resistance law for a spherical particle

$$\mathbf{F}_1 = -3\eta\pi D \mathbf{v} \quad [4]$$

where  $\eta$  is the viscosity of the suspending medium and  $D$  is the particle diameter. Nonspherical particles can be handled in the usual fashion by the introduction of appropriate shape factors.

The buoyant force on the particle is given by

$$\mathbf{F}_2 = - \iint_S p \mathbf{n} \, ds \quad [5]$$

with  $p$  the pressure in the fluid,  $\mathbf{n}$  the outward directed normal at the particle surface, and where the integral is to be evaluated over the surface of the particle.

Green's theorem can now be used to convert the surface integral into an integral over the volume of the particle so that

$$\mathbf{F}_2 = - \iiint_V p \mathbf{n} \, ds = - \iiint_V \text{grad } p \, d\tau. \quad [6]$$

If the particle is sufficiently small so that  $\text{grad } p$  does not change in the region of space occupied by the particle, we obtain finally for the buoyant force

$$\mathbf{F}_2 = -V \text{grad } p \quad [7]$$

where  $V$  is the particle volume.

If the suspending medium is assumed to be an incompressible fluid with density  $\rho_m$ , then the equation of motion for the fluid rotating as a rigid body gives the pressure gradient

$$-\text{grad } p = \rho_m \boldsymbol{\omega} \times (\boldsymbol{\omega} \times \mathbf{P}) \quad [8]$$

Using equations 3, 4, 7, and 8, and taking the volume of the particle (assumed spherical) to be  $\pi D^3/6$  and its mass to be  $\rho_p \pi D^3/6$  with  $\rho_p$  the particle density, we obtain for the equation of motion

$$-\beta \mathbf{v} = k \frac{\partial \mathbf{v}}{\partial t} + 2k \boldsymbol{\omega} \times \mathbf{v} + \boldsymbol{\omega} \times (\boldsymbol{\omega} \times \mathbf{P}) \quad [9]$$

with

$$\beta \equiv 18\eta/(\rho_p - \rho_m)D^2 \quad [10]$$

and

$$k = \rho_p/(\rho_p - \rho_m). \quad [11]$$

The terms on the right-hand side of equation 9 represent, respectively, the particle acceleration in the rotating coordinate system, the Coriolis effect, and the effect of the centrifugal field.

### Transient Time and Coriolis Effect

It is now convenient to specialize to cylindrical coordinates and choose a "z" axis in the direction of  $\boldsymbol{\omega}$ . Then ignoring changes in the "z" direc-

tion, the equation of motion (equation 9) yields the following two equations for the radial velocity,  $v_r$ , and the tangential velocity,  $v_\theta$ , of the particle:

$$-\beta v_r = k \dot{v}_r - r \omega^2 \left( 1 + \frac{2k\Omega}{\omega} + \frac{k\Omega^2}{\omega^2} \right) \quad [12]$$

$$-\beta v_\theta = k \dot{v}_\theta + 2k v_r \omega \left( 1 + \frac{\Omega}{2\omega} \right) \quad [13]$$

where  $r$  is the radial distance of the particle from the axis of rotation and  $\Omega$ , the angular velocity of the particle in the rotating coordinate system has been defined as  $\Omega = v_\theta/r$ . The dots represent differentiation with respect to time.

This coupled pair of equations would be difficult to solve in general because of the nonlinearity in the terms containing  $\Omega^2$  and  $v_r \Omega$ . Fortunately, however, we are interested only in estimating the transient times and Coriolis effects for systems where  $k\Omega/\omega$  and hence  $\Omega/\omega$  are small compared to unity. Hence:

$$-\beta v_r = k \dot{v}_r - r \omega^2 \quad [14]$$

$$-\beta v_\theta = k \dot{v}_\theta + 2k v_r \omega \quad [15]$$

Equation 14 is a second-order linear differential equation for the radial coordinate  $r$  and yields a general solution

$$r = A e^{\alpha_1 t} + B e^{\alpha_2 t} \quad [16]$$

where  $A$  and  $B$  are constants of integration and

$$\alpha_1 = -\frac{\beta}{2k} \left[ 1 - \sqrt{1 + (4k\omega^2/\beta^2)} \right] \quad [17]$$

$$\alpha_2 = -\frac{\beta}{2k} \left[ 1 + \sqrt{1 + (4k\omega^2/\beta^2)} \right] \quad [18]$$

For systems of interest in the present context, the cluster  $4k\omega^2/\beta^2$  is small compared with unity so that we can write

$$\sqrt{1 + (4k\omega^2/\beta^2)} \doteq 1 + (2k\omega^2/\beta^2)$$

and  $\alpha_1, \alpha_2$  are given to a good approximation by

$$\alpha_1 \doteq \omega^2/\beta \quad [19]$$

$$\alpha_2 \doteq -\frac{\beta}{k} \left( 1 + \frac{\omega^2 k}{\beta^2} \right). \quad [20]$$

Thus, we obtain finally for the particle position,  $r$ , as a function of time

$$r = A \exp(\omega^2 t/\beta) + B \exp \left[ -\frac{\beta}{k} \left( 1 + \frac{\omega^2 k}{\beta^2} \right) t \right] \quad [21]$$

$$(4k\omega^2/\beta^2) \ll 1$$

$$(k\Omega/\omega) \ll 1.$$

The contribution of the second term is seen to decrease with increasing time and drops to  $(1/e)$  of its initial value in a time equal to approximately  $(k/\beta)$  seconds. The transient time estimate we have been seeking is given by

$$\text{Transient time constant} = \frac{k}{\beta} = \frac{\rho_p D^2}{18\eta} \text{ seconds} \quad [22]$$

The radial velocity, or sedimentation velocity, of the particle is now obtained by differentiating equation 21 to obtain

$$v_r = \dot{r} = (dr/dt) = A\alpha_1 e^{\alpha_1 t} + B\alpha_2 e^{\alpha_2 t} \quad [23]$$

or, for systems with negligible transient time,

$$v_r = A\alpha_1 e^{\alpha_1 t} = \alpha_1 r = \frac{\omega^2 r}{\beta} = \frac{(\rho_p - \rho_m)D^2}{18\eta} \omega^2 r \quad [24]$$

Equation 24 is recognized as the expression for the sedimentation velocity usually used for a spherical particle.

If the approximations used for the solution of the radial equation are applied to the solution of equation 15 for the tangential velocity, one obtains (ignoring the transient)

$$v_\theta \doteq -\frac{2k\omega^3 r}{\beta^2} = -2\omega^3 \left( \frac{D^2}{18\eta} \right)^2 \rho_p (\rho_p - \rho_m) r \quad [25]$$

Note that the Coriolis effect varies with the cube of the angular velocity and the fourth power of the particle diameter. Further, the Coriolis

effect is such as to make the particle move tangentially in a direction opposite to the direction of rotation of the system.

It is instructive to examine the ratio of the tangential velocity produced by the Coriolis forces to the radial sedimentation velocity in the steady state. From equations 24 and 25

$$\frac{v_{\theta}}{v_r} = - \frac{\rho_p D^2}{9\eta} \omega \quad [26]$$

The relative effect of Coriolis force becomes more important at high speeds of rotation for large, dense particles in a low viscosity medium.

### Summary and Discussion

The general equation of motion for a spherical particle settling through an incompressible fluid in a centrifugal field has been derived with consideration of the time dependence of the sedimentation velocity and the effect of Coriolis force. The result, equation 9, is valid for the analysis of the settling of particles in a centrifuge of any geometry, as long as the Stokes' law of resistance is not violated, *i.e.*, for sufficiently slow settling velocities.

The general equation was then solved in a cylindrical coordinate system and estimates obtained for the transient time constant and the relative effect of the Coriolis force (equations 22 and 26). It was found that the transient time constant is directly proportional to the particle density and to the square of the particle diameter; it is inversely proportional to the viscosity of the suspending medium. The particle tangential velocity produced by the Coriolis effect was found to vary directly with the cube of the rotation angular velocity, the fourth power of the particle diameter, the particle density, the difference in density between particle and suspending medium, and the distance of the particle from the axis of rotation; it varies inversely as the square of the viscosity of the suspending medium. In addition the Coriolis force acts to give the particle a tangential velocity in a direction opposite to that of the rotation of the centrifuge.

Virtually all the biological systems of interest in the program at Oak Ridge are such that transient effects and Coriolis effects are completely negligible. For such cases, equation 24 is used for the sedimentation velocity.

### CENTRIFUGATION IN A CONSTANT DENSITY MEDIUM

The recovery of virus particles from large volumes of culture fluids, tissue extracts, plasma, or natural waters by centrifugal methods is of interest from several points of view. The recent development of zonal centrifuge rotors capable of centrifuging relatively large volumes of fluid (3-5) and seal systems that allow fluids to be pumped into and out of such rotors without aerosol production (6) has raised the question of

the applicability of such rotors to the problem of large-scale virus isolation. In orienting studies (7) the B-II zonal rotor was used to demonstrate that particles could be concentrated and purified by continuous flow centrifugation followed by banding in CsCl in the same rotor. However, the B-II rotor is not ideally suited to continuous-flow centrifugation since the fluid stream in the rotor short-circuits a large part of the rotor volume. In this paper certain theoretical aspects of continuous-flow centrifugation are presented that have been used in the design of a later rotor, B-V. The core of this rotor is intended for instances in which the amount of solid material to be recovered is very small, and where sedimentation against a solid surface has no adverse effect.

### Batch and Semibatch Centrifugation

In a conventional batch technique the rotor is filled with a virus suspension (fig. 1A), and the material is centrifuged for the time required to remove a given fraction of the virus (fig. 1B). By use of the seal system developed for the zonal centrifuge, the depleted suspending medium may be displaced out of the spinning rotor through the edge line with distilled water, which is added through the core line (figs. 1C and D). To recharge the rotor, the direction of flow is reversed (fig. 1E) and a fresh batch of virus suspension is introduced into the rotor through the edge line, displacing distilled water (or other fluid lighter than the virus suspension) out through the core line until the rotor is refilled (text-fig. 1F). After the desired number of batches is run, the sediment that has accumulated on the rotor wall is mechanically removed after the rotor is stopped, or the virus may be banded in CsCl introduced through the edge line during rotation as previously described (7). In the semibatch process the rotor is never completely filled with the virus suspension. Instead, batches are consecutively introduced which fill the rotor to a predetermined thickness (fig. 2A). The remainder of the rotor is filled with distilled water or other fluid that is lighter than the virus suspension. The centrifuge is then run for the time required to remove a given fraction of the virus from the layer (fig. 2B), after which the layer is "backed out" by feeding the light displacement fluid to the rotor center through the core line (fig. 2C), and a second quantity of suspension then introduced through the edge line (fig. 2D). The essential feature of the semibatch method is that each small volume of fluid introduced is oriented in a thin layer close to the rotor wall. An alternative method for achieving this is to add a solute to successive samples so that each displaces the previous, less dense one toward the core. The volume of successive discrete samples may be decreased to the point where the feed stream is introduced as a continuous density gradient. As the density of the stream increases, the sedimentation rate of the suspended particles decreases, approaching zero as the isopycnic density is approached. This is not considered a true continuous-flow method but rather a modification of the semibatch method, since the volume of fluid to be processed is limited.

With all the rotor systems used thus far, a core is used which occupies the rotor axis and defines the minimum radius of the fluid mass in the rotor. The batch and semibatch methods, in effect, differ by changing the volume of the rotor filled with the sample. The question to be answered is: Will greater efficiency be obtained by one or a few batch runs with the rotor full of virus suspension, or by centrifuging many batches which are confined to that part of the rotor having the highest centrifugal force field? This question, whose answer is perhaps intuitively obvious, can be formulated and answered analytically as follows.

Consider a cylindrical centrifuge of radius  $r_2$  and length  $L$ , rotating with angular velocity  $\omega$  radians per second. Initially, the centrifuge may be taken to be filled with distilled water. A layer of suspension containing spherical particles of density  $\rho_p$  suspended in a medium of density  $\rho_m$  is fed to the wall. This layer of thickness  $r_2 - r_k$  occupies a volume  $\pi(r_2^2 - r_k^2)L$ . If the particles are assumed to be uniformly distributed throughout this layer, then any part of this layer, say  $r_2 - r_f$  ( $r_k \leq r_f \leq r_2$ ) contains a fraction  $f$  of the particles where  $f$  is given by

$$f = \frac{r_2^2 - r_f^2}{r_2^2 - r_k^2} \quad [27]$$

A particle at a distance  $r$  from the axis moves toward the wall with a velocity  $v_r$  given by equation 24 as

$$v_r = \frac{dr}{dt} = \frac{\omega^2 r}{\beta}$$

with  $\beta$  defined by equation 10

$$\beta \equiv \frac{18\eta}{(\rho_p - \rho_m)D^2}.$$

For a particle starting at  $r_f$  at time zero, the time required to settle to the wall is obtained by integrating the expression for the velocity. In this integration particle properties are assumed constant during sedimentation and one obtains

$$\int_0^{t_f} dt = \frac{\beta}{\omega^2} \int_{r_f}^{r_2} \frac{dr}{r} \quad \text{or}$$

$$t_f = \frac{\beta}{\omega^2} \ln \frac{r_2}{r_f} = - \frac{\beta}{2\omega^2} \ln \frac{r_f^2}{r_2^2} \quad [28]$$

From equation 27

$$\frac{r_f^2}{r_2^2} = 1 - \left(1 - \frac{r_k^2}{r_2^2}\right)f$$

so that

$$t_f = -\frac{\beta}{2\omega^2} \ln \left[ 1 - \left(1 - \frac{r_k^2}{r_2^2}\right)f \right] \quad [29]$$

In the semibatch process, after this time  $t_f$ , the layer is "backed-out" of the centrifuge and the process repeated. For convenience, the volume of suspension fed in each step is taken to be the same and equal to  $V_p$ . Then,

$$V_p = \pi r_2^2 L - \pi r_k^2 L = \pi r_2^2 L \left(1 - \frac{r_k^2}{r_2^2}\right)$$

or if  $V$  is taken to be the total rotor volume ( $\pi r_2^2 L$ ) one obtains

$$1 - \frac{r_k^2}{r_2^2} = \frac{V_p}{V} \quad [30]$$

Equation 29 for the centrifugation time required in each step to remove a fraction  $f$  of the particulates now becomes

$$t_f = -\frac{\beta}{2\omega^2} \ln \left(1 - \frac{V_p f}{V}\right) \quad [31]$$

If the total volume to be processed is  $V_b$ , then the total centrifugation time  $T$  will be  $(V_b/V_p)$  times  $t_f$  or

$$T = -\frac{\beta V_b}{2V_p \omega^2} \ln \left(1 - \frac{V_p f}{V}\right) \quad [32]$$

Equation 32 can be used to obtain total centrifugation times for either the batch or semibatch process. For the batch process  $V_p$  is taken to be the rotor volume available for liquid, that is  $V - V_c$ , the total rotor volume ( $V$ ) minus the core volume ( $V_c$ ). For the semibatch process  $V_p$  is taken to be some fraction of this, say  $\phi(V - V_c)$  where  $0 \leq \phi \leq 1$ . The total centrifugation time for the batch process is

$$T_B = -\frac{\beta V_b}{2(V - V_c)\omega^2} \ln \left[ 1 - \left(1 - \frac{V_c}{V}\right)f \right] \quad [33]$$

and for the semibatch process is

$$T_s = -\frac{\beta V_t}{2\phi(V - V_c)\omega^2} \ln \left[ 1 - \phi \left( 1 - \frac{V_c}{V} \right) f \right]. \quad [34]$$

It can be shown readily that the minimum time is obtained by making  $V_p$  approach zero in equation 32. This minimum time,  $T_m$ , is

$$T_m = \lim_{V_p \rightarrow 0} T = \frac{\beta V_t f}{2V\omega^2}. \quad [35]$$

It is emphasized at this point that the computed total times represent centrifugation times only and do not include the times required to load and unload the rotor in each step.

A comparison between the batch and semibatch procedures can now be obtained by examining the ratio of the times given by equations 34 and 33. This ratio, which is independent of the total volume of suspension to be processed, of the particle properties, and of centrifuge speed is given by

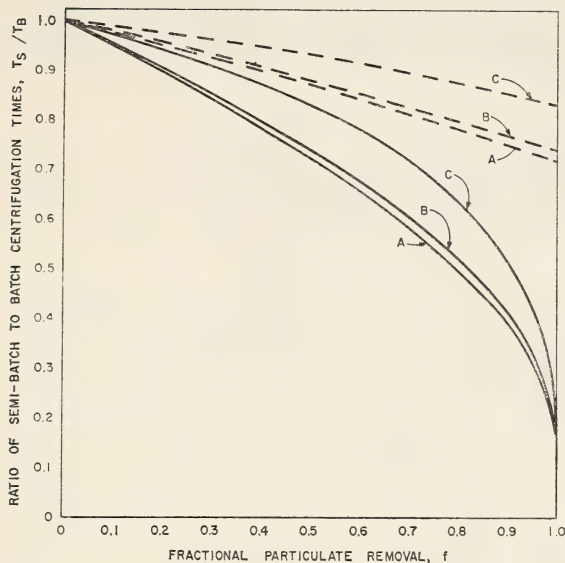
$$\frac{T_s}{T_B} = \frac{1}{\phi} \frac{\ln \{1 - \phi [1 - (V_c/V)]f\}}{\ln \{1 - [1 - (V_c/V)]f\}} \quad [36]$$

and is seen to depend on the ratio of the core volume to total volume ( $V_c/V$ ), the fractional particulate removal  $f$ , and the fraction  $\phi$  of available rotor volume loaded in each step of the semibatch process.

Text-figure 1 gives this ratio for several illustrative cases. The solid curves represent the ratio for a rotor without a core and are given for  $\phi$  equal to 0.1, 0.5, and for  $\phi$  approaching zero. The dashed curves represent the ratio for ( $V_c/V$ ) equal to one half, *i.e.*, for a centrifuge whose core occupies one half of the rotor volume. The latter curves are also given for  $\phi$  equal to 0.1, 0.5, and approaching zero.

The reduced centrifugation time for the semibatch process for the removal of a substantial fraction of particulates is evident from these curves, especially for the case of a rotor without a core. For example, to remove 90 percent of the particulates, the semibatch centrifugation time is about 52 percent of the batch time for a rotor without a core and a  $\phi$  value of 0.5. For a rotor whose core occupies one half of the rotor volume, the corresponding figure is about 85 percent.

In general, semibatch operation would seem to be indicated for hollow rotors but would not necessarily be advantageous for a rotor whose core occupies a substantial portion of the rotor volume since more loading and unloading steps are required to process a given quantity of material by the semibatch technique.



TEXT-FIGURE 1.—Comparison of batch and semibatch processes. *Solid line*, hollow rotor; *broken line*, core volume is one half rotor volume. A,  $\phi=0$ ; B,  $\phi=0.1$ ; C,  $\phi=0.5$  is the fraction of available rotor volume loaded in each step of the semibatch process.

### Continuous Centrifugation

Both processes discussed in the previous section were considered for use in existing B-type rotors. If a design change is permitted in the core of a B-type rotor, then a continuous-flow technique can be considered. In this technique the core almost fills the rotor, leaving a thin annular space between the core and the rotor wall. The medium containing the virus is fed continuously to the annular space at one end of the rotor, flows along the annular space, and is removed at the opposite end of the rotor. The flow rate is adjusted so that a given fraction of the virus is removed.

A solution to this sedimentation problem has been obtained which accounts for the radial variation of the centrifugal field, and for the radial variation in axial flow across the annular space. Viscosity and pressure have been assumed constant in the annular flow channel, and the particles have been assumed to be spherical. It has also been assumed that the particles are uniformly distributed across the annular space at the feed point.

If the radial pressure variation produced by the centrifugal field in annular space between the core and the rotor wall is ignored, then the radial variation of axial velocity in the annulus is given by a well-known solution of the Navier-Stokes' equations of motion:

$$v_z = \frac{dZ}{dt} = \frac{2\bar{v}_z \left[ r_2^2 - r^2 - \frac{r_2^2 - r_1^2}{\ln(r_2/r_1)} \ln(r_2/r) \right]}{r_1^2 + r_2^2 - \frac{r_2^2 - r_1^2}{\ln(r_2/r_1)}} \quad [37]$$

where  $r_1$  is the core radius,  $r_2$  is the rotor radius,  $Z$  is the axial coordinate, and  $\bar{v}_z$  is the average axial velocity defined by

$$\bar{v}_z = \frac{2\pi \int_{r_1}^{r_2} r v_z dr}{\pi(r_2^2 - r_1^2)} = \frac{Q}{\pi(r_2^2 - r_1^2)} \quad [38]$$

with  $Q$  equal to the volume flow rate through the centrifuge. Equation 37 will be taken to be representative of the axial velocity of a particle located at a distance  $r$  from the axis of rotation. The radial velocity of such a particle is given by equation 24. The particle trajectory is obtained by dividing equation 37 by equation 24 to obtain

$$\frac{dZ}{dr} = \frac{2\gamma\lambda}{\rho_p - \rho_m} \frac{r_2^2 - r^2 - 2r_m^2 \ln(r_2/r)}{r} \quad [39]$$

where, for convenience, we have defined

$$\gamma = 9\eta/D^2\omega^2$$

$$\lambda = 2\bar{v}_z/[r_2^2 + r_1^2 - (r_2^2 - r_1^2)/\ln(r_2/r_1)]$$

$$r_m^2 = (r_2^2 - r_1^2)/\ln(r_2/r_1).$$

The effective length of a rotor required to remove a fraction  $f$  of the suspended solids is obtained by integrating equation 39 as follows

$$\int_0^{L_e} dZ = \frac{2\gamma\lambda}{\rho_p - \rho_m} \int_{r_f}^{r_2} \frac{[r_2^2 - r^2 - 2r_m^2 \ln(r_2/r)]}{r} dr \quad [40]$$

where  $L_e$  is the effective rotor length and  $r_f$  is given by equation 27 with  $r_k$  replaced by  $r_1$ . The integration indicated above gives the desired solution to the problem.

The solution relates a cluster of variables,  $U$  (depending on the properties of the centrifuge, the virus, and the suspending medium), to the fraction of the virus to be removed and the inner and outer radii of the annular flow channel:

$$\begin{aligned}
 U &= \frac{\pi r_2^2 \omega^2 L_e}{Q} \frac{D^2 (\rho_p - \rho_m)}{9\eta} \\
 &= \frac{2 \ln R^2}{(1 - R^2) [(1 + R^2) \ln R^2 + 2(1 - R^2)]} \\
 &\quad \times \left\{ \ln \frac{1}{1 - (1 - R^2)f} - (1 - R^2)f \right. \\
 &\quad \left. + \frac{1}{2} \frac{1 - R^2}{\ln R^2} \left[ \ln \frac{1}{1 - (1 - R^2)f} \right]^2 \right\} [41]
 \end{aligned}$$

where  $Q$  is the volume flow rate (cm<sup>3</sup>/sec);  $r_2$ , the outer radius of the annulus (cm);  $R$ , the ratio of the inner to outer radii of the annular flow channel; and  $L_e$ , the effective length of the rotor. The remaining symbols have been defined previously. The effective rotor length  $L_e$  is, in general, shorter than, but approaches, the true length of the annular flow channel as the axial mixing caused by the feed to the rotor approaches zero.

For the radius ratios greater than  $R = 0.8$ ,  $U$  is given with a maximum error of 5 percent by the much simpler expression

$$U = f^2(3 - 2f) - (f^2/2)(5f^2 - 8f + 2)(1 - R^2). \quad [42]$$

These equations permit preliminary design calculations to be made readily, once the required properties of the centrifuge, the particle, and the suspending medium are known.

Text-figure 2 gives  $U$  as a function of the radius ratio  $R$ , for three values of  $f$ , the fraction of virus removed. The text-figure also shows the values of  $U$  obtained from the simple formula valid for radius ratios close to unity. A typical calculation may illustrate the use of the equations:

#### Centrifuge Properties

$$r_2 = 5 \text{ cm}$$

$$L_e = 25 \text{ cm}$$

$$R = (r_1/r_2) = 0.9$$

$$\text{Speed} = 20,000 \text{ rpm}$$

$$\omega = 2.094 \times 10^3 \text{ radians/sec}$$

$$V = 1963 \text{ cm}^3$$

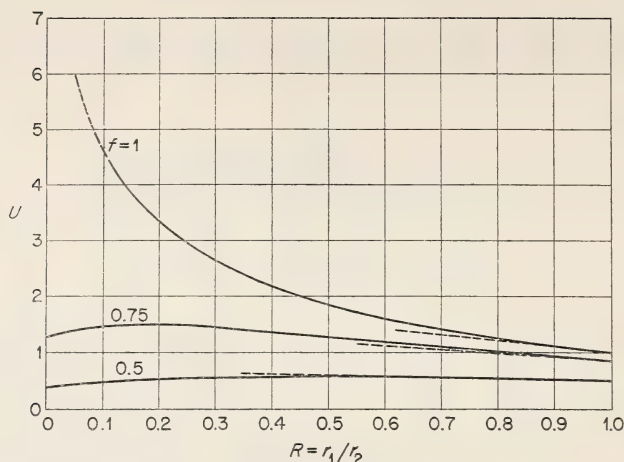
#### Particle and Medium Properties

$$\rho_p = 1.51 \text{ g/cm}^3 \text{ (T3 phage)}$$

$$D = 5.5 \times 10^{-6} \text{ cm (T3 phage)}$$

$$\rho_m = 1.05 \text{ g/cm}^3$$

$$\eta = 0.01519 \text{ poise}$$



TEXT-FIGURE 2.—Flow function  $U$  for continuous-flow centrifuge. Broken line, computed from simplified equation 42 for  $R$  close to unity.

Assume that all the particles must be removed, so that  $f = 1$ . Since  $R$  is close to unity, we can estimate  $U$  from equation 42 to obtain

$$U = 1 - \frac{1}{2}(-1)(1 - 0.9^2) = 1.095. \quad [43]$$

The more accurate equation for  $U$  gives 1.109 for this case, so that the error of the approximation formula in this case is only about 1.3 percent. The feed rate can now be computed from the known value of  $U$ :

$$Q = \frac{\pi r_2^2 \omega^2 L_e}{U} \frac{D^2(\rho_p - \rho_m)}{9\eta} = 2.84 \text{ liters/hr.} \quad [44]$$

Thus 50 liters of suspension can be processed in about 17.6 hours with this centrifuge. If the speed were about 40,000 rpm the flow rate could be increased to about 11.4 liters per hour, and 50 liters could be processed in about 4.4 hours.

Ambler (8) has given an equation relating flow rates, centrifuge properties, and particle properties for a continuous-flow tubular centrifuge. The equation he provides is limited by the assumptions of (a) 50 percent removal of particulates, and (b) the axial velocity in the liquid layer is uniform across the thickness of the layer.

The present work provides the relationships between the desired variables for any fractional removal of particulates and for a laminar velocity distribution in the flowing liquid layer. For the special case of 50 percent removal and thin liquid layer, the present equation gives essentially the same result as that obtained from Ambler's relation. The comments made by Ambler concerning the effects of turbulence and diffusion also apply to the present results.

Equation 41 can be expressed in terms of the sedimentation coefficient defined by

$$S \equiv \frac{1}{\omega^2 r} \frac{dr}{dt} \times 10^{13} \text{ Svedberg units}$$

or for the present case

$$S = \frac{(\rho_p - \rho_m) D^2}{18\eta} \times 10^{13} . \quad [45]$$

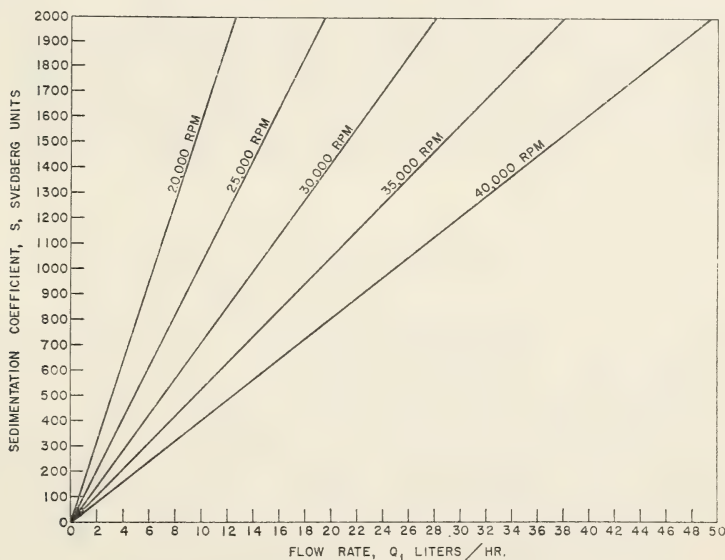
Equation 41 can now be written

$$U = \frac{2\pi r_2^2 \omega^2 L_e}{Q} S \times 10^{-13} \quad [46]$$

If the flow rate is expressed as  $Q_1$  in liters per hour (instead of  $Q$  in  $\text{cm}^3/\text{sec}$ ), and the speed of the rotor is given in revolutions per minute (rpm), then equation 46 provides the following relation between the sedimentation coefficient and the flow rate

$$S = \frac{10^{16} U}{8\pi^3 r_2^2 L_e} \frac{1}{(\text{RPM})^2} Q_1 \quad [47]$$

where  $S$  is in Svedberg units,  $Q_1$  is in liters per hour, and  $U$  is given exactly by equation 41 or approximately (when  $R$  is close to unity) by equation 42.



TEXT-FIGURE 3.—Relation between sedimentation coefficient and flow rate at various speeds. Centrifuge radius, 5 cm; length, 25 cm; core radius, 4.92 cm; fractional removal, 0.95.  $S = \frac{6.50 \times 10^{10}}{(\text{rpm})^2} Q_1$ , where  $S$  is in Svedberg units,  $Q_1$ , liters per hour, and rpm, revolutions per minute.

Text-figure 3 shows the sedimentation coefficient as a function of the flow rate in liters per hour  $Q_1$  for various centrifuge speeds. The calculations were made by using equation 47 with  $r_2 = 5$  cm,  $L_e = 25$  cm,  $R = 0.984$ , and  $f = 0.95$ .

### Summary and Discussion

An analysis has been presented for the calculation of centrifugation times or flow rates required for a given separation task from a knowledge of the centrifuge, particle, and suspending medium properties. Equations 33 and 34 give the total centrifugation times required for conventional batch and semibatch operations, respectively. Equation 47 with the use of the appropriate equation for  $U$  (equation 41 or 42) provides for the rapid calculation of continuous flow rates.

In general, the semibatch process required shorter centrifugation times than the batch process for a given separation task, particularly in a rotor with a small volume core. The advantage of semibatch over batch operation decreases as the core volume approaches the rotor volume.

A fair comparison between the batch processes and continuous operation is not possible since such a comparison would depend in a major way on some assumed times for loading and unloading the rotor for the batch or semibatch operations. Some general statements can be made. For a rotor whose core virtually fills the rotor volume, *i.e.*, a narrow gap rotor, all three methods of operation require about the same centrifugation time for a given separation task with a given centrifuge, particle, and medium. However, even in this case, continuous-flow operation offers the usual practical advantages over batch operation. For rotors with small cores and for tasks that do not require a high percentage of particulate removal, the continuous process leads to shorter operating times than the batch processes.

### ZONAL CENTRIFUGATION (BAND CAPACITY)

The biological centrifuge program at Oak Ridge is concerned primarily with the development of high-resolution and high-capacity centrifugation techniques for a wide variety of materials. A major method under study is zonal centrifugation, which assumes that particles settling through a density gradient can be separated because of differences in their sedimentation rate as well as differences in particle density. In this technique, a "layer" of particles is loaded at the low-density end of a density gradient that has previously been built up in a suitable rotor. The density gradient, which is stabilized by the centrifugal field, is usually obtained by using either sucrose or various salts dissolved in an appropriately buffered water solution. The particles settle through the density gradient at a rate depending on the particle size and shape, the local viscosity of the medium, the particle distance from the axis of rotation, the difference

in density between the particles and the local density of the medium, and the speed of rotation of the centrifuge. Thus, if the original particle layer consisted of a mixture of particles with different properties, these different particles will, after a given period of centrifugation, appear at various points along the density gradient. After a sufficiently long centrifugation time the different particles will be found at points in the density gradient where the local density is equal to the particle density.

Optimum use of the technique for high-resolution, high-capacity particle separations requires the solution of a number of difficult problems concerned with the mechanical design of the centrifuge, with obtaining and maintaining a suitable density gradient in the rotor, with the conditions required for stable settling particle zones, and with unloading the separated particle zones with a minimum of remixing.

The work to be discussed here deals with several theoretical studies on factors that may be of importance in maintaining stable zones of settling particles. These factors, which have come to be known as the "zonal capacity" problem, are of importance since an understanding of them may lead to an estimate of the maximum amount of particles that can be loaded into a given density gradient without the loss of resolution during the settling of the particle zones. Hopefully, a complete understanding would also enable one to specify the best set of operating conditions for any separation task.

Previous work in this area is sparse and limited in scope. Thus, Svensson and co-workers (9) considered the zonal capacity problem with reference to electrophoresis in a density gradient. In this case, the force field is independent of particle position and the particle zone undergoes little dilution during separation. Brakke (10) attempted to test the results of the Svensson analysis and concluded that only a fraction of the theoretical zone capacity, *i.e.*, of the maximum particle loading in a zone, could be attained in practice.

In the work to be described here an attempt was made to include the dilution factor due to migration in a field with cylindrical symmetry, the effect of the varying centrifugal field with position on band width, and the effect of the diffusion of the density gradient producing solute on the local medium density as a function of time.

The presentation will be divided into three sections: (a) the determination of the effect of migration of a finite particle band in a varying centrifugal field on band stability for a given class of density gradients, (b) an extension of the Svensson criterion to include geometry and varying field effects for arbitrary density gradients, and (c) the effect of time dependence of the density gradient on the stability of a migrating particle band. In all cases, the Svensson criterion for stability will be accepted as a reasonable *local* criterion and the effect of the band migration on its stability will be examined.

This *local* stability criterion is simply the requirement that the density anywhere in the migrating band does not exceed the density at any other point located at a greater distance from the axis of rotation. Further,

one considers that the particles in the band contribute to the local density in the band.

I am indebted to Dr. S. Prager of the University of Minnesota for many helpful suggestions and discussions relative to the studies presented in the following sections.

### Density Inversion During Centrifugation<sup>3</sup>

1. *Formulation of problem.*—We consider a centrifuge filled with a solvent whose density,  $\rho_m$ , increases with increasing distance  $r$  from the axis. [These density variations are, of course, produced through a concentration gradient in a suitable solute  $A$  which, following Svensson (9), we consider as part of the solvent.] Into this system we introduce a macromolecular species  $B$  of volume  $\bar{V}$  per molecule and density  $\rho_p > \rho_m$ ; let the initial concentration distribution of  $B$  be  $c_0(r)$ , in molecules per unit volume. The migration of  $B$  particles in the centrifugal field causes their concentration to depend upon time as well as position, so that after a time  $t$  the new concentration distribution will be  $c(r, t)$ . These concentration changes in turn affect the distribution of density in the centrifuge, and give rise to the possibility that the total density of solvent plus  $B$  may in some regions actually decrease with increasing  $r$ , creating a hydrostatically unstable situation. It is with the occurrence of such instabilities, produced in an initially stable system by the sedimentation of  $B$ , that we shall concern ourselves.

To render the problem a little more tractable we make the following assumptions: (a) There is no diffusion, either of  $B$ , or of the solute  $A$ , which produces the density gradient, during the time of a run; (b) the volume fraction  $\bar{V}c$  of  $B$  is everywhere and at all times small compared to unity, so that we can ignore the displacement of solvent by migrating  $B$  particles. With these two assumptions, the solvent density  $\rho_m(r)$  becomes time independent, which greatly simplifies the calculations.

The time dependence of the concentration distribution  $c(r, t)$  is governed by the continuity equation

$$\frac{\partial c}{\partial t} = -\frac{1}{r} \frac{\partial}{\partial r} (rvc) \quad [48]$$

where  $v$ , the migration velocity of  $B$ , is, in the absence of diffusion, given by

$$v = \frac{\omega^2 \bar{V}}{f_0(r)} [\rho_p - \rho_m(r)]r \quad [49]$$

$\omega$  being the angular velocity, in radians per unit time, at which the centrifuge is spinning, and  $f_0$  the friction coefficient for the  $B$  species. Al-

<sup>3</sup> The technique used to study stability as presented in this section is due to Dr. S. Prager, University of Minnesota.

though we shall later assume that  $f_0$  is constant, it must, in general, be considered a function of  $r$ , because of the variation in the solvent viscosity with changing concentration of  $A$ .

Combinations of equations 48 and 49 lead to the partial differential equation

$$\frac{\partial c}{\partial t} = - \frac{\omega^2}{r} \frac{\partial}{\partial r} \left\{ \frac{\bar{V}r^2[\rho_p - \rho_m(r)]c}{f_0(r)} \right\} \quad [50]$$

to be solved subject to the initial condition

$$c(r, 0) = c_0(r) \quad [51]$$

2. *Solution of equation.*—Equation 50 may be solved by the method characteristics. We multiply both sides by  $\bar{V}r^2(\rho_p - \rho_m)/f_0$ , and define a new concentration variable

$$\zeta \equiv \bar{V}r^2(\rho_p - \rho_m)c/f_0, \quad [52]$$

to obtain

$$\frac{\partial \zeta}{\partial t} = - \frac{\omega^2 \bar{V}r[\rho_p - \rho_m(r)]}{f_0(r)} \frac{\partial \zeta}{\partial r} \quad [53]$$

Division by  $\partial \zeta / \partial r$  now gives

$$\left( \frac{\partial r}{\partial t} \right)_{\zeta} = \frac{\omega^2 \bar{V}r[\rho_p - \rho_m(r)]}{f_0(r)} \quad [54]$$

from which the contours of constant  $\zeta$  in the  $(r, t)$  plane may be calculated by integration:

$$\omega^2 t = \int_{r_0(\zeta)}^r \frac{f_0(r) dr}{\bar{V}r[\rho_p - \rho_m(r)]}, \quad [55]$$

where  $r_0(\zeta)$  satisfies the relation

$$\zeta = \bar{V}r_0^2[\rho_p - \rho_m(r_0)] c_0(r_0)/f_0(r_0) \quad [56]$$

Equation 55 is, in implicit form, the desired solution of equation 50.

3. *Example of application.*—Let us consider the particular case of a density gradient of the form

$$\rho_m(r) = \rho_p - \frac{k}{r^n}, \quad [57]$$

where  $k$  and  $n$  are positive constants. Let us further assume that the friction coefficient  $f_0$  and particle volume  $\bar{V}$  are independent of  $r$ . Substitution of equation 57 into 55 then gives

$$\omega^2 t = \frac{f_0}{\bar{V}nk} [r^n - r_0^n(\zeta)] \quad [58]$$

To obtain  $r_0(\zeta)$ , we must specify  $c_0(r)$ , and for this purpose we suppose that at  $t = 0$  a band extending from  $r = r_1$  to  $r = r_2 > r_1$  is loaded with  $B$  to maximum capacity, so that the total density is initially given by

$$\rho_t(r, 0) = \begin{cases} \rho_m(r) & (r < r_1) \\ \rho_m(r_2) & (r_1 < r < r_2) \\ \rho_m(r) & (r > r_2) \end{cases} \quad [59]$$

Clearly, any further loading of  $B$  into the band would produce a density inversion.

The density  $\rho_t$  is related to the concentration  $c$  by the equation

$$\rho_t = \rho_m + c\bar{V}(\rho_p - \rho_m); \quad [60]$$

By combining equation 60 with 52, we obtain

$$\rho_t = \rho_m + \frac{f_0 \zeta}{r^2} \quad [61]$$

The initial position dependence of  $\zeta$  is therefore

$$\zeta(r, 0) = \begin{cases} 0 & (r < r_1) \\ \frac{kr^2}{f_0} \left( \frac{1}{r^n} - \frac{1}{r_2^n} \right) & (r_1 < r < r_2) \\ 0 & (r > r_2) \end{cases} \quad [62]$$

The function  $r_0(\zeta)$  is obtained by inversion of equation 62, and  $\zeta(r, t)$  then follows from equation 58:

$$\zeta(r, t) = \begin{cases} 0 & [(r^n - \tau)^{1/n} < r_1] \\ \frac{k(r^n - \tau)^{2/n}}{f_0} \left( \frac{1}{r^n - \tau} - \frac{1}{r_2^n} \right) & [r_1 < (r^n - \tau)^{1/n} < r_2] \\ 0 & [(r^n - \tau)^{1/n} > r_2] \end{cases} \quad [63]$$

where  $\tau = \omega^2 \bar{V} n k t / f_0$ . At time  $t$  the band containing the  $B$  species thus extends from  $r = (r_1^n + \tau)^{1/n}$  to  $r = (r_2^n + \tau)^{1/n}$ , and within it the density varies according to the relation

$$\rho_t = \left( \rho_p - \frac{k}{r^n} \right) + \frac{k(r^n - \tau)^{2/n}}{r^2} \left( \frac{1}{r^n - \tau} - \frac{1}{r_2^n} \right);$$

$$(r_1^n + \tau)^{1/n} < r < (r_2^n + \tau)^{1/n} \quad [64]$$

A simple criterion for whether density inversion occurs within the band results from a comparison of  $\rho_p$  at its leading and trailing edges. The inequality,

$$\rho_t[(r_1^n + \tau)^{1/n}, \tau] < \rho_t[(r_2^n + \tau)^{1/n}, \tau], \quad [65]$$

must hold to avoid inversion. Substitution of equation 64 into 65 then leads, after simplification, to the stability condition

$$\left( 1 + \frac{\tau}{r_1^n} \right)^{(2/n)-1} > \left( 1 + \frac{\tau}{r_2^n} \right) \quad [66]$$

For  $0 < n \leq 1$ , the inequality equation 66 will always be satisfied, since  $r_1 < r_2$ , while for  $n \geq 2$  the exponent  $\frac{2}{n} - 1$  is zero or negative, so that equation 66 is always violated. We expect, therefore, that the sedimentation of  $B$  will stabilize the initial band in the former case, and destabilize it in the latter. The intermediate situation  $1 < n < 2$  is more complicated. For the initial stability to be maintained, equation 66 must be satisfied for small  $\tau$ , for which the left-hand side of the inequality may be expanded, to give, after simplification

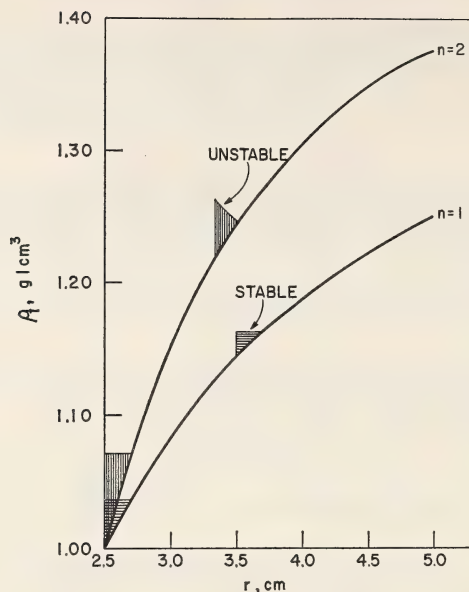
$$\frac{r_1}{r_2} < \left( \frac{2}{n} - 1 \right)^{1/n} \quad [67]$$

However, even if 67 is obeyed, the band will ultimately become unstable. The critical time  $\tau^*$  for the onset of instability may be obtained by finding the nonzero solution of the equation

$$\left( 1 + \frac{\tau^*}{r_1^n} \right)^{(2/n)-1} = \left( 1 + \frac{\tau^*}{r_2^n} \right) \quad [68]$$

Text-figure 4 shows the change in the density distribution of bands migrating in two special choices of density gradient for an equal length of time. The density gradients chosen are of the form given by equation 57 with  $n = 1$  and 2. Both bands start at the same point in the field and are assumed to be loaded to capacity (in the Svensson sense) for their assumed initial band width of 2 mm.

After migration for an equal period of time in their respective density gradients the density distribution as shown in the figure was computed from equation 64. The upper band ( $n = 2$  density gradient) is obviously unstable since its trailing edge has a higher density than its leading edge.



TEXT-FIGURE 4.—Density inversion during sedimentation.

The lower band ( $n = 1$  density gradient) is still stable and will remain so for this density gradient. Not shown in the figure is the behavior of a similar band migrating in a density gradient with  $1 < n < 2$ . For a band which, at  $t = 0$ , has a trailing edge at  $r = 2.5$  cm and a leading edge at  $r = 2.7$  cm, we learn from equation 67 that  $n$  must be less than 1.04 for initial stability at the start of migration. Even if  $n$  were less than 1.04 but still greater than 1.0, instability would still occur after a critical migration time that can be computed from equation 68.

4. *Discussion.*—The detailed calculation of the density variation within a migrating band can become exceedingly difficult for an arbitrary density gradient. Because of this fact, the example chosen for illustration dealt with a special, but not unrealistic, class of density gradients that permitted a solution of the equations with little effort. Still, the treatment just presented of density inversion during migration indicates the importance of the interaction of the band width with the varying centrifugal field seen by a particle band as it sediments. The effect was not included in the analysis given by Svensson. A band that is initially stable when loaded can behave in various ways depending upon the detailed nature of the density gradient through which it is settling. It can remain stable during the whole period of sedimentation; it can become unstable as soon as it begins to migrate; or finally, it can be stable initially and become unstable after some critical time of sedimentation.

### Extension of the Svensson Stability Criterion

1. *General equations.*—In the previous section we examined in detail the density variation within a migrating band and found that density inversions could be produced during migration for an initially stable band. We now ignore the details of the density variation within a band and attempt to estimate the band capacity as a function of time during the migration in a fixed time-independent density gradient.

To avoid the need for considering spherical particles only, we generalize equation 24 for the sedimentation velocity and use

$$v = \frac{dr}{dt} = \frac{\omega^2 \bar{V}(r)}{f_0(r)\eta(r)} [\rho_p(r) - \rho_m(r)]r \quad [69]$$

where  $\bar{V}$  is the volume per particle,  $f_0$  is a drag coefficient to account for nonspherical particle shapes, and the remaining symbols have been defined previously. Note that both the particle properties and the solution properties can, in general, depend on the distance  $r$  from the axis of rotation. A particle starting at  $r_i$  at time zero will have settled to  $r'_i$  at a time given by integrating equation 69, *viz.*,

$$t = \frac{1}{\omega^2} \int_{r_i}^{r'_i} \frac{f_0 \eta}{\bar{V}(\rho_p - \rho_m)} \frac{dr}{r} \quad [70]$$

Consider now a band which at zero time has its trailing edge at  $r_1$  and leading edge at  $r_2 > r_1$ . After a time,  $t$ , the positions  $r'_1$  and  $r'_2$  of the trailing and leading edges, respectively, will be given by solution of the equation

$$\int_{r_1}^{r'_1} \frac{f_0 \eta}{\bar{V}(\rho_p - \rho_m)} \frac{dr}{r} = \int_{r_2}^{r'_2} \frac{f_0 \eta}{\bar{V}(\rho_p - \rho_m)} \frac{dr}{r} \quad [71]$$

provided that all the particles in the band are the same and that the band has remained stable during the time  $t$ .

Given the initial positions of the band edges  $r_1$  and  $r_2$ , and the desired final position of, say, the leading edge  $r'$  equation 71 in principle permits the calculation of the final band width.

We now compute the maximum band capacity. In a band extending from  $r_i$  to  $r_j > r_i$ , the total density varies as

$$\rho_t = c\bar{V}\rho_p + (1 - c\bar{V})\rho_m = \rho_m + c\bar{V}(\rho_p - \rho_m); \quad r_i \leq r \leq r_j \quad [72]$$

where  $c$  is the particle concentration (particles per  $\text{cm}^3$  of solution). The total mass of particles,  $M$ , in the band is

$$M = 2\pi L \int_{r_i}^{r_j} \rho_p c \bar{V} r \, dr \quad [73]$$

where  $L$  is the length of the cylindrical rotor. The *local* stability criterion within the band is

$$\rho_t(r) \leq \rho_m(r_j) \quad r_i \leq r \leq r_j \quad [74]$$

and by equation 72 this condition implies

$$\rho_m(r_j) \geq \rho_m(r) + c\bar{V}(\rho_p - \rho_m) \quad [75]$$

or that the volume fraction of particles be

$$c\bar{V} \leq \frac{\rho_m(r_j) - \rho_m(r)}{\rho_p - \rho_m(r)}; \quad r_i \leq r \leq r_j. \quad [76]$$

This result, along with equation 73, gives for the maximum mass of particles in a stable band

$$M_{\max} = 2\pi L \int_{r_i}^{r_j} \rho_p \frac{\rho_m(r_j) - \rho_m(r)}{\rho_p - \rho_m(r)} r dr. \quad [77]$$

Equations 77 and 71 furnish the tools for testing a migrating band for stability and for computing the maximum band capacity at any time during migration. A given band starting from  $r_1, r_2$  and containing mass  $M$  of particles can be followed along the density gradient by specifying either  $r'_1$  or  $r'_2$  and computing the position of the other edge by equation 71. For each band position, if  $M \leq M_{\max}$ , as given by equation 77, the band is stable.

As mentioned previously, the particle properties can, in general, be functions of position. This is probable for many biological particles. If the dependence of these particle properties on position is known along with the density variation  $\rho_m(r)$ , the integrals can be evaluated and the stability test carried out.

At this point, it is convenient to make a simplifying assumption that will permit the evaluation of the integrals and thus provide a means for a clearer presentation of the qualitative features of the stability of a band during migration.

2. *Thin band approximation.*—The assumption made is that the band remains "thin" during migration. It is felt that the results obtained with this approximation will contain the major features of band stability and capacity during migration. With the approximation of a "thin" band, the integrals in equations 71 and 77 can be evaluated readily. In equation 71 we first change to limits of integration as follows,

$$0 = \int_r^{r'_1} - \int_{r_2}^{r'_2} = \int_0^{r'_1} - \int_0^{r_1} - \int_0^{r'_2} + \int_0^{r_2} = \int_{r_1}^{r'_1} - \int_{r'_2}^{r_2}$$

which permits replacing equation 71 by

$$\int_{r_1}^{r_2'} \frac{f_0 \eta}{\bar{V}(\rho_p - \rho_m)} \frac{dr}{r} = \int_{r_1'}^{r_2'} \frac{f_0' \eta'}{\bar{V}'(\rho_p' - \rho_m')} \frac{dr}{r}. \quad [78]$$

The integrations over large radial regions  $r_1$  to  $r_1'$  and  $r_2$  to  $r_2'$  have thus been replaced by integrals over the "thin" initial and final bands. If unprimed quantities represent averages over the initial thin band, and primed quantities represent averages over the final thin band [78] can be approximated by

$$\frac{f_0 \eta}{\bar{V}(\rho_p - \rho_m) \bar{r}} (r_2 - r_1) = \frac{f_0' \eta'}{\bar{V}'(\rho_p' - \rho_m') \bar{r}'} (r_2' - r_1') \quad [79]$$

where  $\bar{r}$ , and  $\bar{r}'$  are the average radial positions of the initial and final bands, respectively...

The ratio of final to initial band width is now given by

$$\frac{\Delta r'}{\Delta r} = \left( \frac{f_0}{f_0'} \right) \left( \frac{\bar{V}'}{\bar{V}} \right) \left( \frac{\rho_p' - \rho_m'}{\rho_p - \rho_m} \right) \left( \frac{\eta}{\eta'} \right) \left( \frac{\bar{r}'}{\bar{r}} \right) \quad [80]$$

where the initial band width  $r_2 - r_1$  has been designated by  $\Delta r$ , and the final band width  $r_2' - r_1'$  has been designated by  $\Delta r'$ . The way in which the band width changes during migration due to changes in particle properties, solution properties, and band position is clearly shown by equation 80.

In equation 77, the density  $\rho_m(r)$  is expanded in a Taylor series around the point  $r_j$  after which the thin-band approximation gives for the maximum mass in the initial band

$$M_{\max} = \frac{\pi L \rho_p (d\rho_m/dr) \bar{r} (\Delta r)^2}{\rho_p - \rho_m} \quad [81]$$

and the final band

$$M'_{\max} = \frac{\pi L \rho_p' (d\rho_m'/dr)' \bar{r}' (\Delta r')^2}{\rho_p' - \rho_m'} \quad [82]$$

The ratio of these band capacities is

$$\frac{M'_{\max}}{M_{\max}} = \left( \frac{\rho_p}{\rho_p'} \right) \left[ \frac{(d\rho_m/dr)}{(d\rho_m'/dr)'} \right] \left( \frac{\bar{r}'}{\bar{r}} \right) \left( \frac{\rho_p - \rho_m}{\rho_p' - \rho_m'} \right) \left( \frac{\Delta r'}{\Delta r} \right)^2 \quad [83]$$

or by equation 80 for the band width ratio, one obtains

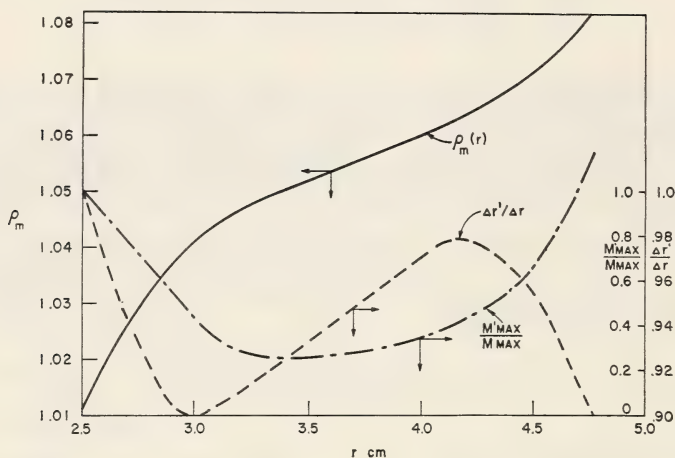
$$\frac{M'_{\max}}{M_{\max}} = \left( \frac{\rho_p}{\rho_p'} \right) \left( \frac{f_0 \bar{V}'}{f_0' \bar{V}} \right)^2 \left[ \frac{(d\rho_m/dr)'}{(d\rho_m/dr)} \right] \left( \frac{\rho_p' - \rho_m'}{\rho_p - \rho_m} \right) \left( \frac{\eta}{\eta'} \right)^2 \left( \frac{\bar{r}'}{\bar{r}} \right)^3 \quad [84]$$

When particle properties are independent of position, one obtains for the ratio of band capacities

$$\frac{M'_{\max}}{M_{\max}} = \left[ \frac{(d\rho_m/dr)'}{(d\rho_m/dr)} \right] \left( \frac{\rho_p - \rho'_m}{\rho_p - \rho_m} \right) \left( \frac{\eta}{\eta'} \right)^2 \left( \frac{\bar{r}'}{\bar{r}} \right)^3 \quad [85]$$

Here again, the dependence of the change in band capacity during migration on particle properties, solution properties, and position in the centrifugal field is clearly shown in equation 84.

3. *Illustrative example.*—Text-figure 5 illustrates the changes in band width and band capacity for a thin band migrating in a typical density gradient.<sup>4</sup> The curves shown in the figure for  $(M'_{\max}/M_{\max})$  and  $(\Delta r'/\Delta r)$  were calculated from equation 85. At time zero the band is assumed to start at a position  $\bar{r} = 2.5$  cm where the solution density is  $\rho_m(\bar{r}) = 1.01$ . It then migrates through the typical density gradient  $[\rho_m(r)]$ , shown by the solid line. The changes in band width and band capacity are also shown.



TEXT-FIGURE 5.—Band capacity and band width changes during centrifugation (thin band approximation).

During early migration the band width decreases primarily because of the steepness of the initial density gradient. The band capacity decreases during early stages of migration because of this decrease in band width. As the band moves into the flat portion of the density gradient, its width begins to increase. However, the band capacity continues to decrease because the band-width increase is not sufficient to overcome the decrease in the density gradient. Finally, as the band moves into the region of increasing density gradient, its width again decreases, but

<sup>4</sup> The gradient shown in the figure is a sucrose gradient that has been used in the B-series zonal rotors at Oak Ridge.

not enough to compensate for the density gradient changes, the density difference changes, and the band-position effect on the band capacity, which is seen to increase in this region. Note that even though band-width changes are of the order of percents, the band capacity changes are large.

4. *Discussion.*—The extension of the Svensson criterion to take into account the effect of migration on band width and band capacity has, in the thin-band approximation, made clear the factors affecting these band properties. Band width varies directly with the volume per particle in the band, the density difference between the band particles and the local solution, and the average radial position of the band. It is found to vary inversely with the drag factor for the particles in the band and the local viscosity of the solution.

Band capacity (maximum mass of particles in the band) varies directly with the particle density, the local solution density gradient, the band position, the square of the band width, and the length of the rotor. It is found to vary inversely with the density difference between the particle and the local solution. [5227]

In addition to the above results, equations were presented which, in principle, would permit the band width and capacity to be computed without the need for any approximation. The additional labor involved in the use of the full equations seems unjustified until the basic concepts used in the theory are verified by experiment.

The results illustrated in text-figure 5 again indicate that a band that is initially stable when loaded can become unstable during migration. Thus, the minimum band capacity for the case shown in text-figure 5 is only about 25 percent of the capacity of the starting band and occurs after the band has migrated about 1 cm.

All the band capacity theory presented to this point has been based on migration in a density gradient which is time independent, *i.e.*, diffusion of the solute molecules producing the density gradient has been ignored. Such a theory could be expected to be reasonable for those cases where the density gradient in the rotor is near equilibrium for the given rotational speed or where particle sedimentation velocities are large compared to solute diffusion velocities. In the next section we will present a preliminary treatment of the band capacity problem when diffusion of solute molecules is important.

### Effect of Solute Diffusion on Band Stability

In some of the zonal centrifugation procedures used in the Oak Ridge program, conditions are such that the diffusion of solute molecules and the consequent time dependence of the density gradient play an important role in determining the stability of a migrating band.

Because of the complexities of the problem only an approximate treatment will be presented here in order to keep the physical facts foremost and to guide future experimental work.

1. *Solution of diffusion equation.*—For many of the “as loaded” density gradients used in the Oak Ridge program a solution of the diffusion equation in rectangular, rather than cylindrical, coordinates gives a sufficiently close approximation to the time dependence of the density gradient that it proves useful in the analysis of band capacity. We also ignore sedimentation of the sucrose molecules. The additional complexity that would arise by the use of cylindrical coordinates and consideration of the sedimentation of sucrose is not justified for the initial estimates desired in the present section. It will be found that the time dependence of the density gradient provided by the rectangular coordinate solution agrees well with the observed time dependence over the region of the rotor in which band migration occurs in some of the Oak Ridge experiments.

For zero time the solute concentration distribution is taken to be

$$c(x,0) = C(x) ; -\infty < x < \infty \quad [86]$$

The solution to the diffusion equation

$$\frac{\partial c}{\partial t} = D_2 \frac{\partial^2 c}{\partial x^2} \quad [87]$$

which satisfies equation 86 is

$$c(x,t) = \frac{1}{2\sqrt{\pi D_2 t}} \int_{-\infty}^{\infty} C(x') \exp - \left[ \frac{(x - x')^2}{4D_2 t} \right] dx' \quad [88]$$

where  $D_2$  is a constant. The following choice of  $C(x)$  approximates, in the region of interest, the initial gradient loaded into the rotor in some of the Oak Ridge experiments.

$$C(x) = \begin{cases} 0 ; x < 0 \\ c_0 + Wx ; x \geq 0 \end{cases} \quad [89]$$

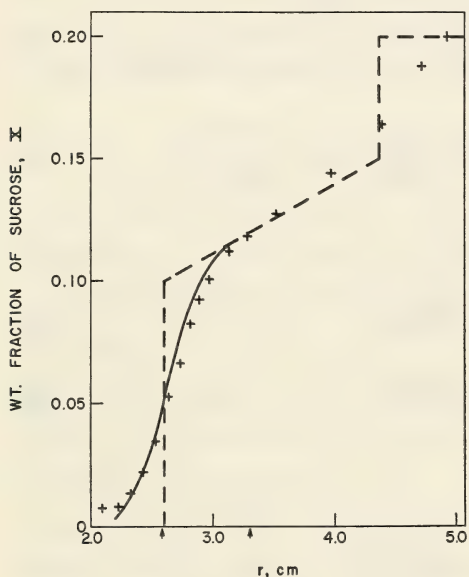
where  $W$  is a constant. With this choice of initial gradient, the integral in equation 88 can be evaluated to give for the dependence of the solute concentration on position and time

$$c(x,t) = \frac{1}{2} (c_0 + Wx) \left( 1 + \operatorname{erf} \frac{x}{\sqrt{4D_2 t}} \right) + \sqrt{\frac{D_2 t}{\pi}} W e^{-x^2/4D_2 t} \quad [90]$$

where

$$\operatorname{erf} \frac{x}{\sqrt{4D_2 t}} \equiv \frac{2}{\sqrt{\pi}} \int_0^{x/\sqrt{4D_2 t}} e^{-y^2} dy \quad [91]$$

Text-figure 6 gives a comparison of the observed and calculated sucrose gradients for 2 hours of centrifugation in a B rotor at high speed. The diffusion coefficient for sucrose has been taken to be  $0.29 \times 10^{-5}$  cm<sup>2</sup>/sec at 5° C. Further, since density variation is small, we have ignored the difference between weight fraction and concentration. One line in the figure represents the initial gradient "as-loaded" into a B-type rotor. Such initial gradients have been measured by loading a B-rotor under operating conditions from a gradient engine, immediately unloading the gradient by displacement, and determining the sucrose weight fraction by refractive index measurements.



TEXT-FIGURE 6.—Effect of diffusion of sucrose gradient. Experimental: broken line, gradient as loaded; plus signs, gradient after 2 hours of centrifugation. Calculated: solid line. The arrows on the "r" axis represent the initial and final positions of a typical 30-S ribosome band after 2 hours of centrifugation.

The solid line represents the predicted gradient after 2 hours of centrifugation as computed from equation 90. The points are experimental, obtained by refractive index measurements.

Also shown on the text-figure are the initial and final positions of a typical 30-S ribosome band that has migrated through the gradient.

Agreement between the computed and measured gradients is good over the region of interest for these experiments. This is taken as confirmation that equation 90 will adequately represent the time dependence of the density gradient for the present purpose.

2. *Effect of diffusion on band capacity.*—The maximum estimated variation in sedimentation velocity for a typical 30-S ribosome band as it moves from its initial to final position is about 10 percent. In computing the effect of diffusion on band capacity we will ignore this change and assume that the band moves at some constant velocity,  $\bar{v}$ , taken to be the total distance traveled by the band center divided by the duration of centrifugation.

The distance,  $x$ , through which the band moves in time,  $t$ , will be taken to be

$$x = \bar{v}t. \quad [92]$$

If this value of  $x$  is substituted into equation 90 and the  $x$  derivative of equation 90, we obtain the concentration and the concentration gradient *at the band position* as a function of time. Thus, the following equations give the concentration and concentration gradient "seen" by the band as it migrates.

$$c(t) = \frac{1}{2} (c_0 + W\bar{v}t) \left( 1 + \operatorname{erf} \frac{\bar{v}t}{\sqrt{4D_2t}} \right) + W \sqrt{\frac{4D_2t}{\pi}} \exp - \left( \frac{\bar{v}^2 t^2}{4D_2t} \right) \quad [93]$$

$$\frac{\partial c}{\partial x} = \frac{1}{2} \left[ W \left( 1 + \operatorname{erf} \frac{\bar{v}t}{\sqrt{4D_2t}} \right) + \frac{c_0}{\sqrt{\pi D_2t}} \exp - \left( \frac{\bar{v}^2 t^2}{4D_2t} \right) \right] \quad [94]$$

We define two characteristic times

$$\tau_1 \equiv c_0^2/D_2W^2 \quad [95]$$

$$\tau_2 \equiv 4D_2/\bar{v}^2 \quad [96]$$

and obtain

$$\frac{c(t)}{c_0} = \frac{1}{2} \left( 1 + \frac{2t}{\sqrt{\tau_1\tau_2}} \right) \left( 1 + \operatorname{erf} \sqrt{\frac{t}{\tau_2}} \right) + \frac{e^{-t/\tau_2}}{\sqrt{\pi}} \sqrt{\frac{t}{\tau_1}} \quad [97]$$

$$\frac{1}{W} \frac{\partial c}{\partial x} = \frac{1}{2} (1 + \operatorname{erf} \sqrt{t/\tau_2}) + \frac{1}{2\sqrt{\pi}} \frac{1}{\sqrt{t/\tau_1}} e^{-t/\tau_2}. \quad [98]$$

In general, depending on the magnitude of the times  $\tau_1$  and  $\tau_2$ , two types of behavior of the concentration gradient seen by the band are possible.

In *case 1* the concentration gradient seen by the band, which is initially greater than the gradient  $W$ , decreases monotonically to  $W$  for long times. In *case 2*, the gradient can drop below  $W$  for some time and then rise again to approach  $W$  asymptotically for long times. The distinction being made here is important since if the band is loaded so that it is stable in a gradient of magnitude  $W$ , it will remain stable in the first case mentioned above, but will become unstable after some centrifugation time in the second case.

The conditions for the occurrence of *case 2* can be obtained readily by differentiating equation 98 with respect to the time, setting the derivative

equal to zero, and solving for the time  $t_m$  at which the minimum gradient is seen by the band. One obtains the following equation:

$$t_m = \frac{1}{2} \frac{\tau_2}{\sqrt{(\tau_2/\tau_1)} - 1} \quad [99]$$

Since  $T_m$  must be positive for *case 2* to occur, we obtain as a condition for this case

$$\sqrt{\frac{\tau_2}{\tau_1}} > 1 \quad \text{or} \quad \tau_2 > \tau_1. \quad [100]$$

By use of the definitions of  $\tau_1$  and  $\tau_2$ , this condition becomes

$$\frac{D_2}{v} > \frac{c_0}{2W} \quad [101]$$

Hence, if the ratio of half the concentration jump at  $x = 0$ ,  $t = 0$ , to the gradient,  $W$ , is less than the ratio of the sucrose diffusion coefficient to the average sedimentation velocity of the particles, an initially stable band loaded to capacity for a gradient,  $W$ , can become unstable during centrifugation.

In general, subject to the approximations made in their derivation, equations 97 and 98 used in conjunction with an equation of type 81 can be used to estimate the band capacity as a function of time for a time-dependent density gradient.

*3. Illustrative example.*—For the initial gradient shown in text-figure 6 we have  $c_0 = 0.1$ ,  $W = 0.0283$  g/cm<sup>4</sup>. Again, we ignore the difference between weight fraction and concentration. From the initial and final positions of a typical 30-S ribosome band we obtain for the average velocity  $\bar{v} = 1.09 \times 10^{-4}$  cm/sec.

The characteristic times  $\tau_1$  and  $\tau_2$  using for sucrose at 5° C,  $D_2 = 0.29 \times 10^{-5}$  cm<sup>2</sup>/sec are:

$$\tau_1 = c_0^2/D_2 W^2 = 4.31 \times 10^6 \text{ sec}$$

$$\tau_2 = 4D_2/\bar{v}^2 = 0.978 \times 10^3 \text{ sec}.$$

To obtain a conservative estimate of band capacity we use the *minimum* band width of  $\Delta r = 0.0217$  cm obtained from a time-independent density gradient calculation for the typical 30-S ribosome band. The following are also used

Length of rotor	$L = 25.6$ cm
Particle density	$\rho_p = 1.5$ g/cm <sup>3</sup> .

From equation 81 we obtain

$$M_{\max} = \frac{\pi(25.6) (1.5) (.0217)^2}{1.5 - \rho_1(t)} \bar{r} (d\rho_m/dr). \quad [102]$$

With concentration,  $c$ , taken to be equal to the weight fraction,  $x$ , and an empirical relation (obtained by least-squares fit to experimental data relating weight fraction to density of sucrose solutions) the following are obtained:

$$\rho_m = 1.000 + 0.3848c + 0.1731c^2 \quad [103]$$

$$\frac{d\rho_m}{dr} = 0.3848 \frac{\partial c}{\partial r} + 0.3462c \frac{\partial c}{\partial r} \quad [104]$$

The relationship between  $x$  and the distance of the band center from the axis of rotation  $\bar{r}$  is (for band center at  $t = 0$  located at  $\bar{r} = 2.583$  cm)

$$x = r - 2.583 = \bar{v}t \quad [105]$$

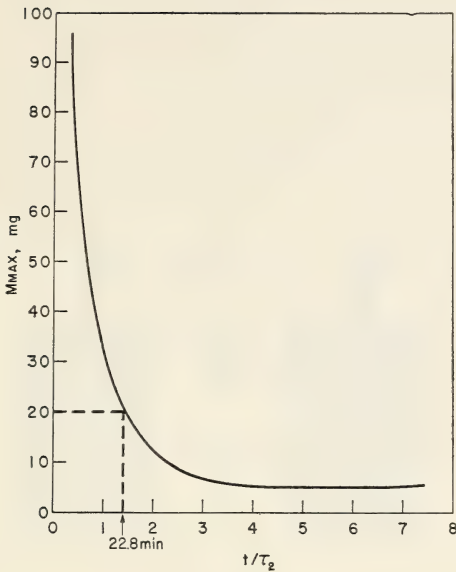
so that  $\bar{r}$  is given as a function of time by

$$\bar{r}(t) = 1.09 \times 10^{-4} t + 2.583 \quad 0 \leq t \leq 7200 \text{ sec} \quad [106]$$

The time dependence of  $c$  and  $\frac{\partial c}{\partial r}$  can now be computed from equations 97 and 98. These values used in equations 103 and 104 lead to the time dependence of  $\rho_m$  and  $\frac{\partial \rho_m}{\partial r}$ . Finally equation 102 is used to compute the band capacity as a function of time. The results of such a computation are shown in text-figure 7. The maximum mass of particles in a stable band is given in milligrams as a function of the reduced time variable  $t/\tau_2$ . For this typical 30-S ribosome estimate, it is seen that the band capacity can fall to about 5 percent of its initial capacity after sufficiently long centrifugation in a time-dependent density gradient.

For the particular example treated here,  $\tau_2 = 978$  seconds so that an initial band containing 20 mg of 30-S ribosomes would become unstable after about 23 minutes of centrifugation.

4. *Discussion.*—The estimates provided by the theory of band capacity in a time-dependent density gradient are subject to direct experimental tests. Care must be exercised in such experiments to assure that only a single type of particle with time-independent particle properties is used, and that the disturbing effects of temperature gradients are eliminated. In such experiments instability would manifest itself in a band width many times that predicted by the theory at a given time of centrifugation.



TEXT-FIGURE 7.—Capacity of a migrating band in a time-dependent density gradient *versus* time of centrifugation.

The major finding of the study just presented is that band capacity can fall to a few percent of that predicted by the Svensson local criterion because of the effects of band migration in a time-dependent density gradient. This appears to be in accord with the findings of Brakke (10) mentioned earlier in this report.

## REFERENCES

- (1) SVEDBERG, T., and PEDERSEN, K. O.: *The Ultracentrifuge*. Oxford, The Clarendon Press, 1940.
- (2) FUJITA, H.: *Mathematical Theory of Sedimentation Analysis*. New York, Academic Press Inc., 1962.
- (3) ANDERSON, N. G., and BURGER, C. L.: Separation of cell components in the zonal ultracentrifuge. *Science* 136: 646-648, 1962.
- (4) ANDERSON, N. G.: The zonal ultracentrifuge. A new instrument for fractionating mixtures of particles. *J Physiol Chem* 66: 1987-1989, 1962.
- (5) ANDERSON, N. G., BARRINGER, H. P., BABELAY, E. F., and FISHER, W. D.: The B-IV zonal ultracentrifuge. *Life Sci* 3: 667-671, 1964.
- (6) ANDERSON, N. G., BARRINGER, H. P., BABELAY, E. F., NUNLEY, C. E., BARTKUS, M. J., FISHER, W. D., and RANKIN, C. T., JR.: The design and operation of the B-IV zonal centrifuge system. *Nat Cancer Inst Monogr* 21: 137-164, 1966.
- (7) ANDERSON, N. G.: Virus isolation in the zonal ultracentrifuge. *Nature (London)*, 199: 1166-1168, 1963.
- (8) AMBLER, C. M.: The theory of scaling up of laboratory data for the sedimentation type centrifuge. *J Biochem Microbiol Techn Eng* 1: 185-205, 1959.
- (9) SVENSSON, H., HAGDAHL, L., and LERNER, K. D.: Zonal electrophoresis in a density gradient. Stability considerations and separation of serum proteins. *Science Tools* 4: 1-10, 1957.
- (10) BRAKKE, M. K.: Density gradient centrifugation and its application to plant viruses. *Advances Virus Res* 7: 193-224, 1960.



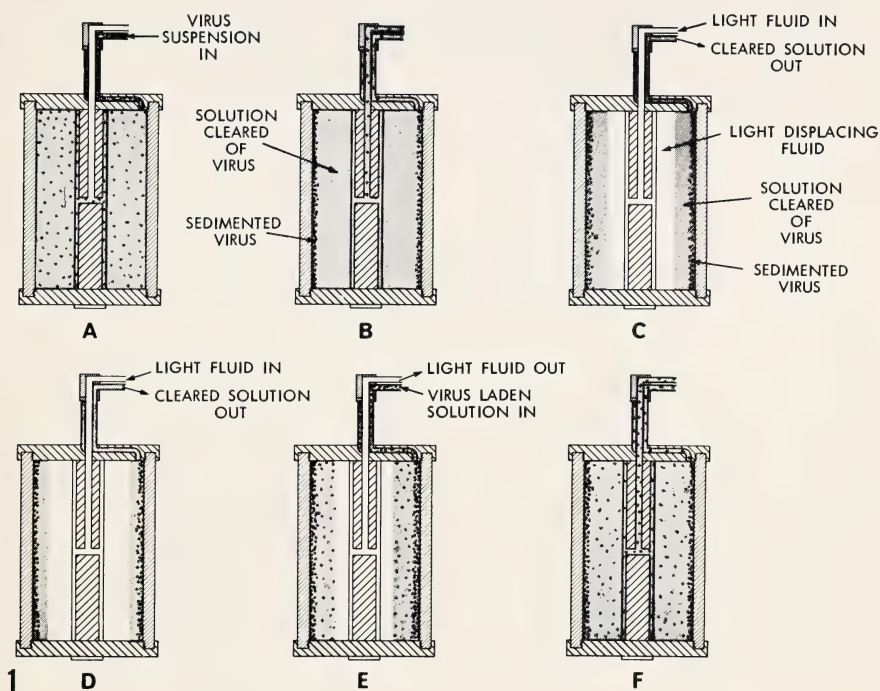


FIGURE 1.—Batch technique for sedimentation of virus particles using B-II or B-IV zonal centrifuge rotor. A, rotor is filled with virus suspension pumped in through edge line; B, particles are centrifuged to wall; C, particle-free suspending medium being displaced out of the rotor through edge line by lighter fluid pumped in through core; D, completion of removal of cleared suspending medium; E, rotor refilled with virus suspension pumped in through edge line. Light fluid displaced out through core; F, rotor completely filled with virus suspension ready for repetition of the sedimentation cycle.

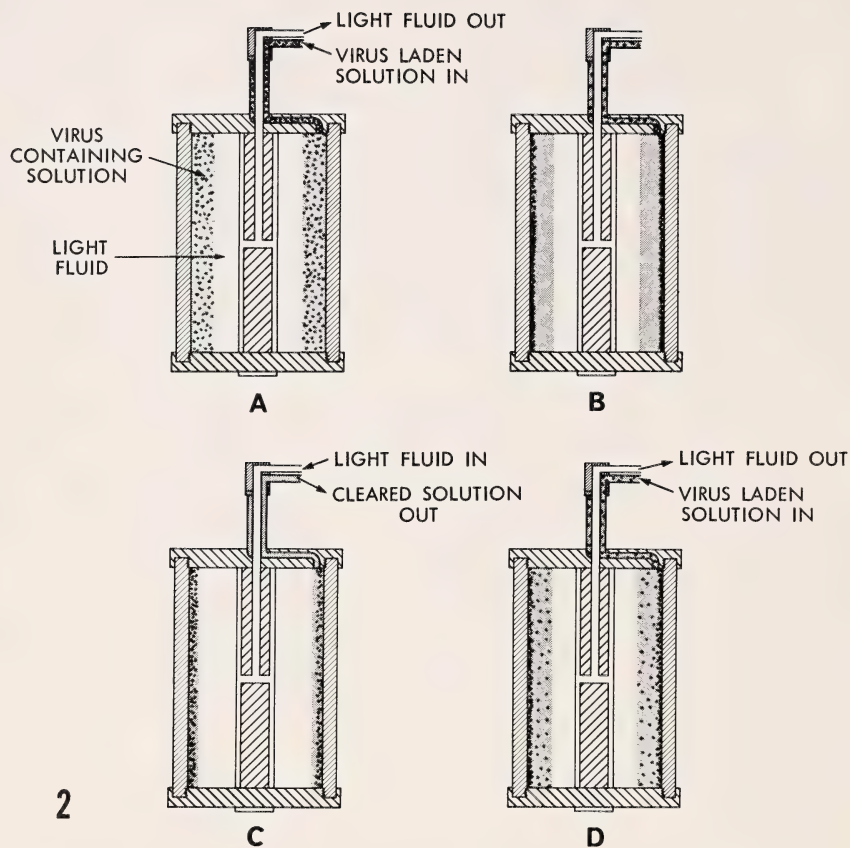


FIGURE 2.—Semibatch method of virus isolation. *A*, rotor partially filled with virus suspension through edge line during rotation, remainder of water filled with light solution; *B*, virus particles sedimented to rotor wall; *C*, particle-free suspending medium removed from rotor through edge line by displacement by light fluid pumped in through core line; *D*, second batch of virus suspension introduced through edge line, displacing out part of light overlying fluid through core line.

# The Design of Zonal Centrifuges<sup>1</sup>

H. P. BARRINGER,<sup>2</sup> *Technical Division, Oak Ridge Gaseous Diffusion Plant,<sup>3</sup> Oak Ridge, Tennessee*

## SUMMARY

The design of zonal centrifuges requires the simultaneous solution of a number of problems which have traditionally been of interest to workers in quite different disciplines. These problems are reviewed in this paper for biologists, physicists, and specialists in several branches of the engineering sciences. Important considerations in the design of several rotors in common use are rotational stability and their physical and momental ellipsoid configurations. These systems are discussed, together with the disturbances causing loss of stability and the resulting mode shapes and frequencies for rigid-body rotor whirl. Self-balancing features and damper-bearing requirements of rotors also are listed. An optimum centrifuge rotor can be designed by use of the stress equations and the equations for the flexural vibration of a freely sus-

pended rotor. Design charts facilitate quick selection of a rotor size and speed. Stress and deflection equations are given for uniform-thickness centrifuge end caps loaded with a parabolic pressure distribution, such as that encountered in biological rotors. Centrifugal wave disturbances are important in a rotor that has been demonstrated to be unstable because of wave formation. Methods are given for preventing these waves. Hybrid rotors, such as those used in zonal centrifugation, necessarily involve many compromises when workers translate theory into design, select specific configurations, evolve methods for maintaining fluid-tight integrity, study new rotor materials, design reliable shaft seals, and use completed systems to investigate specific biological problems.—Nat Cancer Inst Monogr 21: 77-111, 1966.

THE ACCURACY of biophysical measurements and the resolution of biophysical separations are indissociably linked to the design, construction, and operation of the physical systems used. When a new biophysical tool is first developed, interest centers initially on exploring the principles involved. If these are shown to be valid and useful in laboratory practice, interest shifts to the details of the system and to the improvement of the performance to make more refined measurements, observations, or separations.

<sup>1</sup> This research performed under the Joint National Institutes of Health-Atomic Energy Commission Zonal Centrifuge Development Program which is supported by the National Cancer Institute, the National Institute of Allergy and Infectious Diseases, and the U.S. Atomic Energy Commission.

<sup>2</sup> Present address: Stellite Division of Union Carbide Corporation, Kokomo, Indiana.

<sup>3</sup> Operated for the U.S. Atomic Energy Commission by the Nuclear Division of Union Carbide Corporation.

The zonal centrifuge (1) is now past the proof-of-principle stage and is well into the exploratory and developmental phases. The designs that will ultimately prove to be most useful probably have not been conceived. The problem of preparative  $s$ - $\rho$  separations of DNA, for example, will probably require the construction of a whole new series of zonal rotors.

The biological experiments that can be done depend on limitations inherent in the design of high-speed rotors. As the limits of instrumental performance using available theory, materials, and technology are reached, operation of existing systems is reduced to a routine, and the investigator, though well-grounded in the basic principles, often is not familiar in detail with the problems requiring solution during the development of the instrument. For these reasons, it is important to make the development information available in a form which will be useful to both experimental biologists and centrifuge designers. This paper, therefore, describes the design and operation of zonal centrifuges. It also gives the principles which should be considered in selecting rotor systems for specific problems. Centrifuge design information, as presented here, has not been previously available in a concise form. For purposes of comparison, the several types of rotors currently in use will also be discussed.

## ROTORS FOR BIOLOGICAL SYSTEMS

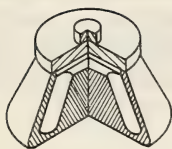
### Angle-Head Rotors

The preparative angle-head rotors (text-fig. 1a) in widest use are simple, rugged units suitable for differential or zonal isopycnic centrifugation. Angle-head centrifuges are fabricated from: (a) rotor body, (b) top, (c) handle, and (d) a tube with cap (2). Commercial models are obtainable with a variety of capacities, speed ranges, and angles of inclination. They are characterized by their solid construction and by their frustum-of-a-cone appearance which gives rotational stability and permits high loads to be carried by the center section of the rotor. The tubes in which the fluid is centrifuged are inclined at different angles for high efficiency, for minimum stirring, or for other reasons.

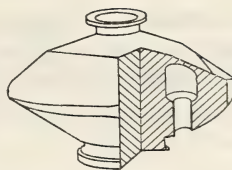
### Analytical Rotors

Analytical rotors (text-fig. 1b) are used to study optically samples being sedimented during centrifugation. They are rugged rotors used to centrifuge milliliter quantities of fluid at high speeds (3). The centrifuges are fabricated from a rotor body, cell holders, quartz or sapphire windows, and sector-shaped compartments.

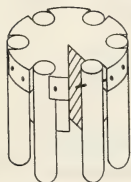
The football-shaped rotors spin about the short L/D (length to diameter) axis. The center section of the rotor is similar to DeLaval high-strength turbine wheels where special contours permit higher than normal peripheral speeds with high stress loads.



(a)  
ANGLE - HEAD ROTOR



(b)  
ANALYTICAL ROTOR



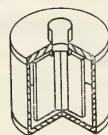
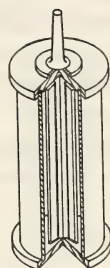
(c)  
SWING BUCKET ROTOR



(d)  
DISK - TYPE CENTRIFUGES



(e)  
TUBULAR CLARIFIER ROTOR



(f) (g)  
ZONAL CENTRIFUGES

TEXT-FIGURE 1.—Cross-sections of centrifuge rotors.

### Swinging Bucket Rotors

The swinging bucket centrifuges (text-fig. 1c) have preparative rotors with movable tubes. The tubes are loaded and unloaded with their axes vertical. During centrifugation the tube axis is nearly horizontal, since positioning of the tubes is done by centrifugal force. The rotor is similar to a spoked wheel with trunnion mounts on the spoke ends for supporting the buckets which hold the centrifuge tubes.

### Disk-Type Rotors

Continuous-flow rotors of the disk type (text-fig. 1d) have conical disks inside a hollow frustum of a cone (4). The fluids pass through

the central sections of the rotor, while the solids sediment against the disk and slide to the periphery of the rotor. These rotors usually have small  $L/D$  ratios, and their high separation capabilities are achieved because of the small distance a particle must sediment before striking a solid wall.

### **Tubular Clarifier Rotors**

Continuous-flow rotors of the clarifier type (text-fig. 1e) have internal dams for separating different strata of a flowing stream (4). These rotors operate at high rotational speeds, high centrifugal fields, and large  $L/D$  ratios. The long rotor length provides adequate distance and time for a radial separation of different materials to be achieved.

### **Zonal Rotors**

Zonal rotors can be made with large  $L/D$  ratios (text-fig. 1f) or small  $L/D$  ratios (text-fig. 1g) and still perform the same function. The operation of these units is explained elsewhere in the text. With the same fluid volume, rotor material, and stress level, the large  $L/D$  rotors produce high centrifugal fields with a sacrifice in radial sedimentation path. However, the small  $L/D$  rotors operate with a larger radial sedimentation path while producing smaller centrifugal fields. The separation desired dictates the rotor speed necessary and, indirectly, the  $L/D$  ratio used for a given volume.

Use of different internal cores in the zonal centrifuge converts the rotor to one or more of the conventional centrifuges described above.

## **ROTOR CONFIGURATIONS**

Choice of rotor configurations must be based on the characteristics of their mass distribution, which is measured by mass moments of inertias rather than considerations of rotor dimensions. The mass moment of inertia is the summation of all the products of mass of an element and the square of the distance from the element to an axis on the body.

Rotor stability is a function of transient and steady-state motion. Transient effects are observed as a whirl (precession or rotation of the rotor center of rotation about a second axis) while steady-state effects consist of rotor runout (rotation of the rotor about an axis different from its geometrical axis) because of mass unbalance. Transient motions can exist for extended periods of time with a resulting unsatisfactory operation of the centrifuge and produce a gradual change in rotor excursion amplitude. This usually occurs with an increase in speed or because of external excitations which add to the motion faster than it can decay in amplitude. Steady-state motion never decays because it is not time dependent. Hence, a stable rotor has a rapid decay of transient motions to a steady-state motion of rotor unbalance without large rotor excursion amplitudes.

### Type of Configurations

The rotors in text-figure 1 can be divided into three types (a fourth type, not shown, is not used for centrifuge devices).

*Type 1.*—The rotors in text-figure 1a, c, d, and g have a principal moment-of-inertia ratio of  $\frac{I_{\text{spin}}}{I_{\text{transverse}}} > 1$ , where  $I_{\text{spin}} > I_{\text{transverse 1}} = I_{\text{transverse 2}}$ .

*Type 2.*—The rotor in text-figure 1b has a principal moment-of-inertia ratio  $\frac{I_{\text{spin}}}{I_{\text{transverse}}} > 1$ , where  $I_{\text{spin}} > I_{\text{transverse 1}} > I_{\text{transverse 2}}$ .

*Type 3.*—The rotors in text-figure 1e and f have a principal moment-of-inertia ratio of  $\frac{I_{\text{spin}}}{I_{\text{transverse}}} < 1$ , where  $I_{\text{spin}} < I_{\text{transverse 1}} = I_{\text{transverse 2}}$ .

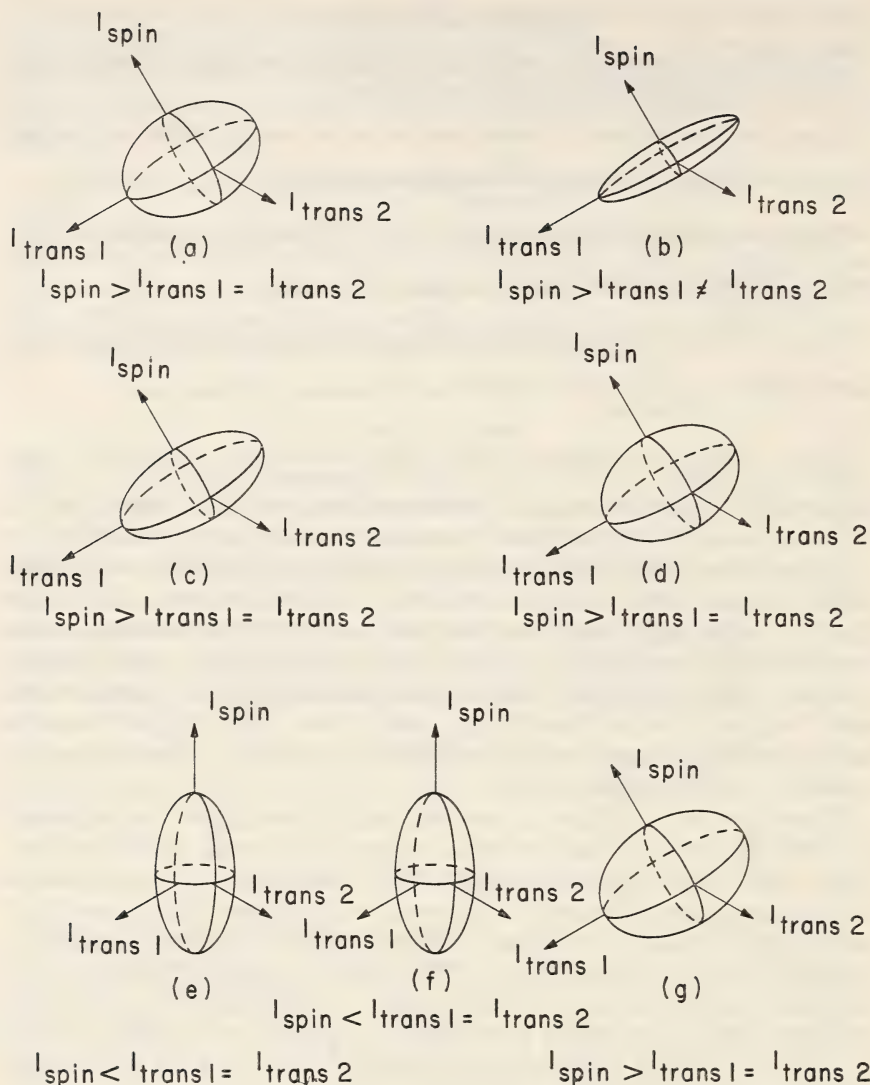
*Type 4.*—This is a spherical rotor where  $\frac{I_{\text{spin}}}{I_{\text{transverse}}} = 1$  and all three moments of inertia are equal. Rotors are most stable for types 1 and 2, of lesser stability for type 3, and of neutral stability for type 4 (5).

Rotor types 1 and 2 require only one constraint (shaft) for controlling oscillation and require simple mechanical driving systems. Rotors of type 3 usually require shafts on each end to control rotor oscillation and thus demand complicated ancillary mechanical damping and support systems. Rotors of type 4 have neutral stability and they are avoided since they have no preferential spin axis; hence, the rotor will tumble in all directions rather than seek a single-spin axis (6). The reasons for stability are discussed below.

The rotors in text-figure 1 are redrawn in text-figure 2 as ellipsoids of inertia in terms of their principal moments of inertia, which are generally called the momental ellipsoids (7). The coordinate axes represent the principal axes of inertia of the rotor body; hence, the moments of inertia with respect to these axes are the principal moments of inertia of the rotor about its mass center. The inertial ellipsoid has the same orientation as the rotor mass distribution. If the rotor is spun about a principal axis, it will rotate about this axis permanently in the absence of any disturbance; however, the three principal axes do not possess equal degrees of rotational stability (8).

Motion of the centrifuge rotor can be represented by a rolling of the momental ellipsoid on an invariant plane (9). Heuristically, if the nonspinning ellipsoid were tossed with its axes completely disoriented onto the invariant plane, it would tend to find a position corresponding to minimum potential energy. This would place the axis of greatest stability perpendicular to the plane, *i.e.*, the centrifuge would prefer to spin about this axis if it were free of constraints.

Suppose the momental ellipsoid were spinning perfectly, *i.e.*, without any disturbance, on the invariant plane about either its greatest or least principal moments-of-inertia axis. In the presence of any disturbance, the ellipsoid will move from the principal axis motion and will roll on the



TEXT-FIGURE 2.—Centrifuge rotor ellipsoids of inertia for rotors shown in text-figure 1.

invariant plane. The motion, due to the roll, traces a curve on the ellipsoid as well as on the invariant plane. The curve traced on the ellipsoid as it rolls on the invariant plane is called the polhode (10).<sup>4</sup> For small oscillation of the ellipsoid, geometrical considerations show that the polhode is a small curve (nearly circular) drawn on the momental ellipsoid around the greatest or least principal axis. Thus, small closed polhodes enclosing a principal axis correspond to a stable rotor motion.

<sup>4</sup> For a rotating rigid body subject to no external resultant torque, the line of intersection of the cone traced out by the angular velocity vector with the momental ellipsoid.

Large oscillations of the ellipsoid correspond to instability, as the body tries to move to a different spin axis. Blass (11) clearly diagrams the polhodes wherein the kinetic energy ellipsoid (derived from similar consideration as the momental ellipsoid) and the angular momentum ellipsoid (not *momental* ellipsoid) intersect to describe the two stable axes and the third unstable axis. The mathematical proof, along with a relevant discussion, is given by Grey (12).

### Selection of Rotor Configurations

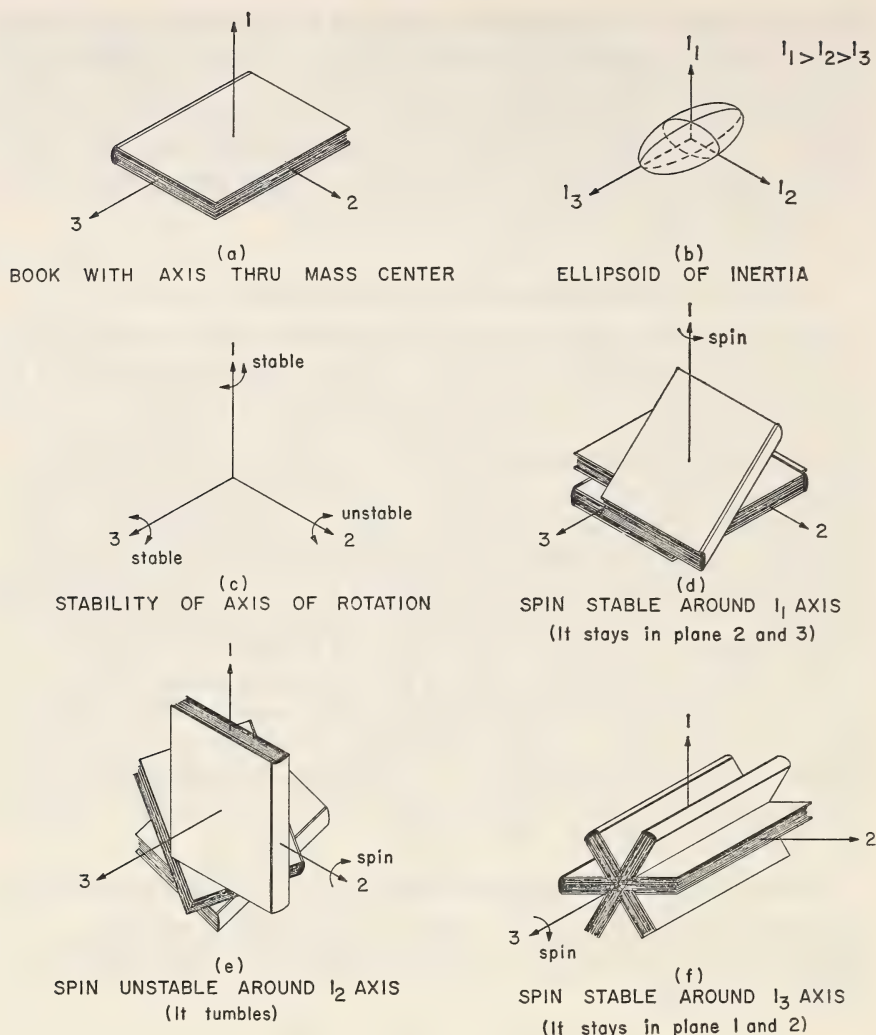
Because most centrifuges are run with flexible shafts for self-balancing of the rotating parts, it is difficult to obtain satisfactory operation of the rotor if an inherently unstable configuration is chosen. The need for choosing a body with a proper ratio of moments of inertia about the spin axis can be vividly demonstrated by the use of a book (text-fig. 3). Choose a book with a large difference in each of its dimensions as in text-figure 3a with the momental ellipsoid shown in text-figure 3b. Toss it into the air with a spin about one axis at a time (text-figure 3c) as shown in text-figure 3d, e, and f, and the resulting motion will demonstrate the rotational stability about the greatest or least moment of inertia, while the axis between the greatest and least will tumble when rotated.

When the largest moment of inertia about the spin axis is chosen, only one shaft is required to hold the spinning body stable. When the least moment-of-inertia axis is chosen, generally two shafts are required to stabilize the rotor at high speeds. Intermediate moment-of-inertia axis or three equal moments of inertia should not be chosen for biological centrifuges since such axes will not provide stability.

Consider the ratio of moments of inertia of  $\frac{I_{\text{spin}}}{I_{\text{transverse}}}$ . For long, tubular rotors, the ratio approaches zero, while for very short, disklike rotors, the inertia ratio approaches two. The midrange, where the ratio is one, should be avoided.

### ROTOR STABILITY

Once a rotor configuration is selected, the problems associated with rotor stability begin to be complex. The word "stability" is not used in the mathematical sense, but refers to any type of motion that would disturb the orientation of the rotor, its contents, or supporting structure by oscillating with undesirable amplitudes, *i.e.*, becomes unstable. By this definition, there are (a) external vibrations, (b) bearing whirl, (c) rigid-body modes of vibration of the rotor in its suspension system, (d) rotor whirl (precession), (e) liquid instabilities, and (f) flexural criticals. All of these factors can cause the rotor to become unstable and none of them are beneficial. The higher the rotational frequency of the rotor, the more difficult it is to provide stability for the whole system.



TEXT-FIGURE 3.—Demonstration of stable and unstable spin axis.

*External vibrations* are associated with both short-term transient vibrations and long-term steady-state vibrations. The external vibrations to excite rotor motions can be as obvious as the vacuum pump, refrigeration equipment, drive system motors, gearing noise, and shock due to bumping the centrifuge or jarring the laboratory floor. Unexpected excitation can be caused by external disturbance as subtle as vibrations transmitted through the earth by nearby moving vehicles and explosions, natural frequency of the centrifuge mounting system, drive shaft critical frequencies, or swaying of the floor on which the system is mounted.

Many of the external vibrations can be reduced or isolated by proper use of conventional vibration isolation techniques. However, the proof

of isolation of supposed destructive vibrations is only found by operation experience once the best isolation has been attempted. Information has been recently compiled on isolation techniques, performance, and testing data (13).

*Bearing whirl* is an effect of hydrodynamic instability in fluid film bearings which causes the shafting, forming a journal, to exhibit high amplitude motion and unexpected frequencies which can be disastrous with high-speed machinery (14). Bearing whirls have been further described as synchronous whirl, half-frequency whirl, fractional-frequency whirl, and resonant whip (15). These instabilities have been described in detail; their effects are always troublesome and sometimes destructive.

Synchronous whirl causes the shaft to be in a continual orbital motion parallel to the shaft axis in synchronism with the rotor speed. Half-frequency (for hybrid journal bearings) whirl causes the shaft center to move from a steady-state position and whirl at a fraction of the shaft speed—eventually the bearings are destroyed by overloading. Resonant whip is a self-supported vibration that couples with the bending critical to resonate at the first critical frequency of the system at higher speeds. It, too, is often destructive.

The above instabilities can be eliminated by hybrid journal bearings—hydrostatic bearings, multilobe bearings, etc.—or by using ball bearings. The use of ball bearings can produce other vibrations because of geometry discrepancies, fatigue, misalignment, etc. Furthermore, ball bearings are limited in their load-carrying abilities at high speeds and by their metal fatigue. High-speed ball bearing speeds are limited on the basis of their  $DN$  values ( $D$  is bearing bore in millimeters,  $N$  is in revolutions per minute) to the following:

- $DN < 300,000$  for grease lubrication,
- $DN < 600,000$  for oil bath lubrication,
- $DN < 850,000$  for wick lubrication, and
- $DN < 1,900,000$  for oil mist lubrication.

*Rigid-body* modes of vibration are passed through as the rotor is accelerated to its operating speed if the system is designed with flexible shafts and mounts. As the rotor speed increases above the rigid-body modes, the rotor seeks to become self-balancing and, hence, quiet-running. The rotation frequency at which the rigid-body vibrations occur depends upon the flexible shaft spring rates, bearing support masses and spring rates, rotor configuration, and stiffness of the rotor. Usually, the first and lowest frequency mode is an orbital translation of the rotor mass center parallel to the system axis, while the second and higher frequency mode is a rotation of the mass center in a conical orbit about the system axis (16). Rigid-body motions can be raised to frequencies above the operating speed range by making the centrifuge system extremely stiff. However, extreme stiffness defeats self-balancing, requires massive structures, and consumes large amounts of power for high speeds (17).

Rotor whirl is an effect of high speed which appears as gyroscopic forces increase. The gyroscopic effects change the observed low frequency modes of vibration and can change the flexural or bending mode frequencies of the rotor and shafts (18). Whirl is observed as a rigid-body translatory or conical rotor movement at a frequency different from the spin frequency. If the damping and stiffness properties of the suspension systems are symmetric about the axis of rotation, then there are four pairs of whirl modes for most centrifuges. These modes are associated with the rigid-body vibration modes; the pair of mode frequencies are increased or decreased with speed changes. Usually the first whirling mode is a translatory motion of the rotor axis about the machine axis. A second whirling mode is conical movement of the rotor axis about the machine axis with a mode near the mass center. The third and fourth types of motion are associated with the suspension system vibrations.

The direction of rotor whirl can be in the same direction as the rotor spin (associated with forward whirl or precession) or in a direction opposed to the rotor spin (associated with backward whirl or precession).

Text-figure 4a, b, c, and d show the rigid-body critical motions, while text-figure 4e shows the whirl frequencies as a function of rotor spin frequency for the B-IV zonal centrifuge rotor. Text-figure 4e was obtained by using Kelley's mathematical model of a centrifuge (19).

The whirl motions of a rotor in forward and backward precession can be illustrated by the method of the body cone rolling on a space cone described by Timoshenko and Young (20). The polhode of the momental ellipsoid and of its axis traces out a body cone in space as the body rolls on the invariant plane. The whirl motion can be visualized in text-figure 5a where the body cone rolls on the outside of the space cone for forward whirl. Text-figure 5b represents the body cone rolling on the inside of the space cone for backward whirl.

Timoshenko and Young (21) point out that a top rotating about a fixed point in space will precess with forward whirl if it is cigar-shaped and precess with a backward whirl if it is disk-shaped. However, for a centrifuge rotor with flexible shafts, the rotor can whirl in both modes depending upon the damping provided in the system (22). Generally, for inadequate damping of a long rotor the whirl mode will be forward, while for too much damping the same rotor will whirl in a backward mode. The whirl frequencies can be estimated by the equation

$$\omega_w = \frac{I_{\text{spin}}}{2I_{\text{transverse}}} \omega \pm \sqrt{\left( \frac{I_{\text{spin}}}{2I_{\text{transverse}}} \omega \right)^2 + \omega_n^2}$$

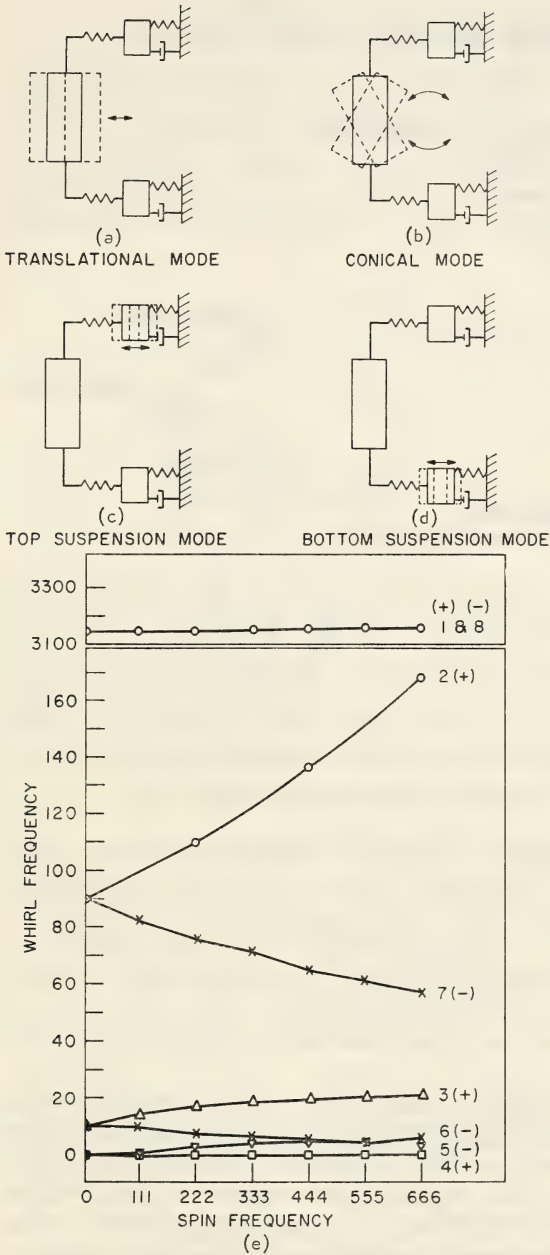
where  $\omega_w$  = whirl frequency,

$\omega$  = spin frequency,

$\omega_n$  = natural frequency of a particular mode,

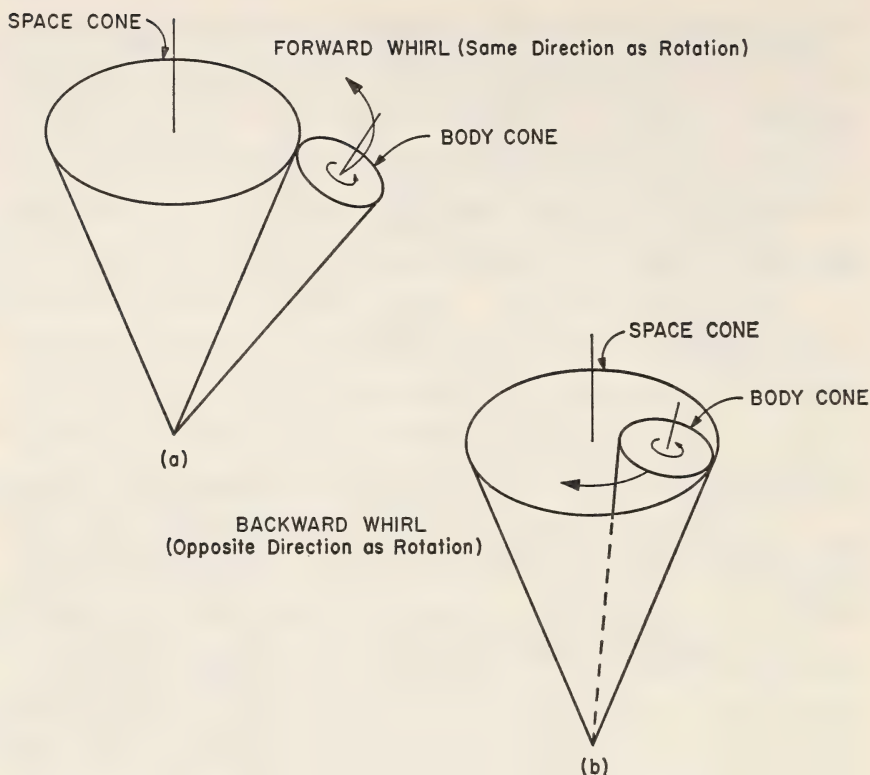
$I_{\text{transverse}}$  = moment of inertia about the transverse axis, and

$I_{\text{spin}}$  = moment of inertia about the spin axis.



TEXT-FIGURE 4.—Motions and frequencies of the B-IV zonal centrifuge rotor. (Spin and whirl frequency in cycles per second.) Upper line in graph at left refers to bottom suspension mode, lines 2 and 7 to top suspension mode, lines 3 and 6 (together at origin) to conical mode, and lines 4 and 5 to translational mode.

*Liquid instabilities* can cause the fluid load of a centrifuge to become unbalanced and vibrate at high frequencies. Centrifugal waves formed on the free surface of a cylindrical rotor have been reduced or eliminated by confining the fluid between rigid cylinders, dividing a cylindrical rotor into sector-shaped compartments, or by reducing the centrifuge



TEXT-FIGURE 5.—Diagram of forward and backward whirl.

operating speed. Centrifugal waves are a natural phenomenon comparable to surface waves on a lake (23). When a centrifuge is constructed to hold an annular section of fluid, the free surface of the fluid can be observed with a stroboscope. Experimentally, we have observed a wave with its crest and trough nearly  $180^\circ$  apart. This wave has its center of mass appreciably displaced from the centrifuge geometric axis, and unbalance of the rotor occurs. This condition is discussed in more detail below.

*Shaft flexural criticals* in the centrifuge drive system can behave as high energy level vibration forcing functions acting on the centrifuge rotor. These flexural criticals cause the shafts to bend into a specific mode shape with resulting unbalance. For example, the rotating flexural critical vibration can cause the shaft to have a banana-shaped curve which rotates off balance, but the bending stress seen by the rotor does not reverse (24). (This is in opposition to a flexural critical of a harp string which, when plucked to vibrate in its flexural critical, has a stress reversal.)

While flexural criticals of the shafting do not present an alternating stress in the shafts, a whirl of the rotor at a speed different than spin speed will produce an alternating stress. Thus, a large number of stress cycles can be accumulated very rapidly to produce shaft fatigue (25).

CRITICAL SPEED OF THE ROTOR<sup>5</sup>

The critical speed of the rotor itself must be determined when the required length-to-diameter ratio of the rotor is large. If flexible shafting is used to support the rotor, it can be demonstrated that the shafting exerts a negligible influence upon rotor critical speed. In such cases, the rotor can be treated quite accurately as a free beam. The Raleigh-Ritz method of analysis can be used to determine this frequency (26):

$$\frac{\partial}{\partial a_i} \int_0^L \left\{ I \left[ \frac{d^2 \phi(x)}{dx^2} \right]^2 - \psi[\phi(x)]^2 \right\} dx = 0, \quad [1]$$

where

$$\phi(x) = \sum_{i=0}^{\infty} a_i (x/l)^{2i},$$

$$\psi = 4\pi^2 \nu^2 (A\gamma / EI g),$$

$\nu$  is the critical frequency (cps);  $A$ , cross-sectional area (in<sup>2</sup>);  $\rho_r$ , density of the rotor (lb/in<sup>3</sup>);  $E$ , Young's modulus (lb/in<sup>2</sup>);  $I$ , area moment of inertia (in<sup>4</sup>);  $g$ , 386 in/sec<sup>2</sup>;  $L$ , length of rotor; and  $l = L/2$ . The  $\phi(x)$  function defines the shape of the rotor when it is operated at its critical speed. Assuming free-free end conditions, the shape function can be determined by invoking the boundary conditions

$$EI \frac{\partial^2 \phi(x)}{\partial x^2} = 0$$

and

$$\frac{\partial}{\partial x} \left[ EI \frac{\partial^2 \phi(x)}{\partial x^2} \right] = 0 \quad [2]$$

at the ends of the rotor. With the midpoint of the rotor as the origin and by application of the boundary conditions to the first four terms of the series,  $\phi(x)$  yields the shape function for a uniform tube

$$\phi(x) = a_0 + a_3 \left( \frac{x^6}{l^6} - \frac{5x^4}{l^4} + \frac{15x^2}{l^2} \right) \quad [3]$$

where  $a_0$  and  $a_3$  are constants.

The total mass of the end plugs will be assumed to be concentrated in a solid plug of uniform density and effective thickness,  $t_{eff}$ . From this

<sup>5</sup> This section was written by D. A. Waters, Technical Division, Oak Ridge Gaseous Diffusion Plant.

assumption,  $t_{eff}$  can be derived from the ratio of the mass of the bowl,  $m_b$ , to the mass of the end plug,  $m_{ep}$  (27):

$$\alpha = \frac{m_{ep}}{m_b} \simeq \frac{\rho_{ep} \pi r^2}{\rho_b \pi A r^2} \frac{t_{eff}}{\ell}$$

or

$$t_{eff} = \frac{\alpha}{K} \ell, \quad [4]$$

where  $K$  is the ratio of the cross-sectional area of the end plug,  $\pi r^2$ , to the cross-sectional area of the bowl,  $\pi A r^2$ .

The range of integration of equation 1 is  $0 = x = l$  for the bowl and  $l = x = l(1 + \alpha/K)$  for the end plug. Furthermore, it will be assumed that the shape of the deflection curve,  $\phi(x)$ , will be constant throughout the end plug, the value of which is equal to the deflection at  $x = l$  or

$$\phi(\ell) = a_0 + 11a_3. \quad [5]$$

Substituting equations 2 through 5 into 1 and integrating over the appropriate ranges, one obtains the following simultaneous equations that can be solved for the critical frequency:

$$a_0(1 + \alpha) + a_3(4.1429 + 11\alpha) = 0, \quad [6]$$

$$0.4063a_3 - \frac{\psi \ell^4}{900} [a_0(4.1429 + 11\alpha) + a_3(28.8504 + 121\alpha)] = 0. \quad [7]$$

These equations can be solved quite easily by hand. However, they have also been included in a computer program to simplify multiple computations for optimum design.

An aluminum rotor weighing 1.34 pounds operates at 2350 cps with a 1.500-inch O.D.  $\times$  1.093-inch I.D.  $\times$  7.5-inch length of the rotor tube filled with cesium chloride. The rotor has a measured natural frequency of 2850 cps and a calculated natural frequency of 2770 cps when:

$$A_{Rotor} = 0.829 \text{ in}^2, A_{Liquid} = 0.940 \text{ in}^2,$$

$$\rho_r = 0.101 \text{ lb/in}^3, \rho_l = 0.060 \text{ lb/in}^3,$$

$$A\rho_r = \sum A_i \rho_{r_i} = 0.14 \text{ lb/in.}$$

$$E_{Rotor} = 10.4 \times 10^6 \text{ lb/in}^2, E_{Liquid} = 0, E = \sum E_i = 10.4 \times 10^6 \text{ lb/in}^2$$

$$\begin{aligned}
 I &= 0.178 \text{ in}^4, \\
 L &= 7.5 \text{ in}, \\
 l &= 3.75 \text{ in}, \\
 m_b &= 1.04 \text{ lb}, \\
 m_{ep} &= 0.30 \text{ lb}, \\
 \alpha &= 0.288, \\
 \psi &= 77.4 \times 10^{-10} \nu^2 \text{ in}^{-4}.
 \end{aligned}$$

## DAMPER BEARINGS

### Loose Mountings

Vibration dampers remove energy from vibratory systems to control maximum amplitudes of the centrifuge when the system is excited by some oscillatory force. There are at least four types of dampers (28): 1) Linear dampers (dash pots) develop a force proportional to the relative velocity across the damper; 2) Coulomb dampers develop a force proportional to the coefficient of friction and force between rubbing surfaces of the damper; 3) eddy current dampers develop a force directly proportional to the velocity of a shorted coil moving through a magnetic field; and 4) hysteresis damping develops a force which is a function of shear strain, frequency, and temperature (29). The force developed by dampers acting through distances and time consumes power, and by dissipating part of the vibratory energy the vibratory amplitude is reduced. The energy removal and, hence, damping constant have a small allowable range which is optimum for the operating speed frequency range. This over-all optimum damping constant is not necessarily an optimum damping constant for specific modes of vibrations.

The damping constant represents a loose connection between the movable parts of the system and ground. Increasing the damping constant stiffens the system by permitting higher forces to be transmitted through the damping material.

The damped member of the system, usually a bearing, is suspended from ground by both springs and dampers. This permits the damper bearing to pass through a critical speed range and become isolated so that vibrations of high frequency are not transmitted to the surrounding system. When the critical speed is passed, the force causing movement and the total restoring forces are out of phase.

### Flexible Shafts

When a rotor has passed through its rigid-body critical vibrations, nearly a 180° phase reversal occurs between the rotor unbalance and spin axis of the shaft (30). Thus, a rotor can become self-balancing. As the rotor becomes self-balancing, the bearing loads required to hold the rotor

in support can be reduced if flexible shafts are provided to bend as the rotor mass center moves to the rotor spin axis. This means that below the rigid-body critical speeds the force causing the unbalance and the rotor runout are in phase, while above the critical speed the force causing unbalance and the rotor runout are  $180^\circ$  out of phase. Self-balancing rotors are quiet running, have lower power losses at high speed, and are preferred over rigid rotors with rigid shafts.

### **Damper Bearing Requirements**

A damper bearing should have some of the following features: 1) optimum weight, 2) variability of damping constant and spring rate, 3) high spring rates between the damper and ground and the damper and rotor, 4) reliable and reproducible operating characteristics, and 5) a sufficiently high frequency and amplitude response to damp high frequency whirl motions. In addition the damper bearing should provide good isolation of rotor vibrations from ground and cause bearing loads to be small. Some of these features are contradictory, such as high spring rates and small bearing loads. A design compromise is required to balance one characteristic against another for satisfactory bearing operation.

Frequency response is of primary concern because the damper bearing must be capable of eliminating high frequency whirl, which is seen in centrifuges with large  $L/D$  ratios. To obtain good frequency response of a damper bearing, it should be designed with its natural frequency of vibration above the maximum whirl frequency expected and with an amplitude of movement equal to that of the rotor. The upper limit of frequency and amplitude response of a damper bearing is reached when the whirl frequency is much greater than the natural frequency of the damper bearing and the damper bearing moves about one tenth of the rotor movement for small displacements; however, a damper bearing pushed to this design limit will usually not perform satisfactorily.

When optimum damping constants are chosen, however, it is still difficult to make the damping stay at the same value over the entire operating frequency range. For this reason the optimal amount of damping must be found experimentally. This must be done by actual operation of the centrifuge in its particular suspension and frame.

### **STRESSES IN ZONAL CENTRIFUGE ROTORS**

The stresses in a zonal centrifuge consist of: 1) a rotational load of the rotor material under a high centrifugal field, 2) a stress from the hydrostatic pressure developed by the fluid in the rotor, 3) bending stresses due to rotor unbalance, and 4) mismatch stresses where end caps are joined to the rotor. Only the first two stresses will be discussed, and they will be related to a cylindrical rotor similar to a zonal centrifuge.

*Rotational stress* in a hollow cylindrical body may be resolved into a number of components (31). The maximum stress is the tangential stress which occurs at the inner edge of the cylinder. This maximum stress,  $\sigma_{t_{\max}}$ , can be written as

$$\sigma_{t_{\max}} = \frac{\rho_r a^2 \omega^2}{g} \left( \frac{3 + \mu}{4} \right) \left[ 1 + \frac{1 - \mu}{3 + \mu} \left( \frac{b}{a} \right)^2 \right] \quad [8]$$

At this point the radial stress is zero.

For hydraulic stress in a cylindrical body pressured on the inside, the tangential stress is a maximum value at the inner edge of the cylinder (32). The maximum stress can be written as

$$\sigma_{t_{\max}} = \left( \frac{\rho_l b^2 \omega^2}{2g} \right) \left( \frac{a^2 + b^2}{a^2 - b^2} \right), \text{ where } \sigma_r = - \left( \frac{\rho_l b^2 \omega^2}{2g} \right). \quad [9]$$

where the first term in parentheses is the maximum pressure at the inner wall formed by spinning the fluid.

From superposition (33) of the two maximum stresses which occur at the same location

$$\sigma_t = \frac{\rho_r a^2 \omega^2}{g} \left( \frac{3 + \mu}{4} \right) \left[ 1 + \frac{1 - \mu}{3 + \mu} \left( \frac{b}{a} \right)^2 \right] + \frac{\rho_l b^2 \omega^2}{2g} \left( \frac{a^2 + b^2}{a^2 - b^2} \right) \quad [10]$$

and

$$\sigma_r = \frac{\rho_l b^2 \omega^2}{2g}.$$

By using the maximum shear stress theory (34) as a criterion for failure the shear stress becomes

$$\tau = \frac{\sigma_t - \sigma_r}{2} = \frac{\rho_l b^2 \omega^2}{g} \left( \frac{3 + \mu}{8} \right) \left[ 1 + \frac{1 - \mu}{3 + \mu} \left( \frac{b}{a} \right)^2 \right] + \frac{\rho_r a^2 \omega^2}{2g} \left( \frac{a^2}{a^2 - b^2} \right) \quad [11]$$

The shear stress can be minimized by setting  $\frac{d\tau}{da} = 0$  to give

$$a = b \left\{ 1 + \left[ \frac{4\rho_l}{(3 + \mu)} \right]^{1/2} \right\}^{1/2} \quad [12]$$

or written in terms of the rotor wall thickness

$$t = b \left\{ \left[ 1 + \left( \frac{4\rho}{(3 + \mu)} \right)^{1/2} \right]^{1/2} - 1 \right\} \quad [13]$$

and the optimized maximum shear stress for an optimum rotor becomes

$$\tau_{\text{opt}} = \frac{b^2 \omega^2}{2g} \{ \rho_r + \rho_l + [(3 + \mu) \rho_l \rho_r]^{1/2} \} \quad [14]$$

Or since the working stress and maximum shear stress are related

$$\sigma_w = 2\tau_{\text{opt}} = \frac{b^2 \omega^2}{g} \{ \rho_r + \rho_l + [(3 + \mu) \rho_l \rho_r]^{1/2} \} \quad [15]$$

- where  $a$  = outside radius of rotor (inches)  
 $b$  = inside radius of rotor (inches)  
 $\omega$  = angular frequency of rotor (radians/sec)  
 $\rho_r$  = density of rotor material (pounds/sq-in)  
 $\rho_l$  = density of fluid filling rotor (pounds/sq-in)  
 $g$  = gravitational constant  
 $\mu$  = Poisson's ratio for rotor material  
 $t$  = rotor wall thickness (inches)  
 $\tau$  = shear stress (pounds/sq-in)  
 $\sigma_t$  = tangential stress (pounds/sq-in)  
 $\sigma_r$  = radial stress (pounds/sq-in)  
 $\sigma_w$  = working stress (pounds/sq-in)

*Bending stress and mismatch stresses* are generally designed to be small and are usually absorbed into the allowable safety factor.

## DESIGN DATA

The selection of a centrifuge rotor material is usually based on: 1) strength-to-density ratio, 2) ease of fabrication, 3) cost and availability, 4) corrosion resistance, and 5) operating temperature. Typical materials considered for use in rotor construction are shown in table 1.

From the information in table 1, a number of materials have been considered (*see* table 2), and the data have been used to construct rotor design curves for various stress levels, assuming dense CsCl solutions are used, as shown in subsequent tables.

The data in table 3 are given where  $N$  is the angular speed of the centrifuge rotor in rpm and where a circumferential wrap is used for the Fiber-glas-epoxy and steel wire-epoxy rotors. With such wraps, a metal liner is used to carry the axial hydraulic load.

With the working stresses shown in table 2 and the stress relations given in table 3, another comparison (table 4) can be made to show the maximum inside peripheral speed of the rotor. The table also points out the penalty for centrifuging heavy liquids.

The data in table 2 have been plotted as design graphs in text-figure 6, with the use of CsCl to determine the proper design of a liquid centrifuge.

TABLE 1.—Typical mechanical properties of various materials

Material	Yield or ultimate strength, $\sigma$ (psi)	Material density, (lb/in <sup>3</sup> ) <sup>r</sup>	Strength- to-density ratio, $\sigma/\rho$ , (inches)	Trade or common name
	$\times 10^3$		$\times 10^6$	
Acetate	138	0.0543	2.54	Fortisan 36
Aluminum	78	0.101	0.773	7.78-T6
Beryllium	144	0.036	4.0	Beryllium wire
Glass	250	0.075	3.34	S-994-HTS
Magnesium	32	0.060	0.534	AZ31B-H24
Plastic	40	0.051	0.784	Mylar T film
Steel	300	0.289	1.04	Maraging steel
Steel	650	0.283	2.30	Rocket motor case wire
Titanium	220	0.175	1.26	13V-11Cr-2Al

TABLE 2.—Typical mechanical properties of materials for liquid centrifuges

Material	Ultimate strength (psi)	(0.2%) yield strength (psi)	Elong- ation (%)	Working stress (psi)	Rotor material density (lb/in <sup>3</sup> )	Strength- to-den- sity ratio*
	$\times 10^3$	$\times 10^3$		$\times 10^3$		$\times 10^6$
7075-T6 aluminum	76	67	11	50	0.101	0.495
Beta-titanium	190	170	4	150	0.175	0.857
Maraging steel	286	280	11	250	0.289	0.865

\*Based on working stress.

## FILAMENT-WOUND VESSELS

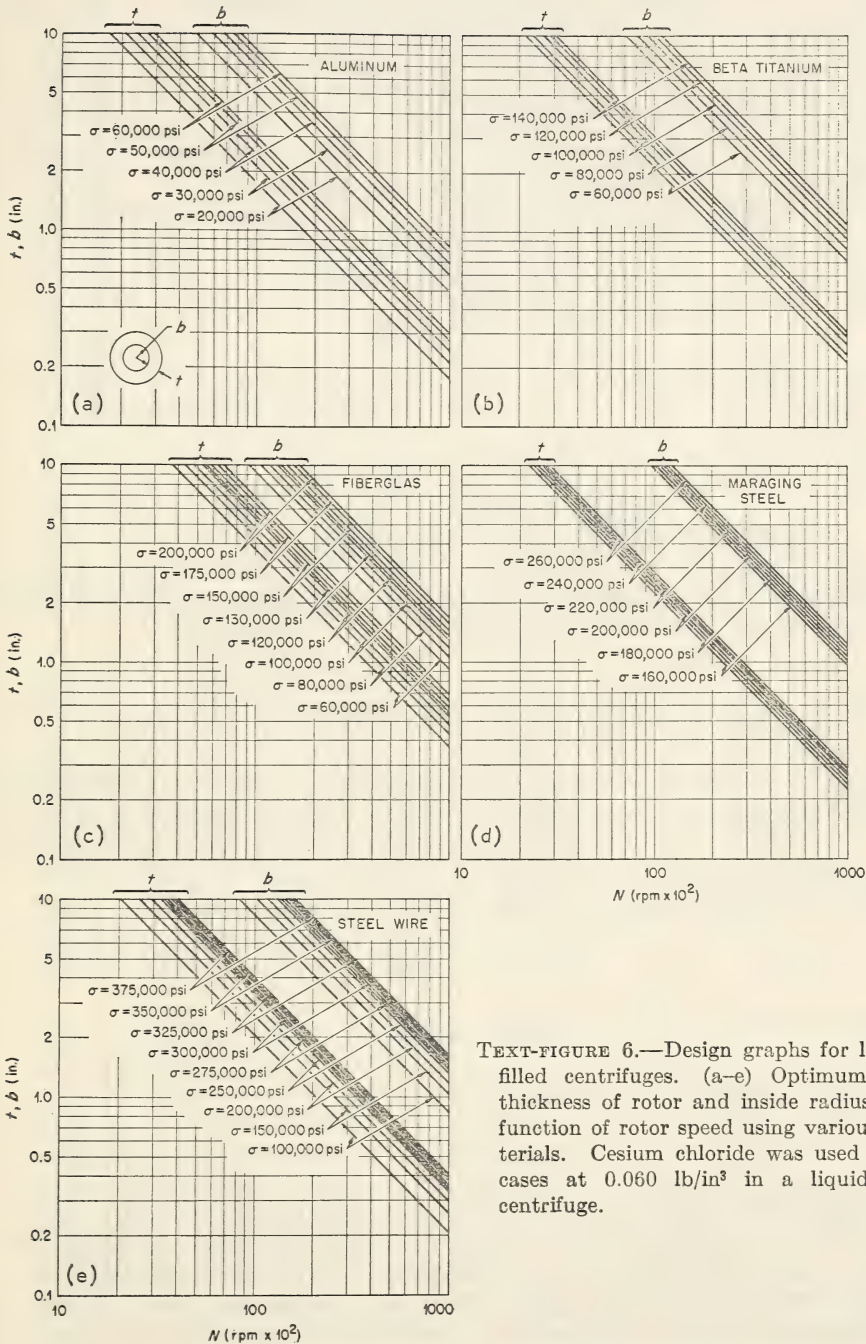
From the data in the preceding section, it is evident that higher peripheral speeds and resulting higher  $g$  fields can be produced by using circumferential wraps of Fiberglas or steel wire over a liner (35). This technique has been used by aerospace firms for rocket motor cases (36) and represents the simplest fabrication method. Two slightly different methods have been used to form rocket motor cases without the use of metal liners. These are 1) the balanced method, which uses sets of longitudinal and circumferential wraps, such as those on the Polaris missile case (37), and 2) the method of winding the cases on a helix angle where the path of the glass or wire filament is that of a geodesic. Techniques for winding vessels with openings on either end of the cylinder, such as would be required with centrifuges, have also been developed for aerospace applications.

TABLE 3.—Optimum working stresses and wall thicknesses for liquid centrifuge rotors

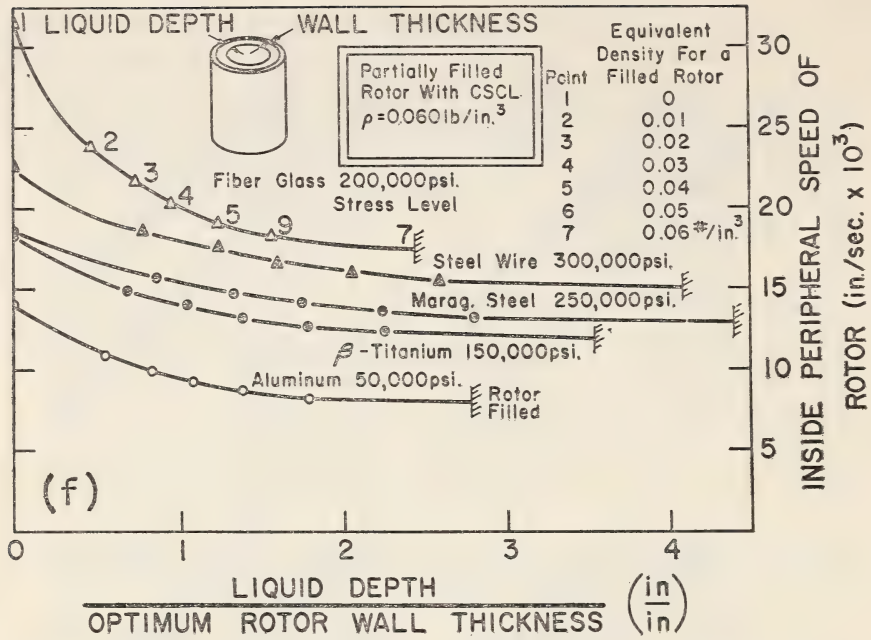
Rotor fluid	7075-T6 aluminum		Beta-titanium		Fiberglas epoxy		Maraging steel		Steel wire epoxy	
	$\sigma$	$t$	$\sigma$	$t$	$\sigma$	$t$	$\sigma$	$t$	$\sigma$	$t$
	$\times 10^{-6} N^2 d^2$		$\times 10^{-6} N^2 d^2$		$\times 10^{-6} N^2 d^2$		$\times 10^{-6} N^2 d^2$		$\times 10^{-6} N^2 d^2$	
CsCl*	8.65	0.36 <i>a</i>	12	0.285 <i>a</i>	7.32	0.14 <i>a</i>	16.8	0.23 <i>a</i>	14.7	0.25 <i>a</i>
66% sucrose†	7.83	0.33 <i>a</i>	11.1	0.255 <i>a</i>	6.6	0.372 <i>a</i>	15.7	0.21 <i>a</i>	13.6	0.22 <i>a</i>
Water‡	7.05	0.29 <i>a</i>	10.1	0.225 <i>a</i>	5.88	0.33 <i>a</i>	14.6	0.18 <i>a</i>	12.5	0.20 <i>a</i>
Empty§	2.88	0	4.98	0	2.13	0	8.24	0	6.74	0

\* $\rho = 0.06 \text{ lb/in}^3$ .† $\rho = 0.0476 \text{ lb/in}^3$ .‡ $\rho = 0.036 \text{ lb/in}^3$ .§ $\rho = 0$ .

ORNL-DWG 65-5356



TEXT-FIGURE 6.—Design graphs for liquid-filled centrifuges. (a-e) Optimum wall thickness of rotor and inside radius as a function of rotor speed using various materials. Cesium chloride was used in all cases at  $0.060 \text{ lb/in}^3$  in a liquid-filled centrifuge.



TEXT-FIGURE 6.—(f) Design graph for liquid-filled centrifuges. Inside peripheral speed compared with fluid density for materials of rotor construction.

TABLE 4.—Maximum inside peripheral velocity for liquid centrifuges\*

Material	Rotor fluid				Working stress (psi)
	CsCl	Sucrose	Water	Empty	
7075-T6 aluminum	(202) 7,950	(211) 8,360	(222) 8,820	(348) 13,800	$\times 10^3$ 50
Beta-titanium	(295) 11,700	(308) 12,200	(322) 12,800	(458) 18,200	150
Maraging steel	(322) 12,800	(333) 13,200	(356) 13,700	(458) 18,200	250

\*Values in parentheses in m/sec, others in in./sec.

Text-figure 7a shows a portion of a rotating centrifuge filled with liquid and helically wrapped with high-strength filaments. Text-figure 7b shows an enlarged view of a filament, with unit width and depth in the direction of the wrap, along with the area of the other surfaces. The stress and force diagrams are shown in text-figure 7c and d from which the helix angle can be found.

The value  $\sigma \sin^2 \phi$  represents the circumferential stress ( $\sigma_\theta$ ) and  $\sigma \cos^2 \phi$ , the axial stress ( $\sigma_A$ ), thus

$$\sigma \sin^2 \phi = \sigma_\theta, \quad [16]$$

$$\sigma \cos^2 \phi = \sigma_A, \quad [17]$$

or

$$\frac{\sigma \sin^2 \phi}{\sigma \cos^2 \phi} = \frac{\sigma_\theta}{\sigma_A}. \quad [18]$$

Then

$$\phi = \tan^{-1} \sqrt{\frac{\sigma_\theta}{\sigma_A}}, \quad [19]$$

where  $\sigma_\theta$  is equation 15; the axial stress is the hydraulic load acting on the end caps of the centrifuge,

$$\sigma_A = \frac{\pi \rho_l \omega^2 a^4 / 4g}{2\pi a t} = \frac{\rho_l \omega^2 \dot{a}^3}{8gt}, \quad [20]$$

where the wall thickness  $t$  is given by equation 13. When equations 13, 15, and 20 are substituted into equation 19, the helix angle becomes

$$\phi = \tan^{-1} \sqrt{\frac{8}{\rho_l} \left[ \sqrt{1 + \sqrt{\frac{4\rho_l}{(3+\mu)\rho_r}}} - 1 \right] [\gamma + \rho_l + \sqrt{(3+\mu)\rho_r\rho_l}]} \quad [21]$$

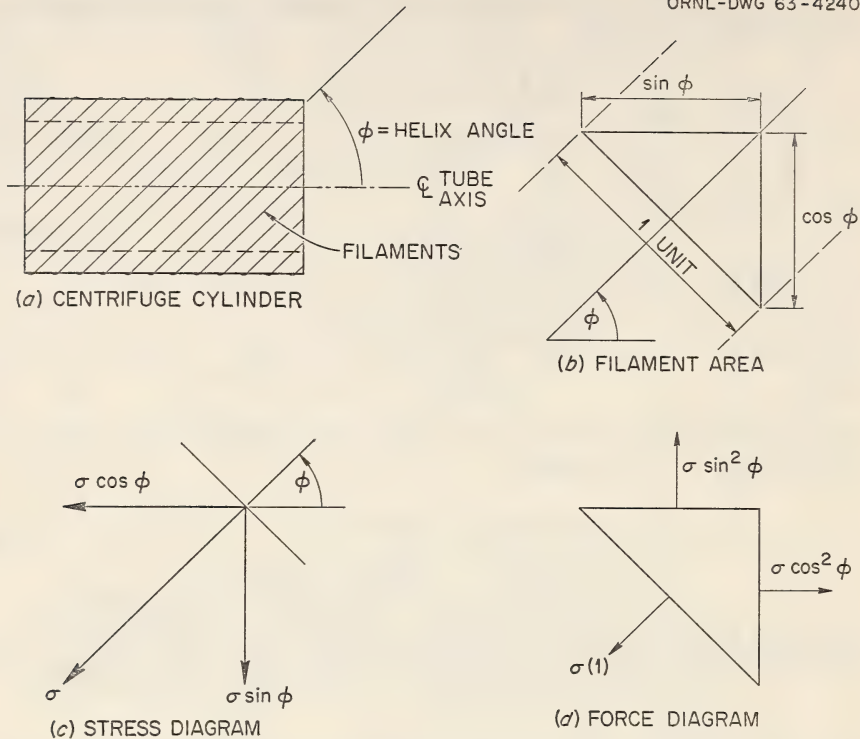
The filament working stress for helically wound rotors can be no higher than for cylindrical wrap; therefore, the circumferential working stress must be reduced by the relation of equation 7.

The data from table 5 have been assembled in the form of design graphs, with the use of CsCl, for finding the proper design of a liquid centrifuge, as shown in text-figure 8.

### END CAP STRESS

Rotational stress and hydraulic stress given above are applicable in some cases to rotor end caps. In other cases, where the end caps have no holes, the equations of stress are much simpler and the tangential stress at the center of the end cap is one half that of an end cap with a hole (38). The end caps can be modified by different contours to increase or decrease their strengths when rotated.

Hydraulic stress causing transverse flexure of the end caps is a more complex situation. Bassali (39) has developed a set of equations to determine the cap deflection and stress due to a parabolic pressure distribution as is the case when a filled rotor is spun. The results are tabulated in



TEXT-FIGURE 7.—Force and stress analysis for helically wrapped rotors. (a) Portion of a rotating centrifuge filled with liquid and helically wrapped with high-strength filaments. (b) Enlarged view of filament, with unit width and depth in the direction of the wrap, together with the area of the other surfaces. (c) Stress diagram from which the helix angle can be found. (d) Force diagram.

TEXT-FIGURE 8.—Design data for Fiberglas and steel wire helically wound centrifuge rotors. Cesium chloride (0.060 lb/in<sup>3</sup>) was used in liquid-filled centrifuges in both cases.

Material	Working stress, $\sigma$	Wall thickness, $t$
	$\times 10^{-6} N^2 a^2$	
Fiberglas (0.075 lb/in <sup>3</sup> )	7.85	0.41a
Steel wire (0.273 lb/in <sup>3</sup> )	15.6	0.25a

ORNL-DWG 63-4241

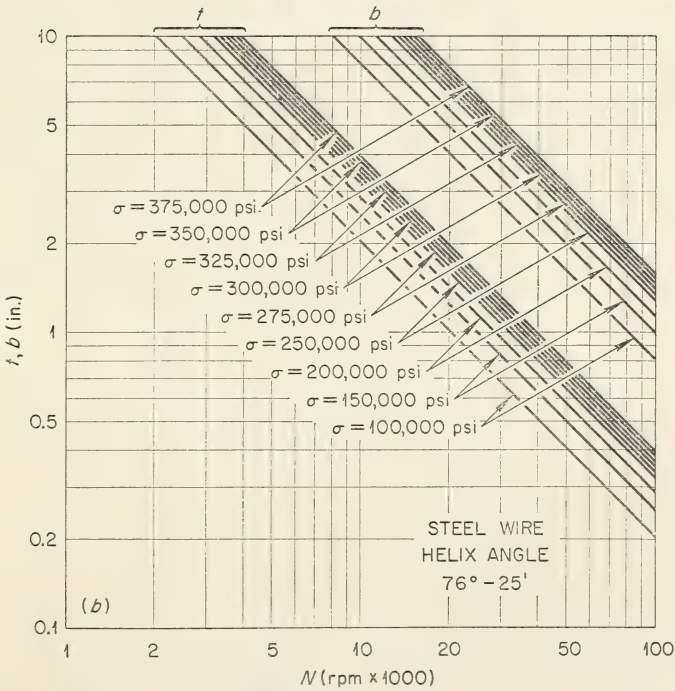
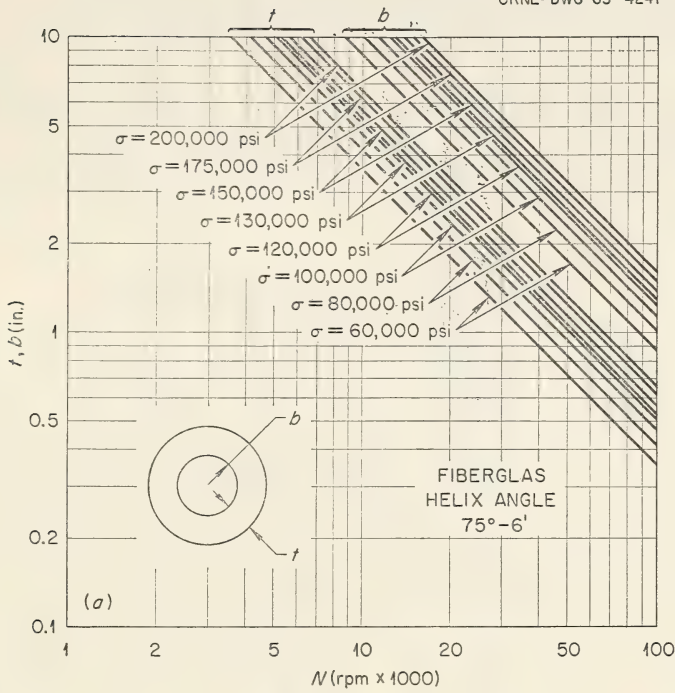


TABLE 5.—Optimum working stresses, wall thicknesses, and helix angles for helically wound liquid centrifuge rotors

Rotor fluid	Helical wrap Fiberglass				Helical wrap steel wire			
	$\sigma$	$t$	$\sigma/\sigma_A$	$\phi$	$\sigma$	$t$	$\sigma/\sigma_A$	$\phi$
	$\times 10^{-6} N^2 a^2$				$\times 10^{-6} N^2 a^2$			
CsCl	7.85	0.41 <i>a</i>	14.1	75°-6'	15.6	0.25 <i>a</i>	17.1	76°-25'
Sucrose	7.06	0.372 <i>a</i>	14.5	75°-17'	14.4	0.22 <i>a</i>	17.7	76°-38'
Water	6.27	0.33 <i>a</i>	15.1	75°-35'	13.2	0.20 <i>a</i>	19.6	77°-19'
Empty	2.13	0	$\infty$	90°	6.74	0	$\infty$	90°

text-figure 9. Other values are given in text-figure 10 for a disk with a hole in the center. The stresses due to transverse deflection of the end caps must be superimposed on the rotational stress for the actual stress condition.

Text-figure 11 compares the results for a disk with uniform pressure loads where the uniform pressure (40) is equal to the maximum parabolic pressure. Text-figure 12 compares the results for a disk with a hole under uniform pressure load (41) with that of a parabolic pressure load.

## CENTRIFUGAL WAVES IN FLUIDS

Some recent work has been done on centrifugal waves, which is of direct interest for centrifuge design in those cases where the rotor is partially filled with a low viscosity liquid (42-45). When a rotating centrifuge has a free liquid surface, the fluid can oscillate with waves of various frequencies and amplitudes, just as water in a pond. In a pond, surface waves are excited by disturbances such as wind gust, but in a centrifuge, which is usually closed, the wind velocity can be negligible and the centrifugal waves are excited by a function of the angular frequency of rotation. Centrifugal waves appearing with the crest and troughs of the first mode shape in the peripheral direction cause the centrifuge to have a severe mass unbalance because the wave crest on one side of the rotor is diametrically opposite to the trough.

Phillips (44) showed experimentally that the axial wave motion was most severe when the fluid depth and speed of rotation produce a wave whose half wavelength in the axial direction is an integral submultiple of the centrifuge length. He also found that for each circumferential wave mode, there are two possible frequencies of excitation (wave frequency less than and greater than the rotational frequency) and the lowest mode is usually excited. The high frequency waves are more heavily damped by viscosity and are difficult to generate. Phillips also found the ratio of circumferential wave frequency to rotational frequency to be reasonably insensitive to what depth the rotor was filled (the ratio varies from 0.6 to 1.0) for the lowest frequency mode. The liquid surface stability can be a problem for surfaces under high acceleration or low acceleration fields (46).

The frequency at which a rotating liquid with a free surface will resonate covers the entire speed range of a centrifuge, *i.e.*, there are no specific natural frequencies as in a rigid-body mechanical system. Hence, the fluid will oscillate at the frequency of excitation. For a centrifuge, the excitation forces are usually at natural vibrational frequencies of the suspension, whirl frequencies, and rotor spin frequencies.

Centrifugal waves can be eliminated by 1) using high viscosity fluids, 2) preventing free fluid surfaces, 3) placing radial septa in the rotor to extend above the fluid surface, or 4) placing circumferential baffles in the rotor to extend above the fluid surface to minimize the axial length of free

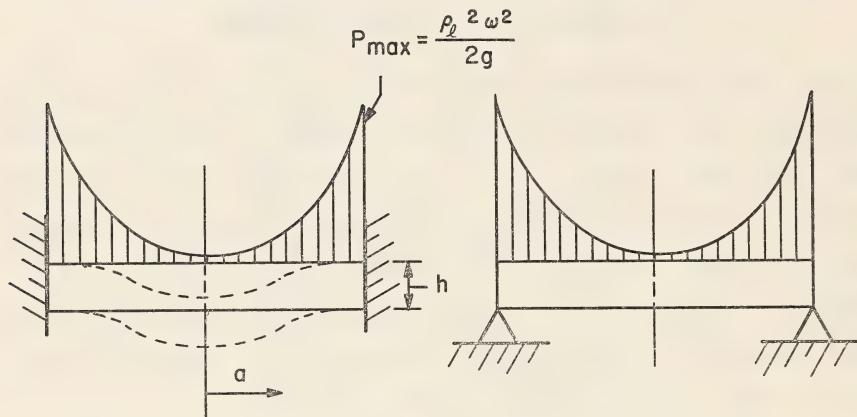
$\rho_L$  = Fluid Density $h$  = Thickness of Disk

$$D = \frac{E h^3}{12 (1 - \mu^2)}$$

 $a$  = Radius of Disk $\mu$  = Poisson's Ratio $\omega$  = Angular Speed $\delta$  = Deflection $P_{\max}$  = Maximum Pressure $g$  = Gravitational Constant $\sigma_r$  = Radial Stress $E$  = Modulus of Elasticity $\sigma_t$  = Tangential Stress

## BUILT-IN EDGES

## SIMPLY SUPPORTED EDGES



Deflection at Center of Disk

$$\delta = \frac{P_{\max} a^4}{288 D}$$

Stress at Center of Disk

$$\sigma_r = \sigma_t = \frac{P_{\max} a^2}{16 h^2} (1 + \mu)$$

Max. Stress Occurs at Outer Edge

$$\sigma_r = \frac{\sigma_t}{\mu} = - \frac{P_{\max} a^2}{4 h^2}$$

Deflection at Center of Disk

$$\delta = \frac{P_{\max} a^4}{288 D} \left( \frac{7 + \mu}{1 + \mu} \right)$$

Stress at Center of Disk (also Max. Stress)

$$\sigma_r = \sigma_t = \frac{P_{\max} a^2}{4 h^2} \left( \frac{5 + \mu}{4} \right)$$

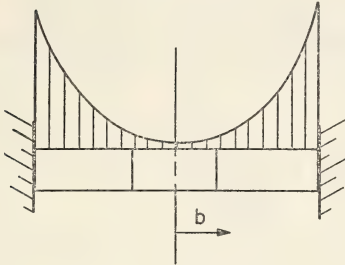
TEXT-FIGURE 9.—Circular disk loaded with a parabolic pressure distribution.

surface so that the oscillations can be damped out. Unfortunately, the theory developed thus far gives the frequencies at which a wave can be excited but does not indicate which particular frequency will cause the most troublesome mode to be excited. Thus, full-scale experiments are the only reliable method of finding which vibration mode and frequency will be excited.

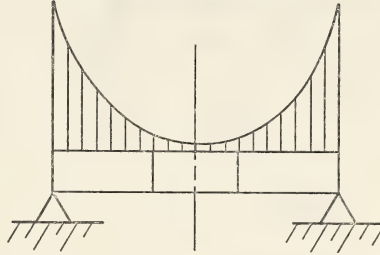
Text-figure 13 shows calculated wave frequencies and mode shapes with the troublesome area due to circumferential waves identified. Text-figure 14 shows a curve of rotor runout versus frequency for the rotor in text-figure 13. At 1300 rpm the wave motion will be excited at 1000 rpm in its lowest mode, and this mode excites the 1000 rpm natural frequency

$$A = \frac{a^4 + 6b^4 + 12b^4 \ln b/a - \left(\frac{7\mu - 1}{1 + \mu}\right)b^4}{b^2(1 + \mu) + a^2(1 - \mu)}, \quad b = \text{Inside Radius, } D = \frac{Eh^3}{12(1 - \mu)^2}, \quad \text{Let } \mu = 0.3$$

BUILT-IN EDGES



SIMPLY SUPPORTED EDGES



Deflection at b:

$$\delta = \frac{P_{\max}}{192D} \left\{ \frac{b^2}{a^2} \left[ b^4 \left( 12 \ln a/b + 19/3 \right) - a^4 \right] + (1 + \mu) b^2 \left( 2 \ln a/b - 1 - b^2/a^2 \right) A + \frac{2a^4}{3} - 6b^4 \right\} = \frac{P_{\max} a^4}{Eh^3} \alpha$$

Stress at Inner Edge:

$$\sigma_t = \frac{P_{\max}}{16h^2 a^2} \left\{ (a^4 - 12b^4 \ln a/b) (1 + \mu) + b^4 (7\mu - 1) - A \left[ b^2 (1 + \mu)^2 + a^2 (\mu^2 - 1) \right] \right\} = \frac{P_{\max} a^2}{h^2} \beta$$

Deflection at b:

$$\delta = \delta_{\text{built-in}} + \frac{P_{\max}}{192D} \left\{ \frac{1}{1 + \mu} - \frac{2b^2 \ln b/a}{(1 - \mu)(a^2 - b^2)} \right\} \left\{ 4a^4 - 12b^4 + 2b^2 (1 + \mu) A \right\} = \frac{P_{\max} a^4}{Eh^3} \gamma$$

Stress at Inner Edge:

$$\sigma_t = \sigma_{t \text{ built-in}} + \frac{P_{\max}}{16a^2 h^2} \left\{ 4a^4 - 12b^4 + 2b^2 (1 + \mu) A \right\} = \frac{P_{\max} a^2}{h^2} \Delta$$

b/a	$\alpha$	$\beta$
0.05	0.0210	0.1614
0.10	0.0221	0.1591
0.15	0.0230	0.1544
0.20	0.0235	0.1473

b/a	$\gamma$	$\Delta$
0.05	0.0971	0.4120
0.10	0.1045	0.4113
0.15	0.1117	0.4094
0.20	0.1211	0.4045

TEXT-FIGURE 10.—Circular disk with a hole loaded with a parabolic pressure distribution.

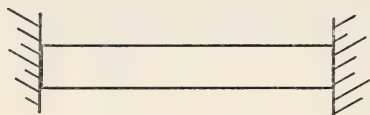
of the system. Wave motion has been eliminated in this rotor by addition of radial septa.

## PROBLEM AREAS

Progression from *theory to prototype* spans a wide gap in building high-speed centrifuges. The comparable gap in building low-speed centrifuges is not as great. This difficulty for high-speed machines stems from 1) the frequency at which the damper bearings must move, 2) shaft flexibility required for high-speed machines, 3) large stresses in the rotors at high

Assume  $P_{\max} \text{Uniform} = P_{\max} \text{Parabolic}$   $\mu = 0.3$

### BUILT-IN EDGES



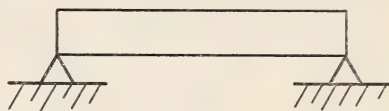
Maximum Deflection

$$\frac{\delta_{\text{parabolic}}}{\delta_{\text{uniform}}} = 0.222$$

Maximum Stress

$$\frac{\sigma_{\text{parabolic}}}{\sigma_{\text{uniform}}} = 0.333$$

### SIMPLY SUPPORTED EDGES



Maximum Deflection

$$\frac{\delta_{\text{parabolic}}}{\delta_{\text{uniform}}} = 0.0611$$

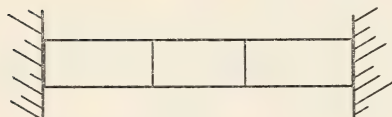
Maximum Stress

$$\frac{\sigma_{\text{parabolic}}}{\sigma_{\text{uniform}}} = 0.201$$

TEXT-FIGURE 11.—Comparison at maximum deflection and stress of a circular disk loaded with a parabolic load and a uniform load.

Assume  $[P_{\max}]_{\text{Uniform}} = [P_{\max}]_{\text{Parabolic}}$   $\mu = 0.3$ ,  $\alpha = 2.875$ ,  $b = 0.500$

### BUILT-IN EDGES



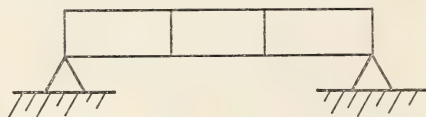
Maximum Deflection

$$\frac{\delta_{\text{parabolic}}}{\delta_{\text{uniform}}} = \frac{1.585 \frac{P}{Eh^3}}{\frac{12.25 P}{Eh^3}} = 0.126$$

Stress at Inner Edge

$$\frac{\sigma_{\text{parabolic}}}{\sigma_{\text{uniform}}} = \frac{1.248 \frac{P}{h^2}}{\frac{P}{h^2}} = 0.208$$

### SIMPLY SUPPORTED EDGES



Maximum Deflection

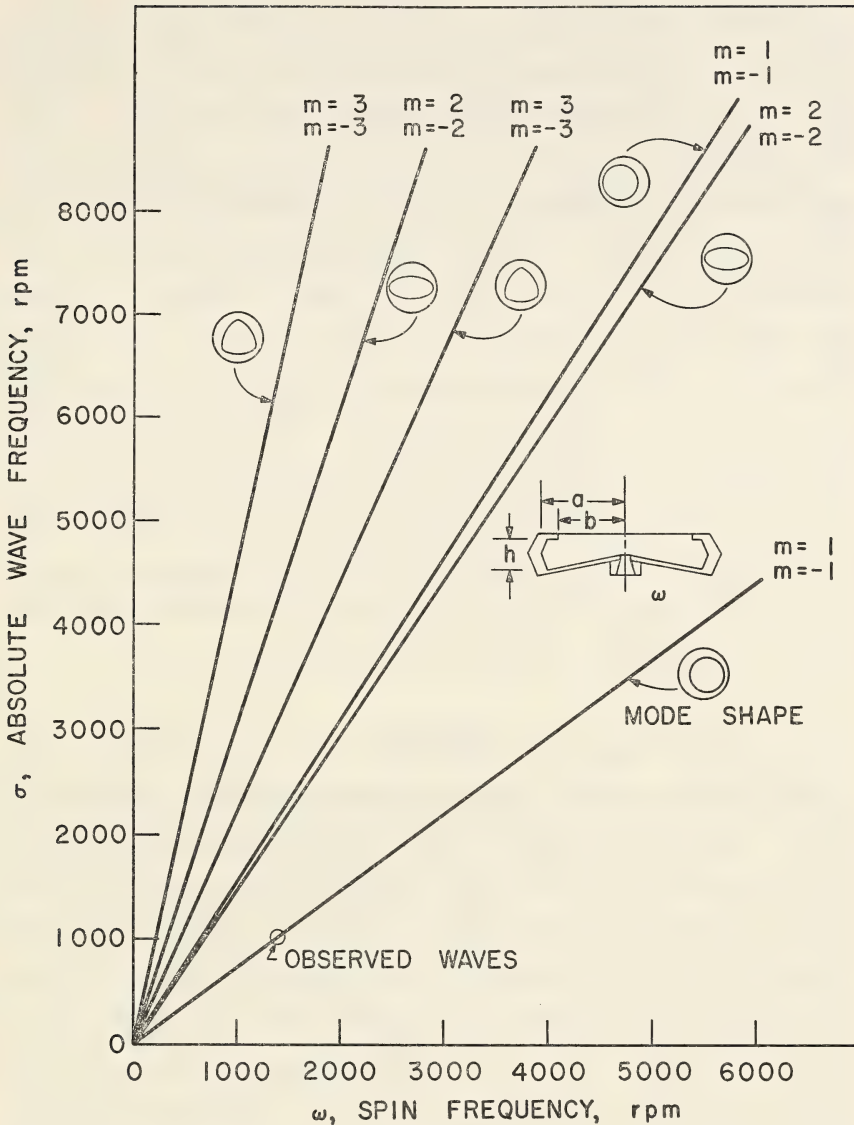
$$\frac{\delta_{\text{parabolic}}}{\delta_{\text{uniform}}} = \frac{7.94 \frac{P}{Eh^3}}{54.9 \frac{P}{Eh^3}} = 0.145$$

Stress at Inner Edge

$$\frac{\sigma_{\text{parabolic}}}{\sigma_{\text{uniform}}} = \frac{3.365 \frac{P}{h^2}}{18.5 \frac{P}{h^2}} = 0.182$$

TEXT-FIGURE 12.—Comparison of maximum deflection and stress of a circular disk with a hole loaded with a parabolic load and a uniform load.

speed, 4) precision required for satisfactory fits of the mating parts, 5) gyroscopic forces to cope with at high angular speeds, and 6) inadequacy of proper mathematical models to describe each type of rotating system. These limitations make the design and fabrication of centrifuges often as much of an art as a science. Years of accumulating information, developing design criteria, and correlating test data are required to advance a given high-speed centrifuge design to a firm basis.



TEXT-FIGURE 13.—Two-dimensional centrifuge waves in the A-XIV rotor/PR-2 drive.

The lack of advancement in commercial centrifuge design for the above reasons is evident from a comparison of machines available today and those available 10 years ago. Because of the difficulty in developing new, satisfactory centrifuge systems, machine design has not radically changed over the years. Instead, improvement is usually noted in the addition of attachments and auxiliary devices.

*A centrifuge configuration* suitable for a number of different separations

has not been obtained nor is a universal centrifuge system likely to be obtained. The conflicts of high centrifugal fields opposed to large rotor volume, a rugged drive system against a high-speed drive, or an analytical rotor contrasted to continuous-flow separation is not likely to be resolved. Each configuration requires too many compromises to solve one problem.

*Threaded joints* and vacuum-tight seals, which are required for high-speed rotors, will be difficult to design for satisfactory field use on centrifuges used for high production processes, such as those used in the pharmaceutical industry. Currently, buttress threads are used to prevent separation of sealing surfaces, but they have no alignment of mating components that have different growth rates, such as rotor bodies and end caps. Simple alignment of threaded surfaces is provided with 60° threads, but axial movement of the sealing surfaces occurs as the growth rates differ.

*Rotor material* for rotors to be used with different fluids is available which can be used at high peripheral speeds. The single rotor material, now available for use with any fluid except hydrofluoric acid, is Zircalloy. This material has not been developed to a sufficient strength, however, to be seriously considered for high-performance machines. Thus, many pieces of rotor hardware are required to fill all the needs in centrifuges. At the current rates of material development, this situation probably will not change appreciably over the next few years.

## SEALS<sup>6</sup>

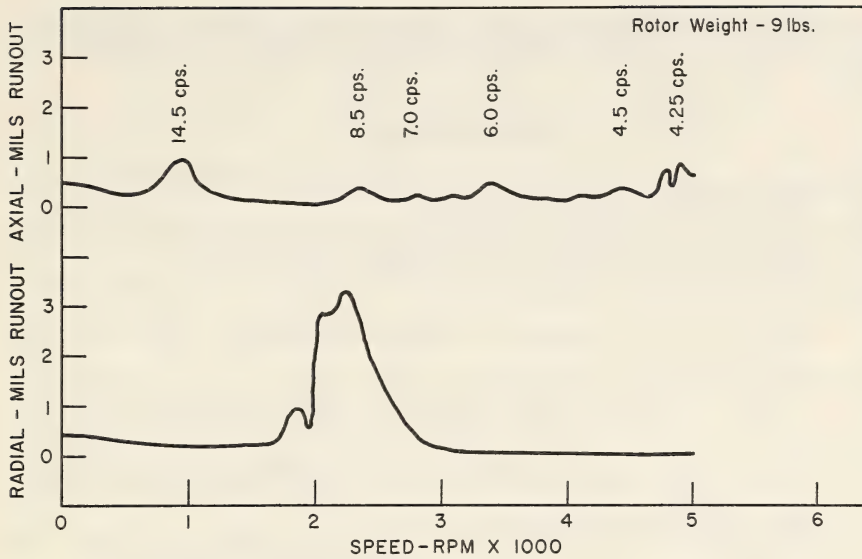
Fluid line seals, which permit the introduction and withdrawal of fluid from a spinning rotor, have been developed thus far for two classes of rotors. The seal designated type A is designed for relatively low-speed rotors (up to 6000 rpm) with a shaft bearing on one end only, usually the bottom. The seal designated type B is designed for intermediate-speed rotors (up to 40,000 rpm) with a shaft bearing on both ends of the rotor. A modification of the type A seal has been developed so it may be attached to a spinning rotor, the gradient and sample loaded, the seal removed, the rotor accelerated to high speed for sedimentation, the rotor decelerated, the seal reattached, and rotor contents displaced while rotor is continuously spinning. The type B seal has been modified with a bleed line for removing gas from the feed line at rotor center during continuous-flow centrifugation. The details of each of these systems are included in subsequent papers on the design of specific rotors.

### Design Principles

The face seal is based on early concepts employed by Pickels at the Rockefeller Institute (personal communication). Sealing is accomplished through contact by the precision-lapped faces of a static seal ring and

---

<sup>6</sup> This section was written by C. E. Nunley, Technical Division, Oak Ridge Gaseous Diffusion Plant.



TEXT-FIGURE 14.—Runout of water-filled A-XIV rotor on PR-2 drive.

dynamic seal ring. Mating faces are in a plane perpendicular to axis of rotating shaft.

Most seal applications involve an accumulation of relative axial motions, arising from such factors as thrust-bearing end play and differential thermal expansion between shaft and housing. Moreover, manufacturing tolerances account for a degree of uncertainty as to the relative axial position of the primary sealing element after assembly. To ensure continuing contact between static and dynamic sealing surfaces, it is necessary to provide a degree of axial freedom for one of the primary sealing members, usually the static seal ring in high-speed seals. This necessity then implies a requirement for an additional, relatively static seal between the static seal ring and the housing. This "secondary seal" may take a variety of forms; however, the O-ring is commonly used in seals for low temperature applications.

To maintain a positive seal during shaft movements and as wear of the sealing faces occurs, there must be some axial driving force to maintain contact between the faces of the static and dynamic seal rings. One or more springs usually provide the required driving force that moves the seal faces into intimate contact during operation.

Wear of the rubbing surfaces depends on many factors and, in most cases, is the factor that determines the useful life of a seal. Some of the factors over which the designer has some control are: 1) loading of seal faces combined with surface speed and ability to remove frictional heat, 2) compatibility of rubbing seal ring materials with each other and process fluids, and 3) surface finish flatness and perpendicularity of sealing faces to axis of rotation. The designer usually has little or no

control over the properties of the contained fluid; however, its corrosion characteristics, viscosity, abrasive content, etc., must be considered.

## REFERENCES

- (1) ANDERSON, N. G.: An introduction to particle separations in zonal centrifuges. Nat Cancer Inst Monogr 21: 9-39, 1966.
- (2) FISHER, W. D., CLINE, G. B., and ANDERSON, N. G.: Density gradient centrifugation in angle-head rotors. Anal Biochem 9: 477-482, 1964.
- (3) SVEDBERG, T., and PEDERSEN, K. O.: The Ultracentrifuge. London, Oxford Press, 1940.
- (4) AMBLER, C. M.: The evaluation of centrifuge performance. Chem Engin Prog 48: 150-158, 1952.
- (5) SUDDATH, J. H.: A Theoretical Study of the Angular Motion of Spinning Bodies in Space, NASA Report R-83, National Aeronautics and Space Administration.
- (6) HILL, P. R., and SCHNITZER, E.: Space-Station Objective and Research Guidelines: A Report on the Research and Technological Problems of Manned Rotation Space Craft, NASA Report TN D-1504, National Aeronautics and Space Administration, 1962, pp 5-8.
- (7) WHITTAKER, E. T.: A Treatise on the Analytical Dynamics of Particles and Rigid Bodies, 4th ed. New York, Dover Publications, 1944, p 24.
- (8) ROUTH, E. J.: Advanced Rigid Dynamics, 6th ed. New York, Macmillan and Co., 1930, vol 2, pp 101-103.
- (9) SMART, E. H.: Advanced Dynamics. New York, Macmillan and Co., 1951, vol 2, pp 284-288.
- (10) ROUTH, E. J.: Advanced Rigid Dynamics, 6th ed. New York, Macmillan and Co., 1930, vol 2, p 94.
- (11) BLASS, G. A.: Theoretical Physics. New York, Meridith Publishing Co., 1962, pp 126-130.
- (12) GREY, A.: A Treatise on Gyrostatics and Rotational Motion. New York, Dover Publications, 1962, pp 377-381.
- (13) HARRIS, C. M., and CREDE, C. E., eds.: Shock and Vibration Control. New York, McGraw-Hill Book Co., 1961, vols I, II, and III.
- (14) PINKUS, O., and STERNLICHT, B.: Theory of Hydrodynamic Lubrication. New York, McGraw-Hill Book Co., 1961, pp 264-285.
- (15) STERNLICHT, B.: Stability and dynamics of rotors supported on fluid bearings. Transactions of the ASME Journal of Engineering for Power, Oct. 1963, pp 331-342.
- (16) HARRIS, C. M., and CREDE, C. E., eds.: Shock and Vibration Control. New York, McGraw-Hill Book Co., 1961, vol 3, 39-8.
- (17) SVEDBERG, T., and PEDERSEN, K. O.: The Ultracentrifuge. London, Oxford Press, 1940, pp 76, 173-180.
- (18) BIEZENO, C. B., and GRAMMEL, R.: Engineering Dynamics. London, Blackie and Son Ltd., 1954, vol III, pp 214-260.
- (19) KELLEY, R. E.: Rigid Rotor Dynamics, University of Virginia (EP-3912-315-63U), 1963.
- (20) TIMOSHENKO, S., and YOUNG, D. H.: Advanced Dynamics. New York, McGraw-Hill Book Co., 1948, pp 337-338.
- (21) ———: *Ibid.*, p 338.
- (22) ARNOLD, R. N., and MAUNDER, L.: Gyrodynamics and Its Engineering Applications. New York, Academic Press Inc., 1961, p 165.
- (23) MILES, J. W., and TROESCH, B. A.: Surface Oscillation of Rotating Liquid. Transaction of the ASME-Journal of Applied Mechanics, 1961, pp 491-496.
- (24) HARRIS, C. M., and CREDE, C. E., eds.: Shock and Vibration Control. New York, McGraw-Hill Book Co., 1961, vol III, 39-7.

- (25) BEYERLE, K.: Patent No. 3,097,167, U.S. Govt Patent Off, July 9, 1963.
- (26) TIMOSHENKO, S.: *Vibration Problems in Engineering*, 3d ed. Princeton, N.J., D. Van Nostrand Co., 1955, pp 386-387.
- (27) PLUNKETT, R.: *Effect of End Disk on Critical Speed of Free-Free Rotor*, Report 60 GL 190, General Electric Co., Schenectady, N.Y., 1960, pp 1-7.
- (28) HARRIS, C. M., and CREDE, C. E.: *Shock and Vibration Handbook*, New York, McGraw-Hill, 1961, vol II, 32-23 to 35.
- (29) UNGAR, E. E., and HATCH, D. K.: *High-Damping Materials*. *Production Engineering*, vol 32, No. 16, April 17, 1961, pp 44-56.
- (30) HARRIS, C. M., and CREDE, C. E., eds.: *Shock and Vibration Handbook*. New York, McGraw-Hill, 1961, vol III, 39-13.
- (31) TIMOSHENKO, S.: *Strength of Materials*, 3d ed. Princeton, N.J., D. Van Nostrand Co., 1956, vol II, pp 214-221.
- (32) ———: *Ibid.*, pp 205-210.
- (33) KARMAN, T. J., and BIOT, M. A.: *Mathematical Methods in Engineering*. New York, McGraw-Hill Book Co., 1940, p 378.
- (34) TIMOSHENKO, S.: *Strength of Materials*, 3d ed. Princeton, N.J., D. Van Nostrand Co., 1956, vol II, p 447.
- (35) ROLSTON, J. A.: Reinforced plastics for rotating structures. *SPE Journal*, 19(4): 387-391 (April 1963).
- (36) ODELL, C. N., and ALBERT, W. E.: The filament-reinforced motor case. *Aero-space Eng* 21(4): 52-53, 1962.
- (37) DARMS, F. J.: Optimum Filament Wound Construction for Cylindrical Pressure Vessels, ASTIA Report AD292010, April 1962, p 12.
- (38) TIMOSHENKO, S.: *Strength of Materials*, 3d ed. Princeton, N.J., D. Van Nostrand Co., 1956, vol II, p 219.
- (39) BASSALI, W. A.: The transverse flexure of a thin circular plate subject to a parabolic loading over a concentric ellipse. *Z Angew Mathematik und Physik* 11: 176-191, 1960.
- (40) TIMOSHENKO, S.: *Strength of Materials*, 3d ed. Princeton, N.J., D. Van Nostrand Co., 1956, vol II, pp 96-99.
- (41) ROARK, R. J.: *Formulas for Stress and Strain*, 3d ed. New York, McGraw-Hill Book Co., 1954, pp 198-199.
- (42) MILES, J. W.: Free surface oscillations in a rotating liquid. *The Phys Fluids* 2: 297-305, 1959.
- (43) STEWARTSON, K.: On the stability of a spinning top containing liquid. *J Fluid Mech* 5: 577-592, 1959.
- (44) PHILLIPS, O. M.: Centrifugal waves. *J Fluid Mech* 7: 340-352, 1960.
- (45) MILES, J. W., and TROESCH, B. A.: Surface oscillation of a rotating liquid. *J Appl Mech* 28: 491-496, 1961.
- (46) MASICA, W. J., DERDULL, J. D., and PETRASH, D. A.: *Hydrostatic Stability of the Liquid-Vapor Interface in a Low Acceleration Field*, NASA Report TN D-2444, National Aeronautics and Space Administration, 1964.



## The Development of Low-Speed "A" Series Zonal Rotors<sup>1</sup>

N. G. ANDERSON, H. P. BARRINGER, N. CHO, C. E. NUNLEY, E. F. BABELAY, R. E. CANNING, and C. T. RANKIN, JR., *Biology Division, Oak Ridge National Laboratory,*<sup>2</sup> and the *Technical Division, Oak Ridge Gaseous Diffusion Plant,*<sup>2</sup> Oak Ridge, Tennessee

### SUMMARY

The evolution of a series of low-speed zonal centrifuge rotors for the separation of cells, bacteria, and subcellular particles visible in the light microscope (Rotors A-V, VI, IX, and XII) is described. All are dynamically loaded and unloaded and may be used for either rate-zonal or isopycnic-zonal separations. Transparent plastic end caps allow direct observation of the separations. The last rotor of the series (A-

XII) has a total rotor volume of 1400 ml and a maximum radius of 17.78 cm. The sample zone volume can be as large as 50 ml, and the density gradient volume is usually one liter. Experimental studies with model particles demonstrate that narrow starting zones and useful separations can be obtained.—*Nat Cancer Inst Monogr* 21: 113-136, 1966.

IN ZONAL centrifugation (1-9) density gradients stabilize the liquid milieu through which particles sediment to allow particles having different sedimentation rates to be separated into discrete zones or bands. Early studies with swinging-bucket rotors demonstrated the feasibility of separation of cell components and viruses in density gradients, but only very small amounts of material could be separated, and considerable time and effort were required to form and recover the gradients.

Since high gravitational fields have a marked stabilizing effect on liquid density gradients, the possibility of forming and recovering gradients during rotation was investigated, and a simple system for distributing a gradient stream into tubes in swinging-bucket rotor was developed (10). These gradients, however, were recovered at rest. The possibility of eliminating centrifuge tubes was next studied, and a hollow-bowl rotor and simple methods for introducing and recovering density gradients were tested (11). The success of this early work prompted the development of rotor systems covering a wide range of speeds and capacities (9). These include the Series A rotors, suitable for the separation of particles ranging from whole cells to mitochondria. In this paper the design and operation of rotors A-V, A-VI, A-IX, and A-XII are described.

<sup>1</sup> This research performed under the Joint National Institutes of Health-Atomic Energy Commission Zonal Centrifuge Development Program which is supported by the National Cancer Institute, the National Institute of Allergy and Infectious Diseases, and the U.S. Atomic Energy Commission.

<sup>2</sup> Operated for the U.S. Atomic Energy Commission by the Nuclear Division of Union Carbide Corporation.

## PRINCIPLES OF OPERATION

Two methods of operation have been explored with the "A" or low-speed rotor series. In the first method the rotor is loaded and unloaded while spinning (fig. 1) at a speed sufficient to stabilize the gradient against the rotor wall (6, 9). Although this method of dynamic loading appears to give very high resolution, it requires precision seal systems. In the second method the gradients are loaded and unloaded at rest, the gradient being reoriented from a horizontal to a vertical configuration during rotation (12, 13) in a hollow rotor containing fixed septa.

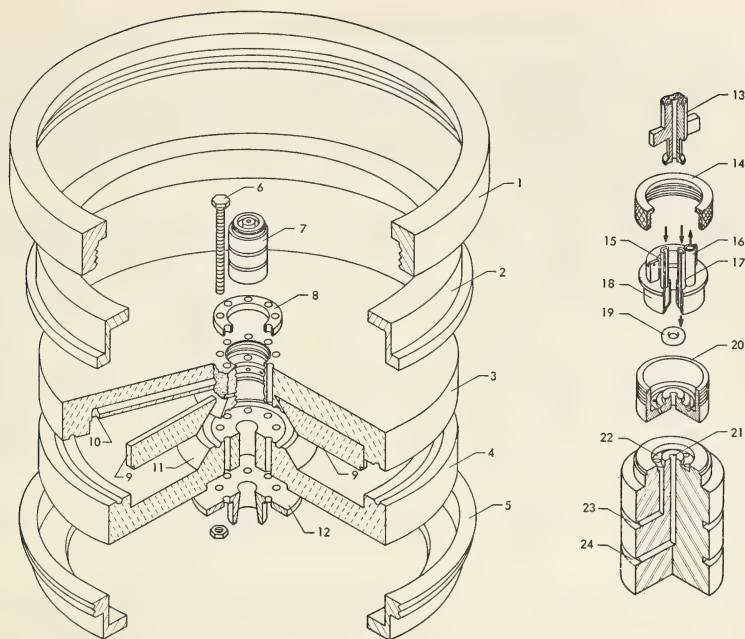
In a reorienting gradient rotor the gradient is introduced to the bottom of the rotor during rest. The sample is introduced by reverse flow through the top and is followed by a light overlay. During gradual acceleration the axial gradient is reoriented to a radial gradient by centrifugal force. After particle separation has been effected, the gradient reorients to the original configuration as it is brought to rest. Gradient recovery is by displacement out the upper fluid line or by drainage out the bottom (12).

The choice between dynamically loaded and reorienting gradient rotors for specific applications cannot be made solely on the basis of theoretical studies (13). It is important to compare experimentally the resolution obtained in the two rotor systems. It should be emphasized that the "A" series includes rotors of both types, but that this paper is limited to dynamically loaded designs.

## ROTOR A-V

Work on rotors A-III and A-IV (9) demonstrated the feasibility of dynamically loaded and unloaded zonal centrifuges. It appeared desirable to (a) observe the entire procedure, (b) detect anomalous sedimentation at various times during the centrifugation, and (c) determine directly the optimal time to unload the gradient. For this reason it was considered desirable to construct the end caps of the more advanced rotors from a transparent plastic.

In dynamically loaded series A rotors, length has been minimized to give a ratio of  $I_{\text{spin}}/I_{\text{transverse}} > 1$  for the moments of inertia (14), which thus provides a configuration spinning about its most stable axis. Rotor A-V was tested at very low speeds (500–1000 rpm). Loading and unloading of rotors at much higher speeds are feasible (6, 15); however, the stabilizing effect of centrifugal force is much less at very low speeds, and the possibility of mixing during introduction of the sample layer is correspondingly increased. Since pressures and stresses are relatively small, large-diameter methacrylate resin end plates could be used. Text-figure 1 is a schematic diagram of the A-V rotor. The interior is divided into 8 sector-shaped compartments, each 2.72 cm deep, with maximum and minimum radii of 13.60 and 3.49 cm. The upper and lower end plates are of 3.26 cm-thick clear plastic, and the internal volume is 1300 ml.



TEXT-FIGURE 1.—Schematic drawing of rotor A-V. (1) Coupling ring; (2) upper retaining ring; (3) upper end plate; (4) lower end plate; (5) lower retaining ring; (6) retaining bolts; (7) filled Teflon rotating seal; (8) bolt locating ring; (9) septa; (10) fluid line to edge of rotor; (11) conical-section core; (12) drive shaft adapter; (13) stationary seal flexible mount and fluid line to center of rotor; (14) stationary seal coupling ring; (15) coolant inlet; (16) coolant outlet; (17) fluid line to edge of rotor; (18) cooling jacket; (19) "O"-ring; (20) stationary seal; (21 and 24) flow passage through rotating seal to center of rotor; (22 and 23) flow passage through rotating seal to edge of rotor.

All parts of a zone of one density in a zonal centrifuge constitute a paraboloid of revolution about the axis of rotation (6, 13). The single conical-section core, therefore, allows the sample layer to slope  $45^\circ$  or more as it approaches the rotor center. The rotating seal was constructed of filled Teflon (Rulon<sup>3</sup>), while the static fluid-line seal was constructed of stainless steel and flexibly mounted to allow alignment to the plane of the rotating seal during operation. Chilled water was circulated through the upper seal to remove frictional heat.

Water was added to the rotor in 100 ml increments, and the position of the meniscus was determined at 1000 rpm. From these data a chart of volume as a function of radius was drawn. The position of any portion of the gradient recovered during unloading could then be related to its original position in the rotor. All work was performed in an International Equipment Company Model PR-2 refrigerated centrifuge with a transparent plastic lid.

<sup>3</sup> Available from the Dixon Corporation, Bristol, R.I.

### Performance

To determine whether density gradients could be introduced into the rotor and recovered without extensive mixing, a density gradient was analyzed refractometrically both before introduction and after spinning in the rotor for 15 minutes at 1000 rpm. Differences between the two gradients were negligible.

A sample zone introduced into the rotor is widened by laminar flow through the tubing and rotor core, by any turbulence or convection in the rotor, and by diffusion. To determine how much widening would occur in practice, a sample zone containing 4 percent bovine serum albumin having a total volume of 20 ml was introduced over a sucrose gradient. When moved to a position just external to the core, the sample had a calculated width of 0.1 cm. The rotor was spun at 1000 rpm at 5° C ( $152 \times g$  at  $R_{max}$  and  $39 \times g$  at  $R_{min}$ ) for 15 minutes. When the gradient was recovered, the absorbance recording of the sample zone showed a peak whose width at half height was equivalent to a zone width of 0.3 cm in the centrifuge. This amount of broadening is not considered excessive.

Three types of experiments were performed to determine the resolution obtainable with this rotor. In the first, ragweed pollen grains were observed during sedimentation. In the second, rat red cells were centrifuged to their isopycnic position, while in a third series of experiments a method for isolating calf thymus nuclei that retained their ability to incorporate amino acids was developed (16). Preliminary experiments with ragweed pollen suggested that more uniform behavior could be obtained if the grains were first fixed in alcohol. Two hundred mg of pollen was suspended in 10 ml of 95 percent ethanol, centrifuged briefly, and the pollen resuspended in 10 ml of 8.5 percent sucrose (w/w). This volume of material was used as the sample layer and was introduced centripetal to a 1200 ml gradient extending from 17 to 55 percent (w/w) sucrose. Fifty-five percent sucrose was also used as the underlay for the gradient. After 10 minutes at 1000 rpm, the gradient was recovered by displacement. Photographs of the rotor during the run are shown in figure 2. When the fractions were examined by dark field phase-contrast microscopy, no particles were observed through the gradient except at the level of the zone observed visually. In experiments with rat red cells, two isopycnic bands were observed repeatedly. The basis for this fractionation has not been determined. These results indicate that the principles previously employed in the Series B zonal centrifuge (6, 15) can be applied to large-particle separations in a low-speed rotor.

### ROTOR A-VI

Rotor A-VI is the largest low-speed zonal rotor thus far constructed. It is designed to explore large-scale nuclear isolation and the separation of different cell types in a mixture such as occurs, for example, in bone marrow suspensions.

The rotor has a 3 liter capacity and is designed for operation at 6000 rpm and a maximal centrifugal force of  $7100 \times g$ . The design specifications were fixed by the speed, permissible diameter, and thrust-bearing capacity of the PR-2 centrifuge. The design does not approach the stress limits of the 7075-T6 aluminum used for the rotor wall. The partially disassembled rotor is shown in figure 3, and the rotor and seal system assembled for use are shown in figure 4. A fairly uniform centrifugal field is achieved with a large-diameter central core to keep the entire gradient close to the rotor edge. The central core diameter is 22.86 cm and the inside rotor diameter is 35.56 cm, which gives a gradient chamber length of 6.35 cm. At the design speed of 6000 rpm with a sucrose density gradient in position, a rather large radial expansion (approximately 0.04 cm) occurs. Since the end caps increase in diameter by only a few thousandths of a centimeter, a mechanism was needed to center the rotor chamber wall with respect to the end caps, and to maintain concentricity to the drive spindle. Plated brass plates (one in each end cap), which expanded during centrifugation at a rate intermediate between that of the rotor wall and the end plates, were used. Without the brass plates, departure from circularity increased from the normal 10 to 25  $\mu$ .

When the rotor was properly constructed, it was in balance. The only metals in contact with the fluid were anodized aluminum, nickel, monel, or stainless steel. "O"-rings were used to seal the rotor chamber and all components in the liquid lines.

Three methods have been investigated for obtaining flow into and out of the centrifuge at operating speed. The use of skimmers as previously suggested (6) was not successful at the relatively low peripheral speed obtained at the edge of the skimmer disks. As a second approach, a self-aligning ball-and-socket rotating seal was tested but was ineffective because of distortion of the ball during attachment to the drive and because of cold-flowing of the reinforced Teflon of the static seal when under pressure. The last design, a flat, modified face seal supported by the centrifuge chamber lid proved effective when the centrifuge was in near-perfect balance. Its alignment with the rotating seal was critical. A self-aligning seal was not designed until the A-IX rotor was developed.

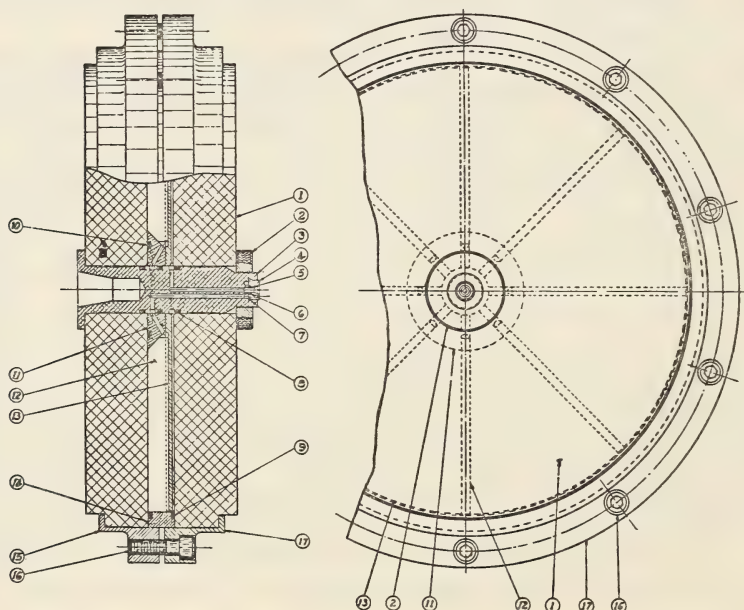
One top end cap for rotor A-VI has been fabricated from Lucite to permit viewing of the rotor contents completely across the rotor diameter. The rotor contents were observed in detail by use of a stroboscopic light. At the center of the rotor, a large nut limits deflection of the cap and reduces the stress. Power limitations of the PR-2 drive motor have restricted the top speed in practice to 5160 rpm. Critical frequencies of the spindle system occur at 700 and 900 rpm, but these have been passed with no difficulty.

The A-V rotor showed that successful separations could be achieved at low speed and demonstrated the utility of a completely transparent system, whereas A-VI showed that plastic end caps could be used at speeds up to 5000 rpm. Our attention was therefore directed toward the de-

velopment of a general purpose rotor with both upper and lower end caps of plastic transparent materials, and with a self-aligning seal that could achieve sufficient speed to separate subcellular particles as small as mitochondria. In addition, an attempt was made to simplify the rotor as much as possible and to provide for its convenient disassembly. [Rotor A-VII has been described (12) and rotor A-VIII, which also utilizes the reorienting gradient principle, is described elsewhere.]

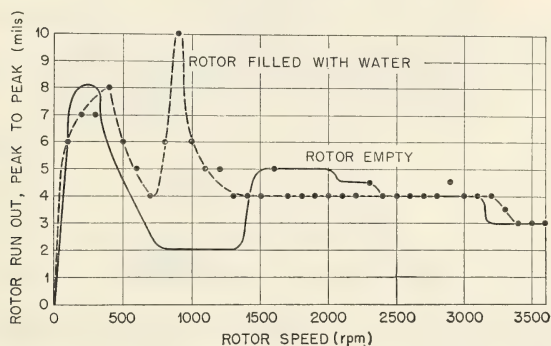
### ROTOR A-IX

Rotor A-IX, shown in figure 5 and text-figure 2, has been designed to replace rotor A-V, but with a higher maximum operating speed and greater stability. The rotor volume of 1300 ml is divided into 8 sector-shaped compartments, each having a depth of 1.49 cm and a maximum radius of 17.78 cm. The central core is a single  $45^\circ$  cone with a maximum radius of 4.79 cm. Flow lines to the rotor edge pass over the septa, which thus allows an unobstructed view of the entire compartment. The rotor weighs approximately 22.68 kg full and is held on the centrifuge drive spindle by its own weight.



TEXT-FIGURE 2.—Diagrammatic representation of rotor A-IX. (1) Upper end plate; (2) nut; (3) spindle; (4) rotating face seal (Rulon); (5) flow channel; (6) "O"-ring; (7) "O"-ring; (8) "O"-ring; (9) "O"-ring; (10) "O"-ring; (11) tapered core; (12) septa; (13) septa holder; (14) spacer ring; (15) lower retaining ring; (16) retaining bolts; (17) upper retaining ring.

The rotor has been spun to 4000 rpm, both empty and filled with water. Design speed of 6000 rpm has not been reached due to the limited power of the drive system. Departure from concentricity was measured by use of an inductance proximity probe<sup>4</sup> placed in the centrifuge chamber close to the edge of the rotor. The resulting signal was amplified and displayed on a calibrated oscilloscope. Rotor runout or wobble when empty and when filled with water is shown in text-figure 3. These rotors have not required balancing to achieve satisfactory performance. The large runouts observed at 400 and 900 rpm when the rotor is filled are rigid-body critical frequencies of the centrifuge system. Flow measurements with water suggested that the centrifuge will serve as a satisfactory continuous flow device for large particles, as well as a rate-zonal centrifuge. Flow rates of 100 ml per minute were easily achieved.



TEXT-FIGURE 3.—Runout of rotor A-IX-b on International Model PR-2 centrifuge drive, expressed in mils ( $10^{-3}$  inches).

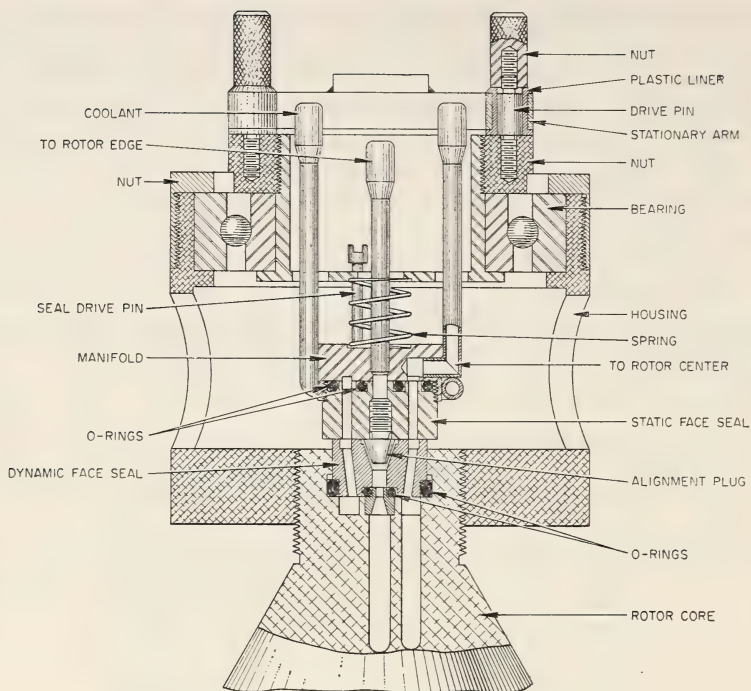
The seal is shown in text-figure 4 and figure 6. A collar attached to the rotor is connected to the static seal through a sealed, stainless steel bearing. Lateral movement of the rotor and the rotating seal is transmitted directly to the static seal. Rotation of the static seal is prevented by a removable arm attached to the centrifuge cooling chamber. The complete A-XII system is shown in figure 7.

### Operation

The rotor is accelerated to approximately 1000 rpm, and the density gradient is pumped in at the rate of approximately 25 ml per minute with a modified Spinco zonal centrifuge gradient pump.<sup>5</sup> For most purposes, gradients ranging from 17 to 55 percent or from 10 to 30 percent (w/w) sucrose are useful. Both the rotor and the solutions used to prepare the gradient are prechilled to 5° C. When the gradient has filled the rotor and begins to emerge through the core line, the gradient pump

<sup>4</sup> Bentley Proximity Probe, Bentley-Nevada Corp., Minden, Nev.

<sup>5</sup> Spinco Division, Beckman Instruments, Palo Alto, Calif.



TEXT-FIGURE 4.—Type "A" seal redesigned to attach to rotor. *See text.* Seal used on low-speed rotors.

is stopped and a drain tube, connected to the line between the pump and the seal, is opened. This allows fluid to escape from the edge of the rotor as the sample layer and the overlay are introduced.

The sample layer (usually 5–20 ml) may be introduced through the rotor center or core line with a large syringe, a small vessel pressurized with air, or with a small peristaltic pump. The sample should have a density less than that of the light end of the gradient, or excessive boundary widening occurs. As soon as the sample layer is in, 100 ml or more of a light fluid, such as a physiological salt solution or a dilute buffer, is pumped in, the drain line between the pump and the rotor edge line closed, and the gradient pump started with the pump set to pump only dense fluid. The excess overlay is then pumped out through the rotor center line into a reservoir containing 75 ml of water. The rotor edge line is then clamped off. As the rotor accelerates, expansion occurs, and fluid to compensate for this increase in volume is drawn from the reservoir. This mechanism assures that the seal does not dry out and that the rotor does not become unbalanced by the introduction of air. The rotor is then accelerated to operating speed.

After the desired separation has been made, the rotor is decelerated to between 200 and 1000 rpm, and the gradient is recovered by pumping dense sucrose into the rotor through the rotor edge line.

Ultraviolet absorbance of the gradient is monitored by a two-wavelength system previously described (17). Forty-milliliter fractions were generally collected. The  $r_i$  of the outer edge of a fraction in the rotor can be deduced from the equation:

$$V_i = h\pi(r_i^2 - r_c^2) + V_{r_c} - Nhw(r_i - r_c)$$

where

$V_i$  = volume collected to reach end of zone or sample  $i$ ,

$V_{r_c}$  = volume from point of collection to outer edge of core,

$r_i$  = radius of zone  $i$  in rotor before unloading,

$r_c$  = radius to edge of core,

$N$  = number of septa,

$h$  = height of sector-shaped compartments, and

$w$  = width of septa.

For rotor A-IX,  $V_{r_c} = 25$  ml,  $r_c = 4.79$  cm,  $N = 8$ ,  $h = 1.49$  cm, and  $w = 0.64$  cm.

To observe the sedimentation of particles, a disk of Lucite having the same outside diameter as the inside of the refrigerated chamber of the centrifuge was mounted under the rotor and painted half white and half black. When the black background was used, particles could be observed by reflected light, whereas particles having appreciable color could best be observed against the white background.

A camera was mounted above the centrifuge, and lights mounted to illuminate the rotor so that photographs could be taken at intervals. An over-all view of the system is shown in figure 7.

### Performance

The A-IX rotor may be used for a variety of purposes (18), and the results obtained will depend largely on the specific conditions employed.

To illustrate the separations that may be obtained, a 1 liter gradient ranging linearly with radius from 10 to 42 percent (w/w) sucrose was introduced into the rotor, and the remainder of the rotor volume was filled with 55 percent sucrose. Twenty ml of a 10 percent brei was prepared from unperfused rat liver and introduced into the rotor at 400 rpm. The sample was moved out beyond the core with 150 ml of pH 7.5 Miller-Golder buffer,  $\mu = 0.1$ . The sedimentation of nuclei, red cells, and mitochondria is shown in figure 8. Phase contrast microscopy was used to identify the various fractions. No cross-contamination between nuclei and mitochondria was observed.

## ROTOR A-XII

After several months of successful use, the acrylic end cap of an A-IX failed. The damage, shown in figure 9, occurred along the outer periphery at low speed (1000 rpm) with a 17 to 55 percent sucrose gradient in the rotor. A complete stress analysis, including studies of the effects of thermal stress, was made and checked in a series of studies on plastic models. To insure as far as possible that further failures did not occur, the rotor was redesigned as the A-XII rotor. In the A-XII rotor, the thickness of the acrylic resin in the area where failure occurred was increased, and a combination of a gasket and a metal-to-metal stop was added to distribute and control the clamping pressure.

### Design Considerations

The A-XII rotor was designed to give the same separation performance as the A-IX, but with improved physical properties. The maximum stress, in terms of the yield values of the materials of construction, the diameter-to-height ratio, and the speed range employed, is in the rotor end caps, and is produced by fluid pressure generated by centrifugal force. The fluid pressure load acting on the end cap is parabolic, increasing toward the periphery of the rotor. The magnitude is governed by the density of the fluid and speed of the rotor. The hyperbolic pressure load, acting upon a a round, thick plate, clamped at the periphery, produces the maximum stress at the periphery. In A-IX, the weakest sectional strength was at this point. Since the rotor end plates are clamped together by the 12 flange screws, the stress caused by the screws also acts on the periphery of the end caps. The clamping stress adds geometrically to the stress caused by the fluid pressure. An uneven clamping pressure applied to the clamping screws tends to concentrate the clamping load in a neighborhood of one or a few screws. To help distribute the clamping pressure evenly, a metal-to-metal stop was used at the periphery, and a gasket added between the end cap and the flange to distribute the load. The gasket also helps to eliminate the possibility of application of a point concentrated load on the plate by dried sucrose droplets or other particles.

The cast thermoplastic acrylic resin used as the end cap is a plastic glass, and like other glasses, its strength is markedly affected by scratches or chips.

The plastic has the maximum stress limitation of about 8000 psi in shear at room temperature with decreasing strength as the temperature decreases. The coefficient of thermal expansion of the material is higher than the aluminum used to clamp the two end caps, whereas the thermal conductivity of the plastic is much lower than aluminum. Generally, the rotor is used at 4° C. If the rotor is assembled at room temperature and then cooled slowly to 4° C, the clamping pressure would tend to decrease. On the other hand, if the rotor is subjected to a rapid temperature drop as well as the hyperbolic fluid load by centrifugation, the net

clamping pressure will increase during the temperature change, because the aluminum clamping flange will react to the temperature change more quickly than the plastic. In addition, if the rotor is left filled with an aqueous solution for a long period, increases in the clamping pressure due to the plate growth caused by the water absorption will be observed. A weight gain of 0.2 percent per day is observed for thin plastic pieces. If the rotor is subjected to a higher temperature after assembly, as may occur if the rotor is left in direct sunlight, increased clamping pressure results. The A-XII rotor should be assembled and stored in a 5° C cold room and placed in a chilled centrifuge immediately before use.

Experiments have also been performed with the A-XII to determine the effect of changing the number of septa. The banding performance obtained with ragweed pollen was examined with 2, 4, and 8 septa. The results with 4 or 8 were indistinguishable, whereas considerable loss in resolution was observed with 2. The number of septa has therefore been reduced to 4 in the A-XII rotor, which results in a small increase in rotor volume.

The A-XII rotors have accumulated several hundreds of hours in operation over a 9-month period without failure. The maximum speed attained was 3900 rpm, a limitation imposed by the PR-2 drive. The rotor is capable of 6000 rpm with 60 percent sucrose in the chamber.

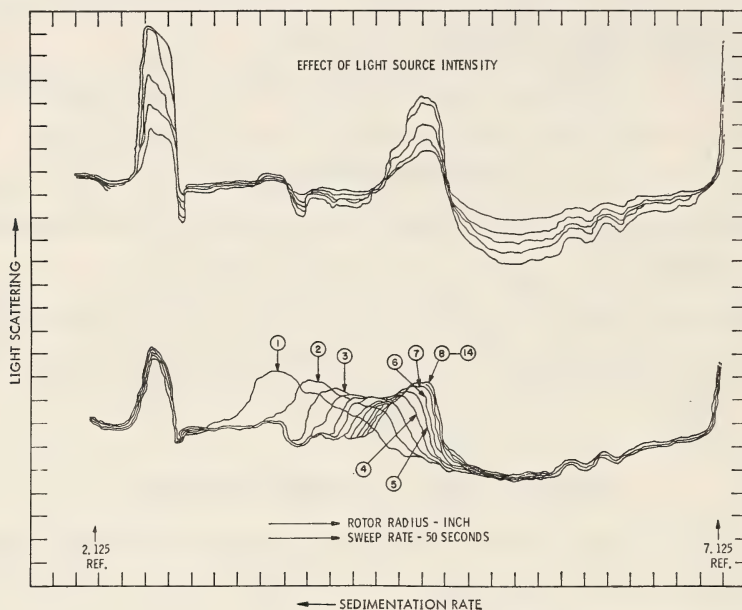
### SCANNER FOR A SERIES ROTORS

The A-XII rotor is capable of yielding precise data on the sedimentation rates of large particles if measurements are made during centrifugation. A simple way of obtaining these measurements is with a photoelectric scanner, as shown in figure 10.

The scanner uses a standard 6-volt lamp and a cadmium selenide photocell. Since most of the decrease in transmission of a particle zone is due to scattered light, the photocell is arranged to scan the rotor with a very narrow beam. The output of the photocell is fed to the Y axis of an X-Y recorder. The position of the photocell on the rotor radius with respect to the rotor axis is measured by a potentiometer, which controls the voltage to the X axis. While the scanner swings through an arc as it traverses the cell, the position-measuring potentiometer is driven through a cam system to produce a voltage output proportional to the true radius. The X-Y recording is thus linear with rotor radius. Scans are repeated at preset intervals, but the recorder pen does not record on the return cycle of the scanner. Normally, the X axis of the recorder is set to give a plot in which the radius is enlarged by a factor of 3 for clarity. The location of sedimenting bands or zones can thus be precisely determined.

The optimum interval between repetitive scans varies markedly with particle sedimentation rate and rotor speed. A timer is incorporated in the scanner to provide a preselected scanning interval of 1, 5, 10, 15, 20, or 25 minutes per cycle. After the completion of 10 scans, the scanner

is automatically shut off. An example of a scan made with this instrument is shown in text-figure 5. Additional scanner features under consideration include measurement of either backward or forward scattered light. For improved visual observation of sedimenting bands, a uniform light source below the rotor is required. A source consisting of three concentric fluorescent lamps with suitable reflectors and diffusers that fit in the International PR-2 centrifuge has therefore been developed.



TEXT-FIGURE 5.—Sequential scan of ragweed pollen particles in 17 to 55 percent sucrose gradient sedimented in the A-XII rotor with a photoelectric scanning device. Changes in transmitted light were recorded in the visible light range spectrum. International PR-2 centrifuge was used at 950 rpm with scanning at 60 seconds per cycle. Numbers denote the scanning order.

## REFERENCES

- (1) BRAKKE, M. K.: Density gradient centrifugation: A new separation technique. *J Amer Chem Soc* 73: 1847-1848, 1951.
- (2) ———: Density gradient centrifugation and its application to plant viruses. *Adv Virus Res* 7: 193-224, 1960.
- (3) HOGEBOOM, G. H., and KUFF, E. L.: Sedimentation behavior of proteins and other materials in a horizontal preparative rotor. *J Biol Chem* 210: 733-751, 1954.
- (4) ANDERSON, N. G.: Studies on isolated cell components. VIII. High resolution gradient differential centrifugation. *Exp Cell Res* 9: 446-459, 1955.
- (5) ———: Techniques for the mass isolation of cellular components. *In Physical Techniques in Biological Research. Cells and Tissues* (Oster, G., and Polister, A. W., eds.). New York, Academic Press Inc., 1956, vol 3, pp 299-352.

- (6) ———: The zonal ultracentrifuge. A new instrument for fractionating mixtures of particles. *J Phys Chem* 66: 1984–1989, 1962.
- (7) ———: Virus isolation in the zonal ultracentrifuge. *Nature (London)* 199: 1166–1168, 1963.
- (8) DE DUVE, C., BERTHET, J., and BEAUFAY, H.: Gradient centrifugation of cell particles. Theory and applications. *Prog Biophys* 9: 325–369, 1959.
- (9) ANDERSON, N. G.: An introduction to particle separation in zonal centrifuges. *Nat Cancer Inst Monogr* 21: 9–39, 1966.
- (10) ALBRIGHT, J. F., and ANDERSON, N. G.: A method for rapid fractionation of particulate systems by gradient differential centrifugation. *Exp Cell Res* 15: 271–281, 1958.
- (11) ANDERSON, N. G.: New fractionation methods for isolating cellular proteins. *Bull Amer Phys Soc Series II* 1: 267–268, 1956b.
- (12) ———: Analytical techniques for cell fractions. IV. Reorienting gradient rotors for zonal centrifugation. *Anal Biochem* 7: 1–9, 1964.
- (13) FISHER, W. D.: Theory of reorienting gradient rotors. In preparation.
- (14) BARRINGER, H. P.: The design of zonal centrifuges. *Nat Cancer Inst Monogr* 21: 77–111, 1966.
- (15) ANDERSON, N. G., BARRINGER, H. P., BABELAY, E. F., and FISHER, W. D.: The B-IV zonal ultracentrifuge. *Life Sci* 3: 667–671, 1964.
- (16) FISHER, W. D., and CLINE, G. B.: A density gradient for the isolation of metabolically active thymus nuclei. *Biochim Biophys Acta* 68: 640–642, 1963.
- (17) ANDERSON, N. G.: Analytical techniques for cell fractions. II. A spectrophotometric column monitoring system. *Anal Biochem* 4: 269–283, 1962.
- (18) CANNING, R. E., and ANDERSON, N. G.: Separation of subcellular fractions with a new zonal rotor. *Amer Zool* 4: 310, 1964.



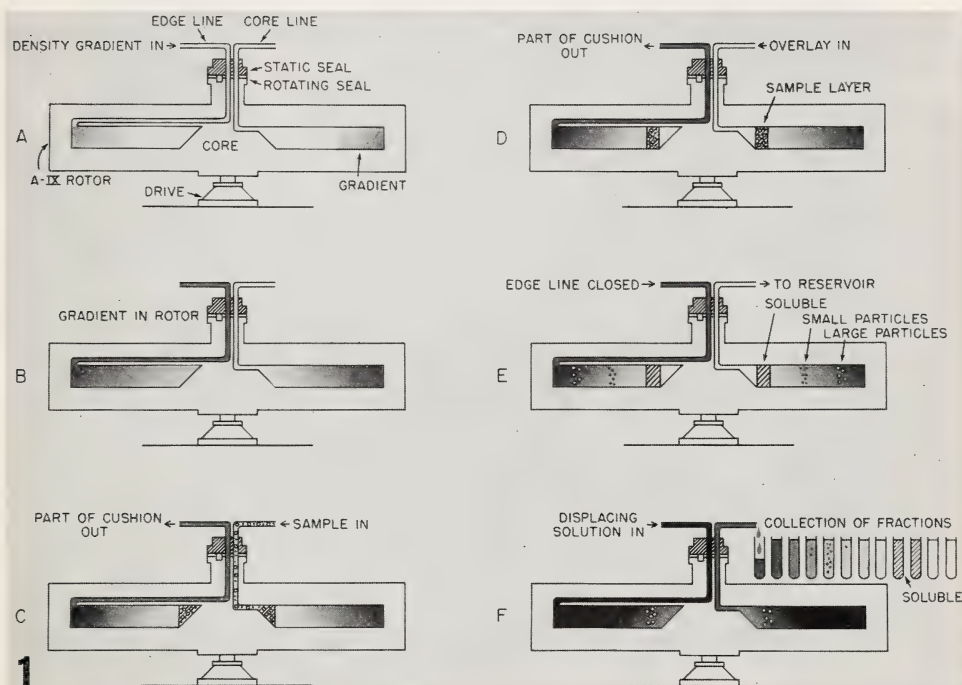


FIGURE 1.—Schematic diagrams of operation of Series A dynamically loaded rotors.

Hollow cavity in the rotor is divided by septa into sector-shaped compartments. Two fluid lines are connected through a flat face seal to the rotor core and the rotor edge in such a manner that fluid may be pumped in either direction through the rotor during rotation. At low speed the rotor is filled by pumping the gradient in through the edge line (A) until the rotor is filled (B). The direction of fluid flow is then reversed, the sample layer pumped in through the core line (C) and then pushed out by a fluid less dense than the sample until the sample layer is free of the core (D). Rotor is accelerated to operating speed to achieve the desired separations (E). Rotor is then decelerated to unloading speed and the gradient displaced out through center core by pumping a dense fluid to the rotor edge (F).

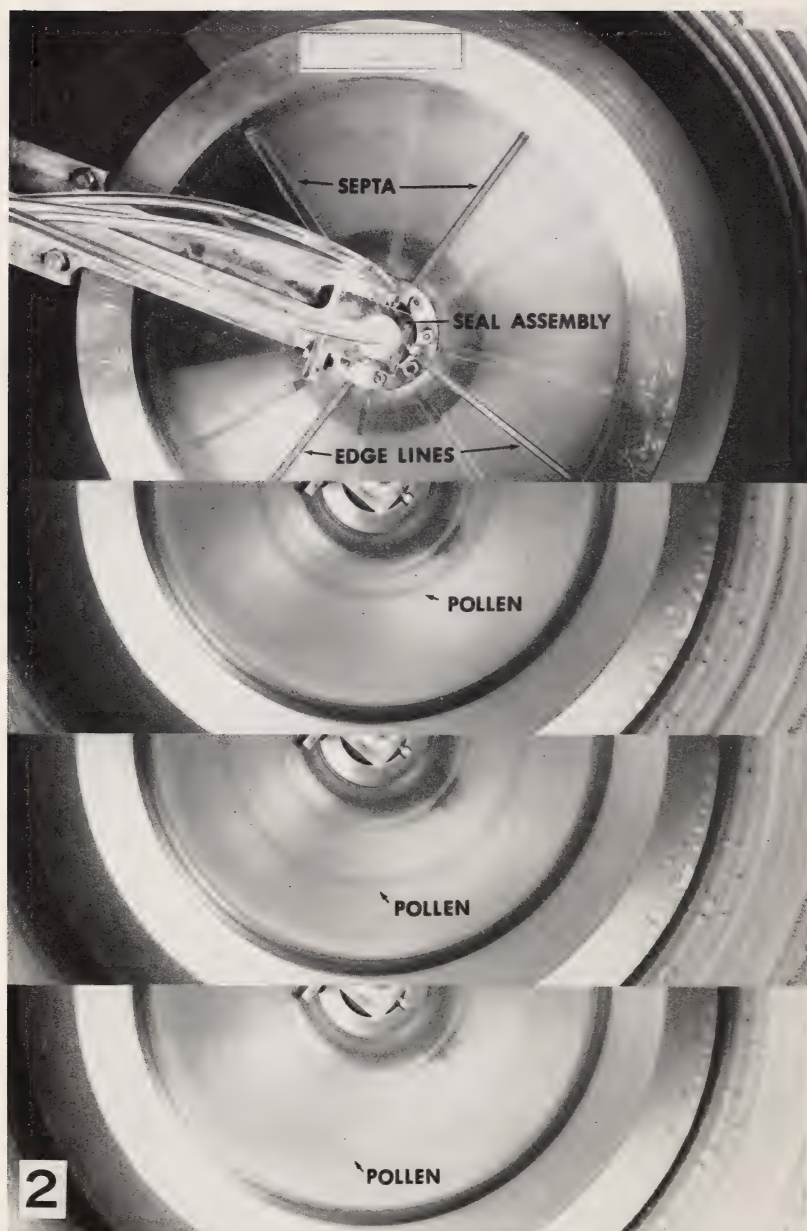


FIGURE 2.—Sedimentation of ragweed pollen in rotor A-V.

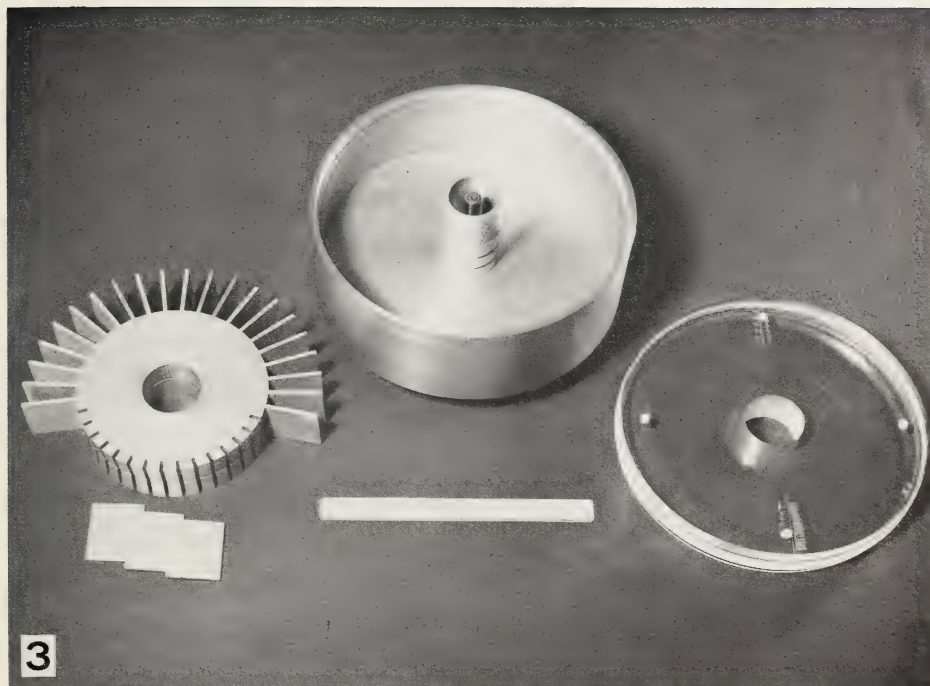


FIGURE 3.—Rotor A-VI partially disassembled. Core with septa shown at *left*, main body of rotor in *center*, with transparent upper end plate at *right*.

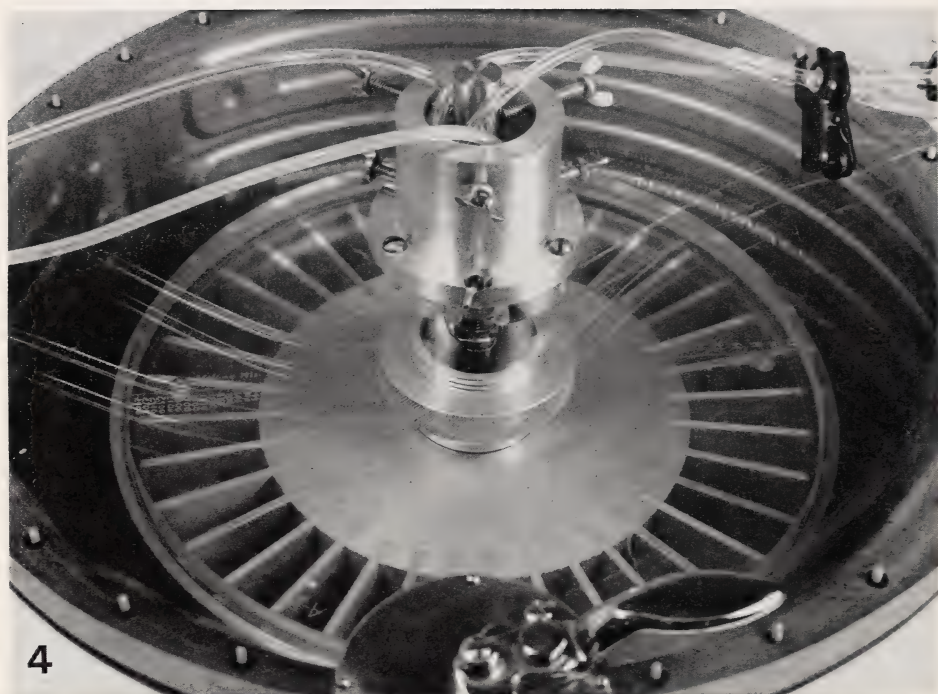


FIGURE 4.—Rotor A-VI and seal assembly mounted in PR-2 centrifuge. The rotor is visible during operation through the plastic top of the centrifuge.

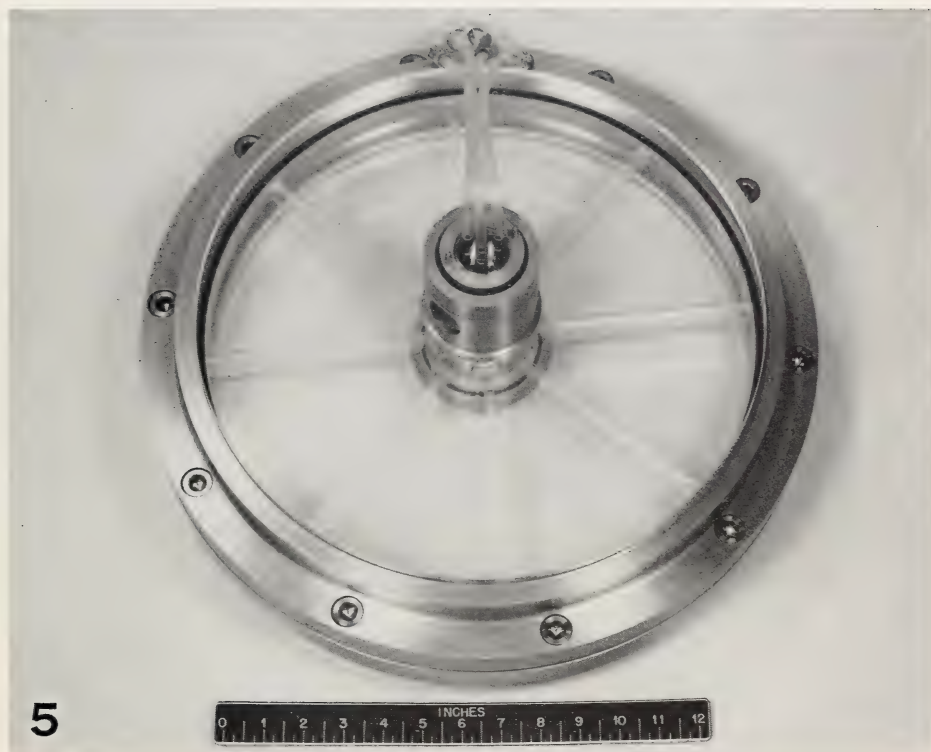


FIGURE 5.—Rotor A-IX; 6000 rpm,  $7150 \times g$ , 1.3 liters.

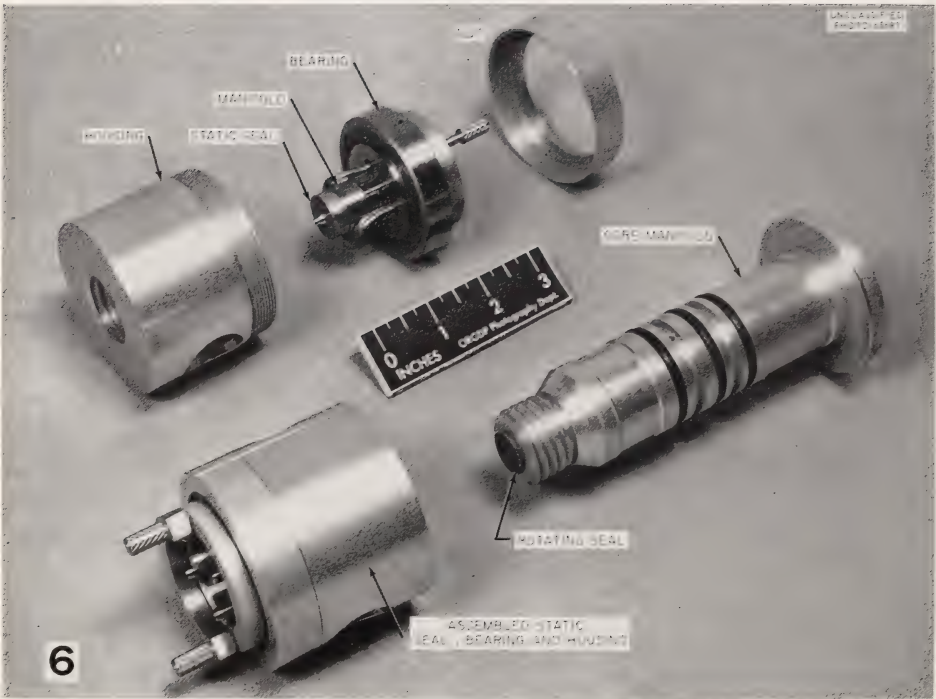


FIGURE 6.—Components of type "A" seal.

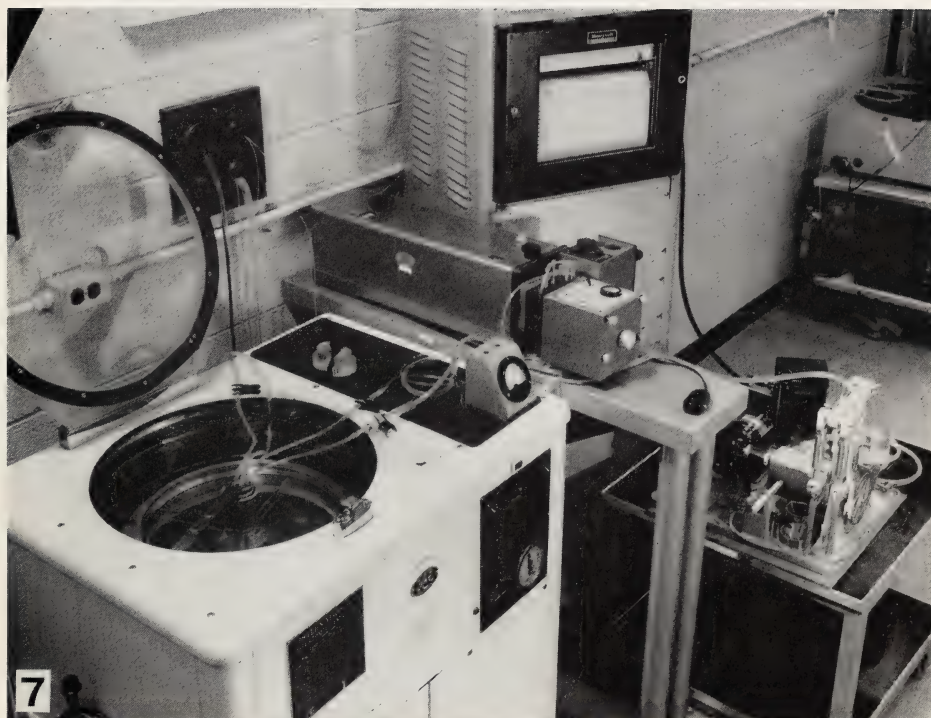


FIGURE 7.—Complete A-XII low-speed zonal centrifuge system. Centrifuge and rotor shown in *left foreground*, with gradient pump at extreme *right*. *Between* are absorbance monitor and recorder.



FIGURE 8.—Separation of rat liver subcellular components in a sucrose gradient in the A-IX rotor.



FIGURE 9.—A-IX rotor after failure at low speed.

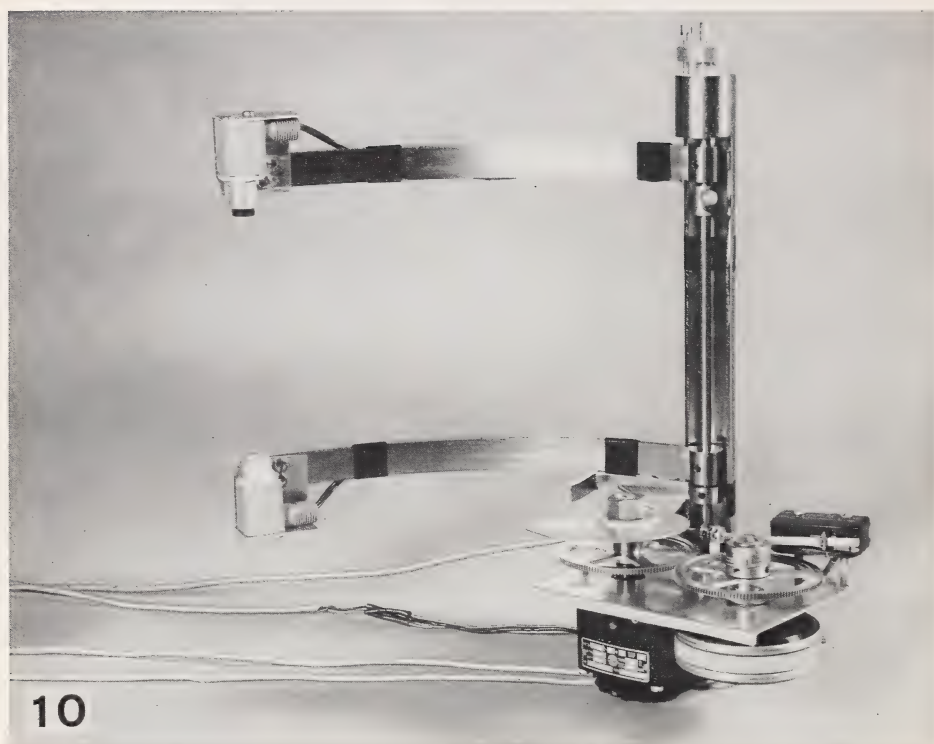


FIGURE 10.—Photoelectric scanner for A series rotors.

# The Design and Operation of the B-IV Zonal Centrifuge System<sup>1</sup>

N. G. ANDERSON, H. P. BARRINGER, E. F. BABELAY, C. E. NUNLEY, M. J. BARTKUS, W. D. FISHER, and C. T. RANKIN, JR., *Biology Division, Oak Ridge National Laboratory,<sup>2</sup> and the Technical Division, Oak Ridge Gaseous Diffusion Plant,<sup>2</sup> Oak Ridge, Tennessee*

## SUMMARY

A zonal centrifuge for either rate-zonal or isopycnic-zonal centrifugation with a total capacity of 1.7 liters useful with sucrose gradients at speeds up to 40,000 rpm (90,000  $\times g$  at  $R_{max}$ ) is described. The rotor is loaded and unloaded during rotation through a coaxial face seal. The core divides the rotor chamber into four sector-shaped compartments and also serves to channel the sample layer into the rotor during loading, and the recovered fractions out of the rotor during unloading. Ancillary instru-

mentation is described for recording the absorbance of the recovered gradient and for integrating the square of the angular velocity during the entire interval between sample introduction and gradient recovery. The centrifuge system has been successfully used to isolate mitochondria, polysomes, ribosomes, ribosomal subunits, macroglobulins, and to fractionate glycogen.—*Nat Cancer Inst Monogr* 21: 137-164, 1966.

SERIES A ZONAL rotors have been designed for the separation of particles ranging in size from whole cells to chloroplasts and mitochondria (1, 2). For the isolation of particles ranging down to very large molecules such as serum macroglobulin, B-series intermediate-speed rotors have been developed (3-5). The present paper describes the B-IV rotor system, which is applicable to the separation of subcellular organelles, including nuclei, mitochondria, microsomes, polysomes, ribosomes, ribosomal subunits, viruses, and macroglobulins. The mass of viral material which may be purified and concentrated with the B-IV and with subsequent rotors in the series designed more specifically for viral isolation (B-V, VIII, IX, and XII) is large; therefore, it has been considered advisable to develop suitable virus-tight enclosures for the upper end of the rotor, the seals, and the ancillary systems that will come in contact with the recovered gradient (6).

The B-II prototype zonal centrifuge previously described (3) has been useful in both the extension of zonal centrifuge theory and in the experi-

<sup>1</sup> This research performed under the Joint National Institutes of Health-Atomic Energy Commission Zonal Centrifuge Development Program which is supported by the National Cancer Institute, the National Institute of Allergy and Infectious Diseases, and the U.S. Atomic Energy Commission.

<sup>2</sup> Operated for the U.S. Atomic Energy Commission by the Nuclear Division of Union Carbide Corporation.

mental studies on particle separation. Instabilities observed with this rotor stimulated an extended study and redesign program (4, 7, 8) that led to the development of the B-IV system. The B-IV rotor has been used routinely at its maximum design speed of 40,000 rpm (5).

## DESIGN OF THE B-IV CENTRIFUGE SYSTEM

A number of problems must be simultaneously solved in the design of an intermediate-speed, dynamically loaded centrifuge rotor (4, 8). The rotor configuration must allow ideal sedimentation to occur in sector-shaped compartments. The compartmentation must also prevent mixing caused by Coriolis forces as fluid moves radially during loading and unloading. Interior surfaces must be arranged to allow the sample layer to spread uniformly over the surface of the density gradient as it flows into the rotor, and for the separated zones to be recovered without appreciable loss of resolution at the conclusion of a centrifuge run. The fluid lines and seals must be arranged to allow fluid to flow into and out of the rotor at low exterior pressure without heating, excessive shearing, spraying, foaming, or cross-leaking. The rotor configuration should be a stable one at all speeds, of as simple design as possible, and easily disassembled for cleaning and inspection. Methods for meeting some of these requirements have been listed previously (4). In long cylindrical rotors, however, more attention must be paid to the problem of funneling the gradient out of the rotor without loss of resolution than in short, flat A-type rotors (2).

The difference in hydrostatic pressure between the centrifugal and centripetal edges of the rotor fluid compartments during high-speed operation is considerable. It is imperative that the fluid pressure in the lines leading to the center and to the edge of the rotor compensate each other. This is done by leading both lines back as close as possible to the axis of rotation and by using a small-radius seal system for the coaxial fluid lines. A schematic presentation of the operating sequence of the B-IV rotor has been included in a previous paper (4).

### The Seal

The coaxial seal developed for the B-II zonal centrifuge (3) worked in a satisfactory manner only at low speeds, since the mass of the stationary portion of the seal was too large to allow it to follow the rotating seal if the plane of the latter was not absolutely normal to the axis of rotation. In addition, fluid leaking out of the seal could form aerosols in the surrounding atmosphere. The seal system has therefore been completely redesigned to reduce the mass and to contain solutions or suspensions which may leak out during operation at high speed.

The seal system developed for the B-IV centrifuge consists of a housing that completely encloses the seal; a manifold to channel the edge, center,

and coolant streams; a two-path, high-speed face seal; and a secondary seal to retain the coolant solution that may also contain a disinfectant (text-fig. 1). The sealing surfaces are preloaded by a coil spring located inside the seal housing. O ring seals at all connections permit the seal to be readily disassembled for cleaning and inspection without the use of special tools or fixtures. The life expectancy of this seal has not been established. One seal has been used for over 100 hours at 40,000 rpm with only minor maintenance. Satisfactory operation at 50,000 rpm has been attained in an experimental test stand constructed to determine whether this seal could be used at higher speeds.

The amount of cross-leakage occurring in the seal during use depends on the condition of the seal, back pressure in the fluid lines, and, possibly, on rotor speed. In continuous flow studies, negligible cross contamination has been observed with viruses. With high flow rates and viscous fluids, cross flow as high as 1 percent may be encountered. In the experiments performed to date, leakage across the seal has not presented a problem.

Fluid leaking out of the primary face seal mixes with the coolant stream, which is contained in a closed loop. For leakage to the outside to occur, the contaminated coolant must also leak past the lower or secondary face seal. Centrifugal force tends to prevent this leakage from occurring.

The seal surfaces are composed of a filled fluorocarbon<sup>3</sup> which presses against stainless steel. The components of the seal are shown in figure 1. It should be noted that the fluid lines do not cross in the seal or manifold in the most recent modification of this centrifuge, the rotor center line flows through the center line of the seal, and the rotor edge line flows through the outer seal line. The sample and the recovered zones are therefore subject to minimal shear during passage through the seal.

Coolant flow through the seal during high-speed operation is essential; if the flow is interrupted the seal will heat up rapidly. It is desirable to have a large squeeze bottle filled with water available to cool the seal externally should this occur.

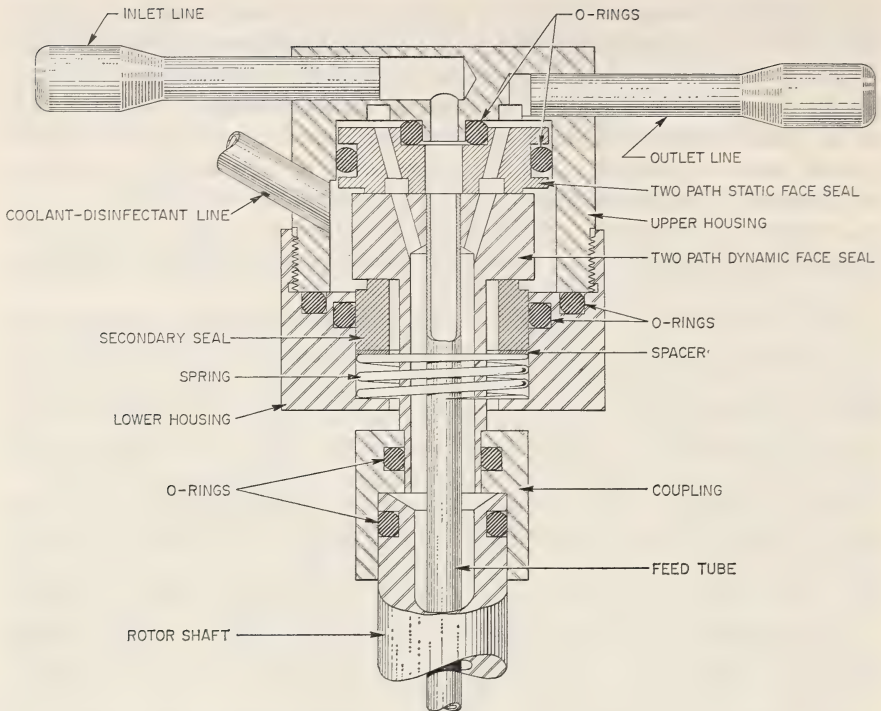
### The Upper Damping Bearing

The B-II zonal centrifuge rotor previously described (3) was destructively unstable in the region of 31,000 rpm. In the original tests, low-speed instability was observed in the region around 5000 rpm. This instability diminished when the number of septa was increased. Initially it was thought that fluid movements in the rotor contributed to this instability, and a large number of septa, 36 in all, were used to achieve a high degree of compartmentalization. The concept that compartmenting would solve the instability problem and that the number of compartments should equal the rotor speed in thousands of revolutions per minute (9) has not been supported by recent work.

In an effort to detect sources of vibration in the system the natural fre-

---

<sup>3</sup> Rulon, available from the Dixon Corporation, Bristol, Rhode Island



TEXT-FIGURE 1.—Enclosed seal for Series B rotors.

quencies were determined for the Spinco Model L drive system, rotor, upper bearing, and the supporting framework of the centrifuge.

For definitive studies, proximity probes<sup>4</sup> have been deployed in four positions to monitor vibrations occurring in the upper bearing, in the top and bottom ends of the rotor, and in the transmission of the centrifuge drive. The outputs are simultaneously displayed on a four-channel oscilloscope or recorded on tape, and photographs taken of oscilloscope traces. The phase relation of the motions at various points may be observed along with the frequencies of vibrations and the amplitudes. As shown by the oscillograms in figure 2, the B-II rotor exhibited a high amplitude precessional motion associated with a natural forward precessional mode of vibration. Efforts to eliminate this vibration involved three areas of the system: (a) drive quill and lower damper bearings, (b) transmission box mounting system, and (c) top centrifuge damper bearing. The first two were investigated in detail and found not to be the primary cause of the instabilities observed at the higher speeds.

The original design of the B-II top bearing was radically revised to incorporate more damping and a lower spring rate between the bearing and the vacuum chamber. Immediate improvements in stability were noted. The maximum amplitude of the instability was reduced from

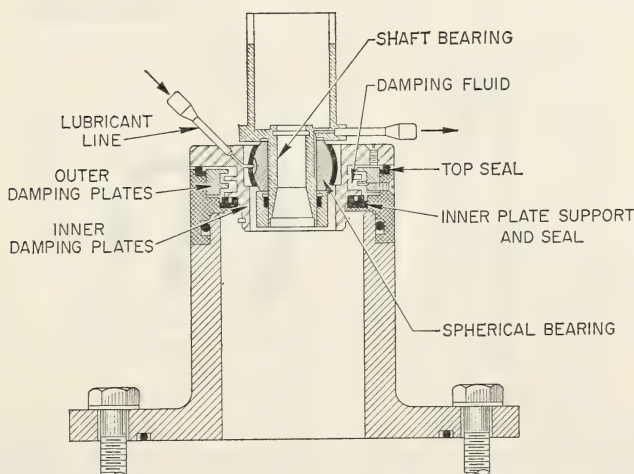
<sup>4</sup> Bentley Nevada Corp., Minden, Nevada, H-3020 and H-1-074-3.

greater than 0.120 inch total indicator reading (TIR) to the maximum amplitude of 0.003 inch TIR, as shown by the oscillogram in figure 3. This amplitude produced no detectable noise, and at about 33,000 rpm the amplitude markedly diminished, permitting the rotor to be driven successfully to 40,000 rpm. The actual value of the runout (variation in distance between the rotor and the probe during rotation) of the original B-II system during unstable operation at 30,000 rpm is not known since the probes positioned 0.060 inch from the rotor were completely destroyed.

This work led to the development of an enclosed journal bearing with the proper damping constants (text-fig. 2 and fig. 4). The bearing is self-aligning and is cooled by a stream of water. Damping is achieved by shearing a viscous oil between parallel plates. One set of plates is attached to the bearing and mounted to allow a small translational movement and by the so-called "squeeze film effect" of the cylindrical surfaces of the damper bearing. The other set of plates is mounted rigidly to the centrifuge top closure. With this bearing, the B-II centrifuge rotor could be rotated at 40,000 rpm filled with water *and without septa*.

### The B-IV Core

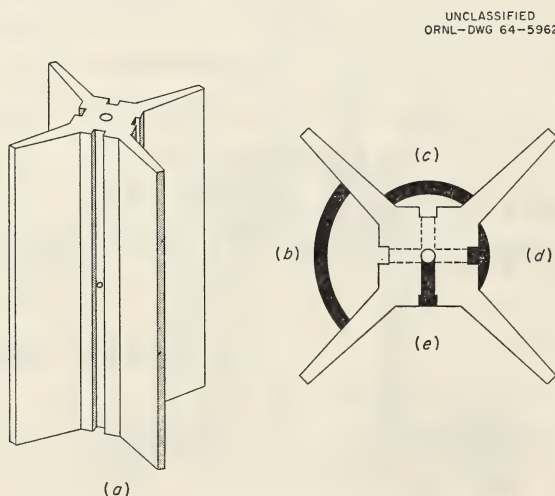
The core of a dynamically loaded zonal rotor serves to divide the rotor volume into sector-shaped compartments, to connect the seal lines to the center and edge of these compartments, and to funnel the gradient into and out of the rotor with minimal mixing and consequent loss of resolution. When it was shown that multiple compartmentation was not necessary to achieve rotor stability, the possibility of using a simple four-vaned core was reconsidered.



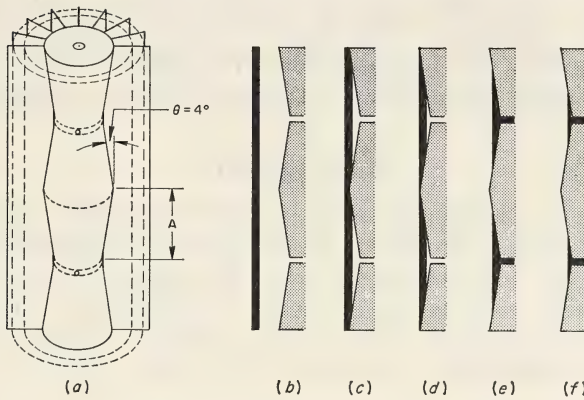
TEXT-FIGURE 2.—Top damper bearing for B-IV rotors.

The B-IV core, shown schematically in text-figure 3, is machined from two pieces of aluminum, which are then permanently joined. Structural considerations require that the vanes taper toward the edges, resulting in a small departure from an ideal sector shape. As a zone approaches the center of the rotor during unloading, it makes contact with the square center section of the core next to the root of the vane. The angle between a given density zone and the flat face of the core is initially  $48.9^\circ$ , resulting in flow of the zone toward the center of the core face. This effectively sweeps each density zone toward one of the four grooves in the center of each core face. Centripetal flow of particle-containing fluids in a centrifugal field has certain characteristics that are used to advantage. Thus, in rate-zonal centrifugation the particle concentration in the film of fluid in contact with the core during unloading is being continually decreased by sedimentation. As a result, laminar flow does not decrease resolution as much as one might expect. The maximum horizontal distance a particle flows in contact with the core face is 1.5 cm. The B-II core is also shown in text-figure 4 for comparison.

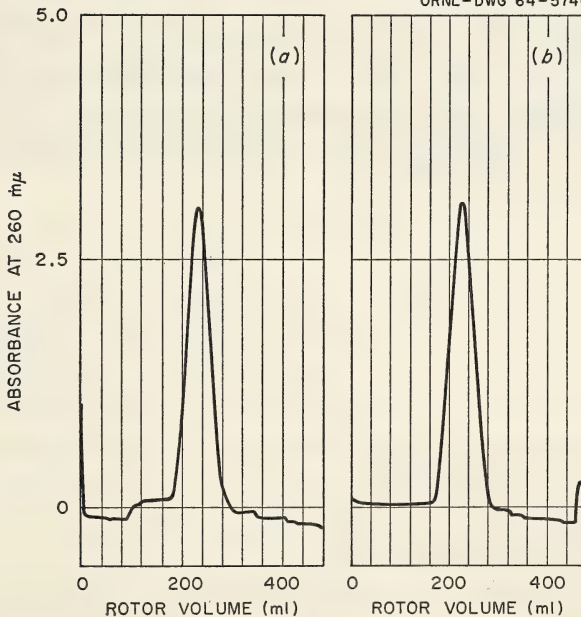
To compare the resolution obtainable with the B-II and B-IV cores, a number of experiments, including the rate separation of T2 and T3 phage under identical conditions, have been performed. No differences were noted. To determine whether the starting zone thickness was comparable in the two rotors, bovine serum albumin samples were run into the two rotors under comparable conditions and unloaded through the ultraviolet (UV) absorbance monitor, as indicated in the legend of text-figure 5. Essentially identical patterns were obtained, a result showing that the volume occupied by the sample was the same in both rotors.



TEXT-FIGURE 3.—Zone recovery in B-IV core. (a) B-IV core; (b-e) zone recovery; (b) zone approaching core; (e) part of zone recovered, part within core.

UNCLASSIFIED  
ORNL-DWG 64-5739

TEXT-FIGURE 4.—Zone recovery in B-II core. (a) Schematic of B-II core, with some septa removed. (b-f) Details of zone recovery in B-II core; (b) zone approaching core, (f) part of zone recovered, part within core.

UNCLASSIFIED  
ORNL-DWG 64-5740

TEXT-FIGURE 5.—Comparison of widths of sample zones in B-II (a) and B-IV (b) rotors. Sample, 25 ml of 2.5 percent bovine serum albumin in 4.2 percent sucrose; overlay, 216 ml of water; gradient, 17 w/w percent sucrose grading into 55 w/w percent sucrose; rotor loaded at 5000 rpm, accelerated to 25,000 rpm, maintained at that speed for 15 minutes, and unloaded at 5000 rpm.

For convenience a plot of rotor volume versus radius is shown in text-figure 6. The sample used in text-figure 5 has a calculated width of 0.07 cm in the rotor. The observed width at half-peak height is equivalent to 0.13 cm, indicating relatively small boundary widening. Equations relating rotor volume to radius are given by Bishop (10).

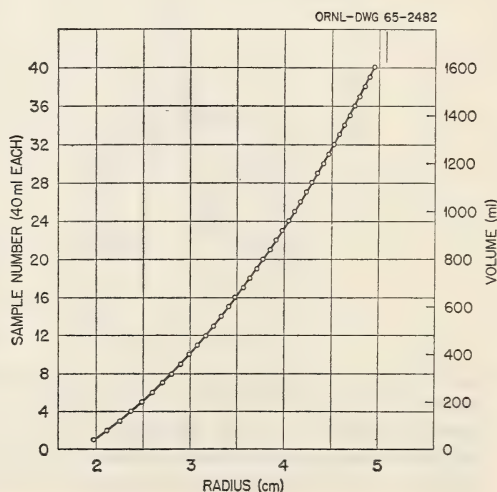
### Rotor Length

The length of a zonal rotor is limited by rotor stability considerations and by the fact that two forces act on particle or density zones during rotation. These are centrifugal and gravitational forces. The net result is that all zones of equal density form paraboloids of revolution about the axis of rotation. The equation for the intersection of an axial plane with the paraboloid of revolution (3) is given by

$$L = \frac{r^2 \omega^2}{2g}$$

where  $L$  (cm) is the height from the apex of the paraboloid of a given point on the isodensity surface,  $r$  (cm) is the radius at that point,  $\omega$  is the angular velocity in radians per second, and  $g$  is the acceleration due to gravity. It is evident that at various heights,  $L$ , isodense zones in a long rotor will be subjected to different centrifugal forces. Indeed, if the rotor is long enough to allow the apex of a zone to be in the rotor, the centrifugal field in a given zone will vary down to zero. For this reason, low-speed rotors generally have a very short height and are of large diameter, while high-speed rotors may be long and narrow. Fortunately, considerations of rotational stability and strength of materials generally favor the same configurations (8).

TEXT-FIGURE 6.—Rotor radius versus rotor volume for the B-IV zonal ultracentrifuge. Volume includes the 11 ml volume of the line leading from the point of fraction collection to the rotor.



### Ancillary Instrumentation

The technique of zonal centrifugation in the B-IV rotor can yield analytical results of considerable precision. However, to realize its full potential it was necessary to develop several ancillary systems. Among these were systems for rotor temperature control, for determining the quantity of sample material recovered in the gradient, and for measuring the total centrifugal force exerted on a particle from the time of its introduction into the rotor until it is recovered in a fraction collector.

All controls (speed, time, temperature, vacuum) are mounted on a rack (fig. 5, right), which also holds the speed indicating and integrating system. The latter presents continuously a digital indication of the integral of  $\omega^2 dt$  or  $G_c$ . A Bentley proximity probe<sup>4</sup> with associated power supply and amplifier,<sup>5</sup> used to detect rotor speed, is sensed by a frequency meter,<sup>6</sup> which provides a *dc* output voltage proportional to rotor speed,  $\omega$ . This voltage drives a slide wire potentiometer,<sup>7</sup> which was modified by the addition of a squaring circuit to give  $\omega^2$ . The squaring circuit output is electronically integrated by an integrator,<sup>8</sup> which provides a digital indication of the time integral of the square of the rotor's angular velocity,

$$\int_{t=t_0}^{t=t_1} \omega^2 dt$$

where  $\omega$  is the angular velocity in radians per second,  $t_0$  is the time at which the sample is moved into the rotor, and  $t_1$  is the time when collection is begun. A calibrating frequency source and locked timer are used for calibrating the entire integrating system. The digital readout is multiplied by  $10^6$  to yield the actual value in units of  $\omega^2$  seconds.

An absorbance monitoring system is arranged so that fluid flows from the rotor seal directly up through a 0.2 cm light path quartz cell (11) mounted in a Beckman DU monochromator. The monochromator has a photomultiplier and amplifier system<sup>9</sup> so that absorbance is indicated linearly on a recording strip-chart potentiometer. The hold-up volume from the point at which fluid leaves the core to collection is 11 ml. The spectrophotometer is mounted on a movable stand so that it may be positioned directly over the upper rotor bearing or may be retracted to allow the bearing and rotor to be moved away from the centrifuge. Forty ml volume fractions are collected by hand using 40 ml calibrated screw-top centrifuge tubes.<sup>10</sup> As the effluent line is moved from one tube to the next, a foot switch is depressed which moves an event-marking pen on the absorbance recorder. The position of any fraction in the

<sup>4</sup> Bentley Nevada Corp., Minden, Nevada, Distance Detector Energizer, Model B-15, and Bentley Distance Detector, Model D-152.

<sup>5</sup> Hewlett Packard, Palo Alto, Calif., Model 500BR.

<sup>6</sup> Leeds & Northrup Co., Philadelphia, Penna., Speedomax Model "H."

<sup>7</sup> Royson Engineering Co., Hatboro, Penna., Lectro Count.

<sup>8</sup> Gilford Instrument Laboratories, Inc., Oberlin, Ohio, Absorbance Indicator Model 220, Light-Source Stabilizer, Model 220, Optical Density Converter Model 220.

<sup>10</sup> Available from Bellco Glass Inc., Vineland, N.J.

absorbance monitor diagram can therefore be determined. For most work the monochromator is set at 260 m $\mu$ , and the amplifier set to record 0 to 2.5 absorbancy full scale. With correction for the short light path, the actual recorded scale is 0 to 12.5 absorbance units. It should be emphasized that when mitochondria and other microscopic particles are separated, a large fraction of the observed absorbance is the result of turbidity.

### Containment

The B-IV system is suitable for work with nonpathogenic materials. For work with virus-containing suspensions, it is desirable to provide additional containment to prevent (a) the inadvertent introduction of contaminants into the fluids being fractionated and (b) the possible leakage of highly concentrated materials into the environment. Experimental containment systems for the B-IV centrifuge have been described by Cho *et al.* (6).

## OPERATION OF THE B-IV CENTRIFUGE SYSTEM

### Assembly of the Rotor System

The components of the B-IV rotor are shown in figure 6. The two end caps of the rotor are sealed with O rings. The four-vaned core is placed in the rotor after the bottom end cap has been screwed on. The O ring for the upper end cap is placed in position in the groove in the body of the rotor, and the manifold plug is screwed into position on the under side of the upper end cap (after the guide for the stem of the seal has been inserted). The top end cap is then screwed down, and the end caps are tightened until small bench marks are aligned. The stem guide is essential to avoid displacing or tearing the O ring, located within the manifold plug, when inserting the seal.

After ethylene oxide sterilization, the assembled rotor is placed in the centrifuge (fig. 7), and the upper chamber closure is screwed into position. The damper and bearing are positioned next. The oil lines for the bearing and the cooling water lines for bearing and seal are visible in figures 8 and 9.

Seals should be handled with care at all times. When the seal is positioned on the assembled rotor it should be pushed gently into running position. Coolant and feed lines should be attached without exerting undue force on the seal housing. *The seal is never operated without a continuous flow of water through both the seal and the upper bearing.*

After the rotor has been accelerated to approximately 3000 rpm, a check is made for (a) excess water in the oil drain line in addition to the few drops normally observed when the rotor is first started, (b) water leaking out the lines leading to the rotor center and the rotor edge, and (c) droplets of liquid in the rotor center line while the gradient

is loaded into the empty rotor. Appearance of droplets indicates leakage across the inner sealing dam if the droplets contain gradient solutes, or leakage across the outer sealing dam if the droplets are coolant fluid. It is important to detect signs of seal failure early, especially if a valuable sample is to be used.

After use, the seal is thoroughly cleaned by passing hot tap water through the seal after it has been removed from the rotor. The seal is then completely disassembled (the seal housing has left-hand threads), and the rubbing surfaces inspected. The lower seal and spring are cleaned carefully and all parts dried in a stream of dry air. Since cesium chloride corrodes stainless steel, the seal is cleaned as soon as possible after an experiment.

Before the seal is reassembled, the rubbing surfaces are inspected for scratches or indentations. Sharp instruments are not used and minimal force is exerted during seal assembly. The long center tube is aligned before insertion into the rotor.

The assembled seal is positioned by gently inserting the stem through the rotor upper shaft extension and, with gentle pressure, moving it through the O ring located inside the manifold plug. The upper portion of the seal is supported partially by the metal ring around the damper and bearing. In practice, an O ring is often used to hold the seal in a given position.

The cooling lines and the oil lines are next connected to the proper outlets provided on the seal and bearing assemblies. The completed assembly at this point is shown in the centrifuge and glove box in figure 8, and outside the centrifuge in figure 9. A schematic diagram of the rotor connections is shown in text-figure 7.

Cooling water flows, respectively, from the pump <sup>11</sup> through the upper rotor bearing, seal, graduated reservoir (not visible in photographs), refrigerated heat exchanger, and back to the pump. The cooling water circulates entirely inside the glove box enclosure, while the refrigerant circulates outside. The graduated reservoir indicates the amount of water in the system and provides visual indication of flow rate.

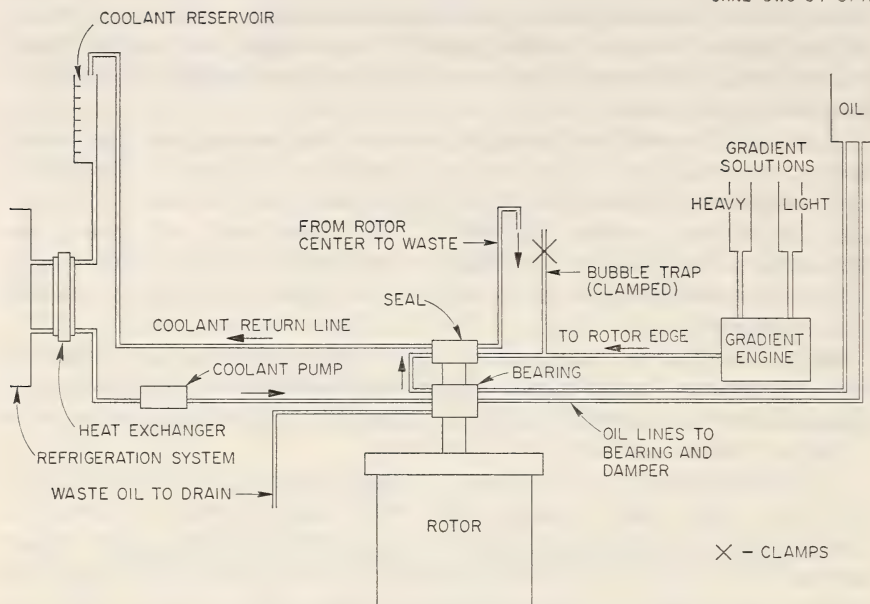
Oil lines from the reservoir within the glove box connect to two inlets on the bearing. The oil not only lubricates the bearing but aids in sealing the vacuum chamber. The overflow oil line from the bearing drains inside the glove box into a small plastic bottle.

### Introduction of Gradient and Sample

After the rotor and associated tubing are positioned, the gradient engine is attached to the gradient solution bottles. The line from the gradient pump to the rotor seal edge line is connected to a glass "T" joint, which serves as a bubble trap and drain line when the sample is being introduced into the rotor.

---

<sup>11</sup> Sigma Pump Model AL 4-300.



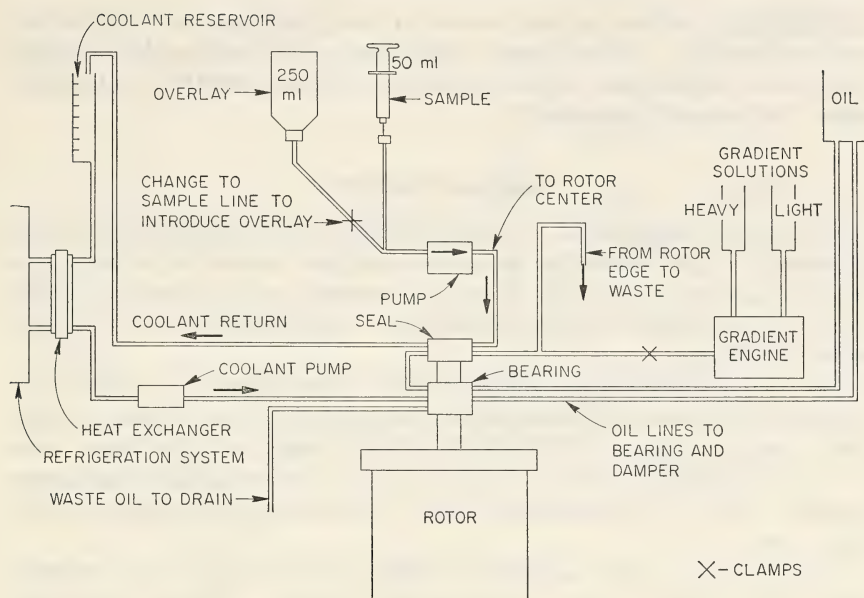
TEXT-FIGURE 7.—Schematic diagram of fluid lines when gradient is loaded into rotor.

At this time the rotor chamber is evacuated, the refrigeration system turned on, and the rotor accelerated to 3000 to 5000 rpm. The gradient, light end first, enters the rotor, is distributed uniformly over the rotor wall and is forced, by denser fluid pumped in subsequently, toward the center of the rotor. The gradient, normally 1000 to 1200 ml, does not fill the rotor completely. An underlay (or "cushion") of fluid denser than that used to form the gradient is pumped in until the first part of the gradient emerges through the center line. At this time, the gradient pump is stopped, and the gradient line is clamped off. The gradient is now ready to receive the sample. This is introduced through the center line (text-fig. 8), so that the sample is placed on top (centripetal end) of the gradient. The sample line is part of an intravenous set.<sup>12</sup>

A small pump<sup>13</sup> on the sample line close to the seal ensures constant flow during sample and overlay introduction. The drip-chamber probe is inserted into the overlay bottle, and the line is clamped. The needle of the sample syringe is inserted into the medicinal entry; this line is clamped also. The clamp on the bubble-trap line between the T and the gradient pump prevents the solution from emerging out of the rotor into the exterior of the glove box. The clamp from the sample syringe line is removed, and the sample is introduced into the rotor with the syringe, displacing part of the underlay from the edge of the rotor through the bubble-trap line to

<sup>12</sup> Intravenous set—Abbott No. 4540; Cutter Code No. 860-08.

<sup>13</sup> New Brunswick PA-56 pump.



TEXT-FIGURE 8.—Schematic diagram of fluid lines during sample introduction into B-IV rotor.

a waste container inside the glove box. To rinse the sample syringe, the clamps are arranged to allow a small amount of overlay solution to be drawn into it. The clamps are then rearranged to allow this rinse to flow into the rotor. When the fluid lines are clear of visible sample, the integrator counter is switched on, the sample syringe line clamped, the overlay line opened, and the small pump turned on and adjusted to pump from the overlay solution bottle to the rotor center.

Approximately 200 ml of overlay is pumped to the rotor (displacing part of the underlay from the edge) to move the sample zone out from the core. An additional 40 ml of overlay is introduced, after which the clamp from the gradient engine is removed and the pump started. The flow from the edge line of the rotor and from the gradient engine both pass through the bubble-trap line to waste. When all overlay solution has entered the rotor, the line from the bottle is clamped, and the sample pump is turned off and removed from the line, the sample syringe line opened, and the bubble-trap line clamped. Flow extends from the gradient engine to the edge of the rotor, and overlay is displaced from the center of the rotor to the syringe. By raising the sample line and tapping it gently, air bubbles are removed from the rotor.

When the 40 ml of overlay is recovered in the syringe, the gradient pump is stopped and the pump line clamped near the rotor. The only line open to the rotor leads from its center to the syringe, which is mounted vertically in a clamp. The rotor is accelerated to achieve the separation desired.

During a run, the level can be observed in the syringe reservoir and leakage can be detected. The volume in the syringe will decrease below 25 ml due to rotor expansion at higher speeds, but after deceleration to unloading speed the volume is restored.

### Gradient Recovery

The rotor is decelerated to a speed of 5000 rpm and emptied by displacement. The rotor center line, which had been connected to the sample introduction syringe during the run, is removed and replaced by a line to the quartz flow cell (0.2 cm light path) and through it to the sample collection tubes.

The Gilford absorbance indicator and optical density converter unit used on the Beckman spectrophotometer and instrument panel, respectively, permit readings of 0.25 to 2.5 optical density units full chart range on the Honeywell recorder. With a 0.2 cm flow cell, the actual range becomes 1.25 to 12.5 absorbance units. Normally, a wavelength of 260  $m\mu$  is used.

The gradient pump is adjusted to pump only the most dense material used (55% sucrose in most virus-isolation studies). The only open lines lead to the rotor edge from the gradient pump and from the core of the rotor to the flow cell (text-fig. 9). As the contents of the rotor are displaced by 55 percent sucrose, the fluid running through the DU monochromator cell is collected in 40 ml centrifuge tubes. As each 40 ml tube is collected, a foot switch is depressed to activate an event-marking pen on the strip-chart recorder. This provides a visual record along the base of the chart which may be used to correlate the presence of a given absorbance peak with its location in the recovered fractions.

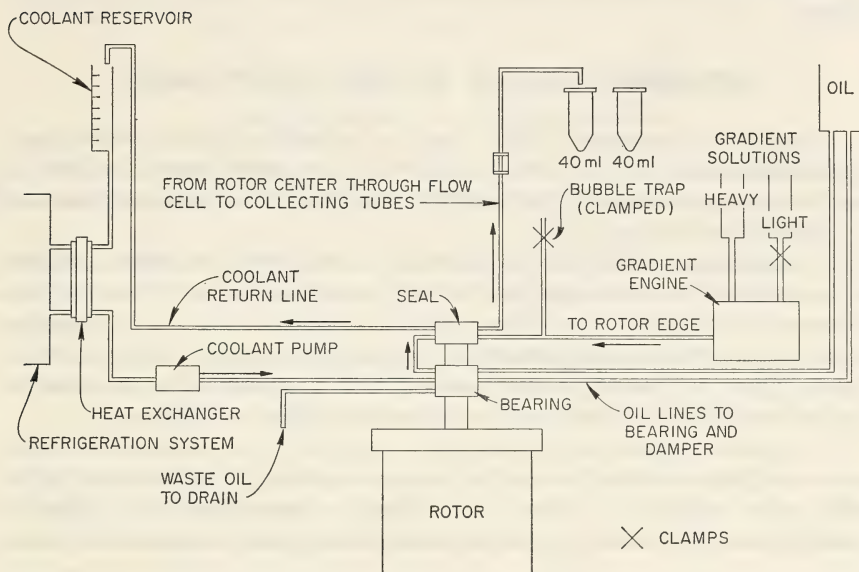
### Density and Refractive Index Determinations

Until recently, the density of the recovered fractions was determined by using a manually operated Abbe-type refractometer. It is extremely difficult to do this aseptically and without contaminating the operator. To provide a semiautomatic method for determining the density of the recovered fractions, a modified torsion balance mounted in the glove box is adjusted to indicate density directly. The 40 ml fractions are shaken with the screw tops in place, opened, and individually placed under the glass bob. (The torsion balance has been modified to electronically read and display the results of the Archimedes measurement on tape outside the glove box. The printout mechanism is activated by a foot pedal.)

### Gradient Pump Assembly

The gradient pump <sup>14</sup> is shown in figure 10. The pump is sterilized with the pistons partially disassembled to permit ethylene oxide exposure.

<sup>14</sup> Available from Beckman Instruments, Spinco Division, Palo Alto, Calif.

UNCLASSIFIED  
ORNL-DWG 64-5749

TEXT-FIGURE 9.—Arrangement of fluid lines during sample collection.

A program cam produces a 1200 ml gradient that is linear with respect to rotor volume. The pump is located outside the glove box. A single Tygon tube carries the gradient to the rotor from the pump and into the glove box through a metal seal. Gradient solutions are kept in sterile bottles and connected to the pump by disposable transfusion tubing connectors.

### Cleaning and Sterilizing

All parts of the system in contact with samples or contaminated must be sterilized. At present, reusable components are treated with formaldehyde where appropriate, washed, and rinsed with distilled water, and either steam- or gas-sterilized. The rotor and its components [including seal, damper bearing, gradient engine and associated tubing, disposable Oak Ridge No. 30 rotor tubes (6), and the glass 40 ml screw-top centrifuge tubes used for gradient recovery] are gas-sterilized in a regular steam sterilizer (American Sterilizer Co.) fitted with an ethylene oxide system. Gas sterilization, which requires approximately 8 hours, is usually done overnight. The components are placed in paper bags, which are opened in the glove box, or in the case of the gradient engine, when the tubes leading to the sterile solutions and to the rotor are ready to be attached.

The glove box in which the rate-zonal centrifuge is housed is sterilized by overnight exposure to ethylene oxide (two 20 oz cans). The outlet valves from the box are closed during this process; filtered air is pumped through the box, beginning early the next morning, to remove residual gas.

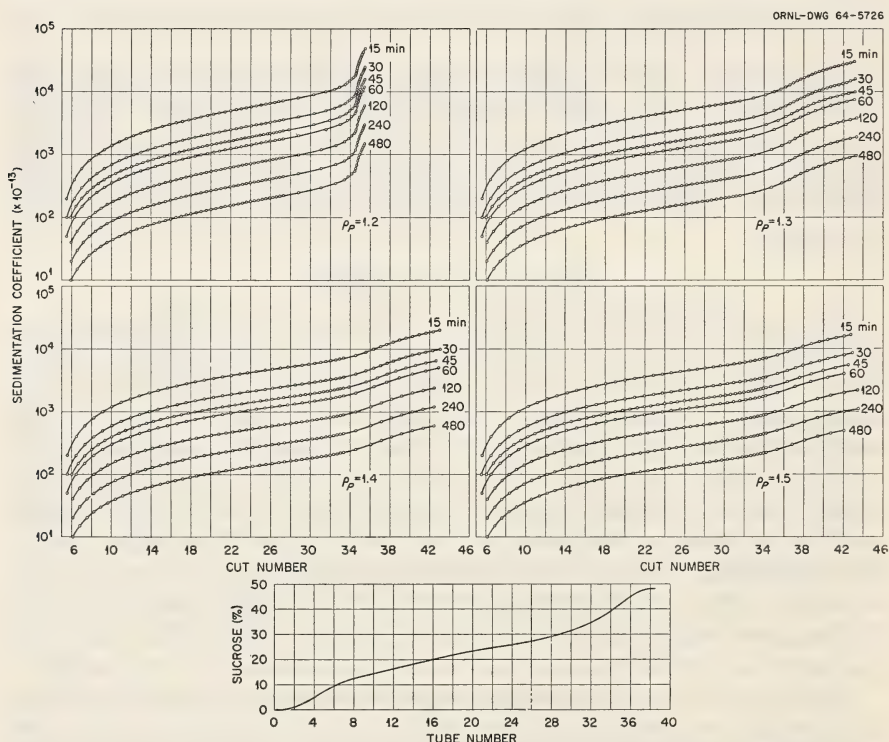
All solutions used are sterilized either by filtration or, when feasible, by steam.

### DETERMINATION OF SEDIMENTATION RATES

A computer program (10) is used to calculate the equivalent sedimentation rates ( $S^*$ ) in water at 20° C of spherical particles that do not behave osmotically. The basic equation is a modification of that used by Martin and Ames (12).

In experiments designed for searching tissue breis for virus particles, it is desirable to centrifuge long enough to spread known virus particles between the soluble protein zone and the mitochondrial zone. Rat liver mitochondria band isopycnicly in sucrose gradients at a density level of 1.203 g per cm<sup>3</sup> [44.5% (w/w) sucrose]. In practice, virus particles are not allowed to reach this density during rate-zonal centrifugation.

The positions that particles having a range of densities and sedimentation coefficients would have after various centrifugation times at 20,000 rpm were calculated. These are plotted in text-figure 10. With the gradient used for these calculations, a suitable spread is obtained in 1 hour



TEXT-FIGURE 10.—Calculated positions in a sucrose density gradient in the B-IV rotor for nonosmotic particles having indicated densities and sedimentation coefficients as a function of centrifugation time at 20,000 rpm.

at 20,000 rpm. This speed and time have been used for most of the studies on viruses, glycogen, and microsomes.

## EXPERIMENTAL SEPARATIONS

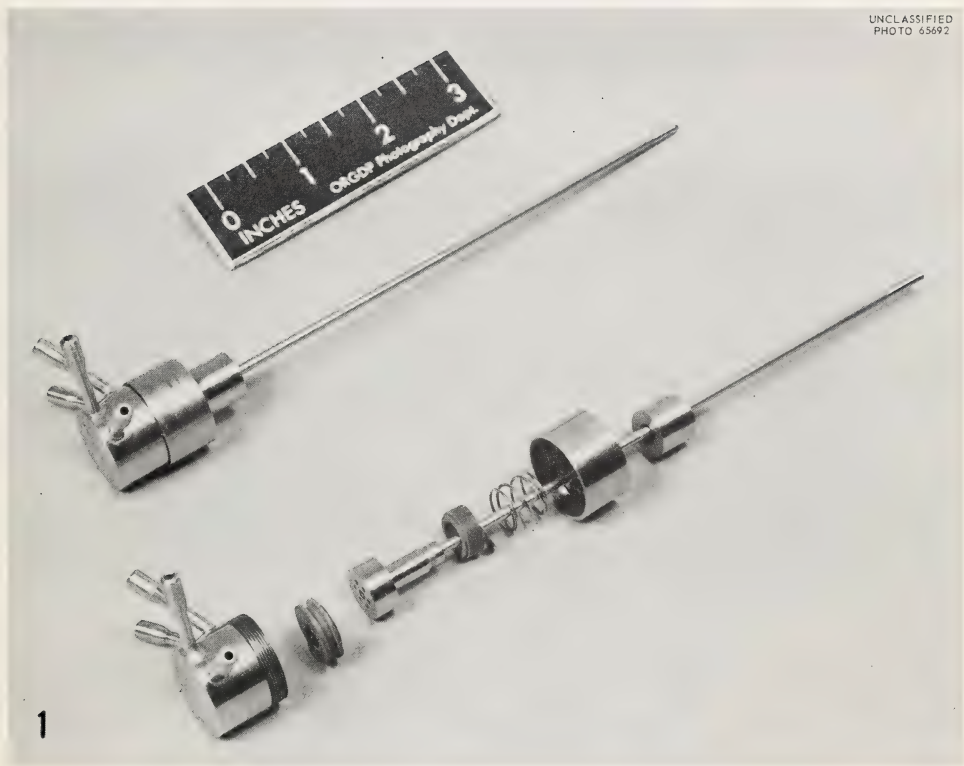
During the development of the B-IV zonal ultracentrifuge a variety of biological materials have been isolated. Among the viruses studied are polio (3, 13), respiratory syncytial virus (14), Rauscher and Moloney mouse leukemia viruses, tobacco mosaic virus, bromgrass mosaic virus, and T2 and T3 coliphages (14, 15). Nuclei, a membrane fraction, mitochondria, microsomes, polysomes, and ribosomes have been separated from rat liver homogenates (16, 17). Cytochrome oxidase was found to be associated exclusively with the mitochondrial peak (18). Polysomes, ribosomes, and ribosomal subunits have been isolated from *Escherichia coli* (5, 19, 20).

By use of the two dimensional  $s$ - $\rho$  technique, viruses added to tissue homogenates have been recovered in a high state of purity (21). The glycogen spectrum has been separated into a series of homogeneous subfractions from liver (22) and from *Tetrahymena pyriformis* (23). Lipid peroxidation has been shown to occur in all membrane fractions in rat liver, brain, kidney, and testis separated in sucrose gradients in the B-IV rotor (24). The relaxing activity in muscle was found to be associated with a particle separable from mitochondria (25). Good separations of serum macroglobulins have been obtained in prolonged runs (26, 27).

## REFERENCES

- (1) CANNING, R. E., and ANDERSON, N. G.: Separation of subcellular fractions with a new zonal rotor. *Amer Zool* 4: 310, 1964.
- (2) ANDERSON, N. G., BARRINGER, H. P., CHO, N., NUNLEY, C. E., BABELAY, E. F., CANNING, R. E., and RANKIN, C. T., JR.: The development of low speed "A" series zonal rotors. *Nat Cancer Inst Monogr* 21: 113-136, 1966.
- (3) ANDERSON, N. G.: The zonal ultracentrifuge. A new instrument for fractionating mixtures of particles. *J Phys Chem* 66: 1984-1989, 1962.
- (4) ———: An introduction to particle separations in zonal centrifuges. *Nat Cancer Inst Monogr* 21: 9-39, 1966.
- (5) ANDERSON, N. G., BARRINGER, H. P., BABELAY, E. F., and FISHER, W. D.: The B-IV zonal ultracentrifuge. *Life Sci* 3: 667-671, 1964.
- (6) CHO, N., BARRINGER, H. P., AMBURGEY, J. W., CLINE, G. B., ANDERSON, N. G., McCauley, L. L., STEVENS, R. H., and SWARTOUT, W. M.: Problems in biocontainment. *Nat Cancer Inst Monogr* 21: 485-502, 1966.
- (7) BERMAN, A. S.: Theory of centrifugation: Miscellaneous studies. *Nat Cancer Inst Monogr* 21: 41-76, 1966.
- (8) BARRINGER, H. P.: The design of zonal centrifuges. *Nat Cancer Inst Monogr* 21: 77-111, 1966.
- (9) STALLMAN, R. C., CARLOS, S., and PICKELS, E. G.: Centrifuge Apparatus. U.S. Patent No. 3,168,474, issued February 2, 1965.
- (10) BISHOP, B. S.: Digital computation of sedimentation coefficients in zonal centrifuges. *Nat Cancer Inst Monogr* 21: 175-188, 1966.

- (11) ANDERSON, N. G.: Quartz flow cells for continuous spectrophotometric analysis of column effluents. *Anal Chem* 33: 970-971, 1961.
- (12) MARTIN, R. G., and AMES, B. N.: A method for determining the sedimentation behavior of enzymes: Application to protein mixtures. *J Biol Chem* 236: 1372-1379, 1961.
- (13) REIMER, C. B., NEWLIN, T. E., HAVENS, M. L., BAKER, R. S., ANDERSON, N. G., CLINE, G. B., BARRINGER, H. P., and NUNLEY, C. E.: An evaluation of the B-V (continuous-flow) and B-IV (density gradient) rotors by use of live polio virus. *Nat Cancer Inst Monogr* 21: 375-388, 1966.
- (14) CLINE, G. B.: Unpublished data, 1965.
- (15) ANDERSON, N. G.: Virus isolation in the zonal ultracentrifuge. *Nature (London)* 199: 1166-1168, 1963.
- (16) SCHUEL, H., and ANDERSON, N. G.: Studies on isolated cell components. XVI. The distribution of acid phenyl phosphatase activities in rat liver brei fractionated in the zonal ultracentrifuge. *J Cell Biol* 21: 309-323, 1964.
- (17) GERIN, J. L.: The effect of thyroid hormones on *in vivo* protein synthesis in rat liver. Ph. D. Dissertation, University of Tennessee, 1964.
- (18) SCHUEL, H., TIPTON, S. R., and ANDERSON, N. G.: Studies on isolated cell components. XVII. The distribution of cytochrome oxidase activity in rat liver brei fractionated in the zonal ultracentrifuge. *J Cell Biol* 22: 317-326, 1964.
- (19) SCHRAM, E.: Etude analytique des ribosomes 30S et 50S d'*Escherichia coli*. *Arch Int Physiol* 72: 695-696, 1964.
- (20) CLINE, G. B., and FISHER, W. D.: Unpublished data.
- (21) ANDERSON, N. G., HARRIS, W. W., BARBER, A. A., RANKIN, C. T., JR., and CANDLER, E. L.: Separation of subcellular components and viruses by combined rate and isopycnic-zonal centrifugation. *Nat Cancer Inst Monogr* 21: 253-283, 1966.
- (22) BARBER, A. A., HARRIS, W. W., and ANDERSON, N. G.: Isolation of native glycogen by combined rate-zonal and isopycnic centrifugation. *Nat Cancer Inst Monogr* 21: 285-302, 1966.
- (23) BARBER, A. A., HARRIS, W. W., and PADILLA, G. M.: Studies of native glycogen from synchronized *Tetrahymena pyriformis*. In press.
- (24) BARBER, A. A., RANKIN, C. T., JR., and ANDERSON, N. G.: Lipid peroxidation in rat tissue particulates separated by zonal centrifugation. *Nat Cancer Inst Monogr* 21: 333-344, 1966.
- (25) SCHUEL, H., LORAND, L., SCHUEL, R., and ANDERSON, N. G.: Isolation of relaxing particles from rat skeletal muscles in zonal centrifuges. *J Gen Physiol* 48: 737-752, 1965.
- (26) FISHER, W. D., and CANNING, R. E.: Isolation of macroglobulin by rate zonal centrifugation. *Amer Zool* 4: 310, 1964.
- (27) ———: Isolation and characterization of rat macroglobulin. *Nat Cancer Inst Monogr* 21: 403-412, 1966.



UNCLASSIFIED  
PHOTO 65692

FIGURE 1.—Assembled and disassembled seal for B-series rotors.

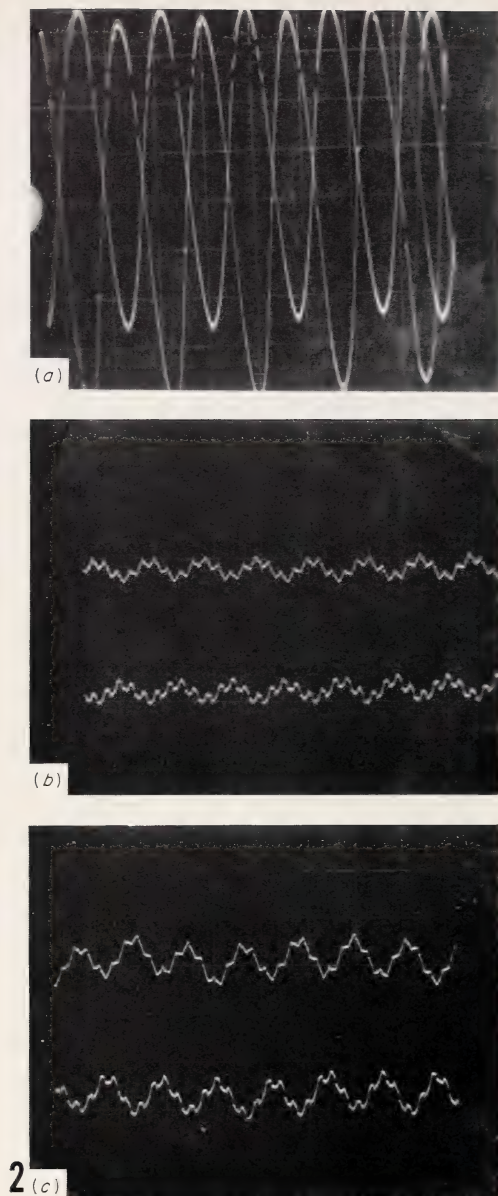


FIGURE 2.—Oscillograms of B-II rotor taken at three speeds. The *upper traces* are monitoring the top end cap, the *lower traces* the bottom end cap. (a) Taken at 28,000 rpm; vertical sensitivity 0.005 in/cm; horizontal sweep rate 0.005 sec/cm; high-amplitude frequency, 114 cps; low-amplitude frequency, not detectable but approximately 28,000 rpm. (b) Taken at 23,500 rpm; vertical sensitivity, 0.005 in/cm; horizontal sweep rate, 0.010 sec/cm; high-amplitude frequency, 86.5 cps; low-amplitude frequency, approximately 23,500 rpm. (c) Taken at 23,000 rpm; vertical sensitivity, 0.005 in/cm; horizontal sweep rate, 0.010 sec/cm; high-amplitude frequency, 87 cps; low-amplitude frequency, approximately 23,000 rpm.

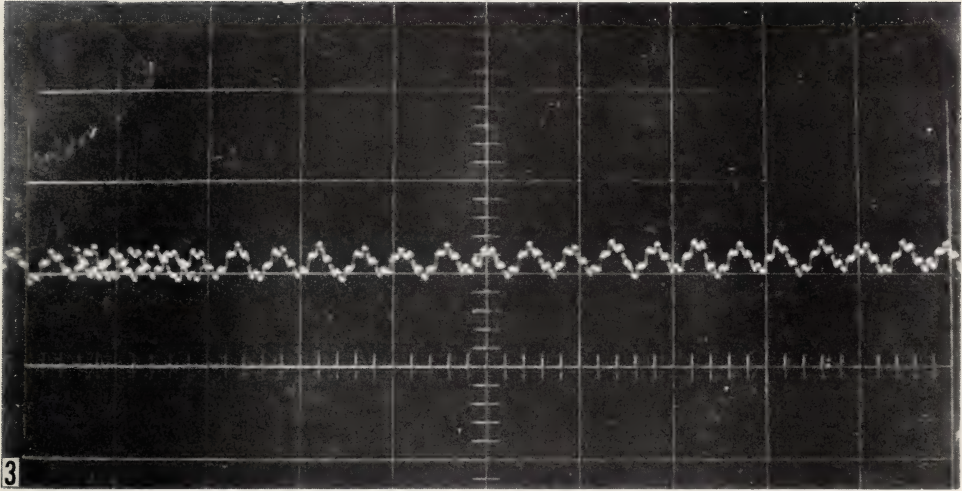


FIGURE 3.—Oscillogram of B-II rotor taken at about 30,000 rpm with modified experimental upper damping bearing. Vertical sensitivity, 0.005 in/cm; horizontal sweep rate, 0.02 sec/cm. The trace is monitoring the bottom end cap. High-amplitude frequency is 111 cps; low-amplitude frequency, about 30,000 rpm.

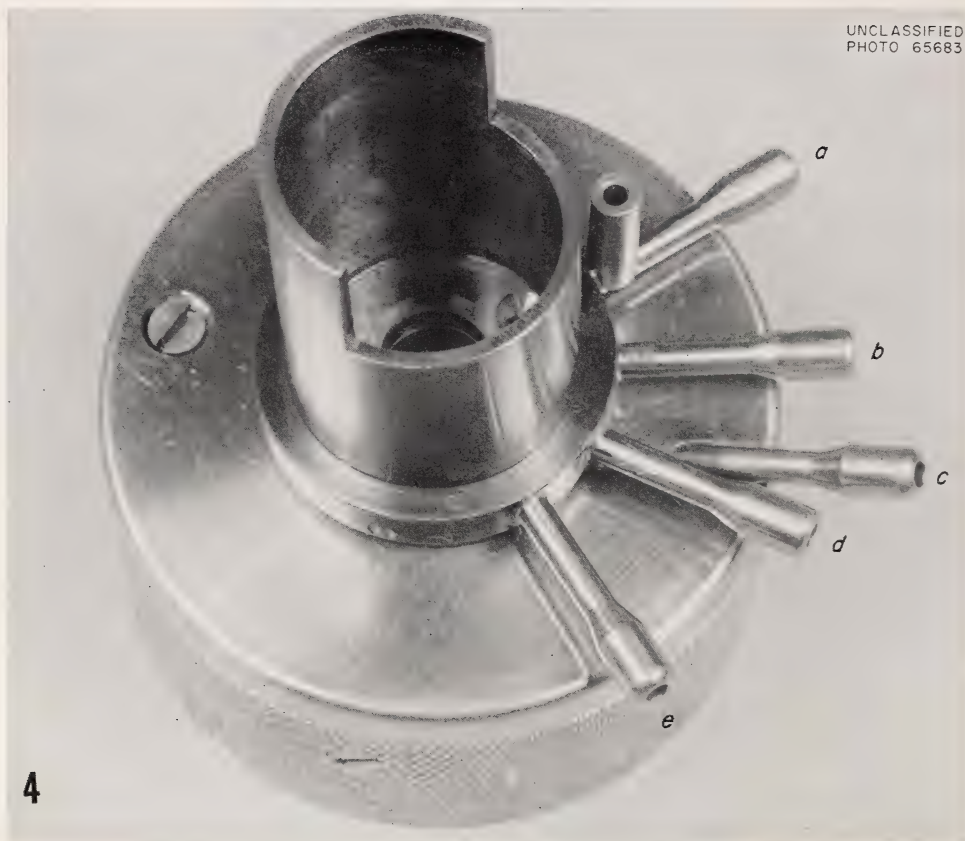


FIGURE 4.—Top damper bearing assembly for B-IV zonal centrifuge. (a) Overflow oil from bearing; (b) cooling water out; (c and d) oil lines into ball joint and bearing; and (e) cooling water in.

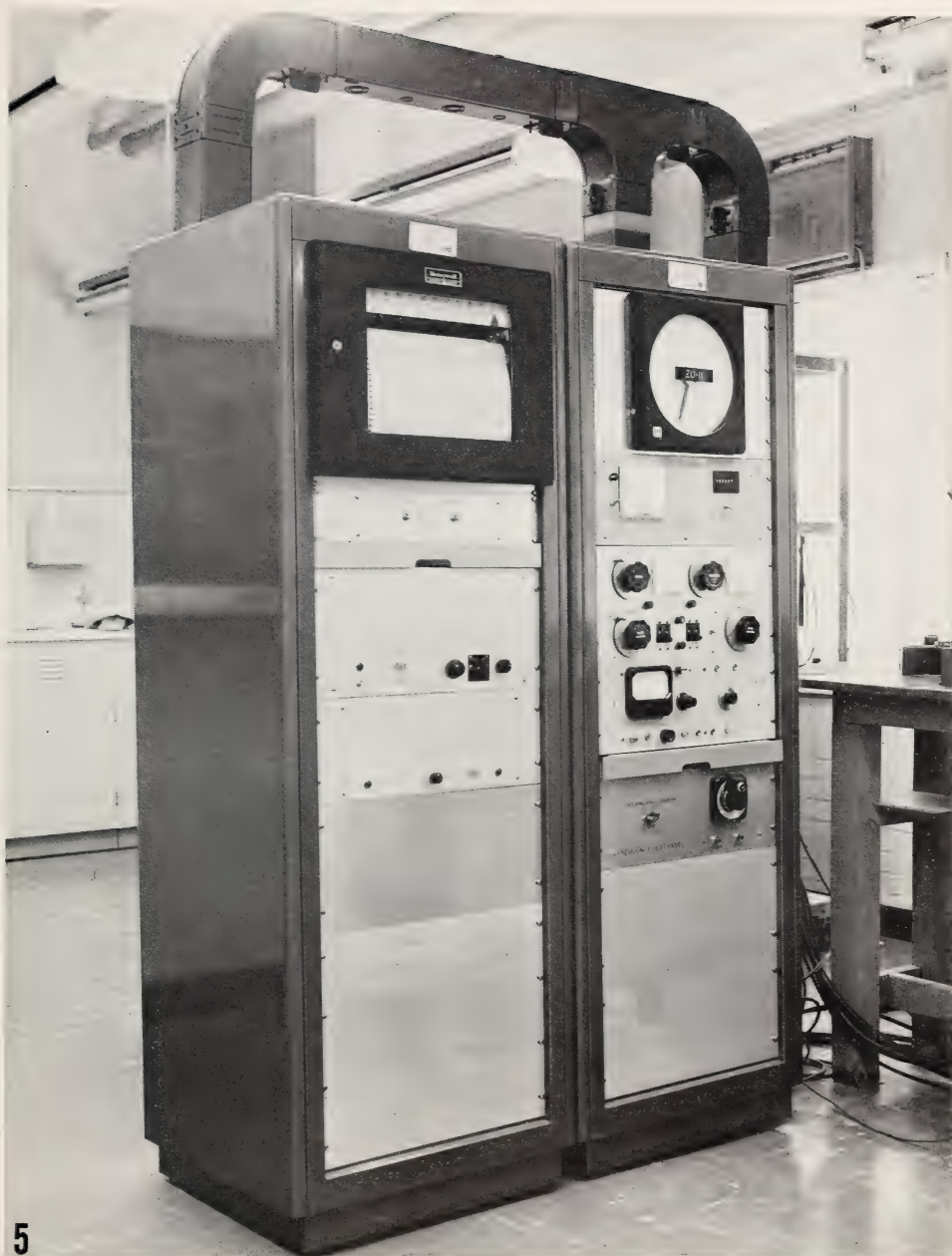


FIGURE 5.—Instrumentation for B- or C-series rotors. *Left rack contains (top to bottom): 1) recorder, 2) switches for gradient pump and accessory, 3) optical density converter including range switch, and 4) hydrogen and tungsten lamp controls. Right rack has (top to bottom): 1) Speedomax rpm indicator, 2) Lectro-counter integrator panel with counter, 3) centrifuge controls (temperature, pressure, above; speed controls and on-off controls, below), 4) frequency meter, and 5) frequency test panel. The last two components are used to calibrate the rpm device.*



FIGURE 6.—Disassembled B-IV rotor with bearing and seal. (a) End cap; (b) seal; (c) bearing and damper; (d) bottom end cap; (e) rotor chamber; and (f) core.



FIGURE 7.—Positioning of the B-IV rotor in centrifuge chamber located in glove box.  
Water pump in background (*right*).



FIGURE 8.—Rotor assembly with cooling, oil, edge, and center lines attached.



9

FIGURE 9.—Rotor assembled outside centrifuge, showing seal, damper bearing, and all lines attached.

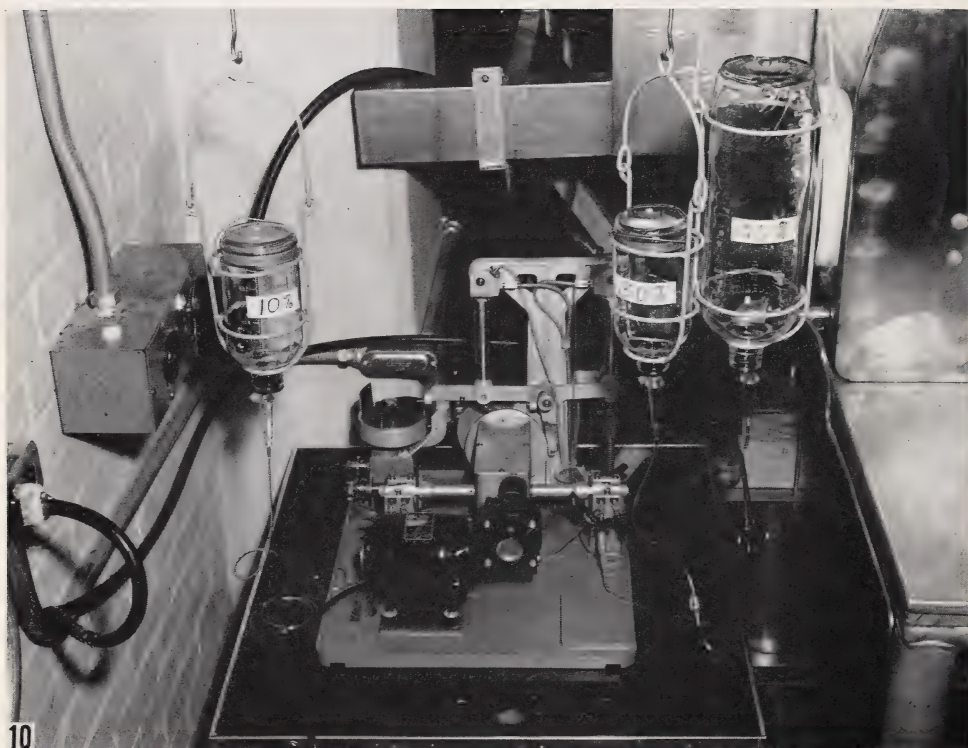


FIGURE 10.—Gradient pump assembly, at rear of glove box, with typical tissue gradient scheme. Program cam, *left rear*; glove box, *right*. Lines used for connection of gradient solution to pump are intravenous injection sets (for 10%, Cutter No. 860-01 or Abbott No. 4622; for 30-55%, Cutter No. 871-00 or Abbott No. 4656).

## Zonal Rotors With Removable Seals: Rotors B-X and B-XI<sup>1</sup>

H. P. BARRINGER,<sup>2</sup> N. G. ANDERSON, C. E. NUNLEY, K. T. ZIEHLKE, and W. S. DRITT, *Technical Division, Oak Ridge Gaseous Diffusion Plant,<sup>3</sup> and the Biology Division, Oak Ridge National Laboratory,<sup>3</sup> Oak Ridge, Tennessee*

### SUMMARY

Two removable-seal zonal rotors, designated B-X and B-XI, have been built and successfully tested for large-volume rate-zonal or isopycnic-zonal centrifugation.—*Nat Cancer Inst Monogr* 21: 165-174, 1966.

THE INITIAL studies in the development of a new biophysical tool must of necessity be directed toward the exploration of principles and the construction of suitable test instruments. If these are successful, then simpler revisions of these tools having comparable resolution may be designed. This paper is concerned with the development of simple zonal rotors for use in existing commercial centrifuges. No modification of the instrument or close attendance during centrifugation is required.

In the previous intermediate-speed B series rotors, the attached upper seal required the use of a bearing, a continuous seal coolant, and an oil supply. The possibility of using a removable seal for loading and unloading the rotor at relatively low speed has been previously suggested (1). This paper describes two new removable-seal rotors (B-X and B-XI) designed for either rate-zonal or isopycnic-zonal centrifugation. They are not readily adaptable to continuous flow centrifugation, as is the case for the B-IV through B-IX centrifuges, except at relatively low speeds.

These rotors have been constructed from conventional aluminum alloy and from a new high-strength steel. The steel rotor is more efficient than the aluminum one but requires that a number of corrosion problems be examined and the feasibility of platings and other resistant finishes be explored.

---

<sup>1</sup> This research performed under the Joint National Institutes of Health-Atomic Energy Commission Zonal Centrifuge Development Program which is supported by the National Cancer Institute, the National Institute of Allergy and Infectious Diseases, and the U.S. Atomic Energy Commission.

<sup>2</sup> Present address: Stellite Division of Union Carbide Corporation, Kokomo, Indiana.

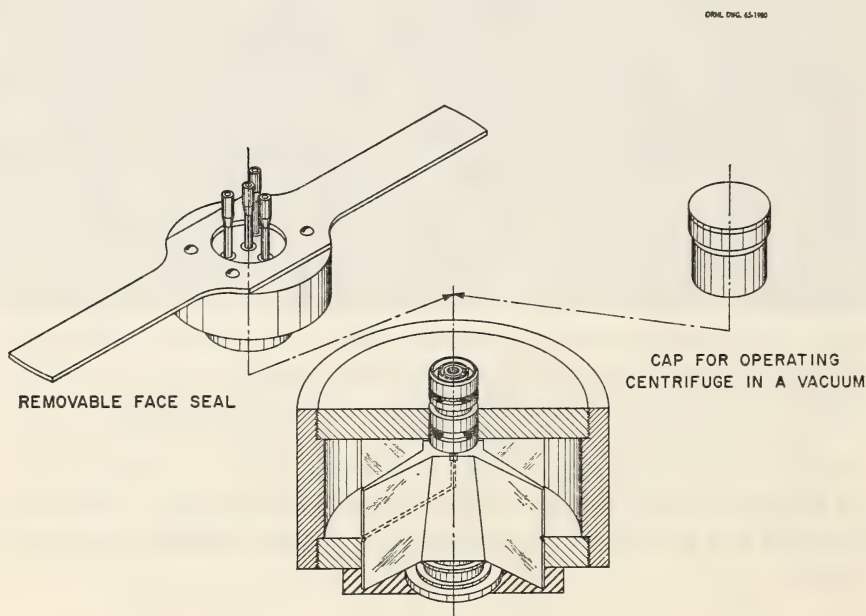
<sup>3</sup> Operated for the U.S. Atomic Energy Commission by Union Carbide Corporation.

## DESIGN CONSIDERATIONS

In the B-IV zonal centrifuge rotor (2, 3), rotor diameter was limited by the yield strength of the aluminum rotor shell at 40,000 rpm. Greater capacity could be gained only by increasing the rotor length to give a configuration requiring an upper shaft and bearing (4). To eliminate the upper shaft and to make the rotor self-balancing, rotor diameter should be somewhat greater than rotor length (4). Under these conditions large capacity can only be attained by increasing the diameter (and proportionately the length), *i.e.*, by using stronger structural materials at the highest stress levels practical.

One-piece configurations having very desirable structural properties have been evolved (5), but fabrication is not practical at present. During operation of a centrifuge at high speed, the chamber wall expands radially more than the end caps, resulting in movement of one relative to the other. This movement can result in loss of alignment or concentricity of the rotor. In addition, the design must insure that a leaktight seal is maintained at all speeds. The basic configuration of the B-XI rotor, shown in text-figure 1, consists of a hollow cylinder with two end caps.

The core (text-fig. 1) comprises 4 tapered septa that divide the rotor chamber into sector-shaped compartments and contain flow lines to the



TEXT-FIGURE 1.—Isometric drawing of B-XI zonal rotor. Removable face seal is attached to the rotor during loading and unloading at low speed. Before acceleration to high speed, the seal is removed and replaced with the cap. The latter is removed before unloading is started at the completion of the run, and the seal replaced.

rotor edge. To channel the gradient into the center exit lines during unloading, the core has flat surfaces that slant in toward the axis of rotation. This core-face slope serves to deflect particle zones upward at the same time that they are concentrated toward the center line of the face due to the parabolic curvature of the zone. A given density zone, therefore, reaches the core face first at the lower corners, and moves up toward the center of the upper edge of the core face to the exit line. This core has no critical unloading speed and functions at a centrifugal force as low as  $1 \times g$ .

### THE REMOVABLE SEAL

An "A" type seal (6) has been modified for attachment or removal from the rotor at speeds from 1000 to 7000 rpm (fig. 1). The seal slips over a central arbor, which extends through the rotor and core. The aligning ball bearing in the seal housing is accelerated to speed by friction, and a seal surface is obtained against the flat rotating Rulon<sup>3</sup> slides and the non-rotating metal stator. The seal housing is held in position by two flexible arms that attach to the centrifuge refrigeration chamber. All operations involving the seal and cap are performed while the rotor is spinning. After the gradient and sample have been introduced into the rotor, the seal is removed by hand and replaced by a cap that prevents evaporation from the rotor during operation in a vacuum. The rotor chamber is then closed and evacuated before acceleration to high speed. When centrifugation has been completed, the rotor is decelerated to unloading speed (500–3000 rpm) and the seal reattached for unloading of the rotor contents by pumping dense fluid to the rotor edge so that the rotor contents are displaced radially inward and then out through the seal.

### ROTOR B-X

The ratio of  $I_{\text{spin}}/I_{\text{transverse}}$  (4) in the B-X rotor is 1.35, similar to that for an angle-head rotor. The rotor chamber contains 685 ml of fluid when completely filled. The rotor components and the assembled rotor are shown in figures 2 and 3. The aluminum test model (7075 aluminum with a T6 heat treatment) may be spun to 31,200 rpm with sucrose gradients. The B-X rotors constructed from Maraging steel may be spun at 40,000 rpm ( $119,000 \times g$  at  $R_{\text{max}} = 6.67$  cm) with a cesium chloride gradient having a maximum density of 1.7. Other operating speeds are shown in table 1.

---

<sup>3</sup> Obtained from the Dixon Corporation, Bristol, R.I.

TABLE 1.—Maximum speeds for B-X and B-XI rotors

Medium	Density	7075-T6 aluminum				18% Nickel Maraging steel			
		Spin frequency (rpm)		$g$ 's at $R_{max}$		Spin frequency (rpm)		$g$ 's at $R_{max}$	
		B-X	B-XI	B-X	B-XI	B-X	B-XI	B-X	B-XI
CsCl	1.7	30,300	22,200	68,000	48,700	40,000	30,000	119,000	89,500
Sucrose	1.2	31,200	23,500	73,500	54,600	42,000	30,300	131,000	95,200
Water	1.0	33,200	24,800	82,100	61,300	43,000	31,800	138,000	101,000

## ROTOR B-XI

The B-XI rotor is comparable in volume to the B-IV zonal centrifuge rotor (2, 3) and resembles the B-X in configuration, but has a larger sedimentation path than either. The aluminum version has been used in experimental studies (7) to 24,000 rpm with sucrose solutions. The Maraging steel version is designed for operation at 30,000 rpm ( $89,500 \times g$  at  $R_{\max} = 8.89$  cm) with 1725 ml of a gradient having a maximum density of 1.7. Other operating speeds are shown in table 1. At top speed this rotor will store 590,000 ft-lb of energy. The components of the disassembled rotors are shown in figure 4.

## CORROSION STUDIES

Stress corrosion has been observed in 7075-T6 aluminum in concentrated cesium chloride at room temperature after immersion for only a few hours. The corrosion resistance of several other materials has therefore been examined. Several samples of polished beta titanium (160,000 psi bending stress level), Kanigen-plated 18 percent nickel Maraging steel (230,000 psi bending stress level), and low phosphorous electroless nickel-plated 18 percent nickel Maraging steel (230,000 psi bending stress level) at stress levels of 95 percent of the estimated yield strengths have accumulated over 6,200 hours test time without failure.

The 18 percent nickel Maraging steel, attractive because of its high strength, is subject to stress corrosion in cesium chloride and therefore requires some type of protection. However, beta titanium is not subject to stress corrosion and needs no protective coating.

Kanigen plating is free from minute cracks that exist in other plating materials, and it readily conforms to contours without build-up at corners. Furthermore, commonly used biological materials do not attack or become poisoned by nickel plating.

## TEMPERATURE CONTROL

Temperature control of the B-X and B-XI rotor is difficult because the rotor is operated in air initially. However, if the rotor is prechilled, the large rotor mass tends to reduce thermal gradients. A Lucite closure minimizes movement of air into and out of the centrifuge chamber during loading and unloading. The rotor chamber door also may be partially closed to leave a small opening for the tubing.

## OPERATION

The loading and unloading procedures are similar to those described for the B-IV rotor (2) except that the seal is removed as soon as the overlay solution is in the rotor. Care is taken to see that both lines to the seal

are clamped before the seal is removed, otherwise fluid will drain into the chamber when the seal surfaces part. The application of these rotors to specific biological separation problems is described in subsequent papers.

*Note added in proof:* Further experimental and design studies have resulted in additional simplification of rotors of this type. B-IX and X have therefore been redesigned as B-XIV and B-XV.

## REFERENCES

- (1) ANDERSON, N. G.: The zonal ultracentrifuge. A new instrument for fractionating mixtures of particles. *J Phys Chem* 66: 1984-1989, 1962.
- (2) ANDERSON, N. G., BARRINGER, H. P., BABELAY, E. F., NUNLEY, C. E., BARTKUS, M. J., FISHER, W. D., and RANKIN, C. T., JR.: The design and operation of the B-IV zonal centrifuge system. *Nat Cancer Inst Monogr* 21: 137-164, 1966.
- (3) ANDERSON, N. G., BARRINGER, H. P., BABELAY, E. F., and FISHER, W. D.: The B-IV zonal ultracentrifuge. *Life Sci* 3: 667-671, 1964.
- (4) BARRINGER, H. P.: The design of zonal centrifuges. *Nat Cancer Inst Monogr* 21: 77-111, 1966.
- (5) BOYLAND, D. A.: Hollow rotors and centrifuges. U.S. Patent No. 3,108,955 issued October 29, 1963.
- (6) ANDERSON, N. G., BARRINGER, H. P., CHO, N., NUNLEY, C. E., BABELAY, E. F., CANNING, R. E., and RANKIN, C. T., JR.: The development of low-speed "A" series zonal rotors. *Nat Cancer Inst Monogr* 21: 113-136, 1966.
- (7) AMBURGEY, J. W., JR., ANDERSON, N. G., and FISHER, W. D.: Experimental studies with the B-X and B-XI removable seal rotors. Unpublished studies.

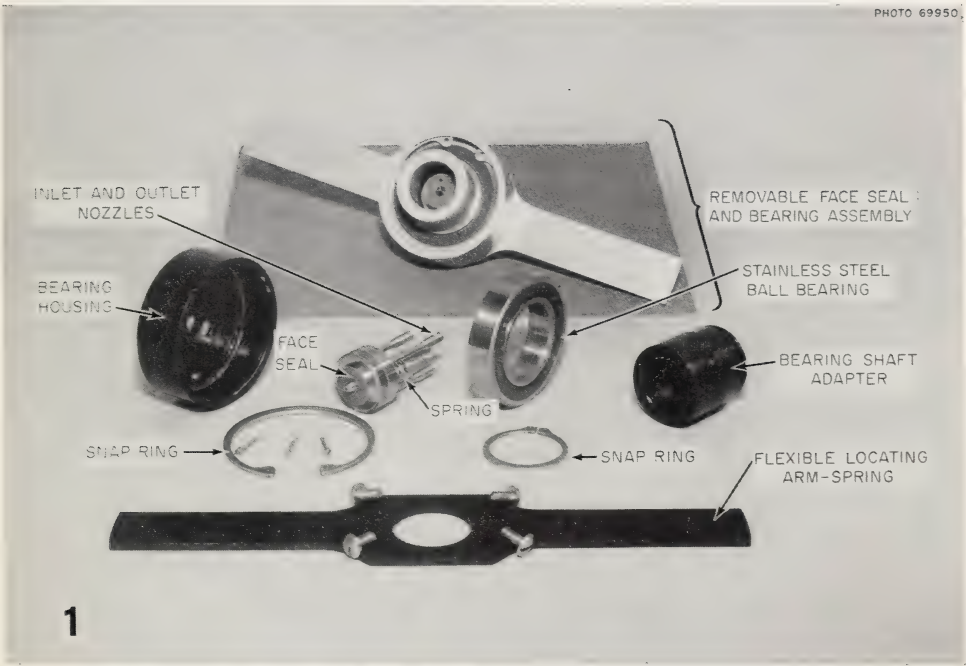


FIGURE 1.—Removable seal for B-X and B-XI rotors.

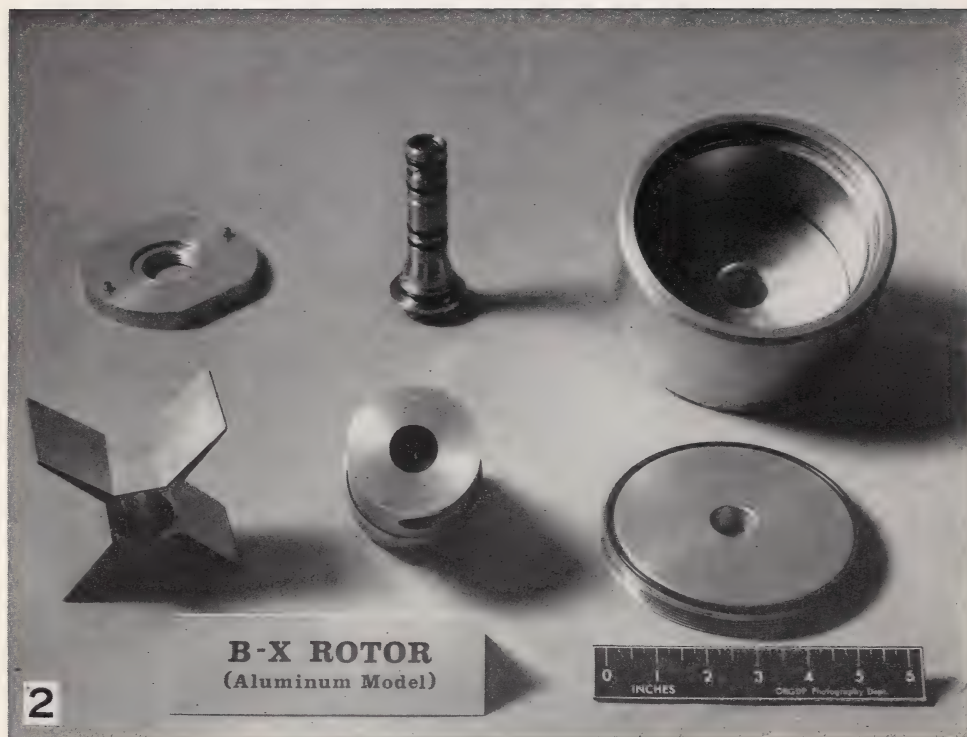


FIGURE 2.—Components of B-X rotor.

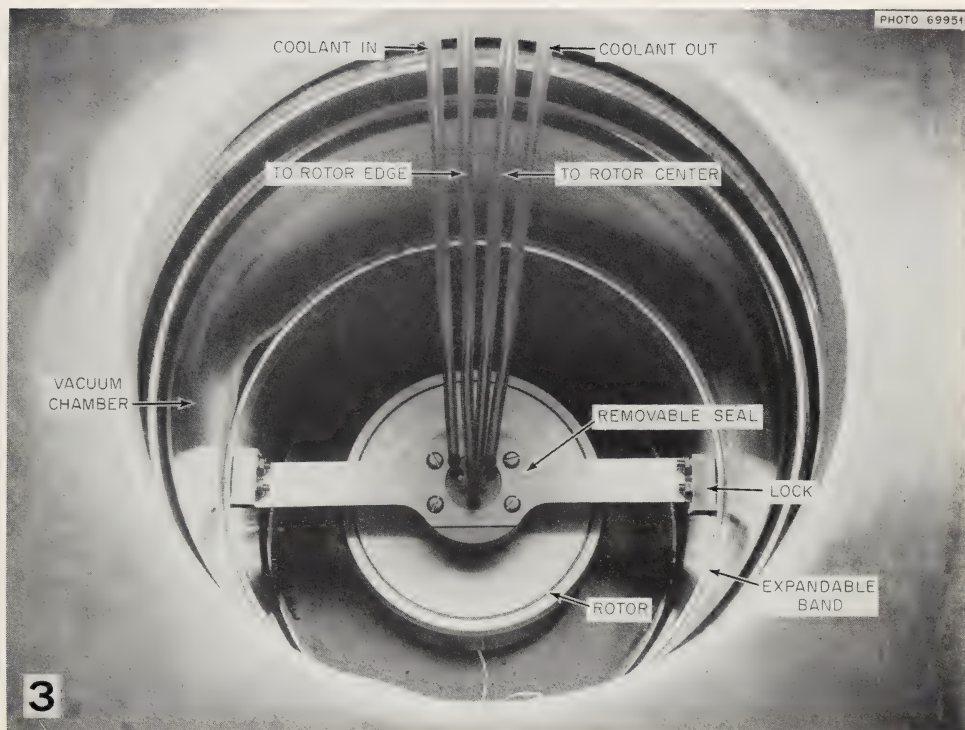


FIGURE 3.—Assembled B-X rotor and seal in centrifuge. The static portion of the seal is kept from rotating by attachment to a fixed band inside the centrifuge refrigeration chamber.



FIGURE 4.—Components of B-XI rotor.

## Digital Computation of Sedimentation Coefficients in Zonal Centrifuges<sup>1</sup>

BARBARA S. BISHOP, *Central Data Processing Facility, Oak Ridge Gaseous Diffusion Plant,<sup>2</sup> Oak Ridge, Tennessee*

### SUMMARY

A system for machine computation and readout of equivalent sedimentation coefficients ( $S^*$ ) in Svedberg units for several B-series zonal centrifuges has been developed using FORTRAN and the IBM-7090 computer. Input data includes the rotor temperature, volume of the sample layer and overlay, sucrose concentration in the collected fractions, volume of the collected fractions, rate of removal of liquid from the effluent rotor stream for simultaneous analysis by automated analytical devices, the rotor temperature, the integral of  $\omega^2 dt$ , the volume in the fluid line between the rotor core and the point of sample collection, the dry particle densities to be used in making calculations of  $S^*$ , and an indication of whether the

sample was introduced as a homogeneous suspension, or in a short gradient. The computer program includes equations for determining the density and viscosity of the sucrose solutions in each recovered fraction at the temperature of centrifugation, the radius of the mass center of the sample layer and of the edge of each collected fraction when in the rotor, and the equivalent sedimentation coefficient,  $S^*$ , for the middle of each collected fraction. A subroutine is included for plotting the position curves for a series of families of particles where each family includes particles having one equivalent sedimentation coefficient at 20° C in water and a range of dry densities.—*Nat Cancer Inst Monogr* 21:175-188, 1966.

RATE ZONAL centrifugation in sucrose gradients centrifuged in swinging bucket rotors has been extensively used to determine the sedimentation constants of viruses, mitochondria, microsomes, ribosomes, nucleic acids, and proteins (1-3).

While zonal centrifuges were initially developed to achieve preparative separations over the same size range (4), the data obtained may also be used to calculate sedimentation coefficients. In rotors A-V, -VI, -IX, and -XII, the sedimentation rate of a visible particle band may be observed while the rotor is spinning (5). In other rotors used for rate zonal separations (B-IV, -X, -XI, and -XII), only the initial and final positions of particle zones in the gradient are known (4, 6).

<sup>1</sup> This research performed under the Joint National Institutes of Health-Atomic Energy Commission Zonal Centrifuge Development Program which is supported by the National Cancer Institute, the National Institute of Allergy and Infectious Diseases, and the U.S. Atomic Energy Commission.

<sup>2</sup> Operated for the U.S. Atomic Energy Commission by the Nuclear Division of Union Carbide Corporation.

The sedimentation rate of a particle in a liquid density gradient is a function of the amount and duration of the applied acceleration, the size and density of the particle, and the density and viscosity of the medium. In a homogeneous medium  $m$ , at temperature  $T$ , the sedimentation coefficient  $s_{T,m}$  is given by the equation (3, 7):

$$s_{T,m} = \frac{(dR/dt)}{\omega^2 R} \quad [1]$$

where  $\omega$  is the angular velocity in radians per second,  $R$  is the distance from the rotor center to the particle, and  $dR/dt$  is the velocity of the particle. The radius is given as  $R$  in this work in place of  $r$  (4) since the computer printout does not include lower case letters.

For comparative purposes the sedimentation coefficient,  $s$ , observed experimentally is usually converted to a standard state defined as the rate in water at 20°C using the equation (3, 7):

$$s_{20,w} = s_{T,m} \frac{\eta_{T,m}(\rho_p - \rho_{20,w})}{\eta_{20,w}(\rho_p - \rho_{T,m})} \quad [2]$$

where  $\eta_{T,m}$  is the viscosity in poises of the medium at the temperature  $T$ ,  $\eta_{20,w}$  is the viscosity of water at 20°C,  $\rho_p$  is the density of the particle in solution,  $\rho_{T,m}$  is the density of the medium at temperature  $T$ , and  $\rho_{20,w}$  is the density of water at 20°C. Since the density of most particles of biological interest varies little with temperature,  $\rho_p$  is considered constant (8). Equations 1 and 2 are applicable to sedimentation in a sucrose gradient, providing the changes in viscosity ( $\eta_{T,m}$ ) and density ( $\rho_{T,m}$ ) are considered (1, 3, 9-11).

Equations 1 and 2 may be combined to give:

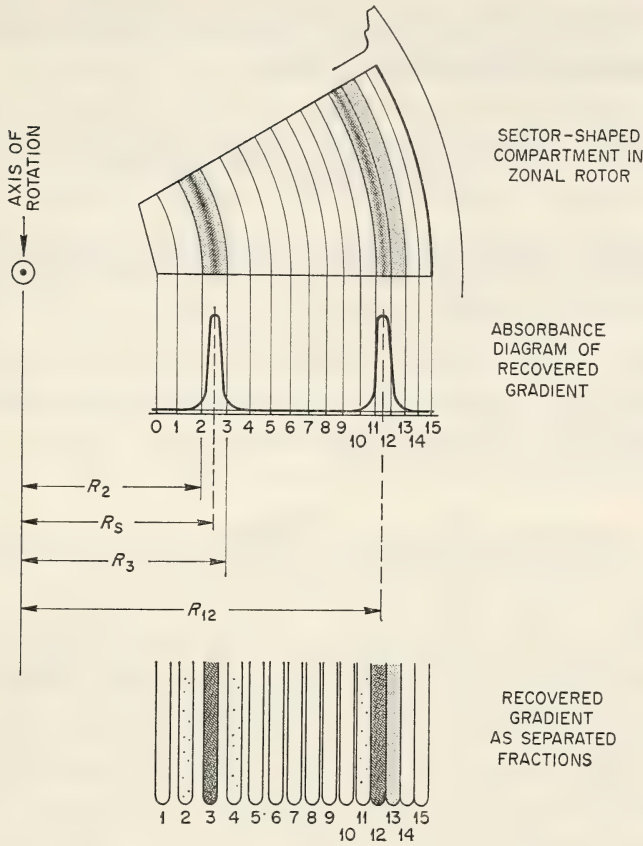
$$s_{20,w} = \frac{(dR/dt)}{\omega^2 R} \frac{\eta_{T,m}(\rho_p - \rho_{20,w})}{\eta_{20,w}(\rho_p - \rho_{T,m})} \quad [3]$$

Methods for evaluating  $s_{20,w}$  in sucrose density gradients have been presented (1, 3, 9-11), and the method described here is adapted from the trapezoidal integration used by Martin and Ames (3). The relation between the ultraviolet absorbance diagram (12), the collected fractions, and the initial positions of zones in the rotor are shown in text-figure 1.

The radius,  $R$ , associated with a given fraction is for the outer edge of the toroidal volume occupied by that fraction when in the rotor. The mass center of the sample zone,  $R_s$ , is calculated by the computer program.

Equation 3 may be rewritten as

$$\omega^2 s_{20,w} dt = \frac{(\rho_p - \rho_{20,w})\eta_{T,m}}{(\rho_p - \rho_{T,m})\eta_{20,w}} \cdot \frac{1}{R} dR \quad [4]$$



TEXT-FIGURE 1.—Relation between the position of zones in the rotor during rotation, ultraviolet absorbance diagram, and collected fractions. Radii are indicated for the end of collected fractions and to the center of the sample zone. *Note* that the center of the sample zone need not be in the center of a fraction as shown.

Integrating the left side of equation 4 gives

$$\int_0^t s_{20,w} \omega^2 dt = s_{20,w} \omega^2 t \quad [5]$$

The right side of equation 4 may be approximated as follows:

$$\frac{(\rho_p - \rho_{20,w})}{\eta_{20,w}} \int_{R_s}^{R_i} F(R) dR = \frac{(\rho_p - \rho_{20,w})}{\eta_{20,w}} \sum_{R_s}^{R_i} F(R_i) (R_i - R_{i-1}) \quad [6]$$

where  $i$  denotes a specific fraction,  $R_i$  the radius at the end of that fraction,  $(R_i - R_{i-1})$  the width of the fraction, and  $R_s$  the radius of the mass center of the sample zone.

Using the equations derived by Barber (13), the density and viscosity of sucrose solutions corresponding to different levels in the gradient are determined and  $F(R)$  evaluated where:

$$F(R) = \frac{\eta_{T,m,f_i}}{[\rho_p - \rho_{T,m,f_i}] (R_i + R_{i-1})/2} \quad [7]$$

In the original method of Martin and Ames (3), a second term is included in equation 6 to take care of the fact that sedimentation coefficients were determined for particles at fixed points along the gradient (along the radius  $R$ ), and that the sucrose concentrations are given for the same fixed points. It was necessary, therefore, to average  $F(R)$  between two consecutive points, and use the average to determine the sedimentation rate of a particle between the two points.

Combining equations 5, 6, and 7:

$$s_{20,w} = \frac{\rho_p - \rho_{20,w}}{\omega^2 t \eta_{20,w}} \sum_{R_s}^{R_i} \frac{\eta_{T,m,f_i}}{(\rho_p - \rho_{T,m,f_i}) (R_i + R_{i-1})/2} (R_i - R_{i-1}) \quad [8]$$

The data actually obtained are the sucrose concentration in each collected fraction, the volume of each fraction, the relation between absorbance and the collected fractions, the temperature of the run, a value for the integral of  $\omega^2 dt$  obtained electronically (12), and the volume of fluid in the lines between the rotor core and the point of fraction collection. Taking the terms in equation 8 in order, therefore:  $\rho_p$  is known or assumed from separate studies,  $\rho_{20,w}$  and  $\eta_{20,w}$  are constants, and  $\omega^2 t$  is determined by the electronic integrator.

The terms beyond the summation sign describe the physical parameters of each fraction collected as they existed in the rotor during centrifugation. The viscosity,  $\eta_{T,m,f_i}$ , and the density,  $\rho_{T,m,f_i}$ , refer to the average viscosity and density of the medium in a collected fraction,  $f_i$ , since the fraction tube is thoroughly mixed before the refractive index is determined. However equivalent sedimentation coefficients are calculated for the end (last drop) of each fraction.

The position of a fraction in the centrifuge is determined from an equation (see below) which relates the volume collected to radius. The radii calculated are the radii for the last drop collected in each tube. The fraction  $f_i$ , therefore, extends from a radius  $R_{i-1}$  to  $R_i$  and the width of the band is equal to the difference between these two values. The centrifugal force, which is directly proportional to the radius, is calculated to the middle of each zone and is therefore proportional to  $\frac{(R_i + R_{i-1})}{2}$ .

The computer program developed to calculate  $s_{20,w}^*$  allows for two different modes of operation when unloading the centrifuge. In the first, the entire rotor contents are unloaded into collecting tubes. The radii

calculated for the beginning and end of a given fraction are for a toroidal section of the rotor volume having the same volume as the fraction collected. In the second mode of operation, only part of the rotor effluent is collected, the rest being diverted at a known and constant rate to an automated analytical system for either chemical or enzymatic analysis (14, 15). The time required to fill each fraction collector tube is recorded and used to calculate the amount of fluid diverted for analysis from each fraction.

The equivalent volume in the rotor represented by each fraction is thus equal to:

$$V_{fr} = V_{fc} + At_v \quad [9]$$

where  $V_{fr}$  is the equivalent volume in the rotor represented by fraction  $f$ ,  $V_{fc}$  the volume of the fraction actually collected,  $A$  the diverted flow rate in ml per minute, and  $t_v$  is the time in minutes required to collect the fraction.

In practice, the position of observed particles in the recovered gradient is not used as a basis for calculations, rather the sedimentation coefficient which a particle would have had if found in a given position and if it had a certain dry density is computed. These are termed equivalent sedimentation coefficients,  $s^*$  ( $S^*$  when given in Svedberg units).

The equations used in this program apply directly to particles described as belonging to Case I (4) which are ideal, anhydrous, spherical, and unaffected by changes in the suspending medium. As pointed out by Trautman (personal communication) the equations also apply to Case II (hydrated, nonosmotic particles) provided that the water of hydration is always in equilibrium with, and has the same density as, the gradient solution in which the particle is suspended.

Since sedimentation coefficients are calculated for distances from the starting zone, the latter must be accurately known. When the sample is introduced as a homogeneous suspension, the volumetric center is considered to be at the radius calculated for a volume equal to the volume of the overlay plus one half the volume of the sample. In some studies, the starting sample has been introduced as a double gradient increasing linearly with volume in sucrose concentration, and decreasing linearly in particle concentration. When the latter type of starting sample is used, the mass center of the starting zone is calculated as being at the radius of a volume equal to the overlay volume plus 0.29 times the sample volume.

## THE PROGRAM

We require a program to calculate sedimentation coefficients,  $S^*$ , corresponding to the end of from 40 to 100 fractions and to report this value correlated with each fraction, using equation 8.

Since computer storage of large tables is not feasible, equations relating the concentration of sucrose (w/w) to density and viscosity as a function of temperature are required. These have been derived by Barber (13). The program at present is applicable only to sucrose gradients but does permit the addition of data for solutions other than sucrose, up to a total of nine solutions. The program also provides for the expansion of rotor types, with a maximum limit of 99. Each time a new rotor is designed it will be necessary to insert the equations to calculate the incremental radii in terms of incremental volume.

The program was written in the FORTRAN II computer language and executed on an IBM-7090 computer. A FORTRAN glossary and listing are not included here but are available from the Biophysical Separations Laboratory.

The program is designed to accept data for a maximum of 100 tubes (cuts). If the quantity of data exceeds this value, the calculations will be completed for the first 100 values and the balance of the data will be ignored.

If further experimental conditions should increase the quantity of data, only minor program changes will be necessary.

The B-II and B-IV rotors have already been incorporated into the program with the following general equations used to calculate the radii: B-II Rotor

$$V = 81.273 R^2 - 74.506 R - 102.082 \quad [10]$$

where  $R$  is the radius in centimeters and  $V$  is the volume in cubic centimeters.

B-IV Rotor

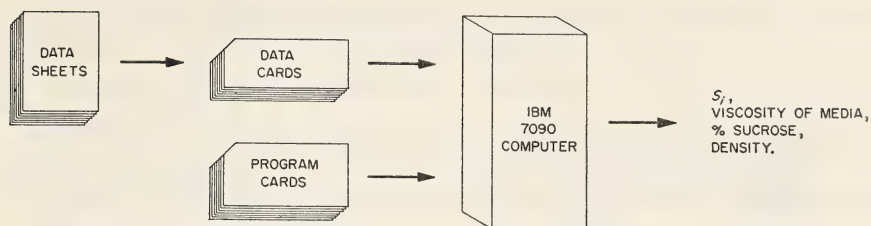
$$R = (\sqrt{0.0018061 V + 0.3282} + 0.16567) \times 2.54 \quad [11]$$

where  $R$  is the radius in centimeters and  $V$  is the volume in cubic centimeters.

The radii are measured from the center of the rotor in all cases. The radius for the center of the sample zone,  $R_s$ , is calculated from the sample and overlay volumes, and the first sedimentation coefficient is calculated for the end of the fraction containing the middle of the sample. The volume-radius relations for rotors B-X and B-XI are calculated by using a more generalized set of equations.

## PREPARING INPUT DATA

A general scheme of data computation is shown in text-figure 2, while a convenient form for presenting the run data is shown in text-figure 3. Although a representative number of cut cards are shown on the data form in text-figure 3, up to 100 may be included. Each case or run is ended with a card with a 998 cut number. Several cases may be submitted



TEXT-FIGURE 2.—Diagrammatic presentation of data-computing scheme.

during one computer run, which is ended with a cut number of 999. A schematic diagram of an input data deck is shown in text-figure 4. If the concentration is negligible, a small positive number (*i.e.*, 0.0000001) is entered for concentration. Each run is also assigned some positive numeric run number. For purposes of plotting, all four of the particle densities are submitted in descending order.

### DISPLAYING OUTPUT DATA

The radius from the center of the rotor to the end of each tube is shown as the first part of the output (text-fig. 5). The mass, radius, and tube number for the center of the sample are given, for example, in this way:

THE SAMPLE MASS CENTER VOLUME IS 316.00 ml  
 THE MIDDLE OF THE SAMPLE ZONE RADIUS IS 2.772 cm  
 THE MIDDLE OF THE SAMPLE ZONE IS IN TUBE 8.10

The calculated sedimentation coefficient for each particle density is then presented. Text-figure 6 is a sample of one density, giving a tabular correlation of cut number, sucrose concentration, viscosity (at 5° C), density (at 5° C), and sedimentation coefficient ( $s^*_{20,w}$ ). The summation page shown in text-figure 7 gives the interpolated values of even sedimentation coefficients correlated to the fractional tube number for each of the input particle densities.

A recently added plotting subroutine, labeled PLTSED, is controlled by column 77 of the identification card for each run. If column 77 is 0 or blank, no plotting will occur; if column 77 is 1, the plotting will be given as binary output. Text-figure 8 is a sample plot. The ORGDP Plotting Package for use with Benson-Lehner plotter is called PLTSED and includes the subroutine BLSCL, ORBL1, and RANGE.

A new even-sedimentation-coefficient subroutine, called SEDEVN, calculates the value that most nearly approaches the center of the tube. (The sample tube is excepted, and the criteria is the middle of the sample zone.) A value is calculated for each tube at the highest density level, and other densities are calculated from the same coefficient.



On the sheet following the last page of output, the number of runs processed in the current job is reported as:

#### LOGICAL RUNS COMPUTED IN THIS JOB.

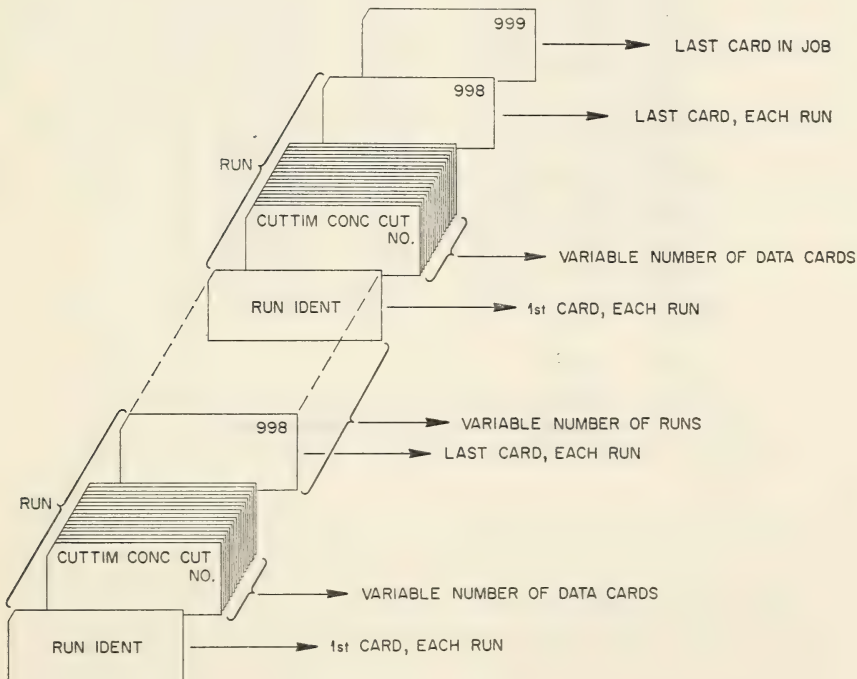
Normally this message will result when all runs are completed; however, some data errors will terminate the computer run with appropriate error messages and only the completed runs will be included in the final message.

### PROGRAM CHECKS

The program may be checked by inserting dummy runs using a sucrose gradient having a negligible increment per fraction [(0.0001%) w/w, for example]. The sedimentation rate calculated to a certain position in the rotor can then be checked using the equation:

$$s = \frac{\ln (R_2/R_1)}{\omega^2 t} \quad [12]$$

When this has been done, the error was found to be less than 1 percent.



TEXT-FIGURE 4.—Data deck for zonal centrifuge computer program.

NATIONAL INSTITUTE OF HEALTH - U.S. ATOMIC ENERGY COMMISSION ZONAL CENTRIFUGE PROGRAM					
ROTOR	E-IV	EXPERIMENT NUMBER	-C	RLN NUMBER 355	DATE OF RUN MAY 26, 1965
ROTOR RADII					
CUT	RADIUS (CM)				
1.CC	1.972				
2.CC	2.116				
3.CC	2.248				
4.CC	2.372				
5.CC	2.488				
6.CC	2.598				
7.CC	2.702				
8.CC	2.802				
9.CC	2.898				
10.CC	2.990				
11.CC	3.079				
12.CC	3.166				
13.CC	3.249				
14.CC	3.331				
15.CC	3.410				
16.CC	3.487				
17.CC	3.562				
18.CC	3.635				
19.CC	3.707				
20.CC	3.777				
21.CC	3.846				
22.CC	3.913				
23.CC	3.979				
24.CC	4.044				
25.CC	4.108				
26.CC	4.170				
27.CC	4.232				

TEXT-FIGURE 5.—Output of radius data.

NATIONAL INSTITUTE OF HEALTH - U.S. ATOMIC ENERGY COMMISSION ZONAL CENTRIFUGE PROGRAM  
 EXPERIMENT NUMBER -0 RUN NUMBER 355 DATE OF RUN MAY 26, 1965

ROTOR B-IV		DENSITY (1 CF 4) # 1.400	
CUT NO.	PERCENT SUCROSE	DENSITY	VISCOSITY
6	9.75CCCC	1.036785	2.007644
7	11.1CCCCC	1.045273	2.157659
8	12.7CCCCC	1.052089	2.292472
9	13.6CCCCC	1.055963	2.374816
10	14.4CCCCC	1.059429	2.452314
11	15.0CCCCC	1.062044	2.513270
12	15.6CCCCC	1.064671	2.576794
13	16.5CCCCC	1.068635	2.677193
14	17.3CCCCC	1.072181	2.771940
15	18.4CCCCC	1.077095	2.911406
16	19.3CCCCC	1.081146	3.034119
17	20.0CCCCC	1.084316	3.135374
18	21.0CCCCC	1.088874	3.289593
19	21.9CCCCC	1.093006	3.438842
20	22.6CCCCC	1.096239	3.562370
21	23.5CCCCC	1.100421	3.731587
22	24.5CCCCC	1.105101	3.934582
23	25.1CCCCC	1.107925	4.064622
24	26.1CCCCC	1.112660	4.296407
25	27.0CCCCC	1.116951	4.522610
26	27.6CCCCC	1.119827	4.683559
27	28.5CCCCC	1.124165	4.941628
28	29.2CCCCC	1.127558	5.157368
29	30.1CCCCC	1.128939	5.456031
30	30.9CCCCC	1.132817	5.743622
31	32.2CCCCC	1.139177	6.261139
32	33.5CCCCC	1.145600	6.850343
33	35.4CCCCC	1.155139	7.868419
34	38.2CCCCC	1.169477	9.816936
35	40.9CCCCC	1.183644	12.419077
36	42.9CCCCC	1.194362	15.012031
37	47.4CCCCC	1.219201	24.270846
38	50.2CCCCC	1.235185	34.015846
39	52.7CCCCC	1.249814	47.560057
40	54.0CCCCC	1.257559	57.393756
41	55.3CCCCC	1.265401	69.987487

SECIMENTATION  
 CCEFFICIENT

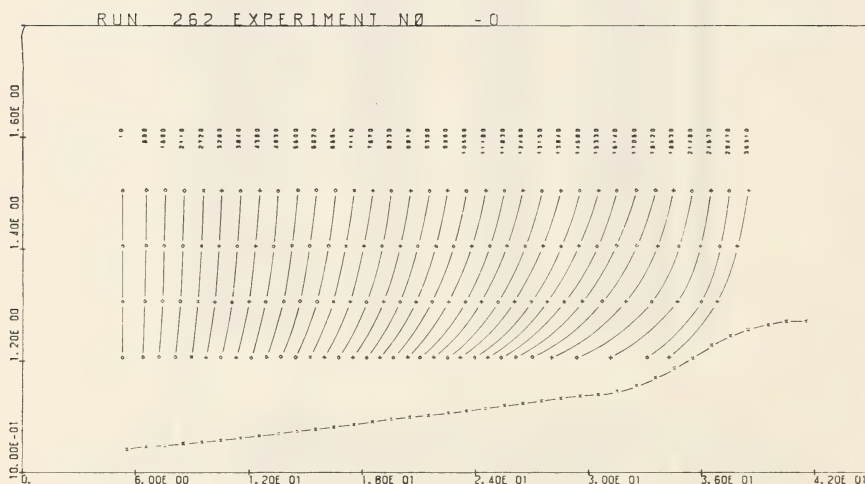
40.76640  
 101.27152  
 161.61296  
 220.19187  
 277.13719  
 332.21019  
 385.72382  
 438.82814  
 491.45767  
 544.75380  
 598.31318  
 651.66938  
 705.99928  
 761.16244  
 816.61025  
 873.24502  
 931.67110  
 990.44687  
 1051.43358  
 1114.44699  
 1178.26218  
 1244.53285  
 1312.45477  
 1382.57175  
 1455.33752  
 1534.35974  
 1620.63373  
 1720.90735  
 1850.42554  
 2020.69052  
 2232.01401  
 2611.47418  
 3181.47000  
 4036.43344  
 5100.41559  
 6443.99951

NOTE CONCENTRATION FOR TUBE 5 IS THE AVERAGE FOR THE SAMPLE ZONE IN TUBE 5.

TEXT-FIGURE 6.—Sample output for one particle<sup>17</sup> density (density 1.4).

NATIONAL INSTITUTE OF HEALTH - U.S. ATOMIC ENERGY COMMISSION ZONAL CENTRIFUGE PROGRAM					
ROTOR	E-IV	EXPERIMENT NUMBER	-C	RLN NUMBER 355	DATE OF RUN MAY 26, 1965
LOCATION IN SAMPLE TUBES					
SED.FAC.	1.4	1.3	1.2	1.1	
1C.	5.49	5.49	5.48	5.47	
8C.	6.65	6.60	6.50	6.22	
14C.	7.64	7.54	7.35	6.92	
20C.	8.65	8.49	8.19	7.38	
25C.	9.52	9.31	8.90	7.83	
31C.	10.59	10.31	9.77	8.35	
36C.	11.52	11.17	10.50	8.78	
42C.	12.64	12.21	11.39	9.29	
47C.	13.59	13.09	12.14	9.70	
52C.	14.54	13.97	12.89	10.11	
58C.	15.66	15.00	13.77	10.59	
63C.	16.60	15.86	14.49	10.99	
68C.	17.52	16.71	15.20	11.39	
74C.	18.62	17.72	16.03	11.85	
79C.	19.52	18.54	16.72	12.22	
85C.	20.59	19.51	17.51	12.65	
91C.	21.63	20.46	18.29	13.06	
97C.	22.66	21.36	19.04	13.45	
103C.	23.65	22.29	19.78	13.83	
109C.	24.61	23.17	20.49	14.17	
115C.	25.56	24.02	21.18	14.50	
122C.	26.63	24.98	21.94	14.86	
128C.	27.53	25.79	22.59	15.14	
135C.	28.54	26.69	23.32	15.46	
142C.	29.52	27.57	24.00	15.76	
150C.	30.58	28.55	24.75	16.09	
158C.	31.55	29.49	25.48	16.40	
167C.	32.52	30.47	26.26	16.73	
179C.	33.56	31.66	27.23	17.11	
194C.	34.55	32.89	28.39	17.53	
212C.	35.51	33.96	29.68	17.96	
241C.	36.50	35.16	31.38	18.49	

TEXT-FIGURE 7.—Summation of output page for zonal centrifuge computer program.



TEXT-FIGURE 8.—Sample of computer output plot (PLTSED). Particle densities are indicated along ordinate, with fraction numbers along abscissa. Each line in the family of curves indicates the position in the gradient of members of one hypothetical group of particles having the same sedimentation coefficients and a range of densities. The lower curve shows the density of the gradient as a function of gradient volume as calculated by the computer from the sucrose concentration of the recovered fractions. In subsequent papers in this volume, the computer output plot is positioned directly below the absorbance diagram of the recovered gradient and is aligned with it.

## DISCUSSION

A computer program has been developed for calculating sedimentation coefficients in sucrose gradients in zonal centrifuges. Initially only particles that do not behave osmotically or change volume in response to physiological variables (Case I and II) have been considered. Future studies will be concerned with programs applicable to the other particle cases previously described (4). While the equivalent sedimentation coefficients,  $S^*$ , are not rigorously applicable to the majority of subcellular particles actually separated, they are useful for comparative purposes, provided they are considered as approximations.

**Note added in proof:** Since the submission of this manuscript, a comprehensive paper on the equations for mass transport in rate-zonal centrifugation has appeared (V. N. Schumaker and J. Rosenbloom, *Fundamental Mass Transport Equations for Zone Sedimentation Velocity*, *Biochemistry* 4: 1005-1011, 1965).

## REFERENCES

- (1) DE DUVE, C., BERTHET, J., and BEAUFAY, H.: Gradient centrifugation of cell particles. Theory and application. *Progr Biophys* 9: 325-369, 1959.
- (2) BRITTEN, R. J., and ROBERTS, R. B.: High resolution density gradient sedimentation analysis. *Science* 131: 32-33, 1960.
- (3) MARTIN, R. G., and AMES, B. N.: A method for determining the sedimentation behavior of enzymes: Application to protein mixtures. *J Biol Chem* 236: 1372-1379, 1961.
- (4) ANDERSON, N. G.: An introduction to particle separations in zonal centrifuges. *Nat Cancer Inst Monogr* 21: 9-39, 1966.
- (5) ANDERSON, N. G., BARRINGER, H. P., CHO, N., NUNLEY, C. E., BABELAY, E. F., CANNING, R. E., and RANKIN, C. T., JR.: The development of low-speed "A" series zonal rotors. *Nat Cancer Inst Monogr* 21: 113-136, 1966.
- (6) ANDERSON, N. G.: The zonal ultracentrifuge. A new instrument for fractionating mixtures of particles. *J Phys Chem* 66: 1984-1989, 1962.
- (7) SVEDBERG, T., and PEDERSON, K. O.: *The Ultracentrifuge*. Oxford, Clarendon Press, 1940.
- (8) EDSALL, J. T.: *The Proteins* (Neurath, H., and Bailey, K., eds.). New York, Academic Press Inc., vol 1, part B, 1953.
- (9) THOMSON, J. F., and MIKUTA, E. T.: Enzymatic activity of cytoplasmic particulates of rat liver isolated by gradient centrifugation. *Arch Biochem* 51: 487-498, 1954.
- (10) THOMSON, J. F., and MOSS, E. M.: The intracellular distribution of a bound acid phosphatase of rat liver as studied by gradient centrifugation. *Arch Biochem* 61: 456-460, 1956.
- (11) THOMSON, J. F., and KLIPFEL, F. J.: Further studies on cytoplasmic particulates isolated by gradient centrifugation. *Arch Biochem* 70: 224-238, 1957.
- (12) ANDERSON, N. G., BARRINGER, H. P., BABELAY, E. F., NUNLEY, C. E., BARTKUS, M. J., FISHER, W. D., and RANKIN, C. T., JR.: The design and operation of the B-IV zonal centrifuge system. *Nat Cancer Inst Monogr* 21: 137-164, 1966.

- (13) BARBER, E. J.: Calculation of density and viscosity of sucrose solutions as a function of concentration and temperature. *Nat Cancer Inst Monogr* 21: 219-239, 1966.
- (14) SCHUEL, H., TIPTON, S. R., and ANDERSON, N. G.: Studies on isolated cell components. XVII. The distribution of cytochrome oxidase activity in rat liver brei fractionated in the zonal ultracentrifuge. *J Cell Biol* 22: 317-326, 1964.
- (15) SCHUEL, H., and ANDERSON, N. G.: Automated determination of protein in the presence of sucrose. *Technicon Sympos*, Sept. 16-18, 1964.

## **Continuous-Flow Centrifuges**



# Design of the B-V Continuous-Flow Centrifuge System<sup>1</sup>

H. P. BARRINGER,<sup>2</sup> N. G. ANDERSON, and C. E. NUNLEY, *Technical Division, Oak Ridge Gaseous Diffusion Plant,<sup>3</sup> and the Biology Division, Oak Ridge National Laboratory,<sup>3</sup> Oak Ridge, Tennessee*

## SUMMARY

A stable, closed, continuous-flow rotor (rotor system B-V) for operation at speeds up to 40,000 rpm has been developed, together with a fluid line seal that allows virus-containing solutions to flow into and out of the rotor without aerosol formation. The rotor is designed specifically for the isolation of virus particles from culture fluids where the mass of material to be isolated is very small (generally less than 1 g) relative to the total fluid volume. Design parameters were based on theoretical studies previously completed in this

laboratory. The virus-containing stream is pumped through a coaxial seal into a narrow annular space in the rotor where sedimentation occurs. The depleted stream returns close to the axis of rotation and flows out through the outer of the two coaxial seal lines. The seal has been modified to allow a small part of the inlet stream and entrained air to bleed out of the seal into the reservoir for the virus-containing sample solution to prevent the high back pressures occurring when air is entrapped in the rotor.—*Nat Cancer Inst Monogr* 21: 191–198, 1966.

BASED ON previous theoretical studies (1), a continuous-flow centrifuge rotor (rotor B-V of the intermediate-speed series) has been developed to explore the isolation of virus particles from large volumes of culture fluid, extracts of tissues, plasma, or natural waters.

## PRINCIPLES OF OPERATION

For the mass isolation of virus particles for experimental or vaccine purposes, a closed continuous-flow centrifuge system is desirable. The requirements are that the feed stream (a) moves continuously into the rotor without heating or spraying, (b) accelerates to the tangential velocity obtaining at the edge of the rotor chamber before entering it,

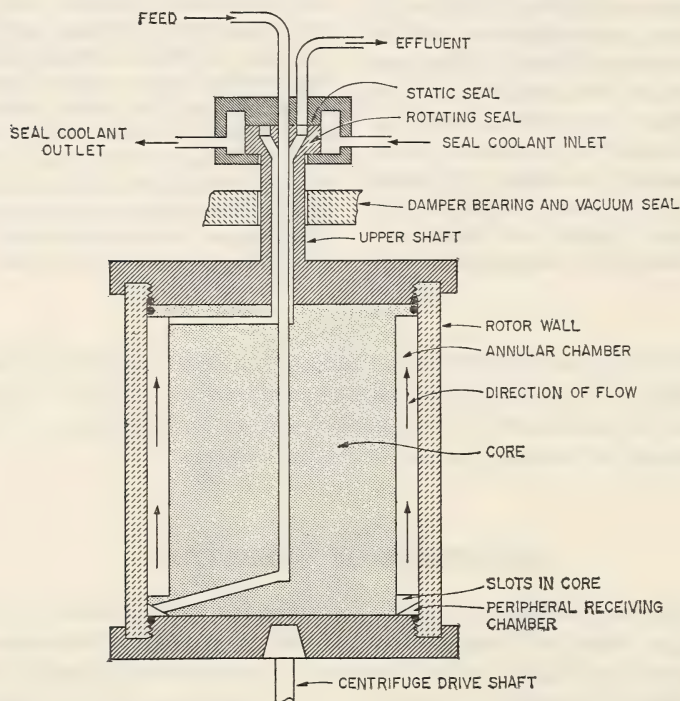
<sup>1</sup> This research performed under the Joint National Institutes of Health-Atomic Energy Commission Zonal Centrifuge Development Program which is supported by the National Cancer Institute, the National Institute of Allergy and Infectious Diseases, and the U.S. Atomic Energy Commission.

<sup>2</sup> Present address: Stellite Division of Union Carbide Corporation, Kokomo, Indiana.

<sup>3</sup> Operated for the U.S. Atomic Energy Commission by the Nuclear Division of Union Carbide Corporation.

and (c) moves evenly across the internal rotor wall surface. Finally, the sedimented virus particles should be easily recovered in sterile containers with no leakage of aerosols.

The configuration chosen is shown in text-figure 1. The virus-laden fluid is brought into the rotor through a face seal by appropriate channels machined in the core and is released into a small peripheral receiving chamber at the lower end of the rotor. The fluid then flows circumferentially to small axial slots in the lower edge of the core and upward in the annular chamber to the exit ports at the top of the core. The latter ports lead back up to the face seal where the fluid is conducted out of the rotor. It should be noted that the four exit channels at the top of the core are rotated  $45^\circ$  with respect to the axial slots at the bottom of the core. The total fluid path is therefore slightly greater than the length of the core. The fluid line seal has been modified to allow a small fraction of the incoming stream and any entrained air to bleed out of the seal into the reservoir. This helps eliminate the high back pressures occurring when air is entrapped in the rotor.



TEXT-FIGURE 1.—Schematic drawing of B-V continuous-flow centrifuge rotor and seal.

Close temperature control of the rotor and fluid stream is not obtained in practice. A change from  $5$  to  $6^\circ\text{C}$  in water flowing through the rotor at  $40,000$  rpm produces an effective force difference of  $2.2\text{ g per cm}^2$ .

We cannot assume that fluid will flow uniformly up the annular space between the core and rotor wall. If denser than the rotor contents, the fluid will rapidly traverse the length of the rotor close to the rotor wall; if lighter, the fluid will flow close to the surface of the core. In either case the fluid will tend to move as a thin sheet.

If the thickness of a fluid layer in a centrifugal field is increased, the time required to sediment particles having a given sedimentation rate will also increase. However, the increased dwell time attributable to the increased cross-sectional area almost exactly compensates for the increased thickness (1). Once the distance between the rotor wall and the core has been reduced to the point where the variation in centrifugal force across the gap is negligible, the width of the gap has little effect on rotor performance, provided it is not so narrow as to produce viscous resistance to flow. It is of little consequence, therefore, whether or not the incoming stream flows as a thin sheet along the core or the rotor wall because of temperature-induced density differences. The quantity of virus in the stream flowing through the rotor assumedly is so small that removing the virus causes no perceptible change in fluid density.

### THE B-V ROTOR

The B-V rotor system includes (a) a hollow centrifuge rotor dimensionally identical to the B-IV zonal rotor previously described (2, 3), (b) an internal core that forms an annular cavity inside the rotor, and (c) a high-speed contact seal for flowing fluids into and out of the rotor during centrifugation at speeds up to 40,000 rpm. The system (text-fig. 1) is driven by a Spinco Model L centrifuge that had been previously modified for use as a zonal centrifuge (2, 4).

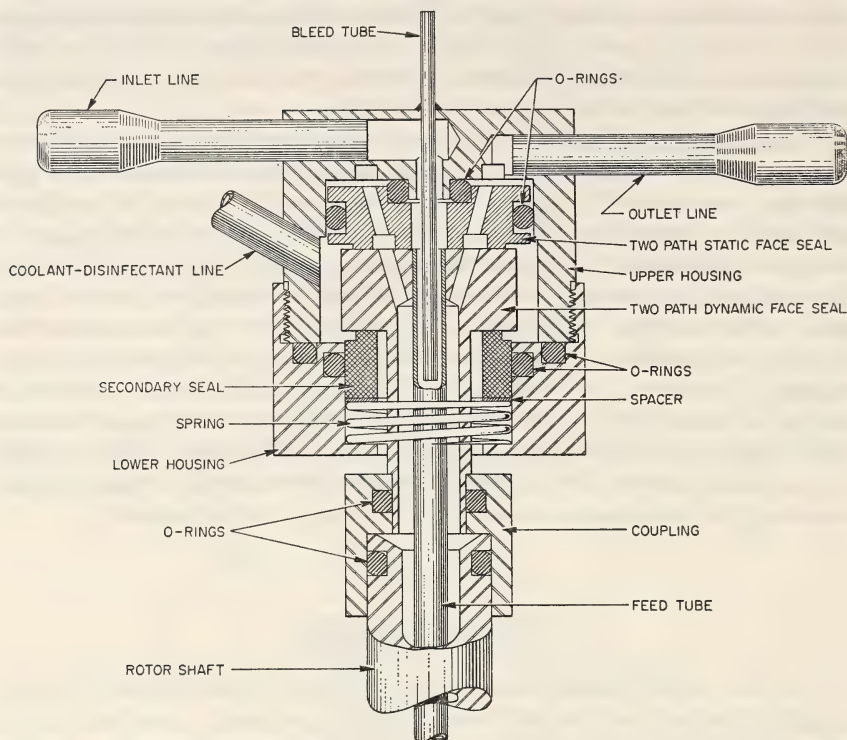
The rotating seal used on the B-V rotor permits one fluid stream to flow on the axis of rotation while the second stream flows as a concentric annular cylinder out-board of the axis of rotation. Text-figure 2 is a sectional view of the high-speed seal. Centrifugal force produces a pressure differential between the two fluid lines as given by the equation

$$\Delta P = \frac{\rho_i \omega^2 r_o^2}{2g} \quad (1)$$

where

- $\Delta P$  = pressure difference between the two seal lines in the rotating part of the seal
- $\rho_i$  = density of the fluid used
- $\omega$  = radial velocity in radians/sec
- $r_o$  = radius of outer fluid line
- $g$  = acceleration due to gravity.

### ZONAL CENTRIFUGE



TEXT-FIGURE 2.—Modified seal for continuous-flow centrifugation.

The radii of the fluid lines are 1.07 and 3.81 mm. If water is flowing through the rotor at 40,000 rpm, the pressure differential would be 18 psi. It is undesirable to pump against this pressure differential, since this would require higher seal face preloads with the accompanying greater wear rates and higher power losses. In the preferred flow direction, the feed stream moves through the center line directly along the axis of rotation and then outward to the bottom of the core. Thus the particle-containing stream has little chance to leak to the outside during continuous-flow centrifugation, since to do so it should also have to leak across the clarified stream flowing in the opposite direction. Rather, leakage that might occur will be more likely to originate from the relatively particle-free effluent stream. In any case seal leakage will be trapped in the cooling fluid surrounding the seal.

The seal has two sliding surfaces that preload each other to prevent leakage. These surfaces are also enclosed in a coolant and disinfectant chamber that prevents the formation of aerosols at high speeds. The seal is attached to the upper shaft of the centrifuge and is centered and the static portion prevented from rotating by a holder, which is an integral part of the damper bearing.

The rotor system is shown disassembled in figure 1. The core, 25 cm long, is separated by a distance of 0.08 cm from the inner rotor wall (radius 5.0 cm) giving a core : rotor ratio of 0.984. The rotor has been operated with seal exposed, or with the entire upper bearing seal, cooling circuit, and all associated lines in a sealed glove box. It has been operated to 40,000 rpm without excessive vibration with the new B-IV damper bearing (2, 3).

The absence of vanes in the annular chamber permits the rotor contents to swirl as the rotor is decelerated, thereby tending to scrub clinging particles from the rotor walls (5).

### RECOVERING SEDIMENTED MATERIAL

To recover sedimented material, the rotor is removed from the centrifuge and placed in a container (fig. 2), which matches the lower rotor end cap and prevents rotor rotation when the upper end cap is removed. The seal and upper end cap are placed in stainless steel containers for disinfection and cleaning. The core is removed and placed in the second section of the container. A sterile rubber policeman on a long stainless steel rod is used to wash particle-containing sediment from the wall into the 120 ml of fluid left in rotor at the end of a run. The fluid is aspirated into a sterile vacuum bottle, all containers are filled with 3 percent formalin, and the glove box used for the entire procedure is sterilized with ethylene oxide. The coolant line fluid (generally distilled water) is also sterilized with formalin.

In an alternate method for making multiple runs, the sedimented particles are resuspended by rapidly decelerating the rotor with an accompanying swirling of the fluid to scrub the surfaces of the annular chamber (5). The rotor contents can then be removed by pumping the fluid out the bottom of the stationary rotor or by displacement with compressed air. Successive runs can then be made without disassembling the rotor. Experimental studies designed to determine whether the B-V rotor performs as predicted by theory (1) are described in other papers in this volume (5, 6).

### REFERENCES

- (1) BERMAN, A. S.: Theory of centrifugation: Miscellaneous studies. Nat Cancer Inst Monogr 21: 41-76, 1966.
- (2) ANDERSON, N. G., BARRINGER, H. P., BABELAY, E. F., and FISHER, W. D.: The B-IV zonal ultracentrifuge. Life Sci 3: 667-671, 1964.
- (3) ANDERSON, N. G., BARRINGER, H. P., BABELAY, E. F., NUNLEY, C. E., BARTKUS, M. J., FISHER, W. D., and RANKIN, C. T., JR.: The design and operation of the B-IV zonal centrifuge system. Nat Cancer Inst Monogr 21: 137-164, 1966.
- (4) ANDERSON, N. G.: The zonal ultracentrifuge. A new instrument for fractionating mixtures of particles. J Phys Chem 66: 1984-1989, 1962.

- (5) REIMER, C. B., NEWLIN, T. E., HAVENS, M. L., BAKER, R. S., ANDERSON, N. G., CLINE, G. B., BARRINGER, H. P., and NUNLEY, C. E.: An evaluation of the B-V (continuous-flow) and B-IV (density gradient) rotors by use of live polio virus. Nat Cancer Inst Monogr 21: 375-388, 1966.
- (6) ANDERSON, N. G., and CLINE, G. B.: Virus isolation for vaccine production. In preparation.

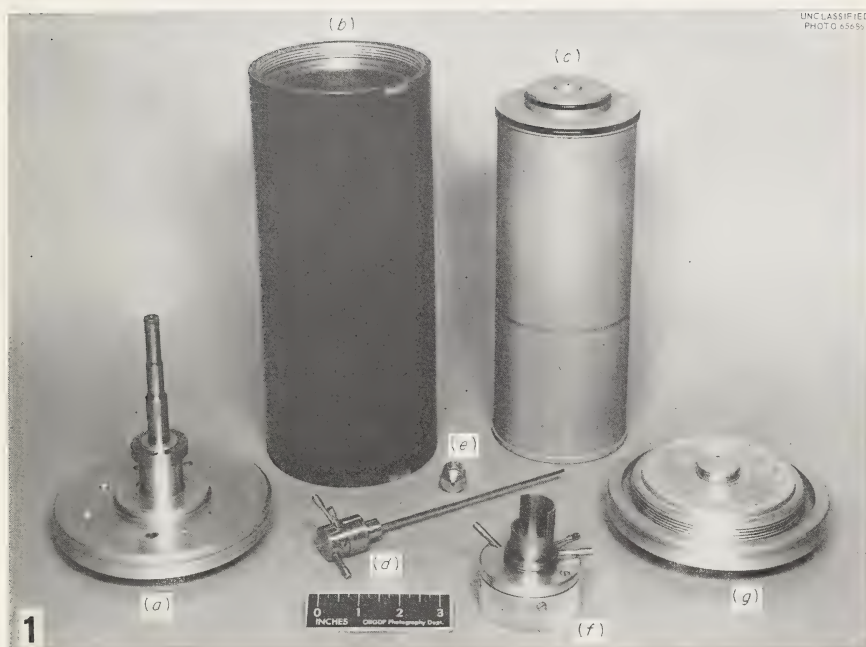


FIGURE 1.—Disassembled B-V rotor system: (a) upper end cap; (b) rotor chamber; (c) rotor core; (d) seal; (e) manifold plug; (f) upper bearing; (g) lower end cap.

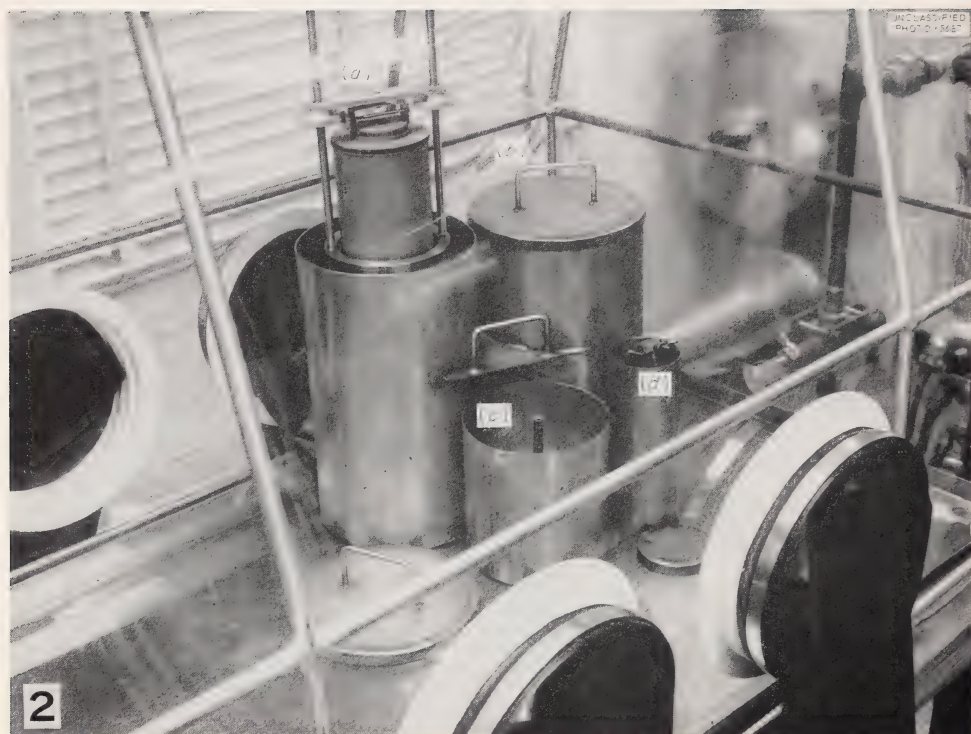


FIGURE 2.—Disassembly of B-V rotor in containers for subsequent disinfection. Photographed in glove box which enclosed the top of the centrifuge chamber. (a) Core being lifted out of rotor chamber; (b) container for disinfecting core; (c) upper end cap in its container; (d) seal container.

## Continuous-Flow Centrifugation Combined With Isopycnic Banding: Rotors B-VIII and B-IX<sup>1</sup>

N. G. ANDERSON, H. P. BARRINGER,<sup>2</sup> J. W. AMBURGEY, JR., G. B. CLINE, C. E. NUNLEY, and A. S. BERMAN, *Biology Division, Oak Ridge National Laboratory,<sup>3</sup> and the Technical Division, Oak Ridge Gaseous Diffusion Plant,<sup>3</sup> Oak Ridge, Tennessee*

### SUMMARY

Pelleting inactivates some viruses and aggregates other dispersed material. Methods for separation should be developed in which desired particles are always kept in suspension. Rotors that combine continuous-flow centrifugation with isopycnic banding can achieve this effect. In our system a liquid density gradient is set up in a spinning rotor next to the wall in each of 4 sector-shaped compartments. The virus-containing suspension is made

to flow over the centripetal surface of the gradient between the gradient and the tapered core of the rotor. Virus particles sediment out of the stream into the imprisoned gradient. At the completion of a run, components of the gradient are recovered by displacing the gradient centripetally with a dense fluid and channeling the gradient out a center line.—*Nat Cancer Inst Monogr* 21: 199-216, 1966.

THE A- and B-series zonal centrifuges allow high-resolution separations of particles ranging from whole cells to large protein molecules to be effected on the basis of sedimentation rate (1-4). Since the resolution obtained in rate-zonal centrifugation is a function of the thickness of the sample zone, and hence its volume, it is often necessary to preconcentrate a dilute suspension of particles so that a reasonable mass of material may be introduced into the rotor as a very narrow zone. This is especially true of virus particles and ribosomes, both of which are usually present in very low concentration. During the operation of a zonal centrifuge, a stream of liquid flows through the rotor during part of the loading cycle and gradient recovery. By use of the theoretical approaches of Berman (5), the B-V core, designed for high-performance, continuous-flow centrifugation was developed (6) and it performed as predicted (7). This rotor, however, is usually disassembled to recover the sedimented particles from the rotor wall. If all the sediment is to be recovered (8), use of this rotor is limited to batch operation and to the separation of particles not damaged

<sup>1</sup> This research performed under the Joint National Institutes of Health-Atomic Energy Commission Zonal Centrifuge Development Program which is supported by the National Cancer Institute, the National Institute of Allergy and Infectious Diseases, and the U.S. Atomic Energy Commission.

<sup>2</sup> Present address: Stellite Division of Union Carbide Corporation, Kokomo, Indiana.

<sup>3</sup> Operated for the U.S. Atomic Energy Commission by the Nuclear Division of Union Carbide Corporation.

by pelleting. Unfortunately, many viruses, especially the myxoviruses, lose biological activity when pelleted. In addition, sedimented particles often do not resuspend properly, and, in subsequent rate and banding experiments, infectivity may be observed in a spectrum of particles—discrete virus particles and clumped or aggregated particles of many different sizes. It was highly desirable, therefore, to develop a centrifugal method for concentrating and purifying virus particles that would keep them suspended at all times. A specific problem in keeping particles suspended, and a major stimulus to the development of these continuous-flow methods, is the possibility of producing effective vaccines which contain only those antigenic proteins necessary to produce immunity. It is evident that both centrifuge development and biochemical problems must be solved during the course of this work. When the B-II rotor was used as a continuous-flow centrifuge, T3 phage particles were recovered from 20 liters of lysate and then banded in the same rotor in a cesium chloride gradient (9). This suggested that rotors could be designed in which the virus stream flowed over a density gradient stabilized at the rotor wall, and was recovered by displacement through the zonal rotor core (9). A group of rotor cores designed to explore these possibilities is discussed in the present paper and have been previously noted in brief communications (10, 11).

### THEORETICAL CONSIDERATIONS

The sequence of steps proposed for the preparation of a vaccine composed only of antigenic viral subunits is as follows:

1. Continuous-flow centrifugation combined with isopycnic banding to concentrate virus particles from up to 100 liters of culture medium using B-VIII or IX rotor cores.
2. Dialysis to lower the density of the virus fraction. (Alternatively the virus may be recovered without banding by use of the B-V core, and then banded in small-volume tubes.)
3. Rate-zonal centrifugation to yield particles having a narrow range of sedimentation coefficients.
4. Dialysis to remove gradient solutes.
5. Dissociation of viral particles to yield suspensions containing antigenic subunits.
6. Rate-zonal centrifugation of dissociated material to yield a purified zone of subunits.
7. Recovery of subunits from the gradient solution.
8. Additional isopycnic banding if required.

It is important to determine at the outset whether the systems have the proper capacities to be used in this sequence, since the particle capacity of a continuous-flow and that of a zonal centrifuge are quite different. The maximum volume of fluid being considered for vaccine production is 100 liters. In practice, the volumes used would probably be

one fourth to one half this amount. The total mass of virus material in a preparation may be predicted from the equation:

$$M_t = TRM_v V \cdot 10^3$$

where  $M_t$  equals the total virus mass in grams,  $T$  the titer in infectious particles per ml,  $R$  the ratio of physical particles to infectious particles,  $M_v$  the mass of one virus particle in grams, and  $V$  the total volume of virus-containing fluid in liters.

For polio, with a mass of  $12 \times 10^{-18}$  g per particle, a titer of  $10^8$ , an infectivity ratio of 100 (12), and a volume of 100 liters, the mass of viral particles would be 12 mg. In a 100 liter volume of influenza culture fluid, having a titer of  $10^8$ , an infectivity ratio of 10 (12), and containing large amounts of other particulate material with the same density as the desired virus, the masses of material expected are well within the limits of the B-IV zonal centrifuge for rate and isopycnic zonal separations. If a continuous-flow centrifuge having sufficiently high flow rates that will also band particles is feasible, then experimental studies on subunit vaccine preparation can be initiated.

In order to design a continuous-flow rotor that will allow viruses to band in a density gradient, we sought to (a) set up the gradient in a spinning rotor, (b) flow large volumes of fluid over the gradient without disturbing it at high speeds, and (c) recover the gradient and suspended particles without loss of banding resolution. Two cores (B-VI and B-VII), consisting of tapered cylinders, were constructed to determine whether stabilizing vanes or septa were necessary. Experimental studies with these cores indicated that excessive mixing occurred between the continuous-flow stream and the gradient. A core having 4 radially arranged vanes (B-VIII) was therefore constructed and tested.

## THE B-VIII CORE

### Description

The B-VIII core shown in figure 1 consists of a solid, tapered conic section and 4 vertical, radially oriented fins. The principles of operation are best understood by the schematic diagrams shown in figure 2. All fluid lines were arranged so that, as far as possible, air bubbles were swept out of the system during operation. The line extending through the annular ring of the seal is connected directly with the top and the outer edge of the fluid compartment. The center seal line extends straight to the bottom of the core and enters the rotor chamber at the lower or smaller diameter end of the core.

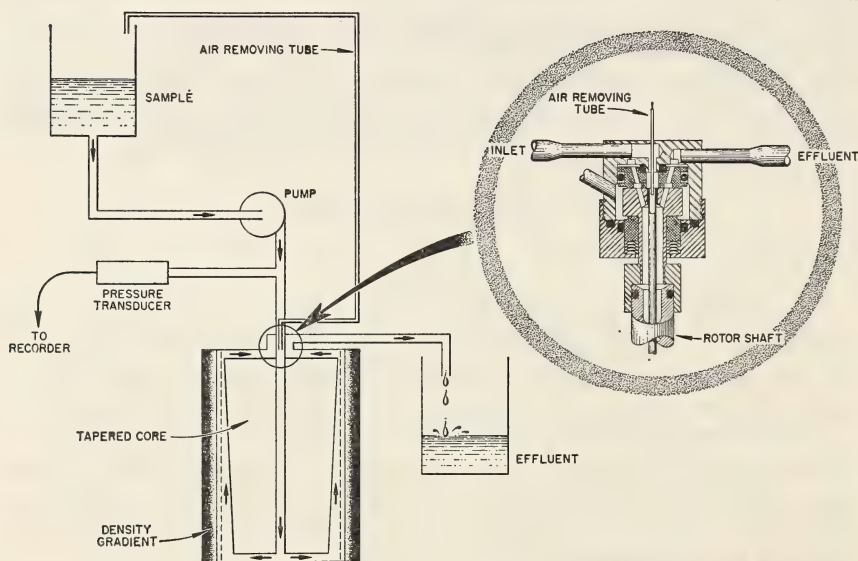
### Operation

Initially, all fluid lines and the rotor chamber are filled with a sterile solution of low density through the center line, and all air in the rotor and lines is expelled. After acceleration to low speed (3000 rpm) the

gradient solution is pumped into the rotor edge (fig. 2b). This solution may be introduced as a gradient or as a volume of fluid of high density. In the latter instance the gradient is formed by diffusion. As the solution moves into the rotor it is held against the rotor wall by centrifugal force, and an equal volume of the fluid is displaced out the center line. The total internal volume of an unmodified B-VIII rotor core is 930 ml; the fluid volume centripetal to the maximum radius of the tapering core is 813 ml.

After a gradient has been set up in the rotor, the direction of fluid flow through the rotor is reversed, and a fluid having approximately the same density as the sample is pumped in through the center (lower) line. Any portion of the density gradient centripetal to the maximum core diameter is displaced out of the rotor through the inner portion of the upper line. While this light fluid is being pumped, the rotor is accelerated to operating speed, and the sample is pumped through the rotor in the same direction (in by the center line, out by the edge line; *see* fig. 2c).

Two points concerning operation of this rotor system should be noted. Any air trapped in the fluid flowing through the rotor is trapped at the narrow (lower) end of the core and rapidly raises the back pressure. To prevent this situation, a bleed line was incorporated in the seal to divert part of the feed stream and any air back into a reservoir (text-fig. 1).



ORNL-DWG 65-9058

TEXT-FIGURE 1.—Schematic diagram of B-VIII-B-IX rotor systems and seal. As the sample stream is pumped into the rotor, hydrostatic pressure is monitored at the entrance of the center line of the seal. A small part of this stream and trapped air bubbles are allowed to flow back into the sample reservoir. The remaining particle-rich stream passes to the lower part of the rotor, back through the tapered region of the core, and out the edge line.

The second point concerns the effect of diffusion of gradient solutes into the fluid stream. Centrifugal force produces a large hydraulic pressure in the rotor chamber. This pressure has a negligible effect on the flow of fluid through the rotor because the pressure gradients in the entrance and exit lines cancel each other out as they are brought back toward the axis of rotation, where the pressure due to centrifugal force is small. In practice the exit line leaves the rotating seal face on a small radius, a situation sufficient to make the rotor a centrifugal pump. This effect is countered by any increase in density of the exit stream because of inward diffusion of the gradient solute. Considerable back pressure is produced by a very small amount of solute during high-speed operation. Since diffusion is a time-dependent process, it is essential to have *a constant flow of fluid through the rotor at all times*. When flow during high-speed operation is interrupted briefly, enough back pressure develops to stop flow, and the rotor speed must be reduced to start flow again.

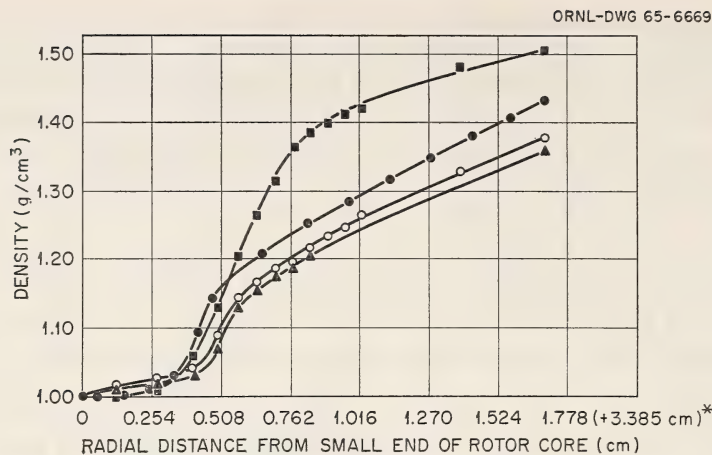
When the continuous-flow portion of an experiment was completed, it was generally desirable to continue centrifugation for 30 minutes to 1 hour to insure that all particles were banded at their proper levels. When there was any danger that enough of the gradient solute had diffused out of the rotor via the exit stream to lower the maximum gradient density below the banding density of the virus, 50 ml of dense gradient solution was pumped to the rotor edge before the final banding period.

The gradient is recovered (fig. 2d) at a speed between 3000 to 5000 rpm. A solution having a density equal to or greater than the maximal gradient density is pumped to the rotor edge, displacing the contents toward the rotor axis. As the banded zones approach the tapered core, they are funneled down to the lower exit line and out through an ultraviolet absorbance monitor. Since a portion of the culture fluid is left in the rotor close to the core, the absorbance initially will be high and will grade out into the separated zones.

The taper of the core, therefore, serves to define the maximum volume of the virus-containing fluid in the rotor (the stream volume) and to guide the gradient out of the rotor at the end of the run (fig. 2e).

## EXPERIMENTAL STUDIES WITH THE B-VIII CORE

To determine whether gradients could be set up and recovered from the B-VIII rotor, solutions of cesium chloride, cesium tartrate, and potassium citrate were introduced into the rotor during rotation. Results are described in text-figure 2. Diffusion produced suitable gradients in a very short space of time. The maximum slope, as expected, occurs close to the interface between the stream and gradient.



TEXT-FIGURE 2.—Density gradients recovered from B-VIII rotor after continuous-flow centrifugation.

Symbol	Gradient			Maximum operating speed (rpm)	Effluent collected (liters)
	Solution	Volume used (ml)	Density ( $\text{g}/\text{cm}^3$ )		
■	Cesium chloride	500	1.62	28,000	~3.5
●	Cesium chloride	300	1.62	28,000	~8.0
▲	Potassium citrate	250	1.54	30,000	~4.5
○	Cesium tartrate	300	1.51	36,000	~4.0

In these experiments relatively small volumes of fluid were run through the rotor. The results show that gradients can be set up and recovered from the B-VIII rotor. However, since a continual removal of gradient material takes place, it may be necessary to add small amounts of concentrated gradient solution at experimentally determined intervals.

Four experimental runs, in which virus-containing media were used, were made with the unmodified B-VIII rotor (table 1). Gradient solutions were established by diffusion of the dense gradient solution into water. The results obtained with adenovirus 2 are shown in text-figure 3. An electron micrograph of a dialyzed sample from the virus peak is shown in figure 3.

The most serious problem with the B-VIII rotor was the high pressure necessary to force fluid through the rotor.

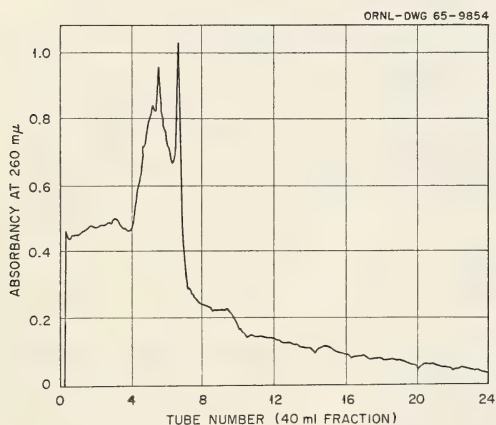
TABLE 1.—B-VIII separation runs

Top operating speed (rpm)	Gradient		Virus particle	Sample volume (liters)	Gradient unloading speed (rpm)	Average flow (liters/hr)
	Material	Loading speed (rpm)				
28,000	Cesium chloride	Statically	Adenovirus 2	3	8000	1.7
36,000	Cesium chloride	2000	Respiratory syncytial	5	8000	1.5
30,000	Potassium citrate	8000	Moloney	3	8000	2.0
30,000	Cesium tartrate	8000	Moloney	2	8000	1.9

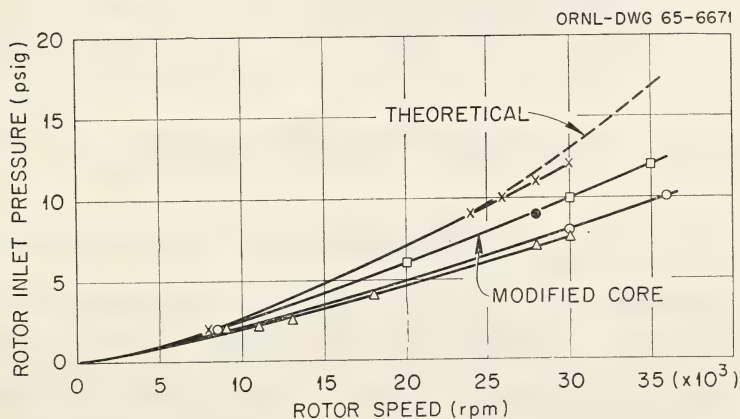
Text-figure 4 shows the pressure of the fluid stream entering the rotor as a function of rotor speed for different gradient solutions of selected volumes and densities. These pressure measurements are reproducible as long as no air is entrained in either of the flow channels. The inlet pressure can also be approximated by comparison of the flow path of the fluid stream through the rotor to a U-tube manometer with a fluid of different density in each of the legs, as illustrated in text-figure 5. Diffusion coefficients are ignored. The calculations are handled as follows:

$$(P_o - P_s)_{\text{atm}} = 0.873 \times 10^{-8} (\text{rpm})^2 [D_2^2 (\bar{\rho}_{2S} - \bar{\rho}_{21}) + D^2 (\bar{\rho}_{21} - \bar{\rho}_{10}) - D_S^2 (\rho_{2S})] \quad (1)$$

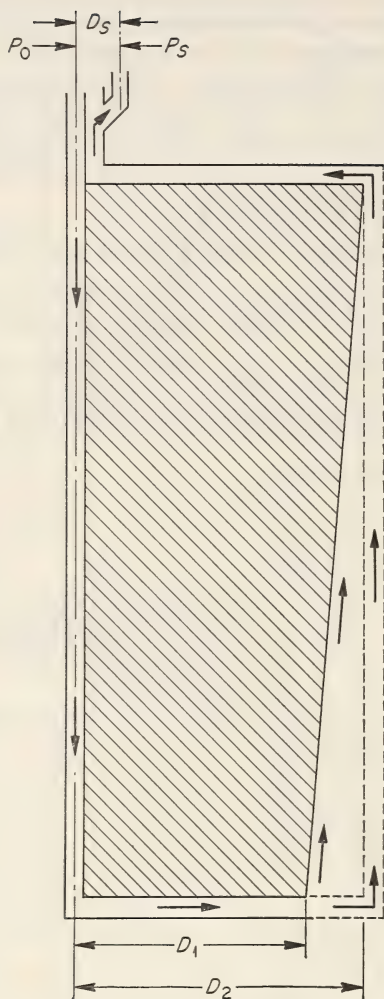
where  $D_1$  = diameter at small end of core taper, inches;  $D_2$  = diameter at large end of core taper, inches;  $D_S$  = smallest diameter at which effluent leaves the rotating system, inches;  $P_o$  = pressure at the axis, atm;  $P_s$  = pressure at  $D_S$ , atm;  $\bar{\rho}_{2S}$  = average density between  $D_S$  and  $D_2$  at the top (measured), g/cm<sup>3</sup>;  $\bar{\rho}_{21}$  = average density between  $D_1$  and  $D_2$  at the



TEXT-FIGURE 3.—Isolation of adenovirus 2 in B-VIII centrifuge. The virus was found in the second (highest) peak.



TEXT-FIGURE 4.—B-VIII rotor system inlet pressure. Average flow, about 3 liters per hour. X: 500 ml cesium chloride, density 1.62 g/cm<sup>3</sup>, theoretical; ●: 300 ml cesium chloride, 1.62; Δ: 250 ml potassium citrate, 1.54; ○: 300 ml cesium tartrate, 1.51; □: 500 ml cesium chloride, 1.62, modified core.



TEXT-FIGURE 5.—Flow path diagram for the B-VIII rotor system.  $D_s = 0.635$  cm;  $D_1 = 6.769$  cm; and  $D_2 = 7.620$  cm or  $6.960$  cm in revised version.

bottom (estimated),  $\text{g/cm}^3$ ;  $\bar{\rho}_{10}$  = average density between axis and  $D_1$  at the bottom (measured),  $\text{g/cm}^3$ .

Two alterations were made in the B-VIII rotor in an attempt to lower the back pressure. First, the free space in the lower end of the core was increased to allow a small amount of mixing between fluid flowing into the rotor and the fluid already in the rotor. A small increase in the density was expected as a result of this mixing. Secondly, the core taper was reduced from  $1^\circ$  to  $\frac{1}{4}^\circ$ . The volume of culture fluid in the rotor was thereby decreased from 117 ml to 30 ml and the dwell time for a given aliquot of fluid proportionately reduced.

The characteristics of the original and modified designs of the B-VIII core are listed in table 2.

TABLE 2.—Characteristics of B-VIII rotor core

Dimension	Original	Modified
Effective core length	24.4 cm	23.5 cm
Total chamber volume	930 ml	1020 ml
Fluid stream volume in chamber	117 ml	30 ml
Gradient volume in chamber	813 ml	990 ml
Maximum core diameter (excluding fins)	7.62 cm	6.96 cm
Minimum core diameter (excluding fins)	6.77 cm	6.77 cm
Core taper	1°	¼°
Unloading speed (minimum)	1178 rpm	2556 rpm

Experimental studies showed that the back pressure was reduced appreciably by these modifications (text-fig. 4). The core angle could not be reduced to such a small angle that particle zones were not funneled out properly. As previously discussed, these zones are sections of a paraboloid of rotation (2, 13). It is important to know whether, at the rotational speeds used for gradient recovery, a zone will contact the core initially at the top and then move down as expected. By use of the equation:

$$L = \frac{r^2 \omega^2}{2g} \quad (2)$$

where  $L$  is the distance from the apex along the axis of a paraboloid of rotation,  $r$  is the radius from the axis of rotation,  $g$  is the acceleration due to gravity, and  $\omega$  is the angular velocity in radians per second. The critical unloading speed, in revolutions per minute, defined as the speed at which a zone will touch the upper and lower ends of the core simultaneously during unloading, may be derived from equation 2 as follows:

$$L_1 - L_2 = \frac{r_1^2 \omega^2}{2g} - \frac{r_2^2 \omega^2}{2g} = \frac{\omega^2}{2g} (r_1^2 - r_2^2) \quad (3)$$

$$\omega = \sqrt{\frac{(L_1 - L_2)2g}{r_1^2 - r_2^2}} \quad (4)$$

and

$$\text{RPM} = \frac{60}{2\pi} \sqrt{\frac{(L_1 - L_2)2g}{r_1^2 - r_2^2}} \quad (5)$$

The critical unloading speeds for the original B-VIII and modified B-VIII cores are 1178 and 2556 rpm, respectively. Even at this speed the flow of fluid across the core face would tend to maintain the resolution of zones.

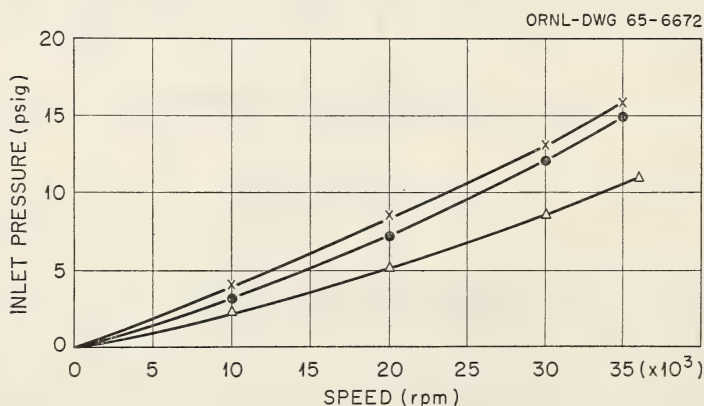
## THE B-IX CORE

The B-IX core was designed to minimize the pressure required to force fluid through the rotor and to reduce the core weight. The rotor characteristics are given in table 3. To reduce the inlet pressure, the core taper was held to the minimum commensurate with a low critical unloading speed and reasonable resolution during unloading. The flow channels through the core were kept as small as possible without restricting flow. The core diameter has been enlarged to increase the centrifugal force across the flowing stream and to reduce the volume of gradient material in the rotor. The weight of the core has been decreased approximately 40 percent by being made hollow.

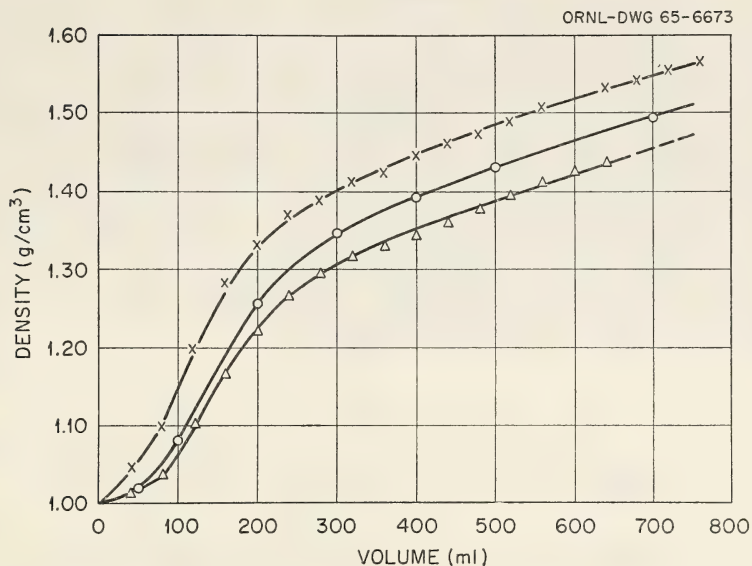
TABLE 3.—Characteristics of B-IX rotor core

Effective core length	24.92 cm
Total chamber volume	749 ml
Fluid stream volume in chamber	79 ml
Gradient volume in chamber	670 ml
Maximum core diameter	8.26 cm
Minimum core diameter	7.84 cm
Core taper	1/2°
Unloading speed (minimum)	1602 rpm

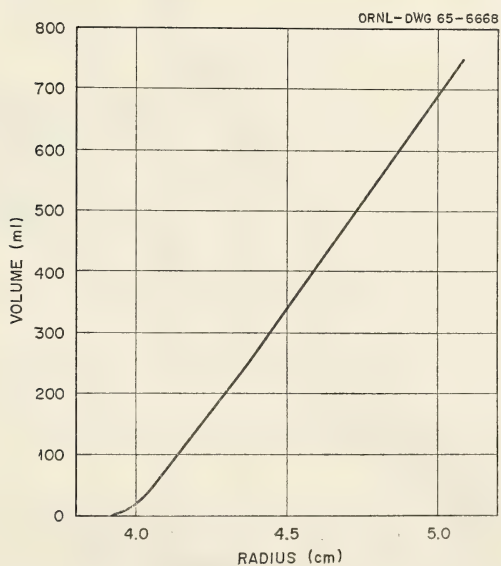
Inlet pressure as a function of rotor speed for a number of gradient volumes and densities is shown in text-figure 6. It is evident that the maximum of 20 pounds per square inch is not exceeded at 40,000 rpm. Gradients set up and recovered from the rotor are shown in text-figure 7. The recovered gradient may be related to radius in the rotor by use of the graph shown in text-figure 8.



TEXT-FIGURE 6.—Inlet pressure in B-IX rotor at an average flow rate of 3 liters per hour. ●: 500 ml of cesium chloride, density, 1.73 g/cm<sup>3</sup>; Δ: 500 ml, 1.63; X: 700 ml, 1.63.



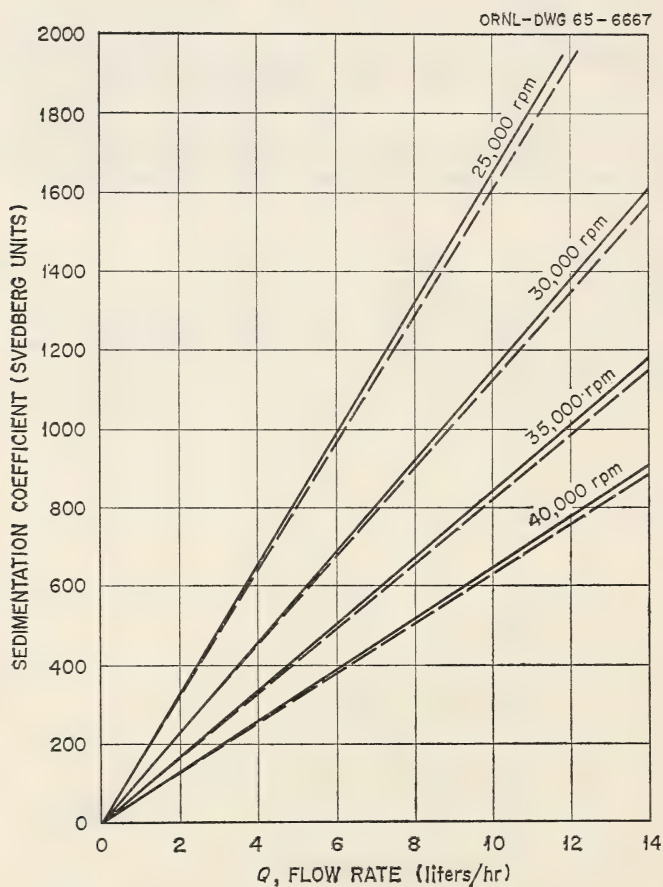
TEXT-FIGURE 7.—B-IX continuous flow centrifuge system. O: 700 ml cesium chloride, density, 1.63 g/cm<sup>3</sup>; X: 500 ml, 1.73; Δ: 500 ml, 1.63.



TEXT-FIGURE 8.—Relation between recovered volume and the radius of the rotor.

The equations previously derived (5) for continuous-flow rotors have been adapted to the B-IX core by the assumption that (a) particles which sediment to a level having a greater radius than the maximum taper remain in the rotor, (b) the fluid stream is confined to the tapered region of the core, and (c) that the tapered region can be approximated by a uniform annular space with a minimum radius equal to the actual minimum taper radius and a maximum radius corresponding to the mean square radius associated with the taper. The calculated performance of the B-IX rotor is shown in text-figure 9, in which curves are plotted for the particle sedimentation coefficient in Svedberg units versus flow rate at several different speeds. Experimental verification of these theoretical curves is presented elsewhere (7).

(e)



TEXT-FIGURE 9.—Calculated performance of the B-IX rotor system. Rotor length, 24.92 cm; mean square core radius, 3.917 cm; minimum core radius, 4.024 cm. Dashed line indicates 95% cleanout; solid line, 99% cleanout.

## DISCUSSION

The development of centrifuge rotors in which particles may be isolated by continuous-flow centrifugation combined with isopycnic banding makes the so-called  $s$ - $\rho$  separations (1) a single-step procedure. By appropriate choice of centrifuge speed, flow rate, and the gradient imprisoned within the rotor, relatively large masses of material may be isolated. In the development of the B-VIII and B-IX centrifuge cores, the specific problem of interest has been the isolation of virus particles from culture media. The principles, however, are applicable to the isolation of nuclei, mitochondria, ribosomes, and other particulate material. By using a series of such rotors operating at increasing speeds, a mixture of particles may be separated into fractions having decreasing sedimentation rates.

For virus isolation in the preparation of vaccines, the B-VIII and B-IX rotors offer a number of advantages. For example, inactivation and agglutination due to pelleting are avoided, and the material is recovered in a suspension which, after dialysis, is suitable for a rate-zonal run. In addition, a number of runs may be made consecutively. At the end of a given run, the rotor is full of the gradient solution, and reintroduction of culture fluid through the center line will re-establish the starting conditions.

In many instances the stream flowing through the centrifuge contains fairly large numbers of particles that are lighter than the virus sought. If the rotor is partially unloaded at intervals, this light band may be removed while the virus band is retained.

## REFERENCES

- (1) ANDERSON, N. G.: An introduction to particle separation in zonal centrifuges. Nat Cancer Inst Monogr 21: 9-39, 1966.
- (2) ANDERSON, N. G., BARRINGER, H. P., BABELAY, E. F., NUNLEY, C. E., BARTKUS, M. J., FISHER, W. D., and RANKIN, C. T., JR.: The design and operation of the B-IV zonal centrifuge system. Nat Cancer Inst Monogr 21: 137-164, 1966.
- (3) ANDERSON, N. G., BARRINGER, H. P., CHO, N., NUNLEY, C. E., BABELAY, E. F., CANNING, R. E., and RANKIN, C. T., JR.: The development of low-speed "A" series zonal rotors. Nat Cancer Inst Monogr 21: 113-136, 1966.
- (4) FISHER, W. D., and CANNING, R. E.: Isolation of macroglobulin by rate zonal centrifugation. Amer Zool 4: 310, 1964.
- (5) BERMAN, A. S.: Theory of centrifugation: Miscellaneous studies. Nat Cancer Inst Monogr 21: 41-76, 1966.
- (6) BARRINGER, H. P., ANDERSON, N. G., and NUNLEY, C. E.: Design of the B-V continuous-flow centrifuge system. Nat Cancer Inst Monogr 21: 191-198, 1966.
- (7) CLINE, G. B., and ANDERSON, N. G.: In preparation.
- (8) REIMER, C. B., NEWLIN, T. E., HAVENS, M. L., BAKER, R. S., ANDERSON, N. G., CLINE, G. B., BARRINGER, H. P., and NUNLEY, C. E.: An evaluation of the B-V (continuous-flow) and B-IV (density gradient) rotors by use of live polio virus. Nat Cancer Inst Monogr 21: 375-388, 1966.
- (9) ANDERSON, N. G.: Virus isolation in the zonal centrifuge. Nature (London) 199: 1166-1168, 1963.

- (10) ANDERSON, N. G., BURGER, C. L., and BARRINGER, H. P.: Virus isolation by continuous flow centrifugation combined with banding. *Fed Proc* 23: 140, 1964.
- (11) AMBURGEY, J. W., JR.: A high capacity centrifuge system for isolating viruses and small particles. *In* Proceedings of the 17th Annual Conference on Engineering in Medicine and Biology, Cleveland, Ohio, November 16-18, 1964. Cleveland, Ohio, Case Institute of Technology, vol 6: 87, 1964.
- (12) WILDY, P., and WATSON, D. H.: Electron microscopic studies on the architecture of animal viruses. *Sympos Quant Biol* 27: 25-47, 1962.
- (13) ANDERSON, N. G.: The zonal ultracentrifuge. A new instrument for fractionating mixtures of particles. *J Phys Chem* 66: 1984-1989, 1962.

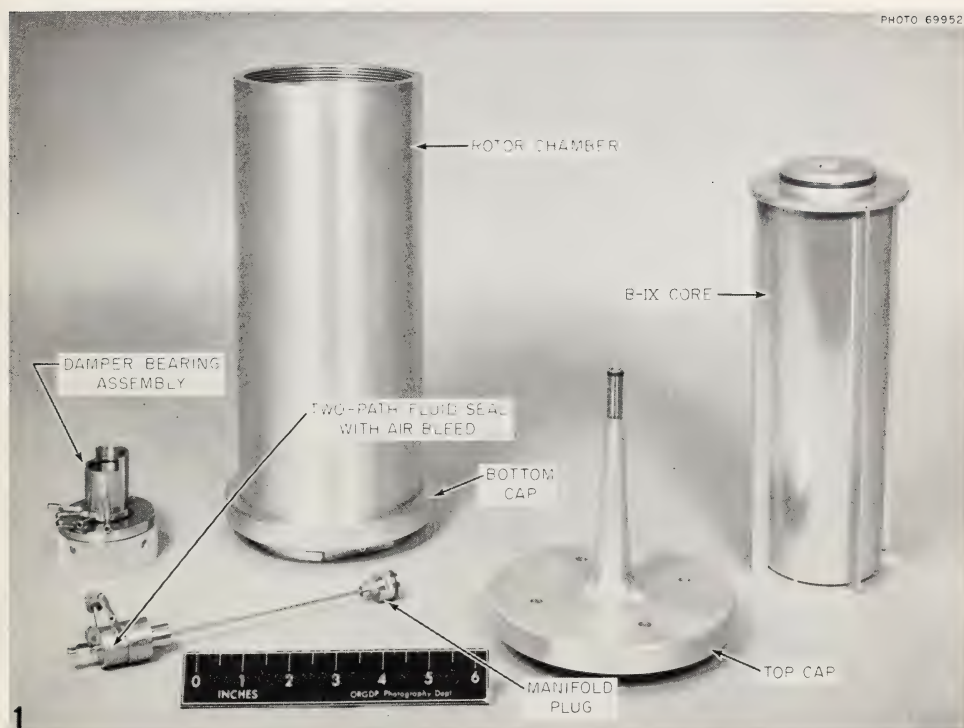
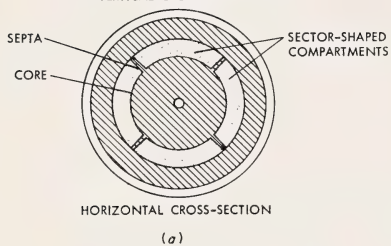
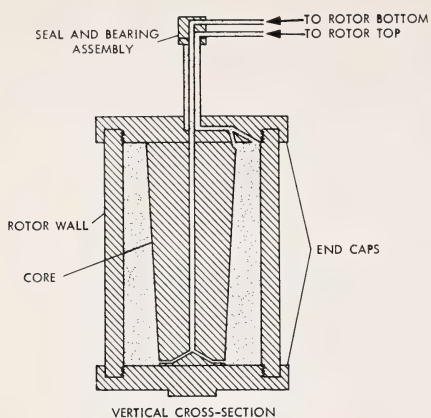
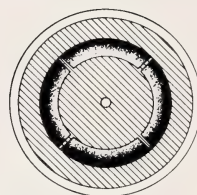
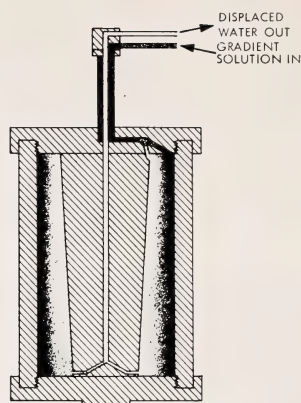


FIGURE 1.—Components of B-IX rotor for continuous-flow centrifugation combined with banding.

ORNL-DWG 65-6674

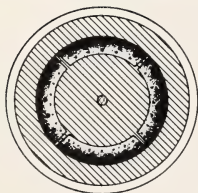
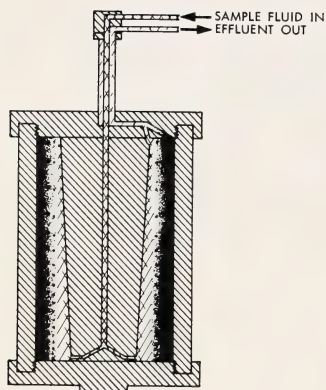


(a)

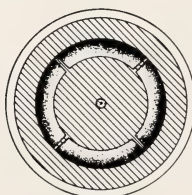
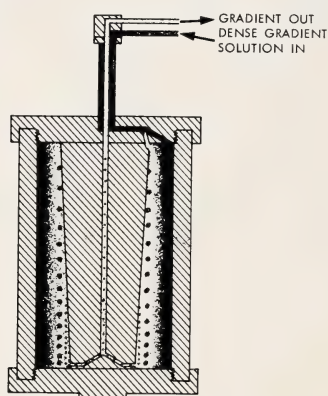


(b)

ORNL-DWG 65-6675



(c)



(d)

ORNL-DWG 65-6676

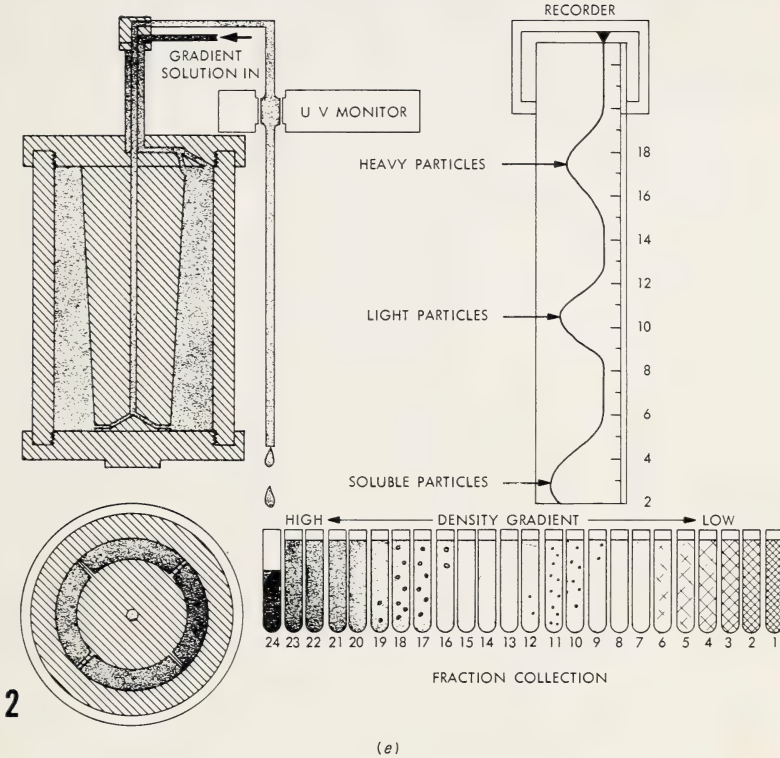


FIGURE 2.—Diagrammatic representation of isopycnic particle banding in a continuous-flow centrifuge rotor. At each stage both vertical and horizontal cross-sections are shown. In (a) the rotor is completely filled with water through the center line (if the rotor is at rest) or the edge line (if it is rotating). During rotation, usually at 3000 rpm, the gradient solution is introduced to the rotor edge (b). During acceleration and at operating speed (c) the particle-rich stream to be cleared flows out the edge line. Particles left in the rotor band isopycnically in the gradient. When the experiment is completed, the gradient is recovered (d) at low speed (3000–5000 rpm) by displacement with a dense fluid pumped to the rotor edge. The gradient and the zones suspended in it are monitored for ultraviolet absorbance and collected as a series of discrete fractions (e).

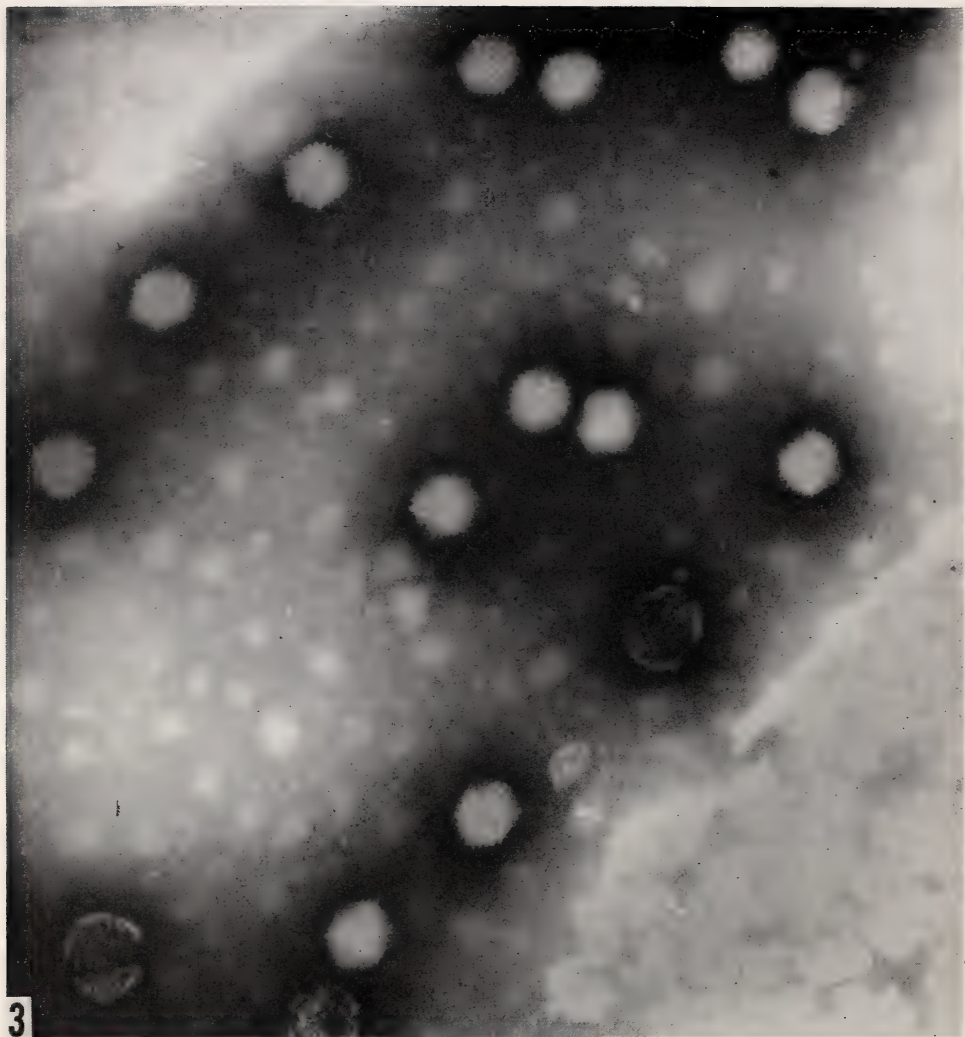


FIGURE 3.—Electron micrograph of adenovirus 2 collected from B-VIII rotor.

## **Studies on Gradient Materials**



# Calculation of Density and Viscosity of Sucrose Solutions as a Function of Concentration and Temperature<sup>1</sup>

E. J. BARBER,<sup>2</sup> *Technical Division, Oak Ridge Gaseous Diffusion Plant,<sup>3</sup> Oak Ridge, Tennessee*

## SUMMARY

In the application of the zonal centrifuge to separation of biological materials, sucrose solutions are often used to produce the gradient. Equations have been developed which permit the calculation of the density and viscosity of sucrose solutions as functions of the composition and temperature for computer programming of the calculation of equivalent sedimentation coefficients. A 9-constant empirical equation expressing the density as a function of the weight fraction sucrose and the temperature is recommended within the actual data range of 0 to 30° C and 0 to 75 weight percent sucrose. For the calculation of density between 30 and 60° C and from 0 to 70 weight percent sucrose, a theoretically based equation that can be extrapolated with confidence is recommended. The former equation reproduces the National Bureau of Standards density data to 7 parts in

10,000 and the latter equation reproduces them within 4 parts per thousand. An Antoine or modified Arrhenius equation was used to correlate the viscosity data of the National Bureau of Standards as a function of the mole fraction sucrose over the data range of 0 to 80° C and 0 to 75 weight percent sucrose. Over the whole set of tabulated data fitted, the standard deviation from the tabulated data was 2 parts per thousand, with a few individual values deviating by as much as 8 parts per thousand. In the range of maximum interest from 5 to 40° C and 5 to 40 weight percent sucrose, no calculated value differed from the tabulated data by more than 3 parts per thousand. The concepts and methods used can be applied to other gradient materials.—*Nat Cancer Inst Monogr* 21: 219-239, 1966.

IN ZONAL centrifuges (1-4) particles sediment through a gradient of increasing density and viscosity at rates determined by the magnitude and duration of the applied acceleration, the size and density of the particle, and the density and viscosity of the suspending medium. To interpret the results obtained, the equivalent sedimentation coefficients

<sup>1</sup> This research performed under the Joint National Institutes of Health-Atomic Energy Commission Zonal Centrifuge Development Program which is supported by the National Cancer Institute, the National Institute of Allergy and Infectious Diseases, and the U.S. Atomic Energy Commission.

<sup>2</sup> I wish to express my appreciation to Mr. Parkhurst B. Wood of Central Data Processing for the development of the least-squares solutions to the nonlinear equations.

<sup>3</sup> Operated for the U.S. Atomic Energy Commission by the Nuclear Division of Union Carbide Corporation.

$S^*$ , in Svedberg units, are calculated and related to analyses made on the recovered samples. A digital computer program (5) is used to calculate  $S^*$  from input data, which includes the rotor temperature and the volume and sucrose concentration in each collected fraction. In a computer program, memory limitations preclude entering a complete tabulation of density and viscosity values as a function of temperature and sucrose concentration; it is necessary, therefore, to develop equations that will give the density and viscosity as functions of these variables.

The ideal material for density gradient preparation should be a chemically inert, readily available, high molecular weight compound that will give solutions of high density and low viscosity (3). Substances actually used do not completely fill these requirements. While sucrose is the compound most commonly used, a variety of other materials may be utilized for density gradient preparations. These include salts (potassium citrate, potassium tartrate, and cesium chloride), nonelectrolytes (dextrans, polyglycols, polyvinylpyrrolidone, other sugars in addition to sucrose), and possibly proteins. For viral isolations, the  $pH$  of the solution should remain between 6.5 and 7.5. Change of the  $pH$  away from neutrality is not a problem with nonelectrolyte gradient materials or with uni-univalent salts of strong acids and strong bases. For all other electrolytes, the effect of deviation of the  $pH$  of the solution from 7.0 on the relation between concentration, density, and viscosity must be considered. The studies done here with sucrose are illustrative of what will be required for other gradient materials. Additional data, as well as a more complex treatment, will be required to achieve the necessary quantitative correlations of density and viscosity with temperature and composition for many of the gradient materials under consideration.

Sedimentation coefficients are determined according to a modification of the trapezoidal approximation of Martin and Ames (5). In a medium,  $m$ , at temperature,  $T$  (in  $^{\circ}C$ ), the sedimentation coefficient is given by:

$$s_{T,m} = \frac{dx/dt}{\omega^2 x} \quad [1]$$

where  $dx/dt$  is the velocity of movement of the boundary,  $\omega$  is the angular velocity of the rotor in radians per second, and  $x$  is the distance from the rotor center to the inflection point of the boundary or center of the zone. It is customary to extrapolate to a standard state, which for biological systems is usually water at  $20^{\circ}C$ , with the equation:

$$s_{20,w} = s_{T,m} \frac{\eta_{T,m}(\rho_p - \rho_{20,w})}{\eta_{20,w}(\rho_p - \rho_{T,m})} \quad [2]$$

where  $\eta_{T,m}$  is the viscosity of the medium at the temperature of centrifugation,  $\eta_{20,w}$  is the viscosity of water at  $20^{\circ}C$ ,  $\rho_p$  is the density of the particle in aqueous solution (equal to the reciprocal of the partial specific vol-

ume)  $\bar{v}$  of the particle,  $\rho_{T,m}$  is the density of the medium at the temperature of centrifugation, and  $\rho_{20,w}$  is the density of water at 20° C. Equation 2 applies to sedimentation in a solvent having either a uniform density or a density gradient; thus, the basic differential equation for sedimentation through a density gradient is obtained by the combination of equations 1 and 2:

$$\omega^2 s_{20,w} dt = \frac{(\rho_p - \rho_{20,w})\eta_{T,m}}{(\rho_p - \rho_{T,m})\eta_{20,w}} \cdot \frac{1}{x} dx \quad [3]$$

where the terms are as defined earlier.

Except for the solution viscosity,  $\eta_{T,m}$ , and density,  $\rho_{T,m}$ , which are intensive properties of the sucrose gradient, all the other terms in equation 3 are either known or are experimental quantities established during an experiment. However, the density and the viscosity of sucrose solutions have been experimentally determined over a range of compositions and temperatures, and reasonably precise tables have been prepared giving these or related properties as functions of the weight percent sucrose and the temperature (4, 6, 7). The data used for the equations developed here are listed in table 1. Since the temperature of centrifugation and the sucrose concentration are accurately determined for each fraction withdrawn from the zonal centrifuge, the density and viscosity of the solution may be computed for each fraction by interpolation of the tables. This approach is impractical, however, because of the large number of samples withdrawn from the zonal centrifuge in the course of even a single run, and means were sought for expression of the density and the viscosity as analytical functions of the temperature and composition which could then be used in a computer program. The relations developed should have an accuracy of about  $\pm 0.5$  percent for the density

TABLE 1.—Absolute density of sucrose solutions

Weight percent sucrose in vacuum	Mole fraction sucrose	Density of solution at indicated temperature (°C), g/cc					
		0	10	15	20	25	30
0	0.00000	1.00000	0.99969	0.99914	0.99823	0.99699	0.99565
5	0.00276	1.02000	1.01976	1.01895	1.01785	1.01654	1.01520
10	0.00582	1.04130	1.04010	1.03929	1.03814	1.03687	1.03527
15	0.00921	1.06300	1.06149	1.06042	1.05916	1.05774	1.05614
20	0.01300	1.08540	1.08368	1.08234	1.08096	1.07940	1.07754
25	0.01726	1.10890	1.10640	1.10506	1.10356	1.10185	1.09999
30	0.02208	1.13280	1.13017	1.12857	1.12698	1.12516	1.12323
35	0.02758	1.15740	1.15473	1.15313	1.15128	1.14940	1.14727
40	0.03393	1.18380	1.18036	1.17849	1.17645	1.17449	1.17210
45	0.04132	1.21030	1.20650	1.20464	1.20254	1.20038	1.19798
50	0.05004	1.23780	1.23398	1.23184	1.22957	1.22732	1.22493
55	0.06049	1.26630	1.26197	1.25984	1.25754	1.25505	1.25266
60	0.07323	1.29550	1.29129	1.28890	1.28646	1.28384	1.28145
65	0.08911	1.32600	1.32140	1.31875	1.31633	1.31369	1.31104
70	0.10946	1.35700	1.35231	1.34965	1.34717	1.34460	1.34168
75	0.13647	1.38930	1.38427	1.38161	1.37897	1.37629	1.37337

and  $\pm 1.0$  percent for the viscosity. The range of temperatures of concern was from 0 to 60° C, and the range of compositions was from 5 to 70 weight percent sucrose. The analysis of the density data and the analysis of the viscosity data, two different problems, are discussed separately. In the development, use was made of Wood's NLLS Program (8) for fitting nonlinear curves by least squares, a program for fitting linear polynomials by least squares, and the OR-SFT programing system (9). The equations that have been derived are discussed first and then the methods for obtaining them.

### EQUATIONS RELATING SUCROSE CONCENTRATION TO SOLUTION DENSITY

Because density data covering only 0 to 30° C were available (4, 7), they were fitted by two equations: an empirical one that is quite accurate within the fitted range but should not be extrapolated, and a theoretically based one that is less accurate within the range but which may be extrapolated to 60° C.

The 9-constant, strictly empirical equation fits the tabulated data covering the concentration range of 0 to 75 weight percent sucrose and 0 to 30° C with a maximum deviation of 7 parts in 10 thousand.

The form of the empirical equation follows with the constants having the values given in table 2:

$$\begin{aligned} \rho_{T,m} = & (B_1 + B_2 T + B_3 T^2) \\ & + (B_4 + B_5 T + B_6 T^2)Y \\ & + (B_7 + B_8 T + B_9 T^2)Y^2 \end{aligned} \quad [4]$$

where

$\rho_{T,m}$  = density of a sucrose solution

$T$  = temperature, °C

$Y$  = weight fraction sucrose

and the  $B_i$ 's are constants.

TABLE 2.—Constants for empirical density calculation

Constant	Value*
$B_1$	1.0003698
$B_2$	$3.9680504 \times 10^{-5}$
$B_3$	$-5.8513271 \times 10^{-6}$
$B_4$	0.38982371
$B_5$	$-1.0578919 \times 10^{-3}$
$B_6$	$1.2392833 \times 10^{-5}$
$B_7$	0.17097594
$B_8$	$4.7530081 \times 10^{-4}$
$B_9$	$-8.9239737 \times 10^{-6}$

\*Values are given to 8 figures for machine calculations; use of the first 5 figures would be sufficient for hand calculations.

The second equation with 6 adjustable constants has a maximum deviation from the tabulated data covering 0 to 30° C and 0 to 70 weight percent sucrose of 4 parts per thousand. It is believed that the accuracy of this equation is the same from 30 to 60° C. No extrapolation beyond the composition limits of the data is required. The form of this equation follows with the constants having the values given in table 3:

$$\rho_{T,m} = \frac{yM_1 + (1-y)M_2}{y(C_1 + C_2T + C_3T^2) + (1-y)(A_1 + A_2T + A_3T^2)} \quad [5]$$

where  $A_1$ ,  $A_2$ , and  $A_3$  are constants that give the molar volume of water determined from independent data on pure water covering the temperature range of interest;  $C_1$ ,  $C_2$ , and  $C_3$  are constants that give the molar volume of liquid sucrose determined from the sucrose solution data;  $M_1$  and  $M_2$  are the molecular weights of sucrose and water; and  $y$  is the mole fraction of sucrose in the solution and is defined as follows:

$$y = \frac{Y/M_1}{Y/M_1 + (1-Y)/M_2} \quad [6]$$

where  $Y$  is the weight fraction sucrose.

The first equation should be used for centrifuge runs at 0 to 30° C and the second one at 30 to 60° C.

TABLE 3.—Constants for extrapolatable density function

Constant	Value*
$A_1$	18.027525
$A_2$	$4.8318329 \times 10^{-4}$
$A_3$	$7.7830857 \times 10^{-5}$
$M_1$	342.30
$M_2$	18.032
$C_1$	212.57059
$C_2$	0.13371672
$C_3$	$-2.9276449 \times 10^{-4}$

\*Values are given to 8 figures for machine calculations; use of 5 figures would be sufficient for hand calculations.

## EQUATIONS RELATING SUCROSE CONCENTRATION TO SOLUTION VISCOSITY

A set of equations giving the viscosity of sucrose solutions has been developed for 0 to 75 weight percent sucrose and 0 to 80° C. The standard deviation in viscosity over the entire range is 2 parts per thousand. No individual value deviates from the tabulated data by more than 3 parts per thousand between 5 to 40° C and 5 to 40 weight percent sucrose. Above 40° C and 40 weight percent sucrose, some individual values may

differ from tabulated values by as much as 8 parts per thousand, but even here the standard deviation is only 3 parts per thousand at any given composition. The set of equations thus gives the viscosity well within the allowed deviation of 1 percent from the tabulated data. The form of the equation also allows treatment of the viscosity of sucrose solutions by the "free volume" approach of Doolittle (10) and Miller (11, 12), which is helpful when effects of pressure on viscosity need to be treated.

The form of the set is shown in equations 7 to 9.

$$\log \eta_{T,m} = A + \frac{B}{T + C} \quad [7]$$

where  $\eta_{T,m}$  is the viscosity of sucrose solution at a given composition and temperature,  $T$  the temperature in °C, and  $A$ ,  $B$ , and  $C$  are constants that depend on composition alone.

The constant  $C$ , which has the dimensions of temperature in °C, is defined as a function of the composition over the whole range of compositions by the equation

$$C = G_1 - G_2 \left[ 1 + \left( \frac{y}{G_3} \right)^2 \right]^{1/2} \quad [8]$$

where  $y$  is the mole fraction of sucrose defined in equation 6 and the  $G_i$ 's are constants given in table 4.

TABLE 4.—Values of the Antoine constant as a function of the composition\*  
( $G_1 = 146.06635$ , \*  $G_2 = 25.251728$ , \*  $G_3 = 0.070674842$ \*)

Weight percent sucrose	Mole fraction sucrose	Antoine constant from equation 18 and tabulated data†	Antoine constant from equation 21 using $G$ -constants	Difference between columns 3 and 4
0	0.000000	122.03	120.81	1.22
5	0.002764	121.92	120.80	1.22
10	0.005818	121.68	120.73	0.95
15	0.009210	120.95	120.60	0.35
20	0.012996	121.17	120.39	0.78
23	0.015491	120.10	120.22	-0.12
25	0.017255	118.14	120.07	-1.93
28	0.020075	118.62	119.82	-1.20
30	0.022077	117.64	119.61	-1.97
33	0.025291	117.85	119.25	-1.40
35	0.027580	117.17	118.96	-1.79
38	0.031276	119.36	118.45	0.91
40	0.033926	119.25	118.06	1.19
45	0.041318	118.44	116.82	1.62
50	0.050042	115.71	115.13	0.58
55	0.060487	113.01	112.83	0.18
60	0.073230	109.92	109.70	0.22
65	0.089113	104.77	105.43	-0.66
70	0.109459	99.11	99.51	-0.40
75	0.136466	91.48	91.16	0.32

\*Numbers as given are for machine calculations. Use of 5 significant figures for hand calculations is adequate.

†Best value from Wood's NLLS Program using tabulated viscosity data at each composition.

The constants  $A$  and  $B$  are defined by a polynomial in the composition of the form

$$A = D_0 + D_1y + D_2y^2 + D_3y^3 + \dots + D_ny^n \quad [9]$$

where  $y$  is the mole fraction defined in equation 6 and the  $D$ 's are sets of constants defining  $A$  (or  $B$ ) for compositions above and below 48 weight percent sucrose. The values of these constants are given in tables 5 and 6.

TABLE 5.—Coefficients\* for calculation of the limiting viscosity or  $A$ -constant as a function of mole fraction sucrose

Coefficients†	Range of equation, weight percent	
	0 to 48	48 to 75
$D_0$	-1. 5018327	-1. 0803314
$D_1$	9. 4112153	-2. 0003484 $\times 10^1$
$D_2$	-1. 1435741 $\times 10^3$	4. 6066898 $\times 10^2$
$D_3$	1. 0504137 $\times 10^5$	-5. 9517023 $\times 10^3$
$D_4$	-4. 6927102 $\times 10^6$	3. 5627216 $\times 10^4$
$D_5$	1. 0323349 $\times 10^8$	-7. 8542145 $\times 10^4$
$D_6$	-1. 1028981 $\times 10^9$	
$D_7$	4. 5921911 $\times 10^9$	

\* Numbers as given for machine calculation.

† Coefficient subscript indicates the exponent of the composition by which the coefficient is to be multiplied.

TABLE 6.—Coefficients\* for calculation for the activation energy or  $B$ -constant as a function of mole fraction sucrose

Coefficients†	Range of equation, weight percent	
	0 to 48	48 to 75
$D_0$	2. 1169907 $\times 10^2$	1. 3975568 $\times 10^2$
$D_1$	1. 6077073 $\times 10^3$	6. 6747329 $\times 10^3$
$D_2$	1. 6911611 $\times 10^5$	-7. 8716105 $\times 10^4$
$D_3$	-1. 4184371 $\times 10^7$	9. 0967578 $\times 10^5$
$D_4$	6. 0654775 $\times 10^8$	-5. 5380830 $\times 10^6$
$D_5$	-1. 2985834 $\times 10^{10}$	1. 2451219 $\times 10^7$
$D_6$	1. 3532907 $\times 10^{11}$	
$D_7$	-5. 4970416 $\times 10^{11}$	

\* Numbers as given for machine calculations.

† Coefficient subscript indicates the exponent of the composition by which the coefficient is to be multiplied.

## DEVELOPMENT AND DISCUSSION OF DENSITY RELATIONS

The density data selected for fitting were those given by de Duve *et al.* (4) and Snyder and Hammond (7) at 0° C and at 10, 15, 20, 25, and 30° C, respectively. The tabulated data of Snyder and Hammond (7) were converted from the weight in air per gallon of solution to absolute densities in grams per cubic centimeter by correction for the weight of the air displaced by the solution and the weights. The absolute density data to be fitted are given in table 1. Since the tabulated data do not cover the entire temperature range of interest, it is necessary not only to

obtain an accurate fit through the range given but to be able to extrapolate the relationship developed to higher temperatures as well. Thus, two equations have been developed. The first was to be as accurate as possible within the temperature range of the data and the second to be extrapolatable with confidence beyond the range temperature of the data.

In developing both equations, it was kept in mind that the change in volume of pure materials with temperature may be accurately expressed over a range of several tens of °C by

$$V = V_0 [1 + \alpha(T - T_0) + \beta(T - T_0)^2] \quad [10]$$

where  $V$  is the volume at temperature  $T$  (in °C),  $V_0$  is the known volume at the reference temperature,  $T_0$ , and  $\alpha$  and  $\beta$  are constants for a given material.

Since the temperature range of interest includes 0° C, equation 10 becomes

$$V = V_0 (1 + \alpha T + \beta T^2) \quad [11]$$

where  $V_0$  is the volume at 0° C.

Because the density is inversely proportional to the volume and  $\alpha$  and  $\beta$  are small with respect to unity, the equation for density in terms of the density at  $T_0$  may also be written

$$\rho_{T,m} = \rho_0 [1 + \alpha'(T - T_0) + \beta'(T - T_0)^2] \quad [12]$$

where  $\rho_{T,m}$  is the density at temperature  $T$ ,  $\rho_0$  the density at temperature  $T_0$ , and  $\alpha'$  and  $\beta'$  are constants for a given material. Again,  $(T - T_0)$  should not exceed a few tens of degrees.

For a reference temperature of 0° C, equation 12 reduces to the following form:

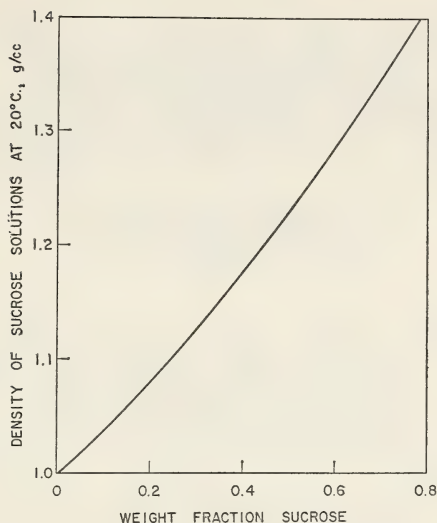
$$\rho_{T,m} = B_1 + B_2 T + B_3 T^2 \quad [13]$$

where the  $B$ 's are constants characteristic of the material.

Since the density of sucrose (m.w. 342.3) is only about 50 percent greater than that of water (m.w. 18.032), a plot of the density of sucrose solutions of varying compositions at a given temperature versus composition expressed in weight fraction may and, in fact, does show only small deviations from linearity as is illustrated in text-figure 1. This means that at constant temperature, density is accurately expressed as a function of the weight fraction by the second-order polynomial

$$\rho_{T,m} = H_1 + H_2 Y + H_3 Y^2 \quad [14]$$

where  $\rho$  is the density of solution of composition  $Y$ ,  $Y$  the weight fraction sucrose, and  $H_1$ ,  $H_2$ , and  $H_3$  are temperature-dependent constants. The constant  $H_1$  is the density of water at the given temperature.



TEXT-FIGURE 1.—Density of sucrose solutions as a function of composition at 20° C.

Combination of the relation in equation 14 with that in equation 13 gives an equation of the form of equation 4, which may be sufficiently accurate. By Wood's NLLS Program (8), the set of constants listed in table 2 were obtained for the set of tabulated data in table 1. The standard deviation over the whole set is 3 parts in 10 thousand and the maximum deviation is 7 parts in 10 thousand.

Equation 4 is sufficiently accurate over the temperature range of the data, but equations of this kind cannot be reliably extrapolated. To be extrapolated with confidence, the confidence limits on the coefficients of the higher power terms in a polynomial must be small. Since this is not the case here, the equation may blow up rapidly outside the range of the data fitted. The available data, therefore, have been examined to see if any reliable method for extrapolation exists. The density of any binary solution at a given temperature may be calculated by the relation

$$\rho_{T,m} = \frac{yM_1 + (1-y)M_2}{y\bar{V}_1 + (1-y)\bar{V}_2} \quad [15]$$

where  $M_1$  and  $M_2$  are the molecular weights of components 1 and 2,  $\bar{V}_1$  and  $\bar{V}_2$  the partial molar volumes of components 1 and 2,  $y$  is the mole fraction of component 1:

$$y = \frac{Y_1/M_1}{Y_1/M_1 + (1-Y_1)/M_2}, \quad [16]$$

and  $Y_1$  the weight fraction of component 1.

The partial molar volumes  $\bar{V}_1$  and  $\bar{V}_2$  may be functions of composition as well as temperature. The molar volumes  $V_1$  and  $V_2$  may be substituted if the volumes of solute and solvent are additive.

Since by definition the molecular weight of one total mole<sup>4</sup> is given by the expression,  $yM_1 + (1 - y)M_2$ , the actual volume of one total mole of the sucrose solution can be calculated from the density by

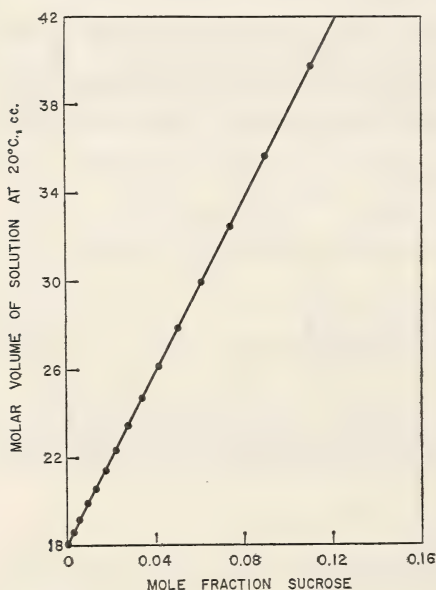
$$V_y = \frac{yM_1 + (1 - y)M_2}{\rho_y} \quad [17]$$

where  $V_y$  is the molar volume at mole fraction  $y$ ,  $\rho_y$  the experimental or tabulated density at the same mole fraction,  $M_1$  and  $M_2$  the molecular weights of sucrose and water, and  $y$  the mole fraction sucrose.

From equation 17, the weights and volumes of one total mole of sucrose solution at the various temperatures for which density data are available were calculated (table 7). A plot,  $V_y$  against  $y$  at 20° C, as illustrated in text-figure 2, was linear within the plotting error so that sucrose solutions may be said to be nearly ideal and the molar volumes substituted for the partial molar volumes in equation 15 to give

$$\rho_{T,m} = \frac{yM_1 + (1 - y)M_2}{yV_1 + (1 - y)V_2} \quad [18]$$

where  $V_1$  and  $V_2$  are the molar volumes of sucrose in the liquid state and water, respectively.



TEXT-FIGURE 2.—Volume of one total mole of sucrose solution at 20° C.

<sup>4</sup> The term one total mole of a solution refers to that quantity of solution which contains just sufficient amount of each component that the sum total of moles of all the components is 1.

TABLE 7.—Weights and volumes of one total mole of sucrose solutions at various temperatures

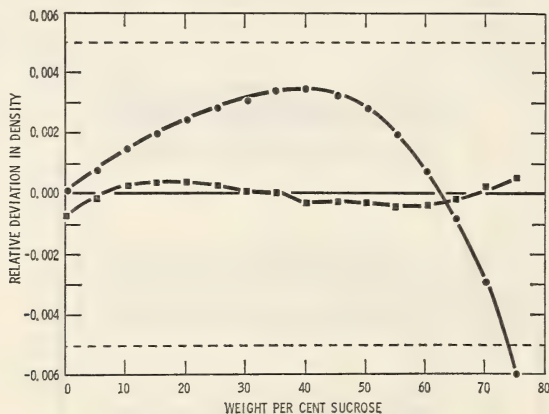
Weight percent sucrose in vacuum	Mole fraction sucrose	Weight of one total mole of solution	Volume of one total mole of solution at indicated temperatures (° C), g/cc						
			0	10	15	20	25	30	
0	0.00000	18.0320	18.0320	18.0376	18.0476	18.0640	18.0864	18.1108	
5	0.00276	18.9269	18.5558	18.5602	18.5749	18.5950	18.6189	18.6435	
10	0.00582	19.9192	19.1292	19.1512	19.1682	19.1874	19.2109	19.2406	
15	0.00921	21.0185	19.7728	19.8009	19.8209	19.8445	19.8711	19.9012	
20	0.01300	22.2475	20.4971	20.5296	20.5550	20.5812	20.6110	20.6466	
25	0.01726	23.6289	21.3084	21.3566	21.3824	21.4115	21.4448	21.4810	
30	0.02208	25.1918	22.2385	22.2903	22.3219	22.3534	22.3819	22.4280	
35	0.02758	26.9753	23.3068	23.3607	23.3931	23.4307	23.4690	23.5126	
40	0.03393	29.0344	24.5264	24.5979	24.6370	24.6797	24.7209	24.7713	
45	0.04132	31.4307	25.9693	26.0511	26.0914	26.1369	26.1840	26.2364	
50	0.05004	34.2584	27.6768	27.7625	27.8103	27.8621	27.9132	27.9676	
55	0.06049	37.6469	29.7298	29.8318	29.8823	29.9369	29.9963	30.0536	
60	0.07323	41.7781	32.2486	32.3538	32.4138	32.4762	32.5415	32.6022	
65	0.08911	46.9275	35.3903	35.5135	35.5848	35.6502	35.7219	35.7941	
70	0.10946	53.5264	39.4446*	39.5814	39.6595	39.7325	39.8084	39.8950	
75	0.13647	62.2849	44.8318*	44.9948	45.0814	45.1677	45.2556*	45.3519*	

\*Value obtained by two-way extrapolation of the tabulated data.

Now both  $V_1$  and  $V_2$  are intensive properties and expressible as second-order polynomials in  $T$ , where  $T$  is in  $^{\circ}\text{C}$ . Further, the data for the molar volume of water are accurately known over the whole temperature range of interest (13) so that  $V_2$  can be determined independently of the set of data for the density of sucrose solutions. Thus the data on the density of sucrose solutions can be used to determine the theoretical molar volume of sucrose in the liquid state as a function of temperature. Since the volume of sucrose should be accurately expressed as a second order polynomial in  $T$ , the density equation will have the form of equation 5.

The  $C_i$ -constants were evaluated from the sucrose solution data with the  $A$ -constants, Wood's NLLS Program (8), and equation 5. All the constants for the extrapolatable density function so developed are given in table 3.

With these constants, the maximum deviation between the calculated and tabulated density values in the range of the data between 0 to 30 $^{\circ}\text{C}$  and 0 to 70 weight percent sucrose is 4 parts per thousand. The relative deviation in the density from the tabulated data at 25 $^{\circ}\text{C}$  is shown as a function of the weight percent sucrose for both equations 4 and 5 in text-figure 3. Equation 5 will suffer very little loss in accuracy when extrapolated to 60 $^{\circ}\text{C}$ , because (a) the molar volume of water is accurately predicted over the range of 0 to 75 $^{\circ}\text{C}$ , (b) the ideality of sucrose solutions increases with increasing temperature, and (c) the relation for the molar volume of sucrose shows very little deviation from linear dependence on temperature.



TEXT-FIGURE 3.—Relative deviation in density equations (25 $^{\circ}\text{C}$ ). ■: equation 4; ●: equation 5.

## DEVELOPMENT AND DISCUSSION OF VISCOSITY EQUATIONS

The viscosity data for sucrose solutions chosen for fitting are those tabulated at the National Bureau of Standards by Swindells and co-workers (6). These data are tabulated as functions of composition at

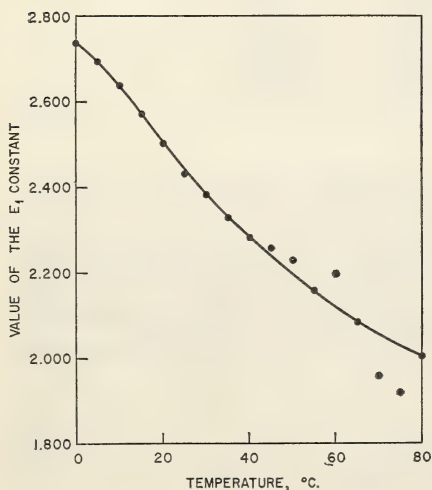
intervals from 20 to 75 weight percent sucrose and of 5° C from 0 to 80° C. Since the only data tabulated between 0 and 20 weight percent sucrose are those presented at 20° C, viscosity values at intervals of 5 percent between 0 and 20 weight percent sucrose were developed at each of the other 5° C intervals in the 80° C range with the NBS equations:

$$\ln \eta_{T,m}/\eta_{T,w} = E_1 \frac{Y}{1-Y} + E_2 Y^2 \quad [19]$$

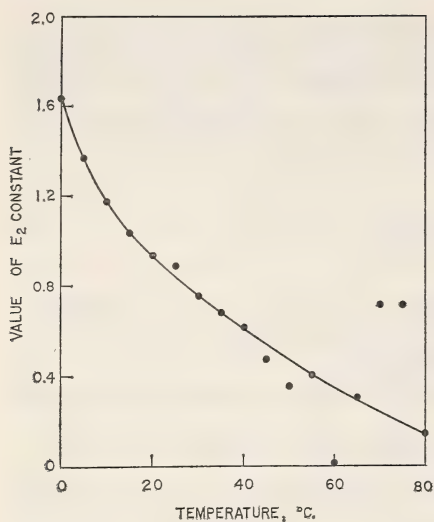
where  $\eta_{T,m}$  is the viscosity of the sucrose solution,  $\eta_{T,w}$  the viscosity of pure water at a given temperature,  $Y$  the weight fraction of sucrose, and  $E_1$  and  $E_2$  temperature-dependent constants.

Values of  $E_1$  and  $E_2$  were computed from the viscosity data for pure water and for sucrose solutions containing 20 and 30 weight percent sucrose at the desired temperature intervals. Text-figures 4 and 5 show values of  $E_1$  and  $E_2$  as functions of temperature. Smoothed values were used to calculate the viscosity values at 5 weight percent intervals between 0 and 20 weight percent sucrose (table 8). Equation 19 cannot be extrapolated beyond the composition range used in computation of  $E_1$  and  $E_2$  with any accuracy. The viscosity data to be fitted by equations giving the viscosity as a function of temperature and composition are those obtained in tables 131, 132, and 133 of NBS 440 (6) supplemented by the data for pure water (13) and the values obtained as outlined above.

In fitting the viscosity data, it is recognized that water is an associated liquid containing clusters of molecules with a high degree of structural order and that sucrose itself is capable of forming hydrogen bonds with the water. Since varying the amounts of sucrose may be expected to affect the structural arrangement of the solution more than varying the temperature, an equation was sought which would accurately describe



TEXT-FIGURE 4.—The  $E_1$ -constant in equation 19 as a function of temperature.



TEXT-FIGURE 5.—The  $E_2$ -constant in equation 19 as a function of temperature.

TABLE 8.—Smoothed values of  $E_1$ - and  $E_2$ -constants in equation 19 as a function of temperature

Temperature (°C)	$E_1$	$E_2$
0	2.7373	1.6373
5	2.6941	1.3697
10	2.6371	1.1748
15	2.5720	1.0325
20	2.5032	0.9362
25	2.4420	0.8450
30	2.3831	0.7568
35	2.3286	0.6834
40	2.2763	0.6117
45	2.2380	0.5440
50	2.1950	0.4780
55	2.1575	0.4043
60	2.1160	0.3510
65	2.0837	0.3044
70	2.0540	0.2460
75	2.0270	0.1930
80	2.0046	0.1433

the change of the viscosity with temperature at constant composition. By use of the "hole" theory of Eyring and associates (14), the Antoine or modified Arrhenius equation so successfully used in vapor pressure treatment was tried. The free volume approach of Doolittle (10) and Miller (12) also leads to similar equations. As related to viscosity, the Antoine equation has the form given in equation 7. This equation may be more familiar in the Arrhenius form

$$\ln \frac{\eta_{T,m}}{\eta_0} = \frac{\Delta H^*}{R(T_A - T_0)} \quad [20]$$

where

$$\ln \eta_0 = 2.303 A \quad [21]$$

$$\frac{\Delta H^*}{R} = 2.303 B \quad [22]$$

$$T_0 = 273.16 - C \quad [23]$$

In these equations,  $\eta_0$  is the limiting viscosity,  $\Delta H^*$  the heat of activation for viscous flow, and  $R$  the gas constant in units compatible with those of  $\Delta H^*$ .  $T_A$  is the absolute temperature in  $^{\circ}\text{K}$ , and  $T_0$  is probably best defined as the temperature in  $^{\circ}\text{K}$  at which the free volume of the solution of the given composition becomes zero (11).

Since the  $C$ -constant in equation 7 is the constant that characterizes this expression as an Antoine equation, the  $C$ -constant will be referred to as the Antoine constant. The zero-free-volume temperature constant may be obtained from the  $C$ -constant by equation 23. Because of the relationships in equations 21 and 22,  $A$  will be referred to as the intrinsic viscosity constant and  $B$  the activation energy constant.

The constants,  $A$ ,  $B$ , and  $C$ , were computed from the tabulated temperature dependence of the viscosity at 0, 5, 10, 15, 20, 23, 25, 28, 30, 33, 35, 38, 40, 45, 50, 55, 60, 65, 70, and 75 weight percent sucrose with Wood's NLLS Program (8). Constants  $A$ ,  $B$ , and  $C$  are found at any of the listed compositions such that the viscosity data as a function of temperature are reproduced to about 3 parts per thousand. Plots of  $A$ ,  $B$ , and  $C$  against composition indicated that these constants were reasonably smooth functions of the composition.

To be certain that equation 7 could not readily be improved for expressing the temperature dependence of viscosity at constant composition, the following equations were also tried:

$$\log \eta_{T,m} = K_1 + \frac{K_2}{T_A} + \frac{K_3}{T_A^2} \quad [24]$$

and

$$\log \eta_{T,m} = \frac{L_1 + L_3 T}{1 + L_2 T + L_4 T^2} \quad [25]$$

where the  $K$ 's and  $L$ 's are constants at any given composition, and  $\eta_{T,m}$ ,  $T$ , and  $T_A$  have the same meanings as before. Misra and Varshni (15) used equation 24 for obtaining an analytical relation to express the viscosity of alcohol-water mixtures as a function of temperature. The empirical equation 25 often gives better fits to curves than does linear polynomials like equation 24.

The fits to the tabulated data obtained with equations 24 and 25 were poorer than the fits with equation 7, and the  $K$ 's and  $L$ 's were not as

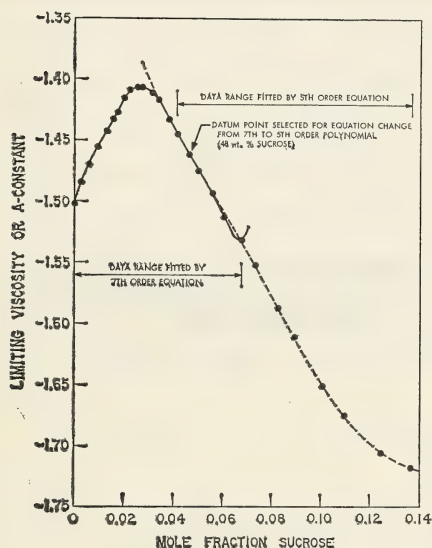
smooth functions of the compositions as were the  $A$ 's,  $B$ 's, and  $C$ 's obtained with equation 7. Since the accuracy of equation 7 is least sensitive to small changes in the  $C$  or Antoine constant, the  $C$ -constant was fitted throughout the temperature range as a function of composition only. With the composition expressed as mole fraction of sucrose, the functional dependence of the  $C$ -constant on mole fraction was shown empirically to be hyperbolic, and the  $C$ -constant determined by the application of equation 7 was fitted as the negative right hand leg of a hyperbola, as indicated in equation 8. The required  $G_i$ -constants, which are independent of both temperature and composition, were developed with the use of the NLLS Program (8). The  $G_i$ -constants and a comparison of the values of the  $C$ -constants calculated from the  $G_i$ -values with the values used to develop the  $G_i$ 's are given in table 4. In developing the  $G_i$ -constants, no restraint was placed on the value at zero concentration sucrose, and the value obtained of 120.8 may be compared with that at 123.2 from  $T_0$  for pure water (11). Since the values of  $C$  decrease with increasing concentration of sucrose, the free volume fraction at any given temperature decreases as the sucrose concentration is increased.

With this functional relationship for the  $C$  value, the other two constants were re-evaluated from the viscosity data at constant composition for following weight percents sucrose with the NLLS Program: 0, 5, 10, 15, 20, 23, 28, 30, 33, 35, 38, 40, 43, 45, 48, 50, 53, 55, 58, 60, 63, 65, 68, 70, 73, 75. There was essentially no loss in the precision of the fit to the tabulated data, which thus indicated the selection of a satisfactory dependence of the  $C$ -constant on composition. The values of the  $A$ - and  $B$ -constants thus obtained plot as smooth functions of the composition expressed as mole fraction of sucrose, but the curves contain some features that are difficult to describe analytically with the use of any simple function.

Attempts to analyze the  $A$  constant in terms of the limiting viscosity concept, with the relations that the reciprocal of the viscosity is the fluidity and that the molar fluidities are additive according to the mole fraction rule, did not result in anything easier to treat analytically than is the  $A$ -constant as a function of mole fraction itself. Attempts to handle the activation energy or  $B$ -constant in terms of molar heats of activation with the additivity rule were similarly unfruitful.

While neither the  $A$ -constant or  $B$ -constant could be expressed as a simple function of the composition, the shape of the  $A$ -constant versus mole fraction sucrose, as shown in text-figure 6, suggested that, if the composition range were broken into two segments, a high-order polynomial could be used to give a satisfactory fit to both segments with an acceptable overlap. A seventh-order polynomial in the mole fraction was found to fit the  $A$ -constant data from 0 to 58 weight percent (0.0–0.0678 mole fraction) sucrose with a standard deviation of  $1.4 \times 10^{-3}$ , and a fifth-order polynomial in the mole fraction was found to fit the  $A$ -constant data from 45 to 74 weight percent (0.0413–0.136 mole fraction) sucrose with a standard deviation of  $1.9 \times 10^{-3}$ . As can be seen from

text-figure 6, these two equations give essentially identical values of the  $A$ -constant over a range of compositions. On the basis of an excellent match of  $A$ -constant and  $dA/dy$  values, a composition of 48 weight percent (0.0464 mole fraction) sucrose was selected for transfer from the seventh- to the fifth-order polynomial equation. The respective values of the  $A$ -constant for the two equations at 0.0464 mole fraction are  $-1.4626$  and  $-1.4629$ . The coefficients for calculating the  $A$ -constant as a function of mole fraction for the two composition ranges are given in table 5.

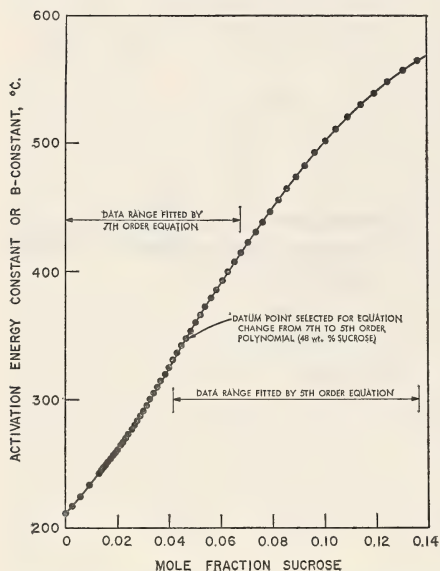


TEXT-FIGURE 6.—Limiting viscosity or  $A$ -constant as a function of mole fraction sucrose.

Identical procedures yielded a seventh-order polynomial and a third-order polynomial description of the  $B$ -constant as a function of mole fraction having the same ranges of application as the  $A$ -constants. However, detailed examination of the behavior of the general set of equations for the viscosity of sucrose solutions indicated that, whereas the tabulated data at temperatures above  $40^{\circ}\text{C}$  were fit about as well as could be expected, the data below  $40^{\circ}\text{C}$  were considerably more accurate than the fit provided by the equations. Study of the fits obtained for the  $A$ - and  $B$ -constants indicated that significant improvement in the fit at individual temperatures and compositions would be obtained by assuming that not only the dependence of the Antoine constant but also the limiting viscosity constant or  $A$ -constant upon the composition were exactly as calculated and by allowing all the errors to be accumulated in the activation energy or  $B$ -constant.

An OR-SFT program was written which calculated mean values of  $B$  for every tabulated composition. A typical calculation is shown in table 9 for 35 weight percent sucrose. Since for every composition the average values of the  $B$ -constant for the two ranges of temperature were the same

within the 95 percent confidence limits, the values over the 0 to 40° C range were chosen for fitting as a function of mole fraction because it was in this temperature range that an improvement in the fit was sought. The values to be fitted and the results of fitting them with the same power polynomials used for the *A*-constant are shown in text-figure 7 as a function of mole fraction. The standard deviation or  $\sigma$  is  $\pm 0.037$  in the range of compositions covered by the seventh-order polynomial and is  $\pm 0.020$  in the range of compositions covered by the fifth-order polynomial. The coefficients to be used in the calculation of the activation energy or *B*-constant as a function of the composition are given in table 9.



TEXT-FIGURE 7.—Activation energy constant or *B*-constant as a function of mole fraction sucrose.

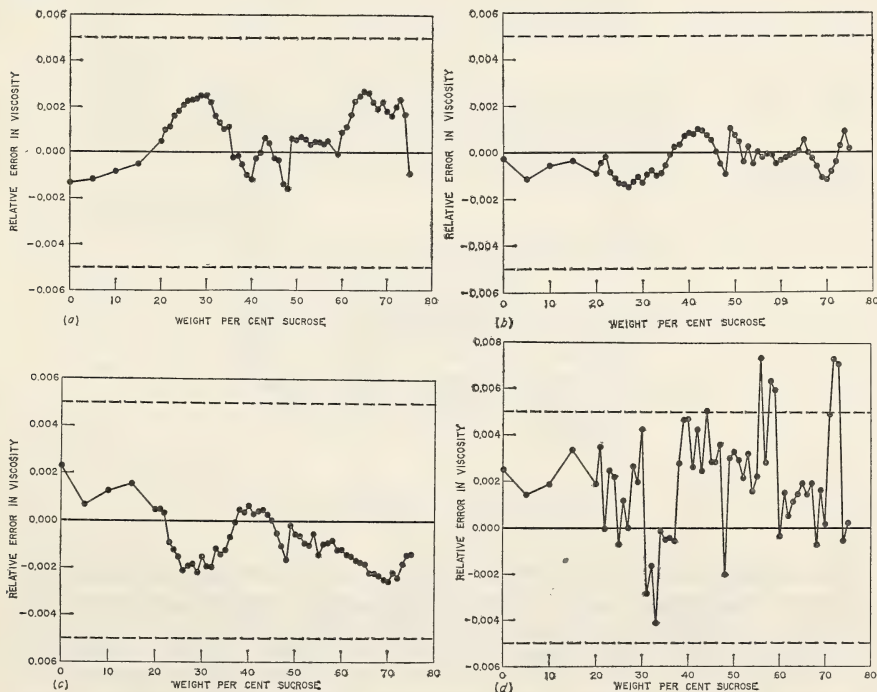
TABLE 9.—Typical results of calculation of activation energy or *B*-constant\* from tabulated data†

Temperature, °C	<i>B</i> -constant, °C
0.00	283.796
5.00	283.786
10.00	283.770
15.00	283.741
20.00	283.721
25.00	283.692
30.00	283.660
35.00	283.663
40.00	283.642
45.00	283.691
50.00	283.482
55.00	283.325
60.00	283.641
65.00	283.792
70.00	283.983
75.00	283.738
80.00	283.947

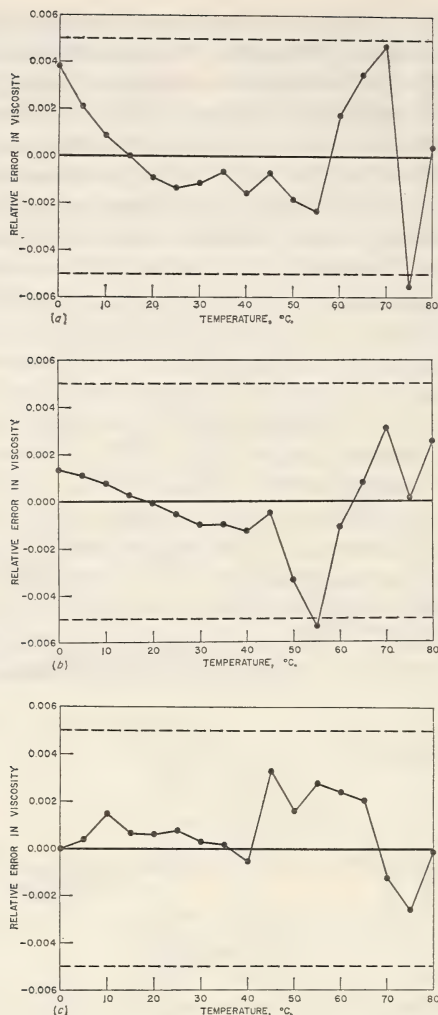
\*Average *B*-constant over 0 to 40° C =  $283.719 \pm 0.035$  °C. Average *B*-constant over 0 to 80° C =  $283.710 \pm 0.069$  °C.

†For 35 weight percent sucrose solution. Mole fraction, 0.027583; *A*-constant,  $-1.40597$ ; *C*-constant,  $118.96$  °C.

By use of the set of equations developed for viscosity, the tabulated viscosity data have been compared with the calculated values. The standard deviation in the viscosity over the entire range of temperature and composition is 2 parts per thousand. No individual value is in error by more than 3 parts per thousand in the temperature and composition ranges of primary interest of 5 to 40° C and 5 to 40 weight percent sucrose. At concentrations above 40 weight percent sucrose and/or at temperatures above 40° C, occasional values deviate from the calculated data by as much as 8 parts per thousand. The relative errors in the viscosity as computed by the equations are illustrated by the seven plots in text-figures 8 and 9. In text-figures 8 a, b, c, and d, the relative deviation between the tabulated and computed values is shown as a function of composition at temperatures of 5, 25, 40, and 45° C, respectively, and in the remaining figures as a function of the temperature at constant compositions of 25, 35, and 50 weight percent, respectively. The error at constant temperature markedly changes between 40 and 45° C. This is a result of a shift of an order of magnitude in the precision with which the tabulated data are stated in the Bureau of Standards tables (6), a shift that occurs between these same two temperatures. The increased deviation between the tabulated and computed viscosities above 40° C is also apparent from text-figures 9 a, b, and c. This set of equations is believed to reproduce the tabulated viscosity data almost within the precision of the tabulated data.



TEXT-FIGURE 8.—Fractional deviation from tabulated values as a function of composition at (a) 5° C, (b) 25° C, (c) 40° C, and (d) 45° C.



TEXT-FIGURE 9.—Fractional deviation from tabulated values as a function of temperature at a constant composition of sucrose weight percent: (a) 25, (b) 35, and (c) 50.

### EFFECT OF PRESSURE

The density and viscosity relations that have been developed are for normal atmospheric pressure. It is recognized that the density of liquids normally increases as the pressure on the liquid is increased. For water at a temperature below that of maximum density, increased pressure decreases viscosity; above the temperature of maximum density, the viscosity increases with increasing pressure (11). Since for water the

increase in density is of the order of  $4.4 \times 10^{-5}$  g/cc-atm, the maximum correction that would need to be applied for the pressures developed in the centrifuge is of the same order as the errors in the equations. Similarly, for water, the errors in the viscosity made by neglect of the pressure correction are within the error in the equations. Since it can be demonstrated that approximately another order of magnitude increase in the pressure would be needed to make the corrections significant for water, it is believed that the pressure correction can be safely neglected for sucrose solutions used in presently available zonal centrifuges.

## REFERENCES

- (1) ANDERSON, N. G.: An introduction to particle separations in zonal centrifuges. *Nat Cancer Inst Monogr* 21: 9-39, 1966.
- (2) ALLFREY, V.: The isolation of subcellular components. In *The Cell* (Brachet, J., and Mirsky, A. E., eds.). New York, Academic Press Inc., 1959, vol I, pp 193-290.
- (3) BRAKKE, M. K.: Density gradient centrifugation and its application to plant viruses. *Advances Virus Res* 7: 193-224, 1960.
- (4) DE DUVE, C., BERTHET, J., and BEAUFAY, H.: Gradient centrifugation of cell particles. Theory and application. In *Progress in Biophysics and Biophysical Chemistry*, 9 (Butler, J. A. V., and Katz, B., eds.). London, Pergamon Press, chap 7, 1959.
- (5) MARTIN, R. G., and AMES, B. N.: A method for determining the sedimentation behavior of enzymes. Application to protein mixtures. *J Biol Chem* 236: 1372, 1961.
- (6) SWINDELLS, J. F., SNYDER, C. F., HARDY, R. C., and GOLDEN, P. E.: Viscosities of sucrose solutions at various temperatures; tables of recalculated values. Supplement to National Bureau of Standards Circular 440.
- (7) SNYDER, C. F., and HAMMOND, L. D.: Weights per United States gallon and weights per cubic foot of sugar solutions. Circular of the National Bureau of Standards C-457.
- (8) WOOD, P. B.: NLLS: A 704 program for fitting non-linear curves by least squares. Union Carbide Corp., Oak Ridge Gaseous Diffusion Plant, Oak Ridge, Tenn., Report K-1440, Jan. 28, 1960.
- (9) KELLEY, J. P., and KNIGHT, G. B.: OR-SFT Programmers Reference Manual. Union Carbide Corp., Oak Ridge Gaseous Diffusion Plant, Oak Ridge, Tenn., Report KOA-612.
- (10) DOOLITTLE, A. K.: *The Technology of Solvents and Plasticizers*. New York, John Wiley and Sons, chap 13, 1954.
- (11) MILLER, A. A.: Free volume and the viscosity of liquid water. *J Chem Phys* 38: 1568-1571, 1963.
- (12) ———: Free volume and viscosity of liquids. Effects of temperature. *J Phys Chem* 67: 1031-1035, 1963.
- (13) HODGMAN, C. D.: *Handbook of Chemistry and Physics*, 28th ed. Cleveland, Ohio, Chemical Rubber Pub Co., 1944, p 1630
- (14) GLASSTONE, S., LAIDLER, K. J., and EYRING, H.: *The Theory of Rate Processes*. New York, McGraw-Hill Book Company, Inc., chap 9, 1941.
- (15) MISRA, B. N., and VARSHNI, Y. P.: Viscosity-temperature relations for solutions. *J Chem Eng Data* 6: 194, 1961.



## Preparation and Recovery of Cesium Compounds for Density Gradient Solutions<sup>1</sup>

R. R. WRIGHT, W. S. PAPPAS, J. A. CARTER, and  
C. W. WEBER,<sup>2</sup> *Technical Division, Oak Ridge Gaseous  
Diffusion Plant,<sup>3</sup> Oak Ridge, Tennessee*

### SUMMARY

Methods have been developed for purifying, recovering, and preparing cesium compounds for biological separations in the zonal centrifuge. Saturated solutions of cesium chloride with absorbancies as low as 0.03 (1 cm path at 260 m $\mu$ ) have been prepared. Serum and other organic impurities were removed by carbonization and filtering. A liquid exchange system was designed for recover-

ing high-purity cesium compounds from impure solutions. In a simple, semicontinuous system the cesium was selectively extracted from metallic impurities, including other alkali metals, with 4-sec-butyl-2-( $\alpha$ -methylbenzyl)-phenol (BAMBP) in Varsol from an alkaline solution and stripped with acid.—*Nat Cancer Inst Monogr* 21: 241-249, 1966.

HIGH PURITY cesium compounds are used in preparing density gradients for isolating viruses, subcellular fractions, and nucleic acids by zonal centrifugation (1, 2). The total divalent cation impurities of these compounds should be less than 100 ppm and total elemental impurities should not exceed 1 percent. Since optical methods are used to monitor the centrifugation separations for particle bands, absorbancy at 260 m $\mu$  of the saturated solutions must be low, preferably less than 0.1 for a 1 cm light path.

This report describes methods for reducing the absorbancy of cesium chloride (CsCl), recovering high-purity cesium compounds from waste solutions, and preparing organic cesium salts.

---

<sup>1</sup> This research performed under the Joint National Institutes of Health-Atomic Energy Commission Zonal Centrifuge Development Program which is supported by the National Cancer Institute, the National Institute of Allergy and Infectious Diseases, and the U.S. Atomic Energy Commission.

<sup>2</sup> We wish to thank R. Aiken and S. A. MacIntyre for recommendations based on their preliminary investigation of the problem, C. M. Preston and Z. Wright for special equipment fabrication, and D. C. S. Randolph and R. D. Rivers for skilled technical assistance.

<sup>3</sup> Operated for the U.S. Atomic Energy Commission by the Nuclear Division of Union Carbide Corporation.

## REDUCING THE ABSORBANCY OF COMMERCIALY AVAILABLE CESIUM CHLORIDE

The absorbancy (1 cm path at 260  $m\mu$ ) of a saturated solution of purified CsCl, purchased from American Potash and Chemical Corporation, was 0.32. Repeated filtration of the solution through Whatman No. 42 paper lowered this value to about 0.2. The dry salt is heated at 450 to 470° C for 30 minutes, cooled, and enough distilled water added to make a saturated solution, which is filtered. Trace organic impurities are destroyed by this procedure, and certain trace metals including iron, calcium, and aluminum are removed as oxides or hydrated oxides. Saturated solutions with an absorbancy as low as 0.03 were prepared in this manner.

## RECOVERY OF WASTE CESIUM CHLORIDE

Both organic and inorganic impurities are introduced into CsCl gradients during centrifugation. Besides the samples introduced into the rotor, such as viruses, homogenates, and other culture fluids, sucrose is used in some experiments. A number of anionic and metallic impurities enter the system with these additives, while others come from trace erosion and corrosion of the rotor and associated components.

To inactivate contaminants, waste solutions from virus experiments are autoclaved twice before handling. Organic contaminants and divalent metals are removed from waste cesium chloride after each run. Since alkali metals are introduced in only trace quantities by serum, and because small amounts of these metals are permissible, several runs are possible with reprocessed CsCl solutions before removal of these metals is necessary.

## Carbonization and Filtration

Waste CsCl solutions were evaporated to dryness in 5 liter boiling flasks by use of Glas-Col heaters. The solids, including organic contaminants, were heated at 450 to 500° C for 2 hours to degrade the organic materials to carbon, which is subsequently removed by filtration through a bed of filter pulp and decolorizing activated carbon on Whatman No. 42 filter paper. Some of the metallic impurities are removed as hydroxides or oxides and by sorption on the carbon during the filtration.

The average absorbancy at 260  $m\mu$  of saturated solutions of CsCl recovered in this way is less than 0.05. Chemical and spectrochemical analyses of recovered cesium chloride are presented in table 1. Except for sodium and potassium, no metallic impurities were detected.

TABLE 1.—Analysis of cesium chloride after carbonization-filtration recovery\*

Spectrochemical		Chemical	
Element	Concentration of each element (ppm)	Measurement	Concentration
Ag, Al, Be, Ca, Cr, Cu, Fe, Mg, Mn, Mo, and V	<1	CsCl	1242 g/liter
Pb and Ti	<5	P as $\text{PO}_4^{3-}$ (colorimetric)	<5 ppm
Bi, Cd, Co, Ni, Si, and Sn	<10	Nitrogen (Kjeldahl)	<25 ppm
P and Zn	<50	Density	1.91 g/ml
Na (flame photometry)	500	Absorbancy at 260 $\text{m}\mu$ vs $\text{H}_2\text{O}$	0.047
K (flame photometry)	80	—	—

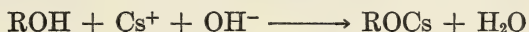
\*The symbol < denotes the lower limit of detection; ppm values are on a CsCl (weight) basis.

## REMOVAL OF METALLIC IMPURITIES INCLUDING ALKALI METALS

### BAMBP Extraction

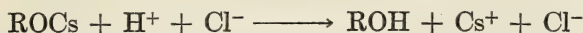
An organic extraction method (3), developed at the Oak Ridge National Laboratory, is used for removing metallic impurities. In this method cesium is separated by liquid cation exchange with 4-sec-butyl-2-( $\alpha$ -methylbenzyl)-phenol, conveniently called BAMBP.

A Varsol solution of BAMBP, in the hydrogen form (ROH), is reacted with the impure cesium chloride solution, made alkaline with sodium hydroxide:



The phenolic BAMBP is a weak acid, so that cesium extraction is sensitive to  $p\text{H}$  and is best at higher  $p\text{H}$  values. The extractant has much more affinity for cesium than for sodium or other metals of interest. According to Arnold and Crouse (4), at  $p\text{H}$  12 to 13 the order of extractability is  $\text{Cs} > \text{Rb} > \text{K} > \text{Na} > \text{Li}$ . In this  $p\text{H}$  region, separation factors as high as 250 for cesium/potassium and several thousand for cesium/sodium are found, depending on the concentrations involved. Under usual process conditions, a maximum solvent loading of 1 mole of cesium per 4 moles of the substituted phenol is attained. According to Egan *et al.* (5), the additional molecules of the substituted phenol are tied up in solvating the salt molecule in the organic phase.

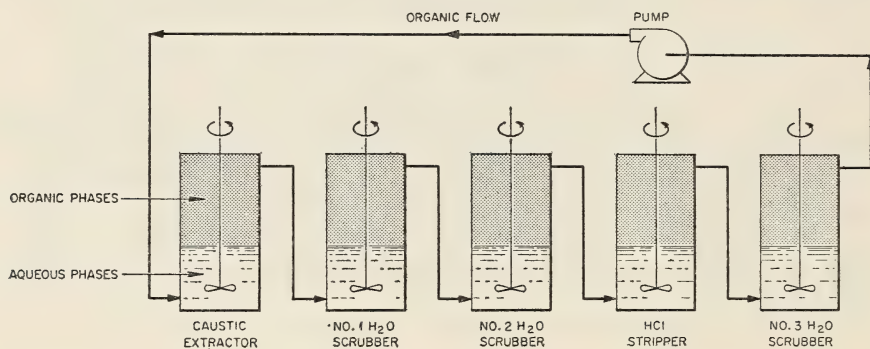
The cesium is recovered from the organic phase with dilute hydrochloric acid in the stripper stage of the recovery system as follows:



Thus, cesium is preferentially transferred from the alkaline feed solution, through the organic phase, to the acid strip solution. The strip system regenerates BAMBP to the hydrogen form in the recycling organic phase. Other metals are excluded from the product solution by scrubbing the loaded BAMBP with water prior to stripping. The water effectively removes metals that are held less firmly than cesium.

### Laboratory Tests and Results

The experimental laboratory-scale system (text-fig. 1) consisted of a feed contactor, three water scrubbers, and an HCl stripper. A solution of BAMBP (1 molar) in Varsol was circulated through the static aqueous phases with a small centrifugal pump. For each mole of CsCl being processed, 1 mole of NaOH was added to the feed contactor and 1 mole of HCl to the stripper. A slight excess of the acid and base was required for complete cesium transfer. Because of the small quantity of BAMBP available at the time of this test, the scale of the studies was limited to 600 ml volume contactors.



ORNL-DWG 63-4249

TEXT-FIGURE 1.—Schematic diagram of laboratory system for recovering cesium chloride from impure solutions. The circulating organic phase transfers cesium from the caustic feed contactor to the acid stripper. Purpose of the water scrubbers is to prevent other metals from reaching the stripper. The cesium salt is recovered in the aqueous phase of the fourth stage.

Results of a cesium extraction test, where the organic phase was circulated at 100 ml per minute for 45 minutes, are presented in table 2. Cesium removal from the feed was 99.8 percent; about 10 percent of the original cesium remained in the scrubbers and the organic phase, as determined by the final cesium concentration in the stripper. The cesium remaining in the system was recovered in subsequent runs. The salt recovered in the fourth stage was better than 99.9 percent pure. The product solution was evaporated to dryness, dissolved in water, and filtered. The absorbancy of the saturated filtrate at  $260\text{ m}\mu$  was 0.31, as recovered, without ignition or decolorization by filtration through carbon.

TABLE 2.—Test data from laboratory BAMBP extraction system for reprocessing cesium chloride

	Organic volume (ml)	Aqueous volume (ml)	Concentration (g/liter) *					Normality		
			CsCl	Na	K	Ca	Mg	Cs <sup>+</sup>	OH <sup>-</sup>	HCl
Extractor										
Initial	330	250	112.1	21.0†	0.1	0.07†	0.003†	0.666	0.86	
Final	330	250	0.25	Strong	0.1	0.001†	0.00005	0.0015	0.06	
No. 1 Scrubber										
Final	455	125	1.1	0.25	0.01	0.02	0.0002		0.015	
No. 2 Scrubber										
Final	455	125	3.0	0.11	0.04	0.01	0.0003		0.012	
Stripper										
Initial	330	50	0	0	0	0	0	0	0	0.875
Final	330	250	101.3	0.03	0.005	0.002	0.0001	0.602		0.19
No. 3 Scrubber										
Final	330	250	1.5	0.006	0.001	0.00076	0.00015			

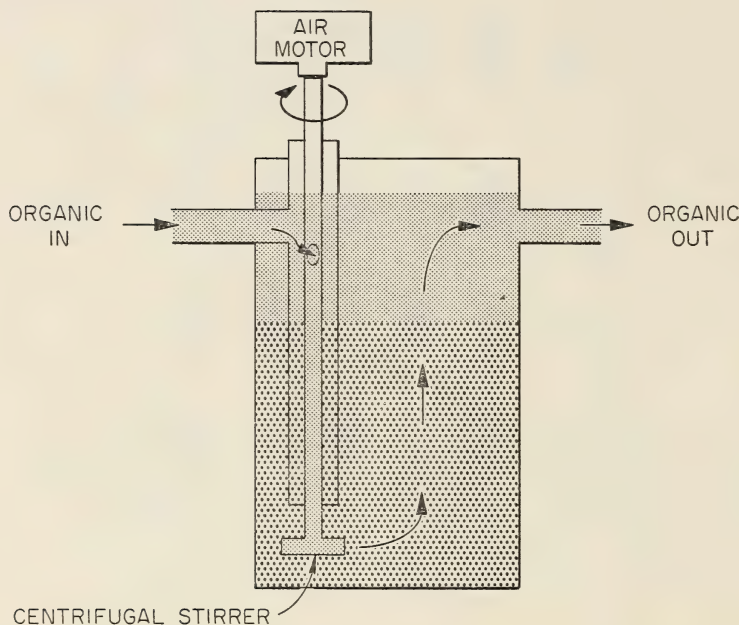
\* Aqueous.

† As NaOH and NaCl.

‡ Prior to filtering where some Mg and Ca were removed.

## PROTOTYPE EXTRACTION SYSTEM

A prototype production-scale liquid exchange system was constructed (fig. 1), which consisted of five Plexiglas contactor stages. In each stage, hollow glass centrifugal stirrers disperse the organic into the aqueous phase as shown in text-figure 2. A differential organic level is developed between the outer and inner compartments of adjacent contactors, effecting transfer of the organic phase without the use of external pumps. The organic-aqueous interface serves as a seal to prevent back-mixing.



TEXT-FIGURE 2.—Schematic of flow within contactor of cesium recovery system. The plastic and glass construction eliminates contamination problems.

## Evaluation Experiments

Four pounds of cesium chloride was contaminated with 500 ppm each (CsCl basis) of  $\text{Al}^{+3}$ ,  $\text{Fe}^{+2}$ ,  $\text{Cu}^{+2}$ ,  $\text{Ni}^{+2}$ ,  $\text{Zn}^{+2}$ ,  $\text{Cd}^{+2}$ ,  $\text{Cr}^{+6}$ ,  $\text{Co}^{+2}$ ,  $\text{Mg}^{+2}$ ,  $\text{Ca}^{+2}$ ,  $\text{Ba}^{+2}$ ,  $\text{Sr}^{+2}$ ,  $\text{Li}^{+1}$ ,  $\text{NH}_4^{+1}$ , and  $\text{PO}_4^{-3}$ . Also added was 1.4 percent  $\text{NO}_3^{-1}$ , 0.15 percent  $\text{SO}_4^{-2}$ , 0.5 percent  $\text{K}^{+1}$ , and a total of 2.7 pounds of sodium as the chloride and hydroxide. This was run through the extraction system. Part of the sodium hydroxide was added during the extraction. The basic solution was filtered before extraction, removing some of the metal impurities. Thirty-four liters of 1 molar BAMBP in Varsol was used, and each scrubber contained an aqueous phase of 6.7 liters; the stripper contained 3 liters of aqueous phase.

Production rates were limited by persistent emulsion formation in the scrub stages. Addition of cesium chloride to these stages, as an emulsion breaker, reduced (but did not eliminate) the problem. Contributing to, and possibly responsible for, the emulsion problem was the slow erosion of the Plexiglas components of the system by the organic extractant. The connecting polyethylene tubing was not attacked, suggesting that future extraction systems should be made of polyethylene or polypropylene.

The BAMBP extraction system was operated with organic solvent flow rates up to approximately 800 ml per minute and production rates as high as 2.5 pounds of cesium chloride per hour. Except for 170 ppm sodium (cesium chloride basis), no detectable metallic impurities were found (see table 1 for limits of detection) in the recovered salt.

By using cesium chloride solution as the feed and substituting the appropriate organic acid in the stripper, solutions of high purity cesium tartrate and citrate were produced. Activated carbon was used to remove traces of the extractant from the final product. The levels of impurities in these salt solutions were comparable to those shown in table 1.

## DISCUSSION

The high-speed, high-capacity rotors now under development for studies on DNA banded in cesium chloride or other cesium salts will require as much as one kilogram of cesium salt per experiment. It will not be feasible to test or use such rotors in the absence of simple methods, such as the one described here, for recovering cesium in a high state of purity.

## REFERENCES

- (1) MESELSON, M., STAHL, F. W., and VINOGRAD, J.: Equilibrium sedimentation of macromolecules in density gradients. *Proc Nat Acad Sci USA* 43: 581-588, 1957.
- (2) ANDERSON, N. G., HARRIS, W. W., BARBER, A. A., RANKIN, C. T., JR., and CANDLER, E. L., JR.: Separation of subcellular components and viruses by combined rate- and isopycnic-zonal centrifugation. *Nat Cancer Inst Monogr* 21: 253-283, 1966.
- (3) HORNER, D. C., CROUSE, D. J., BROWN, K. B., and WEAVER, B.: Recovery of fission products from aqueous solutions by solvent extraction. *Nuc Sci Eng* 17: 234-246, 1963.
- (4) BROWN, K. B., *et al.*: Chemical Technology Division Chemical Development, Section C, Progress Report on Separations Process Research for January-June, 1963, AEC Report ORNL-3496, Oak Ridge National Laboratory, 16-21, October 25, 1963.
- (5) BROWN, K. B., *et al.*: Chemical Technology Division Development, Section C, Status and Progress Report on Separations Research and Development, AEC Report ORNL-3785, Oak Ridge National Laboratory. In press.



## PLATES



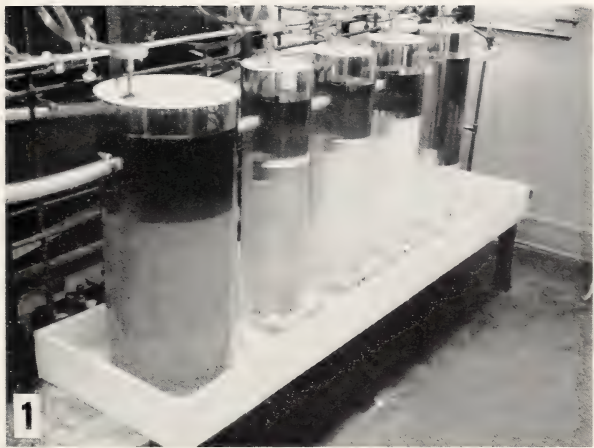


FIGURE 1.—Production-scale cesium recovery system. Three scrubbers were used prior to the stripper, which is the fifth contactor. Containers are Plexiglas.



## **Subcellular Particle Separation by Zonal Centrifugation**



## Separation of Subcellular Components and Viruses by Combined Rate- and Isopycnic-Zonal Centrifugation<sup>1</sup>

N. G. ANDERSON, W. W. HARRIS, A. A. BARBER,<sup>2</sup> C. T. RANKIN, JR., and E. L. CANDLER, *Biology Division, Oak Ridge National Laboratory,<sup>3</sup> and Technical Division and Biophysical Separations Laboratory, Oak Ridge Gaseous Diffusion Plant,<sup>3</sup> Oak Ridge, Tennessee*

### SUMMARY

The re-isolation of trace amounts of virus added to tissue homogenates has been taken as a model problem in the development of high-resolution methods for separating particles. From a review of data on these particles, it was found that, when sedimentation rates are plotted against their banding or buoyant densities, most viruses fall in a "window" which appears to be free of other particles. To examine this concept experimentally, a technique for sequential rate-zonal and isopycnic-zonal cen-

trifugation has been developed which allows this two-dimensional separation to be made and visualized. By use of this so-called *s-ρ* system, trace quantities of T3 phage particles have been recovered and identified from rat liver, brain, and spleen homogenates. The method may be used to isolate trace quantities of virus-like particles that have occasionally been reported in human tumors.—*Nat Cancer Inst Monogr* 21: 253-283, 1966.

AMONG THE properties of subcellular components and viruses that may be exploited by physical separation methods are particle size and density. Two questions arise at once: 1) To what degree are functionally distinct particles physically separable in theory, *i.e.*, to what extent do they have unique size and density distributions, and 2) how well do separations obtainable in practice approximate those predicted on theoretical grounds? In many instances the two questions are inseparable since the physical properties of interest cannot be measured independent of the experimental conditions. Thus it is difficult to determine whether broad zones that may be seen in a zonal centrifuge result from poor centrifugal resolution or from particle heterogeneity. It is of interest to study the behavior of an internal standard of known size and density added to tissue homogenates. The resolution obtained with the standard may then be compared to separations obtained with cell particulates. Virus particles appeared to

<sup>1</sup> This research performed under the Joint National Institutes of Health-Atomic Energy Commission Zonal Centrifuge Development Program which is supported by the National Cancer Institute, the National Institute of Allergy and Infectious Diseases, and the U.S. Atomic Energy Commission.

<sup>2</sup> Department of Zoology, University of California, Los Angeles, Calif. Aided by AEC Contract No. AT(11-1)-34 Project 49.

<sup>3</sup> Operated for the U.S. Atomic Energy Commission by Union Carbide Corporation.

be the most suitable internal standard in the size and density range of interest in connection with the development of intermediate-speed zonal centrifuges.

In this paper we discuss 1) whether, in theory, homogeneous particles such as certain viruses could be re-isolated in a high state of purity from tissue homogenates, 2) the development of methods for achieving high-resolution separations based on particle size and density, and 3) experimental studies using model systems. Since, in addition to serving as a model problem, the isolation of virus particles from tissues, including pathological samples and neoplasms (1-3), is of considerable practical interest, factors limiting the detection of separated virus particles by physical methods will be analyzed. The results may guide attempts to isolate minor cell constituents including, for example, centrioles. Although the major portion of the following discussion concerns viruses, it should be understood that they serve here chiefly as model particles.

## SUBCELLULAR PARTICLES AND VIRUSES

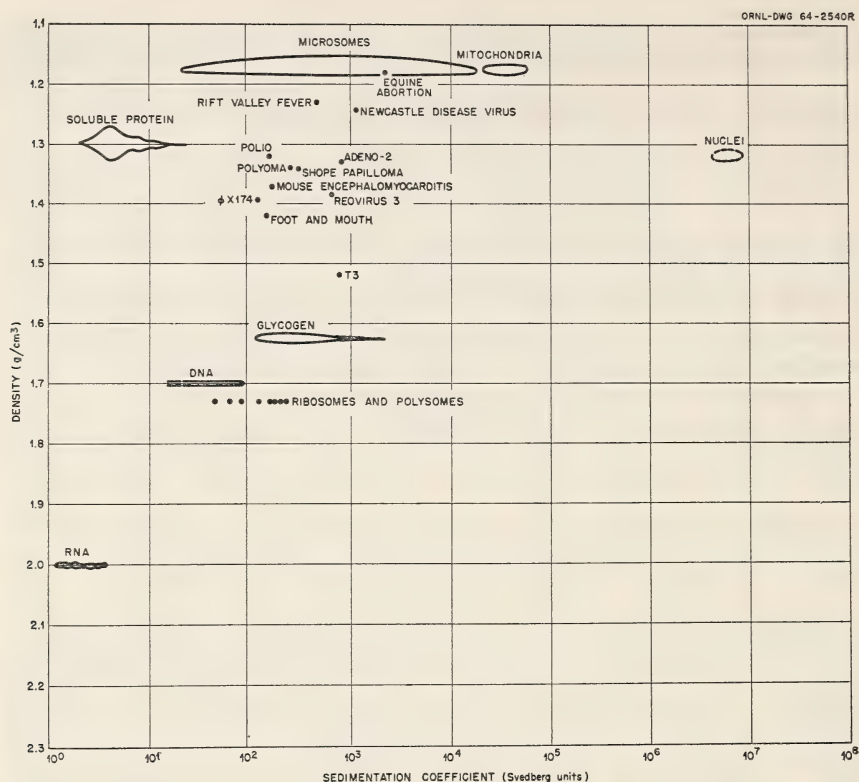
The question to be asked initially is: Are most viruses sufficiently different from the components of a broken cell suspension to allow their isolation in a reasonable state of purity? (Conversely, are most cell constituents sufficiently different from viruses . . . etc.) On purely theoretical grounds, it is evident that particles having quite different densities may have the same sedimentation rates in a given solvent. This follows from the fact that the sedimentation rate of a sphere is proportional to the product of the square of the particle radius and the difference in density between the particle and the suspending medium. Tissues probably contain a spectrum of particles having sedimentation coefficients in the viral range. It is less likely, however, that tissues contain many particles having both the same sedimentation coefficient and buoyant density as a particular virus. Viruses contain appreciable and constant amounts of nucleic acid, whereas very few cell particulates having the same size would be expected to have identical nucleic acid contents. Those few very small viruses that overlap ribosomes and polysomes may be separated by enzymatic digestion or dissociation of the latter structures. *It is concluded, however, that both rate-zonal and isopycnic-zonal separations must be used if maximal resolution is to be obtained.* For convenience, separations in which both of these methods are used have been termed *s-p* separations.

### The Virus "Window" Concept

Available data on the sedimentation rates and densities of viruses and major cell components are given in text-figure 1. The values indicated for the sedimentation coefficients are corrected to water at 20° C. Ex-

perimentally the isopycnic separations were made in salt gradients, and the banding densities, unless otherwise stated, were for cesium chloride gradients. In gradients prepared from other solutes, the values would be numerically different, but the over-all distribution of viral and cellular components would tend to remain the same. The values used for the sedimentation coefficients for proteins are those for rat liver (4) which are similar to the values recorded for rat brain, kidney, and testis. While the banding densities for soluble tissue proteins have not been experimentally determined, they probably do not vary greatly from the value of 1.295 reported for bovine serum albumin and human hemoglobin (5). Values used for the sedimentation coefficients of ribosomes and polysomes were for rabbit reticulocytes (6), while the banding densities were those extrapolated from *Escherichia coli* (7). It is assumed that polysome densities would not be widely different. The range of sedimentation coefficients shown for "microsomes" was that observed experimentally with rat liver in the zonal centrifuge, while the density range was obtained by banding in neutral CsCl. The sedimentation rates for mitochondria are calculated from the data of de Duve *et al.* (8) and of Thomson and Klipfel (9). Nuclear sedimentation coefficients were calculated values for diameters ranging from 6 to 12  $\mu$  and an average density of 1.040 (10) in dilute buffer. The CsCl density was estimated on the assumption that nuclei contained 77 percent protein and 19 percent deoxyribonucleic acid (DNA) (11) and that the isopycnic densities would be the sum of the density of each component times the percentage present. In a salt gradient, nucleoprotein tends to dissociate, at least partially, and probably yields several bands. The nuclear isopycnic density was therefore a calculated value given to indicate a region where separations of nuclear from non-nuclear materials would be difficult. The position of glycogen is taken from studies on the distribution of sedimentation coefficients of material isolated from liver (12-15). The banding density in CsCl was taken from experimental studies carried out in this Laboratory (15) with glycogen isolated from rat liver. The value was slightly higher than that previously reported (13, 16). The position of ferritin is not shown. Ultracentrifuge studies (17) suggest that these particles may be heterogeneous with respect to iron content and therefore would vary in both sedimentation rate and banding density level. Preliminary experiments with ferritin from both human and horse spleen confirm this view.

Also included in text-figure 1 are data on DNA, which would not ordinarily be found free in homogenates of mammalian cells, but would be encountered in bacterial homogenates, and might be extracted from viruses during the preparation of pathological tissues. The banding density range was taken from Schildkraut *et al.* (18), and the range of sedimentation rates includes that of single DNA molecules from T5 phage (19) and a variety of published values. Ribonucleic acid (RNA) has a density in CsCl at the limits of the density available with this salt. The density of 2.0 observed in cesium formate (20) has therefore been used. The sedimentation rate range is taken from a number of sources (21, 22).



TEXT-FIGURE 1.—Sedimentation coefficients and banding densities of cell components and viruses. Sources of data are given in text. Note that most virus particles fall in an area, here termed the "virus window," essentially free of cell constituents.

The accurate positioning of cell components from various tissues in the  $s$ - $\rho$  plot will require much additional experimental work, and some of the values used here must be treated with reservation.

Data on the following viruses are taken from published studies: adenovirus 2 (23, 24); equine abortion virus (25); foot-and-mouth disease virus [(26); R. Trautman and H. L. Bachrach, personal communication]; mouse encephalomyocarditis virus (27, 28); Newcastle disease virus (29, 30);  $\phi$ X 174 (31, 32); polio virus (33, 34); mouse polyoma (35-39); reovirus 3 (40); Rift Valley fever virus (34, 41); Rous sarcoma (42-45); and Shope papilloma virus (42, 46).

It is evident from an examination of text-figure 1 that a large open area, or "window," appears in the center of the  $s$ - $\rho$  plot which includes a small amount of nonviral material and a large fraction of known viruses. In those instances where a virus has the same banding density as a part of the microsomal fraction, it is evident that the virus cannot be completely separated from contaminating material by centrifugal procedures alone. Chemical (47) or enzymatic dissection may then be necessary.

Since the microsomal particles have a wide range of sedimentation rates, however, it should be possible to isolate the virus from most of the microsomal mass. The amount of endoplasmic reticulum giving rise to microsomes varies widely among cells and tissues but is low in many tumors and in some cells used for virus production.

These considerations have prompted us to explore methods for large-scale separation of subcellular constituents which would accomplish the theoretical separations shown diagrammatically in text-figure 1.

### Detection of Virus Particles

Infectivity in a suitable test system is the most sensitive method for detecting virus particles. However, it gives no indication of the purity of the fractions assayed. The physical methods for detecting viruses isolated in a reasonable state of purity include absorbance in the ultraviolet range, light scattering, electron microscopy, and measurement of fluorescence after conjugation with fluorescent antibodies. The usefulness of these methods depends on their sensitivity. By the use of negative-staining techniques, particle-counting methods, or sectioning of pellets, it appears that the identification of virus particles on a morphological basis is feasible at the level of one particle per cell if the virus is obtained in a pure form and in the same concentration in which it existed in the source tissue. For example, if liver containing  $4 \times 10^8$  cells per g is used, then the final virus concentration ( $4 \times 10^8/\text{ml}$ ) would be at the lower limits of detection with spray-counting methods (48, 49) but well within the range of the Sharp counting technique (50-52).

For detection of most viruses by ultraviolet absorbance measurements, somewhat larger amounts of virus are required. The number of absorbance units necessary depends on the absorbancy of the gradient itself, the length of the light path, and the volume in which the virus is recovered. If the lower limit is 0.1 absorbance unit, then  $13 \times 10^{12}$  particles of the small foot-and-mouth disease virus (R. Trautman, personal communication),  $1.2 \times 10^9$  physical particles of pox virus (53), or  $2.3 \times 10^6$  vaccinia particles (54) would be required. This limit may be lowered by the use of long light path (55) cells, electronic methods for extending spectrophotometric ranges, or refined small-volume banding methods. The conclusion is, however, that, if small virus particles are to be detected by ultraviolet absorbance, the concentration per unit volume must be 10 to 100 times higher than that found in the starting tissue, assuming that only one virus particle per cell is found. For very large viruses, however, direct absorbance measurements would probably suffice.

Light scattering as a method of detecting virus-sized particles in gradients is theoretically more sensitive than absorption measurements. In practice, certain compromises must be made. For example, the photographic technique used in this paper involves the use of centrifuge tubes that are designed specifically for virus work, *i.e.*, not to leak or contaminate the operator. They are not as good optically as a glass vessel.

Further, photographic techniques as ordinarily used are not as sensitive as photomultipliers. Considerable improvement in detection sensitivity is therefore possible. The detection limits for virus particles by physical means will actually be set by the quantity of nonviral tissue material found at a given position in the  $s$ - $\rho$  separation.

If methods can be developed to allow isolation of particles having the narrow range of sizes and densities characteristic of a given virus, and if the final particle concentration is equal to or greater than the concentration in the tissue of origin, then virus particles at concentrations possibly as low as one particle per cell could in theory be isolated and described. Since the mass of a virus varies from approximately  $10^{-6}$  (56) to  $10^{-8}$  of that of a cell, the purification (as distinguished from concentration) required is from a million-fold to 10 million-fold.

Available data on the composition and masses of viruses and the absorbance of solutions containing known amounts of particles have been tabulated (57). The latter are calculated values and do not include the increased absorbance caused by scattered light. The increased absorbance due to Tyndall scattering is a function of the refractive index of the suspending medium. Previous studies on light scattering of virus particles have been done in dilute solutions (58) and scattering would be less in dense-banding media. In the calculated absorbancies (57), the effect of scattering on observed total absorbance was neglected. Ultimately it will be necessary to determine the absorbance of suspensions having a known number of physical particles in solutions isopycnic with the particles.

As highly purified virus materials become available for investigation and medical use, it is necessary to consider the units in which concentrations of virus particles are expressed, the relation between these units, and the methods used for analyzing virus suspensions.

The following proposals are internally consistent and would help one to compare different viruses, to analyze given preparations, and to estimate concentration. The basic unit is the weight of an anhydrous virus particle in grams. Fractions of a gram have been given names corresponding to  $10^{-3N}$  g, where  $N$  is a whole number. In keeping with this convention,  $10^{-18}$  has been chosen as the weight unit and might well be termed a "virogram." The viruses thus far described range from approximately 11 to 3500 virograms. Thus whole numbers can be used. In the past, virus concentration has often been expressed as  $\mu$ g of virus per ml of suspension. If a unit of virus concentration containing  $10^{12}$  virus particles per ml is chosen, then the  $\mu$ g of virus per unit concentration is found to be numerically equal to the weight of a single virus in virograms. Thus the weight of a single cowpox virus is 3500 virograms, and a solution containing  $10^{12}$  cowpox virus particles per ml would contain 3500  $\mu$ g of virus per ml. A polio virus with a weight of 12 virograms yields a suspension with 12  $\mu$ g of virus per ml at a concentration of  $10^{12}$  physical particles per ml. In this work, we consider the *physically defined* particle (PP) and not the *infectious unit* (IU). The absorbance at 260  $m\mu$  of virus suspensions at  $10^{12}$  PP per ml is also a useful number. It spans the range of absorbancies usually measured with conventional spectrophotometers, except for the large pox viruses, where dilution by one order of magnitude ( $10^{11}$  PP/ml) is required to make reliable measurements. With these units there are simple correlations between number, particle weight, concentration, and absorbance.

### Search for Viruses by Electron Microscopy

The electron microscope has been invaluable in identifying virus particles in cells. It is important to know whether centrifuge systems may approach, or possibly surpass, the sensitivity of the electron microscope in identifying virus particles in cells. For this discussion we will consider virus concentrations at the limiting level of one particle per cell.

An estimation of the number of photographs that must be examined to find one virus particle per cell is given by the approximation

$$N = \frac{4\pi r^3 M^2}{3TA},$$

where  $N$  is the number of photographs to be examined;  $r$ , the radius of the cell in cm;  $M$ , the electron microscope magnification;  $T$ , the thickness of the section in cm; and  $A$ , the area of the photograph in cm<sup>2</sup>.

For a cell 15  $\mu$  in diameter, approximately six hundred  $8 \times 10$ -inch photographs at 20,000  $\times$ , using 250 A sections, would be required (fig. 1). As the diameter of the cell or the magnification is increased, so is the number of photographs.

It is evident that a statistical study of the number of virus particles in a tissue at this level is inordinately tedious and involves thousands of photographs (6,000 for 10 cells).

### Detection of Virus Particles in Gradients

For detection of virus particles by ultraviolet absorption, the lower limit with present systems is approximately 0.1 absorbance unit. With a small virus, such as polio, this represents approximately  $1.3 \times 10^{12}$  PP; with a large one, such as vaccinia, the same absorbancy is produced by about  $1.4 \times 10^{10}$  PP. If one particle per cell is to be detected, then the number of original cells must be equal to this number of particles. For rat liver as an example, 1 g of tissue contains 2 to  $4 \times 10^8$  cells. The upper limit for tissue used directly in the B-IV rotor is about 10 g, giving about  $3 \times 10^9$  cells. This is one order of magnitude below the ultraviolet absorption limits for vaccinia and three below that for polio.

However, if  $10^8$  virus particles can be isolated from 1 g of tissue free from other contamination and in a volume of 1 ml, then their detection through conventional counting techniques by electron microscopy is fairly simple. Further, if the isopycnic separations can be done in a much smaller volume, the limit of 0.1 absorbance unit may be considerably decreased.

### Use of Negative Staining for Detecting Virus Particles

The negative staining technique of Brenner and Horne (59) is extremely useful for identifying certain viruses, especially where large numbers of samples are to be scanned. While the technique as ordinarily used is

not suitable for the purpose of obtaining accurate counts, it is important to have an estimation of the number of particles required to give the microscopist a reasonable chance of finding them. The following experiment indicates that this simple method, as routinely used in this laboratory, is useful for trace virus isolation.

### *Methods*

A solution of T4 bacteriophage containing  $1.14 \times 10^{10}$  particles per ml was kindly prepared by Dr. Stanley Leibo of the Biology Division of the Oak Ridge National Laboratory. Serial tenfold dilutions were prepared with 0.9 percent NaCl.

A drop of the virus suspension was placed on a carbon-coated Formvar 400-mesh specimen screen. After standing for 2 minutes, the drop was removed by touching to a piece of filter paper, and a drop of 2 percent (w/v) phosphotungstic acid (pH 7.0) was added. Fifteen seconds later the phosphotungstic stain was removed and the screens were allowed to dry in air.

### *Results*

When serial dilutions of the T4 bacteriophage suspension were examined, the following results were obtained.

*10<sup>10</sup> Particles per ml:* estimated average, 12 particles per grid opening. All grid openings had at least 2 particles and some had as many as 50.

*10<sup>9</sup> Particles per ml:* average of 5 particles per grid opening. No particles were found in some openings and the maximum found was slightly greater than 5.

*10<sup>8</sup> Particles per ml:* 3 particles found in 10 grid openings.

*10<sup>7</sup> Particles per ml:* no particles observed with the technique described above. (A very few were found when the drop of test solution was left in contact with the specimen screen for 5 minutes.)

It is concluded that if virus particles are present at the level of 1 per cell, and if all nonviral material could be removed, then the virus could be detected without concentration by this method.

## **RATE-ZONAL SEPARATIONS**

Two gradients have been used for the separation of tissue components, depending largely on the results desired. By use of a gradient extending linearly from 17 to 55 percent w/w sucrose with a 66 percent sucrose underlay, mitochondria are banded isopycnically, while microsomes may be spread out through most of the gradient by a suitable choice of speed and centrifugation time. Ribosomes have been only partially sedimented out of the soluble materials zone, while part of the nuclei is retained by the 66 percent sucrose at the outer end of the gradient.

For the separation of smaller particles directly out of a tissue brei, a shallower gradient has been used which extends from 10 to 30 percent sucrose with either a 47 or 55 percent sucrose as the underlay. In this

gradient, mitochondria are banded at the interface between the dense end of the gradient and the sucrose underlay. In these studies no effort is made to recover nuclei. The centrifugation time and rotor speed could be chosen so that particles in the size range of the virus would be spread out through that portion of the gradient between the sample zone and the mitochondria, or sedimentation may be limited so that virus-like particles would be restricted to a smaller portion of the gradient. For maximal separation and for evaluation of the separations that may be obtained, the former procedure is useful, whereas the latter method is most useful in the search for viruses where very small numbers of particles are expected. In the majority of the studies recorded in this paper, 10 to 30 percent w/w sucrose gradients have been used with a 47 percent sucrose underlay. With this gradient, particles having a density of 1.3 and a sedimentation coefficient of 2000  $S^*$  would appear in the neighborhood of tube 34 after 60 minutes at 20,000 rpm ( $\int \omega^2 dt = 1580 \times 10^7$ ). This time and speed are useful when maximal resolution of virus or virus-like particles is desired. For survey studies, 15 to 30 minutes at the same speed ( $\int \omega^2 dt = 395 \text{ to } 790 \times 10^7$ ) would restrict similar particles to the first 6 to 12 tubes in the gradient below the sample layer.

The choice of whether to use the rate separation or the isopycnic separation first depends on several considerations. Cell nuclei may have protein/nucleic acid ratios, and therefore banding densities, in the range observed for virus particles. If an isopycnic separation is done initially, nuclei may be disrupted and extracted by the high salt concentrations used. Such extracted nucleoprotein would be difficult to separate from smaller particles since it would not behave as intact nuclei do in subsequent rate-zonal separations. Other cell components including ribosomes may also be altered by salt extraction. An additional disadvantage in doing equilibrium studies first is that, with presently available systems, sufficient centrifugal force is not available to band soluble proteins sharply in a relatively short time. Banded virus and other small particles may therefore not be free of contamination by small soluble particles that have not reached their isopycnic points. In addition, isopycnic separations often require more expensive materials than those used in rate runs. The deciding factor, however, is that no way for making large numbers (up to 36) of rate-zonal separations has been devised, whereas this number of isopycnic zonal runs can now be made. In all experimental studies reported here, therefore, rate separations have been made first.

### Protein Distribution in Gradients

It is of interest to know the general distribution of both ultraviolet-absorbing materials and protein through gradients from several tissues to obtain an indication of the amount of the material having sedimentation properties in the viral range.

Homogenates of rat liver, brain, and spleen were therefore examined using the B-IV zonal centrifuge system. The tissue sample preparation

is described in the legend of each figure. Protein was determined by the method of Lowry *et al.* (60). The results are shown in figures 2, 3, and 4.

Each 40 ml fraction in the virus sedimentation coefficient range contains on the average less than 1 percent of the total protein of the homogenate in the case of spleen and liver. In many instances, especially in plant extracts, rate-zonal centrifugation alone will yield a sufficient purification of viruses for many purposes.

### Isopycnic Banding of Cell Components

To translate the theoretical separation shown in text-figure 1 into an experimental technique, it is necessary to make isopycnic zonal or banding separations of a large number of fractions. Rather high centrifugal forces are required to do this in a reasonable length of time. Unfortunately, the available high-speed, swinging-bucket rotors will spin only a small number of samples. Banding of small particles may be done in angle-head centrifuges (61). Thirty-six samples may therefore be run by use of 3 model L preparative ultracentrifuges.

Three different banding techniques have been used to explore  $s$ - $\rho$  separations of tissue components. These are:

- 1) Wide density range banding. Cesium chloride gradients have been used for this purpose and will band nearly all known tissue components. Cesium formate is required if free RNA is to be banded; otherwise CsCl is the solute of choice.
- 2) For particles having buoyant densities less than 1.5 (this would include all viruses that might be expected to occur in animal tissues), potassium citrate has been used.
- 3) For studies on density differences in membrane components banding in sucrose itself is often useful (62). The viscosity of concentrated sucrose solutions at low temperatures is very high. Isopycnic banding of small particles in sucrose solutions therefore requires a longer centrifugation time than when salts are used.

In this paper only the results with wide-range banding are presented. Studies with potassium citrate and sucrose are in process.

#### *Gradient preparation*

Polycarbonate centrifuge tubes for the Spinco No. 30 rotor developed under this program (63) were filled with 10 to 15 ml of undialyzed fractions from the rate-zonal centrifuge runs. Twelve ml of the dense gradient material was then run in to the bottom of the centrifuge tube through a Pasteur pipette. The gradients were allowed to form during centrifugation by diffusion. The steep gradients formed by diffusion are useful for survey studies where particles having a wide range of densities are to be observed. When higher resolution separations of a few components are

required, a step gradient may be formed initially by introducing a series of solutions of increasing density through the pipette.

### *Band detection*

As previously mentioned, light scattering is one of the most sensitive methods available for detecting the presence of particles banded in a centrifuge tube. The refractive index of the gradient in the region of an isopycnic zone approaches that of the particle and, in some instances, may match that of the particle. Particulate subcellular constituents and viruses are not internally homogeneous with respect to either the buoyant density or refractive index of their constituent molecules. This is one reason why viruses and the larger subcellular particles scatter appreciable amounts of light even at their isopycnic level. The number of particles required to give a band that may be identified photographically is a function of particle size, shape, permeability, and composition, the refractive index of the suspending medium, and the optical properties of the centrifuge tube and of the photographic system used for making the photograph or pycnograph.

### *Sensitivity*

To obtain an indication of the amount of material required, T3 phage particles were banded in CsCl, as described, and photographed. The results are shown in figure 5. It is evident that homogeneous virus particles present in fairly small amounts, and having a banding density in the virus window, would not be observed at the level of one particle per cell under the experimental conditions used here, since  $10^{11}$  particles were required to give a visible band. Similar experiments with *E. coli* cells are shown in figure 6, and suggest that particles in this size range would be seen at the one-per-cell level, since  $10^7$  particles could easily be seen.

## **Buoyant Density Separations With Tissues**

The separations obtained with CsCl banding of fractions initially isolated by rate-zonal centrifugation are shown in the lower part of figures 2, 3, and 4. From previous studies with density beads, the density of the endoplasmic reticulum and the density of glycogen are known (15, 64) and are indicated in the figures.

In these experiments the absorbance of the recovered gradient from the B-IV rate-zonal rotor is shown along the upper portion of the diagram. The computer plot of equivalent sedimentation coefficients ( $S^*$ ) is aligned immediately below the absorbance diagram and includes also a plot of the density of the recovered gradient. Along the bottom of the chart is a composite photograph of all of the isopycnic banding tubes, with the density indicated to the left of the photograph. It is evident at once, especially in brain tissue, that a wealth of information is to be gained from the careful examination of the observed bands. For the present purposes, however, the observation of a broad area between the level at

which membranous elements are found and the level of the glycogen band in liver and the absence of any well-defined bands below the membrane level in brain and spleen suggest that the distribution of particulate material seen in figure 1 does in fact occur. We may now be asked whether the so-called virus window area is sufficiently free of traces of particulate matter to allow small amounts of a test virus to be isolated and observed.

For this purpose suspensions containing known numbers of T3 bacteriophage were added to tissue homogenates prior to fractionation by the *s-ρ* system.

### Purification of T3 Phage

A lysate of T3 phage was concentrated by continuous flow centrifugation in the B-V rotor (65) and further purified by banding in CsCl. On examination in the electron microscope, a few larger contaminating phage particles resembling T2 were observed. The sample was therefore purified by rate-zonal centrifugation (fig. 7). Two bands, indicated by arrows, were observed in CsCl. These were recovered and examined. The first band contained only T3, the second only contaminating T2 (fig. 8). The T3 sample was dialyzed against a dilute phosphate buffer and analyzed spectrophotometrically.

### Recovery of T3 From Tissue Homogenates

Ten absorbance units ( $8.5 \times 10^{12}$  physical particles) were added to 20 ml of a rat liver homogenate containing 4 g of tissue (approximately  $1.6 \times 10^9$  cells) to give an average of  $5 \times 10^3$  particles per cell. If the particles had pre-existed in the cell and been uniformly distributed, approximately 10 would have been visible on the average in an  $8 \times 10$  inch electron micrograph at  $20,000 \times$  using 250 Å thick sections. The results of *s-ρ* separation with this sample are shown in figure 9. A band absent from the control, but at the proper position for T3 was observed. Electron micrographs of the recovered band are shown in figure 10. In five  $8 \times 10$  enlargements at  $80,000 \times$  an average of 4 virus particles per micrograph was seen. At the level of 5,000 particles per cell (one part in  $3.3 \times 10^3$ ) the particles are grossly evident and can be easily identified in the banding tubes by light scattering and by electron microscopy. With an improved optical system for observing bands by light scattering, this number could probably be decreased at least an order of magnitude. Similar studies have been done with T2 bacteriophage.

Combined *s-ρ* separations of brain and spleen were also performed as shown in figures 11 and 12, using  $8.5 \times 10^{11}$  phage (one-tenth the amount used above). No well-defined bands were seen by scattered light. However, when samples were taken for electron microscopy at the levels indicated, virus particles were seen (fig. 10). It is evident that at the level of approximately 500 particles per cell virus particles can be detected easily. The lower limit reached in the present studies is 20 T3 phage

particles per average rat liver cell. Demonstration of the particles by negative staining required examination of several fields per particle found, however. If the entire virus window area is removed and examined by the improved method of Geister and Peters (66) which has a lower limit of  $10^5$  particles per ml, the level of one particle per cell could probably be reached. In additional experiments the location of virus particles in the  $s$ - $\rho$  diagram has been confirmed by infectivity studies (unpublished observations).

The problem of whether phage particles sediment in a density gradient independent of the tissue particles has been examined by using  $P^{32}$ -labeled T3 phage added to a liver homogenate. The radioactivity distribution was very similar to that seen in figure 7 for free phage particles in the absence of tissue.

## APPLICATION TO THE SEARCH FOR ONCOGENIC VIRUSES

The methods described here are applicable to the problem of trace virus isolation from tumors, especially if the particles sought have a high nucleic acid content. When the virus particles contain appreciable amounts of lipid and only a low percentage of nucleic acid, the virus particles would tend to band in, or close to, the endoplasmic reticulum band. The Bittner virus, for example, bands at a density level of 1.19 g per ml in potassium tartrate (67) but would probably band at a slightly higher density level in CsCl. However, the virus would generally be much less heterogeneous than the microsomes with respect to both sedimentation rate and density.

The problem of using larger amounts of starting material in the B-IV rotor may be solved by first performing differential centrifugation to isolate only particles in the virus sedimentation-rate range. Mitochondria and nuclei are removed first, and the microsome-virus fraction is then sedimented to remove it from soluble materials. With microsome-poor tissues such as spleen, concentrates from 100 g of tissue may thus be obtained in a sufficiently small volume for use as the starting sample in the rate run. A human breast tumor examined in an exploratory run yielded unidentified particles from the density level at approximately 1.18 (fig. 13). Similar particles have occasionally been seen in a control experiment with normal breast tissue. It is quite evident that no conclusions can be drawn as yet concerning the nature of the particles isolated, but it appears worthwhile to explore human tumors more thoroughly with this technique.

## DISCUSSION

Rate-zonal separations of tissue homogenates followed by isopycnic-zonal centrifugation in angle-head centrifuge tubes have been used to obtain a two-dimensional separation of tissue components.

The gradients, centrifugation times, and the banding densities have been adjusted so that particles in the range of known viruses would be distributed through both gradients. The experimental question asked is: Are relatively homogeneous particles such as viruses separated into discrete bands or zones by this technique? This point is important in evaluating the behavior of particles known to be heterogeneous in size and, in some instances, banding density. The results indicate that good resolution is obtained in both the rate and isopycnic separations.

The absence of appreciable numbers of particles having the physical properties of the smaller viruses has been demonstrated in three tissues. In those instances where virus particles have densities bordering the microsome range, very considerable purification would still be expected on the basis of sedimentation rate alone from liver and spleen. Protein determinations showed that only a small part of the total tissue mass was recovered in each of the fractions in the virus range. In brain, however, a large mass of very light material was recovered in the middle of what has been considered the microsome region. In addition to demonstrating the resolution which may be obtained, these studies lay the groundwork for attempts to isolate viruses and virus-like particles from tissues suspected to contain them.

In the work described, rather steep CsCl gradients have been employed for the isopycnic studies. These covered the range from light membrane particles to glycogen. Careful inspection of these banding patterns reveals a number of bands not as yet identified. These deserve careful study in much shallower gradients capable of giving greater resolution and separation and in gradients prepared with other substances to minimize the possibility of artifacts.

The *s- $\rho$*  separation methods appear to be a useful addition to our biophysical armamentarium for both separating and visualizing subcellular particles and viruses. The exploration of cells and tissues by these methods will require extended efforts which should include electron microscopy and chemical and enzymatic analyses.

## REFERENCES

- (1) BERNHARD, W.: The detection and study of tumor viruses with the electron microscope. *Cancer Res* 20: 712-727, 1960.
- (2) DMOCHOWSKI, L.: The electron microscopic view of virus-host relationship in neoplasia. In *Progress in Experimental Tumor Research* (Homburger, F., ed.). Basel/New York, Karger, 1963, vol 3, pp 35-147
- (3) DMOCHOWSKI, L., GREY, C. E., SYKES, J. A., DREYER, D. A., LANGFORD, P., JESSE, R. H., JR., MACCOMB, W. S., and BALLANTYNE, A. J.: A study of sub-microscopic structure and of virus particles in cells of human laryngeal papillomas. *Texas Rep Biol Med* 22: 454-491, 1964.
- (4) ANDERSON, N. G., and CANNING, R. E.: Studies on isolated cell components. XII. An ultracentrifugal analysis of soluble proteins from rat liver, brain, kidney, and testis. *Exp Cell Res* 17: 465-471, 1959.

- (5) COX, D. J., and SCHUMAKER, V. N.: The preferential hydration of proteins in concentrated salt solutions. II. Sedimentation equilibrium of proteins in salt density gradients. *J Amer Chem Soc* 83: 2439-2445, 1961.
- (6) GIERER, A.: Function of aggregated reticulocyte ribosomes in protein synthesis. *J Molec Biol* 6: 148-157, 1963.
- (7) TISSIERES, A., WATSON, J. D., SCHLESSINGER, D., and HOLLINGSWORTH, B. R.: Ribonucleoprotein particles from *Escherichia coli*. *J Molec Biol* 1: 221-233, 1959.
- (8) DE DUVE, C., BERTHET, J., and BEAUFAY, H.: Gradient centrifugation of cell particles. Theory and applications. *Progr Biophys* 9: 325-369, 1959.
- (9) THOMSON, J. F., and KLIPFEL, F. J.: Fractionation of rat liver particulates using polyvinylpyrrolidone gradients. *Exp Cell Res* 14: 612-614, 1958.
- (10) FALZONE, J. A., BARROWS, C. H., and YIENGST, M. J.: Fractionation of rat liver nuclei into diploid and tetraploid DNA classes by continuous density gradient sedimentation. *Exp Cell Res* 26: 552-561, 1962.
- (11) HALE, A. J., and KAY, E. R. M.: A comparison of nuclear dry weights determined by chemical and by interferometric methods. *J Biophys Biochem Cytol* 2: 147-158, 1959.
- (12) MEYER, F., and ZALTA, J. P.: The state of glycogen in the liver of rats. *C R Soc Biol (Paris)* 247: 357-359, 1959.
- (13) BELL, D. J., GUTFREUND, H., CECIL, R., and OGSTON, A. G.: Physicochemical observations on some glycogens. *Biochem J* 42: 405-408, 1948.
- (14) POLGLASE, W. J., BROWN, D. M., and SMITH, E. L.: Studies on human glycogen. II. Sedimentation in the ultracentrifuge. *J Biol Chem* 199: 105-112, 1952.
- (15) BARBER, A. A., HARRIS, W. W., and ANDERSON, N. G.: Isolation of native glycogen by combined rate-zonal and isopycnic centrifugation. *Nat Cancer Inst Monogr* 21: 285-302, 1966.
- (16) BRYCE, W. A. J., GREENWOOD, C. T., JONES, I. G., and MANNERS, D. J.: Physicochemical studies on starches. XII. The molecular weight of glycogens in aqueous solution. *J Chem Soc*: 711-715, 1958.
- (17) ROTHEN, A.: Ferritin and apoferritin in the ultracentrifuge. Studies on the relationship of ferritin and apoferritin; precision measurements of the rates of sedimentation of apoferritin. *J Biol Chem* 152: 679-693, 1944.
- (18) SCHILDKRAUT, C. L., MARMUR, J., and DOTY, P.: Determination of the base composition of deoxyribonucleic acid from its buoyant density in CsCl. *J Molec Biol* 4: 430-443, 1962.
- (19) HERSHEY, A. D., BURGI, E., and INGRAHAM, L.: Sedimentation coefficient and fragility under hydrodynamic shear as measures of molecular weight of the DNA of Phage T5. *Biophys J* 2: 423-431, 1962.
- (20) DAVERN, C. I., and MESELSON, M.: The molecular conservation of ribonucleic acid during bacterial growth. *J Molec Biol* 2: 153-160, 1960.
- (21) CHENG, P.-Y.: Sedimentation and autoradiographic analyses of rapidly labeled RNAs in human amnion cells. *Biophys J* 2: 465-482, 1962.
- (22) COX, R. A., and ARNSTEIN, H. R. V.: The isolation, characterization and acid-base properties of ribonucleic acid from rabbit reticulocyte ribosomes. *Biochem J* 89: 574-585, 1963.
- (23) GREEN, M.: Studies on the biosynthesis of viral DNA. *Sympos Quant Biol* 27: 219-235, 1962.
- (24) KÖHLER, K.: Gewinnung und Reinigung von Adenovirus-Typ 2 mit Hilfe der CsCl-Gradientenzentrifugation. *Z Naturforsch [B]* 17: 544-547, 1962.
- (25) DARLINGTON, R. W., and RANDALL, C. C.: The nucleic acid content of equine abortion virus. *Virology* 19: 322-327, 1963.
- (26) BREESE, S. S., JR., TRAUTMAN, R., and BACHRACH, H. L.: Analysis by electron microscopy and infectivity of foot-and-mouth disease virus in moving boundary and zone ultracentrifugation. *Arch Biochem* 87: 1-8, 1960.

- (27) FAULKNER, P., MARTIN, E. M., SVED, S., VALENTINE, R. C., and WORK, T. S.: Studies on protein and nucleic acid metabolism in virus-infected mammalian cells. 2. The isolation, crystallization and chemical characterization of mouse encephalomyocarditis virus. *Biochem J* 80: 597-605, 1961.
- (28) HAUSEN, P., and SCHÄFER, W.: Untersuchungen über ein Mäuse-Encephalomyelitis-virus. Reiniguing und physikalisch-chemische Eigenschaften des Virus. *Z Naturforsch [B]* 17: 15-22, 1962.
- (29) ROTT, R., REDA, I. M., and SCHÄFER, W.: Charakterisierung der verschiedenen, nach Infektion mit Newcastle Disease Virus auftretenden, nichtinfektiösen-hämagglutinierenden Teilchen. *Z Naturforsch [B]* 18: 188-194, 1963.
- (30) STENBACK, W. A., and DURAND, D. P.: Host influence on the density of Newcastle disease virus (NDV). *Virology* 20: 545-551, 1963.
- (31) SINSHEIMER, R. L.: Purification and properties of bacteriophage  $\Phi$ X 174. *J Molec Biol* 1: 37-42, 1959.
- (32) EIGNER, J., STOUTHAMER, A. H., VAN DER SLUYS, I., and COHEN, J. A.: A study of the 70s component of bacteriophage  $\Phi$ X 174. *J Molec Biol* 6: 61-84, 1963.
- (33) HOLLAND, J. J., HOYER, B. H., McLAREN, L. C., and SYVERTON, J. T.: Enteroviral ribonucleic acid. I. Recovery from virus and assimilation by cells. *J Exp Med* 112: 821-839, 1960.
- (34) POLSON, A., and LEVITT, J.: Density determination in a preformed gradient of cesium chloride. *Biochim Biophys Acta* 75: 88-95, 1963.
- (35) CRAWFORD, L. V., and CRAWFORD, E. M.: A comparative study of polyoma and papilloma viruses. *Virology* 21: 258-263, 1963.
- (36) HOWATSON, A. F., and CRAWFORD, L. V.: Direct counting of the capsomeres in polyoma and papilloma viruses. *Virology* 21: 1-6, 1963.
- (37) MAYOR, H. D.: Acridine orange staining of purified polyoma virus. *Proc Soc Exp Biol Med* 108: 103-105, 1961.
- (38) MELNICK, J. L.: Papova virus group. *Science* 135: 1128-1130, 1962.
- (39) WINOCOUR, E.: Purification of polyoma virus. *Virology* 19: 158-168, 1963.
- (40) GOMATOS, P. J., and TAMM, I.: The secondary structure of reovirus RNA. *Proc Nat Acad Sci USA* 49: 707-714, 1963.
- (41) NAUDE, W. DU T., MADSEN, T., and POLSON, A.: Different sized infective particles of Rift Valley fever virus. *Nature (London)* 173: 1051-1052, 1954.
- (42) CRAWFORD, L. V., and CRAWFORD, E. M.: The properties of Rous sarcoma virus purified by density gradient centrifugation. *Virology* 13: 227-232, 1961.
- (43) EPSTEIN, M. A.: The identification of the Rous virus. A morphological and biological study. *Brit J Cancer* 10: 33-48, 1956.
- (44) ———: Observations on the Rous virus: Purification and identification of the particles from solid tumours. *Brit J Cancer* 12: 248-255, 1958.
- (45) EPSTEIN, M. A., and HOLT, S. J.: Observations on the Rous virus: Integrated electron microscopical and cytochemical studies of fluorocarbon purified preparations. *Brit J Cancer* 12: 363-369, 1958.
- (46) BREEDIS, C., BERWICK, L., and ANDERSON, T. F.: Fractionation of Shope papilloma virus in cesium chloride density gradients. *Virology* 17: 84-94, 1962.
- (47) KOVACS, E.: Chemical dissection of mammalian cells with liberation of biologically intact viruses. *Z Naturforsch [B]* 17: 234-240, 1962.
- (48) DOORMASHKIN, R. R.: Electron microscopy of polyoma virus: A review. *In Tumors Induced by Viruses: Ultrastructural Studies* (Dalton, A. J., and Haguenau, F., eds.). New York, Academic Press Inc., 1962, pp 151-182.
- (49) BREESE, S. S., JR., and TRAUTMAN, R.: Examination of spray-droplet particle counting as a measure of virus concentration. *Virology* 10: 57-72, 1960.
- (50) SHARP, D. G., and BEARD, J. W.: Counts of virus particles by sedimentation on agar and electron micrography. *Proc Soc Exp Biol Med* 81: 75-79, 1952.
- (51) SHARP, D. G., and OVERMAN, J. R.: Enumeration of vaccinia virus particles in crude extracts of infected tissues by electron microscopy. *Proc Soc Exp Biol Med* 99: 409-413, 1958.

- (52) SMITH, K. O., and BENYESH-MELNICK, M.: Particle counting of polyoma virus. *Proc Soc Exp Biol Med* 107: 409-413, 1961.
- (53) JOKLIK, W. K.: The purification of four strains of poxvirus. *Virology* 18: 9-18, 1962.
- (54) PLANTEROSE, D. N., NISHIMURA, C., and SALZMAN, N. P.: The purification of vaccinia virus from cell cultures. *Virology* 18: 294-301, 1962.
- (55) REIMER, C. B., NEWLIN, T. E., HAVENS, M. L., BAKER, R. S., ANDERSON, N. G., CLINE, G. B., BARRINGER, H. P., and NUNLEY, C. E.: An evaluation of the B-V (continuous-flow) and B-IV (density gradient) rotors by use of live polio virus. *Nat Cancer Inst Monogr* 21: 375-388, 1966.
- (56) RUBIN, H.: Response of cell and organism to infection with avian tumor viruses. *Bact Rev* 26: 1-13, 1962.
- (57) ANDERSON, N. G.: The Joint National Institutes of Health-Atomic Energy Commission Zonal Centrifuge Development Program, Semiannual Report, USAEC Report (ORNL-3502), Special, Oak Ridge National Laboratory, January 1-June 30, 1963.
- (58) PAUL, H. L.: Die Bestimmung des Nucleinsäuregehaltes pflanzlicher Viren mit Hilfe einer spektrophotometrischen Methode. *Z Naturforsch [B]* 14: 427-432, 1959.
- (59) BRENNER, S., and HORNE, R. W.: A negative staining method for high resolution electron microscopy of viruses. *Biochim Biophys Acta* 34: 103-110, 1959.
- (60) LOWRY, O. H., ROSEBROUGH, N. J., FARR, A. L., and RANDALL, R. J.: Protein measurement with the Folin phenol reagent. *J Biol Chem* 193: 265-275, 1951.
- (61) FISHER, W. D., CLINE, G. B., and ANDERSON, N. G.: Density gradient centrifugation in angle-head rotors. *Anal Biochem* 9: 477-482, 1964.
- (62) DALLNER, G.: Studies on the structural and enzymic organization of the membranous elements of liver microsomes. *Acta Path Microbiol Scand (Suppl)* 166: 1-94, 1963.
- (63) CHO, N., BARRINGER, H. P., AMBURGEY, J. W., CLINE, G. B., ANDERSON, N. G., McCauley, L. L., STEVENS, R. H., and SWARTOUT, W. M.: Problems in biocontainment. *Nat Cancer Inst Monogr* 21: 485-502, 1966.
- (64) ANDERSON, N. G., and BARBER, A. A.: Isolation of native glycogen by combined rate-zonal and isopycnic centrifugation. *Abstracts, Biophys Soc*, 140, 1965.
- (65) BARRINGER, H. P., ANDERSON, N. G., and NUNLEY, C. E.: Design of the B-V continuous-flow centrifuge system. *Nat Cancer Inst Monogr* 21: 191-198, 1966.
- (66) GEISTER, R., and PETERS, D.: Ein vereinfachtes direktes Zählverfahren für virus-suspensionen ab  $10^5$  partikel/ml. *Z Naturforsch [B]* 18: 266-267, 1963.
- (67) SYKES, J. A., GREY, C. E., SCANLON, M., YOUNG, L., and DMOCHOWSKI, L.: Density gradient centrifugation studies of the Bittner virus. *Texas Rep Biol Med* 22: 609-627, 1964.



## PLATES



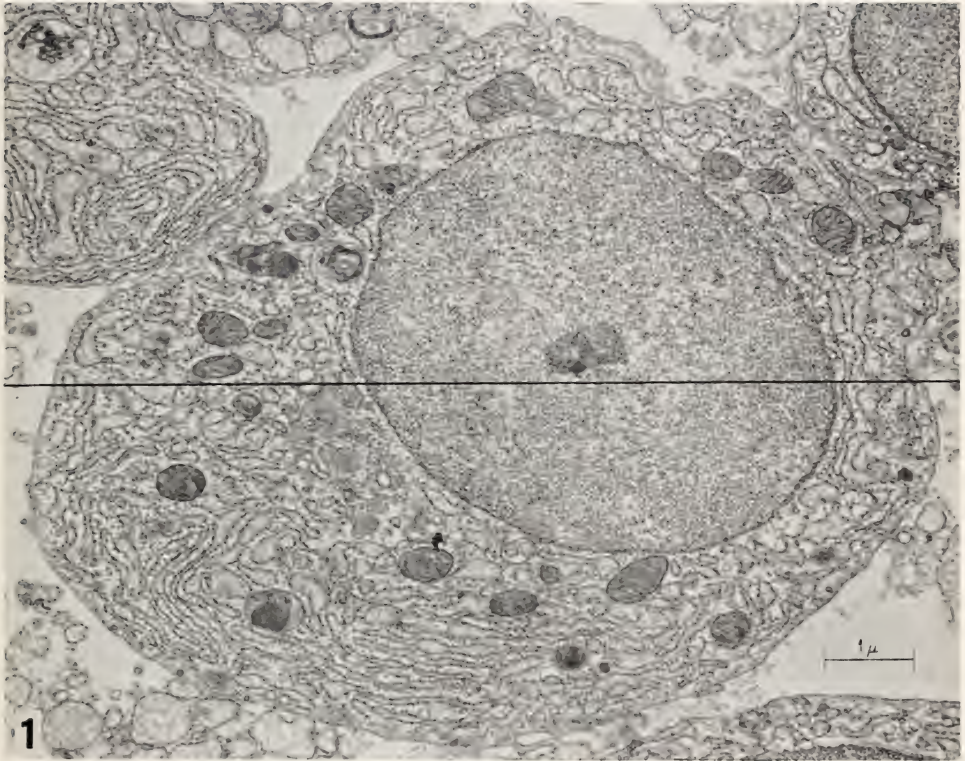


FIGURE 1.—Electron micrograph of section of cell from the lamina propria of the human intestine. The thickness of a 250 Å section is shown as a *solid line*. (Electron micrograph courtesy of Dr. John L. Watson.)

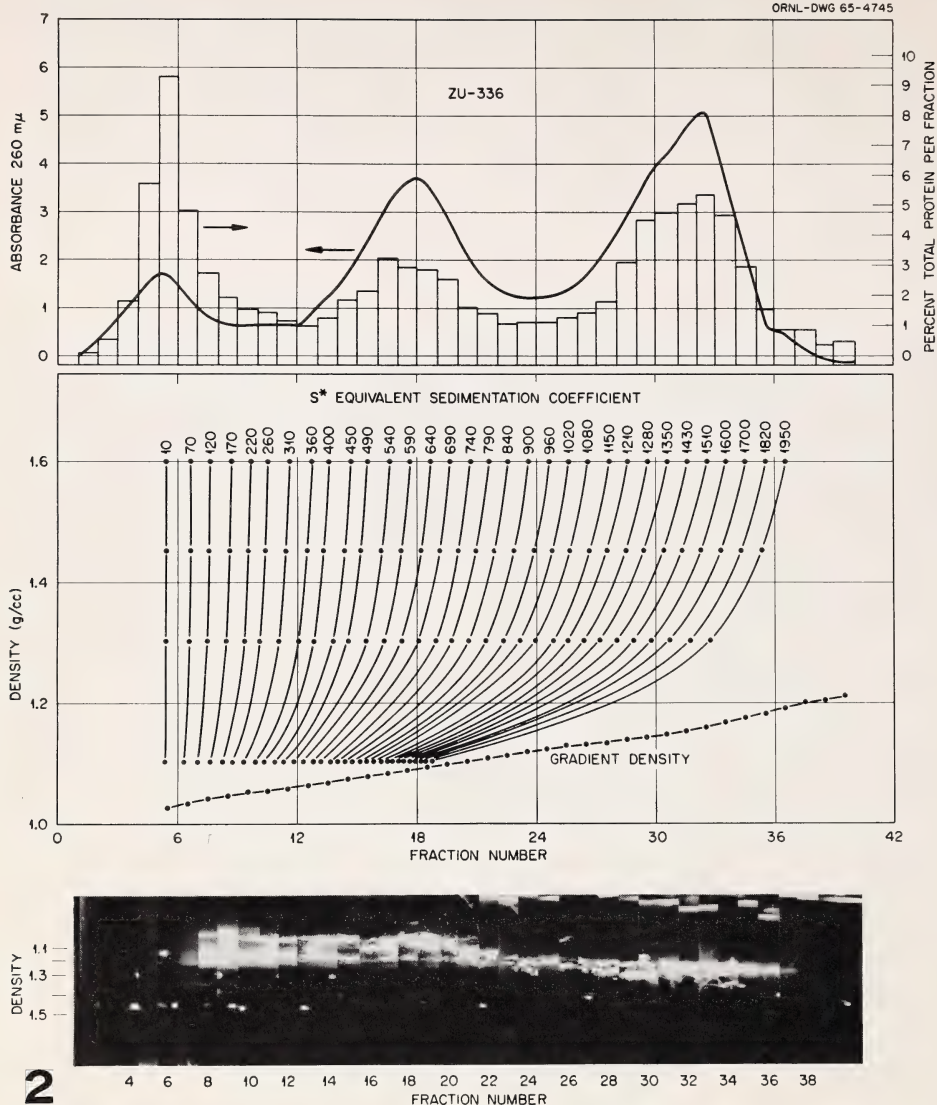


FIGURE 2.—Combined rate-zonal and isopycnic-zonal separation of particles found in a rat brain homogenate. The sample layer was 20 ml of a 20 percent w/v homogenate of fresh unperfused rat brain. The *upper*, *center*, and *lower* sections give, respectively, the results of rate-zonal centrifugation in the B-IV rotor, the computer output for determining equivalent sedimentation coefficients, and the results of isopycnic banding using cesium chloride. In the *upper diagram* the absorbance at 260 mμ was determined with a 0.2 cm light path cell and the observed absorbancies were multiplied by 5. The results of the protein analyses (*bar diagram*) indicate the percent of total homogenate protein found in each fraction. In the computer print-out the positions of hypothetical particles having the densities indicated along the ordinate are plotted together with the density gradient curve. In the lower photograph the banding density pattern in cesium chloride of the fractions previously separated by rate-zonal centrifugation. *White dots* in this composite photograph are plastic density-indicator beads.

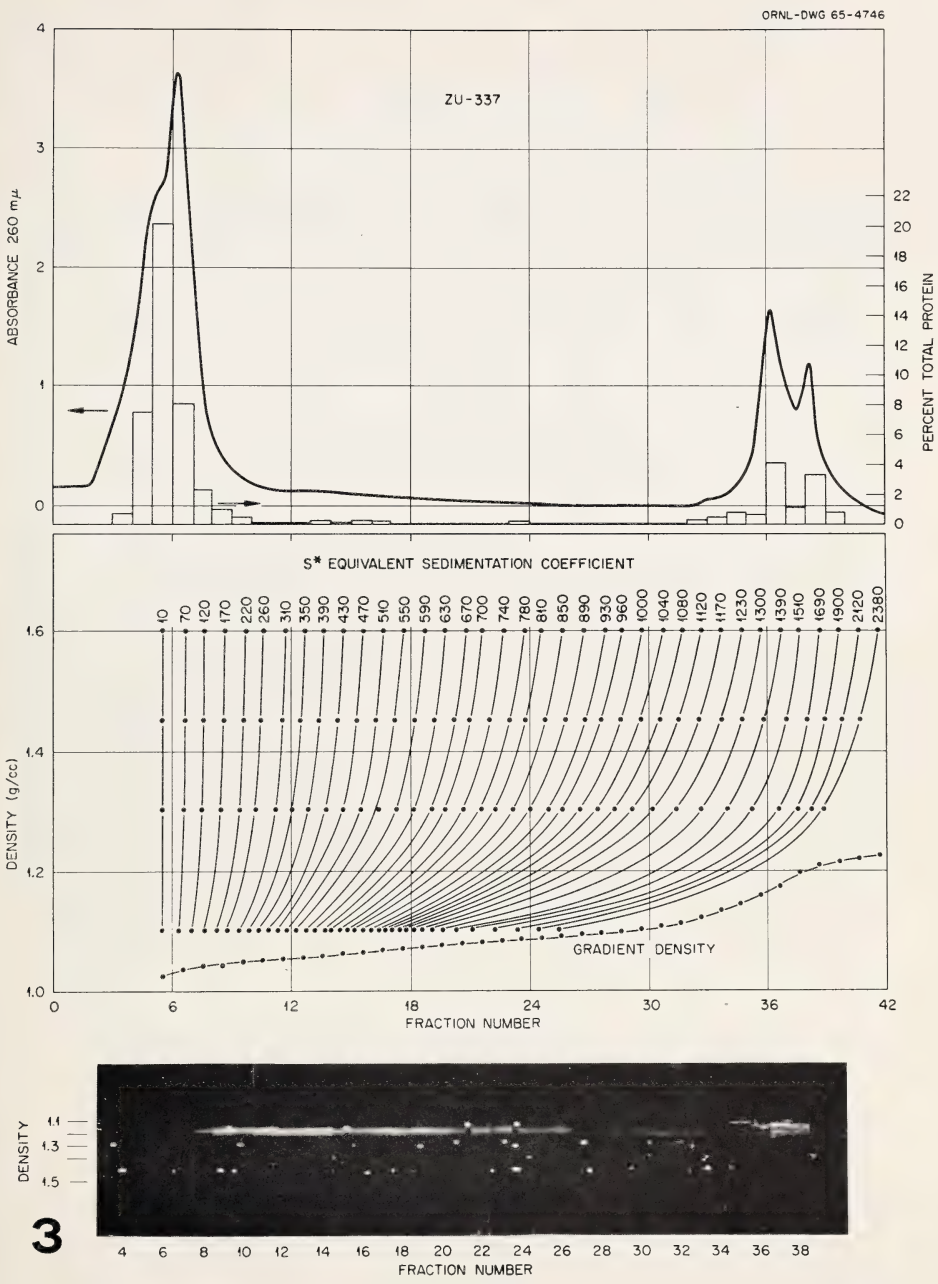


FIGURE 3.—Combined rate-zonal and isopycnic-zonal separation of particles found in a rat spleen homogenate. For details *see* legend of figure 2.

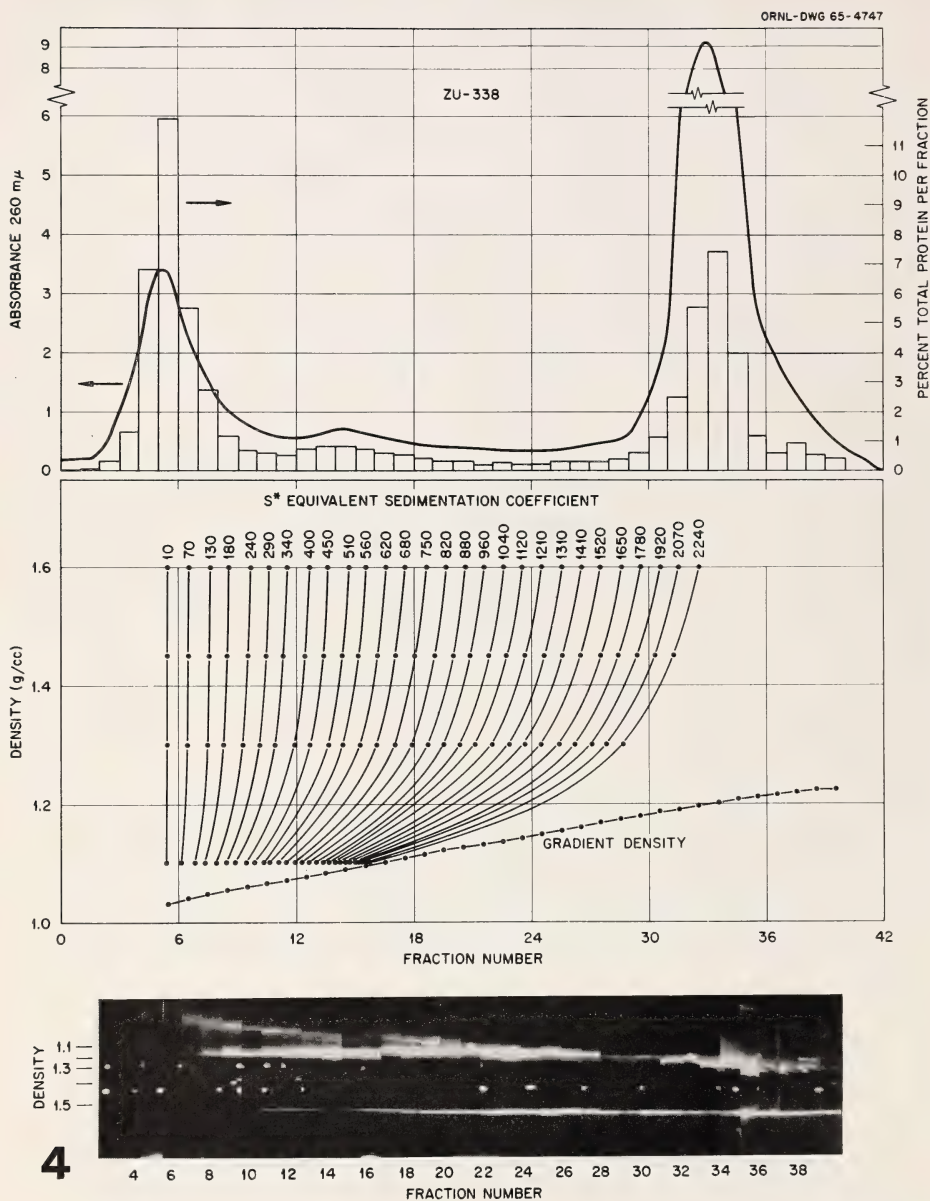


FIGURE 4.—Combined rate-zonal and isopycnic-zonal separation of particles found in a rat liver homogenate. For details *see* legend of figure 2.



FIGURE 5.—T3 phage banded in CsCl and photographed by scattered light. The total number of particles in each tube is indicated. The *band in the center* of all 4 tubes is due to the presence of small numbers of bacteria and serves to indicate the reproducibility of the gradients. The *lower band* clearly seen in the  $10^{12}$  tube is the phage band. It is also visible at  $10^{11}$  but not when only  $10^{10}$  or  $10^9$  particles are present.

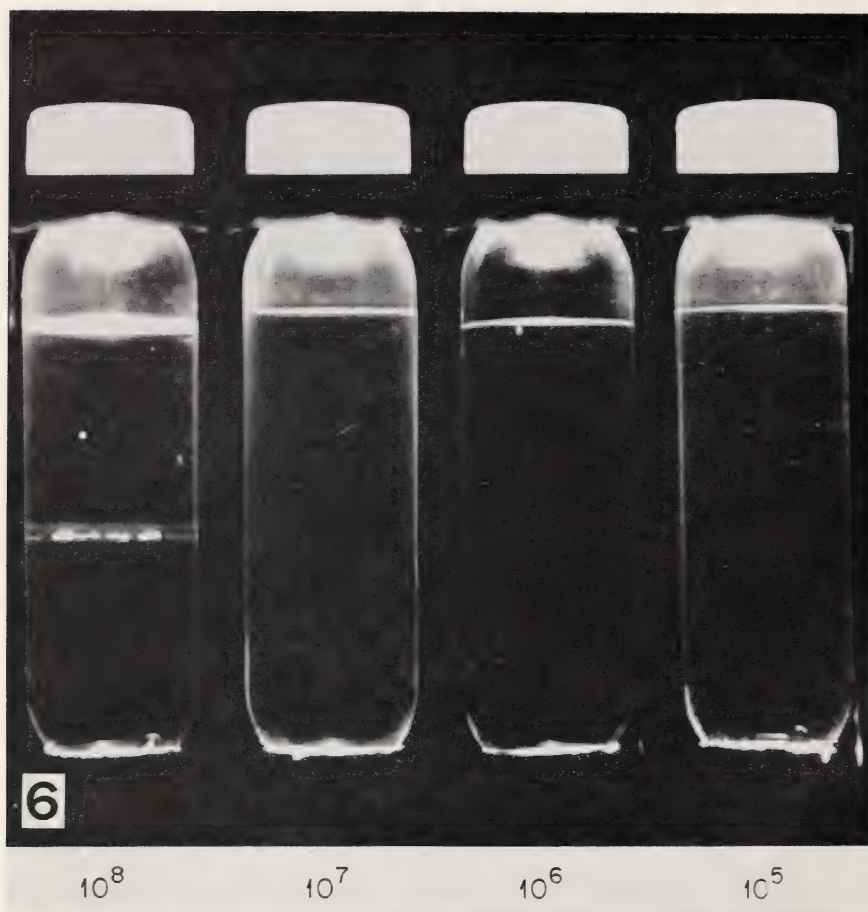


FIGURE 6.—Banding of *Escherichia coli* cells in a potassium citrate gradient. The total number of cells present is indicated. The lower limit of detection appears to be  $10^7$  cells.

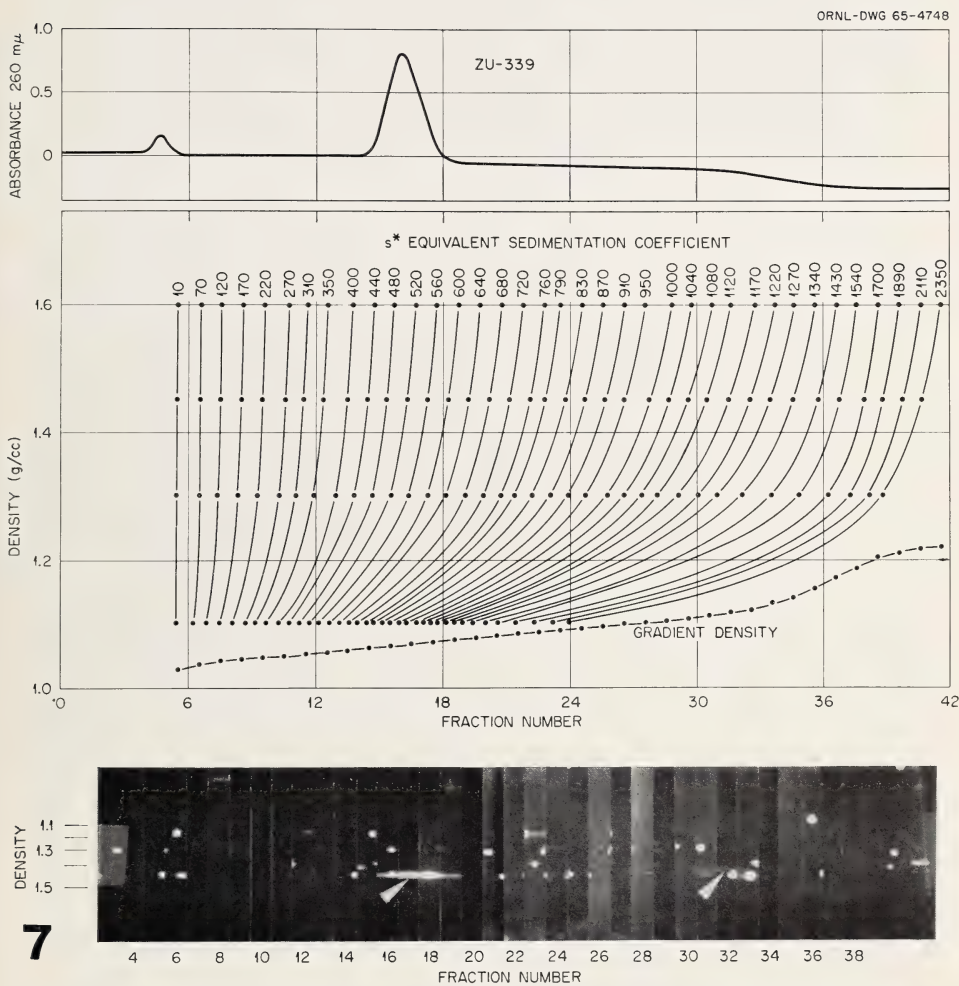


FIGURE 7.—Combined rate-zonal and isopycnic-zonal separation of T3 phage preparation contaminated with T2 phage. Position of the two virus bands indicated by arrows in the lower pycnogram.

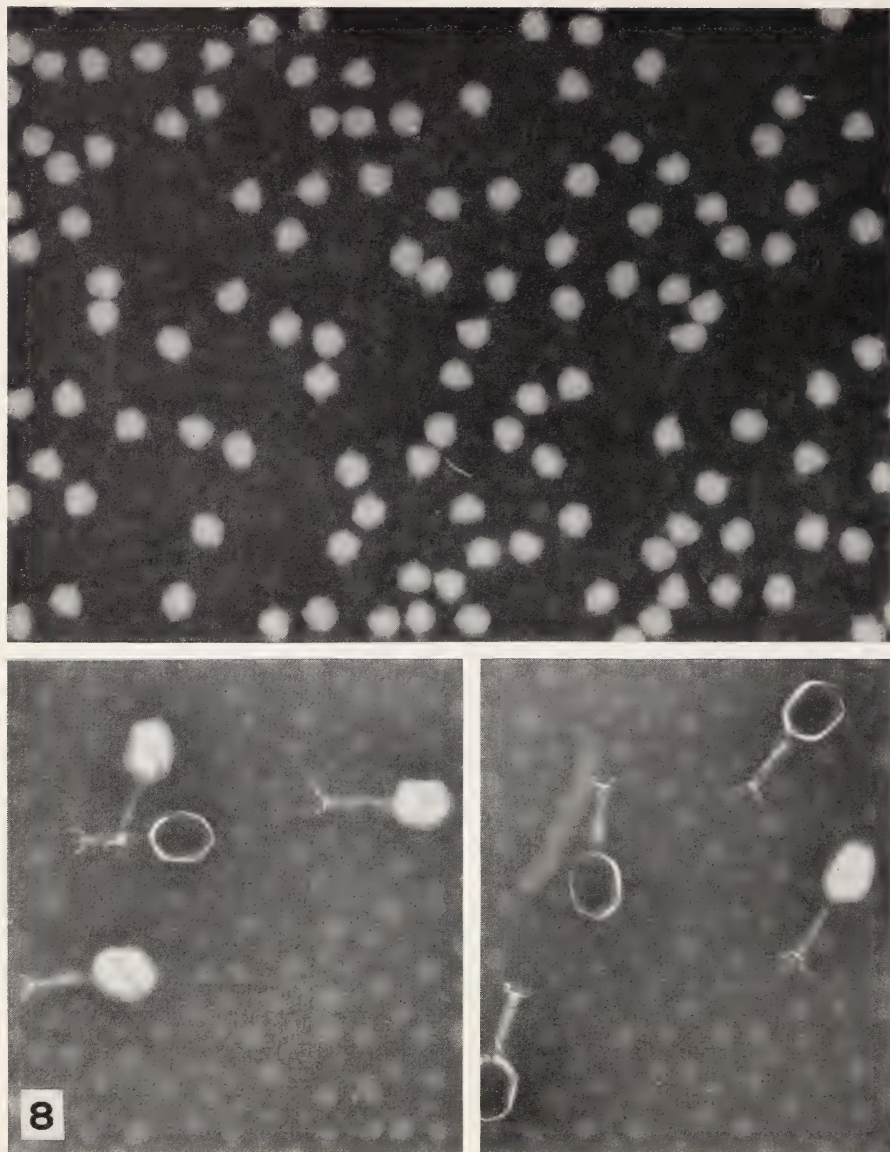


FIGURE 8.—T2 and T3 bacteriophage recovered from bands indicated in figure 7. *Upper micrograph* shows T3 particles from fraction 17; *lower two micrographs* show T2 particles recovered from fraction 32.  $\times 80,000$

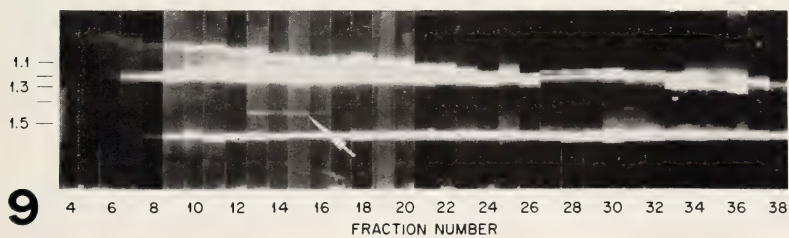
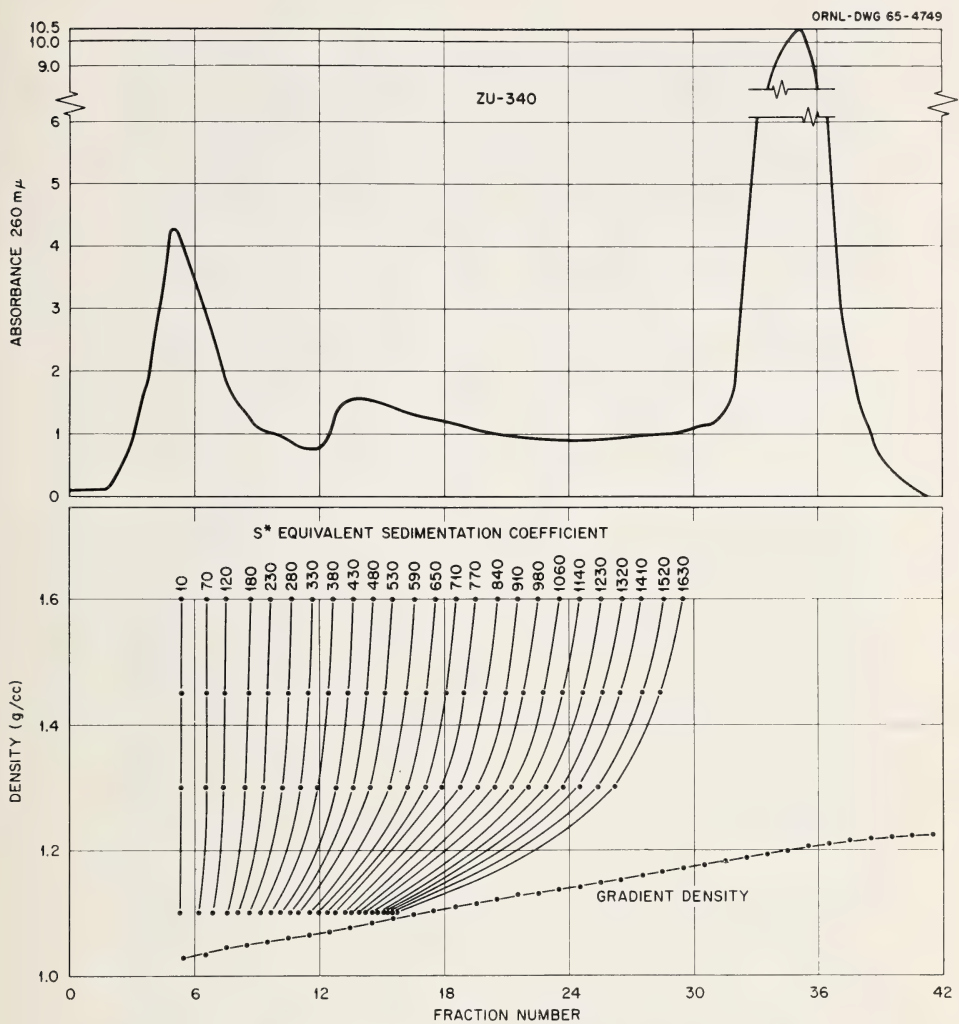


FIGURE 9.—Recovery of added T3 phage from a rat liver brei using the  $s\text{-}\rho$  technique. The particles from the band indicated in the *pycnogram* at the bottom were recovered and are shown in figure 10.

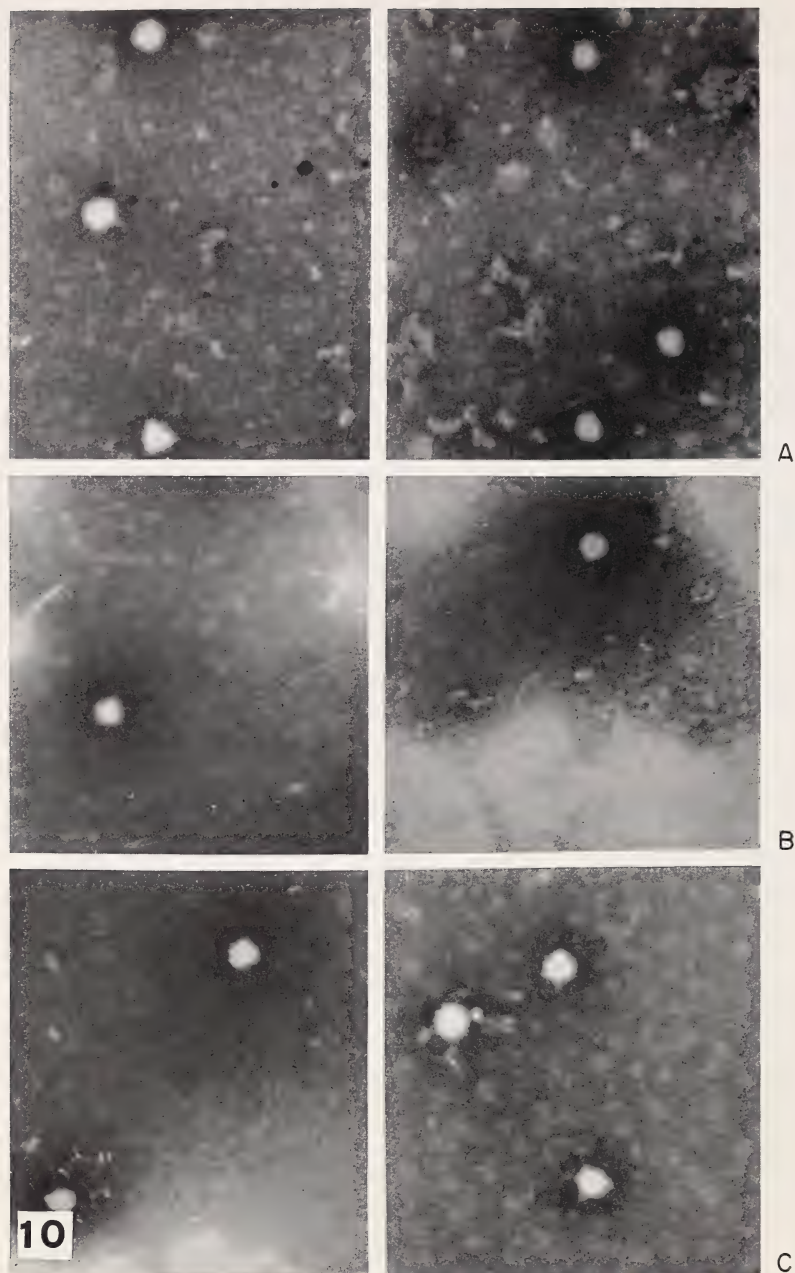


FIGURE 10.—Electron micrographs of T3 bacteriophage recovered from rat tissue homogenates. The positions from which the samples were recovered are indicated in figures 9, 11, and 12. A, liver; B, brain; and C, spleen.

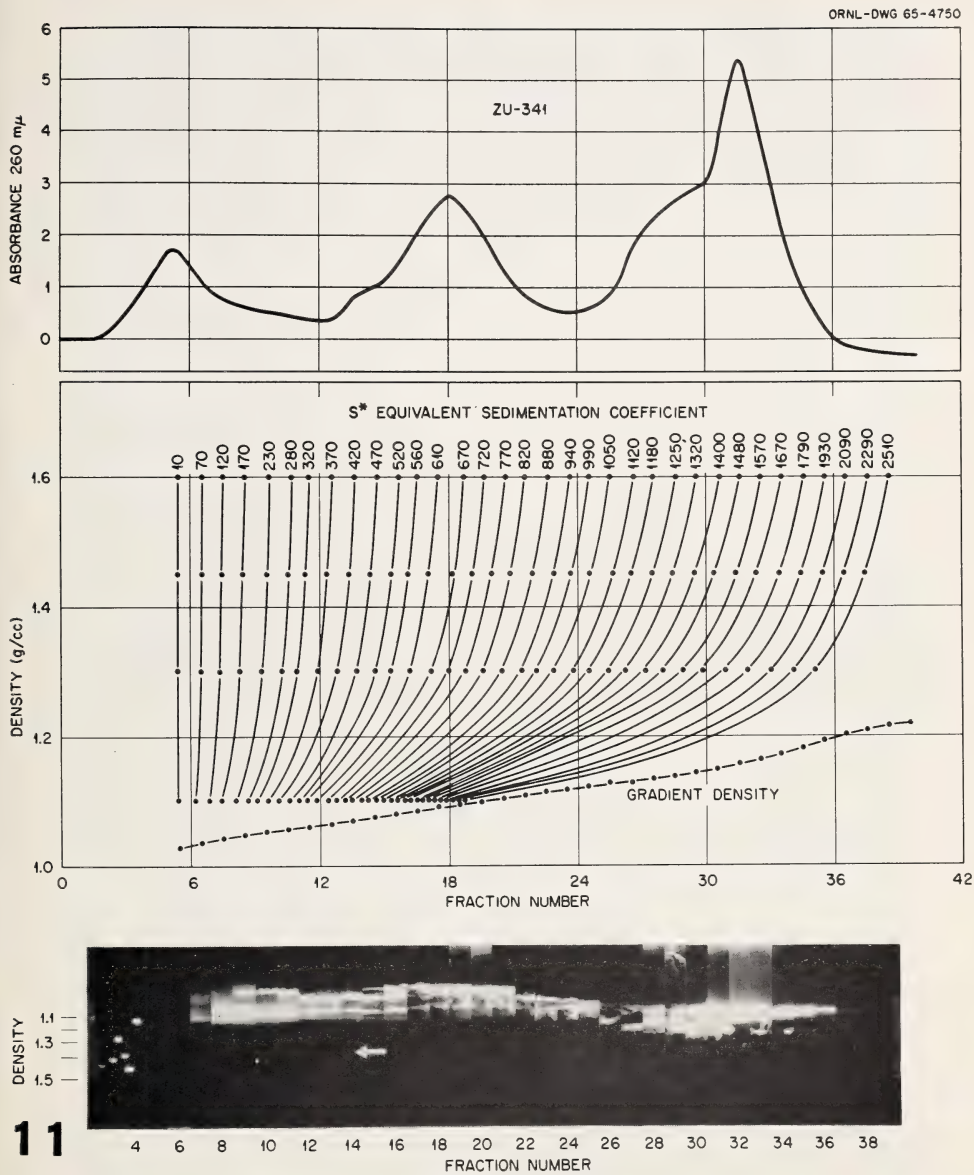


FIGURE 11.—Recovery of added T3 phage particles from rat brain brei using the  $s\text{-}\rho$  technique. Particles recovered from the density level indicated in the pycnogram were recovered, concentrated, and are shown in figure 10.

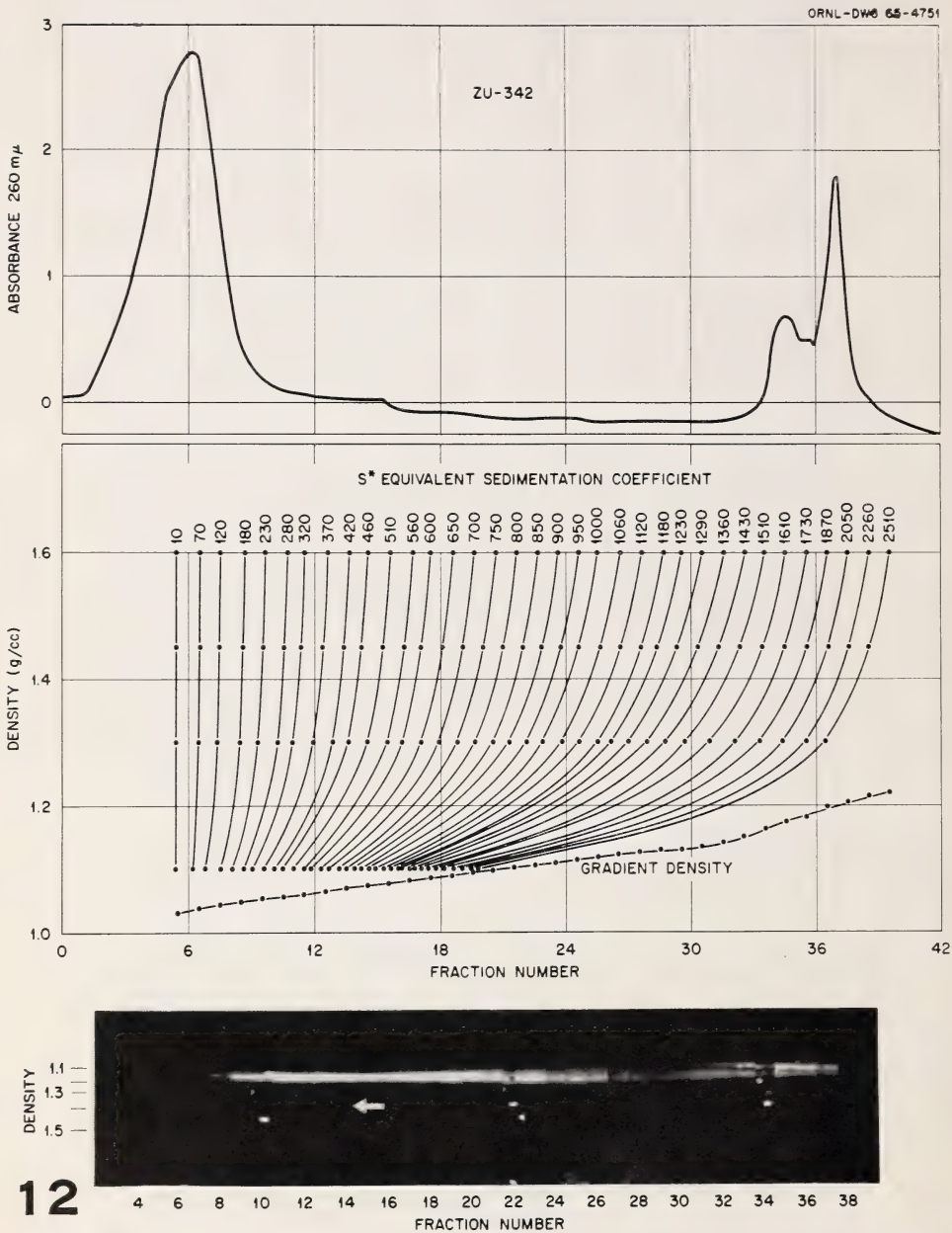


FIGURE 12.—Recovery of added T3 phage particles from a rat spleen homogenate using the *s-p* technique. Particles recovered at the density level indicated in the pycnogram were recovered, concentrated, and are shown in figure 10.

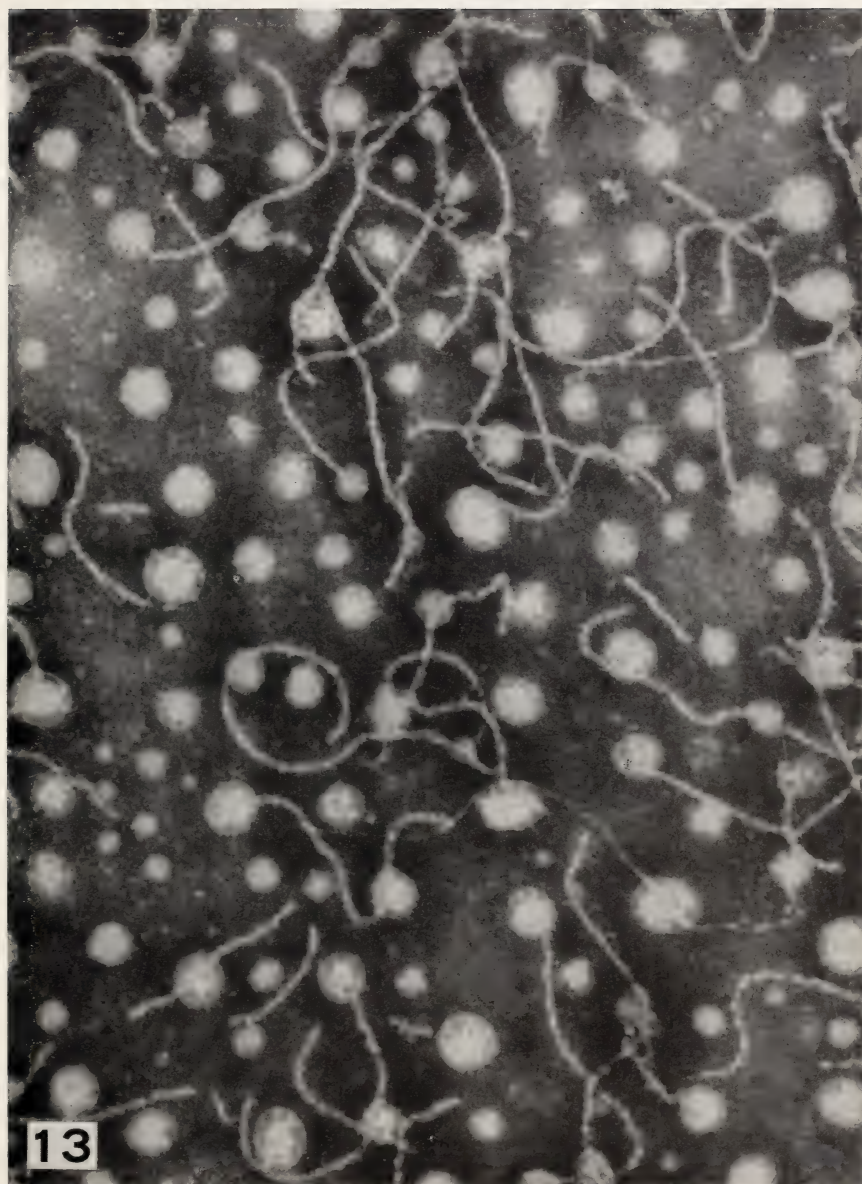


FIGURE 13.—Particles observed in a fraction obtained by rate-zonal centrifugation and isopycnic banding of human breast tumor. Negative staining.  $\times 80,000$



## Isolation of Native Glycogen by Combined Rate-Zonal and Isopycnic Centrifugation<sup>1</sup>

ALBERT A. BARBER,<sup>2</sup> WARREN W. HARRIS, and  
NORMAN G. ANDERSON,<sup>3</sup> *Biology Division, Oak Ridge  
National Laboratory,<sup>4</sup> and the Technical Division, Oak  
Ridge Gaseous Diffusion Plant,<sup>4</sup> Oak Ridge, Tennessee*

### SUMMARY

Rat liver glycogen was separated into fractions of uniform particle size by the rate-zonal centrifugation of homogenates through cesium chloride and sucrose density gradients. Glycogen was then isolated from other cell constituents having similar sedimentation coefficients by isopycnic-zonal centrifugation in CsCl density gradients to effect a density separation. A density of 1.62 to 1.65 was isopycnic for glycogen. A continuous spectrum of particle sizes up to 150 to 200 m $\mu$  was observed, and sedimentation coefficients up to 10,000 were measured. Sedimentation coefficients of particles of different sizes indicated a decrease in molecular packing with increasing cluster size. Microscopically, three levels of glycogen structure were resolved, including fundamental  $\gamma$  particles 2.5 to 3.5 m $\mu$  in diameter, subclusters of  $\beta$  particles 20 to 25 m $\mu$  in

diameter, and  $\alpha$  clusters of increasing size up to maximum diameter of 200 m $\mu$ . The 20 to 25 m $\mu$  subclusters would accommodate the glucose residues required to explain the molecular weight of glycogen particles normally extracted in strong alkali. Membrane fragments were not observed microscopically and specific 260 to 280 m $\mu$  absorption was absent in isolated glycogen fractions. Zonal centrifugation combined with isopycnic banding, therefore, provides a method for isolating large amounts of native glycogen separated into fractions of uniform particle size with a high degree of purity. Such preparations are obviously needed for studies of enzyme binding to glycogen particles and studies of the free and fixed glycogen fractions in tissues.—*Nat Cancer Inst Monogr* 21: 285-302, 1966.

GLYCOGEN, the reserve polysaccharide of animal tissues, consists of chains of (1 $\rightarrow$ 4)-linked  $\alpha$ -D-glucose residues interlinked by  $\alpha$ -D-(1 $\rightarrow$ 6)-glucosidic bonds to form a multibranched structure (1-5). The length of the average chain appears to be 10 to 14 D-glucose residues. These may include or be attached to exterior chains averaging 6 to 9 residues in length, and interior chains 3 to 4 residues long (1, 2, 6). Between 8 and

<sup>1</sup> This research performed under the Joint National Institutes of Health-Atomic Energy Commission Zonal Centrifuge Development Program which is supported by the National Cancer Institute, the National Institute of Allergy and Infectious Diseases, and the U.S. Atomic Energy Commission.

<sup>2</sup> Department of Zoology, University of California, Los Angeles, Calif. Aided by AEC Contract No. AT(11-1)-34 Project 49.

<sup>3</sup> We acknowledge the technical assistance of C. T. Rankin, Jr., for both centrifuge operation and manuscript preparation and of T. W. Bartlett for assistance in the sample preparation and screening for electron microscopy. Operated for the U.S. Atomic Energy Commission by the Nuclear Division of Union Carbide Corporation.

10 percent of all glucosidic linkages are of the (1→6) type. Glycogen has been reported to contain small amounts of protein (7) and RNA (8), while electron microscopic studies have suggested that glycogen particles may be bounded by membranes (9). The low partial specific volume of glycogen ( $\bar{v} = 0.62$ ) suggests either a very open structure completely interpenetrated by water, or very close packing of the polyglucose chains.

The size distribution of isolated glycogen depends to a great extent on the isolation method, of which several have been used. These include extraction with concentrated potassium hydroxide at 100° C (10), trichloroacetic acid (TCA) (11, 12), hot water (13, 14), and cold water (7, 15, 16). Certain shortcomings have been noted with the KOH and TCA methods. For example, concentrated alkali destroys the larger molecular sizes noted when TCA or water is used (12, 17), whereas TCA does not remove all the glycogen present in tissues (12, 18–20). The failure of TCA to extract all the glycogen has led to the concept of free and fixed glycogen fractions within tissues. TCA presumably extracts only the free form. The existence of these two forms as artifacts of extraction, and therefore of no significance, has been reported (21). The complex literature on free and fixed glycogens has been summarized by Stetten and Stetten (3).

Using cold-water extraction, Lazarow (7, 22) reported the isolation of very large glycogen particles in moderately low centrifugal fields and showed that previous extraction methods degraded the large “native” particles. Recent studies support Lazarow’s conclusions and suggest that most of the physical studies previously reported have been done on partially degraded material (17).

Combined rate- and isopycnic-zonal centrifugation ( $s$ - $\rho$  centrifugation) has been applied to problems of cell fractionation (23). The technique is particularly appropriate for isolation of polydisperse cell constituents, such as glycogen. It was therefore used to examine the polydispersity of glycogen separated from rapidly prepared homogenates at neutral pH, and to determine whether glycogen was uniform with respect to banding density. In the case of glycogen, the uniformity of banding density is of interest from the point of view of the uniformity of chain packing. Also, the presence or absence of substances such as protein, lipids, or nucleic acids might be detected by changes in the banding density.

The probability that attached or “fixed” glycogen would band at the same density as free glycogen is small.

Rate- and isopycnic-zonal centrifugation were combined in the present study to separate pure native glycogen into fractions of uniform particle size. The isolation was designed to avoid all procedures using strong alkali or acid, fat solvents, and high temperature. A preliminary report of this work has appeared (24).

## MATERIALS AND METHODS

Rat livers were removed from adult Sprague-Dawley male rats after stunning, decapitation, and exsanguination. Livers were diluted 1:5 (w/v) and homogenized either in 0.25 M sucrose or 0.01 M phosphate buffer at pH 7.0 containing 0.15 M NaCl. All manipulations were carried out as rapidly as possible at 0 to 4° C.

Zonal centrifugation was carried out in the B-IV rotor systems with either cesium chloride or sucrose as the gradient material (25, 26). Twenty ml of homogenate was placed in the rotor containing a gradient volume of 1200 ml. About 300 ml of high-density solution was used as the underlay and 200 ml of buffer as the overlay. Separations were normally carried out at 20,000 rpm for 15 minutes ( $G_c = 4700 \times 10^6$ , including acceleration and deceleration<sup>5</sup>). The rotor contents were emptied by use of high-density solutions, and the eluant was monitored at 260 m $\mu$ . Forty-two fractions of 40 ml each were collected in tubes maintained in ice. The density of each tube was determined from measurements of refractive index with an American Optical refractometer.

Isopycnic banding was carried out by density gradient centrifugation in Spinco No. 30 angle-head rotors (27). Tubes containing CsCl (saturated at 0° C and containing 0.01 M potassium citrate at pH 7.0) layered underneath 18 ml of sample volume were centrifuged at 24,000 rpm for 3 hours in a Spinco Model L ultracentrifuge. Banded samples were photographed with scattered light (23). The glycogen band was removed from some samples with a Band-Recovery Apparatus<sup>6</sup> (BRA I) equipped with a square-tipped spinal needle connected to a 2 ml syringe (23). The total contents of other banded samples were collected in 1 ml portions, starting from the bottom of the centrifuge tube, with a New Brunswick PA-56 pump. The density of each sample was determined from refractive index measurements.

Glycogen was measured by a phenol-sulfuric acid colorimetric method (28), which has been successfully used as a rapid and simple procedure for measuring liver glycogen (29). One ml of 5 percent (w/v) phenol and 5 ml of concentrated reagent-grade (Dupont) sulfuric acid were added to 1 ml samples containing 5 to 40  $\mu$ g of carbohydrate. Absorbancy was measured at 490 m $\mu$  after 1 hour at room temperature and compared with standards prepared from glucose. All spectrophotometric measurements were made with either a Bausch and Lomb Spectronic or a Beckman DB spectrophotometer.

Sedimentation coefficients were read directly from computer plots programmed for sucrose density gradients in the B-IV rotor system (23).

Samples were prepared for microscopy by the negative staining technique of Brenner and Horne (30). Phosphotungstic acid (PTA) has been used successfully for morphological studies of glycogen by negative staining (31, 32). A single drop of sample was placed on each of two

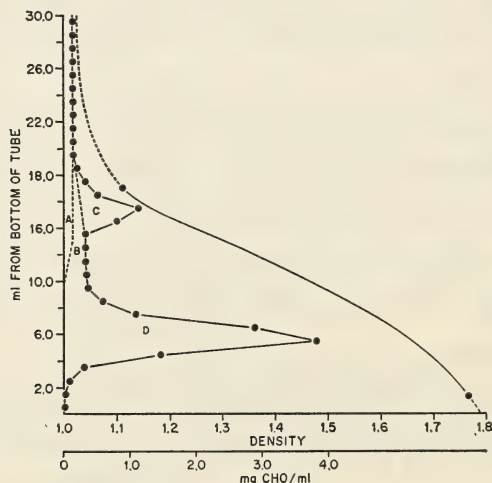
<sup>5</sup> Where  $G_c = \int \omega^2 dt$ .

<sup>6</sup> Information on drawings available from N. G. Anderson.

carbon-coated Formvar specimen screens and allowed to remain on the screen for 2 to 3 minutes in a large petri dish in the presence of osmium vapor. The drop of sample was removed by touching the edge of the screen with filter paper, and a drop of 2 percent (w/v) phosphotungstic acid (adjusted to pH 7.0 with KOH) was added immediately. The PTA was left on the screen approximately 30 seconds, removed, and the screen dried under ultraviolet light. Glycogen was somewhat difficult to examine with the electron microscope because of its low density to electrons. Screens were examined with one or more of the following RCA model electron microscopes: EML, EMU3-F, or EMU3-G.

## RESULTS

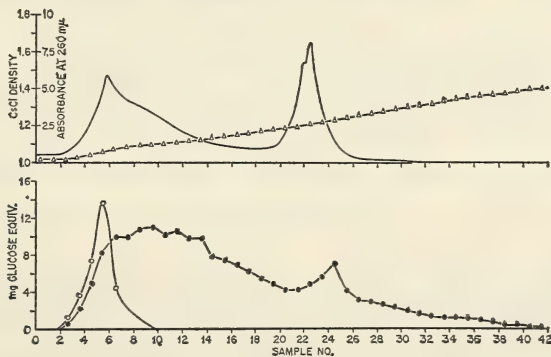
Initially, it was of interest to determine whether all glycogen banded in a narrow zone in CsCl or whether some glycogen was associated with cell structures that banded at a different level. Centrifugation of a rat liver homogenate in CsCl separated the membrane and glycogen fractions into two distinct bands visible with scattered light (fig. 1). The CsCl density and the carbohydrate distributions within the centrifuge tube are plotted in text-figure 1. The banding density of glycogen, under the conditions used, was approximately 1.65. Membrane-associated carbohydrates banded at a density of 1.25. In addition to the banded glycogen (area D, text-fig. 1), representing approximately 65 percent of all carbohydrate, and the membrane-associated carbohydrate (area C, text-fig. 1), representing approximately 12 percent of the carbo-



TEXT-FIGURE 1.—Cesium chloride density and carbohydrate distribution in rat liver homogenate banded in CsCl (same tube as photographed in fig. 1). A total of 16.0 mg of the 16.2 mg placed into the tube was recovered. —●—●—●—●—● Carbohydrate distribution; ----- extrapolated values; ●—●—● CsCl density.

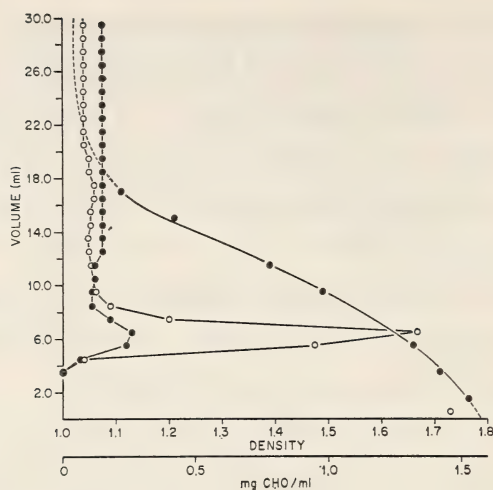
hydrate, two other carbohydrate areas were identified. These included partially sedimented glycogen (area B, text-fig. 1) and unsedimented glycogen. The distribution of nonsedimentable glycogen was determined by measurement of the distribution of glucose in a separate tube centrifuged under similar conditions. As expected, the amount of glycogen banded was less when the centrifugal force was reduced. The ratio between completely and partially banded material, therefore, depended on the centrifugal force and suggested that glycogen exists as a continuous spectrum of particle sizes.

Rate-zonal centrifugation separates mixtures into zones of particles having similar sedimentation coefficients. The polydispersity of native glycogen was confirmed by a rat liver homogenate sedimented in the zonal centrifuge at 17,500 rpm for 15 minutes with CsCl. Cesium chloride was used in place of sucrose because the latter interferes with the analysis for glycogen. Glycogen was sedimented throughout the B-IV rotor (text-fig. 2). The curve of glycogen concentration passed through a maximum a short distance from the starting zone, and a gradual decrease in the concentration was noted in successive samples. An abrupt increase in concentration was noted, however, in the samples containing the larger membrane fractions (tubes 22-26, text-fig. 2). Therefore, as in the banded homogenate, a membrane-associated glycogen fraction was observed. The samples collected from the region of the starting zone contained banded, partially sedimented, and nonsedimented carbohydrate as determined by isopycnic zonal centrifugation in CsCl. Tubes 5 through 12 were banded, since they represented the extremes of glucose distribution under similar conditions of zonal centrifugation (text-fig. 2). The carbohydrate distribution in banded tubes 6 and 10 is plotted in text-figure 3. Sample No. 6 contained only small amounts of banded



TEXT-FIGURE 2.—Distribution of rat liver carbohydrates following density gradient centrifugation in the B-IV rotor at 17,500 rpm for 15 minutes. A total of 20 ml of a 1:5 (w/v) homogenate made in buffer and containing 185 mg of carbohydrate (equivalent to 46 mg/g tissue) was used as sample; 188 mg was measured in the collected samples. ●—● Carbohydrate distribution; △—△ CsCl gradient density; ○—○ glucose distribution determined in a separate run; — absorbance.

#### ZONAL CENTRIFUGE



TEXT-FIGURE 3.—Cesium chloride density and carbohydrate distribution in zonal samples 6 and 10 banded in CsCl. Samples obtained from the experiment described in text-figure 2 were banded as described for text-figure 1. ●—●—●—●—● Sample 6; ○—○—○—○—○ sample 10; ●—●—●—●—● CsCl density.

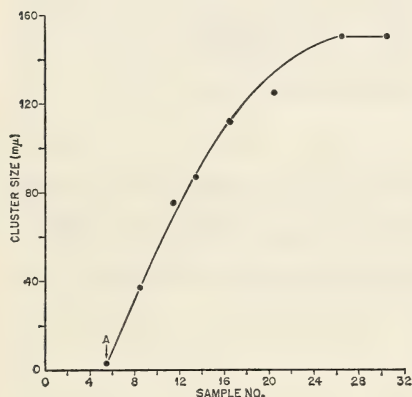
carbohydrate, whereas more than 70 percent of the carbohydrate of sample 10 was banded. The analytical data from the isopycnic banding of tubes 5 through 12 showed that the total amount of nonsedimentable carbohydrate present was similar to that found in homogenates banded directly in CsCl.

Zonal centrifugation of a rat liver homogenate was also carried out with a sucrose density gradient. Each collected sample was then centrifuged in CsCl gradients. The presence of glycogen, banded at its characteristic density level, was determined by photography with scattered light (fig. 2). The presence of glycogen bands throughout the rotor again indicated a continuous spectrum of particle sizes. The equivalent sedimentation coefficient of glycogen particles at various positions within the rotor was read directly from the computer plot, with 1.62 as the density of glycogen. Computer plots of several experiments, with different centrifugal forces and sucrose gradients, indicated an equivalent sedimentation coefficient for the largest glycogen particles of approximately 10,000  $S^*$ . Generally the maximum was somewhat less. Minimum equivalent sedimentation coefficients were not determined in these rate-zonal separations, since the low centrifugal forces used did not sediment the small particles out of the starting zone. A continuous spectrum of particle sedimentation coefficients was observed. Assuming the same shape for the glycogen distribution curves and the same positions of maximum glycogen concentration in sucrose and the CsCl gradients, the peak of glycogen concentration occurred in the particle size range of 500 to 1000  $S^*$ .

Glycogen particles collected in samples from several positions in the rotor demonstrated a progressive increase in particle size as one moves

centrifugally from the starting zone (fig. 3). The particles in any given sample were similar in size. Large  $\alpha$  particles, or clusters (No. 3 in fig. 3), were constructed from subclusters or  $\beta$  particles which measured 20 to 25  $m\mu$  in diameter (No. 2 in figs. 3 and 4). The 20  $m\mu$  subclusters were aggregates of many fundamental  $\gamma$  units 2.5 to 3.5  $m\mu$  in diameter (No. 1 in fig. 4). The latter have been reported to be rodlike and approximately 20  $m\mu$  long (31). However, it is difficult to distinguish rods from beaded aggregates at this level.

The large  $\alpha$  clusters attain sizes of 150 to 200  $m\mu$  in diameter. The progressive increase in cluster size as related to their position in the gradient is plotted in text-figure 4. The largest commonly observed  $\alpha$  particle was 150  $m\mu$  in diameter, its equivalent sedimentation coefficient was approximately 3000. The most rapidly sedimenting particles appeared in the electron microscope to be aggregates of  $\alpha$  clusters. The shape of the curve in text-figure 4 strongly suggests that the largest  $\alpha$  particles existed in the form of  $\alpha$  cluster aggregates in solution.



TEXT-FIGURE 4.—Relationship between glycogen cluster size and sample number after centrifugation in sucrose density gradients. Average cluster size for each sample plotted was determined from figure 3. A, position of sample placed into rotor.

It should be emphasized that the equivalent sedimentation coefficients calculated apply strictly only to the conditions employed in a given experiment. This is shown by simple calculations relating particle size to sedimentation rate using the formula:

$$(2a)^2 = \frac{18\eta s}{\rho' - \rho} \quad (1)$$

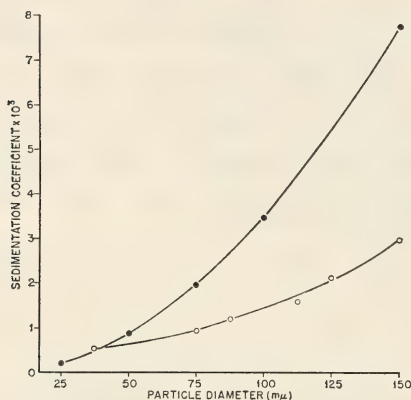
where  $2a$  is the diameter of the particle in cm;  $\eta$  is the viscosity of the medium;  $\rho'$  is the particle density;  $\rho$  is the medium density; and  $s$  is the sedimentation coefficient ( $s \times 10^{13}$  is the sedimentation coefficient in Svedberg units). In water at 20° C the above expression can be reduced to

$$(2a)^2 = \frac{0.18s}{\rho' - 1.0} \quad (2)$$

and for glycogen of density 1.62 the expression further reduces to

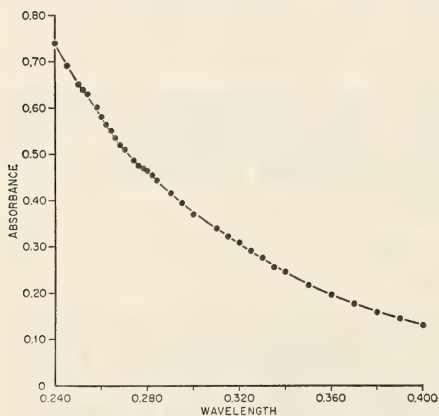
$$(2a)^2 = 0.29s \quad (3)$$

Calculated theoretical sedimentation coefficients for different-sized particles of 1.62 density were compared with experimentally determined values of measured glycogen particles (text-fig. 5). The two curves intersect at a particle dimension of approximately  $37\text{ m}\mu$  but become increasingly divergent with increasing particle sizes. Close packing of glycogen subclusters ( $20\text{--}25\text{ m}\mu$  particles) was therefore indicated, and an increasingly open structure, as observed, must be postulated for the larger clusters.



TEXT-FIGURE 5.—Relationship of size and sedimentation coefficient for theoretical particles having a density of 1.62 compared with the measured size and sedimentation coefficient of glycogen particles of increasing size. Theoretical curve is plotted from the formulation  $(2a)^2 = 0.29 s$  and the experimental curve is plotted from figures 2 and 3. ●—● Calculated; ○—○ observed sedimentation coefficients in conventional Svedberg units.

No membrane elements were observed microscopically in banded glycogen fractions. The absence of membranes was also suggested by the absence of specific 260 or 280  $\text{m}\mu$ -absorbing materials in the collected fractions (text-fig. 6). It therefore appears that glycogen clusters are not held together by membranous elements.



TEXT-FIGURE 6.—Absorption spectrum of glycogen isolated by banding in cesium chloride. Wavelength is in  $\mu$ .

## DISCUSSION

Polydisperse rat liver glycogen was separated into zones of uniform particle size by combined rate- and isopycnic-zonal centrifugation. Forty-two samples were collected following rate-zonal separation and were

banded in CsCl to effect a density separation of the glycogen from other cell constituents having similar sedimentation coefficients. Liver glycogen particles exist as a continuous spectrum of sizes.

Glycogen was identified as the 1.62 to 1.65 density material in banded samples by both chemical analysis and amylase digestion. Phenol-sulfuric acid was used as the chemical method for measuring glycogen on the assumption that all the carbohydrate of liver was present as glycogen. The validity of this assumption was indicated both by comparison of the carbohydrate values of 45 to 50 mg per g tissue with the published values for glycogen (18, 19) and by the results of the carbohydrate distribution in liver homogenates banded in CsCl. Centrifugation in Spinco No. 30 rotors for 3 hours at 24,000 rpm, in the absence of density gradients, totally sediments particles with sedimentation coefficients (in water) of larger than 110. The amount of smaller material sedimented decreases with molecular size. Calculations of the banding profile of a heterogeneous mixture in a density gradient is very complex. However, if one uses particles of  $S^* 100$  as the minimum for banding in the procedures used, the carbohydrates distributed in the partially banded and nonbanded fractions of the banded sample represent the size spectrum of glycogen particles up to this size. This entire spectrum (excluding material which banded with the membrane fraction) would constitute only 23 percent of the total carbohydrates present. Assuming a size distribution curve for particles below  $S^* 100$  similar to that for larger particles, the contribution of non-glycogen carbohydrates to total carbohydrate would be negligible. This would suggest that nearly all carbohydrates of liver are present in the form of glycogen, and glycogen exists in a continuous size spectrum from small molecules to clustered particles containing several million glucose residues. A gradual decrease in concentration occurs with increasing particle size. It is evident that further studies with high-speed zonal centrifuges will be required to determine whether such a size spectrum of small molecules does, in fact, occur, or whether there is a minimum-sized molecule larger than glucose from which larger units are formed.

The three levels of structural organization observed in glycogen were referred to as  $\alpha$ ,  $\beta$ , and  $\gamma$  particles (31). The  $\gamma$  units were spherical or oblong particles 2.5 to 3.5  $m\mu$  in diameter. These were combined into 20 to 25  $m\mu$   $\beta$  particles. Increasing numbers of  $\beta$  particles per cluster resulted in a spectrum of  $\alpha$  particle sizes ranging from 30 to 200  $m\mu$ . The  $\alpha$  particle is the large, sedimentable unit of glycogen described by Lazarow (7, 22). Similar measurements and levels of organization for glycogen were found in this study. The major size differences in these studies concern the  $\gamma$  particle. Drochmans (31) considers them rodlike structures 3 by 20  $m\mu$ , whereas the 3  $m\mu$  particles observed in the present study were primarily spherical and occasionally occurred in short chains.

The large clusters, characteristic of native glycogen from liver, are preserved only by relatively mild isolation procedures. The dissociation of large clusters by KOH and acid treatment has been observed by both centrifugal and microscopic methods (17, 22, 31). TCA extraction meth-

ods cause less breakdown than do methods involving KOH digestion (12). The particles isolated from liver following KOH digestion have molecular weights in the range of 1 to  $8 \times 10^6$  (1), which indicates the dissociation of clusters into smaller units. Drochmans considered the product of KOH digestion normally used for physical studies to be the 3 m $\mu$  particles (31). Particle dimensions and molecular weight calculations, however, indicate the 20 m $\mu$  particle as the product. Assuming a spherical, 3 m $\mu$  particle, the volume occupied by an anhydrous glucose molecule of molecular weight 162 and density of 1.62, the 3 m $\mu$  particle would contain approximately 85 glucose residues. Assuming a 3 m $\mu$  by 20 m $\mu$  cylinder, the particle would contain approximately 850 residues. Neither of these values can be easily correlated with specific units in the branching model proposed for glycogen (1). However, both are too small to represent the glycogen particle studied after KOH extraction. On the other hand, 20 to 25 m $\mu$  spherical particles would contain the appropriate number of glucose residues indicated by the molecular weight of KOH-extracted material. Morphological transition in glycogen structure at the level of the 20 to 25 m $\mu$  particle was indicated by the divergence in the curves of the theoretical and experimental sedimentation coefficients at that point. This divergence could be interpreted as the transition point from a relatively closed to a relatively open structure. The chemical bonds leading to the open structure could be the point of attack of KOH during extraction. The amount of opalescence, used by Drochmans (31) as indicative of the 3 m $\mu$  particle as the digestion product, would likewise be reduced in solutions of 20 m $\mu$  particles.

The particulate glycogen isolated in the present study was collected in fractions of uniform particle sizes throughout the entire spectrum of sizes without appreciable membrane contamination. Such preparations are necessary for studies of enzyme attachment to glycogen particulates. Attachments of  $\alpha$ -glucan phosphorylase and uridine diphosphate glucose-glycogen transferase to glycogen particles have been clearly established (33, 34). The major technical difficulties in these studies involved separation of glycogen particulates from membranous elements. Such difficulties are normally overcome by studies of specific activities during glycogen enrichment. Assuming that the presence of CsCl does not dissociate the bound constituents, isopycnic banding would provide a rapid method for collecting large amounts of uncontaminated glycogen. Rate-zonal separation can also be used to isolate large quantities of the various particle sizes for study of the specificity between particle sizes and amount of enzyme bound. The significance of such studies has been discussed (33).

Free and fixed glycogen fractions in tissues have been isolated by TCA extraction (3). In liver, 10 to 15 percent of the glycogen is considered fixed (18), although the existence of two fractions has been denied (21). In homogenates banded in CsCl, 12 percent of the carbohydrate was associated with the membrane fraction. Rate-zonal separations demonstrated membrane-associated glycogen in the region of mitochondria and

large fragments. No microsomal-bound glycogen was noted in samples banded from the microsomal region. Further studies using rate-zonal and isopycnic centrifugation are needed to determine if this membrane-associated glycogen represents the fixed glycogen fractions identified by TCA extraction.

One problem arising from these studies is the relationship of the three levels of structure observed with the electron microscope to the statistical models of branched glycogen deduced from chemical studies. One published consideration was concerned with the problem of the maximum size reached by a continuously branching open structure (35). Assuming that each chain branches into two at regular intervals, a maximum size of 26 to 40  $m\mu$  was calculated. At this size the entire surface is occupied by the ends of chains and further growth is not possible. The assumption that all chains divide in two is unlikely, since uniform growth probably would not occur. Although the 26 to 40  $m\mu$  size compares favorably with the observed  $\beta$  particle, and  $\alpha$  particles could form from irregularly branched  $\beta$  particles, the chemical nature of the classical branched structure of glycogen cannot be directly correlated with the morphology of the particle.

## REFERENCES

- (1) MANNERS, D. J.: The molecular structure of glycogens. *Advances Carbohydr Chem* 12: 261-298, 1957.
- (2) ———: Enzymic synthesis and degradation of starch and glycogen. *Advances Carbohydr Chem* 17: 371-430, 1962.
- (3) STETTEN, D., JR., and STETTEN, M. R.: Glycogen metabolism. *Physiol Rev* 40: 505-537, 1960.
- (4) CORI, G. T.: Enzymatic structure analysis and molecular weight determination of polysaccharides. *Makromol Chem* 20: 169-180, 1956.
- (5) STETTEN, D., JR., and STETTEN, M. R.: Homopolysaccharides. *In Polysaccharides in Biology* (Springer, G. F., ed.). New York, Josiah Macy, Jr., Foundation, 1957, pp 9-153.
- (6) GREENWOOD, C. T.: Aspects of the physical chemistry of starch. *Advances Carbohydr Chem* 11: 335-393, 1956.
- (7) LAZAROW, A.: Particulate glycogen: A submicroscopic component of the guinea pig liver cell; its significance in glycogen storage and in the regulation of blood sugar. *Anat Rec* 84: 31-50, 1942.
- (8) LOWE, C. W., and GARNER, W.: The isolation from rat liver of a glycogen complex which contains RNA fragments. *Biochem Biophys Res Commun* 3: 196-199, 1960.
- (9) KARRER, H. E., and COX, J.: Electron-microscopic study of glycogen in chick embryo liver. *J Ultrastruct Res* 4: 191-212, 1960.
- (10) SOMOGYI, M.: The solubility and preparation of phosphorus and nitrogen-free glycogen. *J Biol Chem* 104: 245-253, 1934.
- (11) SAHYUN, M., and ALSBERG, C. L.: On rabbit liver glycogen and its preparation. *J Biol Chem* 89: 33-39, 1930.
- (12) STETTEN, M. R., KATZEN, H. M., and STETTEN, D., JR.: Metabolic inhomogeneity of glycogen as a function of molecular weight. *J Biol Chem* 222: 587-599, 1956.

- (13) BELL, D. J., and YOUNG, F. G.: CXXX. Observations on the chemistry of liver glycogen. *Biochem J* 28: 882-889, 1934.
- (14) PETREE, L. G., and ALSBERG, C. L.: A method for the preparation of glycogen and a study of the abalone, *Haliotis rufescans*, Swainson. *J Biol Chem* 82: 385-395, 1929.
- (15) ORRELL, S. A., JR., and BUEDING, E.: Sedimentation characteristics of glycogen. *J Amer Chem Soc* 80: 3800, 1958.
- (16) BUEDING, E., and ORRELL, S. A.: A mild procedure for the isolation of polydisperse glycogen from animal tissues. *J Biol Chem* 239: 4018-4020, 1964.
- (17) ORRELL, S. A., JR., and BUEDING, E.: A comparison of products obtained by various procedures used for the extraction of glycogen. *J Biol Chem* 239: 4021-4026, 1964.
- (18) BLOOM, W. L., LEWIS, G. T., SCHUMPERT, M. Z., and SHEN, T.-M.: Glycogen fractions of liver and muscle. *J Biol Chem* 188: 631-636, 1951.
- (19) GASPAR, Z. N.: Investigation of the physiologically different glycogen fractions in newborn rabbits. *Experientia* 13: 113-114, 1957.
- (20) BRODSKAYA, N. I.: Metabolism of glycogen fractions in brain and liver of rats of different ages. *Fed Proc* 23 (II, Transl Suppl): 1299-1302, 1964.
- (21) HANSON, R. W., SCHWARTZ, H. S., and BARKER, S. B.: "Free" and "fixed" glycogen as physiological entities. *Amer J Physiol* 198: 800-806, 1960.
- (22) LAZAROW, A.: Alterations in particulate glycogen produced by the common glycogen separating agents. *Arch Biochem* 7: 337-343, 1945.
- (23) ANDERSON, N. G., HARRIS, W. W., BARBER, A. A., RANKIN, C. T., JR., and CANDLER, E. L.: Separation of subcellular components and viruses by combined rate- and isopycnic-zonal centrifugation. *Nat Cancer Inst Monogr* 21: 253-283, 1966.
- (24) ANDERSON, N. G., and BARBER, A. A.: Isolation of native glycogen by combined rate-zonal and isopycnic centrifugation. *Abstract 9th Ann Biophys Soc*: 140 (FD3), 1965.
- (25) ANDERSON, N. G., and BURGER, C. L.: Separation of cell components in the zonal ultracentrifuge. *Science* 136: 646-648, 1962.
- (26) ANDERSON, N. G., BARRINGER, H. P., BABELAY, E. F., and FISHER, W. D.: The B-IV zonal ultracentrifuge. *Life Sci* 3: 667-671, 1964.
- (27) FISHER, W. D., CLINE, G. B., and ANDERSON, N. G.: Density gradient centrifugation in angle-head rotors. *Anal Biochem* 9: 477-482, 1964.
- (28) DUBOIS, M., GILLES, K. A., HAMILTON, J. K., REBERS, P. A., and SMITH, F.: Colorimetric method for determination of sugars and related substances. *Anal Chem* 28: 350-356, 1956.
- (29) MONTGOMERY, R.: Determination of glycogen. *Arch Biochem Biophys* 67: 378-386, 1957.
- (30) BRENNER, S., and HORNE, R. W.: A negative staining method for high resolution electron microscopy of viruses. *Biochim Biophys Acta* 34: 103-110, 1959.
- (31) DROCHMANS, P.: Morphologie du glycogène. Etude au microscope électronique de colorations négatives du glycogène particulaire. *Ultrastruct Res* 6: 141-163, 1962.
- (32) MORDOH, J., LELOIR, L. F., and KRISMAN, C. R.: *In vitro* synthesis of particulate glycogen. *Proc Nat Acad Sci USA* 53: 86-91, 1965.
- (33) TATA, J. R.: Subcellular redistribution of liver  $\alpha$ -glucan phosphorylase during alterations in glycogen content. *Biochem J* 90: 284-292, 1964.
- (34) LUCK, D. J. L.: Glycogen synthesis from uridine diphosphate glucose. The distribution of the enzyme in liver cell fractions. *J Biophys Biochem Cytol* 10: 195-209, 1961.
- (35) POLLARD, E. C.: Nucleotides and saccharide synthesis. In *Polysaccharides in Biology* (Springer, G. F., ed.). New York, Josiah Macy, Jr., Foundation, 1957, p 219.

## PLATES

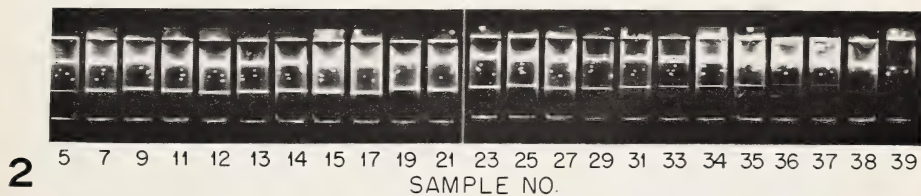
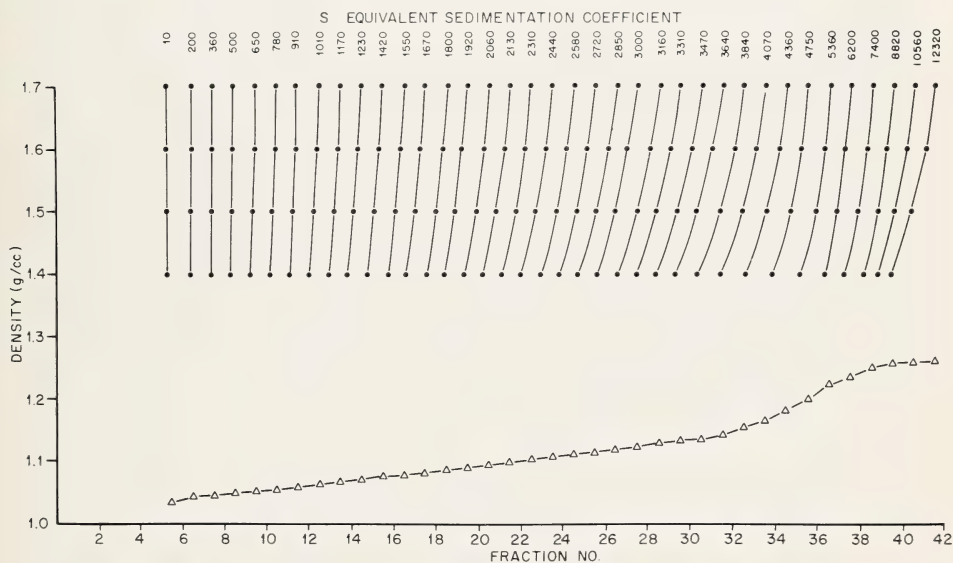
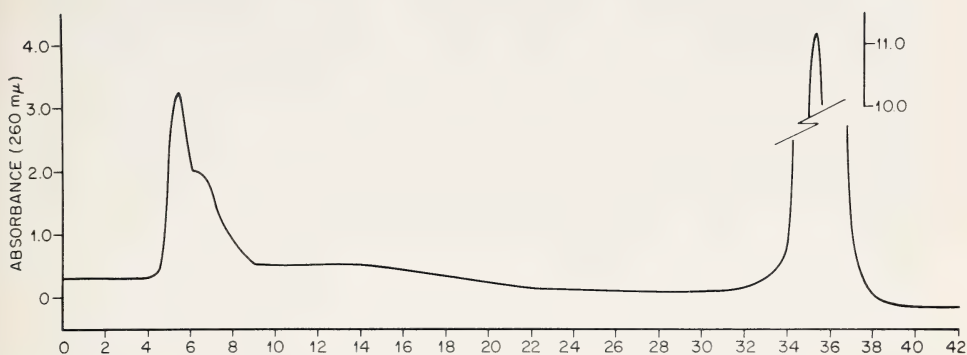




FIGURE 1.—Rat liver homogenate banded in CsCl. A total of 11.0 ml of saturated CsCl was layered beneath 18.0 ml of sample containing a formaldehyde bead of density 1.46. The tube was centrifuged at 24,000 rpm for 3 hours and photographed with scattered light.

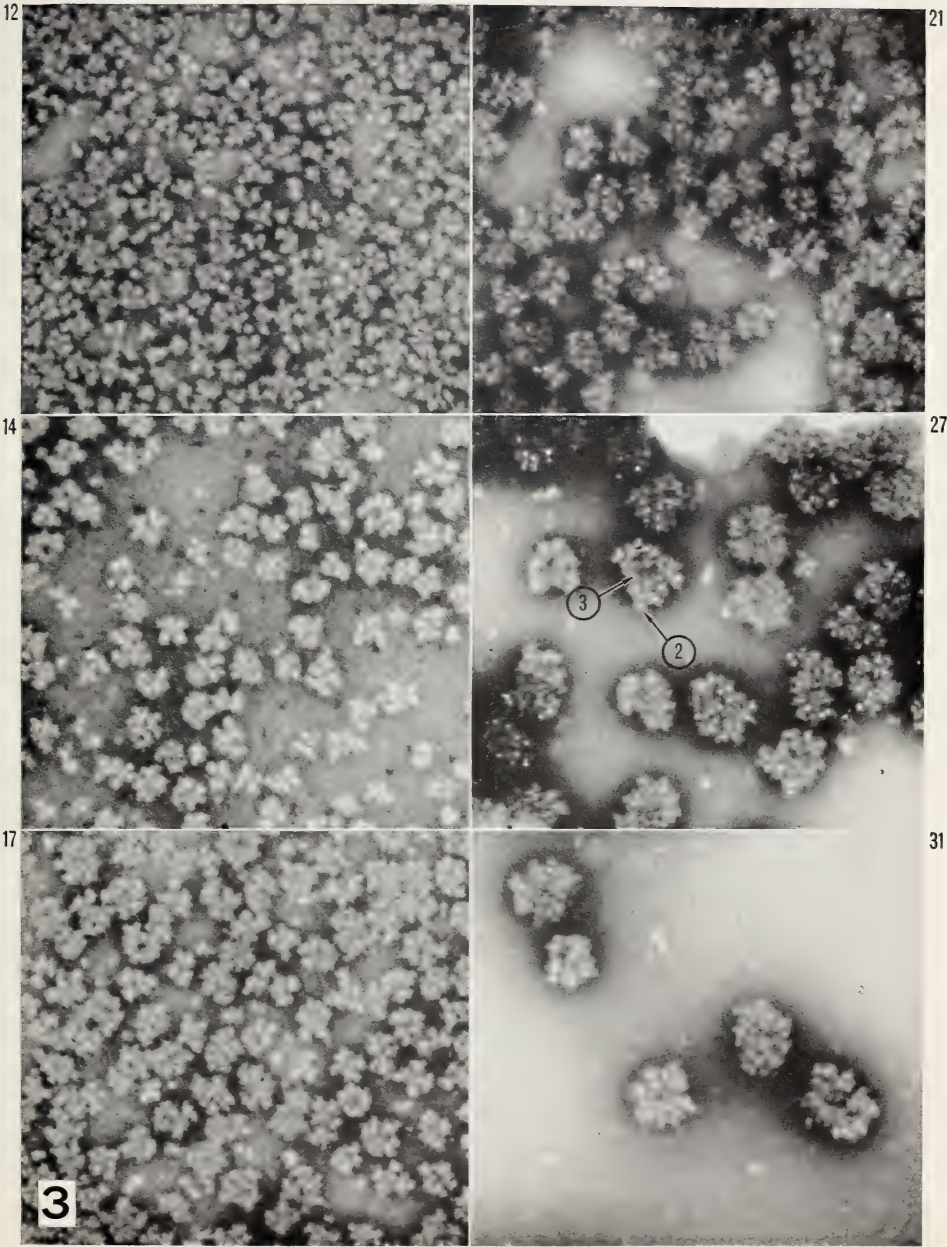
## PLATE 55

FIGURE 2.—Distribtuion of rat liver glycogen following density gradient centrifugation in the B-IV rotor at 20,000 rpm for 15 minutes. A total of 20 ml of a 1:5 (w/v) homogenate made up in 0.25 M sucrose solution was used as the sample. The absorbance of the collected stream was monitored at 260 m $\mu$ . Glycogen distribution was determined by banding collected samples in CsCl as described for figure 1. The banded samples were photographed with scattered light. Relationship between sample number and banded tube is indicated by the numbers below the photographed tubes. The sedimentation coefficients of particles of known density and the sucrose density gradient were computer-plotted. Sedimentation coefficients are in conventional Svedberg units.  $\triangle$ —— $\triangle$  Sucrose density.



## PLATE 56

FIGURE 3.—Electron photomicrograph of negatively stained glycogen. The number in the corner of each photograph indicates the zonal sample number from which glycogen was banded. The lower band of each sample (*see* photograph in fig. 2) was collected, rapidly dialyzed, and viewed following negative staining. Original magnification 80,000. Numbers 2 and 3 refer to the subclusters and clusters of glycogen, respectively (*see* text).



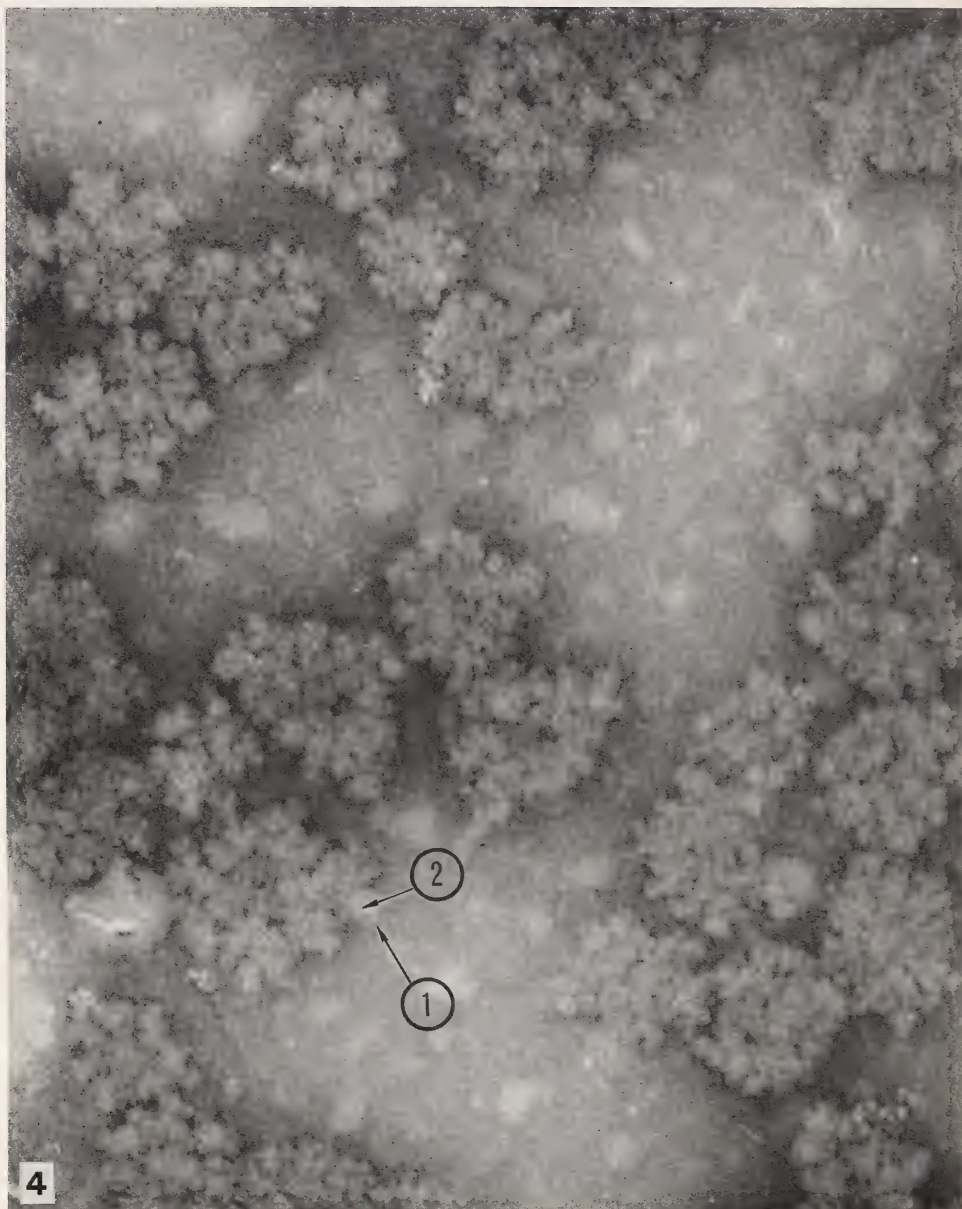


FIGURE 4.—Electron photomicrograph of negatively stained glycogen. Numbers 1 and 2 refer to the fundamental unit and the subclusters of glycogen structure, respectively (*see text*). Original magnification, 320,000

# Isolation of Paramylon From *Euglena Gracilis* Var *Bacillarus* SML-1 by Combined Rate- and Isopycnic-Zonal Centrifugation<sup>1</sup>

ALBERT A. BARBER,<sup>2</sup> THEODORE W. BARTLETT, and BLAINE H. LEVEDAHL,<sup>3,4</sup> Department of Zoology, University of California, Los Angeles, California, and Biology Division, Oak Ridge National Laboratory,<sup>5</sup> and Technical Division, Oak Ridge Gaseous Diffusion Plant,<sup>5</sup> Oak Ridge, Tennessee

## SUMMARY

Paramylon granules were isolated from homogenates of *Euglena gracilis* var *bacillarus* SML-1 (streptomycin bleached) by isopycnic-zonal centrifugation in Spinco No. 30 rotor tubes with cesium chloride density gradients. A combination of isopycnic- and rate-zonal centrifugation in the B-IV rotor with a mixed sucrose-CsCl gradient was also used. The granules were ellipsoid, with major and minor axes of approximately 2.06 by 1.44  $\mu$ , respectively, and banded isopycnically at a density of 1.62. In the presence of 0.25 M KOH the granules were disrupted into large coils of threadlike material, which

banded at the same density. This material was presumed to be the basic form of the glucose polymer stored within the granules. As determined by both chemical and microscopic examination, the paramylon granules were free from other cellular material, and also appeared morphologically similar to the granules observed *in vivo*. The technique of combined rate-isopycnic (*s*- $\rho$ ) zonal centrifugation for the isolation of other cell components from *Euglena* was compared with classical differential centrifugation methods.—Nat Cancer Inst Monogr 21: 303-316, 1966.

PARAMYLON is the storage form of carbohydrate in *Euglena gracilis* and other Euglenoids. A number of workers (1, 2) have established that paramylon is a  $\beta$ -1,3-linked glucose polymer. It is present as large inclusion bodies in *Euglena* and *Astasia* and can be observed by light microscopy. The polymer is also easily identified as rather diverse-sized granules appearing throughout the cytoplasm in electron photomicrographs of both forms. Ringo (3) has reported that the paramylon particles are surrounded by a 60 A membrane in *Astasia*, and while this condition has not been reported directly for *Euglena*, several papers (4-6) contain pic-

<sup>1</sup> This research performed under the Joint National Institutes of Health-Atomic Energy Commission Zonal Centrifuge Development Program which is supported by the National Cancer Institute, the National Institute of Allergy and Infectious Diseases, and the U.S. Atomic Energy Commission.

<sup>2</sup> Aided by AEC Contract No. AT(11-1)-34 Project 49.

<sup>3</sup> Aided by a contract between the Office of Naval Research, Department of the Navy, and the University of California, Los Angeles, Calif., NR 108-673.

<sup>4</sup> We are grateful to Dr. N. G. Anderson for advice and criticism throughout this study. The technical assistance of C. T. Rankin, Jr., is gratefully acknowledged.

<sup>5</sup> Operated for the U.S. Atomic Energy Commission by the Nuclear Division of Union Carbide Corporation.

tures not inconsistent with this observation. However, the presence of a membrane has been questioned (7).

Although paramylon is apparently a stable chemical structure and has been prepared as a rather pure product for investigation, the methods used for its isolation have not been mild ones and the relationship between the storage form in the intact organism and the isolated product is open to question. For example, butanol extraction of homogenates followed by treatment with concentrated urea and chloroform (8) or ethanol-ether extraction followed by treatment with 5 percent KOH and reprecipitation with acid (1, 9) results in apparently pure paramylon preparations, which may well have lost constituents present *in vivo*.

A mild procedure involving combined rate- and isopycnic-zonal centrifugation in cesium chloride gradients has been recently developed for the isolation of glycogen, the glucose polymer that serves as the storage form of carbohydrate in animals (10). The present study was carried out to determine if this technique could be used as a mild isolation procedure for the preparation of paramylon granules. Also, the techniques of differential centrifugation and of combined rate-isopycnic (*s-ρ*) zonal centrifugation were compared in studies of the isolation of other cell components from homogenates of *Euglena*.

## METHOD

*Euglena gracilis* var *bacillarus* SML-1 (streptomycin bleached) were grown in batch culture at 22° C and a pH of 6.9 on a Cramer-Myers (11) media, with either 20 mM acetate or 20 mM succinate as the sole carbon source. Cells were grown in 3 liter Erlenmeyer flasks containing 1000 ml of culture medium. The cells were harvested in log phase growth by centrifugation in a continuous-flow Serval centrifuge. They were then washed twice with M/15 buffer, brought to a final 1:1 dilution with buffer, homogenized at 0° C in a French press, and then stored frozen.

Zonal centrifugation was carried out in the B-IV rotor system, with sucrose and cesium chloride as gradient materials (12). Sixty ml of the cell homogenate (1:6, v/v) was placed in a rotor containing 1200 ml of a 17 to 55 percent sucrose gradient with an underlay of approximately 300 ml of saturated CsCl. The overlay was 160 ml of buffer inboard of the sample layer. Separations were carried out at 7000 rpm for 15 minutes ( $G_c = 440 \times 10^6$  including acceleration and deceleration). The rotor contents were emptied by displacement with saturated CsCl pumped to the rotor edge, and 42 samples of 40 ml each were collected in tubes maintained in ice. The effluent was continuously monitored at 260 mμ during removal. The density of each collected sample was determined from its refractive index. The gradient density in samples 30 through 42 was estimated from the input solution concentration since refractive indices of sucrose-CsCl mixtures could not be used for density determinations.

Isopycnic banding was carried out by density gradient centrifugation in a Spinco No. 30 angle-head rotor (13). Tubes containing 11 ml CsCl (saturated at 0° C and containing 0.01 M potassium citrate at a pH of 7.0) layered beneath 15 ml of sample volume were centrifuged at 24,000 rpm for 3 hours. Centrifuged samples were photographed by use of scattered light. Banded zones of the sample material were collected with a band-recovery apparatus (BRA-1) equipped with a modified flat-end spinal needle attached to a 2 ml syringe (14). The total volume of selected samples was collected in 1 ml aliquots, starting from the bottom of the tube, with a New Brunswick PA-56 pump.

Carbohydrate was measured on either extensively dialyzed or washed paramylon samples, by use of the phenol-sulfuric acid colorimetric method (15). One ml of 5 percent phenol and 5 ml concentrated sulfuric acid were added to each 1 ml sample containing 5 to 50  $\mu$ g of carbohydrate. The absorbancy at 490 m $\mu$  was measured after 1 hour at room temperature with a Bausch and Lomb Spectronic 20 spectrophotometer. A standard curve was prepared with reagent-grade glucose.

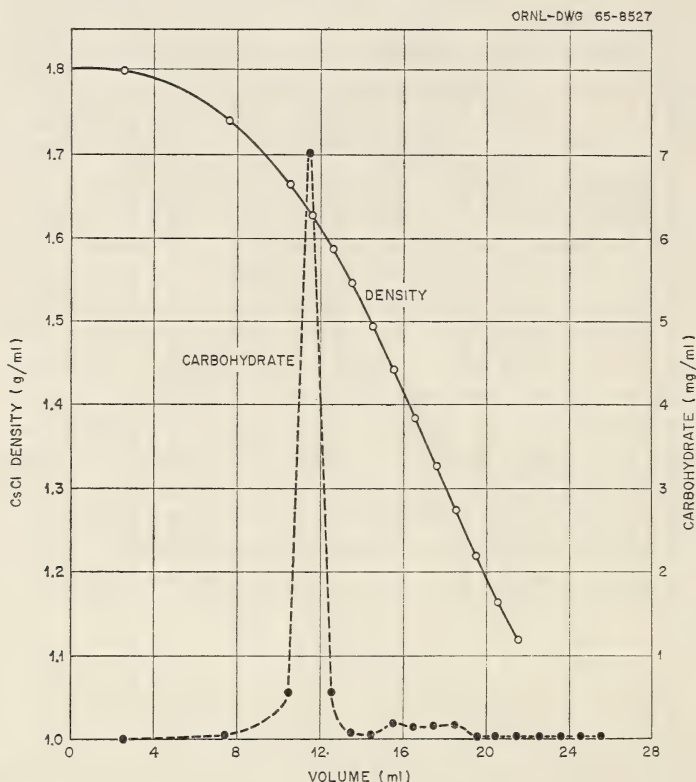
Low-speed differential centrifugation was carried out in an International Model PR-2 refrigerated machine, and high-speed differential centrifugation in a Spinco Model L preparative ultracentrifuge.

Samples were prepared for electron microscopy by the negative staining method of Brenner and Horne (16). Samples were dialyzed and a single drop from each was placed on carbon-coated Formvar specimen screens and allowed to stay on the screen for 20 to 30 seconds in a large petri dish in the presence of osmium vapor. Excess sample material was removed by touching the edge of the screen with filter paper, and then a drop of 2 percent phosphotungstic acid (PTA), adjusted to pH 7.0 with KOH, was added to each screen. The PTA was left on the screen for approximately 30 seconds, and then the screen was dried under ultraviolet light. Screens were examined with either an RCA EML or EMU3-G electron microscope.

## RESULTS

Separation of the subcellular components of *Euglena* in the past (17) has been carried out by the differential centrifugation methods developed for mammalian tissue separations. Failure of this technique to separate *Euglena* fractions, including paramylon, in relatively pure form was verified by banding each of the subcellular fractions prepared by differential centrifugation, in gradients of CsCl (fig. 1). Of all fractions, only the 10,000 rpm supernatant fluid did not contain paramylon. The relative absence of all particulate material from this fraction indicated the reduced amount of small particles in these homogenates. It appears, therefore, that either all subcellular particles of *Euglena* homogenates are relatively large or that they occur as aggregates which are rapidly sedimented at low centrifugal forces. In either case, differential centrifugation as used for mammalian liver fractionation accomplishes little in the isolation and purification of *Euglena* subcellular components.

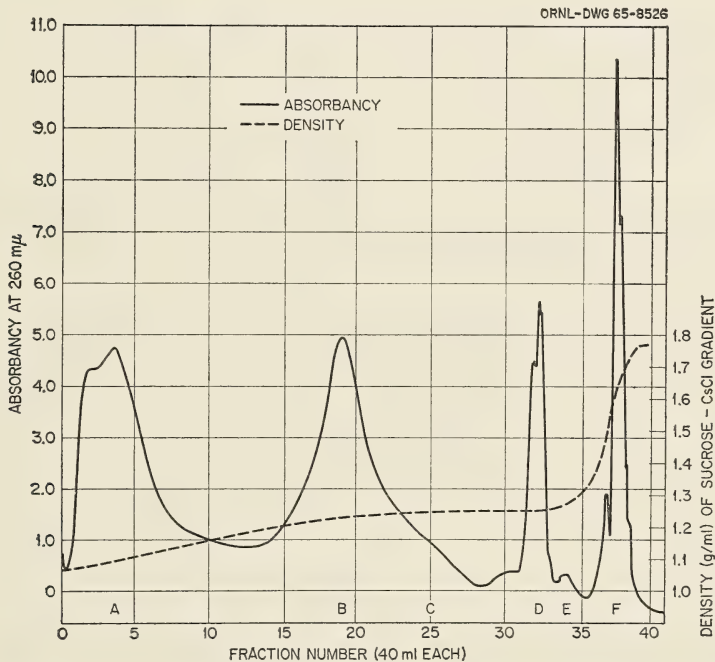
Although paramylon was not separated from other cell constituents by differential centrifugation, it was separated on the basis of density by isopycnic-zonal centrifugation of whole homogenate in cesium chloride density gradients. Paramylon banded at a density of 1.62 near the base of the centrifuge tube; while the membrane fraction banded separately at considerably lower densities (text-fig. 1). The membrane and paramylon separations were similar to those shown in figure 1a. Approximately 85 percent of the total carbohydrate banded in the 1.62 density zone, while the remainder was associated with the membrane zone. Little soluble carbohydrate was present.



TEXT-FIGURE 1.—Cesium chloride density and carbohydrate content in fractions collected following banding of a *Euglena* homogenate in a CsCl density gradient. Fifteen ml of saturated CsCl was layered beneath 11 ml of a *Euglena* homogenate (1:20, v/v). Tubes were centrifuged 3 hours at 24,000 rpm and the entire contents were collected by use of a New Brunswick PA-56 pump.

An attempt to separate subcellular components from a *Euglena* homogenate and to determine the paramylon contamination of each fraction was made by combining rate- and isopycnic-zonal centrifugations in a single B-IV separation by use of a mixed sucrose-CsCl gradient. The centrifugation of an homogenate through a sucrose gradient with a CsCl

underlay resulted in the separation of several distinct fractions (text-fig. 2). Each of the major fractions separated was banded in CsCl gradients and all contained paramylon, although only small amounts remained in the starting boundary (fig. 2). Most of the paramylon, however, was well separated from the other subcellular components and banded isopycnically in the CsCl cushion at the outboard edge of the rotor (*compare* text-fig. 2F and fig. 2F). It is apparent that, except for the paramylon zone, each fraction separated within the sucrose gradient contains a mixture of membrane and paramylon particles. The membrane components, however, were separated into at least three distinct fractions on the basis of their sedimentation in the sucrose gradient (figs. 2A, B, and D). The membranous particles constituting fractions A, B, and D have not been identified. All the yellow pigment of the homogenate was associated with the fraction separated at E (text-fig. 2). The chemical and physical nature of this pigment has not yet been examined. If



TEXT-FIGURE 2.—Distribution of the subcellular components of a *Euglena* homogenate after centrifugation at 7000 rpm for 15 minutes in the B-IV rotor system. The gradient was formed by use of 1200 ml of 17 to 55 percent sucrose with 300 ml of saturated CsCl added as underlay. Sixty ml of homogenate (1:6, v/v) was placed above the gradient and 160 ml of buffer was added as sample overlay. The density curve was determined from refractive index measurements in samples out to number 30. After sample 30, the gradient was estimated from the known volume of CsCl cushion (density, 1.78) placed in the rotor. Density determinations could not be made from refractive index measurements of the region occupied by sucrose-CsCl mixtures. A through F represent the positions of samples banded and photographed in figure 2.

mitochondria of *Euglena* are similar in density to those found in liver homogenates, then mitochondria are presumed to be localized primarily in fraction D (text-fig. 2). Their presence in this fraction, however, has not been confirmed.

The paramylon fraction collected from the CsCl cushion of the B-IV zonal separation (text-fig. 2F) was essentially free of contaminating particles when examined with the electron microscope (fig. 3). The particles were ovoid or elliptical with dimensions of  $2.06 \pm 0.43 \mu$  by  $1.44 \pm 0.35 \mu$  for the major and minor axes, respectively (measurements on 150 particles). The isolation of relatively pure paramylon in this fraction is indicated by its chemical composition (table 1). Approximately one half of its wet weight was due to the presence of carbohydrates, whereas the nitrogen and phosphorus contents were negligible. The absence of other subcellular material was also indicated by banding in CsCl (text-fig. 2F).

TABLE 1.—Chemical content of fractions D and F of *Euglena* homogenates separated in the B-IV rotor\*

Content	D	F
Nitrogen	1.69	0.16
Phosphorus	0.012	0.004
Carbohydrate	25.0	50.0

\*These fractions were obtained by pelleting diluted samples of fractions D and F (text-fig. 2) at 30,000 rpm for 30 minutes. All values are in percent of wet weight.

Because paramylon is known to be solubilized in potassium hydroxide (1), paramylon granules, isolated by isopycnic-zonal centrifugation in the B-IV rotor, were subjected to increasing concentrations of KOH, and the solubilization of these granules was examined both spectrophotometrically and microscopically. A rapid clarification of the paramylon suspension occurred between 0.22 and 0.27 M KOH (fig. 4). This clarification was accompanied by disintegration of the paramylon granules with the subsequent release of long, multiple-stranded structures, presumably the basic form of the glucose polymers stored within these granules. The clarification of the suspension occurred at a KOH concentration that resulted in the disruption of the intact granules. The strands of material released from these granules did not contribute significant opacity to the solutions.

The disruption of paramylon granules releases two distinct components that band separately in CsCl gradients (fig. 5). One component appears composed of relatively large balls of threadlike material. These balls appear to unwind and give rise to individual threads presumed to be strands of glucose polymers (fig. 5c). This component bands at a density of 1.62. The second component is composed of materials that band at a considerably lower density and which have a different structure (fig. 5b). Although the chemical nature of this second component has not been

examined, it appears to be a minor constituent, since its presence does not significantly alter the banding density of the intact granules. Chemical analysis of the paramylon fraction also indicates a very small amount of noncarbohydrate material within the granules.

## DISCUSSION

Results from both rate-zonal and differential centrifugation indicated that little particulate material remains in the supernatant fluid after centrifugation at relatively low speeds. This indicated either aggregation of small particulates or the relative lack of structures in *Euglena* which normally give rise to the microsomal fraction. The relative lack of organized cytoplasmic membranes in *Astasia longa*, a closely related microorganism, would explain the lack of the microsomal fraction in these homogenates (3). It is doubtful, therefore, that previous attempts to isolate mitochondrial fractions from *Euglena gracilis* by differential centrifugation have resulted in much purification of these structures (17), regardless of the number of washings used. The present study indicated that differential centrifugation of *Euglena* homogenates results in the preparation of fractions heavily contaminated with paramylon. Techniques utilizing differential centrifugation, based primarily on results obtained with rat liver homogenates, cannot be successfully used for the separation of cell components from other cells and tissues without a detailed analysis of the sedimentation characteristics of the particles present in the original homogenate. Rat liver fractionation techniques, for example, are not applicable to rat brain fractionation (18). It is not considered likely, therefore, that they would be applicable to the isolation of subcellular components from homogenates of microorganisms. Combined rate- and isopycnic-zonal centrifugation, together with appropriate morphological studies, is a rapid method for establishing the appropriate conditions for isolating subcellular components of specific homogenates by differential centrifugation (14).

The paramylon granules of *Euglena gracilis* isolated by isopycnic-zonal centrifugation are similar in size to those isolated from *Cladophora rupestris* after alcohol-ether extraction and deproteinization by trypsin (1). The granules banded at a density of 1.62 in CsCl. As evidenced by the lack of change in light absorbance in the KOH concentration range 0 to 0.25 M, these granules were ruptured by 0.25 M KOH without appreciable swelling at lower concentrations. Rupture of the granules resulted in the release of large coils of threadlike material which also banded at a density of 1.62 in CsCl. Slightly higher concentrations of KOH resulted in the disruption of the integrity of these coils with the release of long slender threads of material, presumed to represent the glucose fraction of the original granules. The long slender threads also banded at a density of 1.62 in 3 hours at 24,000 rpm. The paramylon granules isolated in the present study do not appear to have a surrounding membrane.

Although such a membrane has been suggested (3), there is little evidence for its presence (7, 8). A strict orientation of the threadlike networks making up the major portion of the granule may be sufficient to maintain its shape.

The polysaccharide component of *Euglena gracilis* is a  $\beta$ -1,3-linked glucose polymer similar in structure to yeast glucan (1,8). In *Tetrahymena pyriformis*, the polysaccharide component is a branched  $\alpha$ -1,4-glycogen containing 8 to 10 percent  $\alpha$ -1,6-interchain linkages similar in structure to animal glycogens (19). The subcellular particles resulting from these two linkage types are very different. The native carbohydrate particle of *Tetrahymena* occurs in sizes up to approximately 40 m $\mu$  and is composed of fundamental units 2 to 3 m $\mu$  in diameter. The native particle of *Euglena*, the paramylon granule, is much larger and is composed of coils which assume the appearance of linear aggregates of threadlike material after treatment by KOH. Correlation of these structural particulates with the known chemical structures of glycogen and paramylon is difficult. The classical extraction procedures used for the isolation of glycogen are known to alter the glycogen particle, and combined rate-zonal centrifugation has been used as a mild procedure for isolating the material in its more native form (10, 20). Preparations of a more native paramylon might also be expected by this technique rather than the extraction procedures normally employed (1, 8). Isopycnic-zonal centrifugation of homogenates prepared in buffer represents a mild isolation technique to prepare large quantities of pure native paramylon for more physiological studies on the chemistry of the granules themselves, while the development of a technique for isolating the threadlike substructures may allow structural analysis by X-ray diffraction.

## REFERENCES

- (1) CLARK, A. E., and STONE, B. A.: Structure of the paramylon from *Euglena gracilis*. *Biochim Biophys Acta* 44: 161-163, 1960.
- (2) KREGER, D. R., and MEEUSE, B. J. D.: X-ray diagrams of *Euglena* paramylon of the acid-insoluble glucan of yeast cell walls and of laminarin. *Biochim Biophys Acta* 9: 699-700, 1952.
- (3) RINGO, D. L.: Electron microscopy of *Astasia longa*. *J Protozool* 10: 167-173, 1963.
- (4) BRANDES, D., BUETOW, D. E., BERTINI, F., and MALKOFF, D. B.: Role of lysosomes in cellular lytic processes. I. Effect of carbon starvation in *Euglena gracilis*. *Exp Molec Path* 3: 583-609, 1964.
- (5) SIEGESMUND, K. A., ROSEN, W. D., and GAWLIK, S. R.: Effect of darkness and of streptomycin on the fine structure of *Euglena gracilis*. *Amer J Botany* 49: 137-145, 1962.
- (6) UEDA, K.: Structure of plant cells with special reference to lower plants. III. A cytological study of *Euglena gracilis*. *Cytologia* 23: 56-67, 1958.
- (7) GIBBS, S. P.: The fine structure of *Euglena gracilis* with special reference to the chloroplasts and pyrenoids. *J Ultrastruct Res* 4: 127-148, 1960.
- (8) LEEDALE, G. F., MEEUSE, B. J. D., and PRINGSHEIM, E. G.: Structure and physiology of *Euglena spirogyra*. III-VI. *Arch Mikrobiol* 50: 133-155, 1965.

- (9) MARZULLO, G., and DANFORTH, W. F.: Composition of ethanol-insoluble assimilatory products of oxidative assimilation of acetate by *Euglena gracilis*. J Gen Microbiol 34: 21-29, 1964.
- (10) BARBER, A. A., HARRIS, W. W., and ANDERSON, N. G.: Isolation of native glycogen by combined rate-zonal and isopycnic centrifugation. Nat Cancer Inst Monogr 21: 285-302, 1966.
- (11) CRAMER, M., and MYERS, J.: Growth and photosynthetic characteristics of *Euglena gracilis*. Arch Mikrobiol 17: 384-402, 1952.
- (12) ANDERSON, N. G., BARRINGER, H. P., BABELAY, E. F., and FISHER, W. D.: The B-IV zonal ultracentrifuge. Life Sci 3: 667-671, 1964.
- (13) FISHER, W. D., CLINE, G. B., and ANDERSON, N. G.: Density gradient centrifugation in angle-head rotors. Anal Biochem 9: 477-482, 1964.
- (14) ANDERSON, N. G., HARRIS, W. W., BARBER, A. A., RANKIN, C. T., JR., and CANDLER, E. L.: Separation of subcellular components and viruses by combined rate- and isopycnic-zonal centrifugation. Nat Cancer Inst Monogr 21: 253-283, 1966.
- (15) DUBOIS, M., GILLES, K. A., HAMILTON, J. K., REBERS, P. A., and SMITH, F.: Colorimetric method for determination of sugars and related substances. Anal Biochem 28: 350-356, 1965.
- (16) BRENNER, S., and HORNE, R. W.: A negative staining method for high resolution electron microscopy of viruses. Biochim Biophys Acta 34: 103-110, 1959.
- (17) BUETOW, D. E., and BUCHANAN, P. J.: Isolation of mitochondria from *Euglena gracilis*. Exp Cell Res 36: 204-207, 1964.
- (18) BARBER, A. A., RANKIN, C. T., JR., and ANDERSON, N. G.: Lipid peroxidation in rat tissue particulates separated by zonal centrifugation. Nat Cancer Inst Monogr 21: 334-344, 1966.
- (19) MANNERS, D. J., and RYLEY, J. F.: Protozoan polysaccharides. J Protozool Suppl 12: 28, 1962.
- (20) BARBER, A. A., HARRIS, W. W., and PADILLA, G. M.: Studies of native glycogen isolated from synchronized *Tetrahymena pyriformis*. J Cell Biol 27: 281-292, 1965.



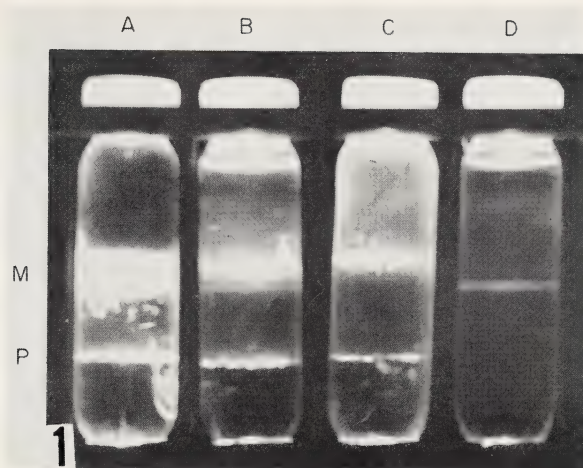


FIGURE 1.—*Euglena* fractions prepared by differential centrifugation and banded in cesium chloride gradients. Eleven ml of CsCl (saturated at 4° C and containing 0.01 M potassium citrate, pH 7.0) was layered beneath 15 ml of the fractions indicated, and the tubes were centrifuged at 24,000 rpm for 3 hours. Tubes were photographed with scattered light. Banded fractions include:

- A, 1000 rpm: 10-minute pellet resuspended
- B, 1000 rpm: 10-minute supernatant fluid
- C, 10,000 rpm: 10-minute pellet of B resuspended
- D, 10,000 rpm: 10-minute supernatant fluid
- M: membrane fraction      P: paramylon fraction

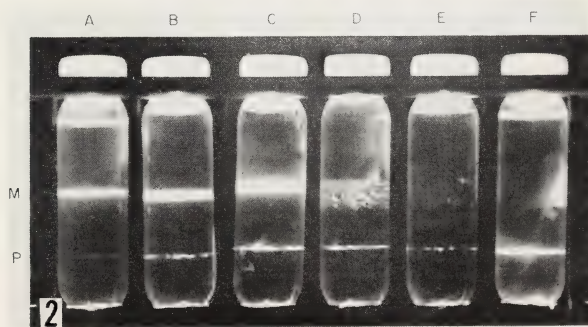


FIGURE 2.—Banding of *Euglena* samples collected from the B-IV rotor. See legend of text-figure 2.



FIGURE 3.—Electron photomicrograph of paramylon obtained by pelleting region F (see text-fig. 2) of the B-IV rotor separated homogenate. Pellet was resuspended in water. Original magnification, 80,000

ORNL-DWG 65-8568

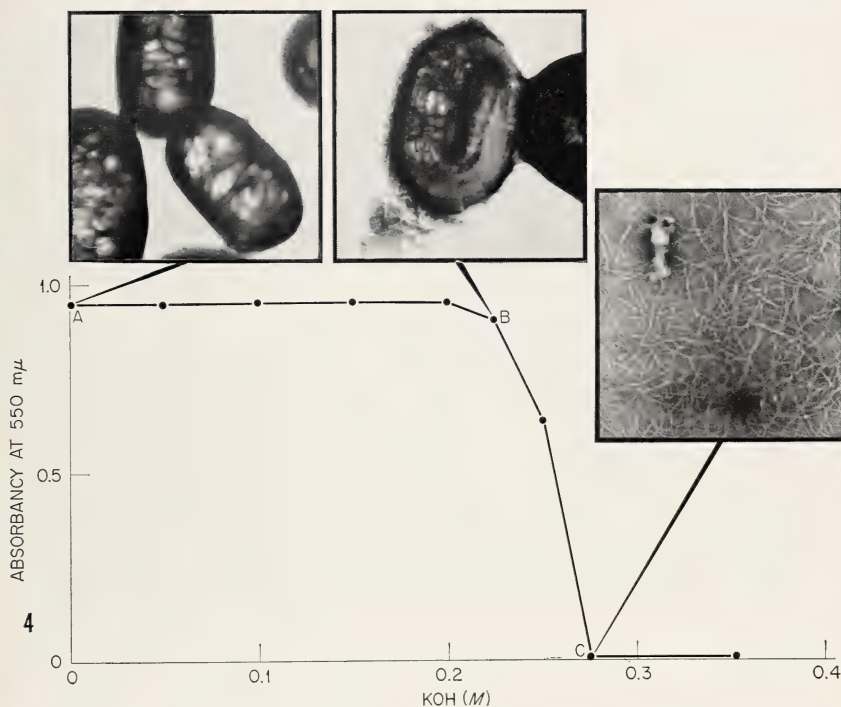


FIGURE 4.—Morphological changes induced in paramylon granules by potassium hydroxide. The paramylon was obtained as a pellet from region F (text-fig. 2) and resuspended in distilled water. Absorbance at 550 mμ was used to follow changes in opacity of the suspended particles. At KOH concentrations represented by A, B, and C, a portion of the sample was removed for microscopic examination. The resultant photomicrographs are depicted above by corresponding letters. Original magnification, 20,000

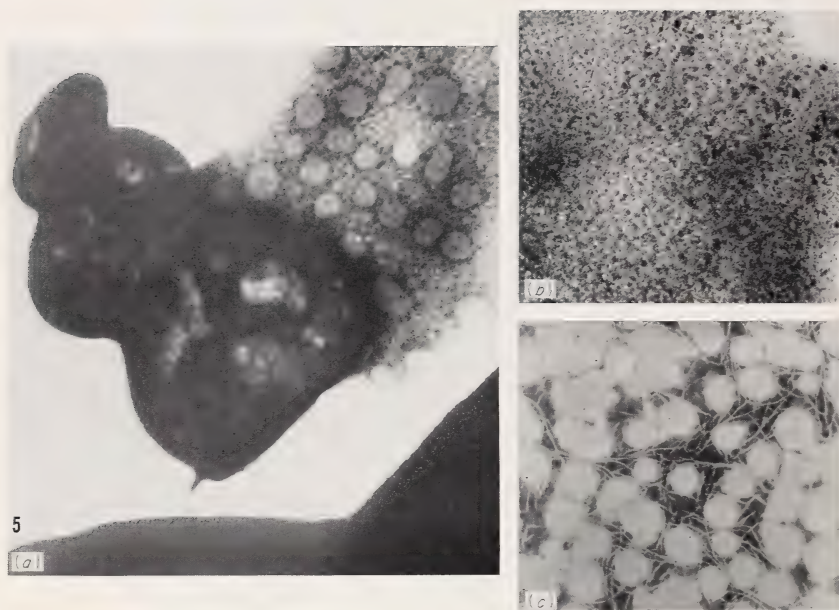


FIGURE 5.—The breakdown of paramylon granules and the components released following treatment by potassium hydroxide. (a) Paramylon granule partially disrupted; (b) the granule component collected near the top of the centrifuge tube (density, approximately 1.2) following the banding of KOH-treated paramylon; (c) the granule component collected at a density of 1.62 following the banding of KOH-treated paramylon in a CsCl density gradient. Original magnification, 80,000

# The Isolation of Oral Structures From *Tetrahymena pyriformis* by Low-Speed Zonal Centrifugation<sup>1</sup>

G. L. WHITSON, G. M. PADILLA,<sup>2</sup> R. E. CANNING, I. L. CAMERON, N. G. ANDERSON, and L. H. ELROD, *Biology Division, Oak Ridge National Laboratory,<sup>3</sup> Oak Ridge, Tennessee*

## SUMMARY

The oral apparatus from indole-lysed *Tetrahymena* has been isolated in sucrose gradients. In the A-XII rotor, kinetosomes and other material band isopycnicly at 12 to 18 percent sucrose and oral structures at 45 to 49 percent sucrose. Macronuclei are found only

when sucrose gradients extending to 63 percent and higher are used. The significance of methods for obtaining large quantities of pure fractions of oral structures is discussed.—*Nat Cancer Inst Monogr* 21: 317–321, 1966.

THE RECENT development of low-speed zonal centrifuge rotors (1) has made possible isolation of the larger subcellular components in considerable quantity and with higher resolution than obtained with conventional differential centrifugation. The cortical organelles and macronuclei of *Tetrahymena* are too large and sediment too rapidly for isolation by rate-zonal centrifugation in the higher speed zonal rotors used for polysome and ribosome isolation. The studies reported here were begun with the purpose of developing methods for isolating oral structures in sufficient quantity for direct biochemical analysis.

## METHODS

Synchronously dividing *Tetrahymena* were grown axenically in modified 2 percent proteose peptone with 0.1 percent liver extract, under the conditions previously described by Padilla and Cameron (2). Cells were removed from these cultures and resuspended in a 40 ml capacity, conical test tube. Ten to 20 ml of packed cells were washed in 0.01 M Tris buffer containing 0.005 M Mg<sup>++</sup> at pH 7.5, repacked, and lysed by addition of an equal amount of saturated indole made up in Tris buffer at pH 7.5.

<sup>1</sup> This research performed under the Joint National Institutes of Health-Atomic Energy Commission Zonal Centrifuge Development Program which is supported by the National Cancer Institute, the National Institute of Allergy and Infectious Diseases, and the U.S. Atomic Energy Commission.

<sup>2</sup> Present address: Babies' Hospital Research Center, Wilmington, North Carolina.

Operated for the U.S. Atomic Energy Commission by the Nuclear Division of Union Carbide Corporation.

Linear sucrose gradients were used. They ranged from 10 to 55 percent (w/w) with a 55 percent underlay, 10 to 66 percent with a 66 percent underlay, and 30 to 66 percent with a 66 percent underlay. These gradients were mixed and pumped into the rotor as described elsewhere (3).

For specific isolation of oral structures and kinetosomes the following method of cell fractionation was used. *Tetrahymena* were collected and lysed with indole, as mentioned.

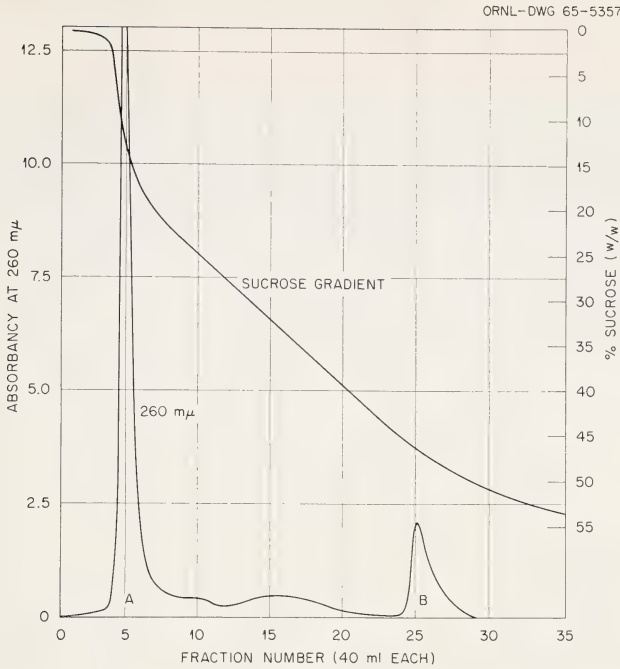
The indole lysate was treated with 4 times its volume of cold 95 percent ethanol (5° C) for 2 to 3 hours and centrifuged; the alcohol-soluble fraction was discarded. The remaining cell lysate was treated with 4 times its volume of cold 1 percent digitonin in 0.4 M KCl as used by Seaman (4). After 1 hour, the lysate was spun at 2000 rpm in a refrigerated International preparative centrifuge for 10 minutes and the supernatant was discarded; the pellet was retreated with cold digitonin for 18 to 24 hours to solubilize any remaining unstable cell fractions. Oral structures and kinetosomes were not solubilized by these treatments. Lysates were centrifuged again at 2000 rpm for 10 minutes and the supernatant was discarded; the pellet was resuspended in 10 percent sucrose.

Each 30 ml sample was added to the A-XII rotor, which contained 1300 ml of the sucrose gradient, while the rotor was rotating at a speed of 900 rpm. An overlay of 100 to 130 ml of Tris buffer at pH 7.5 was used under pressure with nitrogen to push the sample outward from the core of the rotor. The rotor was brought to a final speed of 3800 rpm to separate and band the various cell fractions in the rotor. The time required for a clear separation of these fractions at this speed, determined visually, varied from 30 minutes to a few hours, depending largely upon the gradient used.

After final separation, the rotor speed was reduced to about 900 rpm and the rotor effluent was monitored through a continuous flow cell with a Beckman DU Spectrophotometer as described by Canning and Anderson (3). The percentage of sucrose for each 40 ml sample collected was determined refractometrically, and the contents of each sample were examined with a phase contrast microscope. Cell structures were then related to the absorbance peaks and to their position in the sucrose gradient.

## RESULTS

Saturated indole effectively breaks open *Tetrahymena* and allows the separation of intact oral structures and other pellicular elements. A record of optical density showing the position of the kinetosome-containing fraction and oral structures of *Tetrahymena* in the sucrose gradient is shown in text-figure 1. The gradient used in this run was 10 to 55 percent with a 55 percent underlay. Phase contrast observation of the first peak, which reached an absorbance in excess of 2.5, showed that it contained kinetosomes and other digitonin-insoluble material. The second, smaller peak contained the oral structures, as shown in figure 1. The kinetosomal



TEXT-FIGURE 1.—An optical density profile taken from a recording potentiometer showing 260  $m\mu$  absorbance of the separation of kinetosomes (peak A) and oral structures (peak B). See text for details.

fraction was found in 12 to 18 percent sucrose and the oral structures were sedimented to the 45 to 49 percent sucrose level.

The phase contrast photomicrograph shows that each of the oral structures, or at least their skeletal frameworks, consists of three compound ciliary membranelles (minus their cilia) and an undulating membrane associated with some of these oral structures. The oral fibers or gullet fibers can be seen extending downward and to one side.

Macronuclei can be obtained when Tris buffer is used and lysed cells are placed immediately into the A-XII rotor after collection of *Tetrahymena* and lysing with indole. Pure fractions of macronuclei have not yet been recovered by banding in this rotor. They have, however, been recovered in apparently good morphological conditions from the rotor wall when a sucrose gradient of 10 to 55 percent was used. When recovered from sucrose gradients, macronuclei and some cellular debris have been found in high-density sucrose levels (63% and higher), depending on their size.

Fractions of mitochondria from *Tetrahymena* have not yet been obtained with these methods. Perhaps these structures became contaminated with microsomal material and other vacuolar fractions. Moreover, in high-density sucrose gradients and at low speeds these particles do not sediment or separate from the soluble or kinetosome-containing fraction.

## DISCUSSION

The isolation of oral structures is of interest for several reasons, including the study of the relation of these structures to cell division in synchronized *Tetrahymena* (5, 6). Experimentally, cortical stomatogenesis and cell division can be prevented by the addition of actinomycin D to temperature-synchronized *Tetrahymena* (7). Whether this inhibition of cell division is directly correlated with the prevention of oral morphogenesis is not actually known. Williams (5), however, has found that oral fibers are absent from isolated oral structures after heat-shock treatment and he has suggested that these fibers may be the "division proteins" in *Tetrahymena*.

Since oral structures in *Tetrahymena* may now be isolated by low-speed zonal centrifugation, it should be possible to study structural protein synthesis and protein changes within these cells during the cell cycle or after experimental treatment.

The role of the kinetosome in ciliate morphogenesis has been discussed at length by Chatton and Lwoff (8) and Lwoff (9), and biochemical characterization of these structures has been described by Seaman (4) and Argetsinger (10).

## REFERENCES

- (1) ANDERSON, N. G., BARRINGER, H. P., CHO, N., NUNLEY, C. E., BABELAY, E. F., CANNING, R. E., and RANKIN, C. T., JR.: The development of low-speed "A" series zonal rotors. Nat Cancer Inst Monogr 21: 113-136, 1966.
- (2) PADILLA, G. M., and CAMERON, I. L.: Synchronization of cell division in *Tetrahymena pyriformis* by a repetitive temperature cycle. J Cell Comp Physiol 64: 303-307, 1964.
- (3) CANNING, R. E., and ANDERSON, N. G.: Separation of subcellular fractions with a new zonal rotor. Amer Zoologist 4: 310, 1964.
- (4) SEAMAN, G. R.: Large scale isolation of kinetosomes from the ciliated protozoan *Tetrahymena pyriformis*. Exp Cell Res 21: 292-302, 1960.
- (5) WILLIAMS, N. E.: The development of oral fibers in relation to induced division synchrony in *Tetrahymena*. J Protozool 11 (Suppl) 10, 1964.
- (6) ———: Structural development in synchronously dividing *Tetrahymena pyriformis*. In Cell Division and Growth (Zeuthen, E., ed.). New York, John Wiley & Sons, Inc., 1964, pp 159-176.
- (7) WHITSON, G. L., and PADILLA, G. M.: The effects of actinomycin D on stomatogenesis and cell division in temperature-synchronized *Tetrahymena pyriformis*. Exp Cell Res 36: 667-671, 1964.
- (8) CHATTON, E., and LWOFF, A.: La constitution primitive de la striéciliare des infusoires. La desnodexie. CR Soc Biol (Paris) 188: 1068, 1935.
- (9) LWOFF, A.: Problems in the Morphogenesis of Ciliates. New York, John Wiley & Sons, Inc., 1950.
- (10) ARGESINGER, J.: The isolation of ciliary basal bodies (kinetosomes) from *Tetrahymena pyriformis*. J Cell Biol 24: 154, 1965.

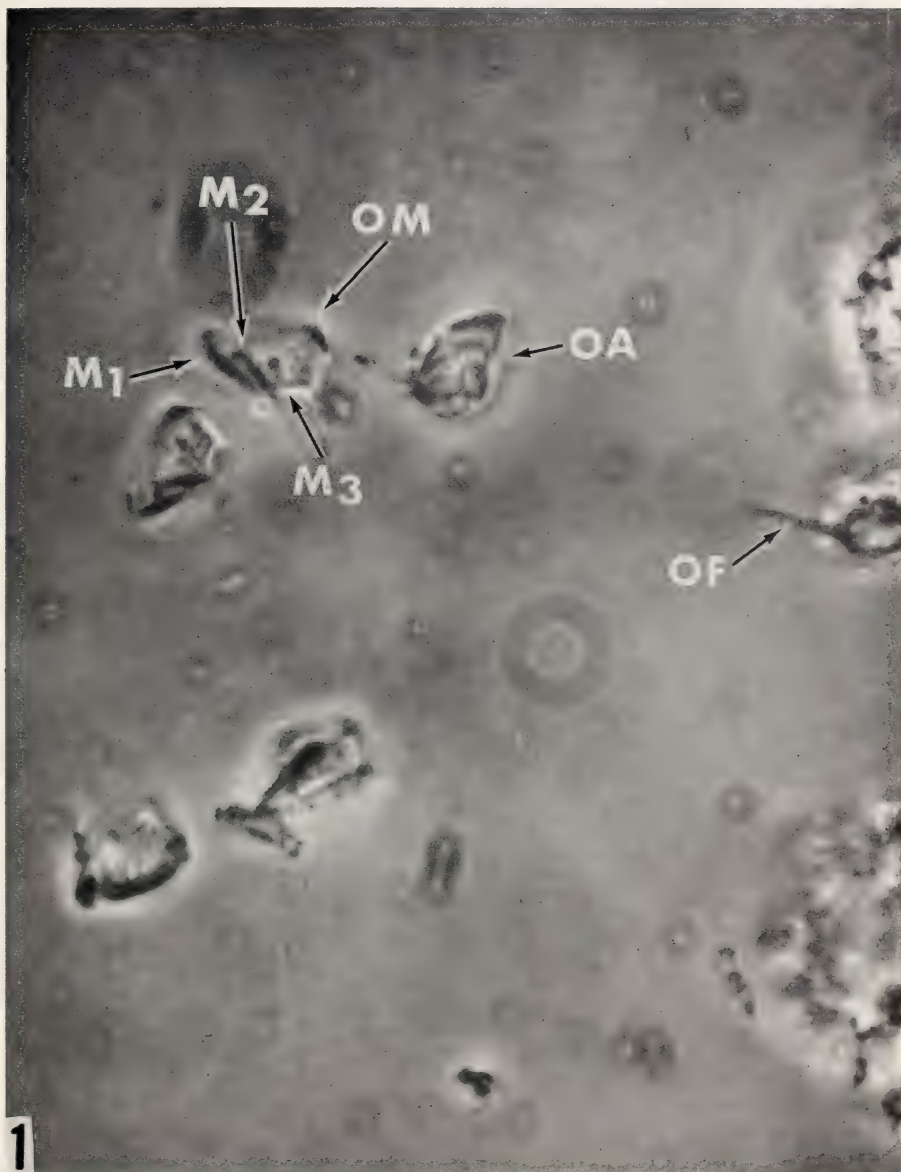


FIGURE 1.—Photomicrograph of the isolated oral apparatus of *Tetrahymena*. Each oral apparatus (OA) consists of an undulating oral membrane (OM), three compound membranelles ( $M_1$ ,  $M_2$ , and  $M_3$ ), and oral fibers (OF). These structures were isolated from peak B of text-figure 1.



## Resolution of the Components in the Microsomal Fraction of Liver in the B-IV Zonal Centrifuge<sup>1</sup>

A. A. EL-AASER,<sup>2,3</sup> E. REID,<sup>3</sup> E. KLUCIS, P. ALEXANDER, J. T. LETT, and JACQUELINE SMITH,<sup>4</sup>  
*Biochemistry Department, Battersea College of Technology, London, S.W. 11, England; Chester Beatty Research Institute, Institute of Cancer Research, Royal Cancer Hospital, London, S.W. 3, England*

### SUMMARY

Liver homogenates, centrifuged to remove nuclei and mitochondria, were analyzed in a zonal centrifuge, over sucrose gradients chosen to resolve the structural components of the microsomal fraction on the basis of isopycnic banding. In sucrose media lacking  $Mg^{2+}$  ions, fractions corresponding to smooth- and rough-surfaced cytomembranes were clearly separated; biochemically and cytochemically both were rich in glucose-6-phosphatase (G-6-Pase). 5'-Nucleotidase (AMPase)—a plasma-membrane enzyme—occurred largely in the smooth-surfaced fraction, though its distribution did not coincide with G-6-Pase, and was absent from the rough-surfaced fractions. Nucleoside diphosphatase (UDPase) showed peaks not quite coincident with

those for G-6-Pase in both the smooth- and rough-surfaced fractions. Nucleoside triphosphatase with ATP as substrate ( $Mg^{2+}$  was the only cation deliberately added in the assay) was found partly in the rough-surfaced fraction but mainly in a region of lower density (1.17). The peaks for inorganic pyrophosphatase (PPase) were such that microsomal PPase could be identical with G-6-Pase. Near the origin there was pronounced activity for all the enzymes studied except ATPase. Data are given for the distribution of RNA and its radioactivity after labeling *in vivo*. Improved separation of AMPase and G-6-Pase was obtained if magnesium was present in all the solutions used.—*Nat Cancer Inst Monogr*, 21: 323-332, 1966.

IN HEPATIC microsomal fractions there is heterogeneity quite apart from that due to any contamination with lysosomes or other organelles. Besides free ribosomes there are membrane fragments of different types, corresponding to smooth-surfaced cytomembranes (including those forming the Golgi complex), rough-surfaced cytomembranes, and plasma-membrane fragments. Fragments of the latter seem to account for

<sup>1</sup> This investigation was supported by grants to the Chester Beatty Research Institute, Institute of Cancer Research, from the Medical Research Council and the British Empire Cancer Campaign, and by U.S. Public Health Service research grant CA-03188 from the National Cancer Institute.

<sup>2</sup> Supported initially by a grant from the United Arab Republic Ministry of Education, then by a grant from the Wellcome Trust. *Present address:* c/o Biochemistry Department, Faculty of Medicine, Cairo University, Cairo, Egypt.

<sup>3</sup> Battersea College of Technology.

<sup>4</sup> Advice from Mr. M. S. C. Birbeck on the electron microscopy is gratefully acknowledged. Mr. R. H. Hinton gave valuable help late in the study.

the 5'-nucleotidase (nucleoside 5'-monophosphatase) activity of microsomal fractions and also for that of crude nuclear fractions (1, 2). Methods have been described [reviewed by Reid (3)] for the isolation from liver of plasma-membrane fragments—the usual starting material being essentially a crude nuclear fraction (4)—and of smooth- and rough-surfaced cytomembrane fractions. The smooth-surfaced elements are obtained free from rough-surfaced elements either by exploitation of differences in density or sedimentation rate (5, 6) or by use of deoxycholate to detach ribosomes (7). The published procedures for isolating smooth- and rough-surfaced cytomembrane fragments from liver are prolonged and delicate and lack information on the fate of plasma-membrane fragments. Some separation of the latter from smooth-surfaced cytomembrane fragments has been reported, without supporting electron microscopy studies, for Ehrlich ascites cells (8).

In the present study, rat liver homogenates free from nuclei and mitochondria were used as starting material. The aim was to separate different microsomal-fraction elements with the zonal centrifuge, the advantages of which include good resolution and high capacity.

## MATERIALS AND METHODS

The rats were "hooded" males weighing about 250 g. They were fasted overnight before autopsy to deplete liver glycogen. Homogenates prepared in 0.25 M sucrose medium (in a Potter-Elvehjem homogenizer) were centrifuged for 15 minutes at  $20,000 \times g$  (value at foot of tube) to remove nuclei and mitochondria. Substitution of 0.88 M sucrose for 0.25 M sucrose, with an initial centrifugation of 20 minutes at  $20,000 \times g$ , was of no advantage. The supernatant, to which deoxycholate (to 0.1%) was added in some experiments, was introduced into the rotor of a B-IV zonal centrifuge (Beckman Instruments), followed by a sucrose solution to give the desired gradient. The sucrose solutions were supplemented with pH 7.4 Tris buffer (to 0.005 M) to reduce the risk of artifacts due to aggregation of particles. In some experiments the liver was taken from rats that 45 minutes previously had been given intraperitoneal injections of 20  $\mu$ g of 6- $C^{14}$ -orotic acid, equivalent to 2  $\mu$ c.

At the end of the zonal run, successive 40 ml samples were removed, with monitoring of absorption 280 m $\mu$  (flow-cell) and of the sucrose concentration (by refractometry). For estimation of RNA by the orcinol procedure, samples were treated in the cold with  $HClO_4$  (to 5%) to give a pellet, which was then washed 5 times, defatted, dried, and extracted with 5 percent  $HClO_4$  at 80° C. This extract was also used for measurement of RNA radioactivity in a liquid scintillation counter. Enzymic activities were assayed by conventional methods at 37°, with final measurement of inorganic phosphate. Glucose-6-phosphatase (G-6-Pase) and inorganic pyrophosphatase (PPase) were assayed in 3,3-dimethyl-

glutarate buffer, pH 6.5. Enzymes concerned with the dephosphorylation of ATP (ATPase), UDP (UDPase), and 5'-AMP (AMPase) were assayed in Tris buffer, pH 8.0, in the presence of  $Mg^{2+}$  ions (0.005 M). The high concentration of sucrose necessarily present caused some inhibition, notably of AMPase (60% with 0.7 M sucrose); the data presented are uncorrected for such inhibitions, which do not invalidate the conclusions.

## RESULTS

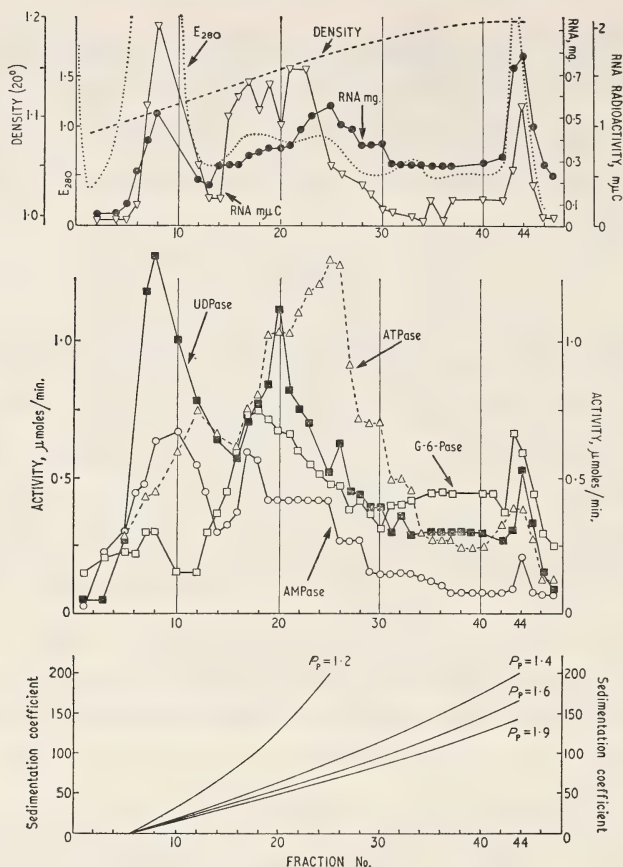
In pilot runs, gradients of different degrees of steepness were tried, either with a brief centrifugation, *e.g.*, 20 minutes at 11,000 rpm, or with prolonged high-speed centrifugation, *e.g.*, several hours at 40,000 rpm, to favor separations based on differences in sedimentation rate and in particle density. These early runs gave AMPase (5'-nucleotidase) mainly as a fairly sharp peak in a position which depended on the conditions chosen; the density of the material appeared to be lower than 1.20. The position of G-6-Pase was the same as that of AMPase, except in some runs where 0.1 percent deoxycholate was added—a concentration known from other work (7) to be too low to solubilize membranous material; in the latter runs G-6-Pase tended to run as a double peak, with AMPase in the dip. Additional peaks for the two activities sometimes occurred, corresponding to those of material with a negligible sedimentation rate or with a density under 1.10.

### Basic Pattern With Isopycnic Conditions for Microsomal Elements

Because of the results of the pilot work, an attempt was made to separate G-6-Pase and AMPase isopycnically, without use of deoxycholate. The tissue material was centrifuged for 6 hours at 40,000 rpm over a gradient kept shallow over a chosen density range. The results of run 9 are shown in text-figure 1.

*Fractions 5 to 14* (density range 1.10–1.12) showed peaks differing in position for RNA (presumably soluble-RNA) the position corresponds to an  $S^*$ , value of  $<10$  and for the various phosphatases studied, other than ATPase. When the contents of these tubes were spun in a conventional centrifuge after dialysis to remove sucrose, the supernatant was almost devoid of AMPase. The small sediment containing most of the AMPase activity showed no membrane structures in the electron microscope; further reference to this material is made below. When zonal centrifugation was performed not on a "mitochondrial supernatant" fraction, as in run 9, but on a resuspended microsomal pellet, obtained in 0.25 M sucrose medium by centrifugation for 5 hours at  $55,000 \times g$ , the fractions near the origin were devoid of the phosphatases and of RNA.

*Fractions 15 to 20* contained a split peak of RNA of high specific radioactivity but quite low in amount; with a density of 1.6 assumed for the unidentified RNA-containing particles, their sedimentation constant



TEXT-FIGURE 1.—Gradient run 9 with tissue corresponding to 5 g of liver, homogenized with only 2 strokes of the homogenizer in 0.25 M sucrose medium, but made up to 0.88 M before loading (25 ml volume). Centrifugation was for 6 hours at 40,000 rpm. Other details are given under Materials and Methods. For each parameter other than  $E_{280}$  and density, the values represent the total per tube. The contents of tubes 45 to 48 represent material that had reached the rotor wall and was dislodged when the rotor was emptied. *Lower part* shows the sedimentation constants, calculated by computer using the Oak Ridge program, for particles of different densities ( $P_p$ ), depending on their position in the gradient.

was in the range  $S = 40$  to  $60$ . The  $S$  values have been calculated by using the Oak Ridge computer program. Tubes 15 and 16 were relatively poor in phosphatases.

Fractions 17, 18, 19 and 20 showed peaks for AMPase, G-6-Pase, PPase (not illustrated), and UDPase, respectively. The sediment obtained from fractions 15 to 20 was examined electron microscopically (fig. 1) and showed abundant smooth-surfaced vesicles, with almost no rough-surfaced vesicles. AMPase and G-6-Pase were both demonstrated cytochemically in the vesicles from this region. On the likely assumption that the particles in fractions 15 to 20 were in their equilibrium position, their

density would be just under 1.15 like the smooth-surfaced membrane fraction prepared by Chauveau *et al.* (6), although other work (3) suggests a value of the order of 1.17 for smooth-surfaced elements.

Fractions 21 to 28 showed progressively diminishing levels of phosphatase activity, except for ATPase which showed a striking peak in fraction 25. This fraction also showed a peak for RNA, but little radioactivity. The RNA presumably resided in free ribosomes. Calculation shows that particles of density 1.6 and  $S^* = 70$  would be found in fraction 25.

Fractions 29 to 40 were relatively low in all constituents studied, except for PPase (not illustrated) which showed, in this run only, a peak in fraction 34. That the peak may represent a mitochondrial PPase (9) is supported by the electron microscopic finding of some damaged mitochondria intermingled with cytomembrane vesicles.

Fractions 41 to 45 showed little AMPase (in other runs no activity was detectable), but there were sharp peaks, almost coincident in fractions 43 and 44, for all other parameters studied. The PPase peak (not illustrated) was remarkably high: 2.0 in the units used for text-figure 1. In accordance with the electron microscopic finding (fig. 2) of abundant rough-surfaced vesicles rich in G-6-Pase, there was a high content of RNA of relatively low specific radioactivity. The literature on rough-surfaced membrane fractions (3) points to a density of the same order as for fractions 41 to 48 (about 1.19).

### Pattern in Presence of $Mg^{2+}$ Ions

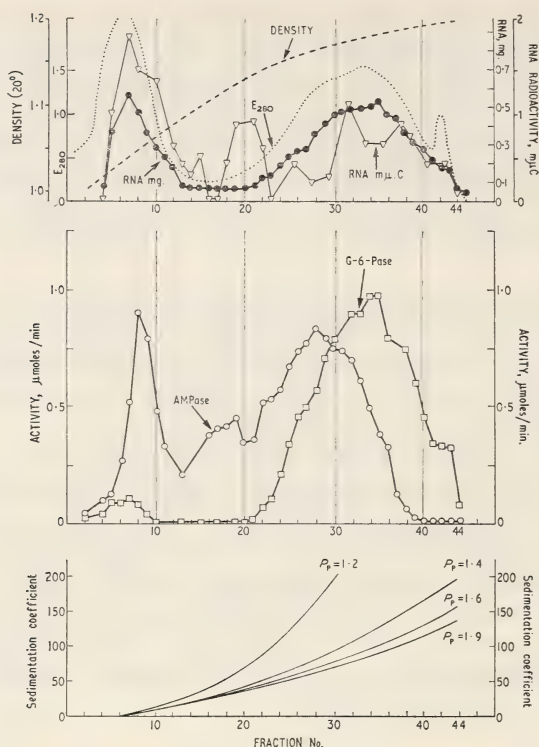
In the above run there was an AMPase peak overlapping with the G-6-Pase of the smooth-surfaced cytomembrane fragments. Trial of a shallower gradient in this region gave improved separation of AMPase and G-6-Pase, but there was still considerable overlap. Runs were then tried with  $Mg^{2+}$  ions added to the homogenizing medium and to the solutions of the gradient. This modification may selectively affect the centrifugal behavior of certain types of membrane fragments (8, 10); plasma-membrane fragments are apparently unaffected, at least in Ehrlich ascites cells (8).

The patterns were similar with  $1.5 \times 10^{-2} M$   $Mg^{2+}$  and  $4 \times 10^{-3} M$   $Mg^{2+}$ , the latter being the concentration used for the run shown in text-figure 2.

Fractions 5 to 12 showed, as before, sharp peaks for RNA and AMPase activity.

Fractions 18 to 22 again contained a small amount of RNA, high in specific radioactivity, but the high concentration of RNA of uncertain identity, seen in run 9, was absent. The electron microscope showed no evidence of membranes.

Fractions 22 to 35 contained a peak of AMPase activity, now around density 1.15, whereas in the absence of  $Mg^{2+}$  ions it was at density 1.17.



TEXT-FIGURE 2.—Gradient run 13 performed under same conditions as for run 9 (text-fig. 1), but with  $MgCl_2$  ( $4 \times 10^{-3} M$ ) present both during homogenization and in the gradient, the latter being slightly different from that in run 9.

In the electron microscope the pooled material from these fractions contained a mixture of rough and smooth membranes and polysome-like structures.

Fractions 36 to 40 showed broad peaks for RNA and G-6-Pase and was clearly identified in the electron microscope as rough-surfaced vesicles.

### Material Near the Origin

As stated for run 9 (text-fig. 1), the AMPase activity in the low density region of the gradient ( $d < 1.12$ ) could be separated after dialysis, against  $10^{-3} M$  Tris buffer,  $pH$  7.4, by high-speed centrifugation into a pellet. By zonal centrifugation of the liver preparation in a gradient starting at a density of  $d = 1.02$ , the AMPase activity could be moved a few tubes from the origin and thereby separated from RNA, UDPase, and UTPase. In general, the enzyme activities found in this region were variable, and the problem of whether they reside in particles of low density or are present as free protein with a tendency to aggregate remains to be resolved.

## DISCUSSION

Most of the published evidence (3) suggests that both smooth-surfaced cytomembranes (other than Golgi) and rough-surfaced cytomembranes contain G-6-Pase, but that ribosomes are almost devoid of enzymes. Separation of these membranes has now been achieved, as judged by electron microscopy and by analyses for G-6-Pase and RNA. There remains the problem of possible contamination with polysomes and ribosomes which is now being investigated, but the data obtained have been interpreted on the basis that the enzymes studied are not associated with these particles.

Plasma-membrane fragments were not identified electron microscopically, and as judged by assays for AMPase (5'-nucleotidase) they were absent from the rough-surfaced membrane fraction. While it would be difficult to identify by electron microscopy fragments corresponding to the nonconvoluted portions of the plasma membrane, bile-canalicular fragments should be recognized. Failure to observe them may be because in the preliminary separation of the microsomal fraction studied here they were removed together with nuclear material. As would be expected from published density values (3), ranging from 1.17 (4) downward, for plasma-membrane fragments, the AMPase position was similar to that of smooth-surfaced membrane fragments in the absence of  $Mg^{2+}$  ions. Sharp separation may call for use of  $Mg^{2+}$  ions, which in accord with ascites cell results (8) may alter the behavior of smooth-surfaced cytomembrane fragments selectively, as in run 13 above; the reported alterations may include aggregation and a change in density (8). As an alternative approach, further trials are planned with deoxycholate, prompted by indications that it "erodes" cytomembrane fragments more readily than plasma-membrane fragments.

The findings for UDPase (nucleoside diphosphatase, active toward GDP, IDP, and UDP) agree with published evidence for a cytomembrane location (11), though the peaks of activity in the smooth- and rough-surfaced membrane fractions did not coincide exactly with those of G-6-Pase. ATPase, located largely in the plasma membrane (4, 11), was found mainly in a fraction (density 1.16) close to, but distinct from, those rich in G-6-Pase (smooth-surfaced cytomembrane fragments) and in AMPase (supposed plasma-membrane fragments, as discussed above). However, the ATPase results must be interpreted with caution, since at least two enzymes exist, differing in susceptibility to activation by cations and to inhibition by ouabain. At least it is evident, from results (not shown) for the low-density material, that UTPase and ATPase are not common activities of a single enzyme (*cf* 11). The results obtained for PPase under a variety of conditions are compatible with the contention (9) that the microsomal enzyme is identical with G-6-Pase.

Zonal centrifugation is thus a powerful tool for the isolation, in fair quantity, of membrane fragments corresponding to different cellular structures. Conditions leading to simultaneous isolation of all the components of the microsomal fraction studied have not yet been achieved.

## REFERENCES

- (1) KU, K-Y., and WANG, C-T.: 5'-Nucleotidase of isolated hepatic cell membrane from rat liver. *Shi Yen Shang Wu Hsueh Pao (Acad Sinica, Shanghai)* 8: 400-407, 1963. Cited in *Chem Abs* 61: 2123, 1964.
- (2) REID, E., EL-AASER, A. A., TURNER, M. K., and SIEBERT, G.: Enzymes of ribonucleotide metabolism in rat-liver nuclei. *Hoppe-Seyl Zeit Physiol Chem* 339: 145-159, 1964.
- (3) REID, E.: Membrane systems. In *Enzyme Cytology* (Roodyn, D. B., ed.). London, Academic Press Inc., 1966. In press.
- (4) EMMELOT, P., BOS, C. J., BENEDETTI, E., and RÜMKE, PH.: Studies on plasma membranes. I. Chemical composition and enzyme content of plasma membranes isolated from rat liver. *Biochem Biophys Acta* 90: 126-145, 1964.
- (5) MOULÉ, Y., ROUILLER, C., and CHAUVÉAU, J.: A biochemical and morphological study of rat liver microsomes. *J Biophys Biochem Cytol* 7: 547-558, 1960.
- (6) CHAUVÉAU, J., MOULÉ, Y., ROUILLER, C., and SCHNEEBELI, J.: Isolation of smooth vesicles and free ribosomes from rat liver microsomes. *J Cell Biol* 12: 17-30, 1962.
- (7) ERNSTER, L., SIEKEVITZ, P., and PALADE, G.: Enzyme-structure relationships in the endoplasmic reticulum of rat liver. *J Cell Biol* 15: 541-562, 1962.
- (8) KAMAT, V. B., and WALLACH, D. F. H.: Separation and partial purification of plasma membrane fragments from Ehrlich ascites carcinoma microsomes. *Science* 148: 1343-1345, 1965.
- (9) NORDLIE, R. C., and ARION, W. J.: Evidence for the common identity of glucose 6-phosphatase, inorganic pyrophosphatase, and pyrophosphate glucose phosphotransferase. *J Biol Chem* 239: 1680-1685, 1964.
- (10) DALLNER, G.: Studies on the structural and enzymic organization of the membranous elements of liver microsomes. *Acta Path Microbiol Scand (Suppl)* 166: 1-94, 1963.
- (11) GOLDFISCHER, S., ESSNER, E., and NOVIKOFF, A. B.: The localization of phosphatase activity at the level of ultrastructure. *J Histochem Cytochem* 12: 72-95, 1964.

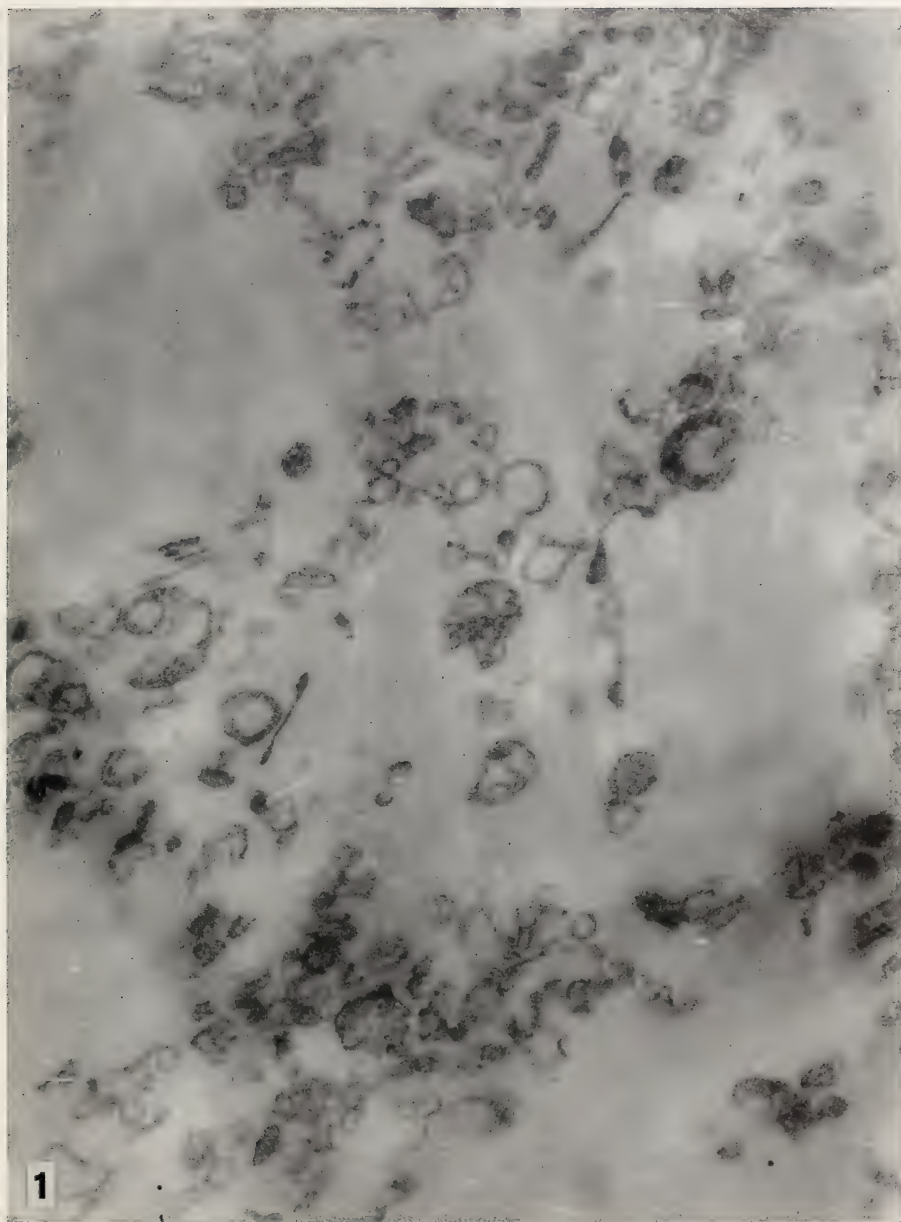


FIGURE 1.—Electron micrograph of pellets isolated from zonal centrifuge fractions 15 to 21, run 9 (*cf* text-fig. 1). Smooth-surfaced vesicles of varying diameter, admixed with a few rough-surfaced vesicles. Osmium-fixed and lead-stained.

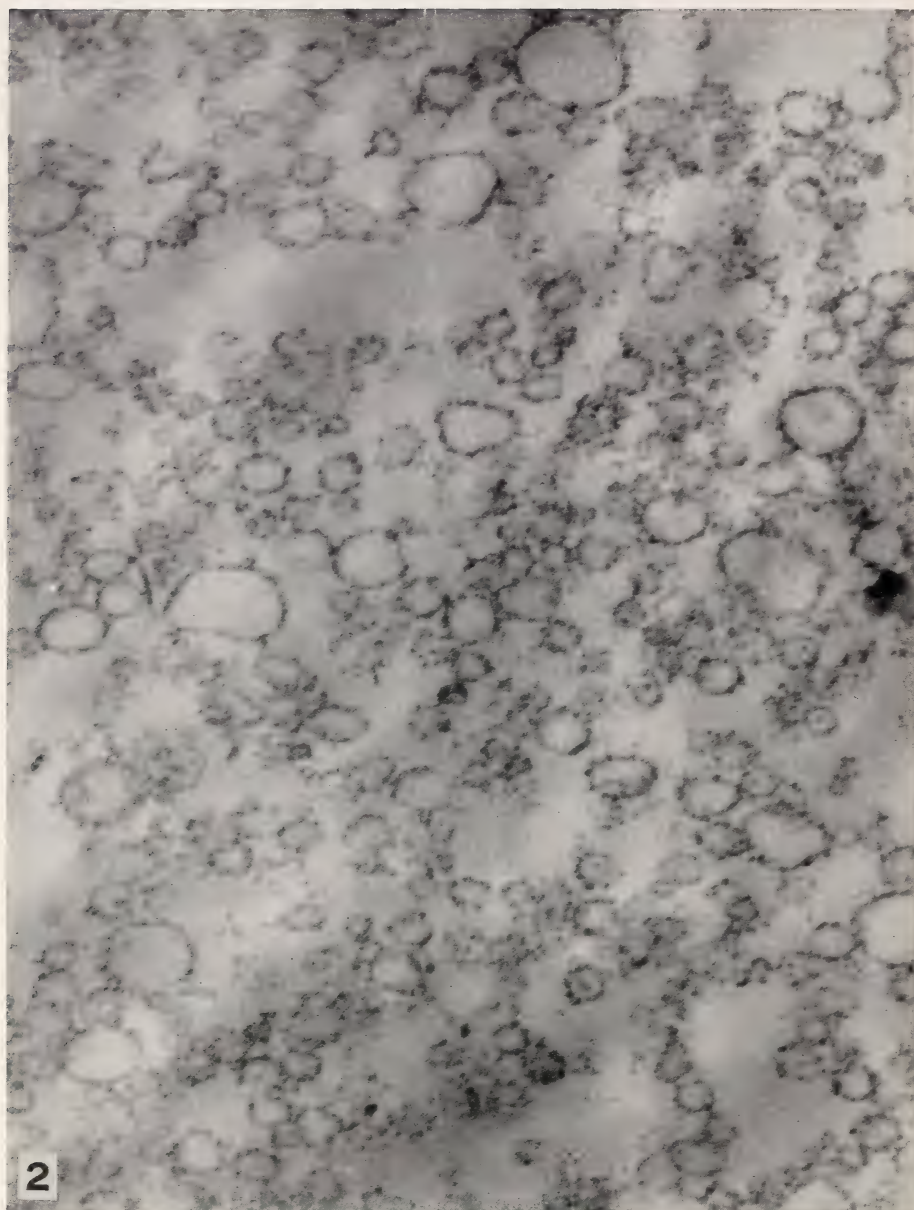


FIGURE 2.—Electron micrograph of pellets isolated from zonal centrifuge fractions 39 to 47, run 9 (*cf* text-fig. 1). Rough-surfaced vesicles. Osmium-fixed and lead-stained.

## Lipid Peroxidation in Rat Tissue Particulates Separated by Zonal Centrifugation<sup>1</sup>

ALBERT A. BARBER,<sup>2</sup> C. T. RANKIN, JR., and N. G. ANDERSON, *Biology Division, Oak Ridge National Laboratory,*<sup>3</sup> Oak Ridge, Tennessee

### SUMMARY

The distribution of protein and lipid peroxidation activity in homogenate fractions of rat liver, brain, kidney, and testis has been determined following zonal centrifugation of these homogenates in sucrose gradients. Lipid peroxidation occurred in nearly all particulate fractions. Differences in the amount of lipid peroxidation between fractions were presumed due to specific differences in their lipid and iron content. The particle profile of brain and testis homogenates differed from that of liver and kidney. Brain had a major particulate fraction with a sedimentation coefficient between those of liver microsomes and mitochondria. Brain

and testis had only small amounts of material corresponding to the mitochondrial zone of liver and kidney. The procedures for the differential centrifugation developed primarily for liver, therefore, are not applicable to all tissue fractionation. The sedimentation characteristics of each tissue particulate fraction must be determined before appropriate procedures for differential centrifugation can be established. Zonal centrifugation, with continuous monitoring of the collected gradient, provides a rapid and efficient method for determining these characteristics.—*Nat Cancer Inst Monogr* 21: 333-344, 1966.

A NONENZYMIC peroxidation of unsaturated lipids occurs when certain rat tissue homogenates are aerobically incubated (1). This reaction does not normally occur *in vivo*. Homogenization and dilution change the tissue antioxidant characteristics sufficiently to allow oxygen attack of the unsaturated lipids.

Preliminary studies, using differential centrifugation, established the subcellular distribution of the components required for lipid peroxidation (2). Lipid peroxidation occurred in all particulate fractions (nuclei, mitochondria, and microsomes) isolated from liver homogenates when incubated with the 105,000  $\times g$  supernatant or with ascorbic acid, but not when incubated alone. Ascorbic acid appears to be the only essential

<sup>1</sup> This research performed under the Joint National Institutes of Health-Atomic Energy Commission Zonal Centrifuge Development Program which is supported by the National Cancer Institute, the National Institute of Allergy and Infectious Diseases, and the U.S. Atomic Energy Commission.

<sup>2</sup> Department of Zoology, University of California, Los Angeles, Calif. Aided by AEC Contract No. AT(11-1)-34 Project 49.

<sup>3</sup> Operated for the U.S. Atomic Energy Commission by Union Carbide Corporation.

component contributed by the supernatant, whereas the particulate fraction contributes both the unsaturated lipids and the iron required for the reaction (2).

The lipid peroxidation reaction has been studied in mitochondrial suspensions (3, 4), microsomal suspensions (2, 5), as well as in pure unsaturated lipid suspensions (6). However, microsomal contamination of mitochondria is difficult to avoid when mitochondria are prepared by differential centrifugation and the contribution by microsomes to lipid peroxidation in mitochondrial fractions has not been established. The peroxidation reaction in isolated mitochondria has been correlated with mitochondrial swelling and lysis (7). Therefore, preparations of mitochondria free of microsomal contamination are obviously necessary for establishing peroxidation as the mechanism involved in swelling and lysis.

The development of zonal centrifugation has made it possible to separate tissue particulate fractions with increased resolution (8). Rate-zonal sedimentation of tissue homogenates in the B-IV rotor system (9), followed by high-speed centrifugation of the collected samples by conventional means, results in the separation of particulate materials on the basis of their sedimentation properties. The present study was designed to separate tissue fractions in a sucrose gradient and to determine the extent of lipid peroxidation in all fractions by aerobically incubating similar volumes of each with ascorbic acid. The membrane and lipid peroxidation profiles from rat liver, brain, kidney, and testis homogenates are compared.

## MATERIALS AND METHODS

Liver, brain, kidney, and testis obtained from exsanguinated Sprague-Dawley male rats were homogenized in 0.25 M sucrose. Twenty ml of homogenate was placed in the B-IV rotor system containing a gradient volume of 1200 ml extending from 10 to 30 percent sucrose. About 300 ml of a 55 percent sucrose solution was used as the outboard cushion with 200 ml of buffer placed inboard of the sample layer. Separations were carried out at 10,000 rpm for 15 minutes ( $G_c = 1100 \times 10^6$ , including acceleration and deceleration) in all cases but one, which was at 20,000 rpm for 60 minutes ( $G_c = 17,000 \times 10^6$ ). The rotor contents were emptied by displacement with 55 percent sucrose and the eluant was monitored continuously at 260 m $\mu$ . Forty-two fractions containing 40 ml each were collected in tubes maintained in ice. The percent sucrose was measured with an American Optical Company refractometer calibrated to read w/w percent sucrose directly and proteins were measured colorimetrically by the method of Lowry *et al.* with bovine serum albumin as the standard (10).

Twenty-five ml of each collected sample was placed in polycarbonate centrifuge tubes and 3 ml of water added. All samples were centrifuged for 90 minutes at 30,000 rpm in a Spinco Model L ultracentrifuge. Pellets were rinsed twice with 0.01 M phosphate buffer (containing 0.15 M NaCl)

at pH 7.0 and resuspended to the original volume by homogenizing in buffer. Proteins were analyzed in all resuspended pellets and an aliquot of each was used to measure lipid peroxidation.

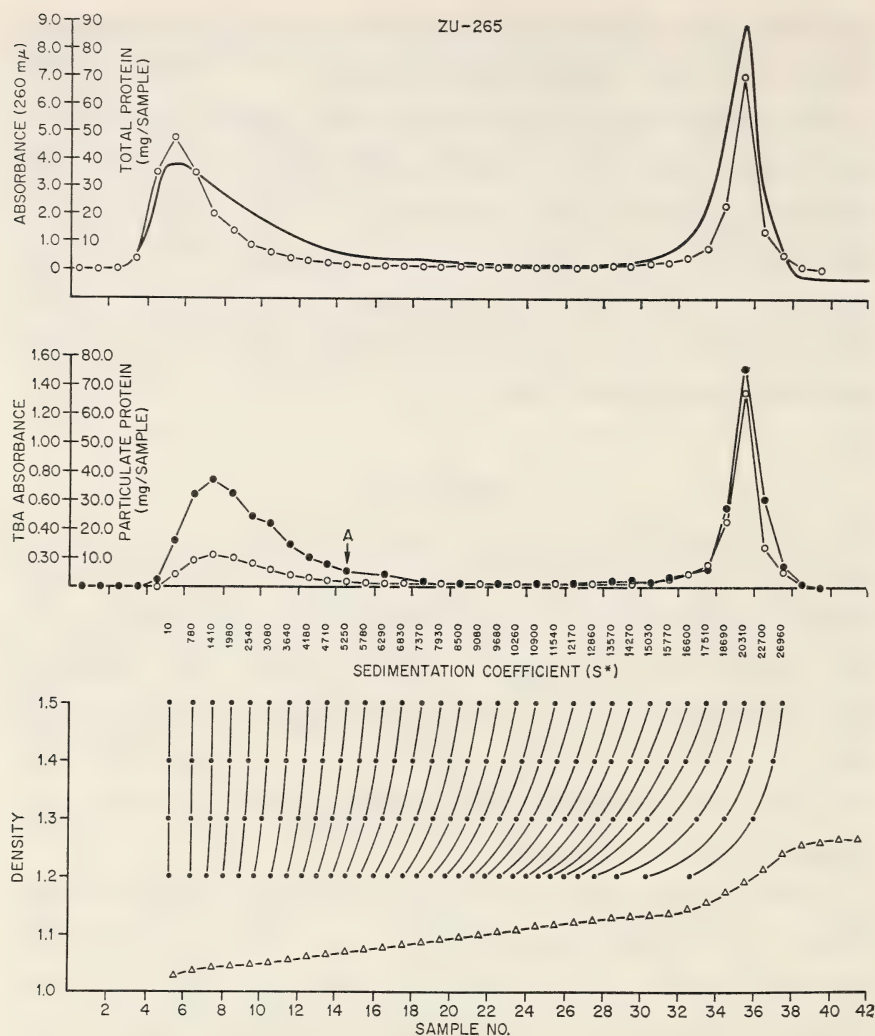
Lipid peroxidation was measured by placing equal portions of resuspended pellets in 20 ml beakers; 30  $\mu$ g of ascorbic acid was added to each beaker, and the final volume was adjusted to 4.0 ml with buffer. Beakers were incubated for 90 minutes at 37° C in a Dubnoff Metabolic Shaker oscillating at 100 cycles per minute. The thiobarbituric acid (TBA) test was used to measure lipid peroxidation (11). Results were expressed directly as the TBA absorbance measured at 530 m $\mu$  on a Beckman Model DB Spectrophotometer rather than as units of malonaldehyde, since the relationship between the TBA color and malonaldehyde continues to be questioned (12).

## RESULTS

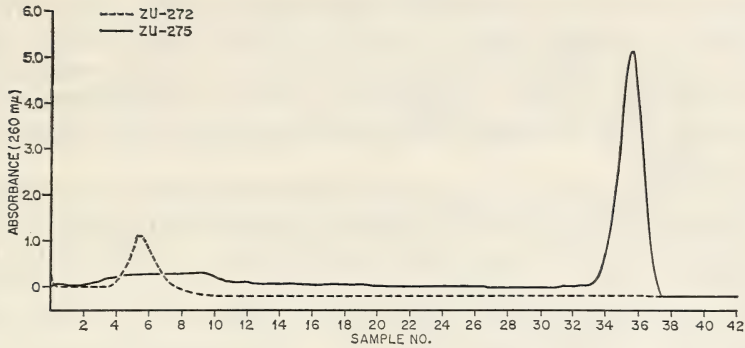
Sedimentation of a 10 percent rat liver homogenate in the zonal centrifuge for 15 minutes at 10,000 rpm resulted in the separation of two major ultraviolet (UV) absorbing fractions (text-fig. 1, top diagram). The soluble protein represented 41 percent of the homogenate protein and was recovered from the starting zone (sample 6). The microsomal fraction sedimented slightly from the starting zone (text-fig. 1, middle diagram). The mitochondria and larger particles sedimented to their isopycnic level at the outboard edge of the rotor (sample 36). Some particulate material was distributed between the microsomal and mitochondrial fractions. Assuming similar particle densities, a continuous spectrum of sizes was indicated.

The distribution of lipid peroxidation activity in liver fractions was similar to the distribution of particulate protein (text-fig. 1, middle diagram). The specific activity (TBA absorbance/100  $\mu$ g protein) of the microsomal fraction (samples 6–15) was greater than that of the larger fragments (samples 33–36) and was also slightly higher than the activity of microsomes isolated by differential centrifugation (table 1). This difference in specific activity was not due to the particle size differences since sonication of large fragments from liver did not change the specific activity of lipid peroxidation (0.051 TBA absorbance/100  $\mu$ g protein) but did disrupt the larger fragments to particles which centrifuged in the microsomal zone (text-fig. 2).

The microsomal pellet prepared by centrifuging a 10,000 rpm-15-minute supernatant (No. 30 rotor of a Spinco Model L ultracentrifuge) at 40,000 rpm for 60 minutes contained 14 percent of the protein of the homogenate. In the zonal centrifuge diagram shown in text-figure 1, 14 percent of the particulate protein is found to the left of point A. Particles at this experimentally determined point have an equivalent sedimentation coefficient of approximately 6300  $S^*$  assuming a density of 1.2. The particle fraction collected between the starting boundary



TEXT-FIGURE 1.—Distribution of ultraviolet absorbance, total protein, particulate protein, and lipid peroxidation activity in a rat liver homogenate subjected to 10,000 rpm for 15 minutes in the zonal centrifuge; 20 ml of homogenate (1:10 w/v in 0.25 M sucrose) placed in B-IV rotor and overlaid with 200 ml of buffer. Starting zone at sample 6; 40 ml collected in each tube; 25 ml of each sample, diluted with 3 ml of water, was centrifuged for 90 minutes at 30,000 rpm. Pellets were rinsed twice and resuspended in phosphate buffer (0.01 M, pH 7.0) containing 0.15 M NaCl. Lipid peroxidation was measured in 20 ml beakers by using 2 ml of resuspended pellet and 30  $\mu$ g ascorbic acid brought to a final volume of 4 ml. Incubation was for 90 minutes at 37° C. TBA reaction run was previously described (1). See text for explanation of A. Please note that ordinate units differ in subsequent figures. These changes were necessitated by the large differences in the amount of material present in each tissue: ○—protein (total in upper and particulate in middle diagram); ●—TBA absorbance at 530 mμ; △—sucrose gradient density.



TEXT-FIGURE 2.—Sedimentation of normal and sonicated mitochondria at 10,000 rpm for 15 minutes in the zonal centrifuge. To obtain the isopycnic rebanding of normal mitochondria, 38 ml of a mitochondrial suspension obtained from zonal centrifugation of a liver homogenate was diluted to 150 ml with buffer and reloaded into the B-IV rotor. For examining the effects of sonication, 40 ml of a pelleted sample was resuspended in buffer, sonicated for 2 minutes, and 20 ml was placed into B-IV rotor.

—— Normal      - - - - - Sonicated

TABLE 1.—Comparison of lipid peroxidation activity in particulate fractions of rat tissue homogenates. Values represent the TBA absorbance/100  $\mu$ g protein developed during 90 minutes of aerobic incubation at 37° C with 30  $\mu$ g of ascorbic acid in each flask. Final volume of each flask was 4.0 ml

Tissue	Microsomes*	Microsomes†	Large fragments‡ (including mitochondria)
Liver	0.115	0.136	0.051
Brain	0.100	0.086	0.050
Kidney	0.060	0.071	0.044
Testis	0.043	0.056	0.025

\*Microsomes prepared by differential centrifugation. A 10,000 rpm-15-minute supernatant solution was centrifuged at 40,000 rpm for 60 minutes. Pellets were resuspended in 0.01 M phosphate buffer, pH 7.0, containing 0.15 M NaCl.

†The combined specific activities of all particles between tubes 6 and 15 collected after zonal centrifugation, as described in the legend of text-figure 1. This total fraction contained approximately the same amount of protein as in microsomes collected by differential centrifugation.

‡The combined specific activities of the particulates between zonal samples 33 and 36, except for brain where it represents the material between samples 18 and 22.

and point A of text-figure 1 is therefore roughly comparable to the particles retained in the supernatant fluid following differential centrifugation at 10,000 rpm for 15 minutes in Spinco No. 30 rotors. It should be recalled that the pellet in differential centrifugation contains *all* particle species present but in different amounts. The supernatant also contains different amounts of each species excepting those completely sedimented. If microsomes and mitochondria represented two particle populations whose sedimentation coefficient distribution curves did not overlap, then clean separations could be made in the zonal centrifuge but not in single step differential centrifugation. The distribution between pellet and

supernatant fluid in differential centrifugation cannot, therefore, be indicated by a single point in zonal centrifuge run diagrams. The particle fraction collected between the starting boundary and point A is therefore only roughly comparable to the particles retained in the supernatant fluid following differential centrifugation at 10,000 rpm for 15 minutes.

Zonal centrifugation of a 1:5 (w/v) brain homogenate at 10,000 rpm for 15 minutes separated six UV-absorbing components (text-fig. 3). The soluble protein fraction represented approximately 18 percent of the total homogenate protein, compared to 41 percent in liver. The microsomal fraction was similar to that of liver but the characteristic mitochondrial fraction was a smaller fraction of the total. The major particulate fraction of brain sedimented with an  $S^*$  of approximately 12,000 (assuming a density of 1.2) and constituted nearly half of the particulate protein. The last UV-absorbing peak (sample 37) was made up primarily of red blood cells. The particulates to the left of point B in text-figure 3 correspond roughly to the microsomal fraction remaining in the supernatant of brain homogenates centrifuged at 10,000 rpm for 15 minutes in a Spinco No. 30 rotor.

Lipid peroxidation occurred in brain particulate samples throughout the rotor (text-fig. 3). The microsomal fraction had the highest specific activity, which was only slightly less than that of microsomes collected by differential centrifugation (table 1). The lack of an increase in the peroxidation reaction in samples 15 to 25, as compared with the samples preceding and following, suggests that the particles responsible for this reaction may be uniformly distributed through this region. An additional population of particles may be present, which accounts for the peak in tube 21 observed in the absorbance monitor but which does not contribute to the peroxidation reaction. No peroxidation occurred in the particulates from tube 37, the fraction containing primarily red blood cells. Zonal centrifugation at higher speeds for longer times resulted in isopycnic banding of the 12,000  $S^*$  fractions in 38 percent sucrose.

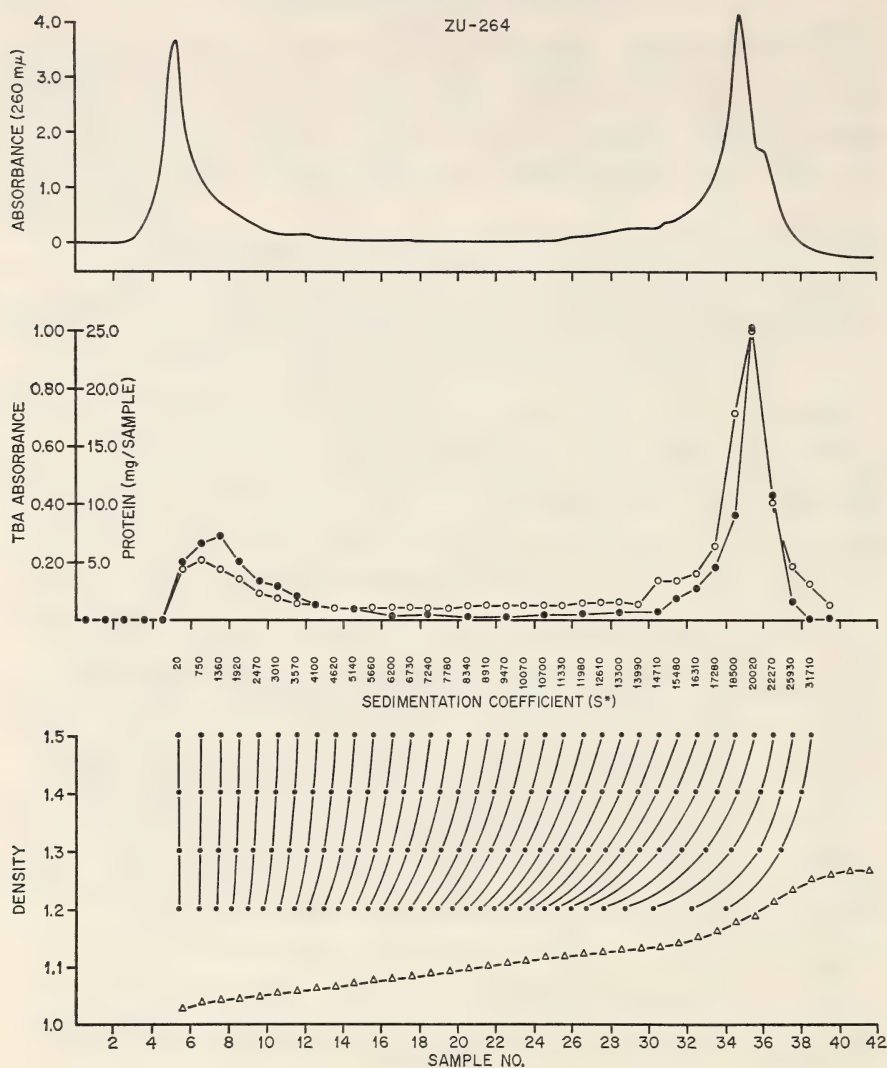
Zonal sedimentation of a 1:5 (w/v) kidney homogenate at 10,000 rpm for 15 minutes resulted in a distribution of UV-absorbing material and total protein similar to liver (text-fig. 4). The soluble protein represented 41 percent of the homogenate protein and the microsomal fraction was again well separated from the larger particulates. Small amounts of particulate material were again sedimented throughout the gradient. Lipid peroxidation occurred in all particulate fractions with the highest specific activity material associated with the microsomal particles. The specific activity of the kidney microsomal fraction was slightly more than that of a similar fraction prepared by differential centrifugation but was only about half that of similar fractions prepared from liver (table 1). The specific activity of the larger fragments was only slightly less than that of similar fragments from liver.

The profile of particulate materials obtained by the zonal centrifugation of a 1:5 (w/v) testis homogenate was different from liver, brain, or kidney



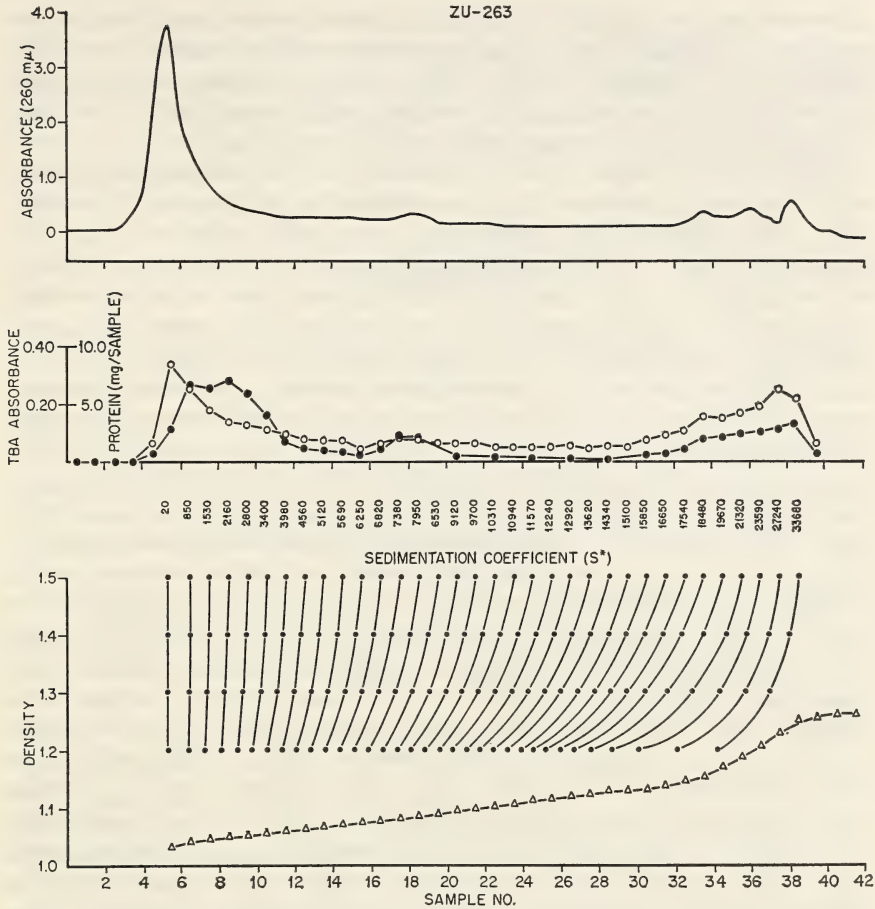
TEXT-FIGURE 3.—Distribution of ultraviolet-absorbing material, particulate protein, and lipid peroxidation activity in a rat brain homogenate (1:5 w/v) centrifuged at 10,000 rpm for 15 minutes in the B-IV rotor. Conditions similar to those described in the legend for text-figure 1 except that lipid peroxidation was tested by using 1 ml of resuspended pellet: ○—particulate protein; ●—TBA absorbance at 530 mμ; △—sucrose gradient density.

(text-fig. 5). The soluble protein constituted approximately 40 percent of the total homogenate protein and the microsomal fraction (samples 6–15) represented the largest single particulate fraction. No large mitochondrial fraction was noted, but several small distinct peaks were noted between samples 33 and 39. One small peak of particulate material was also noted at sample number 19 (~11,000  $S^*$  assuming a density of 1.2).



TEXT-FIGURE 4.—Distribution of ultraviolet-absorbing material, particulate protein, and lipid peroxidation in a rat kidney homogenate (1:5 w/v) subjected to 10,000 rpm for 15 minutes in the zonal centrifuge. Conditions similar to those described in text-figure 1, except that lipid peroxidation was tested by using 2.0 ml of resuspended pellet: ○—particulate protein; ●—TBA absorbance at 530 mμ; △—sucrose gradient density.

Lipid peroxidation occurred in nearly all samples. The specific activity of the small particulate fraction was lower than in other tissues (table 1), but was probably due to the presence of a large amount of particulate material in sample 6, which was very low in activity. The particles distributed in samples 8 to 10 were comparable in activity to similar samples obtained from other tissues. The nature of this material in sample



TEXT-FIGURE 5.—Distribution of ultraviolet-absorbing material, particulate protein, and lipid peroxidation activity in a rat testis homogenate (1:5 w/v) subjected to 10,000 rpm for 15 minutes. Conditions similar to those described in legend for text-figure 1 except that lipid peroxidation was tested by using 3.0 ml of resuspended pellet: ○—particulate protein; ●—TBA absorbance at 530 mμ; △—sucrose gradient density.

6 is unknown. The specific activity of the larger fragments is also approximately half that noted for similar fragments obtained from other tissues.

## DISCUSSION

The thiobarbituric acid test for lipid peroxidation was used in the present studies since it is a very sensitive measure of the oxidation of polyunsaturated fatty acids (13). Linolenic and arachidonic acids are the important biological fatty acids measured by this test. The peroxidation reaction in homogenates, in isolated particulates, and in pure fatty acid emulsions can use iron in various forms, such as cytochrome, hematin,

or ferrous ions as a catalyst (2, 6, 14). Ascorbic acid is utilized in the reaction to maintain iron in its catalytically active reduced form (3). Although iron interferes with the TBA reaction, the amount of catalytic iron required in the presence of ascorbic acid is considerably less than that which causes interference with the TBA test (14, 15).

All particulate fractions of liver and kidney, which include mitochondria and microsomes, underwent lipid peroxidation in the presence of ascorbic acid. The mitochondrial preparations were well separated from the microsomal fractions and peroxidation in mitochondria was not due to contamination by this fraction. Swelling and lysis of mitochondria accompanied by lipid peroxidation are, therefore, not necessarily due to microsomal contamination (7). Brain and testis each had one major particulate fraction with low peroxidation activity. In brain this component centrifuged to the center of the rotor and had an  $S^*$  of approximately 12,000 assuming a density of 1.2. The testis component was a small particle which did not migrate appreciably from the starting boundary. The lack of peroxidation activity has not been explained for either component. The presence of unsaturated lipids as structural components in biological membranes suggests that most particulate fractions would undergo peroxidation and is compatible with these results. However, the extent of lipid peroxidation differed greatly between different fractions of the same tissue, as well as between fractions with similar sedimentation properties obtained from several tissues. These differences in peroxidation appear to depend on the lipid and iron constituents of the membrane fraction and not on the membrane size, since sonication of large membranes into smaller fragments did not change their specific activity. Several iron forms are associated with membrane fractions (16-18), and the binding of cytochromes by membrane structural protein has been demonstrated (19). The catalytic activity of various membrane fractions might be different, therefore, depending on the specific iron form available. The specificity of the TBA test itself for the higher polyunsaturated fatty acids could also explain differences in the extent of peroxidation in various membranes. Membranes with large amounts of linolenic and arachidonic acids would undergo more measurable peroxidation with the TBA test (13).

The successful use of differential centrifugation for liver fractionation is due, in part, to the large differences in sedimentation coefficients for the microsomal and mitochondrial fractions and the conspicuous absence of intermediate materials, as shown in the present studies. Microsomes and mitochondria can, therefore, be prepared without excessive cross contamination of particles. Brain, however, has a typical microsomal fraction as well as a major particle fraction of approximately 12,000  $S^*$ . Preliminary observations indicated that this fraction contained the synaptosomes described by Whittaker *et al.* (20). Minor variations in differential centrifugation would result in differences in the amounts of this fraction remaining in the supernatant fluid. The specific activity of this fraction, therefore, would change markedly as a result of the slight variations in the centrifugal force used in this range. These results

emphasize the necessity of establishing the centrifugal distribution of the particles of homogenates from all tissues before specific differential centrifugation methods for the preparation of their fractions are used (21, 22). Zonal centrifugation with continuous monitoring of the collected gradient provides a rapid and efficient method for establishing membrane profiles.

## REFERENCES

- (1) BARBER, A. A., and WILBUR, K. M.: The effect of X-irradiation on the anti-oxidant activity of mammalian tissues. *Radiat Res* 10: 167-175, 1959.
- (2) BARBER, A. A.: Addendum: Mechanisms of lipid peroxide formation in rat tissue homogenates. *Radiat Res (Suppl)* 3: 33-43, 1963.
- (3) OTTOLENGHI, A.: Interaction of ascorbic acid and mitochondrial lipids. *Arch Biochem* 79: 355-363, 1959.
- (4) HUNTER, F. E., JR., SCOTT, A., HOFFSTEN, P. E., GUERRA, F., WEINSTEIN, J., SCHNEIDER, A., SCHUTZ, B., FINK, J., FORD, L., and SMITH, E.: Studies on the mechanism of ascorbate-induced swelling and lysis of isolated liver mitochondria. *J Biol Chem* 239: 604-613, 1964.
- (5) TAPPEL, A. L., and ZALKIN, H.: Inhibition of lipid peroxidation in microsomes by vitamin E. *Nature (London)* 185: 35, 1960.
- (6) TAPPEL, A. L.: The mechanism of the oxidation of unsaturated fatty acids catalyzed by hematin compounds. *Arch Biochem* 44: 378-395, 1953.
- (7) HUNTER, F. E., JR., GEBICKI, J. M., HOFFSTEN, P. E., WEINSTEIN, J., and SCOTT, A.: Swelling and lysis of rat liver mitochondria induced by ferrous ions. *J Biol Chem* 238: 829-835, 1963.
- (8) ANDERSON, N. G., and BURGER, C. L.: Separation of cell components in the zonal ultracentrifuge. *Science* 136: 2-4, 1962.
- (9) ANDERSON, N. G., BARRINGER, H. P., BABELAY, E. F., and FISHER, W. D.: The B-IV zonal ultracentrifuge. *Life Sci* 3: 667-671, 1964.
- (10) LOWRY, O. H., ROSEBROUGH, N. J., FARR, A. L., and RANDALL, R. J.: Protein measurement with the Folin phenol reagent. *J Biol Chem* 193: 265-275, 1951.
- (11) WILBUR, K. M., BERNHEIM, F., and SHAPIRO, O. W.: The thiobarbituric acid reagent as a test for the oxidation of unsaturated fatty acids by various agents. *Arch Biochem* 24: 305-313, 1949.
- (12) SASLAW, L. D., ANDERSON, H. J., and WARAYDEKAR, V. S.: Ultraviolet photolysis of unsaturated fatty acids in relation to the thiobarbituric acid test. *Nature (London)* 200: 1098-1099, 1963.
- (13) DAHLE, L. K., HILL, E. G., and HOLMAN, R. T.: The thiobarbituric acid reaction and the autoxidations of polyunsaturated fatty acid methyl esters. *Arch Biochem* 98: 253-261, 1962.
- (14) BARBER, A. A.: Inhibition of lipid peroxide formation by vertebrate blood serum. *Arch Biochem* 92: 38-43, 1961.
- (15) WILLS, E. D.: The effect of inorganic iron on the thiobarbituric acid method for the determination of lipid peroxides. *Biochim Biophys Acta* 84: 475-477, 1964.
- (16) TAPPEL, A. L., and ZALKIN, H.: Lipide peroxidation in isolated mitochondria. *Arch Biochem* 80: 326-332, 1959.
- (17) THIERS, R. E., and VALLEE, B. L.: Distribution of metals in subcellular fractions of rat liver. *J Biol Chem* 226: 911-920, 1957.
- (18) DALLNER, G.: Studies on the structural and enzymic organization of the membranous elements of liver microsomes. *Acta Path Microbiol Scand (Suppl)* 166: 1-94, 1963.

- (19) CRIDDLE, R. S., BOCK, R. M., GREEN, D. E., and TISDALE, H. D.: Specific interaction of mitochondrial structural protein (S.P.) with cytochromes and lipid. *Biochem Biophys Res Commun* 5: 75-80, 1961.
- (20) WHITTAKER, V. P., MICHAELSON, I. A., and KIRKLAND, R. J. A.: The separation of synaptic vesicles from nerve-ending particles (synaptosomes). *Biochem J* 90: 293-303, 1964.
- (21) BARBER, A. A., HARRIS, W. W., and ANDERSON, N. G.: Isolation of native glycogen by combined rate-zonal and isopycnic centrifugation. *Nat Cancer Inst Monogr* 21: 285-302, 1966.
- (22) ANDERSON, N. G., HARRIS, W. W., BARBER, A. A., RANKIN, C. T., JR., and CANDLER, E. L., JR.: Separation of subcellular components and viruses by combined rate- and isopycnic-zonal centrifugation. *Nat Cancer Inst Monogr* 21: 253-283, 1966.

## Extraction of Contractile Proteins from Myofibrils Prepared by Rate-Zonal Centrifugation<sup>1</sup>

MARY LEE S. BARBER and ROBERT E. CANNING,<sup>2</sup>  
*Biology Division, Oak Ridge National Laboratory,<sup>3</sup> Oak Ridge, Tennessee*

### SUMMARY

Conventional actomyosin extractions involve whole muscle homogenates, which include many cell components other than myofibrils as well as the relaxing factor system. In this study, myofibrils were separated from other cell components by rate-zonal centrifugation. Myosin, but not actomyosin, can be extracted with adenosine triphosphate-concentrated salt solution from

such myofibrils. Recombining the small particles with these myofibrils under the same conditions results in the extraction of actomyosin. These particles may be relaxing factor granules that could augment dissociation of actomyosin with resulting changes in the solubility properties of actin or myosin—*Nat Cancer Inst Monogr* 21: 345-359, 1966.

ACTOMYOSIN is conventionally extracted from muscle tissue by suspending ground muscle in saline solution (1). Although ground muscle contains many subcellular components besides myofibrils, it has been assumed that actomyosin is extracted directly from the myofibrils. The role of other components such as sarcoplasmic reticulum, mitochondria, nuclei, and soluble enzymes in the extraction of actomyosin has not been investigated.

Extraction of contractile proteins from isolated myofibrils is desirable because of evidence of nonspecific binding by myosin. Adenylic deaminase and ribonucleic acid (RNA) (2) and a water-soluble protein (3) are contaminants in extensively reprecipitated myosin preparations. Purified myosin binds deoxyribonucleic acid (DNA) or congo red (4). Adenosine triphosphatase enzymes having widespread distribution on various sizes of isolated frog muscle membrane components (5) might bind with myofibrillar proteins, an event resulting in a confused enzyme picture.

The presence of the relaxing factor in whole muscle homogenate (6) causes myofibrils to react differently from those suspended in saline. This

<sup>1</sup> This research performed under the Joint National Institutes of Health-Atomic Energy Commission Zonal Centrifuge Development Program which is supported by the National Cancer Institute, the National Institute of Allergy and Infectious Diseases, and the U.S. Atomic Energy Commission.

<sup>2</sup> We wish to thank Dr. Norman G. Anderson for his encouragement and valuable advice throughout these studies; W. W. Harris and T. W. Bartlett for the electron microscopic studies; and Dr. Albert A. Barber for his constant help with and discussion of the problem.

<sup>3</sup> Operated for the U.S. Atomic Energy Commission by the Nuclear Division of Union Carbide Corporation.

factor was later recovered on a particulate component (7, 8). Refinement of differential centrifugation procedures for muscle breis and electron micrographic identifications have shown this particulate fraction to be vesicular and of sarcoplasmic tubular origin (5, 9, 10). The relaxing factor system (RFS) not only has a relaxing effect, increasing the fiber volume of myofibrils in the presence of ATP (6), but also inhibits myofibrillar adenosinetriphosphatase (6, 11), controls reactions of isolated contractile proteins (12, 13), inhibits interaction of actin and myosin (14), and dissociates actomyosin into actin and myosin (9). The RFS may exert some or all of these effects due to its adenosinetriphosphatase properties and the active removal of calcium. It would exert these effects in whole muscle breis used for the preparation of actomyosin. Extraction of isolated myofibrils with concentrated salt solution might then result in quite different preparations from those extracted from whole muscle. Conventional techniques for isolation of myofibrils (15) leave RNA (16) and membrane components (17) attached to them. High-resolution separations of subcellular components have been recently accomplished by rate-zonal centrifugation in a sucrose gradient (18). Myofibrils were prepared by use of this method of centrifugation and were extracted with concentrated salt solution. The resulting proteins were compared to those extracted from whole ground muscle, and to those extracted from combinations of other subcellular particulates with the isolated myofibrils fraction.

## MATERIALS AND METHODS

Frog hind leg muscles were removed from pithed female *Rana pipiens* (C. H. Mumley, Alburg, Vt.) and homogenized in 3 volumes of a solution containing 0.25 M sucrose, 0.0018 M  $\text{CaCl}_2$ , and 0.001 M Tris buffer at pH 8 with a Waring blender for 3 minutes in the cold room. The resultant homogenate was further homogenized by use of 25 double strokes with a coaxial homogenizer. The homogenate (pH 6.5) was strained through cheesecloth; a portion was used for extraction of actomyosin and the remainder for the isolation of components by zonal centrifugation.

Actomyosin was extracted from pellets of whole homogenates centrifuged at  $78,000 \times g$  for 90 minutes. The pellets were suspended in a solution of 0.5 M KCl, 0.01 M Tris (pH 8),  $2 \times 10^{-4}$  M ATP, and allowed to extract overnight. The extracts were centrifuged at 20,000 rpm for 30 minutes. The extract supernatant was decanted and diluted with 9 volumes of glass-distilled water. The resultant actomyosin or myosin precipitate was pelleted by  $1600 \times g$  for 30 minutes and the pellet resuspended in a final concentration of 0.5 M KCl, 0.01 M Tris at pH 8. All manipulations were carried out at 4° C.

Zonal centrifugation was carried out with the A-XII rotor (19). A total of 60 ml of muscle homogenate was layered over a sucrose gradient made by layering 200 ml of 13 percent sucrose over a 700 ml gradient of 33 to 54 percent sucrose with an underlay of 300 ml of 55 percent sucrose.

An overlay of 140 ml of 0.0018 M  $\text{CaCl}_2$  and 0.001 M Tris at pH 8 was introduced over the sample. Loading was done at 1000 rpm. The rotor was then accelerated to either 1500 or 2000 rpm and maintained for either 10 or 20 minutes. The rotor was decelerated to 1000 rpm and unloaded from the center by pumping 55 percent (w/w) sucrose into the outer edge. The effluent stream was monitored at  $280 \text{ m}\mu$  by a Beckman spectrophotometric system (19) and collected in 40 ml fractions. The sucrose concentration of each fraction was measured refractometrically. The 40 ml fractions were pelleted at  $78,000 \times g$  for 90 minutes and extracted for actomyosin as the whole homogenate pellets.

Adenosinetriphosphatase studies of actomyosin and myosin were carried out by measuring the released phosphate (20). The reaction mixture contained 0.1 mg per ml protein, 0.05 M KCl, 5mM  $\text{CaCl}_2$  or  $\text{MgCl}_2$ , 0.05 M Tris at pH 8, and 2 mM ATP, unless otherwise specified. The reaction was terminated after 2 to 3 minutes at  $28^\circ \text{C}$ .

Protein concentrations were determined colorimetrically (21).

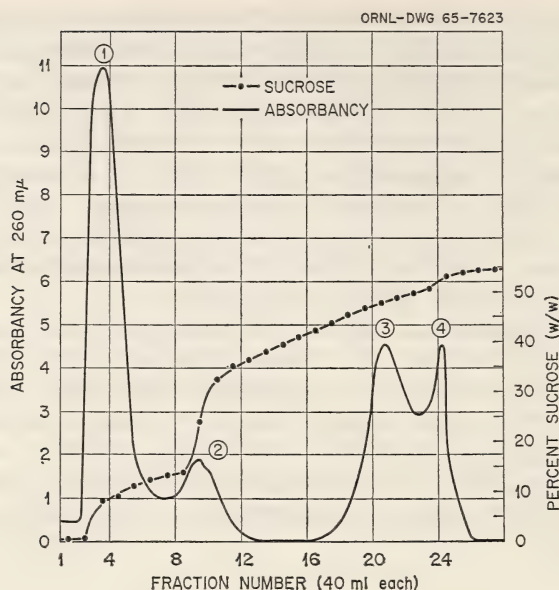
Ultracentrifugal analyses were carried out with a Spinco Model E ultracentrifuge.

## RESULTS

Frog muscle homogenates separated into four distinct zones of material following centrifugation at 1600 rpm for 4 minutes plus 2000 rpm for 6 minutes in the A-XII rotor (fig. 1). The material displaced from the rotor also has four distinct peaks as shown by a continuous recording of absorbancy at  $260 \text{ m}\mu$  (text-fig. 1). This pattern is a characteristic one, although peaks 3 and 4 do overlap to a greater extent in some experiments. Peak 1 (fractions 2-5) contains the soluble proteins and smaller particulates. The particulate material sedimented from this fraction includes vesicles of the size of the relaxing factor system (17) as well as filaments  $2 \text{ m}\mu$  in diameter (fig. 2). Peak 2 (fractions 8-10) contains larger vesicles, which are fragments of mitochondria and 2 to  $12 \text{ m}\mu$  diameter filaments. Particulates from peaks 3 (fractions 19-21) and 4 (fractions 23, 24) include myofibrils and collagen fibers (figs. 3 and 4). Myofibrils from peak 4 have many more elements of the sarcoplasmic tubular system ( $v^2$ ) attached than do those from peak 3 (fig. 3). These vesicles can be dispersed by treatment of the peak 4 myofibrils with deoxycholate.

Muscle homogenates and the particulate fractions (peaks 1 through 4) obtained by zonal centrifugation of whole homogenates were pelleted at  $78,000 \times g$  for 90 minutes and the pellets extracted for contractile proteins. Only extracts from whole homogenates, peak 3, peak 4, precipitated upon dilution with 10 volumes of water, indicating the presence of contractile proteins. The enzymatic and sedimentation properties of the extracted contractile proteins are summarized in tables 1 and 2.

The adenosinetriphosphatase activity of extracts of whole homogenate pellets was 0.55 to  $0.76 \text{ }\mu\text{M P}$  per mg protein per minute and was approximately doubled upon reprecipitation (table 1). The actomyosin from



TEXT-FIGURE 1.—Absorbing material (at 260  $m\mu$ ) displaced from A-XII rotor. Same separation as in figure 1. The sucrose gradient is also plotted.

TABLE 1.—Adenosinetriphosphatase enzyme activities of contractile proteins

Fraction extracted	Activity
Whole homogenate pellet	0.55 0.762 1.565*
Peak 3 pellet	0.44 0.166 0.103
Peak 4 pellet	0.403 0.470 0.702*
Peak 3 + peak 1 combined pellets	0.601 0.668 0.686 0.666
Peak 3 + peak 2 combined pellets	0.353 0.460 0.433 0.373

Samples were extracted from the  $78,000 \times g$  pellets of various peaks of muscle separated in the A-XII rotor, followed by precipitation, by dilution with water, and resuspension in concentrated salt solution. Activity is expressed in  $\mu\text{M P}$  per mg protein per minute. Medium† contained 0.05 M KCl,  $2 \times 10^{-3}$  M ATP, 5 mM  $\text{CaCl}_2$ , 0.05 M Tris at pH 8, and 0.1 mg per ml protein. Reactions were run for 2 to 3 minutes at 28° C.

\*Reprecipitated by dilution with water twice instead of once.

†The medium used for adenosinetriphosphatase measurements contained calcium but no magnesium since calcium activates maximally from pH 6.2 to 8.0, whereas magnesium becomes increasingly inhibitory with increasing pH values. Also, low ionic strength (0.05) was used because adenosinetriphosphatase activity decreases markedly with increasing ionic strength (22).

TABLE 2.—Sedimentation coefficients of contractile proteins in 0.5 M KCl, 0.01 M Tris at pH 8, 20° C. Adenosine triphosphate (ATP), when used, was 0.01 M. The contractile proteins were extracted from the 78,000  $\times g$  pellets of the various peaks of frog muscle separated in the A-XII rotor. These extracted proteins were precipitated by dilution with water and redissolved in the usual manner

Fraction	Sedimentation coefficient* of sample numbers $\times 10^{-13}$					
	0-7	7-10	10-13	13-16	16-19	19-40
Whole homogenate†			11.75	13.61‡		
Whole homogenate + ATP†	4.99‡				18.12	
Peak 3§	5.39					
	5.97‡	7.83				
	5.78					
	6.66‡	8.23				
Peak 4	5.88	6.97		15.87		
Peak 4 + ATP	5.19‡	7.25		15.77		
Peak 3 + peak 1§						30.65
Peak 3 + peak 1	4.80					33.10‡
Peak 3 + peak 1	6.56					26.93‡
Peak 3 + peak 1 + ATP	5.29‡			15.67		
Peak 3 + peak 1 + ATP	5.39‡				18.51	
Peak 3 + peak 2	5.88‡					35.94
Peak 3 + peak 2 + ATP	5.78					

\*These groupings are arbitrary, by range of  $S_{20}$ , and are not meant to show the number of possible proteins. The  $S_{20}$  of actomyosin, for example, varies with concentration and can appear in the last three columns along with those of F-actin. Myosin  $S_{20}$  values are in the first column, myosin dimers  $S_{20}$  values are in the second.

†See figure 5a.

‡Main component.

§See figure 5b.

||See figure 5c.

the whole homogenate pellet has an  $S_{20} = 13.61$  for the main component. Two components with  $S_{20} = 4.99$  and 18.12 appear upon addition of adenosine triphosphate (ATP) (table 2 and fig. 5a).

Myosin, but not actomyosin, is extracted from peak 3, even with overnight extraction. The  $\text{Ca}^{2+}$ -activated enzyme activity is only about 20 percent that of actomyosin extracted from the pellet of whole muscle homogenate (table 1). The  $S_{20}$  values in 0.5 M KCl (table 2 and fig. 5b) are from 5.39 to 6.66 for the main components. These are in the range reported for other vertebrate myosins (23-26). The  $S_{20}$  values for the minor components are within the range reported for myosin dimers (27).

The extract from peak 4 contains actomyosin. The enzyme activity is slightly lower than that of actomyosin from the whole homogenate pellet, presumably due to the myosin present (table 1). The  $S_{20}$  values of the three peaks present are in the range of those of myosin, myosin dimer, and actomyosin (table 2). Upon addition of 0.01 M ATP at pH 7, the concentration of the heavy component ( $S_{20} = 15.87$ ) diminishes and that of the lighter one ( $S_{20} = 5.19$ ) increases (table 2). After treatment of peak 4 myofibrils with deoxycholate, actomyosin is no longer extracted.

Much heavier protein components ( $S_{20} = 26$  to 33) are extracted from pellets of peak 3 when peak 1 is added before extraction (table 2, figs.

5b, c). The extracted protein reacts like actomyosin since the heavy peak disappears upon addition of ATP with the appearance of two new components having  $S_{20}$  values of 5.3 and 15.67 to 22.0 (fig. 5c). The adenosinetriphosphatase activity of the protein extracted from the combined peaks 1 and 3 is comparable to that of actomyosin extracted from whole homogenate pellets and slightly higher than that extracted from peak 4 (table 1).

A heavy actomyosin ( $S_{20} = 35.94$ ) is also extracted from the pellet of peak 3 when the pellet of peak 2 is added before extraction (table 2). However, unlike the heavy component obtained from combined peaks 1 and 3, which is the major component, the myosin peak is the major component extracted from combined peaks 2 and 3. Also, the enzyme activity (table 1) is higher than the activity of myosin and slightly lower than the activity of actomyosin, indicating a mixture of the two proteins.

The augmentation of extraction of actomyosin, instead of myosin, when the pellets from peak 1 or 2 are combined with that of peak 3 is destroyed by prior treatment of the peak 1 or 2 pellets with 3 mM deoxycholate for 5 minutes in the cold.

## DISCUSSION

A number of results suggest that actomyosin can be extracted from frog muscle myofibrils only when other particulate components are present in the extraction medium: 1) Actomyosin is extracted only from pellets of whole homogenates and the heavy myofibril fraction prepared by zonal centrifugation, both of which contain the small particles; 2) myosin alone is extracted from the pellets of the light myofibrils, which do not contain this fraction; and 3) the addition of these small particles to the light myofibril fraction results in the extraction of actomyosin.

The active components in the small particles which augment actomyosin extraction are not known. The possible involvement of the relaxing factor system (RFS) is indicated, since relaxing factor activity has been demonstrated in this fraction (28) containing vesicles similar in size and deoxycholate lability to the sarcoplasmic tubule elements of the RFS. Myosin extractibility decreased when rabbit myofibrils, separated from homogenate RFS, remained contracted after ATP depletion (29). Two well-known properties of the RFS are facilitation of dissociation of actomyosin and calcium uptake. Actomyosin extraction might, therefore, be facilitated by RFS due to a dissociation of the complex resulting in an increased solubility or extractibility of the actin molecule. This dissociation would occur in the presence of RFS and high ATP concentrations (14), and the reassociation into actomyosin would occur on standing when the ATP level was reduced by the naturally occurring adenosinetriphosphatase activity in the extracts. However, dissociation itself does not appear to be the sole mechanism involved since the ATP of the extraction medium would dissociate actomyosin at the salt con-

centrations used during extraction. No extraction was noted with ATP alone. It is possible that the particles serve to intensify the dissociation of actomyosin by ATP (30). The possible mechanism of RFS action by the removal of calcium from ATP (31) or the medium, promoting dissociation of actomyosin, also seems unlikely. The preservation of the  $\text{Ca}^{2+}$  removal activities of RFS depends on the presence of oxalate in the particle medium (10), and oxalate was not included in the medium. In addition, RFS granules do not remove appreciable calcium from myofibrils (9).

Peak 1 particles combined with light myofibrils (peak 3) result in the extraction of a "large" actomyosin with a higher sedimentation rate than the "natural" actomyosin (myosin B), which is extracted from homogenate or from peak 4. This rate change is even more than the considerable concentration effect on  $S_{20}$  noted for actomyosin by Johnson and Landolt (24). Perhaps the ratio of actin to myosin is not optimal in the "natural" actomyosin extracted from whole homogenates or from peak 4 myofibrils. The optimal combination proportions of 4 myosin to 1 of F-actin, by weight (32), may be limited by the length or branching of the actin polymers. Length or branching of F-actin may be affected when peak 1 is present during extraction.

Since peak 1 particles are in whole homogenates, similar proportions of myosin to actin should be reached. The present study suggests that the amount of actomyosin extracted depends on the particle-to-fibril ratio. The more particles, the heavier the actomyosin extracted. The relaxing effect of the granules also depends on a granule-to-fibril ratio rather than absolute concentration of granules (9).

Myosin is extracted from myofibrils independently of actin in the absence of particles. Myosin was also found more easily extracted from actomyosin pellets than actin (33). Perhaps several myosin molecules can dissociate from an actomyosin complex without changing the solubility or extractibility properties of the remaining actomyosin, which would still not be free to diffuse out. The extraction of actomyosin from myofibrils upon addition of the particles allows these possible explanations: 1) Actin is not solubilized by the usual ATP-concentrated salt extraction procedures, but is solubilized by a factor from RFS, or 2) actin is extracted from particulates different from myofibrils. The second explanation is not probable since myofibrils can subsequently undergo syneresis after exposure to deoxycholate, which disperses the particles (34). Actin is necessary for this syneresis if the system is comparable to threads prepared *in vitro*, so it must be in the myofibrils treated for the removal of other particles.

An increase of enzyme activity occurs when increasing amounts of actin are added to the same quantity of myosin *in vitro*, with a plateau of activity reached at a myosin-to-actin weight ratio of 4:1 (33, 35). If "large" actomyosin is a result of additional actin, the enzyme activity seems to have reached this plateau in "natural" actomyosin since the heavier enzyme had no more activity per mg than natural actomyosin.

The  $\text{Ca}^{2+}$  activation and  $\text{Mg}^{2+}$  inhibition of frog actomyosin at higher  $p\text{H}$  has been previously reported (22, 36, 37), in contrast to the  $\text{Mg}^{2+}$  activation of rabbit actomyosin. The decrease in adenosinetriphosphatase enzymatic activity with increasing ionic strength is similar to that for dog actomyosin and is probably due to a similar ATP dissociation of actomyosin at higher ionic strengths, leaving only myosin adenosinetriphosphatase present (35).

"Natural" actomyosin is dissociated by addition of 0.01 M ATP (without the  $\text{Mg}^{2+}$  classically used for dissociation) into two peaks that have  $S_{20}$  values different from the starting actomyosin. Previous workers (24, 38, 39) demonstrated a disappearance of the actomyosin peak and increase in the myosin but not the appearance of the second peak shown in the present studies. This second peak may be F-actin. Its  $S_{20}$  value is different from frog G-actin, which has an  $S_{20}$  of 2.84 (40). The ATP-dissociated "large" actomyosin shows the same  $S_{20}$  values for the resulting two peaks, a result suggesting that no new components in the molecule are responsible for the increase in size and weight of the "large" actomyosin. Since the  $S_{20}$  of the faster dissociation peak is smaller than the  $S_{20}$  of the original actomyosin, it cannot be just an actomyosin peak with reduced concentration.

Zonal centrifugation appears to be useful for separating myofibril preparations free from contaminating RFS. These preparations would be useful for extraction of pure myosin, which is extremely difficult to do when using whole frog muscle extracts (22, 41). The difficulty in the whole muscle extract appears to be the contamination of myofibrils with small particles and resulting actomyosin extraction. Extraction of myosin from muscles ground before and after stimulation showed no change in extractibility after activity (42). Dissociation during extraction caused by the relaxing factor particles present in all samples could have masked any solubility changes due to activity. Extractibility of myosin was decreased in muscle frozen after contraction (43).

Pure myosin has been extracted by a glycerin medium containing EDTA. However, these preparations have lost their adenosinetriphosphatase activity (22). Glycerin extraction might have inactivated the RFS needed for actomyosin extraction. The difficulty in extracting actomyosin during rigor mortis could also be due to the inactivation of the RFS, as indicated by the loss of relaxing ability.

## REFERENCES

- (1) SZENT-GYORGYI, A.: *Chemistry of Muscular Contraction*, 1st ed. New York, Academic Press Inc., 1947.
- (2) PERRY, S. V.: The chromatography of L-myosin on diethylamino-ethylcellulose. *Biochem J* 74: 94-101, 1960.
- (3) TAKAHASHI, K., HASHIMOTO, Y., and TONOMURA, Y.: Water-soluble subfraction in myosin A preparation. *J Biochem* 54: 550-552, 1963.
- (4) ENGELHARDT, W. A.: Mechanochemistry and enzymology. *In* Conference on the Chemistry of Muscular Contraction. Tokyo, Igaku Shoin Ltd., 1957.

- (5) MUSCATELLO, U., ANDERSSON-CEDERGREN, E., AZZONE, G. F., and VON DER DECKEN, A.: The sarcotubular system of frog skeletal muscle. *J Biophys Biochem Cytol* 10: 201-218, 1961.
- (6) MARSH, B. B.: The effects of adenosine triphosphate on the fiber volume of a muscle homogenate. *Biochim Biophys Acta*: 247-260, 1952.
- (7) PORTZEHL, H.: Die Bindung des Erschlaffungsfaktors von Marsh an die Muskelgrana. *Biochim Biophys Acta* 26: 373-377, 1957.
- (8) EBASHI, S.: A granule-bound relaxation factor in skeletal muscle. *Arch Biochem* 76: 410-423, 1958.
- (9) NAGAI, T., MAKINOSE, M., and HASSELBACH, W.: Der physiologische Erschlaffungsfaktor und die Muskelgrana. *Biochim Biophys Acta* 43: 223-238, 1960.
- (10) EBASHI, S., and LIPMANN, F.: Adenosine triphosphate-linked concentration of calcium ions in a particulate fraction of rabbit muscle. *J Cell Biol* 14: 389-400, 1962.
- (11) BRIGGS, N. G., and PORTZEHL, H.: The influence of relaxing factor on the pH dependence of the contraction of muscle models. *Biochim Biophys Acta* 24: 482-488, 1957.
- (12) MAKINOSE, M., and HASSELBACH, W.: Die Abhängigkeit der Granawirkung von der Art des Aktomyosinsystems und Gergely's Cofaktor. *Biochim Biophys Acta* 43: 239-248, 1960.
- (13) PARKER, C. J., JR., and GERGELY, J.: Soluble relaxing factor from muscle. *J Biol Chem* 235: 3449-3453, 1960.
- (14) BARANY, M., and JAISLE, F.: Kontraktionszyklus und Interaktion zwischen Aktin und L-Myosin unter der Wirkung spezifischer Interaktions-inhibitoren. *Biochim Biophys Acta* 41: 192-203, 1960.
- (15) PERRY, S. V., and GREY, T. C.: A study of the effects of substrate concentration and certain relaxing factors on the magnesium-activated myofibrillar adenosine triphosphatase. *Biochem J* 64: 184-192, 1956.
- (16) PERRY, S. V., and ZYDOWO, M.: The nature of the extra protein fraction from myofibrils of striated muscle. *Biochem J* 71: 220-228, 1959.
- (17) MUSCATELLO, U., ANDERSSON-CEDERGREN, E., and AZZONE, G. F.: The mechanism of muscle-fiber relaxation adenosine triphosphatase and relaxing activity of the sarcotubular system. *Biochim Biophys Acta* 63: 55-74, 1962.
- (18) ANDERSON, N. G., and BURGER, C. L.: Separation of cell components in the zonal ultracentrifuge. *Science* 136: 646-648, 1962.
- (19) ANDERSON, N. G., BARRINGER, H. P., CHO, N., NUNLEY, C. E., BABELAY, E. F., CANNING, R. E., and RANKIN, C. T., JR.: The development of low-speed "A" series zonal rotors. *Nat Cancer Inst Monogr* 21: 113-136, 1966.
- (20) NANNINGA, L. B.: Investigation on the effect of calcium ions on the splitting of ATP by myosin. *Biochim Biophys Acta* 36: 191-202, 1959.
- (21) LOWRY, O. H., ROSEBROUGH, N. J., FARR, A. L., and RANDALL, R. J.: Protein measurement with the Folin phenol reagent. *J Biol Chem* 193: 265-275, 1951.
- (22) BARBER, M. L.: Characterization of adult muscle proteins and of related proteins during development in *Rana pipiens*. Ph.D. dissertation, University of California, Los Angeles, 1962.
- (23) VON HIPPLE, P. H., GELLERT, M. F., and MORALES, M. F.: Some physical enzymatic phenomena in solutions of myosin B. *In* Conference on the Chemistry of Muscular Contraction. Tokyo, Igaku Shoin Ltd., 1957.
- (24) JOHNSON, R., and LANDOLT, R.: Muscle proteins and their interaction with adenosine triphosphate. *Nature (London)* 165: 430-432, 1950.
- (25) MOMMAERTS, W. F. H. M., and PARRISH, R. G.: Studies on myosin II. Some molecular-kinetic data. *J Biol Chem* 209: 901-903, 1954.
- (26) HOLTZER, A., and LOWEY, S.: The molecular weight, size and shape of the myosin molecule. *J Amer Chem Soc* 81: 1370-1377, 1959.

- (27) LOWEY, S., and HOLTZER, A.: The aggregation of myosin. *J Amer Chem Soc* 81: 1378-1383, 1959.
- (28) SCHUEL, H., LORAND, L., SCHUEL, R., and ANDERSON, N. G.: Isolation of relaxing particles from rat skeletal muscles in zonal centrifuges. *J Gen Physiol* 48: 737-752, 1965.
- (29) MOMMAERTS, W. F. H. M., and MILLER, C. H.: Role of relaxation factor in determining extractibility of myosin. *Fed Proc* 13: 266, 1954.
- (30) HASSELBACH, W.: Relaxing factor and the relaxation of muscle. *Prog Biophys Molec Biol* 14: 167-222, 1964.
- (31) SEIDEL, J. C., and GERGELY, J.: Concerning the existence of a soluble muscle relaxing substance. *Abstr 8th Ann Mtg Biophys Soc., Chicago, Abstract Fe7*, 1964.
- (32) GERGELY, J., and KOHLER, H.: Light scattering studies on the stepwise formation and dissociation of actomyosin. *In Conference on the Chemistry of Muscular Contraction*. Tokyo, Igaku Shoin Ltd., 1957.
- (33) MARUYAMA, K., and GERGELY, J.: Interaction of actomyosin with adenosine triphosphate at low ionic strength. *J Biol Chem* 237: 1095-1106, 1962.
- (34) BRIGGS, F. N., and FUCHS, F.: The nature of the muscle-relaxing factor. I. An improved assay system. *J Gen Physiol* 46: 883-891, 1963.
- (35) HASSELBACH, W.: Die Umwandlung von Aktomyosin—ATPase in L-Myosin-ATPase durch Aktivatoren und die resultierenden Aktivierungseffekte. *Z Naturforschung* 7B: 163-174, 1951.
- (36) DE VILLAFRANCA, G. W.: Frog myofibrillar adenosine triphosphatase activity. *Comp Biochem Physiol* 13: 87-95, 1964.
- (37) NASS, M. M. K.: Developmental changes in frog actomyosin characteristics. *Develop Biol* 4: 289-320, 1962.
- (38) MOMMAERTS, W. F. H. M.: Does adenosinetriphosphate cause a contraction or a disaggregation of dissolved actomyosin? *Exp Cell Res* 2: 133-136, 1951.
- (39) WEBER, A.: The ultracentrifugal separation of L-myosin and actin in an actomyosin sol under the influence of ATP. *Biochim Biophys Acta* 19: 345-351, 1956.
- (40) CARSTEN, M. E., and KATZ, A. M.: Actin: A comparative study. *Biochim Biophys Acta* 90: 534-541, 1964.
- (41) DE VILLAFRANCA, G. W., and HOCHGRAF, H. L.: Adenosine triphosphatase activity of frog myosin B. *Comp Biochem Physiol* 6: 147-163, 1962.
- (42) SERAYDARIAN, M. W., ABBOTT, B. C., and WILLIAMS, E. G.: Studies on the frog's sartorius at different stages of activity. *Biochim Biophys Acta* 46: 355-363, 1961.
- (43) DUBUISSON, M., and JACOB, J.: L'électrophorèse des protéines des muscles striés, normaux et fatigués, de la grenouille. *Rev Canad Biol* 4: 426-451, 1945.

## PLATES



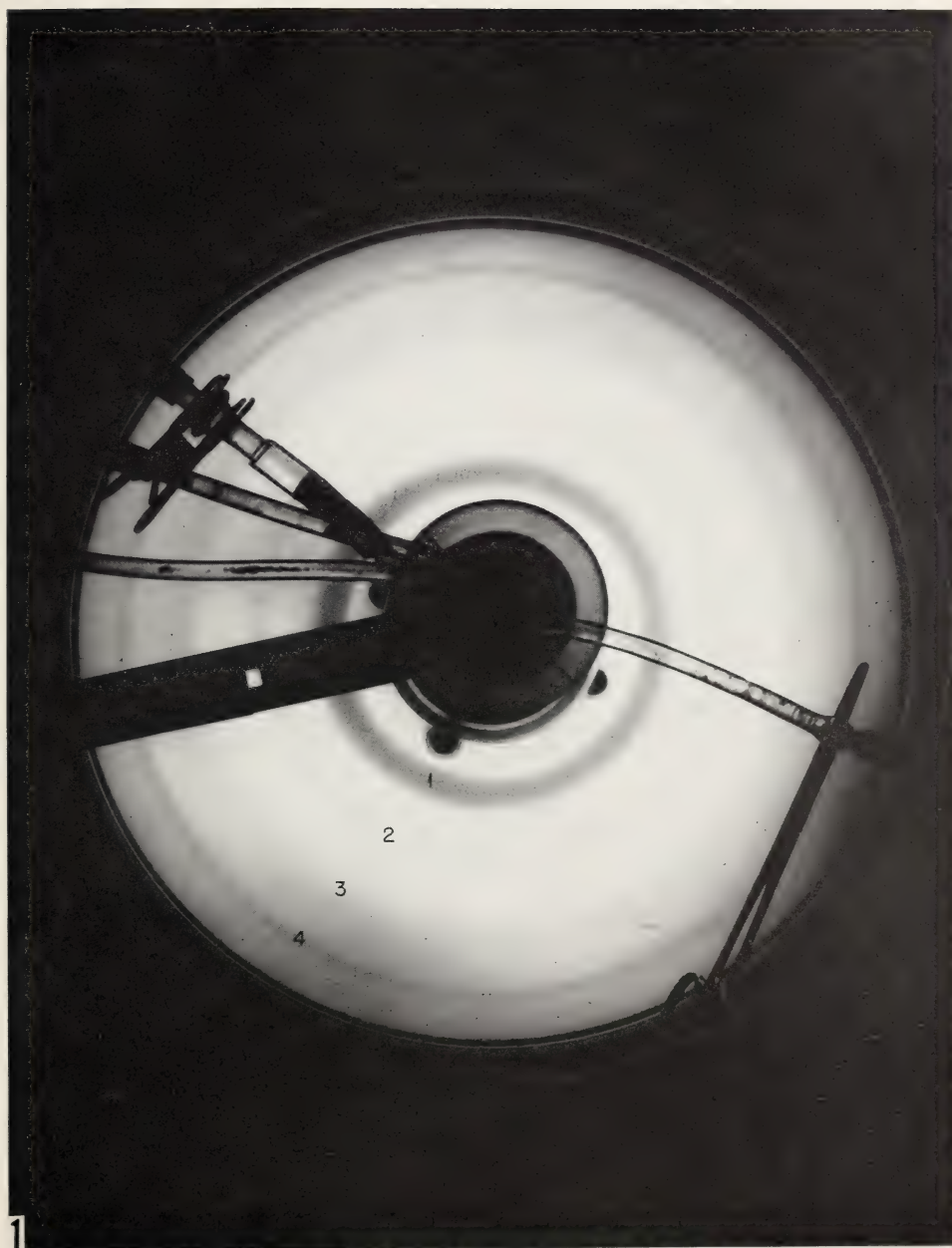


FIGURE 1.—A-XII rotor as seen from above with bands from a muscle homogenate (1/4/65) after 4 minutes at 1600 rpm plus 6 minutes at 2000 rpm. Band numbers correspond to those in text-figure 1.

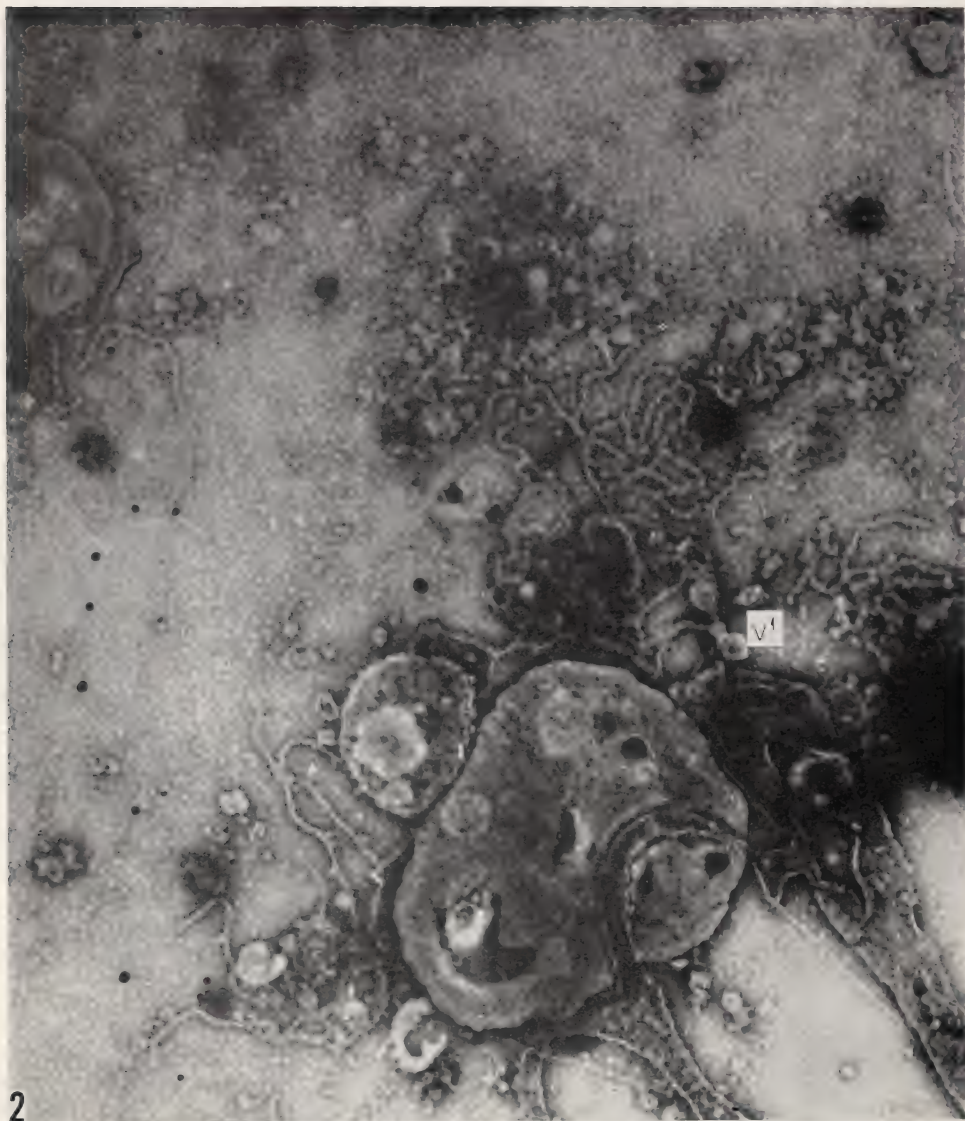


FIGURE 2.—Representative field of particulate material from peak 1 which makes possible actin extraction from peak 3 myofibrils.  $\times 50,000$ . Placed directly on carbon-coated grid and negatively stained with phosphotungstic acid. Note vesicles ( $v^1$ ).

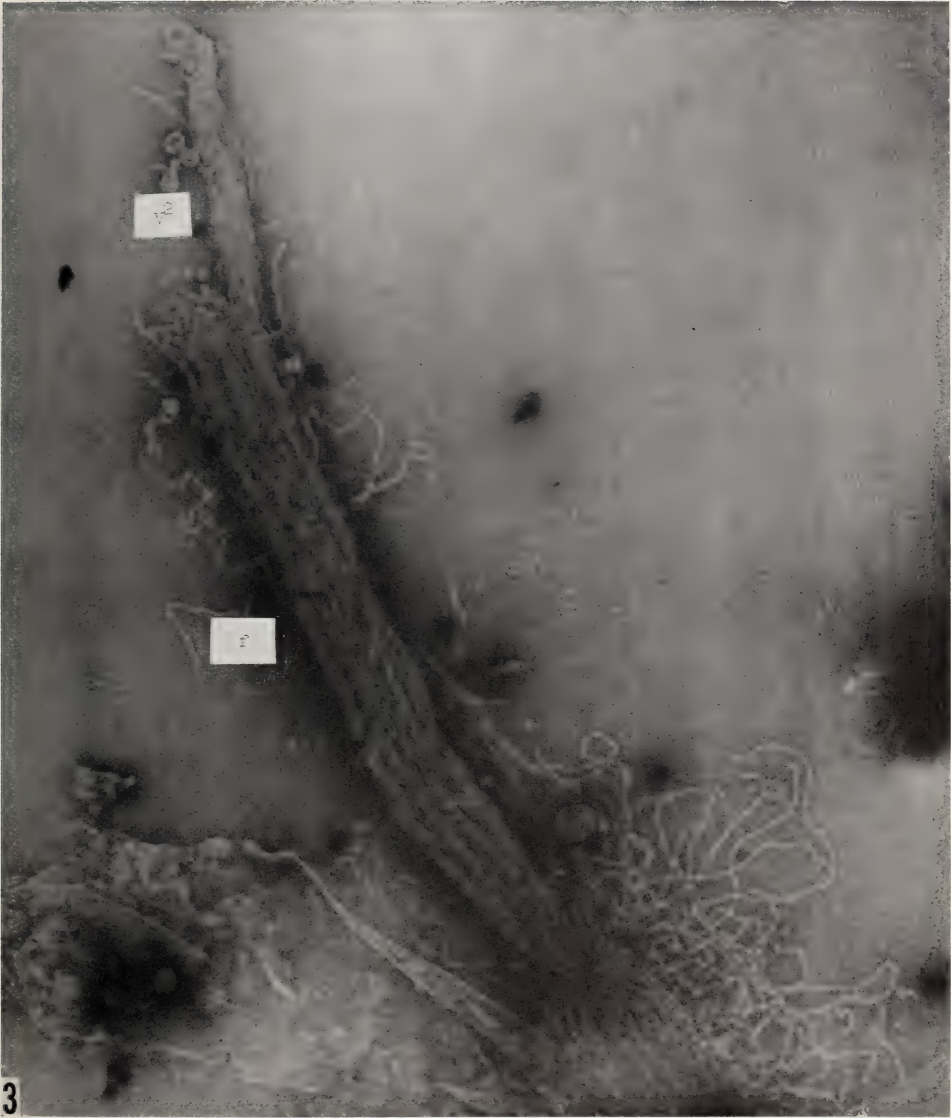


FIGURE 3.—Representative electron micrograph of particulate material from peak 3. Note myofibril (300 m $\mu$ ), vesicles (v<sup>2</sup>) (100 to 130 m $\mu$ ) and myofilaments (f) (12 to 20 m $\mu$ ).  $\times$  50,000. Same conditions as figure 2.

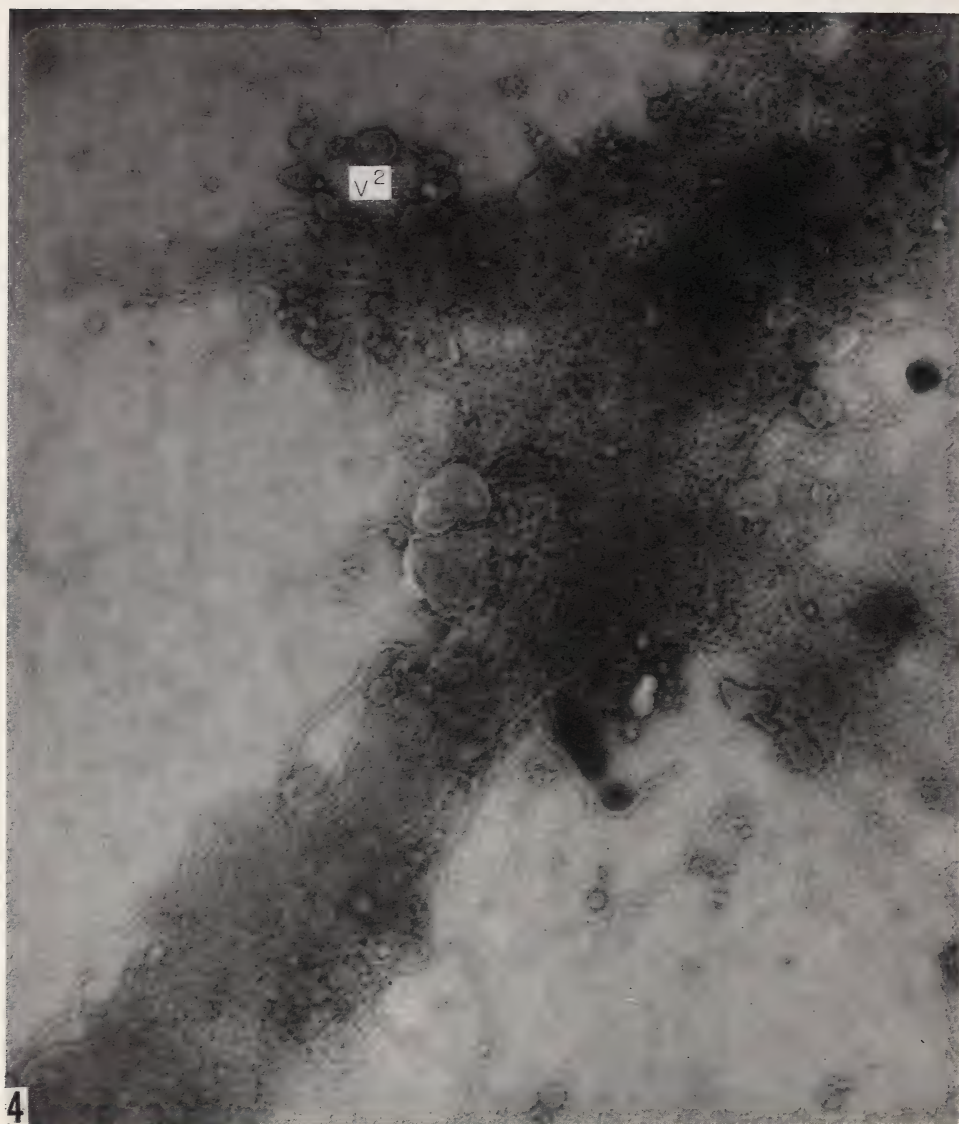


FIGURE 4.—Representative electron micrograph of material from peak 4. *Note* myofibril (660 m $\mu$ ) and vesicle (v<sup>2</sup>).  $\times 50,000$ . Same conditions as figure 2.

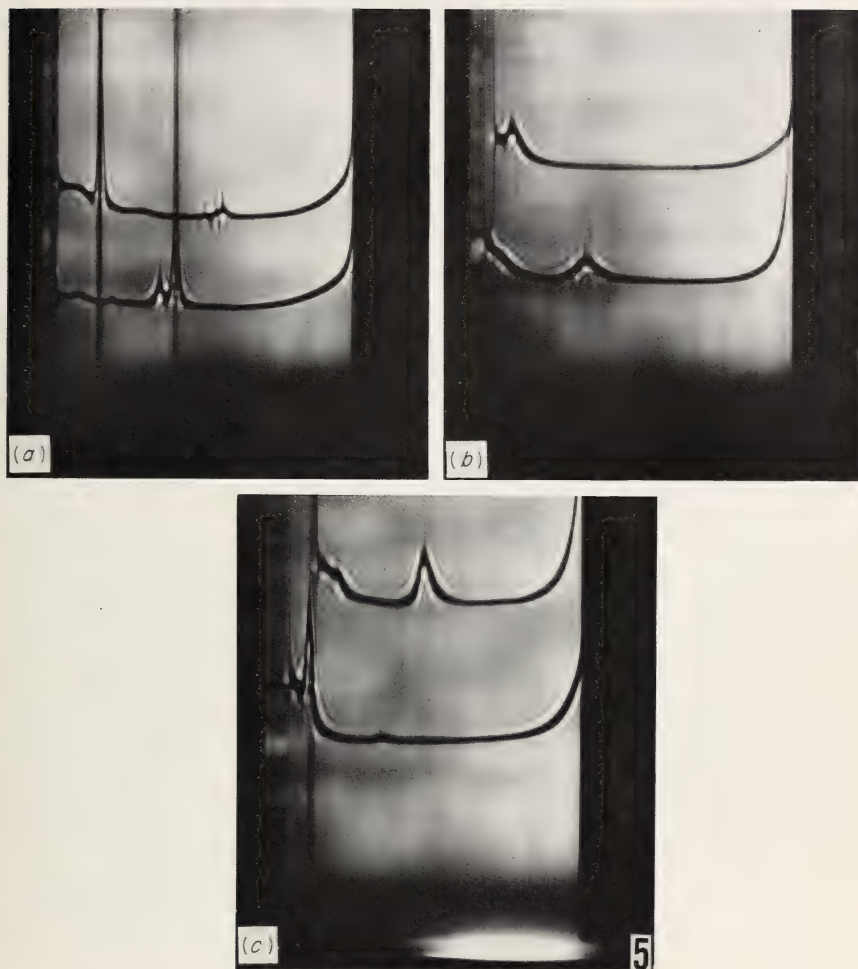


FIGURE 5.—Sedimentation patterns of actomyosin and contractile proteins. (a) Actomyosin (*lower*), with  $S_{20} = 11.75$  and  $13.61$  and actomyosin in  $0.01$  M ATP (*upper*) with  $S_{20} = 4.99$  and  $18.12$ . Actomyosin was extracted from whole homogenate pellet, precipitated twice, and redissolved in  $0.5$  M KCl, and  $0.01$  M Tris at pH 8. Centrifugation was done at  $59,780$  rpm,  $20^\circ$  C, and 24 minutes. Protein concentration was  $3.42$  mg per ml. (b) Contractile proteins. The *upper* pattern ( $S_{20} = 5.39$ ) is protein extracted from peak 3 ( $1$  mg/ml). The *lower* pattern ( $S_{20} = 30.65$ ) is protein extracted from peak 3 together with peak 1 ( $2.15$  mg/ml). Proteins were in  $0.5$  M KCl,  $0.01$  M Tris at pH 8. Centrifuged at  $59,780$  rpm at  $20^\circ$  C for 8 minutes. (c) Contractile proteins. The *upper* pattern ( $S_{20} = 6.56$  and  $26.93$ ) is from protein extracted from peak 3 + peak 1. The *lower* pattern is from the same extract as the *lower* pattern of figure 6 (peak 3 + peak 1) but after addition of ATP ( $S_{20} = 5.29$  and  $15.69$ ). Same conditions as b, after 8 minutes.



## Polysomes From *Tetrahymena* Following Pyrimidine Deprivation and Replacement<sup>1</sup>

I. L. CAMERON, G. B. CLINE, G. M. PADILLA, O. L. MILLER, JR., and P. A. VAN DREAL, *Biology Division, Oak Ridge National Laboratory, <sup>2</sup> Oak Ridge, Tennessee*

### SUMMARY

Polysomes from indole-lysed suspensions of the logarithmically growing ciliated protozoans *Tetrahymena pyriformis* were successfully separated on sucrose gradients in the zonal ultracentrifuge. After the centrifugal run ( $G_0=10^{11}$ ), the effluent stream from the spinning rotor reveals peaks of 260 m $\mu$  ultraviolet-absorbing material. The profile of 260 m $\mu$  ultraviolet absorbance shows a "fraction of low S components" followed by peaks of computed sedimentation coefficients of 72, 117, 148, 186, 203 S units. This is followed by an isopycnic so-called "membrane fraction." The macronuclei are not ruptured during indole lysing and during centrifugation pass through the sucrose gradient to the rotor wall. Electron micrographs confirm the polyosomal nature of the isolated particles.

Nongrowing (72-hour pyrimidine-starved) cells show overlapping of the polysome peaks. Forty minutes after replacement of the required pyrimidines the cells show an increase in ultraviolet-absorbing material near the "membrane fraction." Labeling of growing and nongrowing cells with C<sup>14</sup>-leucine for a brief time (10 minutes) leads to greater incorporation of radioactivity into polysomes than into the monosomic particles. The lack of P<sup>32</sup> incorporation into monosomes shows that there are few or no ribosomes formed and transferred to the cytoplasm in a 20-minute exposure interval. These findings are taken as an indication of *in vivo* involvement of polysomes in protein synthesis.—*Nat Cancer Inst Monogr* 21: 361-371, 1966.

A TEMPORAL PATTERN of cellular responses has emerged from studies of unbalanced growth in microorganisms. This pattern shows a rapid increase in cellular RNA after a shift from a poor nutrient medium to a rich medium; protein synthesis follows, then DNA synthesis, and finally cell division. *Tetrahymena pyriformis* appear to follow this same pattern of events (1, 2), and it is important to know if and how polyribosomes (polysomes) are involved in this adaptive process.

Although ribosomes from *Tetrahymena* have been isolated and studied

<sup>1</sup> This research performed under the Joint National Institutes of Health-Atomic Energy Commission Zonal Centrifuge Development Program which is supported by the National Cancer Institute, the National Institute of Allergy and Infectious Diseases, and the U.S. Atomic Energy Commission.

<sup>2</sup> Operated for the U.S. Atomic Energy Commission by Union Carbide Corporation.

(3-6), the isolation and separation of polysomes have apparently not been accomplished.

Two new developments suggested the possibility of isolating and studying the polysomes from *Tetrahymena*. 1) Lyttleton has shown that ribosomes can be gently released from *Tetrahymena* by placing the cells in a saturated indole solution. 2) The availability of the recently developed zonal ultracentrifuge by Anderson *et al.* (7-10) affords the following advantages over the conventional swinging bucket rotors: ideal sedimentation in sector-shaped compartments, large capacity, rapid gradient formation in the rotor with minimal stirring or convection, sharp starting or sample boundary, and rapid recovery of the gradient after centrifugation without loss of resolution.

This report describes the method developed for the isolation of polysomes from *Tetrahymena* and preliminary studies of the properties and functional activities of the polysomes in protein synthesis under conditions of pyrimidine deprivation.

## MATERIALS AND METHODS

*Tetrahymena pyriformis* (strain HSM) were grown at 29° C in half-liter volumes in 2.5 liter low-form culture flasks (Sargent Co.). A chemically defined medium (11), supplemented with 400 mg per liter of proteose peptone (Difco), was used (table 1). Only cultures in the exponential growth phase, at population densities of less than  $10^5$  cells per ml, were sampled for pyrimidine deprivation.

In the pyrimidine-deprivation experiments, the cells were aseptically collected by centrifugation for 2 minutes at 2000 rpm and washed 3 times

TABLE 1.—Modified medium for *Tetrahymena pyriformis*\*

Compound	Amount (mg/liter)	Compound	Amount (mg/liter)
Arginine	150.0	FeSO <sub>4</sub> ·7H <sub>2</sub> O	0.50
Histidine	110.0	CuCl <sub>2</sub> ·2H <sub>2</sub> O	0.50
Isoleucine	50.0	Riboflavin	0.10
Leucine	70.0	Ca pantothenate	0.10
Lysine	35.0	Niacin	0.10
Methionine	35.0	Folic acid	0.01
Phenylalanine	50.0	Thictic acid	0.01
Serine	90.0	Adenine	25.0
Threonine	90.0	Guanidine	25.0
Tryptophan	20.0	Cytidine	25.0
Valine	30.0	Uridine	25.0
K <sub>2</sub> HPO <sub>4</sub>	100.0		
MgSO <sub>4</sub> ·7H <sub>2</sub> O	10.0		
Zn(NO <sub>3</sub> ) <sub>2</sub> ·6H <sub>2</sub> O	5.0		
Thiamine	1.0		
Pyridoxine HCl	2.0		
Glucose	1000.0		
Na acetate	1000.0		
Cholesterol	1.0		

\*Modified from Elliott, Brownell, and Gross, 1954 (11).

with sterile medium, which lacked both the pyrimidines and the proteose peptone. The cells were resuspended in a half liter of this incomplete medium for 48 hours, then another half liter of incomplete medium was added and the culture maintained for another 24 hours (total of 72 hours). This period of deprivation gradually brings the cells to a nongrowing, but viable and mobile state (1, 2, 12). For regrowth the required pyrimidines and the proteose peptone are added to a final concentration equaling that of the complete medium. Prior studies have shown that refeeding with exogenous pyrimidines permits the cells to increase RNA synthesis almost immediately; however, an increase in protein synthesis does not begin until 60 to 90 minutes after pyrimidine replacement (1, 2). No dividing cells are found until 6 hours after refeeding (1, 2).

Starved and control cells from 1 liter cultures were concentrated to a 40 ml volume by a 2-minute centrifugation (2000 rpm) in a custom-made, large-capacity, hollow angle-head rotor. After a single washing with sterile medium (lacking pyrimidines and proteose peptone for the starved cells), the cells were resuspended in 20 ml volumes of the same medium and maintained at 27°C. In the regrowth experiment, cells were harvested 40 minutes after refeeding. The cells were labeled for 20 minutes with 0.175 mc per ml of  $P^{32}$ -orthophosphate (sp. act. 30 c/mm, Oak Ridge National Laboratory) and for the last 10 minutes with 100  $\mu$ c per ml of  $C^{14}$ -L-leucine (sp. act. 198 mc/mm, New England Nuclear Corp.). The number of cells subjected to lysing in each experiment, shown in text-figure 1, respectively, from top to bottom were:  $41.3 \times 10^6$ ,  $56.9 \times 10^6$ , and  $57.1 \times 10^6$  cells. Cell counts were measured with the model B Coulter counter.

After labeling, the cells were harvested by centrifugation at 2000 rpm, washed once with growth medium, and repelleted, yielding approximately 1 ml of packed cells. Resuspension of these packed cells in 10 ml of a buffer solution (10 mM Tris, pH 7.5) containing 0.5 mM  $MgCl_2$  and saturated with indole caused rupture of the cells within 5 minutes. Lysis was accelerated by stirring for 15 seconds with a Vortex Jr. stirrer (Scientific Industries Inc.). Phase microscopic observation of the lysate revealed complete lysis of the cells but not the nuclei.

The 10 ml suspension of broken cells was introduced into the B-IV rotor previously filled with 1728 ml of a 10 to 30 percent sucrose gradient made with 10 mM Tris buffer pH 7.5  $\times$  0.5 mM  $MgCl_2$  (10). The gradient was separated from the rotor wall with a cushion of 55 percent sucrose. Separation of the cell particulates was performed by subjecting the sample to a total force time field of  $10^{11}$  G $_o$  (roughly equivalent to centrifugation at 40,000 rpm for 2.5 hours). The temperature was maintained at 8°C throughout the centrifugation.

At the end of the run, the effluent stream from the spinning rotor was automatically and continuously monitored at 260 and 280 m $\mu$  with a Beckman DB spectrophotometer. Coincidentally, the refractive index which gave a record of the sucrose gradient profile was also monitored with a Waters Associates Model 35 H refractometer. The ultraviolet

(UV) absorption and refractive index were recorded on a Brown multipoint recorder. The effluent stream was separated into 40 ml fractions. Samples for electron microscopy from the stream fractions were deposited on carbon-coated grids, stained with uranyl acetate, and examined with a Siemens Elmiskop I. One-half ml aliquots of the fractions were suspended in scintillation solution (13) and counted for  $P^{32}$  in a dual channel Packard Tricarb Liquid Scintillation Counter. Carbon- $^{14}$  counts were similarly performed on samples of the fractions which were pelleted by overnight centrifugation at 30,000 rpm in the 40 W rotor of the Beckman Model L Spinco centrifuge.

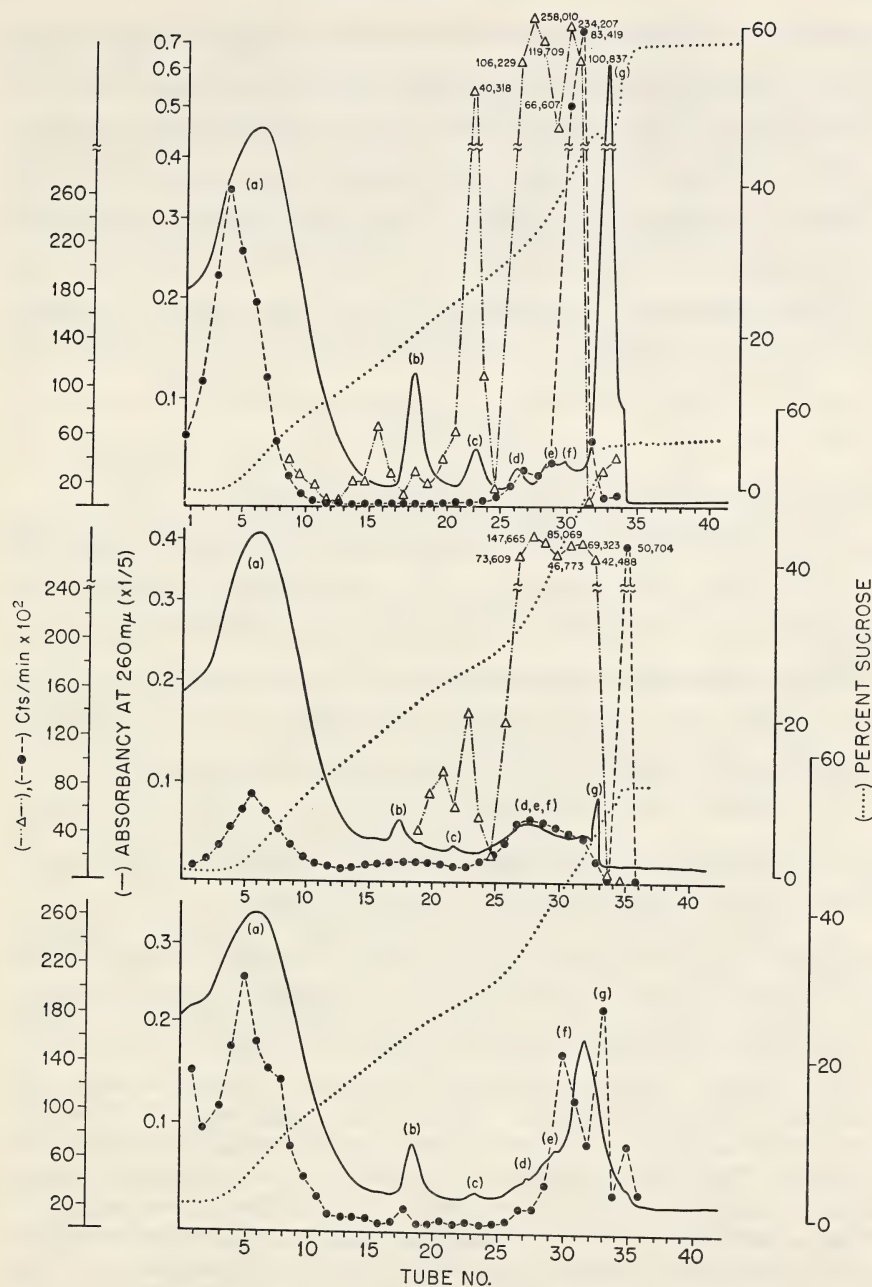
For computation of polysome sedimentation coefficients, freshly lysed *Tetrahymena* and sucrose-free pellets from the zonal centrifuge were analyzed in the Beckman Model E ultracentrifuge by Schlieren optics. These analyses were performed in 5 to 10 mM Tris buffer (pH 7.3) with 0.5 mM  $MgCl_2$  at speeds varying from 24,600 to 39,460 rpm at 20° C in different experiments. One ml of packed cells was sufficient for such analyses.

Equivalent sedimentation coefficients for the various fractions were estimated from a computer analysis based on a program especially set up for this B-IV rotor. The computer program, based on equations devised by Martin and Ames (14) for computing equivalent sedimentation coefficients,  $S^*$ , has been previously described (15).

## RESULTS

Text-figure 1, top, shows the 260  $m\mu$  UV absorbance effluent profile obtained after centrifugation of the lysed suspensions of exponentially growing cells. The initial peak *a* represents a fraction of low *S* value components and is analogous in its centrifugation behavior to the soluble materials fraction described by Anderson (7, 9). This soluble component is followed by several peaks (*b* through *g*), the last of which is isopycnic and comparable to the "membrane fraction" in rat liver homogenates (7). However, our "membrane fraction" does not actively incorporate  $C^{14}$ -leucine and thus differs from the comparable fraction of rat liver homogenate. Examination of scrapings off the rotor wall after the centrifuge run, by use of phase microscopic observation, verifies that the macronuclei and other large particulate material pass through the 55 percent sucrose cushion and move to the rotor wall.

On the basis of the Model E ultracentrifuge analysis we have found that ribosomes from indole lysates of *T. pyriformis* in 0.5 mM  $MgCl_2$  have sedimentation values of approximately 73 S and 125 S. The 125 S value is higher than might be expected if dimers were produced by the compact aggregation of monomers, but might be due to a difference in shape of true polysomal dimers. These values are slightly higher than the *S* values assigned to *Tetrahymena* ribosomes by Plesner (4, 5). If these two ribosome fractions represent monomers and dimers, they correspond to



TEXT-FIGURE 1.—Separation of the particles from a lysate of *Tetrahymena pyriformis* in the B-IV zonal ultracentrifuge rotor. The *top* graph was obtained from logarithmically growing cells, the *middle* graph from 72-hour pyrimidine-starved cells, the *bottom* graph from pyrimidine-starved cells that were refed their required pyrimidines for 40 minutes. In each run the cells were pulsed with  $P^{32}$ -orthophosphate for 20 minutes before lysing and also with  $C^{14}$ -leucine for 10 minutes prior to lysing. Counts per minute  $P^{32}$  (●—●),  $C^{14}$ -leucine (△—△).

ZONAL CENTRIFUGE

peaks *b* and *c* separated by zonal centrifugation (*cf.* text-fig. 1, top). Evidence that peaks *b* and *c* are monomer and dimer fractions that persist during unloading of the rotor is afforded by electron micrographs of these peaks (figs. 1 and 2). However, when fraction *b* is pelleted and analyzed on the Model E ultracentrifuge, two components with *S* values of 86 and 130 appear (the sedimentation values were not extrapolated to infinite dilution). Electron micrographs of this pelleted fraction confirm the change from a homogeneous (fig. 1) to a heterogeneous (fig. 5) mixture of particles.

Having determined the nominal *S* values for the monomer and dimer ribosomes, as measured by the analytical ultracentrifuge analysis, we have assigned nominal *S* values of 73 and 125 to fractions *b* and *c* from the zonal run. These *S* values are in close agreement with 72 *S*\* and 117 *S*\* values determined by use of the computer program with an assumed density of 1.6 for the monomer unit. By extrapolation, fractions *d*, *e*, and *f* have computed *S*\* values of 148, 186, and 203.

Electron micrographs (figs. 1, 2, 3, and 4) prepared directly from the effluent stream show peak *b* to constitute a homogeneous suspension of single particles, peak *c* primarily double particles, peak *d* primarily triple particles, etc. The average diameter of the monomeric particles is about 210 Å.

The inclusion of data on pyrimidine-starved cells, as well as pyrimidine-refed cells, is given only for general comparison to the logarithmically growing culture. Understanding that the findings are of preliminary nature, we wish to point out the following general observations:

The 72-hour starved *Tetrahymena* (text-fig. 1, middle) show little or no change in peak *a*, but considerable diminution in peaks *b* and *c*. The *d*, *e*, and *f* peaks are not resolved. The reason for this lack of resolution is not known. The last fraction *g* is greatly reduced.

In cells that are refed for 40 minutes (text-fig. 1, bottom), one sees no apparent change in the low *S* fraction *a* but an increase in the *b* peaks, as compared with starved cells. With the exception of the *c* peak, the UV absorbance in the polysome region (including the region *d*-*g*) increases.

Analysis of the  $P^{32}$  radioactivity distribution shows that for the log cells (text-fig. 1, top) label is found in the low *S* fraction *a* and in the polysome peaks *e* through *f* as well as in the trailing edge of fraction *g*. In the starved cells (text-fig. 1, middle), the label in the low *S* fraction is reduced. The polysome fraction is labeled, but in contrast to the log cells it lacks the discrete, high peak of radioactivity corresponding to tubes numbered 29 and 30. In addition, there is a peak of  $P^{32}$  incorporation to the right of fraction *g*, where the 260  $m\mu$  absorption is low. The major features in the distribution of  $P^{32}$  in the refed *Tetrahymena* are: 1) Fraction *a* shows a higher activity than the starved cells; 2) there may be a slight peak of incorporation corresponding to the monomer fraction *b*; 3) two peaks of radioactivity straddle the last UV peak, possibly corresponding to the *f* and *g* regions of the control cells; and 4) the last radioactive peak (found in tube No. 35 of the refed cells) appears de-

creased in magnitude when compared to the corresponding cut from the starved cells.

To determine how pyrimidine deprivation affects the incorporation of amino acids by polysomes, both the control and starved cells were labeled with  $C^{14}$ -leucine. The results of these experiments are shown in text-figure 1, top and middle portions. Two points emerge from these data: 1) The polysome peaks (*c, d, e, f*) from the control cells contain much more radioactivity per unit 260  $m\mu$  UV-absorbing material than does the monomer fraction *b*. 2) There is little radioactivity in fraction *g* of the control cells (in the starved cells the incorporation of  $C^{14}$ -leucine associated with the polysome region overlaps peak *g*; see text-fig. 1, top and middle).

## DISCUSSION

The excellent polysomal separations achieved by use of the zonal ultracentrifuge, as demonstrated in text-figure 1, top, and the electron micrographs figures 1, 2, 3, and 4, attest to the value of this machine in future work of this type.

In the pyrimidine replacement experiment (text-fig. 1, bottom), the reappearance of UV-absorbing material in the region of peak *g* is quite obvious. Just what kind of material this peak contains has not been determined.

The incorporation of  $C^{14}$ -leucine, and to a lesser extent  $P^{32}$ , into the polysome fractions is in agreement with past studies of pyrimidine-starved cells, which showed that the starved cells still actively "turn over" endogenous protein and RNA (2).

It is tempting to think that the  $P^{32}$  peak in tubes 29 and 30 of both the log and the pyrimidine-refed cells is caused by the newly synthesized messenger RNA produced under these growth conditions, but there is no direct evidence that this is RNA. Its apparent absence or diminution in the starved cells may reflect the cell's diminished production of messenger RNA under nongrowth conditions. Indeed, analysis of this  $P^{32}$  peak may be a rewarding area for future study, especially in view of the separation of different classes of polysomes afforded by zonal ultracentrifugation. Moreover, in this study we are probably dealing solely with cytoplasmic polysomes. The macronuclei are not ruptured or swollen by the lysing or centrifugation procedures employed and pass unbroken to the rotor wall. Thus the possibility of contamination of the centrifugal separations with nuclear polysomes seems unlikely. If this is the case, previous work on the fate of labeled RNA precursors in cellular components of *Tetrahymena* may have some bearing on our results. For example, at least 12 minutes elapse between introduction of labeled RNA precursors ( $H^3$ -uridine,  $H^3$ -cytidine) and their appearance in the cytoplasm (16, 17). Thus pulsing with  $P^{32}$  (used as an indicator of RNA synthesis) would not be expected to label much of the structural RNA of the ribosomes originating in the nucleus. In turn, a 10-minute

labeling with C<sup>14</sup>-leucine (used as a precursor and therefore an indicator of protein synthesis) would not be expected to contribute any appreciable label to the structural protein of such ribosomes. Therefore, the cytoplasmic C<sup>14</sup>-leucine label associated with the dimer and higher polysome fractions probably is nascent protein which is still attached to the polysomes. A higher rate of C<sup>14</sup>-leucine incorporation into the polysome fractions, as compared with the monomer fraction, lends support to the idea that this incorporation reflects protein synthesis associated with these polysomes rather than absorption of C<sup>14</sup>-leucine-labeled proteins that have already been made and released to the soluble fraction. This would be in agreement with the role assigned to these subcellular components in other systems (18-20).

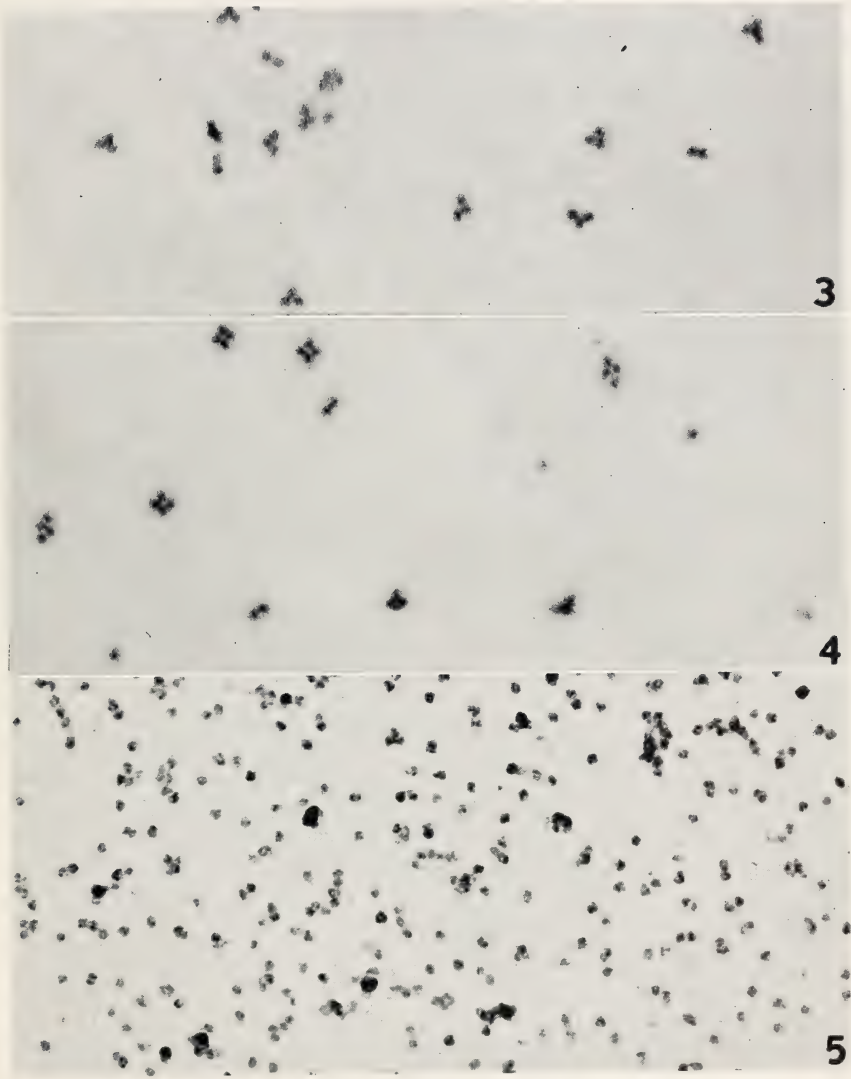
## REFERENCES

- (1) CAMERON, I. L.: Macromolecular events leading to cell division in *Tetrahymena pyriformis* after replacement of required pyrimidines. *J Cell Biol* 19: 12A, 1963.
- (2) ———: Macromolecular events leading to cell division after removal and replacement of required pyrimidine. *J Cell Biol* 25: 9-18, 1965.
- (3) LITTLETON, J. W.: A simple method of isolating ribosomes from *Tetrahymena pyriformis*. *Exp Cell Res* 31: 385-389, 1963.
- (4) PLESNER, P.: Changes in ribosome structure and function during synchronized cell division. *Sympos Quant Biol* 26: 159-162, 1961.
- (5) ———: Nucleotide metabolism and ribosomal activity during synchronized cell division. In *Symposia on Cell Growth and Cell Division*, International Society for Cell Biology (Harris, H., ed.). New York, Academic Press Inc., 1962, pp 77-91.
- (6) SCHAECHTER, M.: Bacterial polyribosomes and their participation in protein synthesis *in vivo*. *J Molec Biol* 7: 561-568, 1963.
- (7) ANDERSON, N. G.: The zonal ultracentrifuge: a new instrument for fractionating mixtures of particles. *J Physiol Chem* 66: 1984-1989, 1962.
- (8) ANDERSON, N. G., and BURGER, C. L.: Separation of cell components in the zonal ultracentrifuge. *Science* 136: 646-648, 1962.
- (9) ANDERSON, N. G.: Virus isolation in the zonal ultracentrifuge. *Nature (London)* 199: 1166-1168, 1963.
- (10) ANDERSON, N. G., BARRINGER, H. P., BABELAY, E. F., and FISHER, W. D.: The B-IV zonal ultracentrifuge. *Life Sci* 3: 667-671, 1964.
- (11) ELLIOTT, A. M., BROWNELL, L. E., and GROSS, J. A.: The use of *Tetrahymena* to evaluate the effects of gamma radiation on essential nutrilites. *J Protozool* 1: 193-199, 1954.
- (12) LEDERBERG, S., and MAZIA, D.: Protein synthesis and cell division in a pyrimidine-starved protozoan. *Exp Cell Res* 21: 590-595, 1960.
- (13) BRAY, G. A.: A simple efficient liquid scintillator for counting aqueous solutions in a liquid scintillation counter. *Anal Biochem* 1: 279-285, 1960.
- (14) MARTIN, R. G., and AMES, B. N.: A method for determining the sedimentation behavior of enzymes: application to protein mixtures. *J Biol Chem* 236: 1372-1379, 1961.
- (15) BISHOP, B. S.: Digital computation of sedimentation coefficients in zonal centrifuges. *Nat Cancer Inst Monogr* 21: 175-188, 1966.
- (16) PRESCOTT, D. M.: RNA synthesis in the nucleus and RNA transfer to the cytoplasm in *Tetrahymena pyriformis*. In *Biological Structure and Function*, II

- (Goodwin, T. W., and Lindberg, O., eds.). New York, Academic Press Inc., 1961, pp 527-536.
- (17) ———: Synthetic processes in the cell nucleus. II. Nucleic acid and protein metabolism in the macronuclei of two ciliated protozoa. *J Histochem Cytochem* 10: 145-153, 1962.
- (18) RICH, A.: Polyribosomes. *Sci Amer* 209: 44-53, 1963.
- (19) RICH, A., WARNER, J. R., and GOODMAN, H. M.: The structure and function of polyribosomes. *Sympos Quant Biol* 28: 269-285, 1963.
- (20) SCHERBAUM, O. H.: Chemical prerequisites for cell division. *In The Cell in Mitosis* (Levin, L., ed.). New York, Academic Press Inc., 1963, pp 141-147.



FIGURES 1 THROUGH 5.—Electron micrographs of zonal ultracentrifuge fractions from the *top* graph on text-figure 1: figure 1, peak *b*; figure 2, peak *c*; figure 3, peak *d*; figure 4, peak *e*; figure 5, peak *b* after pelleting and resuspension.  $\times 77,000$





## **Virus Isolation by Centrifugal Methods**



## An Evaluation of the B-V (Continuous-Flow) and B-IV (Density Gradient) Rotors by Use of Live Polio Virus <sup>1</sup>

C. B. REIMER, T. E. NEWLIN, M. L. HAVENS, and R. S. BAKER, *Lilly Research and Biological Development Laboratories, Indianapolis, Indiana*, and N. G. ANDERSON, G. B. CLINE, H. P. BARRINGER, and C. E. NUNLEY, *Biology Division, Oak Ridge National Laboratory,<sup>2</sup> and Technical Division, Oak Ridge Gaseous Diffusion Plant,<sup>2</sup> Oak Ridge, Tennessee*

### SUMMARY

The B-V (continuous-flow) and B-IV (density gradient) centrifuge rotors have been evaluated in the Spinco zonal centrifuge, using polio virus, type 3 Saukett strain. The B-V rotor can sediment live polio virus from raw tissue culture harvest fluids with 99 percent capture efficiency at flow rates up to 2.5 liters per hour. Fractions obtained had been purified more than 30-fold and concentrated more than 100-fold. Practical aspects, such as virus harvest without rotor disassembly and process

interruption, were investigated. Five-fold further purification of B-V processed live polio virus was effected by rate-zonal sedimentation in the B-IV rotor. Virus recovered in high yield after centrifugation in the B-IV rotor contained additional impurities, including polysomes. Decontamination failure was observed when virus was allowed to dry in the presence of 20 percent (w/w) sucrose in medium 199.—*Nat Cancer Inst Monogr* 21: 375-388, 1966.

THIS JOINT EFFORT, at the Lilly Research and Biological Development Laboratories in collaboration with the Oak Ridge National Laboratory, was undertaken to evaluate new centrifuge rotors and systems being developed at the Oak Ridge National Laboratory.

We desired to determine the efficiency of these systems for separating small animal viruses from the relatively large amounts of impurities commonly found in such preparations. Polio virus was chosen as a model because of its small size, our prior experience, technical facilities, and readily available supplies of live virus material.

For the B-V rotor, the following information was desired:

1. Is virus capture adequate at useful flow rates?
2. Can one efficiently harvest the concentrated virus midway in a run without rotor disassembly?
3. Is it possible to stop a centrifugation for several hours and then successfully resume centrifugation without sacrifice?

<sup>1</sup> This work was performed under a contract between Union Carbide Corporation, Nuclear Division, and the Lilly Research Laboratories, and was also jointly sponsored by the National Institutes of Health and by the U.S. Atomic Energy Commission under contract with the Union Carbide Corporation.

<sup>2</sup> Operated for the U.S. Atomic Energy Commission by Union Carbide Corporation.

We also wished to compare the performance of the B-IV rotor in separating live polio virus to that of the B-II rotor in separating inactivated polio virus (1). Finally, we wanted to know if safety precautions for virus containment were adequate.

## MATERIALS AND METHODS

*Virus.*—All experiments were performed with a single production lot of live, unfiltered, type 3 polio virus (Saukett strain), grown in Maitland tissue cultures of rhesus monkey kidney.

*Virus titration.*—Appropriate tenfold serial dilutions of each sample were prepared in medium 199 containing sodium bicarbonate buffer with neomycin the only antibiotic. One half ml of each dilution of virus, along with 1.5 ml of fresh medium, was inoculated into each of ten 8-day-old roller tube cultures of primary rhesus monkey kidney cells. Cultures were incubated at 36° C in roller drums, and examined for 4 + CPE on the 4th and 7th days. The TCID<sub>50</sub> titer of each sample was calculated on the 7th day by the method of Reed and Muench (2).

*Protein determinations.*—Protein analysis was made by the method of Lowry *et al.* (3).

*Instrumentation.*—A prototype Spinco zonal centrifuge was used for all experiments (1, 4). This instrument was modified for remote control operation by remounting the instrument panel controls and indicators in a chassis located in an adjacent room, cabling all connections back to the instrument (fig. 1). The mechanical tachometer-odometer was left in its original location. The vacuum control was relocated on the top panel for more convenient operation. This prototype instrument was further modified for 40,000 rpm operation by the temporary installation of an oil-dampened, water-cooled, upper bearing and improved seal assembly.<sup>3</sup> The B-V (continuous-flow) rotor (5-8) was an experimental rotor made at ORNL. The first B-IV (density gradient) (8, 9) run was made with an ORNL developmental rotor, other B-IV runs with a rotor obtained from the Spinco Division of Beckman Instruments Company.

The upper-bearing cooling water was recycled from a refrigerated tank held at 4° C. Generally, unless otherwise stated in this report, the operational procedures adopted were those previously described (6-8, 10). B-V runs were made at 40,000 rpm. The flow-rate of tissue culture infectious material was controlled by regulation of air pressure on the liquid surface in a sealed tank with dip tube.

A Spinco gradient-producing engine was used to form the linear density gradients used with B-IV fractionations. Specially purified, sterile solutions of 60 percent (w/w) sucrose, which had an absorbancy less than 0.25 at 260 m $\mu$  in a 10 cm cell, were used.<sup>4</sup> The 1200 ml gradient started

<sup>3</sup> These modifications are now standard for recent Spinco zonal centrifuges.

<sup>4</sup> Obtainable from Elanco Products Co., a Division of Eli Lilly and Company, Indianapolis, Ind., as Gradient Solution No. 1, Item number 1019.

with 10 percent (w/w) sucrose and ended with 30 percent (w/w) sucrose in phosphate-buffered ( $\frac{I}{2} = 0.1$ ) saline (1% NaCl) at pH 7.0 throughout. This gradient rested on an unbuffered 60 percent (w/w) sucrose underlay. Fifty ml of sample containing 3 percent (w/w) sucrose was placed on top of the gradient and overlaid by 200 ml of distilled water or phosphate-buffered saline. The rate-zonal B-IV fractionations were made either in 60 minutes at 40,000 rpm or in 90 minutes at 30,000 rpm, as indicated in the text-figures. Either 20 or 40 ml fractions were automatically collected in 50 ml vaccine vials.

The gradient was analyzed by refractometry either with a calibrated Milan Liquid Analyzer or by direct analysis of the fractions with a Bausch and Lomb Abbe Refractometer. A Cary Model 15 Recording Spectrophotometer was used to obtain absorbancy throughout the ultraviolet range with fused-silica cells up to 10 cm in path length.

Virus counts were made by a modification of Sharp's procedure, wherein virus was spun directly onto carbon films supported by 200 mesh grids, which, in turn, were supported by silicone rubber cushions in the Spinco SW-39 swinging bucket rotor. Appropriate tenfold serial dilutions of virus in 0.2 M ammonium acetate were sedimented onto these films in a stepwise procedure wherein a supernatant fluid from a prior sedimentation at a relatively slower speed of shorter duration was carefully removed and respun at a higher speed or for longer duration. Essentially all virus was collected by the following sequential centrifugations: 5000 rpm for 15 minutes; 39,000 rpm for 60 minutes; 39,000 rpm for 120 minutes. Electron micrographs ( $3\frac{1}{4} \times 4$  inches) on randomly selected fields of the platinum-shadowed films were made with a calibrated RCA-EMU-3E electron microscope with 30  $\mu$  objective aperture, using 32,000 ( $\pm 2\%$ ) electronic magnification (11).

These micrographs were optically projected onto a ruled grid for virus counting.

*Virus containment.*—Salk polio virus immunization was required for all persons involved in this experiment. The centrifuge was sealed within a walk-in, stainless-steel, dry-box ( $7.5 \times 6 \times 8$  ft) and operated by the previously mentioned remote controls and/or by rubber gloves sealed to ports (fig. 1). This dry-box contained six 30-watt germicidal ultraviolet lights. It was maintained at negative pressure (0.5 inch water) by means of a fan, which vented infectious aerosols to the outside through a flame (700° C). During fractionation, infectious samples could be introduced from or withdrawn to the outside through tubing. In the event of failure of any critical system, appropriate controls automatically seal the centrifuge room. The entire room and its contents could be sterilized overnight both before and after each run by raising the temperature in the room to 55° C and introducing 7.1 kg of a mixture of 12 percent ethylene oxide and 88 percent Freon 12 (Matheson) volatilized with a heat exchanger. The ethylene oxide concentration was monitored by infrared absorbancy at 3.3  $\mu$  by use of 10 cm cell with NaCl windows. Starting with 100 mg per

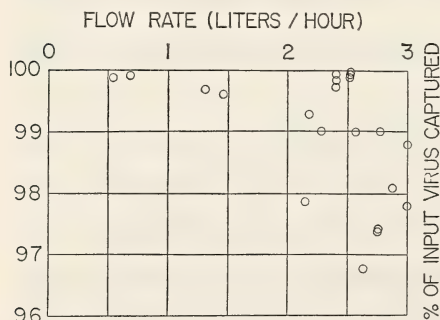
liter of ethylene oxide, the concentration generally dropped to 60 mg per liter in 20 hours.

The effectiveness of room decontamination procedures was tested for a virus spill that dried (dry spill) and for a spill which did not dry (wet spill). To test the wet spill, 5 ml aliquots of polio virus were pipetted into Falcon plastic tissue culture flasks and a loose cotton plug was inserted in the necks. The depth of fluid was 3 mm when a flask was placed on its side in the dry-box. To test the dried spill, 1 ml of polio virus in medium 199 with 20 percent sucrose was distributed as droplets in petri dishes and allowed to dry at 20° C for 20 hours before introduction to the dry-box. The room was then brought to the sterilizing condition described, and flasks or petri dishes were withdrawn at various times during sterilization. Material in flasks was titered directly and dried material in petri dishes was resuspended in 10 ml of medium 199 and titered.

## RESULTS

### B-V (Continuous-Flow) Rotor

In all, 60 liters of raw, unfiltered tissue culture polio-infected fluid were processed by this continuous-flow rotor. In text-figure 1 we have plotted the percent of input virus captured by the rotor as a function of flow rate through the system. These values are derived from titration data of randomly selected, 40 ml effluent samples. The loss of titer actually represents virus removed from the continuously flowing stream ("clean out"). The tacit assumption of this plot is that titer loss represents recoverable virus rather than virus destroyed by the process.



TEXT-FIGURE 1.—Efficiency of polio virus capture at various flow rates through the B-V (continuous-flow) rotor.

Table 1 gives the purification and concentration data of harvested fractions. The column "original virus" gives data relative to the starting material. Fraction 1 was obtained by rotor disassembly and rinse after 15 liters had been processed at a mean flow rate of 2.5 liters per hour. Fractions 2 through 7 were taken without rotor disassembly during the course of a 4-day run. During the 1st day, 10.6 liters of original virus were passed through the rotor at a mean flow rate of 3 liters per hour. Effluent titer was  $10^{-3.5}$ . At the end of the working day the sample flow

was stopped and the rotor was allowed to decelerate to zero rpm without dynamic breaking. The rotor and its contents were kept refrigerated *in situ* at 4° C overnight. The next morning the rotor was accelerated to full speed before the sample flow was resumed. The first 40 ml of effluent titered  $10^{-6.4}$ . By the time an additional 120 ml had flowed, virus concentration had dropped to  $10^{-3.6}$  in the effluent. This transient loss was inconsequential. Effluent titer remained at a low level throughout the 2d day when an additional 16.7 liters of raw fluid were passed through the rotor at an average flow rate of 2.4 liters per hour. At the close of the 2d day the rotor was again decelerated to zero rpm in the manner just described.

At the start of the 3d day, an attempt was made to harvest the virus that had accumulated on the rotor wall. To wash virus from the wall, the rotor was accelerated to 10,000 rpm and immediately decelerated to zero rpm with the brake on and with the fluid flow stopped. This process was repeated 3 more times. Fractions 2, 3, and 4 (table 1) were taken successively by discharging the turbid rotor contents through the disconnected input tube by means of air forced into the output tube with a syringe. The rotor was at rest during this harvest. Virus yield of these 3 samples accounted for one half the total virus which had been accumulated at that time. The rotor was rinsed by filling with original virus suspension (titer  $10^{-6.5}$ ) and back-flushing with air as above. Titters of 3 successive 40 ml rinses were  $10^{-7.4}$ ,  $10^{-6.8}$ , and  $10^{-6.5}$ , representing less than 1 percent of the accumulated virus.

The rotor was again accelerated to 40,000 rpm and a mean flow rate of 2.7 liters per hour resumed throughout the 3d day until an additional 13.5 liters had been processed. During the 3d day, effluent titer gradually increased from  $10^{-4.9}$  to  $10^{-5.7}$ , indicating less efficient virus retention. As before, the system was closed down at the end of the 3d day. During the 4th day, an additional 4.5 liters were processed at a mean flow rate of 3.2 liters per hour. Effluent had a mean titer of  $10^{-5.0}$ . The rotor was decelerated from 40,000 rpm to 1000 rpm with the brake on. It was then cycled between 15,000 and 1000 rpm 3 times and stopped. We were unable to pump out the rotor contents by forward flow of medium 199 at 10 lb/in<sup>2</sup> pressure because the rotor had become plugged. We successfully discharged fractions 5, 6, and 7 of table 1 by back-flush with air as previously described.

The rotor was removed from the centrifuge, opened, and the core withdrawn. We observed that three quarters of the available annular space was occluded with solid material, and that probably only one of the four radial fluid flow channels at the base of the core remained clear. This solid material was resuspended in medium 199 and constitutes fraction 8 of table 1.

Fractions 1 through 8 account for two thirds of the virus employed in this experiment.

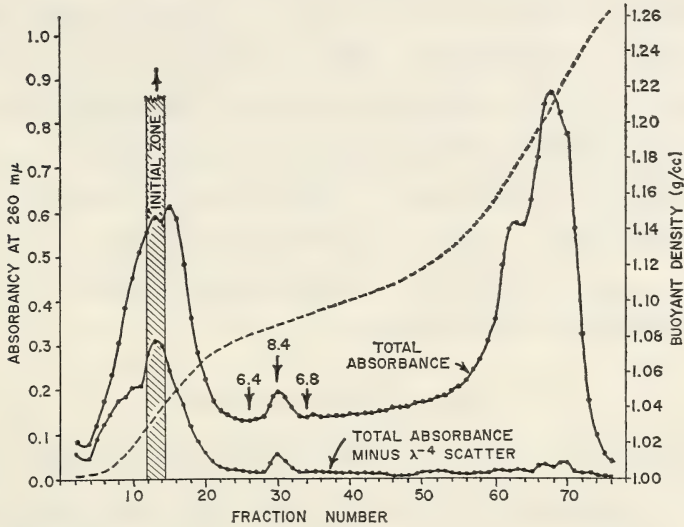
TABLE 1.—Harvested polio virus fractions from B-V centrifugation

Harvest fraction No.	Original virus	1	2	3	4	5	6	7	8
Volume (ml)	60,000	150	30	55	40	40	40	40	100
Titer—(log 10) per ml	6.5	8.6	8.4	8.6	8.4	8.2	8.4	8.6	8.2
Concentration factor (based on infectivity)									
Lowry protein (mg/ml)	1×	100×	89×	120×	88×	56×	73×	126×	51×
Specific infectivity	0.029	Not done	0.211	0.097	0.208	0.100	0.089	0.119	1.044
Specific infectivity ( $\frac{\text{infectious virus}}{\text{mg protein}}$ )	$2.13 \times 10^8$	—	$2.60 \times 10^9$	$7.68 \times 10^9$	$2.6 \times 10^9$	$3.48 \times 10^9$	$5.3 \times 10^9$	$6.55 \times 10^9$	$3.05 \times 10^8$
Purification factor (based on specific infectivity)	1×	—	12×	36×	12×	16×	24×	31×	1.4×

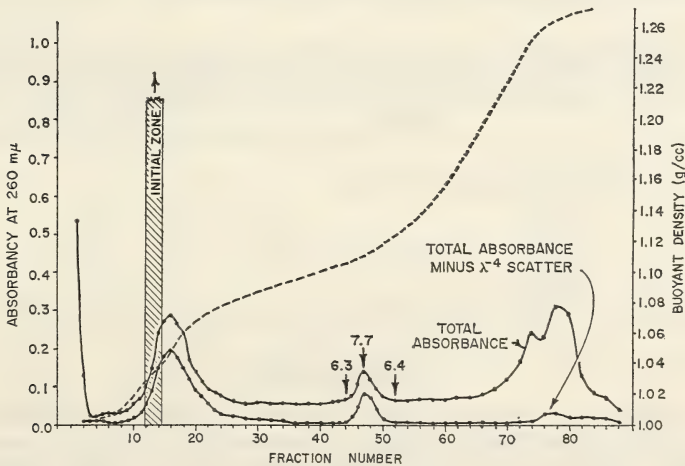
## B-IV (Density Gradient) Rotor

Text-figure 2 shows the sedimentation profile of 50 ml of fraction 1 of table 1 when spun for 90 minutes at 30,000 rpm. The infectivity peak corresponds to the 260 m $\mu$  peak at fraction 30.

Text-figure 3 shows the sedimentation profile of 50 ml of pooled fractions 3 and 7 of table 1 when spun for 60 minutes at 40,000 rpm. This



TEXT-FIGURE 2.—Sedimentation profile for 50 ml of fraction 1 of table 1: B-IV rotor, 30,000 rpm for 90 minutes. Titters in  $\log_{10}$  infectious particles per ml indicated for three 20 ml fractions.



TEXT-FIGURE 3.—Sedimentation profile for 50 ml of pooled fractions 3 and 7 of table 1: B-IV rotor, 40,000 rpm for 60 minutes. Titters in  $\log_{10}$  infectious particles per ml indicated for 3 fractions.

50 ml represents essentially all the virus but only 3 percent of the protein present in 6150 ml of raw, infectious tissue culture fluid. The infectivity peak corresponds to the 260  $m\mu$  peak at fraction 47. The additional purification achieved by the B-IV rotor is obvious (in this case, fivefold with respect to protein). Figure 2 is an electron micrograph of the starting material of the B-IV run (pooled fractions 3 and 7 of table 1) and figure 3 is an electron micrograph of fraction 47. Both micrographs were made under identical conditions for particle counting (1/100 dilution, spun onto carbon films in SW-39 rotor at 39,000 rpm for 1 hour after preclarification at 5000 rpm for 15 minutes). The B-IV purification is strikingly self-evident in these micrographs. Figure 4 shows a polysome. These structures are found occasionally in microscopic fields from fraction 47.

Electron microscopic particle counts of pooled fractions (3 and 7 of table 1) gave the value of  $10^{11.8}$  physical particles per ml. Fraction 47 had  $10^{11.6}$  physical particles per ml. On the basis of our previous experience in counting this virus, the difference probably is not significant. Fraction 47 had 22  $\mu$ g protein per ml. Virus titer of the pooled fractions (3 and 7 of table 1) was  $10^{-8.6}$ . Fraction 47 had a titer of  $10^{-7.7}$ , a statistically significant infectivity loss.

### Room Decontaminations

For the case of a wet spill, flasks containing type 2 polio virus were withdrawn at 3, 4, 6, and 12 hours. Control titer was  $10^{-7.3}$ . We were unable to demonstrate live virus in any experimental flask. Similar sterilization was also obtained with T2 bacteriophage and SV2, a Coxsackie-like simian enterovirus.

Table 2 lists our findings where virus was allowed to dry in medium 199 containing 20 percent sucrose before sterilization.

TABLE 2.—Residual titer before and after drying and after exposure to ethylene oxide in the dry state. Polio virus type 3 dried in medium 199 containing 20 percent sucrose

Sample	—Log <sub>10</sub> titer
Undried virus	6.7
Dried virus exposed to ETO for:	
0 hours	4.6
2 hours	2.2
4 hours	2.0
8 hours	1.9
20 hours	1.0

### DISCUSSION

The results with the B-V rotor, as listed in table 1, although limited, indicate that this device permits the processing of large amounts of unfiltered, relatively impure and dilute polio virus to give a concentrated and purified product in high yield. In some cases virus was concentrated more than 100-fold and purified more than 30-fold. The ability to

interrupt the process or to harvest by a simple procedure at any time during a run is a practical advantage. The process began to degenerate during the 3d day, as revealed by less efficient virus retention; this probably resulted from occlusion of the rotor with tissue debris. The occluding material (fraction 8) had a high titer but low specific infectivity, a result indicating that relatively large amounts of nonviral material were filling the rotor. This suggests the need for prefiltration of material processed by the device and possibly the need for greater hold-up volume capacity in future designs.

The two B-IV runs generally confirm earlier findings of Anderson (1) regarding the efficient purification of polio virus by zonal centrifugation. The sedimentation profile reveals the complexity of the starting material. The B-V starting material harvested by back-flush with air is relatively cleaner than is the B-V starting material harvested by terminal rotor disassembly and resuspension. This is revealed by a comparison of the profiles of our two B-IV runs. We do not know why infectious titer decreased in the second B-IV separation (text-fig. 3).

In contrast to this study, the starting material for Anderson's previous study was formalin-inactivated virus purified and concentrated by the nucleic acid method (12). The B-V purified and concentrated material had relatively less soluble, 260 m $\mu$  absorbing impurity than did the nucleic acid-purified material. The B-IV profile revealed relatively more large or dense light-scattering material than did the nucleic acid-purified vaccine.

Our inability to decontaminate the polio virus, dried in the presence of 20 percent sucrose in medium 199, with ethylene oxide is disturbing (table 2). It is probable that the virus was encapsulated within a sucrose crystal, which protected the virus from ethylene oxide. If so, it is likely that aerosolized droplets may also dry to produce infectious dusts. New equipment should be designed to permit heat sterilization of all contaminated parts.

*NOTE:* After the completion of this work, and as a result of it, the seal used for continuous-flow centrifugation was modified to include a bleed tube for removing air bubbles from the seal inlet line (13).

## REFERENCES

- (1) ANDERSON, N. G.: The zonal ultracentrifuge: A new instrument for fractionating mixtures of particles. *J Phys Chem* 66: 1984-1989, 1962.
- (2) REED, L. J., and MUENCH, H.: A simple method of estimating fifty percent end-points. *Amer J Hyg* 27: 493-497, 1938.
- (3) LOWRY, O. H., ROSEBROUGH, N. J., FARR, A. L., and RANDALL, R. J.: Protein measurement with the folin phenol reagent. *J Biol Chem* 193: 265-275, 1951.
- (4) ANDERSON, N. G., and BURGER, C. L.: Separation of cell components in the zonal ultracentrifuge. *Science* 136: 646-648, 1962.
- (5) ANDERSON, N. G.: Virus isolation in the zonal ultracentrifuge. *Nature (London)* 199: 1166-1168, 1963.

- (6) ANDERSON, N. G.: The Joint National Institutes of Health-Atomic Energy Commission, Zonal Centrifuge Development Program Semiannual Report, ORNL-3415, July 1-December 31, 1962.
- (7) ———: *Ibid.*, ORNL-3502, January 1-June 30, 1963.
- (8) ———: *Ibid.*, ORNL-3656, July 1-December 31, 1963.
- (9) ANDERSON, N. G., BARRINGER, H. P., BABELAY, E. F., and FISHER, W. D.: The B-IV zonal ultracentrifuge. *Life Sci* 3: 667-671, 1964.
- (10) ANDERSON, N. G.: The Joint National Institutes of Health-Atomic Energy Commission, Zonal Centrifuge Development Program Semiannual Report, ORNL-3752, January 1-June 30, 1964.
- (11) REIMER, C. B.: Simple gauge for obtaining pre-selected magnification with the electron microscope. *Rev Sci Inst* 33: 1126-1127, 1962.
- (12) CHARNEY, J., MACHLOWITZ, R., TYTELL, A., SAGIN, J. F., and SPICER, D. S.: The concentration and purification of poliomyelitis virus by the use of nucleic acid precipitation. *Virology* 15: 269-280, 1961.
- (13) BARRINGER, H. P., ANDERSON, N. G., and NUNLEY, C. E.: Design of the B-V continuous-flow centrifuge system. *Nat Cancer Inst Monogr* 21: 191-198, 1966.



FIGURE 1.—Control room for remote operation of zonal centrifuge.

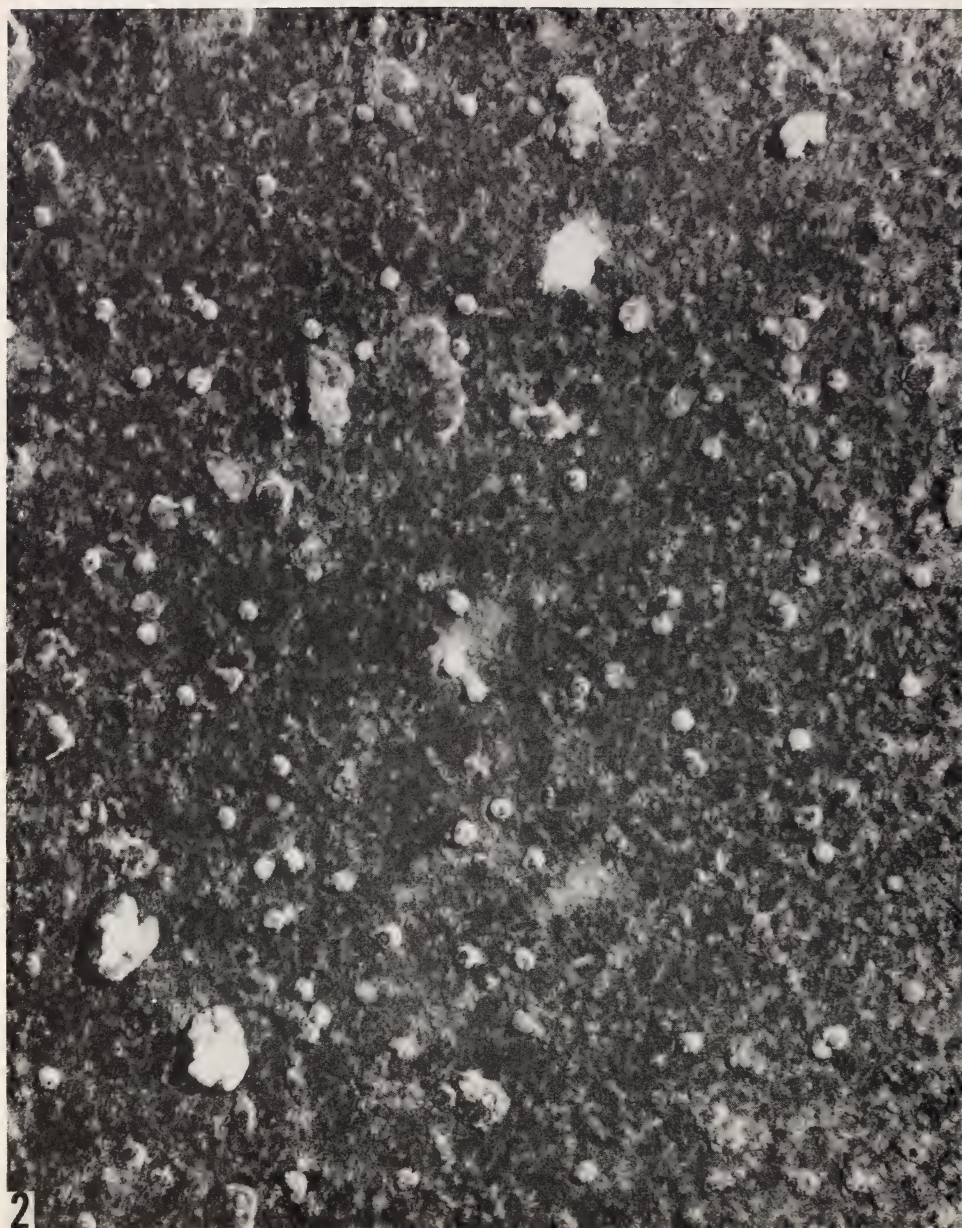


FIGURE 2.—Electron micrograph of starting material of B-IV run shown in text-figure 3. Magnification: 96,000, 1/100 dilution spun onto electron microscopic grids in SW-39 (swinging bucket) rotor at 39,000 rpm for 60 minutes, after preclarification at 5000 rpm for 15 minutes.

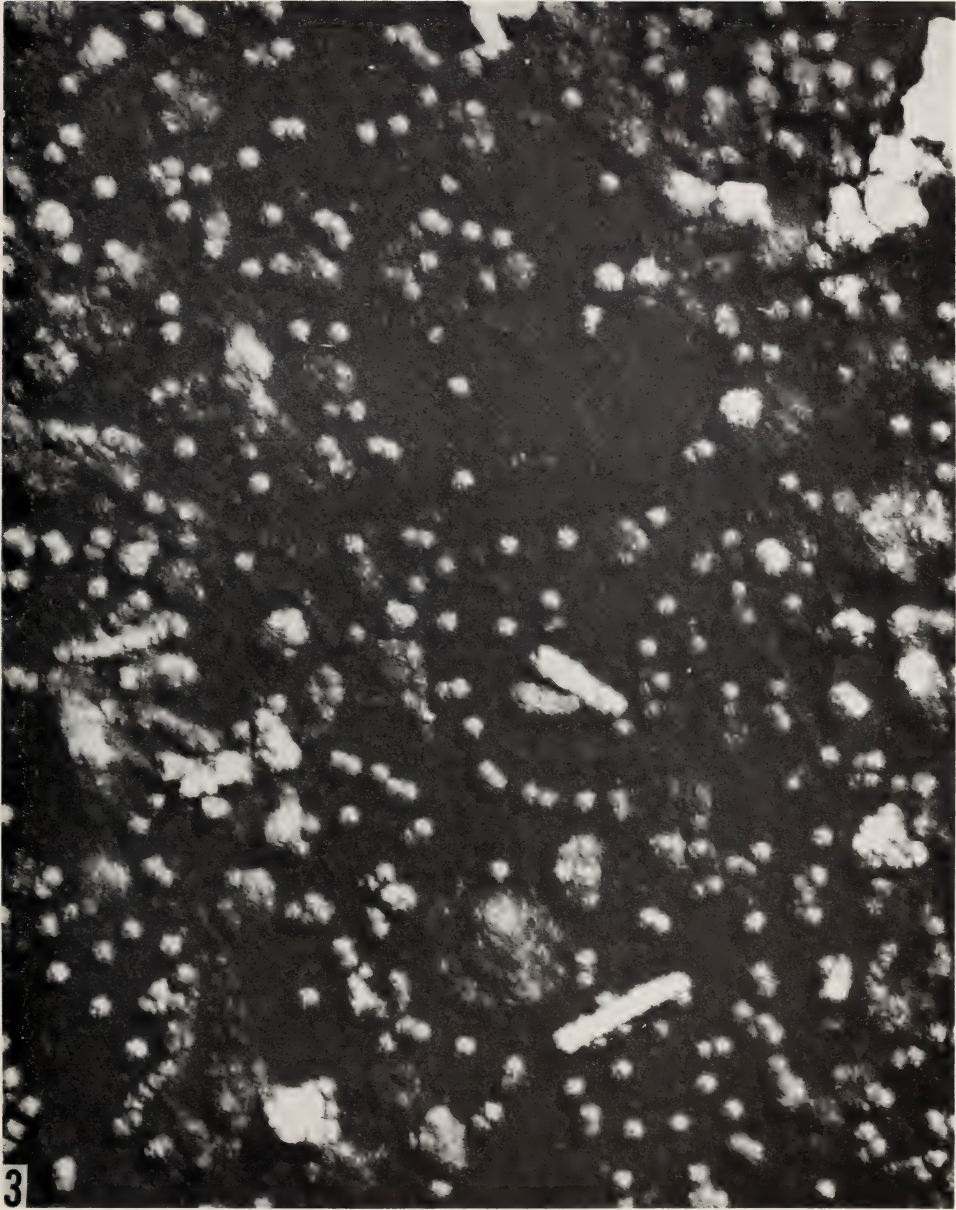


FIGURE 3.—Electron micrograph of the peak fraction 47 of the B-IV run shown in text-figure 3.  $\times 96,000$ . Same treatment as in figure 2.

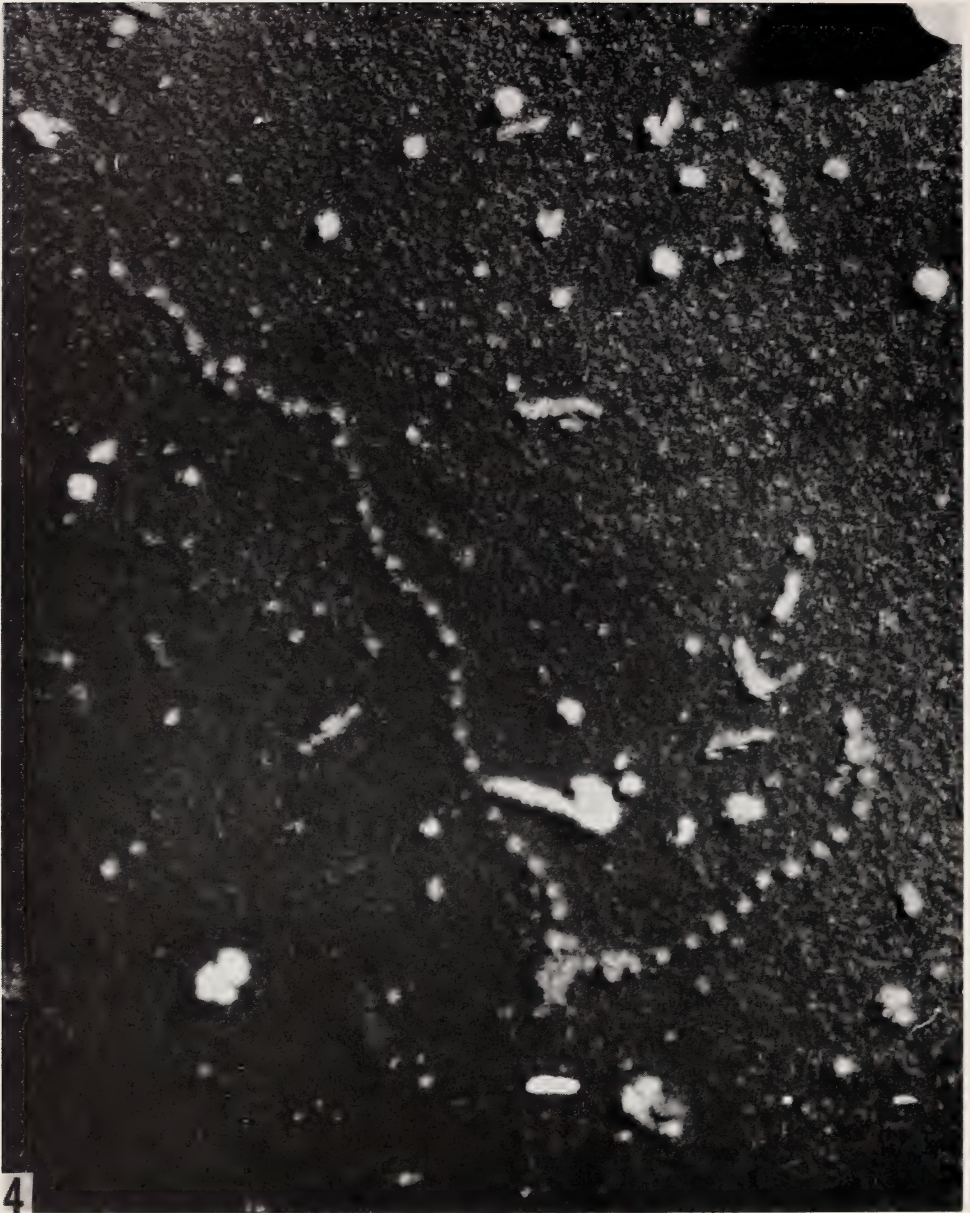


FIGURE 4.—Electron micrograph of a polysome, found in occasional fields from fraction 47.  $\times 96,000$

# Unusual Particles in Human Plasma From Leukemia and Lymphosarcoma<sup>1</sup>

W. W. HARRIS, N. G. ANDERSON, T. W. BARTLETT, ELIZABETH L. RUTENBERG, L. L. McCAULEY, and R. M. KNISELEY, *Biology Division, Oak Ridge National Laboratory,*<sup>2</sup> *Biophysical Separations Laboratory, Oak Ridge Gaseous Diffusion Plant,*<sup>2</sup> and *Oak Ridge Institute of Nuclear Studies, Oak Ridge, Tennessee*

## SUMMARY

Plasma of 2 patients out of 255 with either leukemia or lymphosarcoma yielded large numbers of 10 and 25 m $\mu$  particles in phosphotungstate negatively stained preparations. For 1 of the 2, repeated sampling over a period of

months showed continuing high particle incidence until death. The particles were unlike any found in a survey of over 300 human plasma samples.—*Nat Cancer Inst Monogr* 21: 339–394, 1966.

VIRUS-LIKE PARTICLES in human leukemic plasma, bone marrow, and lymph nodes have been reported by numerous investigators (1–9). After initial observations on particles in human plasma (6) in this laboratory, a survey of over 300 human plasma samples was undertaken. The total sample for statistical analyses was 302, of which there were 141 leukemias, 114 lymphomas, and 47 miscellaneous controls including hospital patients and normals. There were 55 chronic lymphocytic leukemias and 24 lymphocytic lymphosarcomas within the total sample. Eleven different physicians and institutions participated. Results of the large survey will be reported elsewhere.

However, during the survey, plasma of 2 patients, now deceased, showed unique particles in high concentrations which are discussed here. Diagnosing physicians reported the first, patient A, to be chronic lymphocytic leukemia, and the second, B, to be lymphocytic lymphosarcoma.

## MATERIALS AND METHODS

Patient A was under treatment in a Nashville, Tennessee, hospital, and B was a patient at the Oak Ridge Institute for Nuclear Studies, Medical Division. Sample collection was under the supervision of Dr. R. M.

<sup>1</sup> This research performed under the Joint National Institutes of Health-Atomic Energy Commission Zonal Centrifuge Development Program which is supported by the National Cancer Institute, the National Institute of Allergy and Infectious Diseases, and the U.S. Atomic Energy Commission.

<sup>2</sup> Operated for the U.S. Atomic Energy Commission by the Nuclear Division of Union Carbide Corporation.

Kniseley of the latter hospital. He supplied the following data pertaining to the two cases discussed here.

*Patient A:* F N2-T6212163

Diagnosis: F820 AMA SNDO<sup>3</sup>

Age: 44

Date onset: 3/60

Date sample: 2/64

Status: Outpatient

Local radiotherapy over 1 year before

No total body radiotherapy

Steroid therapy completed within 1 year of sample

Alkylating agents—on treatment at time of sample

No cytotoxic agents

No known virus infection

*Patient B:* F 111242

Diagnosis: 830<sup>3</sup>

Age: 41

Date onset: 1/61

Date sample: 3/64, 8/64

Status: Inpatient

No surgery or total body radiation

Radiotherapy, local over 1 year prior

Steroid treatment—on treatment at time of samples

Alkylating agents—completed over 1 year before

Antimetabolites—none

Cytotoxic agents—none

Virus infection—unknown or unclassified organism

### Sample Preparations

In patient A, plasma prepared by the originating institution from whole heparinized blood was forwarded packed in ice; plasma of patient B was prepared in this laboratory from whole heparinized blood. The clarification procedure was that of Burger *et al.* (6).

Plasma volume of each was 4 to 6 ml, prepared as follows: The plasma was placed into a Spinco No. 40 rotor tube and the tube filled with sodium citrate 0.15 M pH 6.7. The sample was centrifuged for 1 hour at 38,000 rpm in the Model L centrifuge. The brake was not used. The pellet was resuspended in 2 ml 0.15 M pH 6.7 sodium citrate buffer, transferred to a No. 30 rotor tube, brought to 27 ml with 0.15 M sodium citrate, and the tube was capped. With a Pasteur pipette, 10 ml of  $\rho = 1.66$  cesium chloride solution was added to the bottom of the tube and centrifuged for 2 hours at 24,000 rpm. The tube was photographed and the band corresponding to  $\rho = 1.24$  was withdrawn with a probe admitted through the tube cap and pumped through a gradient analyzer which plotted the refractive index of the solution. The band at  $\rho = 1.24$  was transferred to a No. 40 rotor, made to volume with 0.05 M pH 7.0 sodium citrate, and centrifuged 1 hour at 38,000 rpm. The pellet was used for electron microscopy.

<sup>3</sup> Standard Nomenclature of Diseases and Operations, American Medical Association, Fifth Edition.

### Negative Staining

The pellet was resuspended in a drop of 0.15 M sodium citrate. An aliquot of this sample was placed directly onto a Formvar-carbon coated specimen grid and stained with 1 percent phosphotungstate (PTA), pH 7.0.

## RESULTS

Particulate spherical objects were observed in negatively stained electron micrographs of plasma of the 2 patients after differential centrifugation and banding. In each sample particle size distribution was bimodal, one of 10 m $\mu$  diameter and the other 25 m $\mu$ , as shown by arrows in figure 1. The larger particles are shown at higher magnification in figure 2. No regular internal structure was observed at higher magnifications in either PTA negatively stained or uranyl acetate positively stained preparations. Rodlike structures, figure 2, were also observed in the two cases.

## DISCUSSION

Had these particles been observed only once in each of these 2 of the 302 patients examined, some preparative artifact would have been suspected, as indeed it was until samples from patient B taken over a period of several months repeatedly showed the same pattern.

Interaction of heparin and citrate was ruled out indirectly by the fact that plasma of patient B was processed within an hour after withdrawal, while that of patient A was in transit for several hours, and also by the fact that over 200 other plasma samples which did not show these particles were in transit for varying times, even up to 1 day or so. A direct test in which whole heparinized blood was allowed to stand overnight did not produce the particles.

The biochemical nature of the particles is not known. The fact of recovery in a density gradient of 1.24 eliminates heavy particles such as ferritin (10) or glycogen (11-13), nor do the particles have the proper morphology for either of these compounds. The largest of these ether-insensitive particles (25 m $\mu$ ) is smaller by almost a factor of 4 than the smallest mycoplasma elementary bodies reported by Hummeler *et al.* (14) for mycoplasma isolated from human leukemia.

Whether the particles described here are related to cell debris, virus, or mycoplasma is incidental to the fact that physical particles of unusual homogeneity of size and high incidence were observed in plasma of 2 patients of nearly the same age at onset of disease, the same sex, and who had received treatment for a leukemoid condition. These results suggest a possible source of particles for physical and biological study.

## REFERENCES

- (1) DMOCHOWSKI, L., and GRAY, C. E.: Electron microscopy of tumors of known and suspected viral etiology. *Texas Rep Biol Med* 15: 704-753, 1957.
- (2) ———: Studies on submicroscopic structure of leukemias of known or suspected viral etiology. *Blood* 13: 1017-1042, 1958.
- (3) BEARD, J. W.: Virus tumors in cancer research. *In* Stern Symposium. New York, Feb. 24-25, 1958.
- (4) BRAUNSTEINER, H., FELLINGER, K., and PAKESCH, F.: On the occurrence of virus-like bodies in human leukemia. *Blood* 15: 476-479, 1960.
- (5) ALMEIDA, J. D., HASSELBACK, R. C., and HAM, A. W.: Virus-like particles in blood of two acute leukemia patients. *Science* 142: 1487-1489, 1963.
- (6) BURGER, C. L., HARRIS, W. W., ANDERSON, N. G., BARTLETT, T. W., and KNISELEY, R. M.: Virus-like particles in human leukemic plasma. *Proc Soc Exp Biol Med* 115: 151-156, 1964.
- (7) PORTER, G. H. III, DALTON, A. J., MOLONEY, J. B., and MITCHELL, E. Z.: Association of electron-dense particles with acute human leukemia. *J Nat Cancer Inst* 33: 547-556, 1964.
- (8) SMITH, K. O., BENYESH-MELNICK, M., and FERNBACH, D. J.: Studies on human leukemia. II. Structure and quantitation of myxovirus-like particles associated with human leukemia. *J Nat Cancer Inst* 33: 557-570, 1964.
- (9) BENYESH-MELNICK, M., SMITH, K. O., and FERNBACH, D. J.: Studies on human leukemia. III. Electron microscopic findings in children with acute leukemia and in children with infectious mononucleosis. *J Nat Cancer Inst* 33: 571-579, 1964.
- (10) FARRANT, J. L.: An electron microscopic study of ferritin. *Biochim Biophys Acta* 13: 569-576, 1954.
- (11) DROCHMANS, P.: Morphologie du glycogène. Etude au microscope électronique de colorations négatives du glycogène particulaire. *J Ultrastruct Res* 6: 141-163, 1962.
- (12) BARBER, A. A., HARRIS, W. W., and ANDERSON, N. G.: Isolation of native glycogen by combined rate-zonal and isopycnic centrifugation. *Nat Cancer Inst Monogr* 21: 285-302, 1966.
- (13) BARBER, A. A., HARRIS, W. W., and PADILLA, G. M.: Studies of native glycogen isolated from synchronized *Tetrahymena pyriformis* (HSM). *J Cell Biol.* 27: 281-292, 1965.
- (14) HUMMELER, K., TOMASSINI, N., and HAYFLICH, L.: Ultrastructure of a mycoplasma (Negroni) isolated from human leukemia. *J Bact* 90: 517-523, 1965.

## PLATES



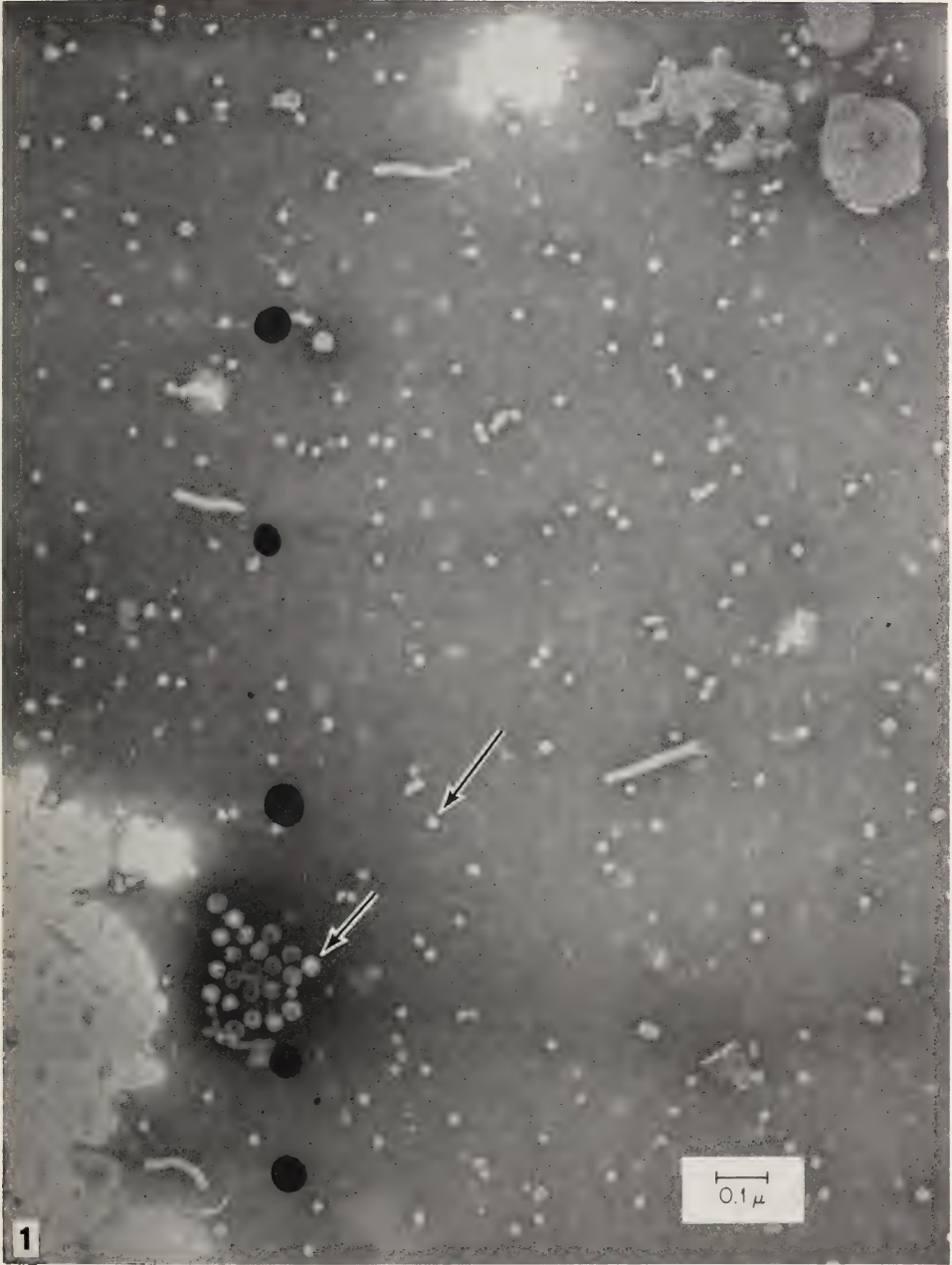


FIGURE 1.—Typical field showing 10  $\mu$  and 25  $\mu$  particles found in plasma of both patients A and B. Phosphotungstate negative stain.  $\times 80,000$

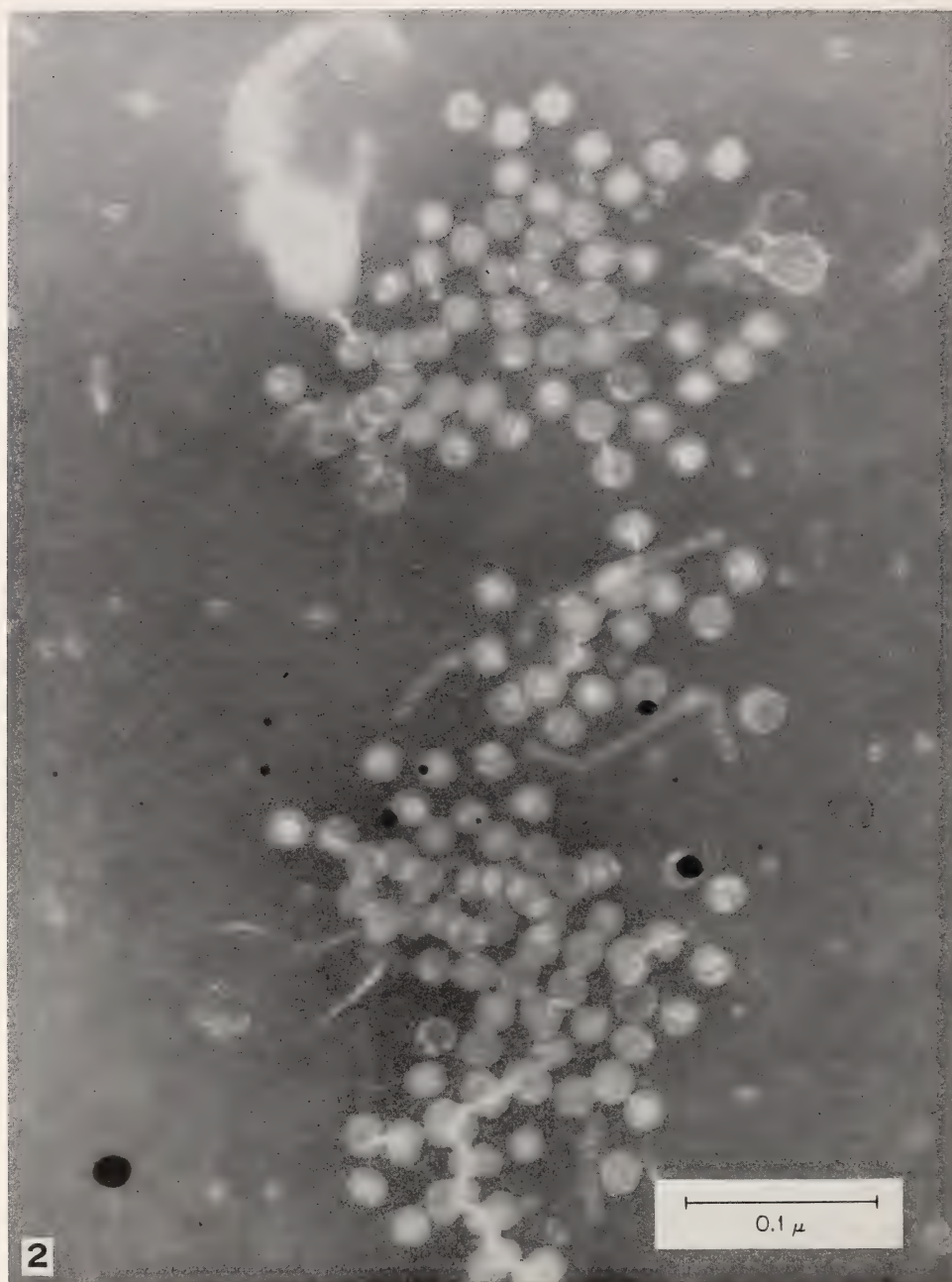


FIGURE 2.—25 m $\mu$  particles from plasma of patient with lymphocytic lymphosarcoma. Phosphotungstate negative stain.  $\times 300,000$

## **Molecular Separations in Zonal Centrifuges**



## Use of the Zonal Centrifuge to Separate Components of Ribosomal RNA<sup>1</sup>

J. R. B. HASTINGS, J. H. PARISH, K. S. KIRBY, and E. KLUCIS,<sup>2</sup> *Chester Beatty Research Institute, Institute of Cancer Research: Royal Cancer Hospital, London, England*

THE NATURE and function of ribosomal ribonucleic acid (rRNA) have been mainly studied through the isolation of the whole complex which, in general, has been shown to consist of two components of different sedimentation constants. Bacterial rRNAs have *S* values of 23 and 16, whereas mammalian sources have *S* values of 28 and 18 (1). Why these differences exist is not clear. The inability to remove all ribonucleases from most rRNA preparations presents a difficulty which has necessitated the use of a detergent (sodium dodecylsulfate) or bentonite in the gradient (2, 3).

We have recently been able to separate rRNAs that are stable to strong salt from *Escherichia coli*, from *Drosophila melanogaster* (4), and from rat liver and a hepatoma (5). These rRNAs can be centrifuged in sucrose density gradients and their components can be recovered without recourse to ribonuclease inhibitors. However, only a few milligrams of the components may be isolated by the conventional gradient on the Spinco Model L or the M.S.E. Superspeed 50 centrifuge. The zonal ultracentrifuge (6, 7) presented us with the means of separating these components in greater quantities.

The sucrose gradient used for the separation was based largely on our previous experience. Centrifugation for a 6-hour period at 40,000 rpm was found suitable for separation of the main components, but, in addition, it became clear that other components, which had been suspected from previous work, were also present.

The amount of these minor components had been too small to be isolated.

A good separation was achieved with about 40 to 80 mg material dissolved in 20 to 80 ml 0.1 M sodium acetate (pH 7), containing 2.5 percent sucrose. The sample was layered onto a linear (with radius) gradient containing 5 to 20 percent w/v sucrose and 0.1 M sodium acetate (pH 7), backed by a pad of similarly buffered 30 percent w/v sucrose.

<sup>1</sup> This investigation was supported by grants to the Chester Beatty Research Institute from the Medical Research Council, the British Empire Cancer Campaign, and by U.S. Public Health Service research grant CA-3188 from the National Cancer Institute.

<sup>2</sup> We wish to thank Dr. N. G. Anderson for making the zonal centrifuge available to the Chester Beatty Research Institute and Dr. P. Alexander for cooperation in the use of it.

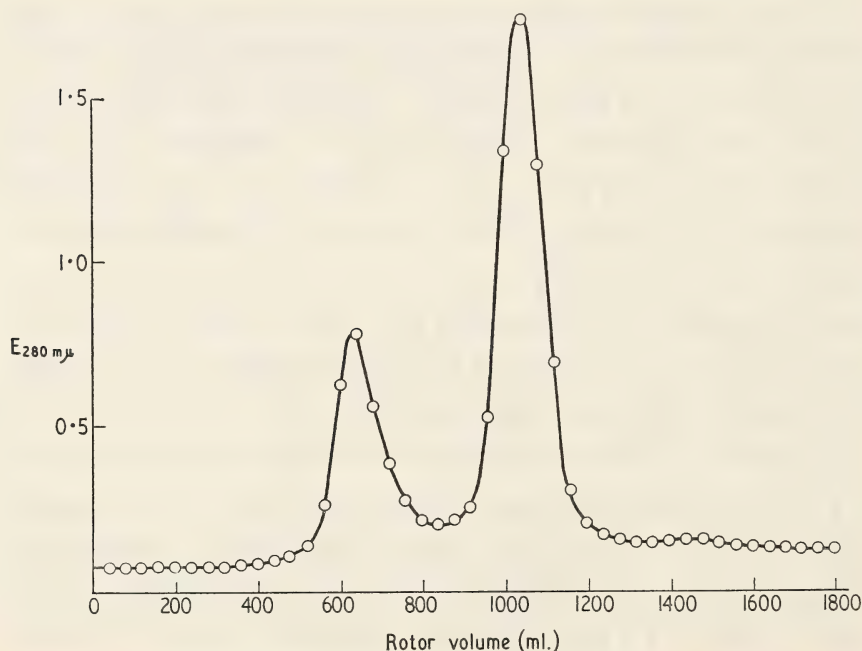
The sample was then overlaid with a small volume of buffered 1 percent w/v sucrose. After centrifugation, the gradient was displaced by 30 percent w/v sucrose introduced at the perimeter. The ultraviolet absorption of the effluent was recorded automatically and fractions of 40 ml were collected.

The separation curves for 5 separate rRNAs and a characteristic rerun of the principal fast and slow components separated from the rRNA of *E. coli* are shown in text-figures 1 through 6.

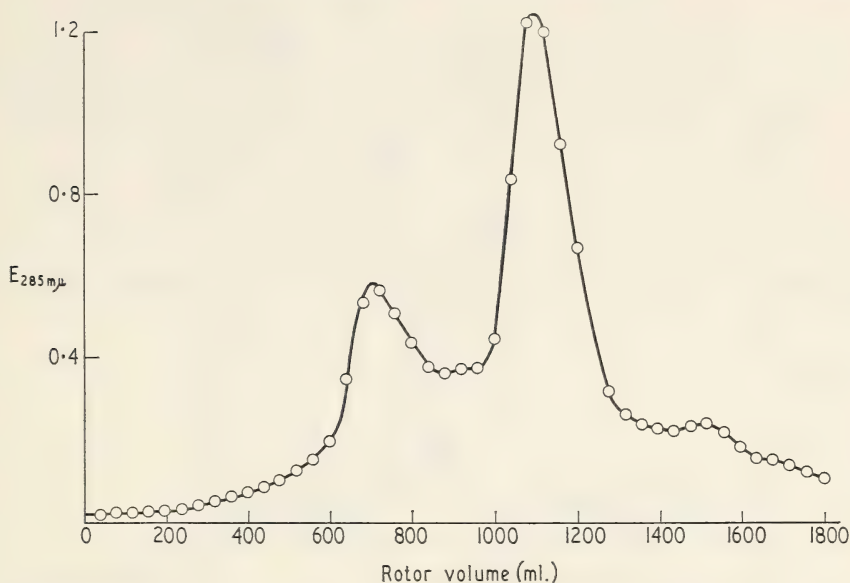
The patterns for rRNA from *Drosophila melanogaster* and from *E. coli* show an excellent separation between the two major components and the presence of a small amount of a component in *E. coli* sedimenting faster than the 23 S component. The two curves for rRNA obtained from livers of rats fed 20 and 12 percent protein, respectively, show noteworthy differences, the significance of which is under investigation.

The various components have been recovered by addition of sodium acetate and precipitation with acetone, and RNA can be thus isolated in dried form in at least a 75 percent yield from solutions containing as little as 20  $\mu$ g per ml. The curves for the 23 and 16 S components separated from *E. coli* shown in text-figure 6 indicate the purity of the fractions and the stability of the material.

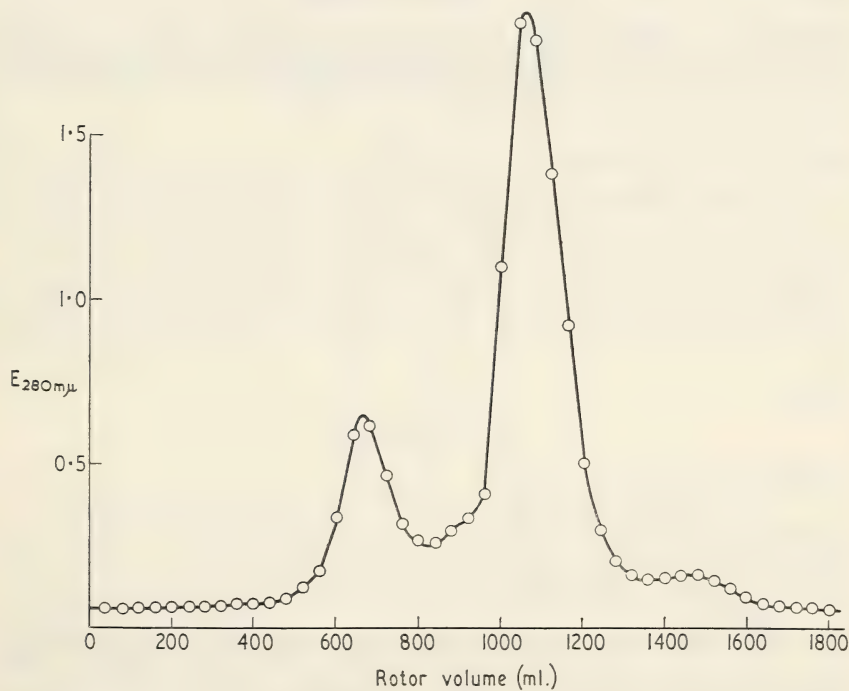
The advantages of the zonal ultracentrifuge in this work on rRNA are clear: first it is possible to accumulate larger quantities than before of



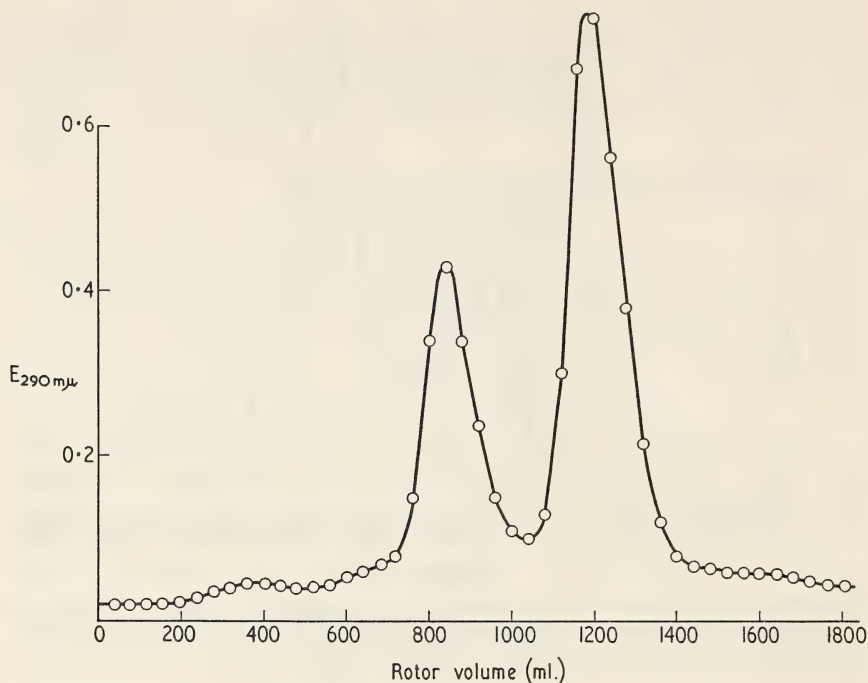
TEXT-FIGURE 1.—Ribosomal RNA from rat liver, 20 percent protein diet. 44 mg RNA dissolved initially in 40 ml 0.1 M sodium acetate pH 7, 2.5 percent w/v sucrose. Centrifuged 6 hours at 40,000 rpm, ZU B-IV rotor.



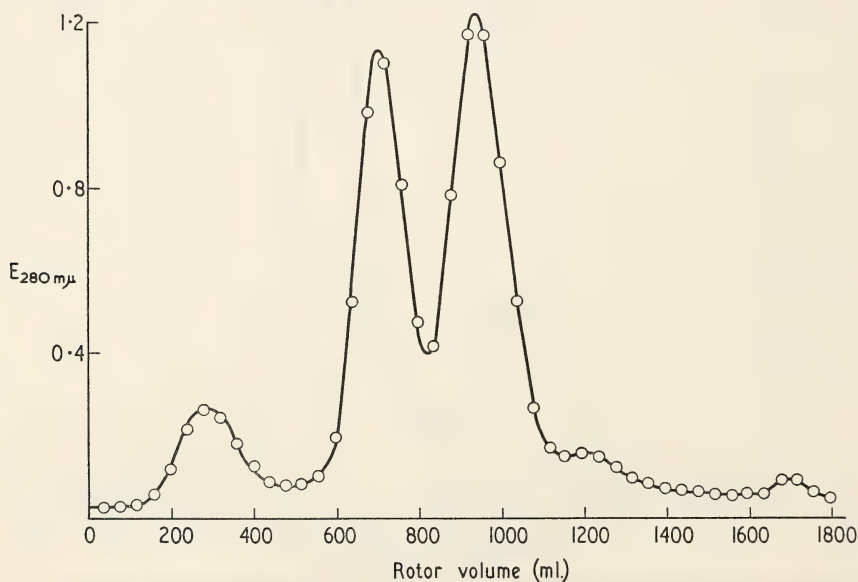
TEXT-FIGURE 2.—Ribosomal RNA from rat liver, 12 percent protein diet. 80 mg RNA dissolved initially in 40 ml 0.1 M sodium acetate pH 7, 2.5 percent w/v sucrose. Centrifuged 6 hours at 40,000 rpm, ZU B-IV rotor.



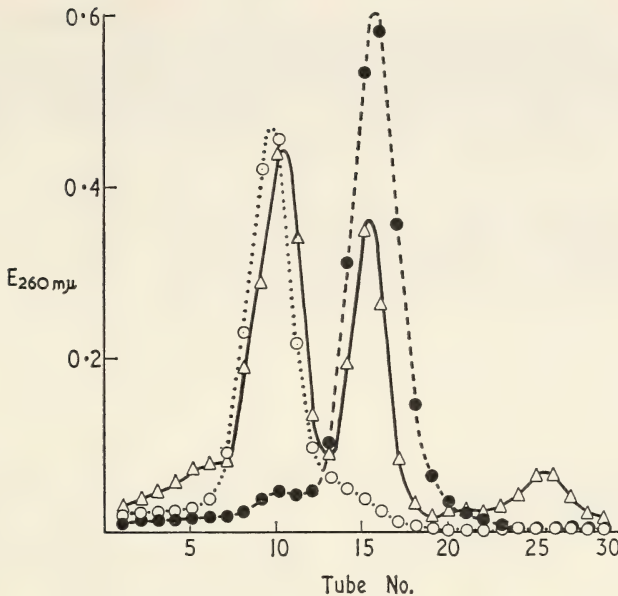
TEXT-FIGURE 3.—Ribosomal RNA from subcutaneously transplanted rat hepatoma originally induced by feeding *p*-(*p*-fluorophenylazo)-*N,N*-dimethylaniline. 60 mg RNA dissolved initially in 40 ml 0.1 M sodium acetate pH 7, 2.5 percent w/v sucrose. Centrifuged 6 hours at 40,000 rpm, ZU B-IV rotor.



TEXT-FIGURE 4.—Ribosomal RNA from *Drosophila melanogaster*, adult flies. 80 mg RNA dissolved initially in 20 ml 0.1 M sodium acetate pH 7, 2.5 percent w/v sucrose. Centrifuged 6½ hours at 40,000 rpm, ZU B-IV rotor.



TEXT-FIGURE 5.—RNA from *E. coli*. 60 mg RNA dissolved initially in 40 ml 0.15 M sodium acetate pH 7, 2.5 percent w/v sucrose. Centrifuged 6 hours at 40,000 rpm, ZU B-IV rotor.



TEXT-FIGURE 6.—RNA from *E. coli*. Rerun of fractions recovered from ZU run shown in text-figure 5. Centrifuged 14½ hours at 24,500 rpm in Model L, S.W.25 rotor. 5 to 20 percent w/v sucrose gradient containing 0.15 M sodium acetate pH 7. —△—△— 0.7 mg of original material as run in text-figure 5. --●--●-- 0.4 mg of material recovered from 600 to 800 ml cut (16 S) . . . ○ . . . ○ . . . 0.4 mg of material recovered from 840 to 1080 ml cut (23 S).

the major components for further studies on structure and function, and secondly minor components can be more easily recognized and work on the physical characteristics of these is also on hand.

The improved separation in this type of centrifuge is probably due to the higher speed and shorter time involved, thus decreasing the effects of diffusion and consequent masking or overlapping of minor components by major components.

## REFERENCES

- (1) HALL, B. D., and DOTY, P.: Preparation and physical properties of ribonucleic acid from microsomal particles. *J Molec Biol* 1: 111-126, 1959.
- (2) STAEBELIN, T., WETTSTEIN, F. O., OURA, H., and NOLL, H.: Determination of the coding ratio based on molecular weight of messenger ribonucleic acid associated with ergosomes of different aggregate size. *Nature (London)* 201: 264-270, 1964.
- (3) FRAENKEL-CONRAT, H., SINGER, B., and TSUGITA, A.: Purification of viral RNA by means of bentonite. *Virology* 14: 54-58, 1961.
- (4) HASTINGS, J. R. B., and KIRBY, K. S.: Isolation of nucleic acids from *Drosophila melanogaster*. Submitted for publication.
- (5) KIRBY, K. S.: Isolation and characterization of ribosomal ribonucleic acid. *Biochem J.* In press.

- (6) ANDERSON, N. G., BARRINGER, H. P., BABELAY, E. F., and FISHER, W. D.: The B-IV zonal ultracentrifuge. *Life Sci* 3: 667-671, 1964.
- (7) ANDERSON, N. G., BARRINGER, H. P., BABELAY, E. F., NUNLEY, C. E., BARTKUS, M. J., FISHER, W. D., and RANKIN, C. T., JR.: The design and operation of the B-IV zonal centrifuge system. *Nat Cancer Inst Monogr* 21: 137-164, 1966.

## Isolation and Characterization of Rat Macroglobulin<sup>1</sup>

W. D. FISHER, and R. E. CANNING,<sup>2</sup> *Biology Division, Oak Ridge National Laboratory,<sup>3</sup> and Biophysical Separations Laboratory, Oak Ridge Gaseous Diffusion Plant,<sup>3</sup> Oak Ridge, Tennessee*

### SUMMARY

A homogeneous rat macroglobulin can be prepared on sucrose density gradients in the B-IV zonal centrifuge. Hundred mg quantities are readily isolated in a single run. Data from

physicochemical studies and chemical analysis of the macroglobulin are reported.—*Nat Cancer Inst Monogr* 21: 403-412, 1966.

OF THE VARIOUS gamma globulins of plasma possessing antibody activity, the 7S- $\gamma$  globulins (IgG) have been extensively studied with respect to structure and biological activity; the 19S macroglobulins (IgM) are more difficult to isolate in quantity and have been less extensively studied (1). Excellent analytical separations of macroglobulins have been obtained in sucrose density gradients with swinging-bucket rotors with a method introduced by Edelman *et al.* (2). The major deficiency in this technique is low yield. Jacquot-Armand *et al.* (3) purified a rat macroglobulin by centrifugation but subsequently abandoned this approach in favor of preparative electrophoresis followed by chromatography on Sephadex and diethylaminoethyl (DEAE) cellulose (4).

In this paper we report the isolation of rat macroglobulin on large sucrose density gradients in the B-IV zonal centrifuge (5). The high capacity of the rotor gives yields large enough for extensive chemical and physicochemical characterization of the macroglobulin.

### MATERIALS AND METHODS

*Sample preparations.*—Male Sprague-Dawley rats were bled from the throat into 0.1 M sodium ethylenediaminetetraacetate at a pH of 7 (0.5 ml/10 ml of blood) and the plasma was collected after centrifugation. The plasma was defibrinated after the addition of a stoichiometric amount of 0.1 M CaCl<sub>2</sub>.

<sup>1</sup> This research performed under the Joint National Institutes of Health-Atomic Energy Commission Zonal Centrifuge Development Program which is supported by the National Cancer Institute, the National Institute of Allergy and Infectious Diseases, and the U.S. Atomic Energy Commission.

<sup>2</sup> We wish to acknowledge the technical assistance of Mrs. Aaron Rutenberg and Mr. Tom Grizzard.

<sup>3</sup> Operated for the U.S. Atomic Energy Commission by the Nuclear Division of Union Carbide Corporation.

A globulin fraction from frozen, pooled serum was prepared by two precipitations with 40 percent saturated ammonium sulfate. The precipitate was dissolved in cold 0.15 M NaCl and exhaustively dialyzed against running tap water in a 4° C cold room. The resulting fraction was spun in an International Model PR-2 centrifuge (#253 head) for 10 minutes at 2000 rpm ( $1000 \times g$ ) and the supernatant fluid made to one fifth the original serum volume in 0.1  $\mu$  Miller-Golder (6) buffer (pH 7.5). Ten ml of the sample was separated with the B-IV zonal ultracentrifuge on a 1 liter gradient (5–15% sucrose in 0.1  $\mu$  Miller-Golder buffer) by use of 400 ml of buffer as overlay. Centrifugation was to  $\int_0^t \omega^2 dt = 35 \times 10^{10}$  (approximately 6 hours at 40,000 rpm). Samples were recovered from the sucrose gradient and concentrated by pressure dialysis against 0.1  $\mu$  Miller-Golder buffer.

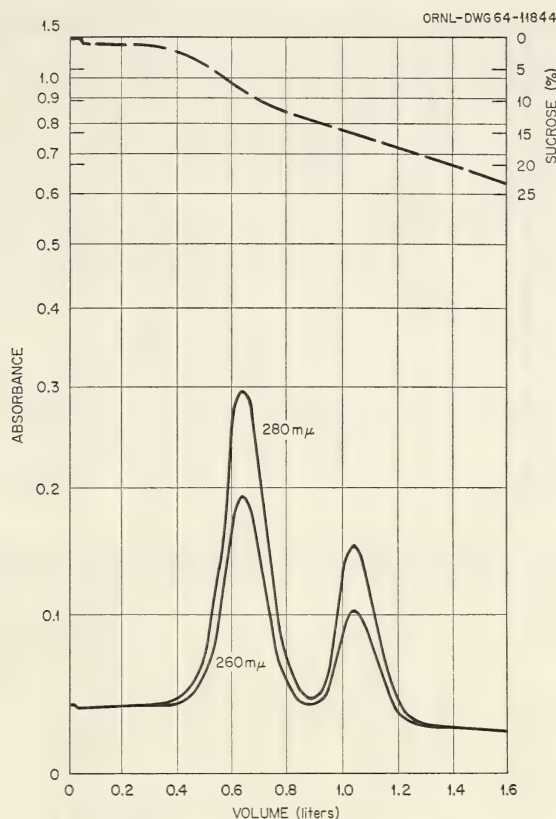
*Monitoring of gradient.*—The gradient was monitored at 260 and 280 m $\mu$  by passage through a 0.2-cm Oak Ridge flow cell by use of a Beckman DB spectrophotometer modified as described by Anderson (7). A model 34H Waters refractometer in the flow stream was used to measure the refractive index. The effluent was collected in 40 ml fractions.

Sedimentation measurements were made in an An-D rotor by use of 4° 12-mm cells in a Spinco Model E analytical ultracentrifuge. Data were evaluated as described by Schachman (8). Electrophoretic and diffusion measurements were performed with a Spinco Model H unit with 11 ml cells. Diffusion data were evaluated as described by Schachman (8) and electrophoretic data as described in Beckman Bulletin 95-B. Immunoelectrophoresis was done by the method of Grabar and Williams (9). The Folin method with a Technicon autoanalyzer was used for protein analysis of the ammonium sulfate fractions. The protein concentrations of the purified macroglobulin were calculated from the nitrogen determination (10). Mercaptoethanol treatment was done as described by Deutsch and Morton (11). Carbohydrate was determined with an anthrone reagent by the method of McCready *et al.* (12). Amino acid analysis was performed by the method of Spackman *et al.* (13) by use of a Spinco 120 analyzer on 24- and 48-hour hydrolysates. Element analysis was done by the Galbraith Laboratories Inc., Knoxville, Tennessee.

## RESULTS

From a starting sample of 4800 mg of protein, the two ammonium sulfate fractionations yielded 700 mg of protein, which, on ultracentrifugal analysis, showed two major peaks with sedimentation constants of approximately 6S and 19S.

One separation of rat serum proteins in the B-IV rotor is shown in text-figure 1. The right-hand peak is the macroglobulin. The starting sample (10 ml of a 2.8% solution) represents 50 ml of rat plasma; the yield was approximately 85 mg of macroglobulin. After concentration by pressure dialysis, the leading peak appeared to be ultracentrifugally

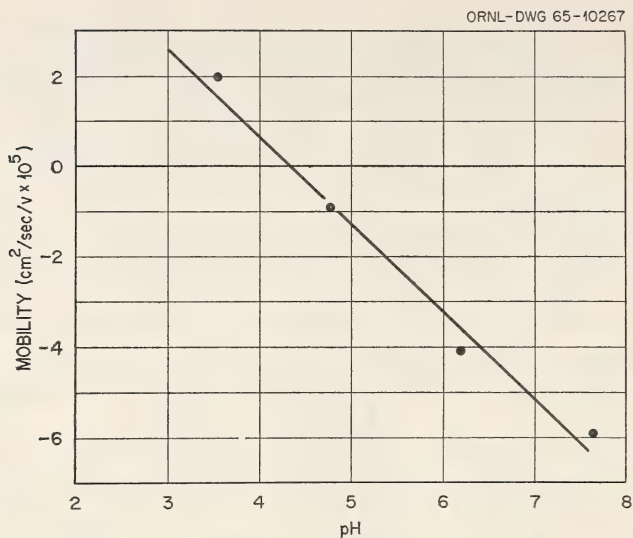


TEXT-FIGURE 1.—Separation of rat macroglobulin in B-IV zonal centrifuge. *Upper curve*, sucrose concentration; *lower curves*, absorbance (0.2 cm light path).

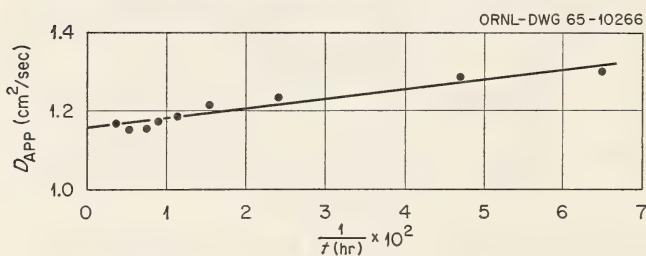
(fig. 1a) and immunoelectrophoretically homogeneous (fig. 2). In other runs, as much as 250 mg of macroglobulin has been purified in a single experiment.

Data on electrophoretic mobility are given in text-figure 2. The isoelectric point is 4.38. The preparation migrated as a single homogeneous peak over the entire  $pH$  range (3.5–7.7). A typical electrophoretic pattern is shown in figure 1b. Data from diffusion experiments are presented in text-figure 3. The data corrected to standard conditions give the value  $D_{20,w} = 2.22 \times 10^{-7}$  cm<sup>2</sup> per second. A diffusion pattern is shown in figure 1c.

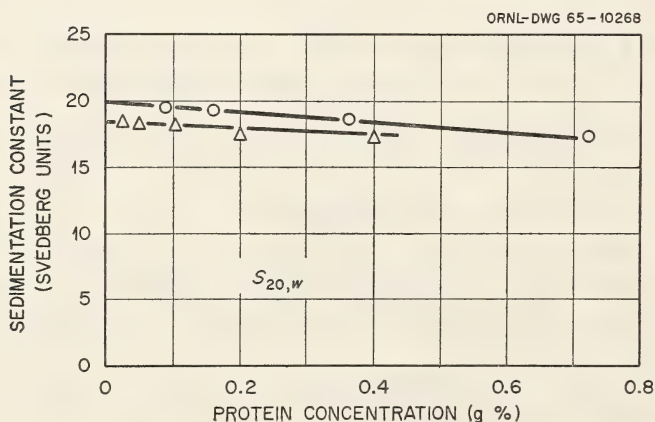
Determination of the sedimentation coefficient at various protein concentrations is shown in text-figure 4. Use of Svedberg's equation and the values of  $S_{20,w} = 18.5$ ,  $D_{20,w} = 2.22 \times 10^{-7}$  and  $\bar{V} = 0.73$  ml per g (calculated from amino acid and carbohydrate composition) gives a molecular weight of 768,000.



TEXT-FIGURE 2.—Electrophoretic mobility of rat macroglobulin as a function of  $pH$  in Miller-Golder buffer,  $\mu = 0.1$ .



TEXT-FIGURE 3.—Diffusion analysis of rat macroglobulin in Miller-Golder buffer,  $pH$  4.38,  $\mu = 0.1$ .



TEXT-FIGURE 4.—Values of the sedimentation constant of rat macroglobulin plotted against protein concentration.  $\circ$  Miller-Golder buffer,  $pH$  7.5,  $\mu = 0.1$ ;  $\triangle$  Miller-Golder buffer,  $pH$  4.4,  $\mu = 0.1$ .

The physicochemical properties of the sample are summarized in table 1. Chemical analysis of the sample gave the following results: carbohydrate content 10.3 percent; N, 13.17 percent; S<0.1 percent.

TABLE 1.—Physicochemical properties of rat macroglobulin

Sedimentation constant, $S_{20,w}^{\circ}$	18.5
Diffusion constant, $D_{20,w}$	$2.22 \times 10^{-7}$ cm <sup>2</sup> /sec
Calculated partial specific volume, $\bar{V}$	0.730 ml/g
Molecular weight ( $s$ , $D$ , $\bar{V}$ )	768,000
Electrophoretic mobility at pH 6.2 phosphate buffer, $\mu = 0.1$	$-4.22 \times 10^{-5}$ cm <sup>2</sup> v <sup>-1</sup> sec <sup>-1</sup>
Isoelectric point	pH 4.38

Treatment with 0.1 M mercaptoethanol dissociated the macroglobulin into subunits of approximately 7S. The subunits were not studied further.

An amino acid analysis is given in table 2.

TABLE 2.—Amino acid composition of rat macroglobulin

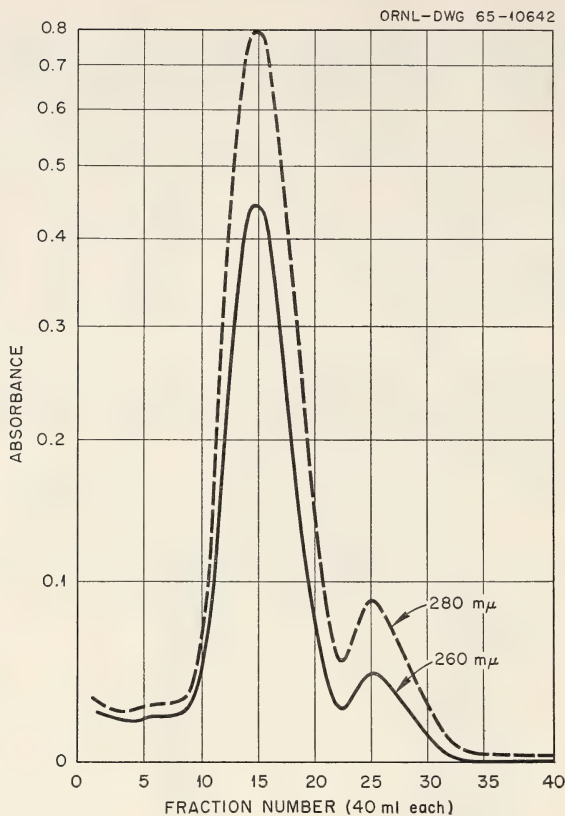
Amino acid	g/100 g protein
Glycine	2.77
Alanine	3.75
Serine	4.74
Threonine	4.38
Proline	3.72
Valine	5.58
Isoleucine	3.65
Leucine	7.06
Phenylalanine	5.39
Tyrosine	5.29
Half cystine	0.75
Methionine	1.71
Aspartic acid	7.16
Glutamic acid	10.47
Arginine	2.91
Histidine	2.00
Lysine	5.69

A separation of macroglobulin from rat serum without previous fractionation by ammonium sulfate is shown in text-figure 5. The starting sample was 19 ml of serum and the yield of macroglobulin (leading peak) approximately 45 mg. Purity was checked by immunoelectrophoresis and was the same as the other preparations. No further studies were done on this sample.

## DISCUSSION

The protein described in this report is a typical macroglobulin (14); it contains approximately 10 percent carbohydrate and has a sedimentation coefficient of 18.5S and a molecular weight of 768,000. It is dissociated by mercaptoethanol as first reported for human macroglobulins by Deutsch and Morton (11). Its isoelectric point (4.38) is low when compared with values reported for human macroglobulins (15, 16).

A homogeneous rat macroglobulin from Wistar rats designated  $\alpha_{IM}$  has been studied by Boffa *et al.* (4). It is immunoelectrophoretically



TEXT-FIGURE 5—Separation of rat macroglobulin from whole serum on a sucrose density gradient in the B-IV zonal centrifuge.

similar to our preparation. The only physicochemical information given by these authors is the sedimentation coefficient  $S_{20,w}^{\circ} = 18.3$ , which compares to a value of  $S_{20,w}^{\circ} = 18.5$  for our preparation.

The data reported show that the B-IV zonal centrifuge can be used to prepare a homogeneous rat macroglobulin in preparative quantities, with either whole serum or samples partially purified by ammonium sulfate fractionation. The large capacity of the zonal centrifuge overcomes the deficiency of low yield in separation in swinging-bucket rotors. Separation in swinging-bucket rotors has been an extremely useful tool for the study of immunological relationships of various antibodies in plasma using very small samples. In conjunction with the protein chromatographic method, large-scale zonal centrifugation should be a useful tool in the study of immunological relationships of the various antibodies in plasma, especially the 20S antibodies, which by previous methods are the more difficult to isolate in quantity.

We have also used the zonal centrifuge to obtain mouse, hamster, and fish macroglobulin directly from whole serum. Physicochemical data on these preparations will be reported subsequently.

## REFERENCES

- (1) PORTER, R. R.: Chemical structure of  $\gamma$ -globulin and antibodies. *Brit Med Bull* 19: 197-201, 1963.
- (2) EDELMAN, G. M., KUNKEL, H. G., and FRANKLIN, E. C.: Interaction of the rheumatoid factor with antigen-antibody complexes and aggregated gamma globulin. *J Exp Med* 108: 105-120, 1958.
- (3) JACQUOT-ARMAND, Y., BOFFA, G. A., and FINE, J. M.: Isolement d'une macroglobuline  $\alpha_1(\alpha_{1M})$  dans le serum du rat normal. *C R Soc Biol (Paris)* 255: 590-592, 1962.
- (4) BOFFA, G. A., JACQUOT-ARMAND, Y., and FINE, J. M.: Constantes de sédimentation caractères électrophorétiques et immunologiques de deux protéines isolées du serum de rat: l'albumine et l' $\alpha$ -macroglobuline. *Biochim Biophys Acta* 86: 511-518, 1964.
- (5) ANDERSON, N. G., BARRINGER, H. P., BABELAY, E. F., and FISHER, W. D.: The B-IV zonal ultracentrifuge. *Life Sci* 3: 667-671, 1964.
- (6) MILLER, G. L., and GOLDBERGER, R. H.: Buffer of pH 2 to 12 for use in electrophoresis. *Arch Biochem* 29: 420-423, 1950.
- (7) ANDERSON, N. G.: Analytical techniques for cell fractions. II. A spectrophotometric column monitoring system. *Anal Biochem* 4: 269-283, 1962.
- (8) SCHACHMAN, H. K.: Ultracentrifugation, diffusion, and viscometry. *In Methods Enzymology IV* (Colowick, S. P., and Kaplan, N. O., eds.). New York, Academic Press Inc., 1957, pp 32-103.
- (9) GRABAR, P., and WILLIAMS, C. A.: Méthodes permettant l'étude conjuguée des propriétés électrophorétiques et immunochimiques d'un mélange de protéines. Application au sérum sanguin. *Biochim Biophys Acta* 10: 193-194, 1953.
- (10) MA, T. S., and ZUZAAGA, C.: Micro-Kjeldahl determination of nitrogen. *Ind Eng Chem, Anal Ed* 14: 280-282, 1942.
- (11) DEUTSCH, H. F., and MORTON, J. I.: Human serum macroglobulin and dissociation units. I. Physico-chemical properties. *J Biol Chem* 231: 1107-1118, 1958.
- (12) MCCREADY, R. M., GUGGOLZ, J., SILVERIA, V., and OWENS, H. S.: Determination of starch and amylose in vegetables. *Anal Chem* 22: 1156-1158, 1950.
- (13) SPACKMAN, D. H., STEIN, W. H., and MOORE, S.: Automatic recording apparatus for use in the chromatography of amino acids. *Anal Chem* 30: 1190-1206, 1958.
- (14) KUNKEL, H. C.: Macroglobulins and high molecular weight antibodies. *In The Plasma Proteins* (Putnam, F. W., ed.). New York, Academic Press Inc., vol 1, 1960, pp 279-307.
- (15) McDougall, E. I., and DEUTSCH, H. F.: A comparison of the native and monomer forms of macroglobulin from pathological human serum with particular reference to electrophoretic mobility differences. *Biochem J* 90: 163-170, 1964.
- (16) ALBERT, A., and JOHNSON, P.: Macroglobulins. 1. Studies on the isolation and physical properties of pathological macroglobulins. *Biochem J* 81: 658-671, 1961.



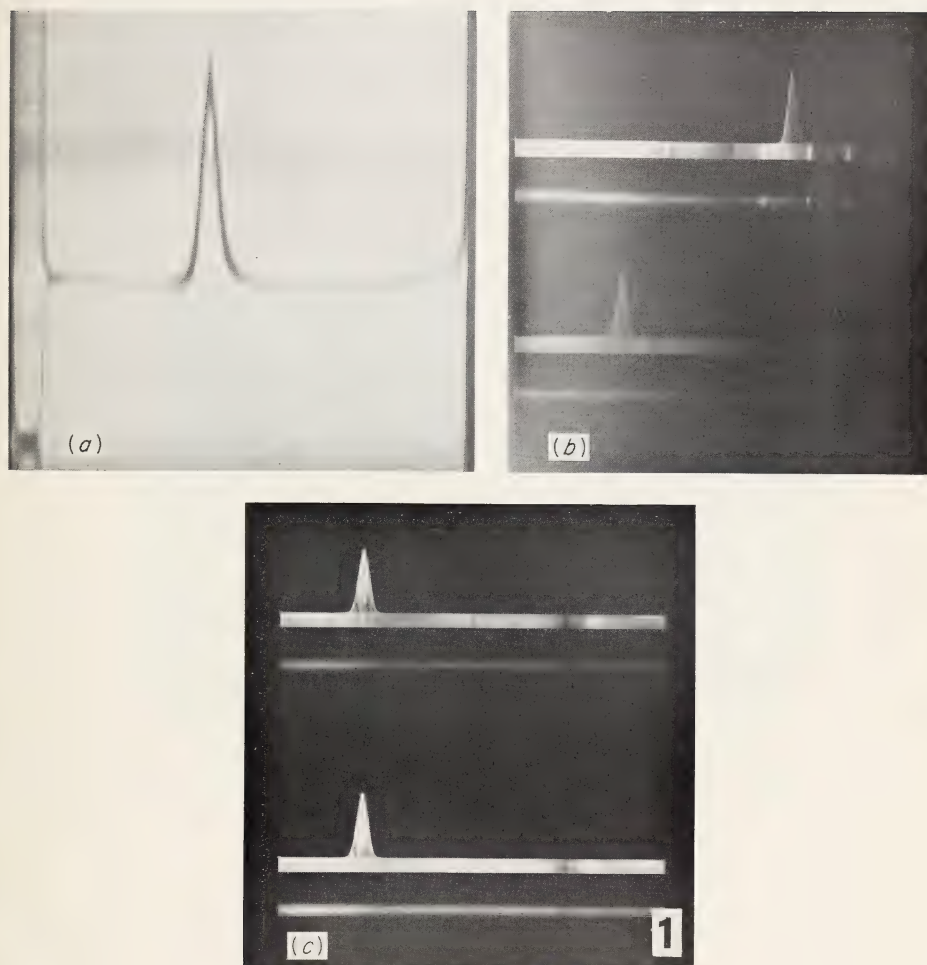


FIGURE 1.—Rat macroglobulin patterns. (a) Ultracentrifuge pattern in  $0.1 \mu$  Miller-Golder buffer after 20 minutes at 59,780 rpm. (b) Ascending (*top*) and descending (*bottom*) electrophoretic patterns at pH 6.2 in  $0.1 \mu$  Miller-Golder buffer. (c) Diffusion pattern 15.3 hours in Miller-Golder buffer at pH 4.38,  $0.1 \mu$ .



FIGURE 2.—Immunoelectrophoretic pattern of (a) macroglobulin and (b) rat serum. In both cases the *upper trough* contains rabbit-anti-whole-rat serum and the *bottom trough* rabbit-antirat macroglobulin.

## **Ancillary Studies**



## Centrifugal Freezing. I. A System for Rapid Freezing of Aqueous Cell Suspensions<sup>1</sup>

N. G. ANDERSON, JOHN G. GREEN,<sup>2</sup> and PETER MAZUR,<sup>2</sup> *Biology Division, Oak Ridge National Laboratory,<sup>3</sup> and Technical Division, Oak Ridge Gaseous Diffusion Plant,<sup>3</sup> Oak Ridge, Tennessee*

### SUMMARY

A centrifugal method for ultrarapid freezing of cells and subcellular particles has been developed, in which small droplets are centrifuged at high speed through liquid nitrogen. When material such as water or blood was injected from a syringe into a rotor, increased rotor speeds gave progressively smaller frozen droplets. Droplet

size of materials introduced from a sprayer was uniform, smaller than the smallest droplets obtained from a syringe injection, and independent of rotor speed. Cell survival was found to be inversely related to increasing droplet size and directly related to rotor speed and warming rate.—*Nat Cancer Inst Monogr* 21: 415-430, 1966.

THE TWO chief causes of injury in frozen and thawed cells appear to be the concentration of solutes produced during freezing and the physical consequences of ice crystal formation within the cell (1). Intracellular ice formation can be avoided by cooling cells sufficiently slowly so that they dehydrate (2), but they then may succumb to concentration of intracellular and extracellular solutes. Conversely, damage from solutes can be eliminated by increasing the cooling velocity to shorten the exposure time, an expedient that may result in the formation of intracellular ice and cell death.

Some years ago, Luyet and Gehenio (3), proposed that if cells were cooled rapidly enough, it might be possible to vitrify the intracellular water to avoid lethal injury. It now appears unlikely that truly amorphous ice can be produced by cooling water in bulk; however, high cooling velocities can produce very small ice crystals and may, in fact, produce ice that is partly crystalline, partly amorphous—especially in cells and tissues. Electron microscopy of rapidly cooled cells shows that crystal size decreases with increasing velocity, and that the highest velocities result in specimens in which ice crystals or spaces left by ice crystals are not resolvable (4, 5).

<sup>1</sup> This research performed under the Joint National Institutes of Health-Atomic Energy Commission Zonal Centrifuge Development Program which is supported by the National Cancer Institute, the National Institute of Allergy and Infectious Diseases, and the U.S. Atomic Energy Commission.

<sup>2</sup> We are indebted to Janice J. Schmidt and E. Jane Holloway for performing all the cell survival assays.

<sup>3</sup> Operated for the U.S. Atomic Energy Commission by the Nuclear Division of Union Carbide Corporation.

The survival of ultrarapidly cooled cells is much higher than that of cells cooled at intermediate velocities. Meryman and Kafig (6), Rinfret and Doebbler (7), and Luyet *et al.* (8) observed this effect with red blood cells, Doebbler and Rinfret (9) with a variety of microorganisms, and Moore and Mühlethaler (5) with yeast.

Small and imperfect ice crystals produced during rapid cooling will remain so only if they are warmed and thawed rapidly. If they are warmed slowly they grow by recrystallization (10, 11). Such slow warming is usually lethal to cells (12).

A specimen must have a high surface-to-volume ratio in order to be cooled or warmed rapidly. One attractive way of achieving this high ratio in suspensions of cells is to subdivide the suspension into droplets and spray the droplets into a coolant. Meryman and Kafig (6) introduced a technique, subsequently used by Rinfret and Doebbler (7), of spraying from a syringe into flowing liquid nitrogen.

One difficulty with the use of boiling liquid nitrogen as a coolant is that the warm, immersed specimen immediately becomes surrounded by a layer of gaseous nitrogen, and heat transfer through a vapor is much slower than through a liquid. However, the density of the vapor is much less than that of the liquid, and this difference suggested a method by which the vapor layer around the specimen could be reduced or prevented. In this method the cell suspension is directed into liquid nitrogen under centrifugal acceleration.

An aqueous fluid stream directed against liquid nitrogen spinning at a reasonably high speed in a hollow-bowl rotor will break up into very small droplets as it is accelerated by the moving liquid nitrogen surface. Centrifugal force will then move the droplets centrifugally at a speed dependent upon the rotor velocity and the density and viscosity of the liquid nitrogen. At high speeds, no insulating gas layer should exist around the aqueous droplets. Instead, the liquid nitrogen may form gas bubbles behind the sedimenting droplets or the gas may be stripped from the droplets as it is formed because of its low density and the velocity of the droplets. In addition, the boiling point of the liquid nitrogen would tend to be depressed near the rotor edge as a result of the pressure gradient.

The reverse problem, rapid thawing, may be approached by allowing the frozen droplets to fall against a warm aqueous solution spinning in a hollow-bowl rotor similar to the one used for freezing. In this case the frozen particles move rapidly through the warm fluid during acceleration to the tangential velocity of the liquid surface. With the proper choice of densities, the frozen droplet will float back to the surface since the density of ice (0.917 g/cc) is lower than that of the surrounding water, even at 37° C (0.9934 g/cc). Cold fluid at the surface of the frozen particle will be denser than either the particle or the suspending medium, and, in a centrifugal field, will tend to move rapidly away.

The question to be asked is simply: Will this technique permit cells and particulate material to be frozen and thawed rapidly enough to observe experimentally the theoretical advantages of ultrarapid cooling?

## MATERIALS AND METHODS

### Rotor Design

Three rotor designs were used. The first was designated "rotor F-I-f"<sup>4</sup> and is similar to that shown in figure 1. The brass outer shell of the rotor fits the drive spindle of a refrigerated centrifuge.<sup>5</sup> The shell supports a closely fitting inner cup machined from methacrylate plastic and drives it by friction. The cup must be made from a solid piece of plastic, since glued models invariably crack at low temperatures.

To allow rapid transfer of frozen droplets to the thawing bath, the original cup was modified to accept a plastic transfer cap. This second rotor type, F-II-f, is shown in figure 1. The opening at the top of the cup is a truncated cone, and the conical surface extends to the cup. A film of silicone stopcock grease was applied to the threads and sealing surface before attachment of the rotor. Rotor F-II-f has been especially useful for the transfer of suspensions into rotor F-III-t (fig. 2), which was built to evaluate the effect of centrifugal warming on the frozen suspensions. This rotor was fabricated by hollowing out a Duralumin angle-head rotor.<sup>6</sup> In use, cell suspensions frozen in rotor F-II-f were expelled into phosphate plating diluent held in rotor F-III-t, which is spun at 1800 rpm.

### Freezing Procedure

The rotor was mounted in the centrifuge and chilled by repeatedly pouring in liquid nitrogen. Before the sample was introduced, the rotor was taken to operating speed and again filled with liquid nitrogen to the top lip of the insert.

Two methods of introducing samples into a rotor were used. Initially aqueous suspensions were pulse-injected into the rotor through a 23-gauge cannula fitted to a hypodermic syringe inclined to the axis of rotation. A typical injection is shown in figure 3. Observation of the procedure, positioning of the syringe, and protection of the experimenter were facilitated by a transparent plastic cover fitted to the centrifuge. Syringe injection did not yield particles of uniform size. A sprayer, shown in figure 4, was fabricated to produce small droplets in aerosol form. Formation of the aerosol had no apparent effect on the viability of yeast. Filtered air was used to form the spray, and the flow of air was controlled by a needle valve placed at the filter.

The yeast, *Saccharomyces cerevisiae*, used in the survival studies was cultured as described by Mazur (13) and used while in stationary growth phase. The cells were washed free of culture medium by centrifugation and diluted in triply distilled water to a volume containing approximately  $4 \times 10^8$  cells per ml. In each experiment, approximately 4 ml of sus-

<sup>4</sup> The upper case letter indicates the rotor series, the numeral the modification, and the lower case letter the use, i.e., freezing or thawing.

<sup>5</sup> Model PR-2, International Equipment Company, Boston 35, Mass.

<sup>6</sup> Number 855, International Equipment Company.

pension was introduced into a rotor. The exact amount was variable because some material was lost during transfer into the rotor or into warming solutions.

### Thawing Procedure

Frozen droplets were recovered from rotor F-I-f by pouring the liquid nitrogen and suspended particles from the insert or by spooning them out with a chilled spatula after the coolant had evaporated. Frozen droplets were recovered from rotor F-II-f by first removing the insert from the brass shell and then attaching the chilled transfer cap. When nearly all of the liquid nitrogen had evaporated from the rotor, it was inverted and the contents expelled by gas pressure arising from vaporization of the remaining coolant.

To obtain relatively rapid thawing of frozen droplets, three warming procedures were used. Early in this study, droplets in liquid nitrogen were transferred from a rotor to a small aluminum dish in the bottom of a 1500 ml beaker. When nearly all coolant had evaporated, 1 liter of 0.067 M potassium phosphate solution was poured rapidly into the beaker over the droplets. In subsequent experiments, the droplets were transferred in liquid nitrogen to an insulated cup. When approximately 10 ml of suspension in liquid nitrogen remained, the droplets in approximately 1 ml aliquots were transferred to a beaker containing 1 liter of diluent at 35° C stirred by a propeller agitator. Reproducibility of results was maximal when the agitator was positioned near the wall of the beaker and driven at 2000 rpm.

In a centrifugal warming procedure, the cell suspension injected from a syringe and frozen at 5000 rpm in rotor F-II-f was expelled into 1 liter of 0.067 M diluent at 35° C in rotor F-III-f at 1800 rpm. The diluent containing the thawed cells was transferred immediately to beakers for subsequent viability assay.

To obtain slow thawing of droplets, the frozen suspension was left in the plastic rotor at room temperature until melted.

### Evaluation Techniques

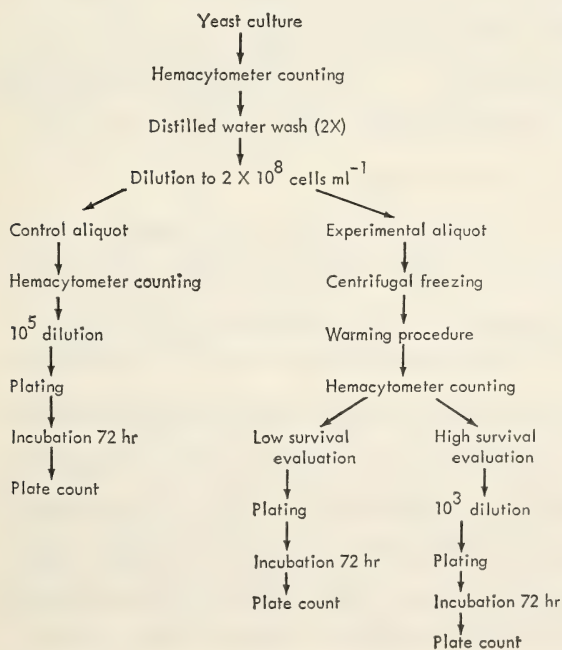
*a. Droplet formation and freezing.*—Experiments were performed with three materials to evaluate the performance of the centrifugal freezing techniques—distilled water, whole blood, and yeast suspensions. In an initial series of tests designed to study the mechanics of droplet formation at various speeds, distilled water was pulse-injected into a rotor, the frozen droplets recovered by pouring them in coolant into a chilled petri dish, and the dish observed under a low-power microscope. At the moment the last vestiges of coolant had evaporated, the droplets were photographed. In another series of experiments, rat blood, treated

with a chelating anticoagulant, was injected from a syringe into the rotor to evaluate the droplet freezing process with a cell suspension. The same photographic technique was used.

*b. Assay of cell viability.*—Cell viability was assayed by plating techniques described by Mazur (13), which are shown in text-figure 1. Triplicate samples were plated either directly from the thawing medium, or, when high survival rates were anticipated, from 1000-fold dilutions. Because the total number of cells recovered after freezing and thawing was somewhat variable, the determination of percentage of survival required some modifications. The total number of cells in aliquots of the thawed suspension and in unfrozen controls was determined by hemacytometer counts, and the total number of viable cells by agar plating. Percentage of survival,  $S$ , was calculated as:

$$S = \frac{F_v C_t}{F_t C_v} \times 100 \quad (1)$$

where  $F_v$  and  $F_t$  represent the number of viable frozen and total frozen cells per ml and  $C_v$  and  $C_t$  the number of viable and total control cells per ml, respectively. Appropriate multipliers were introduced for dilution factors. To offset the possibly deleterious effects of aerosol formation, control samples were sprayed into a liter of diluent, when that mode of sample injection was used.



TEXT-FIGURE 1.—Diagrammatic representation of experimental procedure with yeast suspensions.

## RESULTS AND DISCUSSION

### Droplet Formation

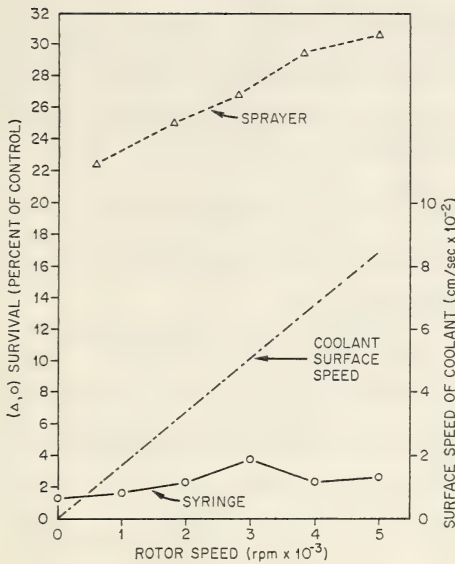
Photographs of droplets obtained when water was injected into liquid nitrogen in rotor F-I-f at rest and at speeds of 1000, 3000, and 5000 rpm are shown in figure 5. When the rotor was stationary, particles varying from 0.1 to 10 mm in diameter were formed, and, although smaller droplets were spherical, larger droplets were irregularly shaped. When the rotor was driven at increasingly greater speeds, successively smaller and, generally, spherical particles were produced. Figure 6, a photograph of whole blood injected into rotor F-I-f at 5000 rpm, illustrates that the injection technique yielded a spectrum of sizes of frozen particles. Many of the larger droplets cracked during photography. Such fracturing was peculiar to cell suspensions and did not occur when distilled water was frozen and warmed.

The following sequence of events during centrifugal freezing was inferred from photographic studies. On contact with the surface of the liquid nitrogen in a spinning rotor, a large droplet breaks into many smaller droplets, which remain fluid until surface tension produces a spherical shape. The particles are engulfed in the coolant and then accelerate and move to the rotor wall. Owing to the initial inertia of a particle and the velocity it attains in the centrifugal field, it is unlikely that a normal insulating gas envelope forms, but, rather, that either the particle leaves a trail of superheated liquid nitrogen in its wake, which vaporizes after the particle has passed, or that movement of the particle in the coolant and the lesser density of vaporized fluid results in reduction or removal of the gas. Heat transfer is probably rapid, since the absence of clumping and the relative sphericity of the frozen droplets indicate that they are sufficiently solidified to prevent distortion when they contact the rotor wall after passage through 1.2 cm of liquid nitrogen.

### Cell Survival

Preliminary evaluation of centrifugal freezing with respect to cell survival has involved varying three parameters—droplet size, rotor speed, and rewarming rate of frozen suspensions. The effect of variation in the first two interrelated parameters may be inferred from the data in text-figure 2, and the gross effect of rewarming may be determined from table 1.

*Particle size effects.*—From the spraying mode of sample injection frozen droplets small and uniform in size were obtained. In contrast, syringe injection gave a spectrum of particle sizes at each rotor speed. The consistently higher survival values obtained from the spraying mode probably reflect the greater cooling and rewarming rate of the smaller droplets resulting from steeper thermal gradients. In addition, physical stress, such as shearing, is probably less with small droplets than with large droplets, which are fragmented at the surface of the coolant.



TEXT-FIGURE 2.—Survival of centrifugally frozen cells injected or sprayed into rotor F-I-f at various speeds.

TABLE 1.—Effects of warming and sample introduction mode on the survival of centrifugally frozen yeast

Experimental series	Rotor	Sample introduction mode	Relative warming rate	Percent survival*
Warming rate effects	F-I-f	Injected from syringe	Slow	0.002
		"	Rapid, diluent pouring	10.5
		"	Rapid, centrifugal	6.8
Sample introduction effects	F-II-f F-III-t F-I-f	"	Rapid, agitation	5.09†
	"	Sprayed	"	16.32†

\*Corrected for viability of controls.

†Average of 8 experiments.

*Rotor speed effects.*—In general, as shown in text-figure 2, the survival of the cells increased with increasing rotor speed. With samples injected from a syringe, the survival rate rose to a maximum at 3000 rpm and declined. Although differences were small, results were consistent within experiments. With samples sprayed into the coolant, the survival rate rose throughout the rotor speed range.

*Warming rate effects.*—Mazur (2) showed that at high cooling rates yeast cells freeze internally since water cannot diffuse from them rapidly enough to prevent freezing. Survival of such cells depends upon the rewarming rate. So, too, does the survival of centrifugally frozen yeast cells. As shown in table 1, rapid warming yielded 5,000 times as many viable cells as slow warming did.

With optimum delivery procedures and rotor speed, the centrifugal freezing-rapid warming technique yielded survivals of 33.8 percent

(text-fig. 2). For comparison, Doebller and Rinfret (9) obtained survivals of 42 percent by spraying suspensions of yeast on a moving surface of liquid nitrogen and Moor and Mühlethaler (5) reported survivals of 30 percent when a 0.2 mm<sup>3</sup> droplet on a copper disk was immersed in liquid propane at -190° C. Neither group, however, examined the effects of slow warming.

Although Rinfret (14) has calculated that the edge and center of a 1 mm droplet of water introduced into liquid nitrogen will cool at 60° and 300° C per second, respectively, from 0° to -60° C, no one has yet devised a method for actually measuring the cooling rates.

The survivals with the centrifugal freezing technique were not superior to those reported in other published procedures for rapid freezing. This could mean that, contrary to our expectations, centrifugal freezing did not produce a higher cooling velocity. Or it could mean that not more than 40 to 50 percent of the yeast cells will survive no matter how rapidly they are cooled. Two pieces of evidence argue against this last statement. One is that Moor and Mühlethaler (5) reported that 100 percent of yeast survived cooling in liquid helium II at an estimated (but unmeasured) cooling velocity of 10<sup>4</sup> °C per second. The other is that, in the present experiments, there appears to be a slow progressive rise in survival with increasing rotor speed.

The matter of cooling velocity is one of the unanswered questions with centrifugal freezing. The present technique yielded respectable survivals with yeast, and suggests that centrifugal freezing may be a valuable tool, especially when large quantities of rapidly frozen material are required. The data also indicated some avenues for improving percentages of survival. These include improvements in the techniques for forming and delivering small, uniformly sized droplets; methods for increasing the velocity of the liquid nitrogen surface; more attention to the matter of achieving still higher and more reproducible warming rates (*e.g.*, centrifugal warming); determining the applicability of centrifugal freezing to cells other than those of yeast, to subcellular particles and viruses, and to other techniques such as the preparation of materials for electron microscopy.

## REFERENCES

- (1) MAZUR, P.: Causes of injury in frozen and thawed cells. *Fed Proc* 24 (2) Suppl 15, Part III, pp S 175-S 182, 1965.
- (2) ———: Kinetics of water loss from cells at subzero temperatures and the likelihood of intracellular freezing. *J Gen Physiol* 47: 347-369, 1963.
- (3) LUYET, B. J., and GEHENIO, P. M.: Injury and death by low temperature. *Biodynamica* 3: 33-99, 1940.
- (4) REBHUN, L. I.: Applications of freeze-substitution to electron microscope studies in vertebrate oocytes. *J Biophys Biochem Cytol* 9: 785-798, 1961.
- (5) MOOR, H., and MÜHLETHALER, K.: Fine structure in frozen-etched yeast cells. *J Cell Biol* 17: 609-628, 1963.
- (6) MERYMAN, H. T., and KAFIG, E.: Rapid freezing and thawing of whole blood. *Proc Soc Exp Biol Med* 90: 587-589, 1955.

- (7) RINFRET, A. P., and DOEBBLER, G. F.: Observations on the freezing and thawing of blood in droplet form. *Biodynamica* 8: 181-193, 1960.
- (8) LUYET, B. J., RAPATZ, G. L., and GEHENIO, P. M.: On the mode of action of rapid cooling in the preservation of erythrocytes in frozen blood. *Biodynamica* 9: 95-124, 1962.
- (9) DOEBBLER, G. F., and RINFRET, A. P.: Survival of microorganisms after ultra-rapid freezing and thawing. *J Bact* 85: 485, 1963.
- (10) MERYMAN, H. T.: Physical limitations of the rapid freezing method. *Proc Roy Soc [Biol], Series B*, 147: 452-459, 1957.
- (11) MENZ, L., and LUYET, B. J.: An electron microscope study of the distribution of ice in single muscle fibers frozen rapidly. *Biodynamica* 8: 261-294, 1961.
- (12) MAZUR, P.: Physical and chemical basis of injury in single-celled microorganisms. *In Low Temperature Research in Biology* (Meryman, H. T., ed.). London, Academic Press, Inc. In press.
- (13) ———: Physical and temporal factors involved in the death of yeast at subzero temperatures. *Biophys J* 1: 247-264, 1961.
- (14) RINFRET, A. P.: Factors affecting the erythrocyte during rapid freezing and thawing. *Ann NY Acad Sci* 85: 576-594, 1960.



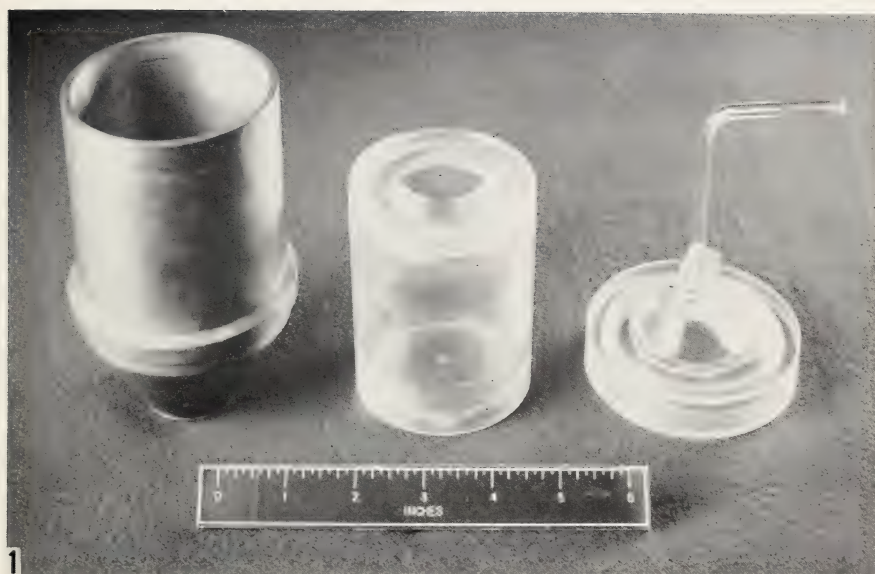


FIGURE 1.—Components of Rotor F-II-f. Rotating brass holder shown *at left*, plastic cup used to contain liquid nitrogen shown *in center*, and transfer cap used to transfer the frozen particles is shown *at right*.

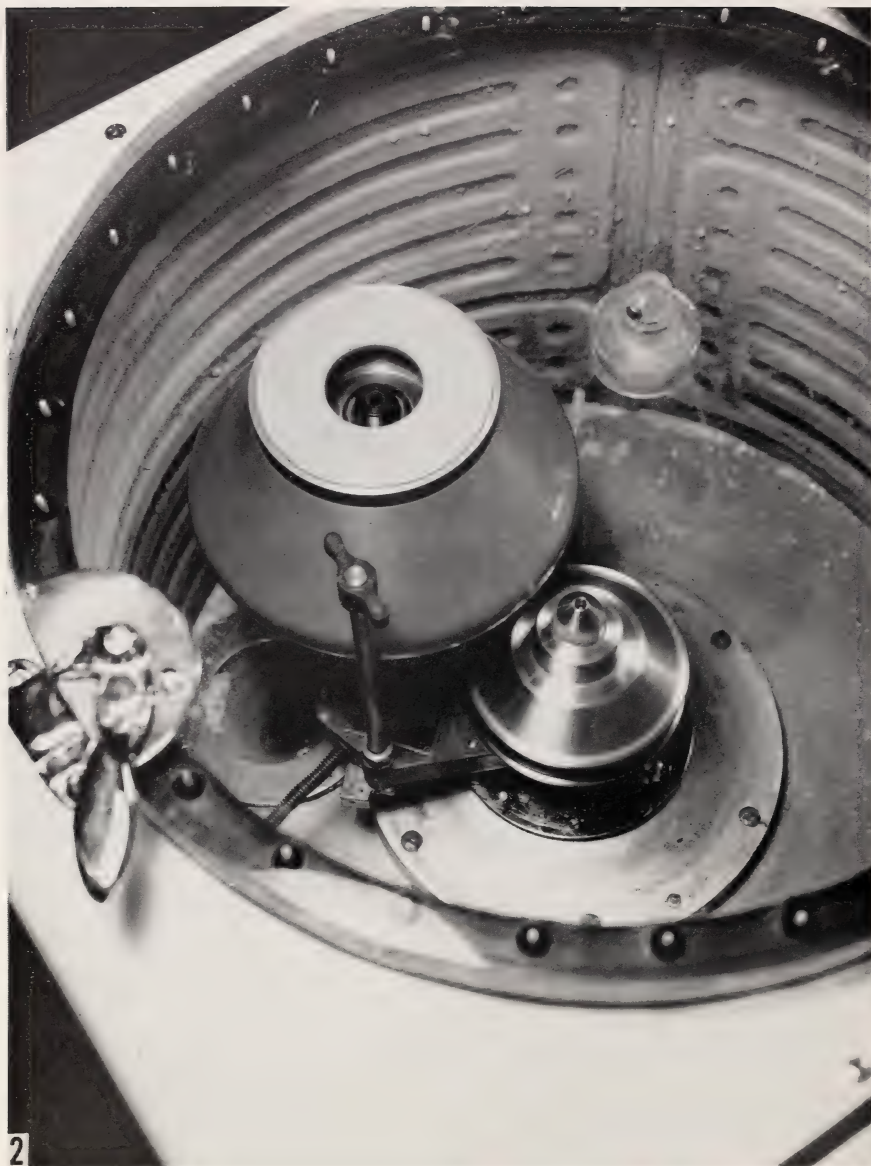


FIGURE 2.—Rotor F-III-t in the PR-2 centrifuge. Rotor is hollow and is used for rapidly thawing cells.



FIGURE 3.—Shows technique for centrifugal freezing of cell suspensions by injection of sample into liquid nitrogen in a spinning rotor.



FIGURE 4.—Sprayer used to obtain fine droplets of cell suspension in aerosol form. Flask *on right* contains cotton filter and has needle valve on the outlet side. Sprayer *on left* includes small reservoir for cells connected by a plastic tube to the air jet. Direction of spray would be to left.

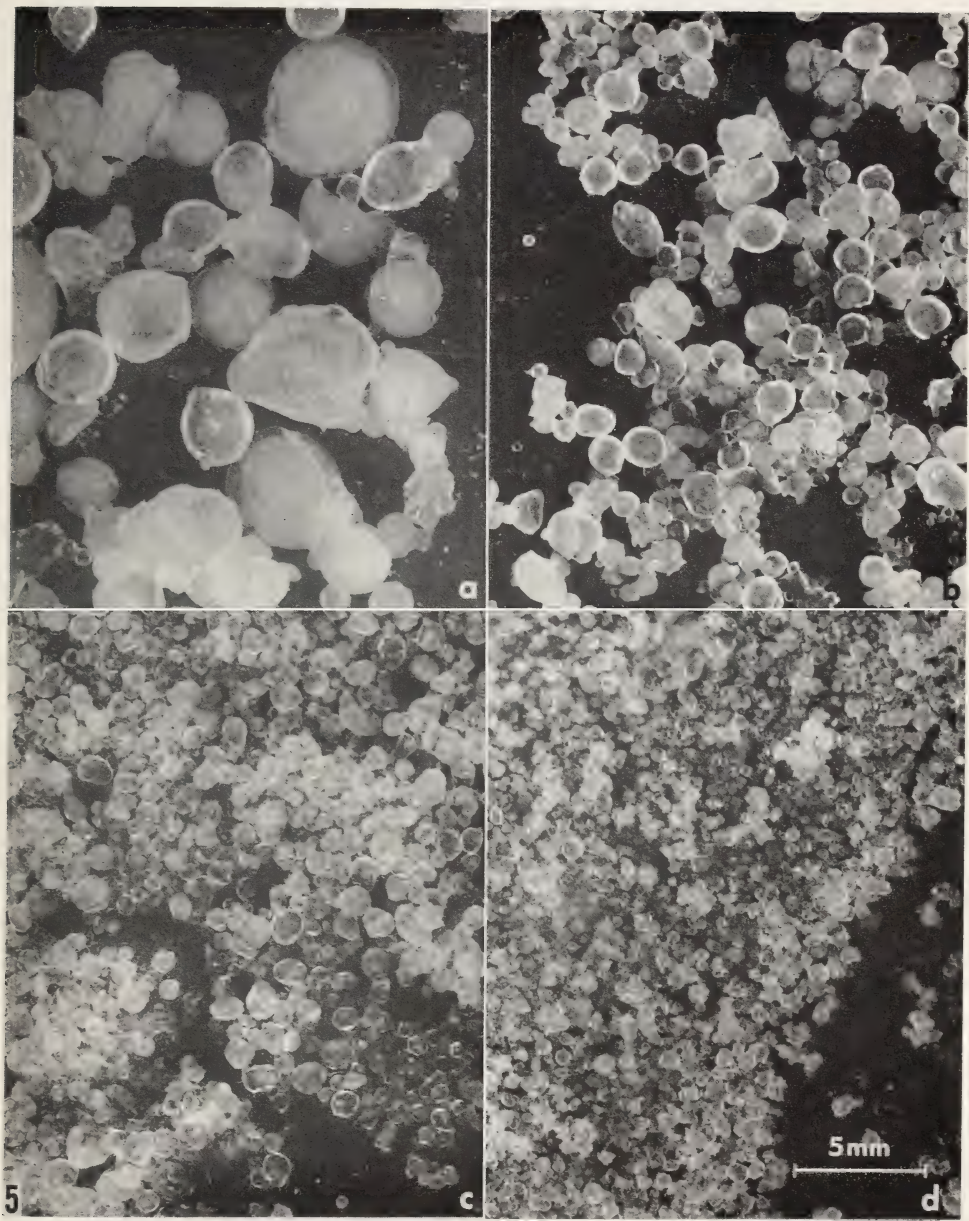


FIGURE 5.—Water injected into liquid nitrogen at rest (a) and in rotor F-I-f at 1000 rpm (b), 3000 rpm (c), and 5000 rpm (d).

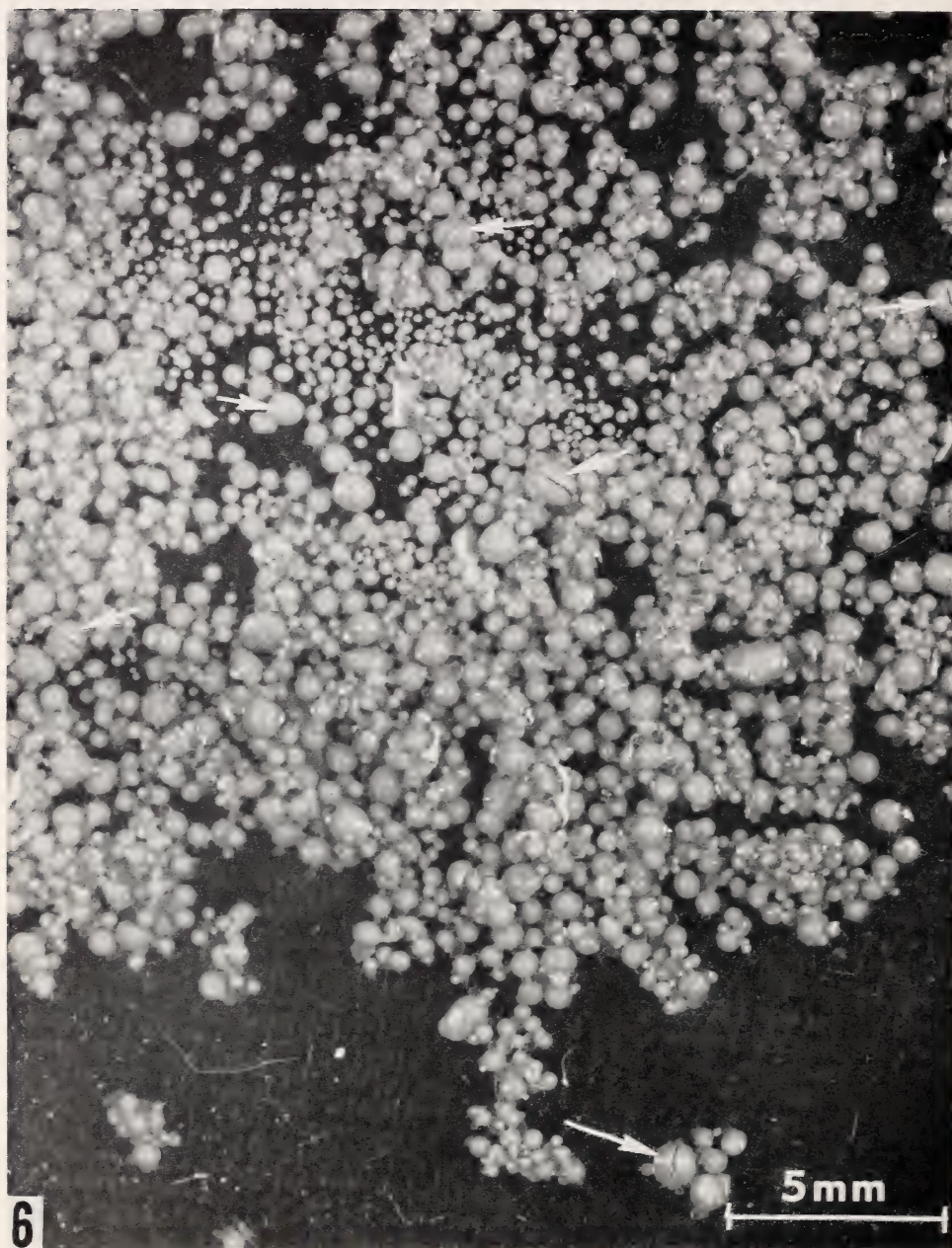


FIGURE 6.—Whole, versenated rat blood injected into liquid nitrogen in rotor F-I-f at 5000 rpm. Arrows denote cracking that appears in larger particles during observation.

# High-Pressure Column Chromatography. I. Design of Apparatus and Separation of Bases, Nucleosides, and Nucleotides<sup>1</sup>

J. G. GREEN, C. E. NUNLEY, and N. G. ANDERSON,  
*Technical Division, Oak Ridge Gaseous Diffusion Plant,<sup>2</sup>  
and the Biology Division, Oak Ridge National Laboratory,<sup>2</sup> Oak Ridge, Tennessee*

## SUMMARY

Theoretical studies suggest that the resolution obtained with ion exchange columns increases when the size of the ion exchange resin particles and the diameter of the column are decreased. In the development of precise, automated microanalytical systems for the analysis of complex biological mixtures, these, as well as other parameters, must be explored. Very high pressures are required to obtain adequate flow rates through fine resin beds. An experimental system capable of performing separations at 4000 lb/in<sup>2</sup> (psig) is described and its application to the separation of bases, nucleosides, and

related materials is discussed. The system consists of a high-pressure variable volume pump, a steel column, and a spectrophotometric monitoring system. Elutions of base and nucleoside mixtures and simulated ribonucleic acid hydrolysates have been performed with acetate buffers. At high pressure, superior resolution is obtained and elution times are shorter than with previously described systems. In addition, fractionated sample components elute in small volumes of buffer.—*Nat Cancer Inst Monogr* 21: 431-440, 1966.

FOLLOWING THE introduction of the automated amino acid analyzer (1), automatic systems have been developed for the analysis of other classes of substances, including nucleotides and nucleotide derivatives (2, 3) and simple carbohydrates (4), on ion exchange column. In these instances, the sample sizes, though small, are still intermediate between those used in laboratory-scale preparative columns and those required for truly ultramicroanalytical procedures. For many research purposes, including clinical survey studies, no preparative requirements exist, and interest shifts in the direction of speed of analysis, precision, decrease in sample size, and miniaturization of the purely analytical equipment. Refinements permitting considerable reduction in sample mass and analysis time have been described for the amino acid analyzer (5, 6) and have been studied during the development of the carbohydrate analyzer

<sup>1</sup> This research performed under the Joint National Institutes of Health-Atomic Energy Commission Zona Centrifuge Development Program which is supported by the National Cancer Institute, the National Institute of Allergy and Infectious Diseases, and the U.S. Atomic Energy Commission.

<sup>2</sup> Operated for the U.S. Atomic Energy Commission by the Nuclear Division of Union Carbide Corporation.

(4). Of the many complex problems that must be solved in the development of miniature ion exchange analyzers, that of obtaining high-resolution separations in a short time has been examined first.

An expression for determination of the effective theoretical plate height,  $H$ , of a column in elution development of trace quantities is (7):

$$H = 1.64 r_o + \frac{0.14 + r_o^2 v}{\bar{D}(\lambda_i'' + \beta)^2} + \frac{0.266 \lambda_i''^2 r_o^2 v}{D(1 + 70 r_o v)(\lambda_i'' + \beta)^2} + \frac{D\beta\sqrt{2}}{v}$$

where

$H$  = effective theoretical plate height

$r_o$  = particle radius

$v$  = linear flow rate (ml cm<sup>-2</sup> min<sup>-1</sup>)

$D$  = diffusion coefficient in interstitial liquid

$\bar{D}$  = interdiffusion coefficient in the ion exchanger

$\lambda_i''$  = column distribution ratio

$\beta$  = fractional void volume in the resin bed

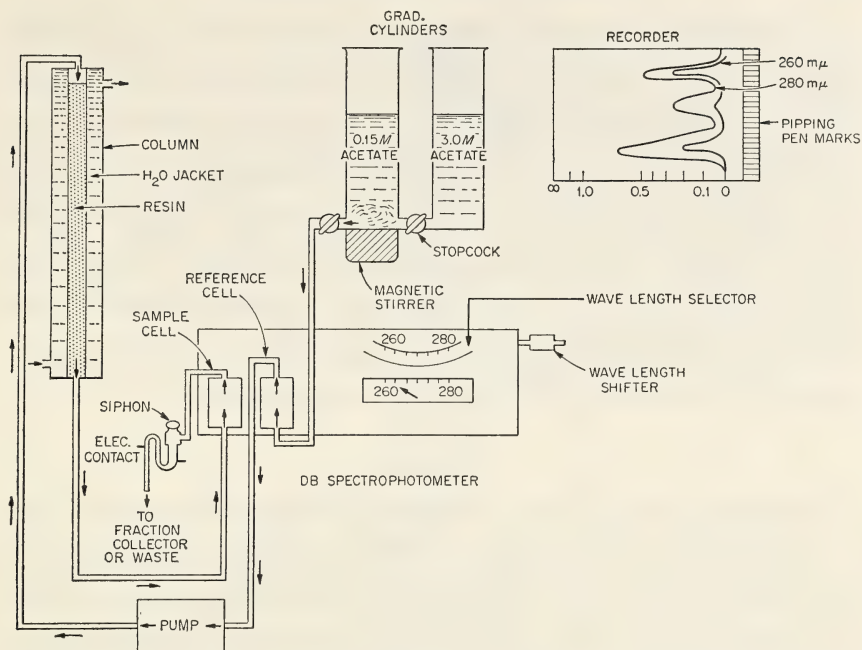
The four terms of the equation express the effects of particle size, slow particle diffusion, slow film diffusion, and longitudinal diffusion, respectively. The best separations are obtained when the value of each term is at a minimum and, thus, the number of theoretical plates for a given column is at a maximum. For uniform operating conditions a reduction in exchanger particle size,  $r_o$ , reduces the value of the first three expressions. In practice, the value of the particle size effect is usually doubled to allow for imperfect column packing (7). Such compensation can be reduced by use of spherical resins of uniform particle size and by reduction of the diameter of the column. When separations are optimal, band widths are minimal and flow rates may be increased to reduce the time required for an analysis. In addition, increased recorded peak heights result in a net over-all increase in the sensitivity of a system.

Reductions in column diameter and resin particle size increase flow resistance. Higher pressures are required to maintain flow rates, and such pressures can surpass the capabilities of systems using glass columns. The purpose of this work has been to examine the performance and define the problems of chromatographic systems that operate at high pressures. For comparison with our existing conventional system (3) and for elimination of the development of an eluate processing procedure, the high-pressure modification was applied to the separation of bases and nucleosides. Elution principles and the spectrophotometric monitoring system have been described previously (2, 3).

## DESIGN AND OPERATION

### Design

The analytical system, diagrammed in text-figure 1 and shown in figure 1, consists of (a) a system to form concentration gradients and to



TEXT-FIGURE 1.—Diagram of an experimental system for the evaluation of high-pressure elution techniques.

deacerate the elution buffer, (b) a pump to deliver the buffer to the column, (c) a metal column to support an anion exchange resin bed, and (d) a spectrophotometric system to monitor the ultraviolet absorbance of the eluate at two wavelengths.

Linear or convex gradients are formed by using connected cylinders, with the terminal cylinder heated to deacerate the buffer. To minimize evaporation from this cylinder, a drop-shaped condenser is placed in the top opening. The cylinders are interconnected through capillary stopcocks, and the gradient system is connected to the inlet of the pump through a 3-way stopcock, which allows the system to be drained.

Buffer is delivered to the column by a diaphragm pump<sup>3</sup> capable of delivering liquids at pressures to 5000 lb/in<sup>2</sup> (psig) at adjustable rates. Influent pressure is indicated by a gauge<sup>4</sup> having wetted parts of stainless steel and a range of 0 to 5000 lb/in<sup>2</sup>. The gauge serves as a damper and reduces undesirable hydraulic shock to a minimum. The pump, gauge, and column are joined by ¼ inch O.D. by ⅛ inch I.D. tubing and appropriate tube fittings of 316 stainless steel. To prevent the back flow of particulate material into the pump, a valve is incorporated in the line connecting the pump to the column.

<sup>3</sup> Laboratory Feed Pump Model LP10 with 5 mm plunger and 30:1 gear ratio. Whitey Research Tool Co., 5525 Marshall St., Oakland, Calif.

<sup>4</sup> Acragage with shockstop and capillary bleed. Robertshaw Controls Co., Fulton Syphon Division, Knoxville, Tenn.

The column is pictured in figure 2 and diagrammed in text-figure 2. The main column is fabricated from  $\frac{3}{8}$  inch O.D. by  $\frac{1}{8}$  inch I.D. 316 stainless steel. The fitting<sup>5</sup> at the top of the column allows direct access without disconnecting the buffer inlet. The resin is supported on a sintered stainless-steel disc of 5  $\mu$  porosity which is sealed to the column by an O-ring. Eluate passes from the column through hypodermic tubing and Teflon tubing (AWG 22). A metal water jacket is incorporated into the column assembly by the use of heat exchanger tube fittings. Heated water is supplied to the column jacket from a circulating constant temperature water bath, passes from the column to the water jacket of the terminal gradient cylinder (not shown), and returns to the bath.

The absorbancy of the column eluate was monitored by a Beckman DB spectrophotometer at 260 and 280  $m\mu$  and recorded.

### Operation

Two separate lots of Dowex 1- $\times$ 8 anion exchange resin have been used in the evaluation of the system. Initially, a portion of a pilot plant production from the manufacturer<sup>6</sup> was fractionated hydraulically to yield material with a mean particle size of 10  $\mu$  and a size range for 90 percent of the particles of 9  $\mu$ . Subsequently, an analytical-grade fractionated resin was obtained from a commercial source.<sup>7</sup> The latter exchanger possessed a settling rate of 0.27 cm per minute in water at room temperature, a mean particle size of 13  $\mu$ , and a size range of 7 to 28  $\mu$  for 90 percent of the particles. Before use, a resin was washed with 6 N HCl, converted to the hydroxyl form with NaOH, and then to the acetate form with sodium acetate buffer. It was packed in the column in increments from a 50 percent slurry in stock acetate buffer, by use of the buffer pump.

Separations have been performed with sodium acetate buffers at  $pH$ 's from 4.1 to 4.6. Stock buffer was obtained by mixing 3 M sodium acetate and 3 M acetic acid in correct proportions to obtain the desired  $pH$ , and elution buffers were diluted from this solution.

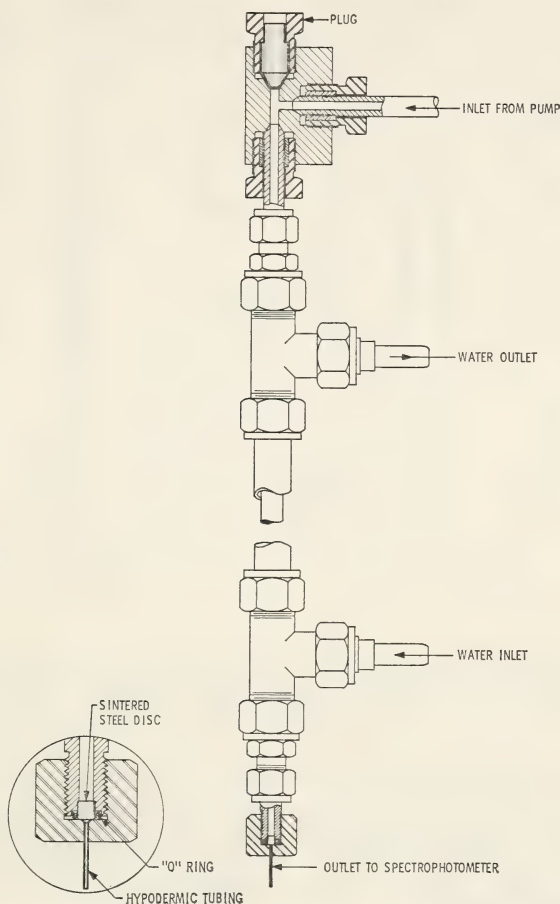
Two methods of placing a sample on the resin have been used. In one procedure, the sample was absorbed on a bit of cotton and carefully tamped on the surface of the exchanger. The remainder of the volume was filled with buffer, the column sealed, and the elution begun. In the alternate procedure, buffer was removed from the column by aspiration and the sample, in a volume of 75  $\mu$ l or less, was placed directly on the resin surface. Finally, the column was sealed and elution begun.

Two standard solutions, 10 mM with respect to each component except guanine, which is 1.0 mM, have been used. One contained cytosine, cytidine, uracil, uridine, thymidine, inosine, adenine, adenosine, guanine, and guanosine. The other, simulating an alkaline ribonucleic acid (RNA) hydrolysate, contained the mixed 2' and 3' monophosphate ester isomers of cytidine, adenosine, and guanosine, and the 3' ester of uridine.

<sup>5</sup> Catalogue No. 45-4321, American Instrument Co., Inc., Silver Spring, Md.

<sup>6</sup> Lot No. 5893-35, Dow Chemical Co., Midland, Mich.

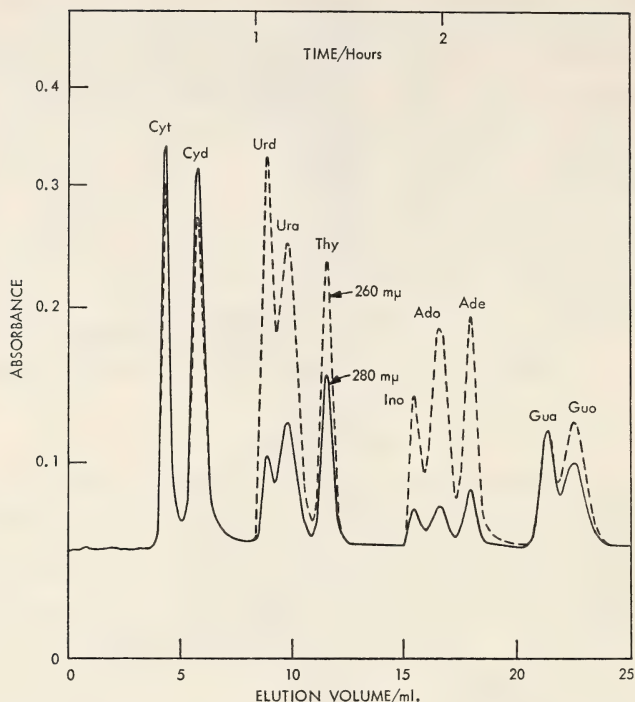
<sup>7</sup> Lot No. B2082, Bio-Rad Laboratories, 32d and Griffin Ave., Richmond, Calif.



TEXT-FIGURE 2.—High-pressure ion exchange column. Except where noted in the text, the assembly is fabricated from readily available tube fittings and accessory components. The sintered disc is machined from a larger disc obtained from Crawford Fitting Company, Cleveland, Ohio.

## RESULTS AND DISCUSSION

For acceptable separations of bases and nucleosides in this system, it has been necessary to elute with both  $pH$  and concentration gradients at low flow rates and to establish a temperature program. A chromatogram obtained from an elution involving variation of these parameters is shown in text-figure 3. Elution was accomplished with buffers of low concentration, and the  $pH$  change involved in this elution should not affect molar absorbancy values. As a result of using a small-bore column, eluted peaks were contained in minimal amounts of buffer. For example, cytosine eluted in 1.26 ml and guanosine in 2.52 ml of liquid. An analysis was completed in less than 3 hours; a comparable elution requires 6.5



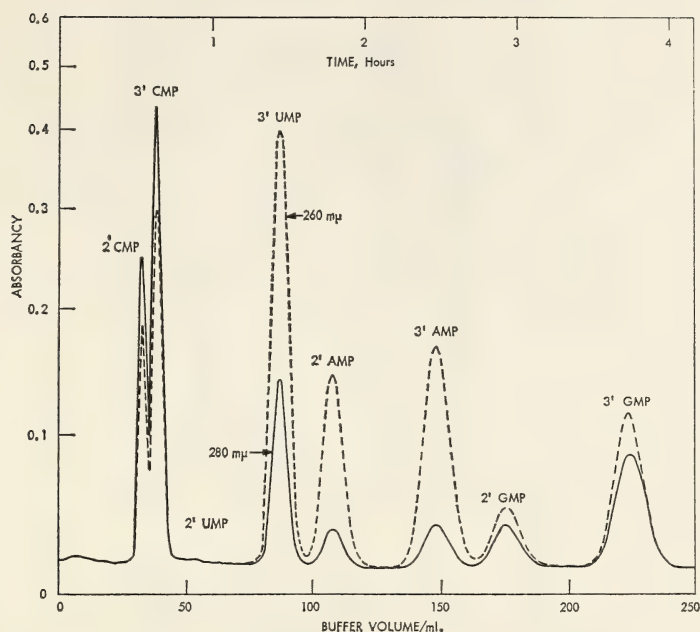
TEXT-FIGURE 3.—Separation of bases and ribonucleosides with a high-pressure elution system. At 72 minutes from the start of the analysis, the temperature was shifted from 30 to 50° C at 4° C per minute. The elution gradient was composed of 40 ml of  $1.5 \times 10^{-3}$  M (acetate ion) buffer at pH 4.4 in the mixing cylinder and 40 ml of  $3 \times 10^{-3}$  M (acetate ion) buffer at pH 3.9 in the back cylinder. Sample was 0.25  $\mu$ mole of each component. Column diameter and length were, respectively, 0.125 inch and 36.0 inches.

hours in the system described previously (3). Although separation of eluted peaks was not ideal, quantitation was possible.

The analysis of a simulated RNA hydrolysate is shown in text-figures 4 and 5. When unusual components are anticipated or separation of isomers is desired, the 4-hour elution can be used, but when rapid analyses are desired, the 2-hour program is applicable. Temperature and pH programming were not required for these elutions.

With the present system, separations have been performed at pressures to 4000 lb/in<sup>2</sup>. Presently, the capability of the pump limits the pressure at which the system may be operated and, consequently, the minimal bead size of the resin that may be used.

Introducing a sample into the high-pressure column remains a problem. When the sample was sorbed on cotton, total transfer to the resin was not obtained. The layering technique has been satisfactory, but sample



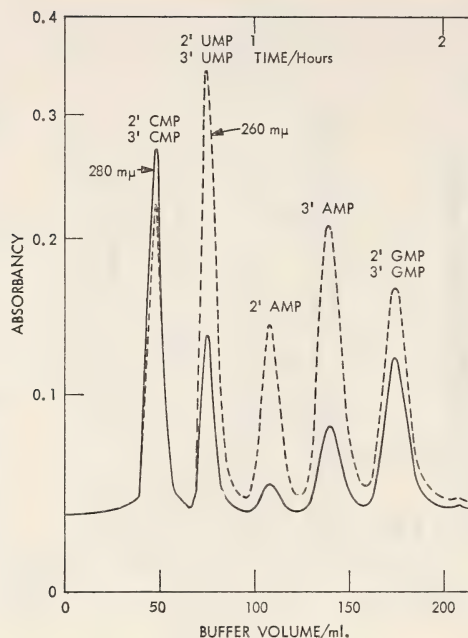
TEXT-FIGURE 4.—Analysis of a simulated ribonucleic acid hydrolysate by normal elution procedure. Gradients, expressed as acetate ion, were 120 ml each of 0.05 M and 1.0 M buffer at pH 4.1. Sample sizes were  $0.5 \mu\text{M}$  of each component. Elution temperature was  $45^\circ \text{C}$ .

size is severely limited. Ultimately, a variable volume sample injection system with very high reproducibility would alleviate this problem.

As found in other chromatographic systems, the quality of resolution is limited by the performance of the ion exchanger. The mechanical design of the system can only exploit the properties inherent in the resin. Of several resins examined, only lot B-2082 gave satisfactory resolution in this system. However, with careful control during manufacture, materials may be produced that are adapted to specific separations.

Reduced elution times permit increasing the number of analyses that may be performed in a given time. Shorter columns mean smaller systems and reduced requirement for expensive—perhaps especially synthesized—resins. Eluted peaks appearing in minimal volumes required reduced postelution processing for recovery. Additional refinements may make the system a useful laboratory tool for both analysis and studies on the effect of particle size on resolution.

Cell fractions obtained by zonal centrifugation with the combined rate-isopycnic banding technique (8) do not yield large quantities of each of the many fractions seen. The analysis of these fractions for nucleic acids and nucleic acid derivatives will be greatly facilitated by the development of automated analytical systems requiring very small samples.



TEXT-FIGURE 5.—Analysis of a simulated ribonucleic acid hydrolysate by accelerated elution procedure. Gradients, expressed as acetate ion, were 100 ml each of 0.15 M and 0.30 M buffer at pH 4.4. Sample sizes were 0.5  $\mu$ M of each component. Elution temperature was 45° C.

## REFERENCES

- (1) SPACKMAN, D. H., STEIN, W. H., and MOORE, S.: Automatic recording apparatus for use in the chromatography of amino acids. *Anal Chem* 30: 1190-1206, 1958.
- (2) ANDERSON, N. G.: Analytical techniques for cell fractions. II. A spectrophotometric column monitoring system. *Anal Biochem* 4: 269-283, 1962.
- (3) ANDERSON, N. G., GREEN, J. G., BARBER, M. L., and LADD, SISTER F. C.: Analytical techniques for cell fractions. III. Nucleotides and related compounds. *Anal Biochem* 6: 153-169, 1963.
- (4) GREEN, J. G.: Automated carbohydrate analyzer: Experimental prototype. *Nat Cancer Inst Monogr* 21: 447-467, 1966.
- (5) PIEZ, K. A., and MORRIS, L.: A modified procedure for the automatic analysis of amino acids. *Anal Biochem* 1: 187-201, 1960.
- (6) HAMILTON, P. B.: Ion exchange chromatography of amino acids. A single column, high resolving, fully automatic procedure. *Anal Chem* 35: 2055-2064, 1963.
- (7) HELFERRICH, F.: *Ion Exchange*. New York, McGraw-Hill Book Co., Inc., 1962, 624 pp.
- (8) ANDERSON, N. G., HARRIS, W. W., BARBER, A. A., RANKIN, C. T., JR., and CANDLER, E. L., JR.: Separation of subcellular components and viruses by combined rate- and isopycnic-zonal centrifugation. *Nat Cancer Inst Monogr* 21: 253-283, 1966.

## PLATES



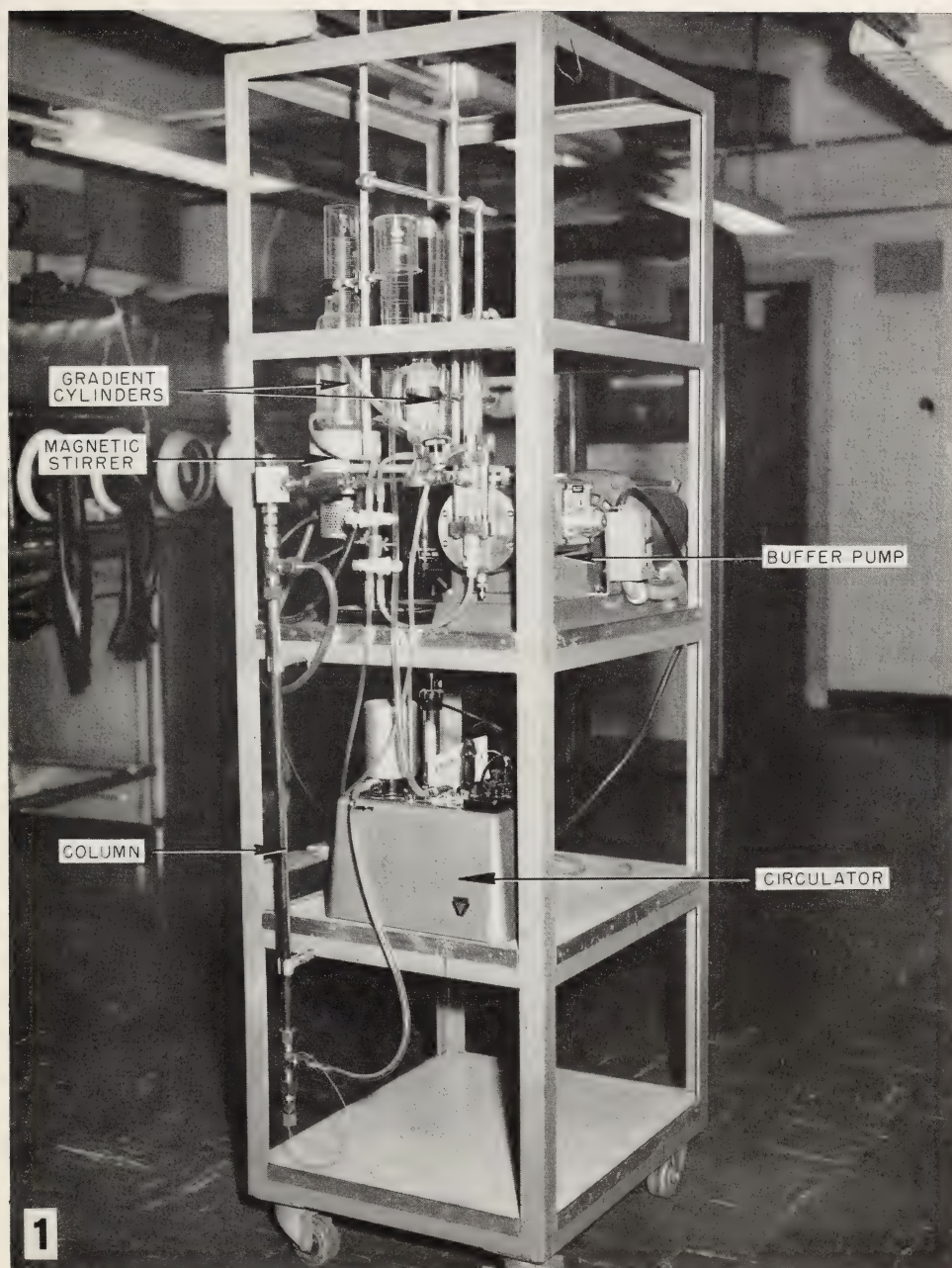


FIGURE 1.—The column module of the high pressure system. Eluate is conducted from the column to the spectrophotometric column through capillary Teflon tubing. The monitor module is not shown but has been described elsewhere (2).

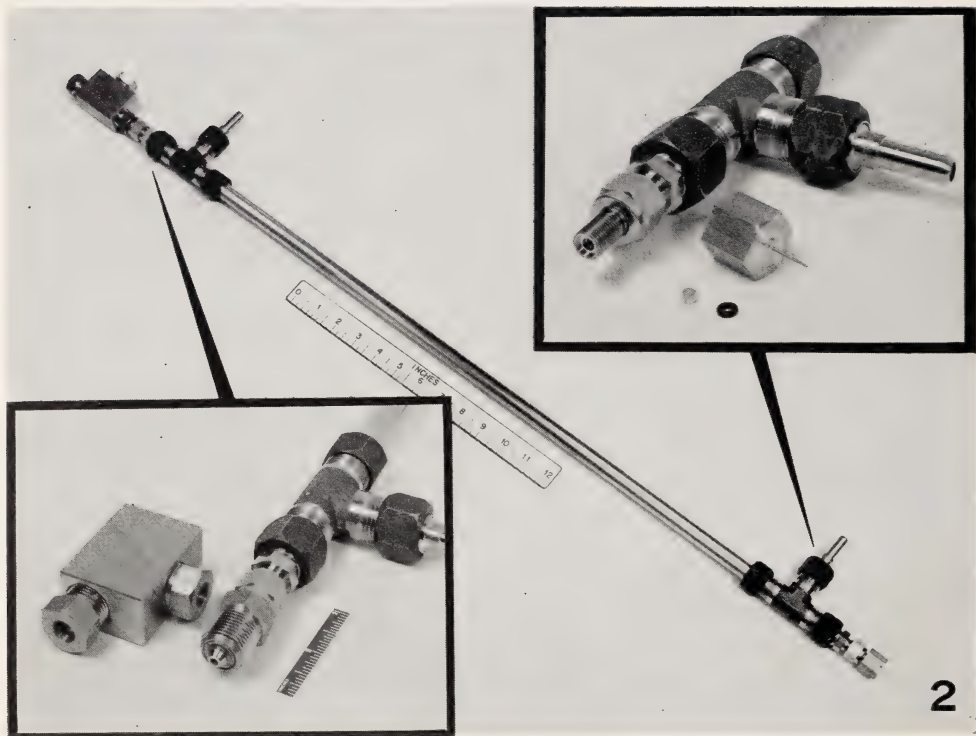


FIGURE 2.—Column used for the study of high-pressure elution techniques.

## Separation of Acid-Soluble Nucleotides From Yeast With the Nucleotide Analyzer<sup>1</sup>

IVAN L. CAMERON<sup>2</sup> and WILLIAM D. FISHER,<sup>3</sup>  
*Biology Division, Oak Ridge National Laboratory,<sup>4</sup> Oak Ridge, Tennessee*

### SUMMARY

An anion exchange chromatographic method has been used for the separation of material extracted by cold acid from a strain of yeast requiring uracil and adenine. The results indicate that deprivation of uracil and adenine does not change appreciably

the number of nucleotides extracted, although the amounts of uracil derivatives are decreased and those of adenine derivatives are slightly increased. *Nat Cancer Inst Monogr* 21: 441-446, 1966.

OUR UNDERSTANDING of the role of nucleotides and their metabolism has been hindered by the difficulty in separating and quantifying purine and pyrimidine bases, nucleosides, and nucleotides. Ideally these compounds should be separated on one chromatographic column at one *pH* so that they can be identified and quantified by relatively simple procedures. Anderson *et al.* (1) and Anderson (2) have devised a separation method that satisfies the above conditions and have developed an automatic spectrophotometric system to monitor and record continuously the column effluent at two wavelengths. The method has been tested on mixtures of known bases, nucleosides, and nucleotides (1), but has not yet been applied to cell or tissue extracts. The present report demonstrates the applicability of this technique to biological investigations.

Yeast was selected for this study for two reasons: (a) Preliminary tests showed that the nucleotide pool of yeast is less complex than that of protozoa and identifications are easier, and (b) the availability of yeast mutants that require uracil and adenine suggested a possible way to alter the composition of this pool.

<sup>1</sup> This research performed under the Joint National Institutes of Health-Atomic Energy Commission Zonal Centrifuge Development Program which is supported by the National Cancer Institute, the National Institute of Allergy and Infectious Diseases, and the U.S. Atomic Energy Commission.

<sup>2</sup> Present address: Anatomy Department, State University of New York, Syracuse, N.Y.

<sup>3</sup> We wish to thank Dr. T. R. Manney for helpful advice about this project and Dr. P. A. Van Dreal, who stimulated our interest in the automatic nucleotide analyzer

<sup>4</sup> Operated for the U.S. Atomic Energy Commission by the Nuclear Division of Union Carbide Corporation

The present experiment was designed to analyze the nucleotide pool of an adenine-requiring and uracil-requiring strain before and after removal of these bases from the synthetic medium.

Briefly, removing adenine and uracil decreased the cellular pool of uracil and its derivatives, uridine, UMP,<sup>5</sup> and UDP, and increased the cellular pool of adenine and its derivatives, AMP and ADP.

## METHODS AND MATERIALS

A haploid strain of the yeast *Saccharomyces cerevisiae*, S1238D, was kindly supplied by Dr. T. R. Manney. This mutant strain requires adenine, uracil, and histidine for continued growth and reproduction. Its genotype is *a ur<sub>1</sub> ad<sub>3</sub>*. The *ad<sub>3</sub>* mutation leads to the requirement for both adenine and histidine ( $\beta$ ). Cells were grown in a synthetic medium consisting of dextrose (20 g/liter) and Difco yeast nitrogen base (MV) without amino acids (6.7 g/liter), supplemented where indicated with adenine (20 mg/liter), uracil (20 mg/liter), and histidine (20 mg/liter). They were grown at 30° C in 5 liters of medium in a Micro Ferm Model MF 105 fermenter and harvested in log phase ( $1 \times 10^7$  cells/ml) by centrifugation. The culture was continuously aerated (4000 ml/min) and rapidly agitated. The harvested cells were washed twice with sterile distilled water. Half of the cells were saved for extraction, and the rest were resuspended in 5 liters of preheated and preaerated synthetic medium without adenine and uracil.

A pellet of 5 ml of packed cells was obtained from the first harvest, and half of this pellet increased to 4 ml of packed cells in the deficient medium in 6 to 8 hours (60% increase in cell number). No further increase in packed cell volume or in cell number occurred, even after 16 hours. Cultures to be analyzed were harvested after 8 hours.

The cells were extracted with 1.75 volumes of ice-cold 0.5 N HClO<sub>4</sub> for 15 minutes, with intermittent stirring. The pH was then adjusted to 7 with about 3 to 4 drops of cold saturated KOH. The precipitate was spun down in a prechilled centrifuge cup (2500  $\times$  g) for 3 minutes. The supernatant was saved and 3 to 4 drops of 4 M sodium acetate (NaAc) were added to a concentration near 0.15 M and a pH of 4.4. The extract was then ready to be placed on the column. Samples of about 3 to 6 ml were used.

As our chromatographic procedures do not differ significantly from the method of Anderson *et al.* (1), we will give only a brief outline of the procedure. The column was 0.9  $\times$  155 cm of Dowex 1- $\times$ 8; the flow rate was initially 0.715 and changed to 1.10 ml per minute after 3.5 hours; absorbance was recorded at 260 and 280 m $\mu$  in a 1-cm Oak Ridge flow cell with a modified Beckman DB spectrophotometer. The

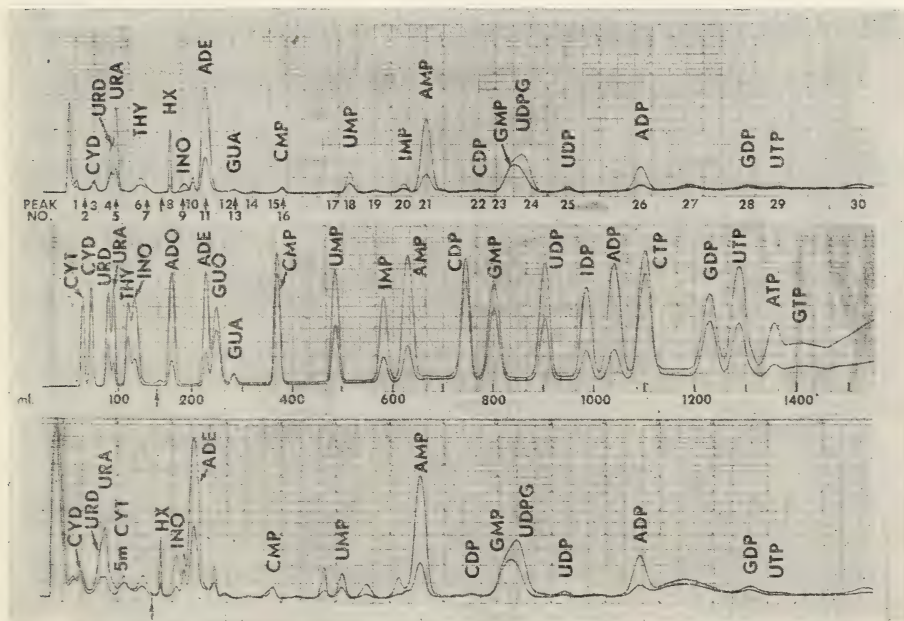
<sup>5</sup> Abbreviations for nucleotides and other compounds used in this paper are the accepted usage of the *Journal of Biological Chemistry*. [See vol 241 (1): 5-8, 1966.]

sample was eluted with an 1800 ml convex gradient of NaAc at pH 4.4 (0.15–3 M). Compounds were identified by comparison of the times at which they were eluted with the times for elution of known standards run on the same column, and on the basis of 280 to 260 m $\mu$  absorbance ratios at pH 4.4. The compounds were quantified according to previously described techniques (1, 2).

## RESULTS

Repeated freezing, cold storage, and thawing of an extract did not change the chromatographic profile noticeably. Extractions of a culture gave superimposable chromatographic profiles. Repetition of the entire experiment on different days gave essentially the same chromatographic profile.

The chromatographic separation of a standard mixture of bases, nucleosides, and nucleotides is shown in text-figure 1, center chart. Standard solutions (containing several compounds) were made up at a concentration of 2 mM for each compound except guanine, which was 0.2 mM. A



TEXT-FIGURE 1.—Chromatograph of bases, nucleosides, and nucleotides from yeast.

(a) *Upper chart:* chromatograph of an ice-cold 0.5 N HClO<sub>4</sub> extract of log phase yeast. The column was eluted with an 1800 ml convex gradient of NaAc at pH 4.4 (0.5–3.0 M). Absorbance is shown at 280 and 260 m $\mu$ . A 1-cm quartz flow cell was used. The identifiable compounds are indicated. (b) *Center chart:* separation of a known mixture of bases, nucleotides, and nucleosides by the same system (see text for mixing composition). (c) *Lower chart:* separation of the extracted nucleotides from nongrowing yeast deprived of required adenine and uracil. Pump flow rate was changed from 0.715 to 1.10 ml per minute after 3.5 hours of run.

standard mixture for chromatography contained 0.1 ml of a mixture of Cyt, Cyd, Urd, Ura, and Thy; 0.2 ml of a mixture of Ino, Ado, Ade, Guo, and Gua; 0.4 ml of CMP, UMP, IMP, AMP, and GMP (all 5' isomers); 0.5 ml of CDP, UDP, ADP, and GDP; and 0.8 ml of CTP, UTP, ITP, ATP, and GTP. The chromatographic separation of this standard solution demonstrates the resolving power of the procedure. The separation is good, but some tailing is evident after the elution of UTP.

Although several changes are notable in the chromatographic profile of acid-soluble nucleotides from log phase yeast and from nongrowing yeast deprived of required adenine and uracil for 8 hours, in general, the profiles are similar (*cf* text-fig. 1a, c).

The absorbance ratios of the peaks from the column effluent at pH 4.4 are given in table 1. Ratios are given for the log phase yeast culture, the nongrowing culture (without adenine and uracil), and the standards. The peaks on the chromatograph from the log phase culture are numbered for easy reference. After adenine and uracil deprivation, a new peak appears after Urd, between peak 5 and 6 (it has the chromatographic and optical properties of 5 methyl-*d* Cyt or uric acid), and increases are seen in the peak just preceding hypoxanthine ("Hx") in the peaks on either side of Ade and in the peaks on either side of UMP.

TABLE 1.—Absorbance ratios (280/260 m $\mu$ ) from the column effluent at pH 4.4

Peak No.	Compound	Grown in MV + hist + ad + ur	Grown in MV + hist	Observed from standard run
1				
2	Cyd			
3				
4	Urd	0.365	0.35	0.35
5	Ura	0.214	0.2	0.20
6	Thy (?)	0.51		0.55
7				
8	Hx	0.09	0.17	0.11*
9	Ino	0.29	0.214	0.25
10		0.74	0.55	
11	Ade	0.229	0.214	0.22
12			0.455	
13	Gua	~1	~1	1.0
14				
15				
16	CMP	>1	>1	1.53
17			0.61	
18	UMP	0.394	0.398	0.38
19			0.27	
20	IMP	0.25	0.2	0.24
21	AMP	0.192	0.186	0.174
22	CDP	>1	>1	1.7
23	GMP	0.7	0.7	0.66
24	UDPG (?)	~0.4	0.35	0.38†
25	UDP	0.4	~0.4	0.39
26	ADP	0.2	0.2	0.187
27				
28	GDP			
29	UTP			
30				

\*Taken from Anderson *et al.* (1).

†Pabst Research Biochemical, Specifications Circular OR-17, Milwaukee, Wis.

Table 2 lists the cellular content of various identifiable nucleotides from these cultures. Uracil and its derivatives, Urd, UMP, and UDP, are all substantially decreased, while adenine and its derivatives, AMP and ADP, are slightly increased. The cellular content of hypoxanthine is decreased and GMP shows little quantitative change.

TABLE 2.—Quantification of yeast nucleotide pool compounds (expressed in mmoles/10<sup>10</sup> cells)

Compound	Grown in MV + hist + ad + ur	Grown in MV + hist	Increase or de- crease (%)
Urd	0.249	0.196	-27
Ura	0.374	0.189	-98
Hx	0.112	0.048	-133
Ade	0.489	0.540	+12
UMP	0.080	0.054	-48
AMP	0.290	0.373	+42
GMP	0.173	0.169	
UDP	0.027	0.012	-125
ADP	0.091	0.117	+29

## DISCUSSION

The excellent chromatographic separations of mixtures of bases, nucleotides, and nucleosides, as well as the yeast nucleotide pools, attest to the value of this system. The nucleotide pool of growing and non-growing yeast does not undergo appreciable qualitative changes even after being deprived of required adenine and uracil. Perhaps the yeast cell is able to adjust nucleic acid synthesis to maintain or slightly increase adenine and nucleotide derivatives. It is known that exogenous hypoxanthine can satisfy the adenine requirement in this yeast (3). That the hypoxanthine pool is decreased during deprivation suggests that adenine derivatives may stem in part from a hypoxanthine reserve. The usefulness of maintaining adenine derivatives for glycolysis and oxidative phosphorylation has been pointed out by Burns (4). Yeast may be able to stop nucleic acid synthesis while continuing carbohydrate metabolism. On the other hand, uracil and its derivatives are decreased, which suggests that the regulation of purine and pyrimidine pools may not be controlled in the same manner. Our results suggest that uracil, and not adenine, may be limiting to growth.

## REFERENCES

- (1) ANDERSON, N. G., GREEN, J. G., BARBER, M. L., and LADD, F. C.: Analytical techniques for cell fractions. III. Nucleotides and related compounds. *Anal Biochem* 6: 153-169, 1963.

- (2) ANDERSON, N. G.: Analytical techniques for cell fractions. II. A spectrophotometric column monitoring system. *Anal Biochem* 4: 269-283, 1962.
- (3) DORFMAN, B. Z.: Complementation and meiotic recombination at the *Ad-5-7* locus in *Saccharomyces cerevisiae*. Ph.D. Thesis, Yale University, 1964.
- (4) BURNS, V. W.: Regulation and coordination of purine and pyrimidine biosynthesis and its relation to transient changes in intracellular nucleotide levels. *Biophys J* 4: 151-166, 1964.

## Automated Carbohydrate Analyzer: Experimental Prototype<sup>1</sup>

JOHN G. GREEN,<sup>2</sup> *Biophysical Separations Laboratory, Technical Division, Oak Ridge Gaseous Diffusion Plant,<sup>3</sup> and the Biology Division, Oak Ridge National Laboratory,<sup>3</sup> Oak Ridge, Tennessee*

### SUMMARY

Although carbohydrate materials have important roles in biological structure and metabolism, a fully satisfactory system for the automatic fractionation and detection of complex mixtures of sugars has not been devised. In the system described here, such mixtures of sugars, which may be found in extracts or hydrolysates, are fractionated as borate complexes on strongly basic anion exchange resin in borate form by elution with borate buffers. The eluate is processed continuously by phenol-sulfuric acid colorimetry, and the ab-

sorbancy of the processed stream is monitored and recorded to give a permanent record of the fractionation. The analytical system has been applied satisfactorily to the analysis of simulated extracts and hydrolysates and to the assay of microbiological growth media. In addition, the analyzer is applicable potentially to the analysis of phosphorylated and alkylated derivatives and to the study of polysaccharides.—*Nat Cancer Inst Monogr* 21: 447-46, 1966.

THE DEVELOPMENT of automated systems for the analysis of amino acids (1) and nucleotides and related materials (2) has facilitated greatly the study of these compounds in biological systems. Although carbohydrates have important roles in the structure and metabolism of organisms, an analogous system for their quantitative separation and analysis has not been described previously. An experimental prototype of a suitable system is described here. A preliminary report of this work has appeared (3).

Paper and thin-layer chromatographic procedures, as applied to the analysis of sugars, do not yield satisfactory separations of many complex mixtures, are not adapted to preparative-scale separations, and do not give quantitative results. Adsorption chromatography has been applied to the separation of sugars and oligosaccharides on charcoal (4, 5) and on

<sup>1</sup> This research performed under the Joint National Institutes of Health-Atomic Energy Commission Zonal Centrifuge Development Program which is supported by the National Cancer Institute, the National Institute of Allergy and Infectious Diseases, and the U.S. Atomic Energy Commission.

<sup>2</sup> The author was supported by U.S. Public Health Service Postdoctoral Fellowship GPD-15,703 during a part of the developmental period.

<sup>3</sup> Operated for the U.S. Atomic Energy Commission by the Nuclear Division of Union Carbide Corporation.

cellulose columns (6-8). In addition, oligosaccharides have been separated by gel filtration (9). Many sugars do not exist normally as charged species; however, they will combine with anions, such as borate (10), tungstate, and molybdate (11), to yield ionizing complexes susceptible to ion exchange chromatography.

The well-known reaction between borate ions and polyhydroxy compounds to give negatively charged complexes has been used to develop ion exchange methods for the analysis of compounds in various sugar mixtures (12-18). In a related approach, mixtures of sugars have been fractionated by partition chromatography on ion exchange resins with ethanolic elution (19).

In most ion exchange applications, the presence of sugars in column eluates has been detected by manual colorimetric assay. Recently, automated colorimetric procedures have been applied, including anthrone or cysteine assay (18), acid hydrolysis and ferricyanide reduction (19), and chromate oxidation (20). Gas chromatography has been applied to the separation of sugar derivatives (21). Although fractionations are very good, volatile sugar derivatives must be prepared. In addition, large-scale preparative separations are difficult to achieve with this method.

## DESIGN AND MATERIALS

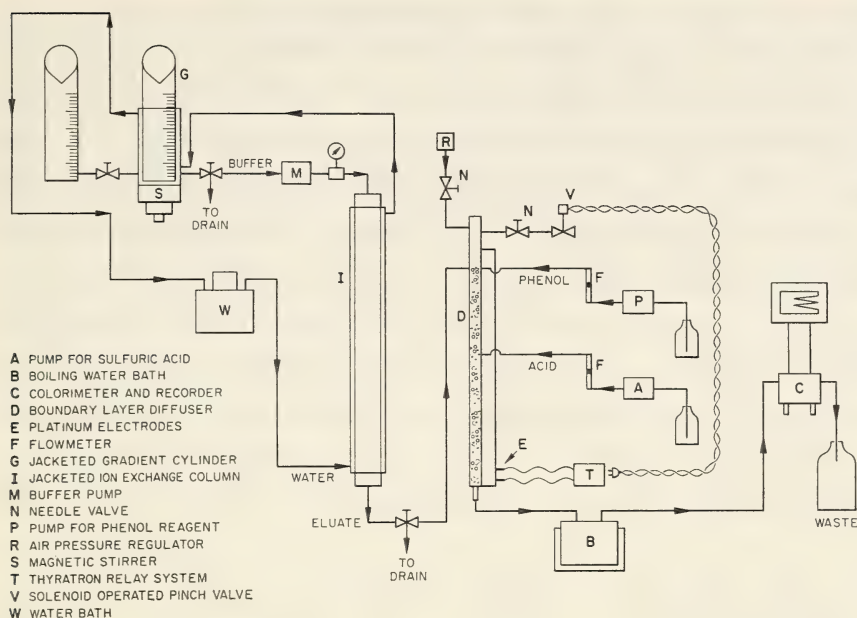
In the system depicted schematically in text-figure 1 and figure 1, sugars obtained from simple extracts or carbohydrate hydrolysates are fractionated by elution with borate buffers from a strongly basic anion exchange resin in borate form. The eluate is processed automatically by use of a phenol-sulfuric acid assay procedure (22) and a recorder to obtain a permanent record of the elution. On a typical chromatogram (text-fig. 2), eluted sugars appear as slightly asymmetrical peaks whose sequence is constant for a given elution schedule.

*Resin.*—Satisfactory separations have been obtained with Dowex 1- $\times$ 8 anion exchange resins, which have strongly basic quaternary ammonium groups on a polystyrene lattice. The initial separations were performed with a commercially fractionated<sup>4</sup> material (Lot 5495-33, B-1440), which is here arbitrarily designated S-I. Additional resins S-II (Lot 5893-35) and S-III (Lot 5743-7), obtained directly from the manufacturer,<sup>5</sup> have been fractionated hydraulically (23) to yield fine-mesh resins that increase the resolving capability of the system. Of the ion exchangers used thus far, S-III has given the best results.

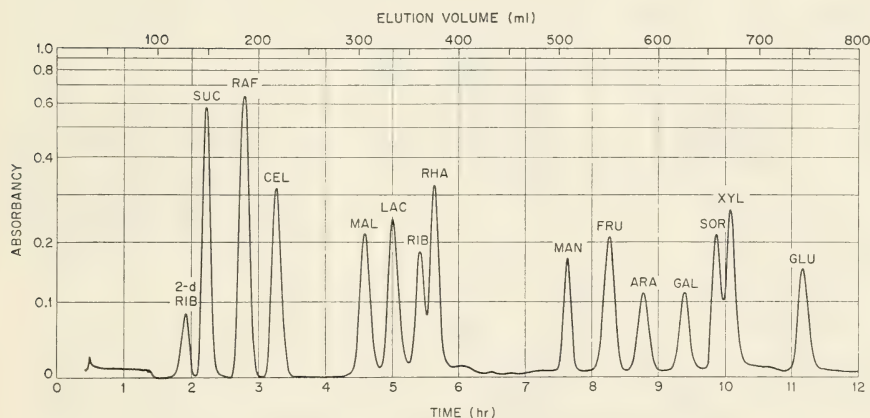
After fractionation, unprocessed resins were washed successively with 6 *N* sulfuric acid, anhydrous methanol, normal hydrochloric acid, normal sodium hydroxide, and borate elution buffer. The first two reagents were not used in the treatment of analytical-grade resins. Between each

<sup>4</sup> Bio-Rad Laboratories, 32d and Griffin Ave., Richmond, Calif.

<sup>5</sup> The Dow Chemical Co., Midland, Mich.



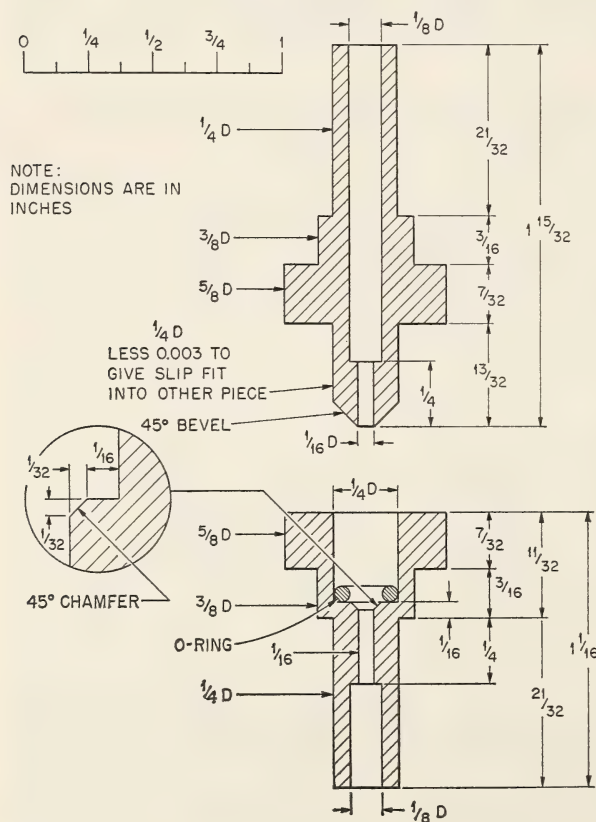
TEXT-FIGURE 1.—Schematic diagram of the carbohydrate analyzer.



TEXT-FIGURE 2.—Elution curve of a 15-component standard ( $0.75 \mu\text{M}$  of each sugar on a  $0.81 \times 158 \text{ cm}$  column. Gradient: 400 ml of  $0.142 \text{ M}$  sodium borate containing  $0.283 \text{ M}$  boric acid emptying into 400 ml of  $0.028 \text{ M}$  sodium borate containing  $0.057 \text{ M}$  boric acid. Flow rates (ml/min) are 1.14, 0.43, and 2.65 for buffer, phenol, and sulfuric acid, respectively. Absorbance at  $482 \text{ m}\mu$ . 2-d Rib = 2-deoxyerythropentose (2-deoxy-D-ribose); Suc = sucrose; Raf = raffinose; Cel = cellobiose; Mal = maltose; Lac = lactose; Rib = D-ribose; Rha = rhamnose; Man = D-mannose; Fru = D-fructose; Ara = D-arabinose; Gal = D-galactose; Sor = D-sorbose; Xyl = D-xylose; Glu = D-glucose.

solution change, the material was washed free of excess reagent with distilled water and finally suspended in borate buffer.

**Columns.**—Initially, jacketed glass columns measuring  $0.9 \times 150$  cm or  $0.9 \times 60$  cm fitted with ball and socket joints were used;<sup>6</sup> however, these columns are not suitable for pressures exceeding 80 psig. The use of fine-mesh resins requires columns fabricated from  $\frac{3}{8}$ - and  $\frac{1}{2}$ -inch O.D. heavy-walled borosilicate glass tubing and Swagelock<sup>7</sup> tubing fittings for operation at higher pressure. The fitting at the base of the column (fig. 2) is carefully machined to accept a sintered stainless steel disc of  $5 \mu$  porosity.<sup>7</sup> To reduce the internal volume of the fitting to a minimum an insert machined from rigid polyvinylchloride plastic was fitted against, the sintered disc. Eluate is taken from the column through AWG 22 Teflon tubing attached to the plastic insert by a swivel fitting.<sup>8</sup> The fitting at the top of the column is not altered; however, entry into the column requires loosening the fitting with a wrench to permit removal of the buffer inlet insert. An alternate arrangement, which does not require the use of wrenches, is shown in text-figure 3.



TEXT-FIGURE 3.—Column connector and seal. When a column is in use, the two parts of the seal are held together by a size 12A screw clamp.

<sup>6</sup> Scientific Glass Apparatus Co., Inc., Bloomfield, N.J.

<sup>7</sup> Fittings 810-6-4-316 and 600-6-4-316 from Crawford Fitting Co., 884 East 140th St., Cleveland, Ohio.

<sup>8</sup> Part 120-311 from Spince Division, Beckman Instruments, Inc., Palo Alto, Calif.

In accordance with the manufacturer's instructions, Teflon front and nylon back ferrules are used to attach the fittings to the carefully squared end of the glass tubing, and the tubing is seated against  $\frac{1}{32}$ -inch thick Teflon washers or  $\frac{1}{16}$ -inch O rings to cushion it against high-point pressures. Standard glass water jackets with screw caps and rubber bushing seals are used. Since the Teflon front ferrule tends to flow under compression, it is necessary to tighten the fittings periodically during the first 50 hours of service. These columns have been used at pressures up to 600 psig; however, to prevent lifting of the top fitting at pressures exceeding 400 psig, it is necessary to roughen the glass at the top of the larger column by wet sanding.

A circulating water bath supplies heated water to jackets on both the columns and the terminal gradient cylinder described below. A 3-way stopcock permits the selective warming of either column, limiting the total exposure time of a column to elevated temperatures to little more than the time necessary to make a separation.

Resins suspended in approximately 2 volumes of dilute buffer are packed in the column with pressurized air or buffer. For reprocessing, they may be removed from the columns by a combination washing and suction procedure. Air and vacuum for these operations are obtained from line sources or from a suitably trapped combination air and vacuum pump.

*Elution system.*—The sodium borate elution buffer is delivered from two 1000 ml graduated cylinders connected in parallel to permit the formation of simple concentration gradients. To deaerate the buffer, and thus prevent the appearance of dissolved air at the base of the warm columns, the terminal cylinder is fitted with an integral, partial water jacket. Water passes from a constant-temperature, circulating water bath through the column jacket, through the cylinder jacket, and then returns to the bath. Evaporation of water from the buffer is minimized by a simple inverted drop-shaped glass condenser placed at the top opening of the terminal cylinder. To permit filling without mixing of the two solutions, the cylinders are connected through stopcocks with Teflon plugs, and, to permit draining or flushing, the contents of the terminal cylinder may be directed through a 3-way stopcock either to the drain or to a pump. The buffer is delivered to the column by a piston-type metering pump<sup>9</sup> through  $\frac{1}{8}$ -inch O.D. by 0.030-inch wall Teflon tubing. A pressure gauge with stainless steel movement and wetted parts permits visual monitoring of the buffer pressure and prevents sudden hydraulic shocking of the glass columns. All wetted parts in the elution system are glass, Teflon, or 316 stainless steel.

*Colorimetric system.*—The colorimetric stream-processing system consists of pumps to deliver reagents, a pulse-dampening system associated with each pump, a boundary layer diffuser where mixing and degassing occur, a boiling water reaction bath, a colorimeter and single pen recorder, and associated tubing and connectors.

<sup>9</sup> Minipump, CHMMI-B-29R, Milton Roy Co., 1300 E. Mermaid Lane, Philadelphia, Penna.

Reagent-grade concentrated sulfuric acid is dispensed from 9-pound bottles, and the pump lead is transferred to another bottle when one is emptied. Sixty ml of reagent-grade liquefied phenol (approximately 88%) is diluted to 1-liter to obtain the phenol reagent. The liquefied phenol is dispensed directly from a 2-liter bottle with a self-filling burette, and each bottle is checked by running a calibration standard through the analyzer. Since phenol solutions are sensitive to light, they are stored and dispensed from brown or opaque-glass containers.

The phenol is delivered by a solution metering pump (Beckman Model 74601),<sup>10</sup> which has not been altered. The acid is metered by a similar pump (Model 74603), which is fitted with Teflon-coated valve diaphragms that are available in kit form from the manufacturer. To render the latter pump suitable for dispensing sulfuric acid, it is necessary to replace the valve and cylinder retainers with parts fabricated from corrosion-resistant material, such as filled Teflon.<sup>11</sup> A pulse-dampening system (fig. 3) is mounted with each pump. A pump delivers a reagent through a glass-ball check valve<sup>12</sup> to an air dome-reservoir, and the reagent passes from the reservoir through a needle valve<sup>13</sup> to the remainder of the system. The selection of pumps with high stroking rates and careful adjustment of the needle valves yield flow rates that vary only 3 percent during a pump cycle. The check valves isolate the pumps from back pressure of the system except during the delivery portion of their cycles.

Flow rates are measured by timed delivery from modified burettes and by observation of variable area flowmeters.<sup>14</sup> Delivery from the burettes may be used to calibrate the flowmeters, and the latter afford a visual check of the effectiveness of dampening the reagent flow.

Mixing of the phenol and eluate, addition of the acid, and initiation of color development occur in the boundary layer diffuser (fig. 4). The device is fabricated from 6 mm I.D. borosilicate glass tubing and filled to the level of the phenol and sample inlet tubes with borosilicate glass beads 3 mm in diameter. The phenol and eluate are introduced at the top of the bead column through short lengths of 4 mm glass tubing. They mix during flow as a thin film over the surface of the beads in the first 22 cm of the column. At the 22 cm level, the sulfuric acid is added to the flowing stream through a short length of 4 mm glass tubing. Heating of the stream upon the addition of the acid affords very rapid mixing; however, gas is released during the reaction. The additional 42 cm length of the diffuser allows the gas to diffuse from the flowing film. To prevent entry of gas into the stream monitoring system, the gas is vented from the diffuser through a metering stopcock with a Teflon plug.<sup>15</sup> The process stream is pooled to a depth of 2 cm at the base of the bead column, and the level of the pool is sensed by two platinum electrodes (fig. 5a), inserted

<sup>10</sup> Scientific and Process Instruments Division, Beckman Instruments, Inc., Fullerton, Calif.

<sup>11</sup> Rulon, obtained from the Dixon Corporation, Bristol, R.I.

<sup>12</sup> Catalogue No. M-309900, H. S. Martin and Son, 1916 Greenleaf St., Evanston, Ill.

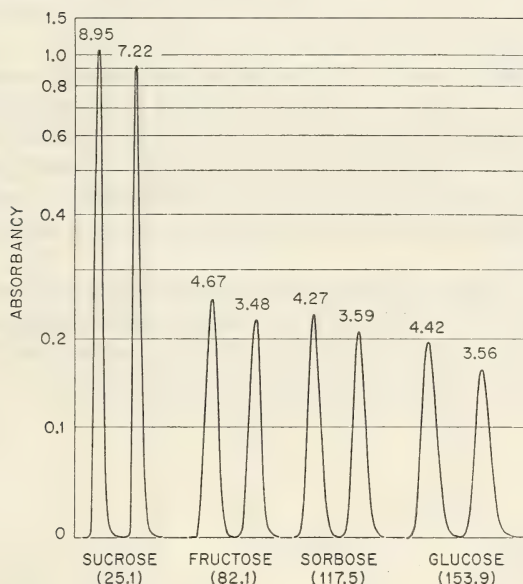
<sup>13</sup> Catalogue No. 795-500, Fisher and Porter Co., Warminster, Penna.

<sup>14</sup> Catalogue Nos. F1100 and F1200, Kontes Glass Co., Vineland, N.J.

<sup>15</sup> Catalogue No. 790-006, Fisher and Porter Co.

through Teflon union fittings,<sup>16</sup> controlling the function of a normally open, thyatron-controlled relay system. When the pool level rises to close the sensing circuit across the electrodes, the venting system is closed by the action of a solenoid-actuated pinch clamp (fig. 5b). When the pool level is depressed by accumulated gas to open the sensing circuit, the venting system is opened. The maximum pool depth may be adjusted by repositioning the upper electrode, and the metering valve is adjusted to give a bleed rate slightly exceeding the rate of gas generation.

Although the process may be monitored directly from the diffuser, color intensity is enhanced by passing the stream through a simple boiling-water bath. The bath consists of a 2-liter borosilicate glass bottle heated by a mantle supported by a stainless steel beaker. The heat output of the mantle is adjusted by a variable transformer to maintain gentle boiling of the water, and water vapor from the flask is condensed in a short metal coil formed from soft copper tubing (0.5 inch in diameter) and is returned to the bath. The reagent stream passes through a 6-meter length of  $\frac{1}{8}$ -inch O.D. by 0.030-inch wall Teflon tubing



TEXT-FIGURE 4.—A composite curve illustrating the effect of the reaction bath on the color intensity of  $1 \mu\text{M}$  sugar samples eluted under identical conditions. In each pair, the curve on the right was produced when the reaction bath was bypassed. The figures in parentheses denote the retention volumes in milliliters, and the figures at top of curves denote the approximate areas under each curve. In each case, this value is reduced approximately 20 percent by removal of the reaction bath from the system. A negligible effect of passage of the stream through the bath on peak width is shown only with sucrose, which elutes quickly in this system.

<sup>16</sup> Catalogue No. 830204, Scientific and Process Instruments Division, Beckman Instruments, Inc., Fullerton, Calif.

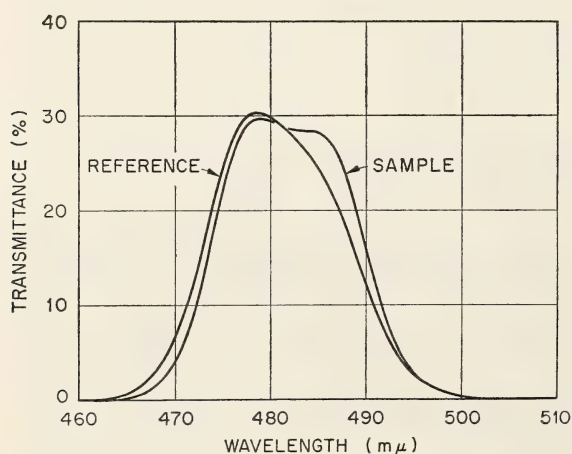
randomly coiled in the water bath. The effect of the addition of the incubation bath is shown in text-figure 4, and increasing the length of tubing beyond 6 meters has not enhanced the color development.

The absorbancy of the processed stream is monitored with a Technicon<sup>17</sup> colorimeter-recorder system fitted with the tubular flow cell with a 15 mm light path. The stream is conducted to and from the cell through Acidflex<sup>17</sup> tubing, but since this tubing hardens somewhat in use, permitting seepage to occur, it is anchored to the cell inlet and outlet with O rings slipped over the tubing on the glass nipples of the cell. Occasionally air bubbles arise, but no attempt is made to remove them from the stream. The outlet tubing from the cell is passed directly to a simple antisiphon device connected to a waste receptacle or acid-resistant drain.

In the colorimetric system used here, where pentoses absorb maximally at about 480 m $\mu$ , and hexoses and di- and oligosaccharides at 485 to 490 m $\mu$ , a selected interference filter having a broad-peak transmittance from 479 to 485 m $\mu$  was used. The sample and reference filters were supplied by Technicon to suit this application, and transmission spectra are shown in text-figure 5. The reference aperture is selected to place the 100 percent transmittance adjustment near mid-range, and the recorder chart speed is set at 2 inches per hour.

Filtered air, reduced to 8 psig and admitted through a metering stopcock, is introduced into the stream-processing system at the top of the diffuser. By suitable manipulation of the 3-way stopcocks at the base of the diffuser and at the pulse-dampening modules, any portion of the system may be purged with air prior to disassembly. In addition, air may be admitted to the diffuser at the start of each analysis to adjust the pool level.

The phenol reagent is transmitted through neoprene tubing ( $\frac{1}{4}$ -inch O.D.  $\times$   $\frac{1}{8}$ -inch I.D.), which slips over 4 mm glass tubing or into 6 mm Teflon tube fittings. The sulfuric acid is carried by (a) Teflon tubing



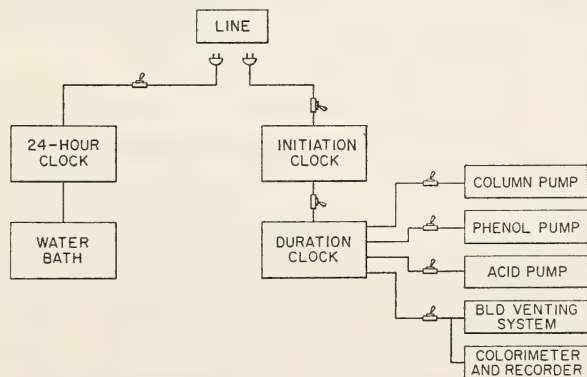
TEXT-FIGURE 5.—Transmission spectra of the interference filters used in the colorimetric monitoring system.

<sup>17</sup> Technicon Instruments Corporation, Research Park, Chauncey, N.Y.

( $\frac{3}{16}$ -inch O.D.  $\times$  0.030-inch wall), which slips tightly over 4 mm glass tubing for nonpressurized applications or into 4 mm tube fittings and (b) Teflon tubing ( $\frac{1}{8}$ -inch O.D.  $\times$  0.030-inch wall), which is fitted into 4 mm tube fittings with sleeves of Acidflex tubing slipped over the Teflon. Where 4 mm unions are used to join  $\frac{1}{8}$ -inch O.D. Teflon tubing in the stream-processing system, the tubing is cut square, passed through Acidflex tubing sealing sleeves, and butt-joined in the center of the fitting.

A simple programing system (text-fig. 6) controls operation of the analyzer. The water bath is given a single on-off cycle during a 24-hour period and may be shut down entirely for extended periods. Two 20-hour clocks<sup>18</sup> control the elution programing cycle: 1) an initiating timer, which is OFF while timing, turns on the second clock; 2) a duration timer, which is ON while timing. In the preanalysis column equilibration operation, the water bath is cycled to turn on 1 hour before the duration timer; only the column pump is switched to the ON position, and the column eluate is valved to drain. To program a sample analysis, the initiation timer is bypassed, and the switches are turned on for the column pump and the colorimeter-recorder and venting system. Elution is begun by closing the duration timer master switch, which turns on the pump and monitoring system. The eluate is valved to the boundary layer diffuser, and at 2-minute intervals first the phenol pump and then the acid pump are started. Finally, the pool level in the diffuser is adjusted with air as described previously. At the termination of an analytical run, the duration timer automatically shuts down the entire chromatographic system. Programing of the water circulation system is not essential but does limit to a desirable minimum the exposure of columns and buffers to elution temperatures.

Only borate elution buffers have been used in the present system where the  $pH$ , and thus the relative composition, of the buffer is selected to give optimum resolution with each resin lot. The buffer is prepared as a stock solution, and dilutions are made as necessary. The relative concentrations of sodium borate ( $Na_2B_4O_7 \cdot 10 H_2O$ ) and boric acid ( $H_3BO_3$ )



TEXT-FIGURE 6.—Schematic diagram of the programing system.

<sup>18</sup> Type HA Microflex, Eagle Signal Co., Moline, Ill.

required depend on the resin lot used and are, respectively, 0.157 and 0.186 M for resin S-I and 0.142 and 0.283 M for the others.

Standard solutions containing up to 15 commonly occurring sugars have been prepared, 5 mm with respect to each sugar, in stock borate buffer. They have been stable for as long as several months at room temperature. If refrigerated storage is desired, they should be prepared in diluted buffer to prevent salt crystallization at reduced temperatures. The sugars used in resolution studies (24) are listed in the legend of text-figure 2.

## RESULTS AND DISCUSSION

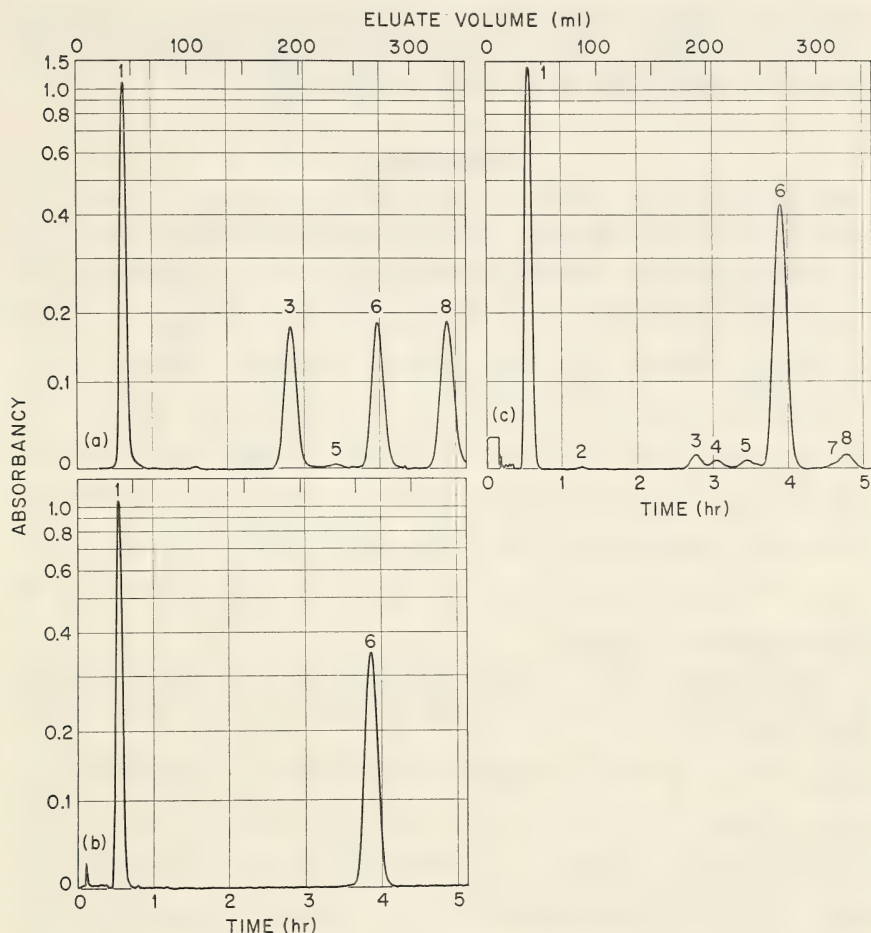
### Chromatography

A chromatogram obtained from a full standardization analysis is shown in text-figure 2. The least satisfactory separations are (a) D-ribose and rhamnose, and (b) D-sorbose and D-xylose. The former separation is pH sensitive, and the latter is dependent on the resin batch used; however, the separations are sufficient to permit quantitation with resin lot S-III. Full standard runs were completed in less than 12 hours, and less complex mixtures were run faster, as shown in text-figure 7.

The resolving capability of the chromatographic system is a function primarily of the resin. In this system, using a borate buffer for elution, Dowex-2 resin yielded separations of sugars inferior to those obtained with Dowex-1 and unsuitable for complex mixtures. Although greater separation of eluted peaks was obtained with Dowex-1 with a 4 percent cross-linked resin, the latter tends to compress under pressure. Resins having 8 percent and higher cross-linkage values show little or no compression at pressures as great as 450 psig. The most substantial improvement in resolution has been obtained by using resins with fine particle size; however, when these materials are used, the pressure required to maintain a specified flow rate increases. The mean diameter and size range for 90 percent of the particles in each lot used thus far are  $36 \pm 11 \mu$  for S-I,  $33 \pm 8 \mu$  for S-II, and  $13 \pm 6 \mu$  for S-III.

The resolving capability of the specified Dowex 1- $\times$ 8 resin varies with each lot. Lot S-II has a somewhat different affinity for the sugar complexes than the other two lots tested, and to obtain equivalent performance, elutions on S-III should be performed with buffers having a lower pH than buffers used with S-I. Changes in the pH and ionic strength of the buffer may equalize the performances of the resins.

While many analyses may be made with simple elution techniques, complex samples, such as the 15-component standard, require gradient elution and careful control of the pH and temperature of the elution systems. Most elutions are performed at pH values of 8.5 to 8.7, which are obtained by varying the relative proportions of sodium borate and boric acid in the buffers. In general, lowering pH tends to accelerate the



TEXT-FIGURE 7.—The effect of sterilization on Fries' *Neurospora* culture medium with sucrose and sorbose as carbon sources. The chromatograms are: (a) standard solution containing  $1\ \mu\text{M}$  of each sugar, (b) filter-sterilized medium, and (c) heat-sterilized medium. The sugars are: 1) sucrose, 2) unknown, 3) fructose, 4) unknown, 5) unknown, 6) sorbose, 7) unknown, and 8) glucose. Gradient elution was employed. Absorbancy at  $482\ \text{m}\mu$ .

passage of bands through the column; however, for each resin lot, an optimal pH appears to exist for maximal resolution.

The resolving capability of the system is affected by the temperature at which the elution is performed. In this system, the width of an eluted band decreases with temperature increase from room temperature to  $55^\circ\text{C}$ , and complex separations cannot be achieved at temperatures below  $40^\circ\text{C}$ . Little improvement is obtained by performing elutions at temperatures higher than  $55^\circ\text{C}$ , and at temperatures above  $65^\circ\text{C}$  some sugars, notably fructose and maltose, appear to degrade partially during passage

through the column. Routinely, elutions are performed at 50° C or, for increased resolution, at 55° C. At the latter temperature, resolution is optimal and degradative losses are inconsequential.

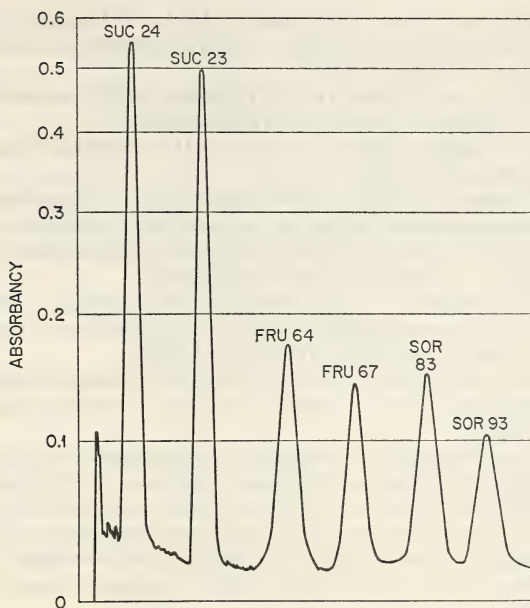
### Colorimetry

The phenol-sulfuric acid assay (22) is the most suitable method for the assay of the column effluents. Many colorimetric methods that utilize the reducing property of sugars are unsuitable because nonreducing sugars and polysaccharides cannot be assayed directly. Where a hydrolytic process has been used in conjunction with such a colorimetric process, only partial hydrolysis has been obtained on-stream. Anthrone colorimetry offers carbohydrate specificity but absorption maxima vary somewhat for each sugar (25), maximal color development requires variable incubation times depending on the sugar assayed (26), and colors tend to fade after reaching a maximum. In cases where the anthrone assay has been used to monitor column effluents, supplemental assays, such as the reaction with orcinol (16) or with cysteine (18), give a satisfactory analysis. In addition, the phenol-sulfuric acid method may be used to monitor phosphorylated and alkylated derivatives as well as long-chain polysaccharides.

A fluorometric method for microdetermination of carbohydrates (27) has been reported but requires a long incubation at 125° C to achieve stable endpoints.

To obtain data suitable for quantitative studies, it is imperative that the flow rate for the addition of the phenol reagent be controlled precisely, since maximal color development for each sugar depends on the relative concentration of this reagent. In the present system, the absolute flow rates for the eluent, phenol, and sulfuric acid are 1.14 ml per minute, 0.43 ml per minute, and 2.65 ml per minute, respectively. In this application, these proportions yield elution peaks with nearly equal areas for equimolar standards within each class of sugar. Other flow rates may be used for columns of different diameters if the relative concentrations of the reagents are maintained. For large flow rates, a stream-splitting assembly is used.

In the boundary layer diffuser, mixing is achieved by inducing turbulent flow due to boundary layer effects in the flowing liquids. It is essential, therefore, to maintain the liquid film yet to allow gas diffusion and flow space. The dimensions given in the preceding section are critical and allow best stacking of the glass beads. Increasing the diameter of the bead column yields peaks with greater band width; however, as demonstrated in text-figure 8, increasing the length of the column has virtually no effect on the resolution of the system. The band width of an elution curve and the degree of tailing appear to be directly related to the pool volume at the base of the bead column. At the start of an analysis, when the diffuser is cold, higher stream viscosity allows liquid bridging to occur between the beads and the wall; however, after the system



TEXT-FIGURE 8.—A composite curve illustrating the effect of bead column length in the boundary layer diffuser. The curve on the left was developed on a  $0.7 \times 14$  cm column and the curve on the right on a  $0.6 \times 34$  cm column. Numbers at each peak denote elution volume to maximum peak height. Variations in peak form are attributable to differences in concentration and elution volume for each pair rather than to length of the bead column. Absorbancy at  $482\text{ m}\mu$ . Suc = sucrose; Fru = D-fructose; Sor = D-sorbose.

becomes hot and the pool level is established initially by admitting pressurized air, bridging is eliminated. Alternate systems are under consideration, though the present system is effective and requires no maintenance. The platinum electrodes are unaffected by the hot acidic solutions after many hours of use, but the detector section of the relay unit must operate with very low currents, 5 ma or less, to prevent electrolysis. The concept of the boundary layer diffuser may be adaptable to other uses, such as on-stream mixing or hydrolytic and digestion procedures.

Reagent handling and waste disposal pose problems, since the reagents and waste are corrosive. Presently, the waste is collected in polyethylene bottles which are emptied, rinsed, and reused. A corrosion-resistant pump may be used to transfer the sulfuric acid from a large container to a machine reservoir. Where acid-resistant drains are available, the waste material may be drained directly.

### REFERENCES

- (1) SPACKMAN, D. H., STEIN, W. H., and MOORE, S.: Automatic recording apparatus for use in the chromatography of amino acids. *Anal Chem* 30: 1190-1206, 1958.
- (2) GREEN, J. G., and ANDERSON, N. G.: Prototype automatic carbohydrate analyzer. *Fed Proc* 24: 606, 1965.

- (3) ANDERSON, N. G., GREEN, J. G., BARBER, M. L., and LADD, Sister F. C.: Analytical techniques for cell fractions. III. Nucleotides and related compounds. *Anal Biochem* 6: 153-169, 1963.
- (4) WHISTLER, R. L., and DURSO, D. F.: Chromatographic separation of sugars on charcoal. *J Amer Chem Soc* 72: 677-679, 1950.
- (5) ALM, R. S.: Gradient elution analysis. II. Oligosaccharides. *Acta Chem Scand* 6: 1186-1193, 1952.
- (6) HOUGH, L., JONES, J. K. N., and WADMAN, W. H.: Quantitative analysis of mixtures of sugars by the method of partition chromatography. Part IV. The separation of the sugars and their methylated derivatives on columns of powdered cellulose. *J Chem Soc*: 2511-2516, 1949.
- (7) BOGGS, L. A., CUENDET, L. S., DUBOIS, M., and SMITH, F.: Simple fractionating device for chromatographic analysis. Application to the study of carbohydrates. *Anal Chem* 24(7): 1148-1151, 1952.
- (8) THOMA, J. A., WRIGHT, H. B., and FRENCH, D.: Partition chromatography of homologous saccharides on cellulose columns. *Arch Biochem Biophys* 85: 452-460, 1959.
- (9) FLODIN, P., and ASPBERG, K.: Separation of oligosaccharides with gel filtration. In *Biological Structure and Function* (Goodwin, T. W., and Lindberg, O., eds.). New York, Academic Press Inc., 1961, vol 1, pp 345-348.
- (10) BOESKEN, J.: The use of boric acid for the determination of the configuration of carbohydrates. In *Advances in Carbohydrate Chemistry* (Pigman, W. W., and Wolfrom, M. L., eds.). New York, Academic Press Inc., 1949, vol 4, pp 189-210.
- (11) ANGUS, H. J. F., BOURNE, E. J., SEARLE, F., and WEIGEL, H.: Complexes between polyhydroxyl-compounds and inorganic oxy-acids. Tungstate complexes of sugars and other cyclic polyhydroxy compounds. *Tetrahedron Letters* 1964: 55-60, 1964.
- (12) KHYM, J. X., and ZILL, L. P.: The separation of sugars by ion exchange. *J Amer Chem Soc* 74: 2090-2094, 1952.
- (13) NOGGLE, G. R., and ZILL, L. P.: The quantitative analysis of sugars in plant extracts by ion-exchange chromatography. *Arch Biochem Biophys* 41: 21-28, 1952.
- (14) KHYM, J. X., and COHN, W. E.: Separation of sugar phosphates by ion exchange with the use of the borate complex. *J Amer Chem Soc* 75: 1153-1156, 1953.
- (15) ZILL, L. P., KHYM, J. X., and CHENIAE, G. M.: Further studies on the separation of the borate complexes of sugars and related compounds by ion-exchange chromatography. *J Amer Chem Soc* 75: 1339-1342, 1953.
- (16) PARR, C. W.: The separation of sugars and sugar phosphates by gradient elution from ion exchange columns. *Biochem J* 56: XXVII-XXVIII, 1954.
- (17) HALLÉN, A.: Chromatographic analysis of sugars as complex borate ions. *Acta Chem Scand* 14: 2249-2250, 1960.
- (18) SYAMANANDA, R., STAPLES, R. C., and BLOCK, R. J.: Automatic analysis of sugars separated by column chromatography. *Contrib Boyce Thompson Inst* 21: 363-369, 1962.
- (19) SAMUELSON, O., and SWENSON, B.: Partition chromatography on ion exchange resins. Separation of sugars. *Acta Chem Scand* 16: 2056-2058, 1962.
- (20) SAMUELSON, O., and WALLENIS, L. O.: Anion exchange separations of aldobionic and aldonic acids. *J Chromatogr* 12: 236-241, 1963.
- (21) WELLS, W. W., SWEeley, C. C., and BENTLEY, R.: Gas chromatography of carbohydrates. In *Biomedical Applications of Gas Chromatography* (Szymanski, H. A., ed.). New York, Plenum Press, 1964, pp 169-223.
- (22) DUBOIS, M., GILLES, K. A., HAMILTON, J. K., REBERS, P. A., and SMITH, F.: Colorimetric method for determination of sugars and related substances. *Anal Chem* 28: 350-356, 1956.

- (23) VASSILIOU, B., and KUNIN, R.: Fractionation of fine particle-sized ion exchange resins. *Anal Chem* 35: 1328-1329, 1963.
- (24) Revised Tentative Rules, IUPAC Biological Chemistry Division, Information Bulletin No. 20, pp 13-29, 1963 (July).
- (25) KOEHLER, L. H.: Reaction of deoxy sugars with anthrone. *Anal Chem* 26: 1914-1916, 1954.
- (26) ———: Differentiation of carbohydrates by anthrone reaction rate and color intensity. *Anal Chem* 24: 1576-1579, 1952.
- (27) TOWNE, J. C., and SPIKNER, J. E.: Fluorometric microdetermination of carbohydrates. *Anal Chem* 35: 211-214, 1963.



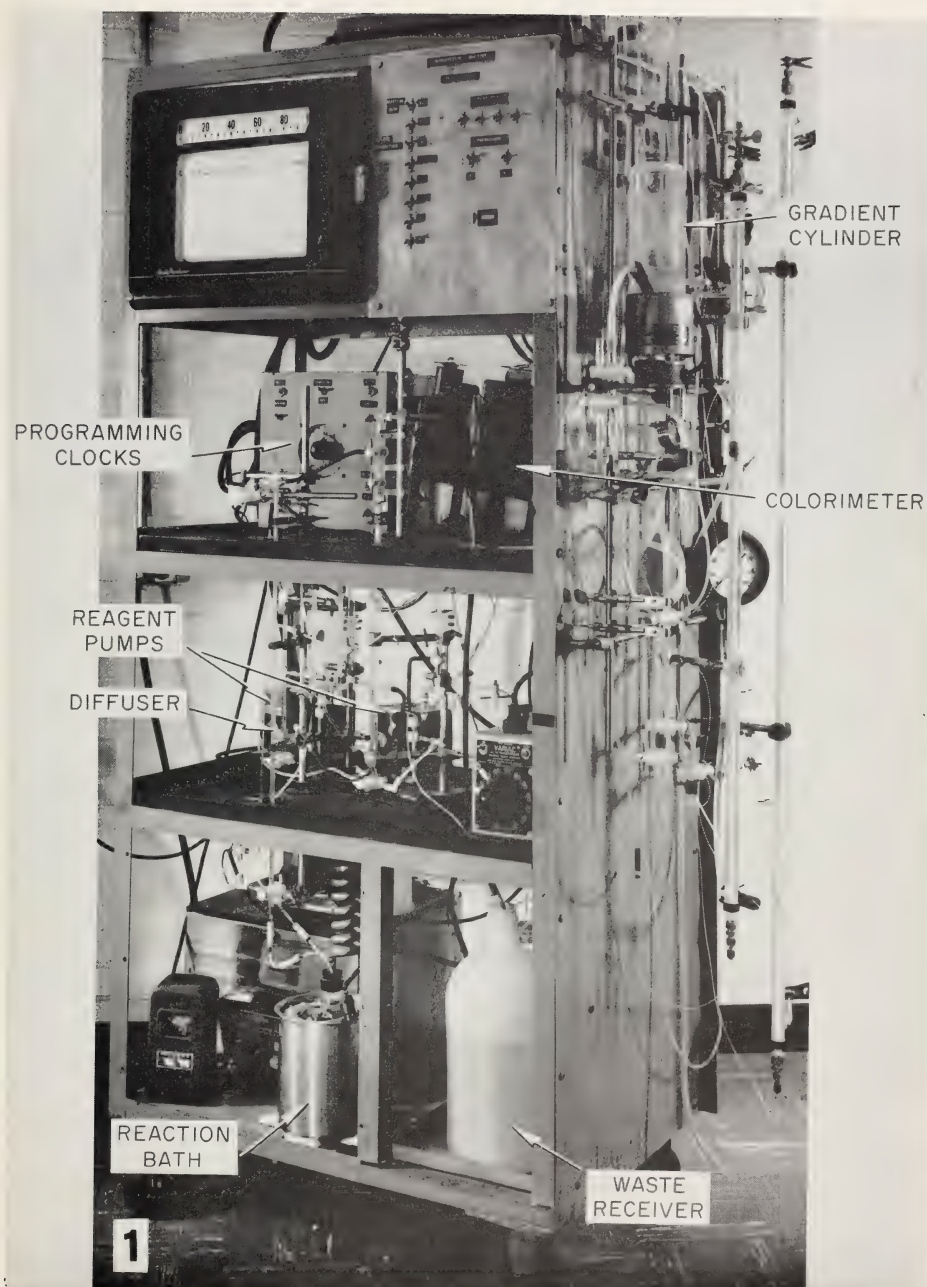


FIGURE 1.—Prototype carbohydrate analyzer.

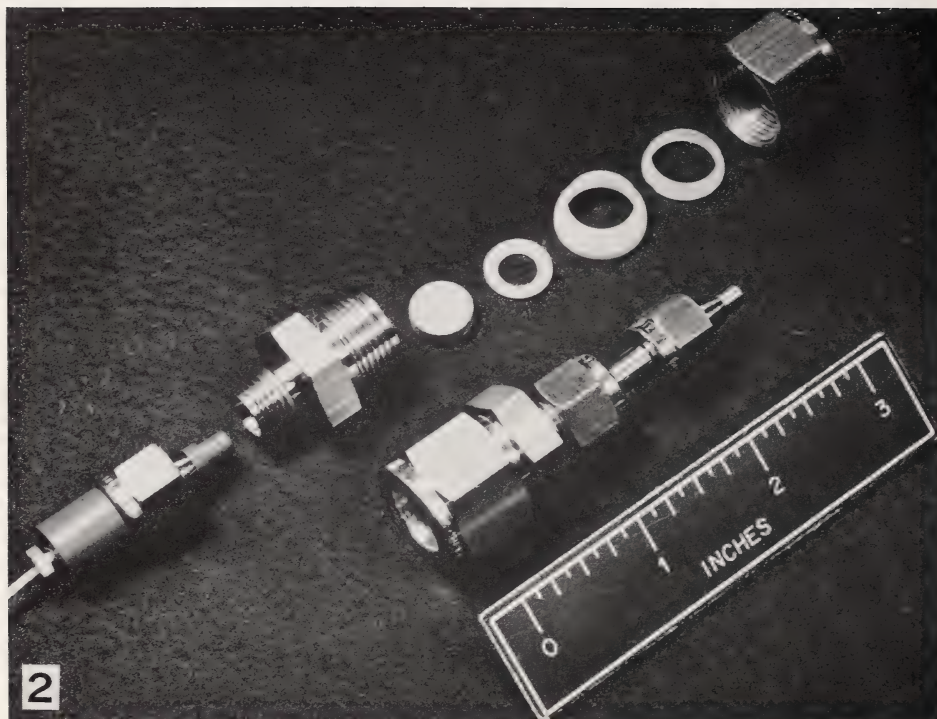


FIGURE 2.—Modified tube fittings used to adapt heavy wall glass tubing to high-pressure ion exchange studies. The basal fitting is disassembled to show ferrules, sintered stainless steel disc, and plastic insert with Teflon line attached through a swivel fitting.

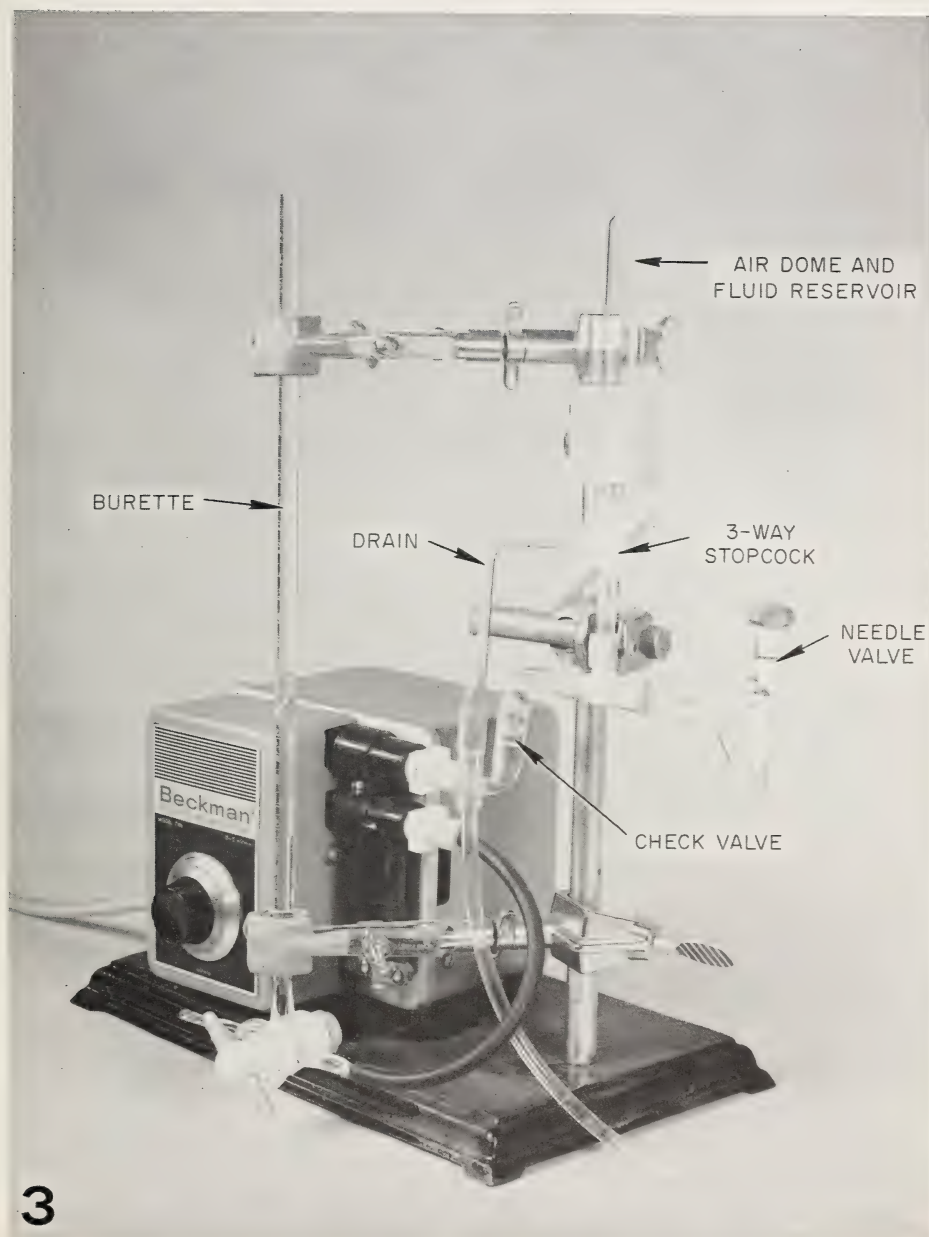


FIGURE 3.—Reagent pumping module. The pulsing output from the pump is pneumatically dampened to yield nearly constant reagent flow.



FIGURE 4.—Evolution of the boundary layer diffuser. The diffuser in use is at the *right*. An intermediate form used a manually operated gas bleed. The parts shown are (a) sample inlet, (b) phenol reagent inlet, (c) air inlet, (d) acid inlet, (e) gas bleed valve (metering stopcock), (f) 3-way stopcock, (g) electrodes in capillary sidearm.

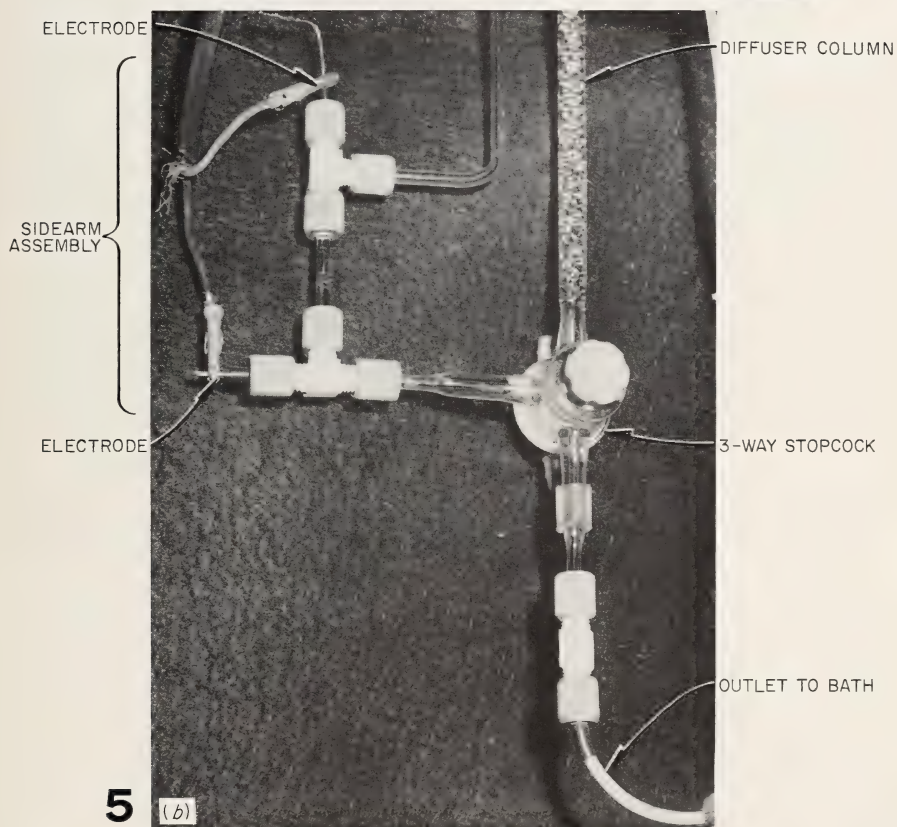


FIGURE 5.—Detail of top and base of the boundary layer diffuser showing the parts associated with (a) gas-venting and (b) fluid level-sensing.



## A Flame Ionization Analyzer for the Continuous, Rapid Determination of Carbon in Liquid Streams or Solid Samples<sup>1</sup>

R. H. STEVENS,<sup>2</sup> *Technical Division, Oak Ridge Gaseous Diffusion Plant,<sup>3</sup> Oak Ridge, Tennessee*

### SUMMARY

A flame ionization analyzer, capable of analyzing submicrogram-sized samples and liquid streams for carbon on a continuous, rapid basis, has been developed. Nongaseous samples can be introduced into the detector without the use of a separate pyrolysis chamber or a gas chromatography column. Samples are placed on a slowly moving loop of iridium-rhodium alloy wire and traversed horizontally into the flame. Problems arising from the loss of sample from the wire by evaporation or pyrolysis when proximal to the flame, but outside the flame envelope, have been overcome through the use of a horizontally fed flame jet that allows the wire to pass through the jet opening itself. Volatilized constituents are swept into the combustion zone of the flame by a nitrogen gas flow in close time synchrony with the less volatile sample components. The instrument has a fast time response, 0.125 second (63%), which permits individual analysis of discrete particular matter in the  $10^{-9}$  to  $10^{-6}$  g range, e.g., single biological cells, pollen grains or spores, and dust particles, even when closely spaced on the wire. The organic solute residues from the evaporation of microliter-sized droplets of solution hung on the wire have been analyzed, as well as drops of liquid simulating the effluent from liquid exchange columns.—*Nat Cancer Inst Monogr* 21: 469-483, 1966.

THE INTRODUCTION of the flame ionization detector by McWilliam and Dewar (1) in 1958 provided a very sensitive and specific means for quantitating carbon in organic materials in the gas phase. Since biological materials exist primarily in the liquid and solid phases, a direct and preferably continuous method for the analysis of these types of samples is desirable. Janak (2) and Keulemans and Perry (3), among others, have shown that solid samples of high-boiling points can be analyzed quantitatively by a pyrolysis-gas chromatography technique using a flame ionization detector. Karmen *et al.* (4) have obtained a nonspecific, "total" carbon determination of lipid material in the 5 to 100  $\mu$ g sample

<sup>1</sup> Research performed under the Joint National Institutes of Health-Atomic Energy Commission Zonal Centrifuge Development Program which is supported by the National Cancer Institute, the National Institute of Allergy and Infectious Diseases, and the U.S. Atomic Energy Commission.

<sup>2</sup> I wish to thank Mr. H. Rosander and Mr. C. Lovejoy for their excellent work in the fabrication of the wire-handling hardware and the coaxial jet

<sup>3</sup> Operated for the U.S. Atomic Energy Commission by the Nuclear Division of Union Carbide Corporation.

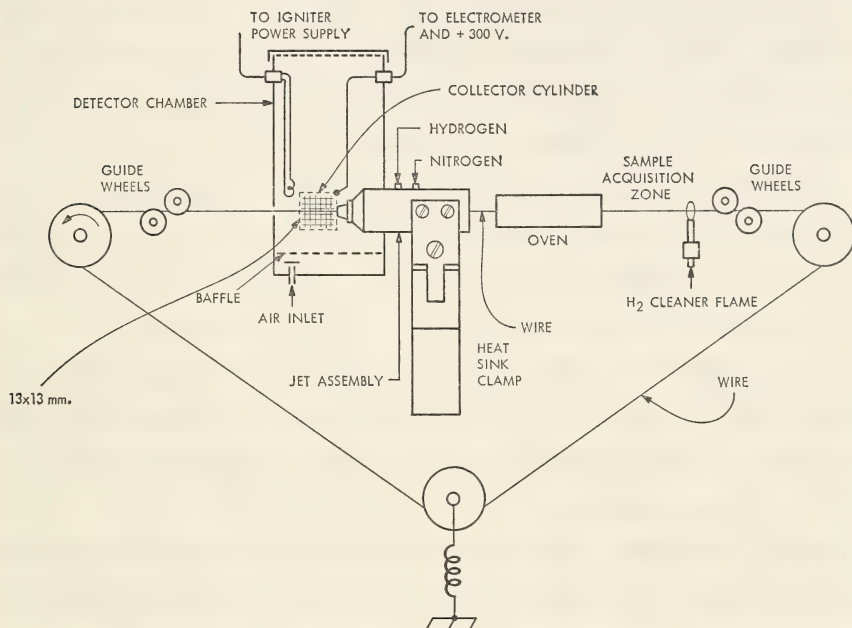
range by using a temperature-programed, uncoated, miniature column as a medium for removing solvent from a solute that is then pyrolyzed directly into a flame ionization detector. James *et al.* (5) have also described a liquid column monitor that acquires a thin film of solution by passing an iron wire through the column discharge, then pyrolyzes the sample from the wire into an argon stream flowing to an argon ionization detector. In all of these applications, the sample is introduced into the detector as a gas and, for solid samples, pyrolytic equipment is batch-operated and requires reloading a new sample before each analysis. Recently, means for introducing liquid samples continuously and directly into the flame of a flame ionization detector were developed by Haahti and Nikkari (6) and, independently, by Anderson and Stevens (7, 8) for solid and liquid samples. Haahti uses a continuous loop of gold chain to pick up solution from a liquid chromatography column, which then passes through a small oven to remove solvent, and finally into the flame of the detector. The analyzer described here is functionally similar to that of Haahti and Nikkari. This analyzer, however, uses a continuous loop of noble metal wire and a new coaxial jet design in which the wire and the fuel pass through the same nitrogen-swept channel to retain sample components volatilized from the wire when the sample approaches, but is still outside of, the flame envelope. This precombustion evaporation effect, also noted by Haahti, is caused by the conduction of heat from the flame along the wire and results in a considerable loss from samples in the  $10^{-9}$  to  $10^{-6}$  g range. The nitrogen-swept channel used here becomes the jet itself at the end of the flow path to assure that all volatile sample constituents will be swept into the combustion zone by the nitrogen gas.

The analyzer is characterized by a fast time response (0.125 sec), permitting rapid individual analysis of discrete particulate matter in the  $10^{-9}$  to  $10^{-6}$  g range, *e.g.*, single biological cells, pollen grains or spores, and dust particles, even when closely spaced on the wire. Organic materials in solution have been analyzed by evaporating the solvent from 1  $\mu$ l droplets of the solution hung on the wire, followed by movement of the residue into the flame. The use of the analyzer for monitoring column effluents has also been investigated.

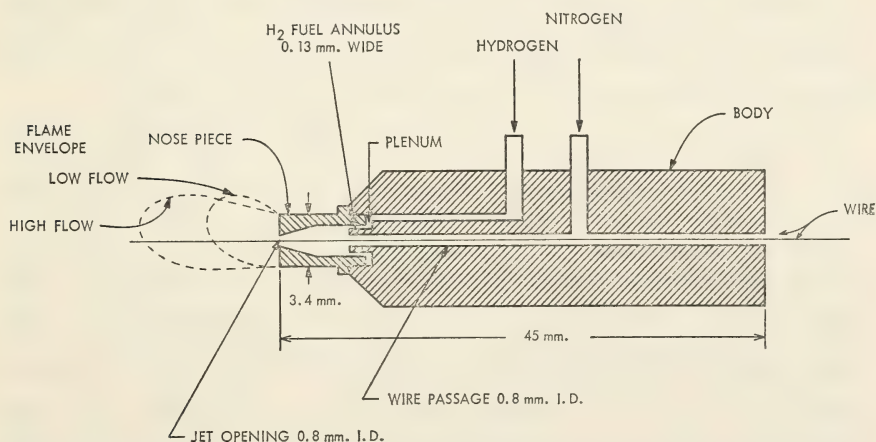
Flame ionization detectors operate by collecting either the electron or the positive ion current produced by carbon during the combustion of gaseous organic material in a hydrogen flame. The electrical signal obtained from the combustion of a given sample is, within wide limits, a linear function of the rate of carbon introduction to the flame (9, 10). This paper will deal with (a) the effects observed when a wire and solid samples are placed in the detector flame, (b) the conditions for best operation with solid samples, (c) the differences in magnitude of positive and negative ionization currents produced by a given sample on the wire, (d) methods for reproducibly sampling solutions and liquid flows, and (e) the results obtained with several types of samples and sampling techniques with the coaxial jet design.

## INSTRUMENTAL DESIGN

In the experimental apparatus used for the present studies (fig. 1 and text-fig. 1), a continuous loop of 0.13 mm diameter iridium-50 percent rhodium alloy wire (Englehard Industries, Newark, N.J.), 116 cm in circumference, is moved from a sample acquisition zone, through an oven to dry off solvents, and through a coaxial jet assembly (text-fig. 2)



TEXT-FIGURE 1.—Schematic diagram of flame ionization analyzer for carbon determination in solid and liquid organic samples.



TEXT-FIGURE 2.—Cross-sectional view of coaxial jet assembly.

into the flame. The nitrogen gas introduced into the assembly flows in both directions from the point of entry along the wire. The gas serves to assist in removing volatile solvents from the wire (gas flow to right) and to cause sample constituents volatilized from the wire when approaching the flame to be swept into the flame envelope. Hydrogen is also introduced into the jet assembly and burns around the wire as it passes out of the assembly channel. The wire within the flame envelope reaches a dull red color (approximately 500–600° C).

A heated aluminum block with U-slot along its top serves as an oven through which the wire passes. The oven accelerates the evaporation of solvent from droplets of solution hung on the wire, or from the thin coating of solution acquired by the wire when passing through a drop at the end of a liquid chromatography column.

A second small diffuse hydrogen flame about 3 mm high is used to clean the wire of "background" material picked up during its passage around the loop. The wire is normally traversed to the left at about 2.5 mm per second providing a total "hot" time from both the detector and cleaning flames for any spot on the wire of approximately 3 seconds per revolution. One revolution requires about 7.5 minutes.

The electrometer (Aerograph Model 500, Wilkins Instrument and Research, Inc.) was modified to provide input resistance in decade steps from  $10^6$  to  $10^{10}$  ohms, and the ignitor coil circuit was grounded. The wire and coaxial jet assembly are also grounded in normal operation. The collector screen is biased to either (+) or (–) 300 volts DC to collect the current of interest.

A small electrostatic precipitator has been used to collect air-dispersed particulate matter onto the sample transport wire. A corona discharge is established so that particles in the air flowing into the precipitator pass through the corona and acquire a negative charge by electron impingement. The wire (positively charged) then attracts the negatively charged particles and holds them until they pass into the detector.

A Sanborn Model 150 two-channel recorder (Sanborn Co., Cambridge, Mass.) has been used to record the current pulses from the ionization chamber, and pulse integration was performed manually with an Ott Model 131L planimeter (Keuffel and Esser Co., New York).

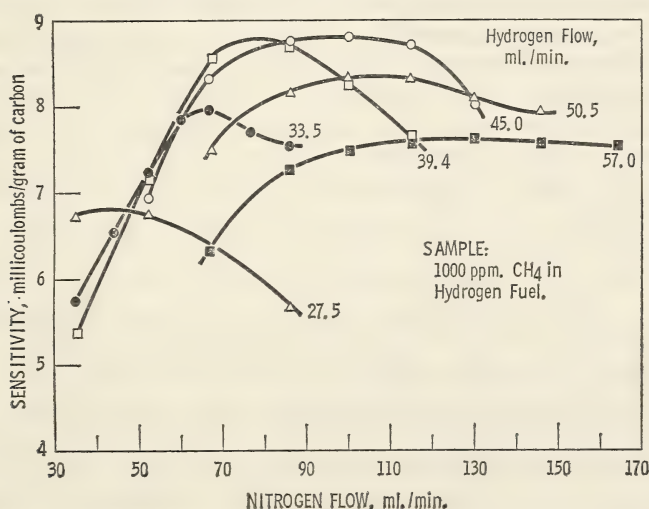
The requirements to be met in designing are: (a) all sample constituents vaporized from the wire when the sample nears the flame envelope should be retained and swept into the envelope in close time synchrony with the less volatile components; (b) the sample should be completely evaporated or pyrolyzed from the wire in a single pass through the detector flame; (c) the response of the detector to solid samples should be specific for carbon; and (d) the response of the entire system should be sufficiently fast to collect and record faithfully the rapid pulses of current produced during the combustion of discrete samples, such as individual cells. All of these requirements have been met for the most part in the detector described here when hydrocarbon samples are used; however, anomalies have been observed when a metallo-

organic sample (sodium acetate) is used, and additional improvements are needed to linearize the output and increase the sensitivity of the system.

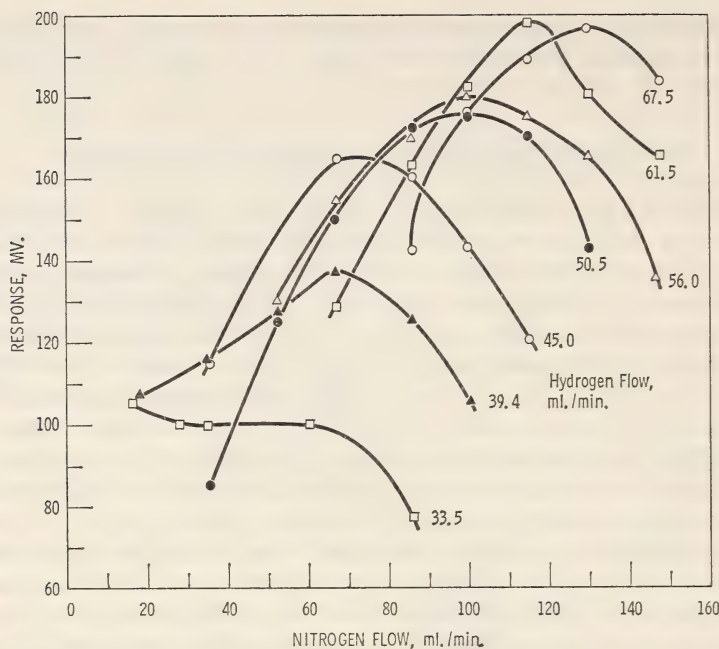
### NEGATIVE CHARGE CARRIER COLLECTION

The detector was initially operated with gas samples to compare its performance with other conventional detectors. Response data were taken by varying the nitrogen flow to the flame at several hydrogen flow levels using a 1000 ppm methane sample in the hydrogen fuel, with the wire removed from the chamber. Text-figure 3 is a plot of the results, which compare favorably in form with those obtained by McWilliam (11) and Sternberg *et al.* (9) for vertical jet detectors. A sensitivity of 0.0088 coulomb per g carbon was obtained under the best flow conditions. This is somewhat less than the 0.02 coulomb per g carbon (0.24 coulomb/g atom carbon) reported by Sternberg and probably results in part from flame cooling because of the massive jet design.

The conditions for optimum response to solid samples were examined by placing a thin coating of bovine serum albumin on the wire and moving it through the jet body and into the flame at a constant rate of 6.3 mm per second (text-fig. 4). The coating was acquired by passing the wire through a drop of solution of 0.1 percent albumin in distilled water. Except for the variations in the hydrogen and nitrogen flows, the operating conditions were the same as those used for the detector evaluation with a gaseous sample. The recorder response is given in millivolts because the actual feed rate of the solid sample was unknown. Although the form of this family of curves is similar to that in text-figure 3, the hydrogen and nitrogen flow rates required for maximum response are higher. Com-



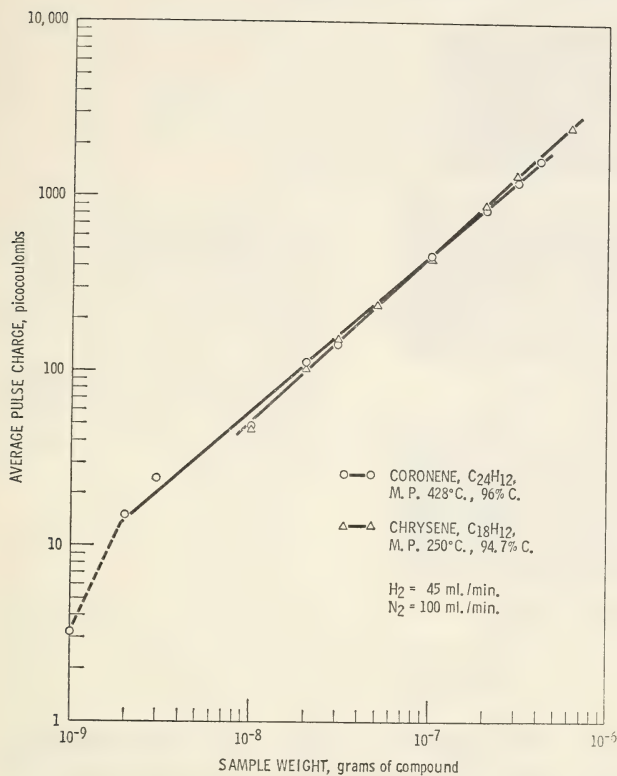
TEXT-FIGURE 3.—Effect of hydrogen and nitrogen flows on the sensitivity of the coaxial jet for a gas sample.



TEXT-FIGURE 4.—Effect of hydrogen and nitrogen flows on the sensitivity of flame ionization detector with bovine serum albumin continuously dried on the sample wire.

plete removal of the sample from the wire was obtained during the test as determined by reversing the direction of wire movement for a short period and observing the detector output. Perhaps the greatest difference observed in the performance of the detector when operated under the two sets of optimum conditions for gas and solid samples was the increase of noise seen in the output for the solid sampling condition.

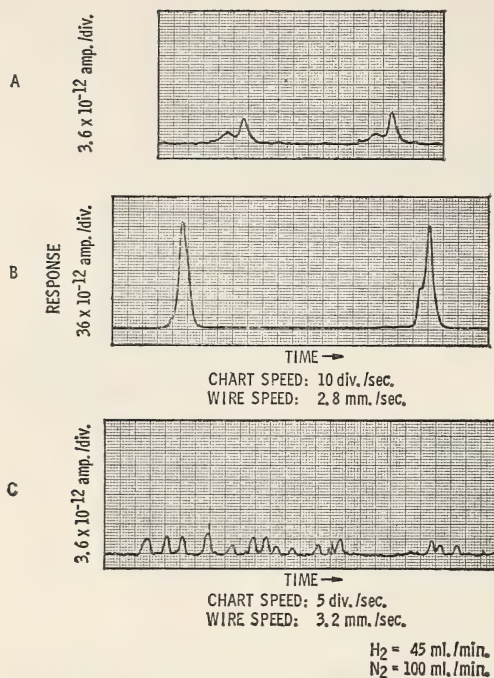
Known samples of pure hydrocarbons were placed on the wire by a hanging-drop solvent evaporation technique to evaluate the usable sample weight range and linearity of response possible with this type of material introduction. The hydrocarbons, *viz*, coronene,  $C_{24}H_{12}$ , mp  $428^{\circ}C$ , and chrysene,  $C_{18}H_{12}$ , mp  $250^{\circ}C$ , were dissolved in RACS-grade carbon tetrachloride at decade concentrations of  $10^{-6}$  to  $10^{-4}$  g per ml and  $1\ \mu l$  droplets of each were "hung" on the wire over the oven until the solvent evaporated. By this technique samples as small as  $10^{-9}$  g could be located within a 1 to 1.5 mm length along the sample transport wire (text-fig. 5). Table 1 gives the average charge obtained per sample for electron collection and the sensitivity calculated for the weight of carbon burned. In each case, the average charge from the residues from  $1\ \mu l$  droplets of the carbon tetrachloride solvent was subtracted from the gross value to obtain the net charge given in table 1. Since the net charge recorded for the  $1 \times 10^{-9}$  g coronene sample is of the same magnitude as that from the solvent, and considering the small chart areas integrated to obtain these



TEXT-FIGURE 5.—  
Effect of sample  
size on linearity  
for discrete, solid  
hydrocarbon sam-  
ples.

numbers (about 13 sq mm), little accuracy can be assigned to the sensitivity value calculated for this sample. For the rest of the data, the accumulative errors from sampling and integration are estimated to be less than about  $\pm 6$  percent of the value. Text-figure 6A shows two typical pulses recorded from duplicate  $2 \times 10^{-9}$  g coronene samples, and text-figure 6B shows the pulses from duplicate  $1 \times 10^{-7}$  g samples of the same compound. Note that the ionization currents were collected over periods of 1.5 and 1.0 seconds, respectively. The system time response (63%) for the conditions used was 0.125 second for the A, and 0.02 second for the B recording. The double peak structures for both of the smaller samples and the shoulder on one peak for the larger samples are frequently seen, and represent both the material evaporated shortly before the sample spot reaches the combustion zone (left peak and shoulder), and the remainder of the sample which reaches the flame immediately thereafter when the sample spot leaves the jet opening (right peak in text-fig. 6A).

It is evident from the data that the sensitivity decreased as the sample weight increased and that a sensitivity range of slightly over 2:1 was obtained. Overloading can be rejected on the basis of results given by Sternberg *et al.* (9) as a cause of sensitivity decrease. A more likely explanation is that the air supply to the flame was limited by reason of flow paths present within the chamber. This effect was noted by van



TEXT-FIGURE 6.—Chart recordings of the signals obtained from discrete solid samples. A: duplicate  $2 \times 10^{-9}$  g coronene samples; B: duplicate  $1 \times 10^{-7}$  g coronene samples; C: individual *Tetrahymena pyriformis* cells, each having a calculated carbon content of  $1 \times 10^{-9}$  g.

der Craats (12) and was confirmed here when a significant sensitivity increase was obtained by raising the detector chamber lid to assist in the removal of the flame combustion products.

It is interesting to note the differences in the amount of sample actually reaching the flame envelope when: (a) no jet is used, *i.e.*, when the wire is completely exposed inside the detector; (b) a thin-walled tube entering the flame on one end is placed over the wire with and without a nitrogen purge into the flame; and (c) the coaxial jet is used (table 2). A sensitivity gain of at least 127 was achieved by the use of the coaxial jet over that obtained with the exposed-wire arrangement in the  $10^{-7}$  to  $10^{-6}$  g sample range.

Since the purpose of this investigation was to provide a rather versatile analyzer capable of both rapid response to discrete matter and a slower response to continuous sample flow, as in the case of column monitoring, a simple test for solute acquisition was made by passing the wire through a drop of an aqueous solution of serum albumin at several concentrations. Different amounts of solution are acquired and held by the wire, depending on the angle of departure between the wire and the surface of the drop at the point of wire exit. For example, when the angle of departure was about  $90^\circ$ , the maximum sample was obtained. If this quantity is taken as unity, the sample acquired when the wire passed through the top half of the drop (angle of departure about  $45^\circ$ ) was 0.83, and a minimum sample value of 0.73 occurred when the wire passed through the very top of the drop. For this reason, the wire was positioned at  $90^\circ$  to

TABLE 1.—Sensitivity test with solid hydrocarbon samples

Weight of compound (g)	Average charge per sample (picocoulomb)	Calculated sensitivity (coulomb/g of carbon)
Sample: coronene, $C_{24}H_{12}$ , mp 428° C		
$4 \times 10^{-7}$	1526.0	0.00397
$3 \times 10^{-7}$	1209.0	0.00419
$2 \times 10^{-7}$	871.0	0.00453
$1 \times 10^{-7}$	462.0	0.00480
$3 \times 10^{-8}$	147.0	0.00509
$2 \times 10^{-8}$	112.0	0.00582
$1 \times 10^{-8}$	48.9	0.00508
$3 \times 10^{-9}$	24.4	0.00846
$2 \times 10^{-9}$	15.07	0.00783
$1 \times 10^{-9}$	3.25	0.00338
Sample: chrysene, $C_{18}H_{12}$ , mp 250° C		
$6 \times 10^{-7}$	2551.0	0.00448
$3 \times 10^{-7}$	1336.0	0.00470
$2 \times 10^{-7}$	895.0	0.00472
$1 \times 10^{-7}$	453.0	0.00478
$5 \times 10^{-8}$	244.0	0.00515
$3 \times 10^{-8}$	153.0	0.00538
$2 \times 10^{-8}$	103.0	0.00543
$1 \times 10^{-8}$	48.5	0.00512
1 $\mu$ l $CCl_4$ blank	4.63	
Test conditions: Hydrogen flow = 45 ml/min Nitrogen flow = 100 ml/min Wire speed = 3 mm/sec Detector sensitivity to 1000 ppm $CH_4$ in fuel = 0.0079 coulomb/g carbon		

TABLE 2.—Samples losses from precombustion evaporation. Sample: chrysene,  $C_{18}H_{12}$ , mp 250° C

Weight of compound (g)	Detector arrangement	Average charge collected (picocoulomb)	Calculated sensitivity (coulomb/g carbon)
$1 \times 10^{-6}$	<sup>a</sup> Exposed wire (no tube)	35	0.000037
$1 \times 10^{-6}$	<sup>a</sup> Tube* over wire	220	0.00023
$1 \times 10^{-6}$	<sup>a</sup> Tube* over wire plus $N_2$ purge into flame	533	0.00056
$2 \times 10^{-7}$	<sup>a</sup> Sample withdrawn from quartz jet. <sup>†</sup> No $N_2$ purge	311	0.0032
$2 \times 10^{-7}$	<sup>b</sup> Coaxial jet with $N_2$ purge	871	0.00472
Test conditions:			
		a	b
		Hydrogen flow = 37 ml/min	45 ml/min
		Nitrogen flow = Zero or at unknown rate	100 ml/min
		Charge collection = Negative	

\*1 mm I.D.  $\times$  0.13 mm wall  $\times$  26 mm long platinum-20% rhodium tube entering flame envelope on one end.<sup>†</sup>Sample was placed on a 0.13 mm diameter wire and lowered vertically into a flameless quartz jet (0.46 mm I.D.). The flame was lighted and the sample withdrawn upward into the flame with presumably no loss.

the drop for maximum sampling in subsequent tests. Table 3 gives the results obtained at four albumin concentrations. Assuming that the same volume rate of solution was acquired by the wire for all solution concentrations, the same sensitivity decrease with increasing sample size as noted in table 1 is again apparent.

In protein chromatography, organic buffer solutions used to elute these materials could completely mask the signal from solutes even at their higher concentrations. Inorganic buffers or eluents would be necessary, and as a limiting case for test purposes, the background response from a 0.5 M ammonium dihydrogen phosphate solution was determined by the same wire-through-drop technique employed in obtaining the data in table 3. The output signal from the buffer solution was equal to that from the 0.1 percent albumin solution. In addition, the signal was extremely noisy, having at least 100 millivolts of noise superimposed upon the signal level. No explanation is presented for this noise other than rapid loss of water of hydration in the flame. Such noise has also been observed when analyzing discrete sodium acetate samples placed on the wire by the evaporation of droplets of a water solution.

As a test of the instrument performance in detecting very small particulate matter suspended in solution, the wire was passed through a drop of culture containing *Tetrahymena pyriformis* cells at a lineal speed of 3.2 mm per second. Individual cells are dragged out of the solution by the wire, and the water evaporates almost instantaneously (text-fig. 6C). The average pulse seen here represents about  $7.8 \times 10^{-12}$  coulomb of charge for an average cell size of about  $30 \times 44 \mu$ . For these cells Plesner *et al.* (13) reported a dry weight of  $1.7 \times 10^{-9}$  g per cell. Using a sensitivity of 0.008 coulomb per g carbon and the average charge collected per cell, a carbon content of about  $1 \times 10^{-9}$  g is calculated. This is believed to be in good agreement with the dry weight, considering the variability in cell size, the different culture used in the dry-weight measurement, and the fact that carbon does not account for all the cell dry mass. Although these cells are larger by a volume factor of about 5 than the largest white cells in human blood, these results suggest strongly that an instrument of this type could be used to analyze for the carbon content of cells removed from blood and perhaps provide, by means of pulse

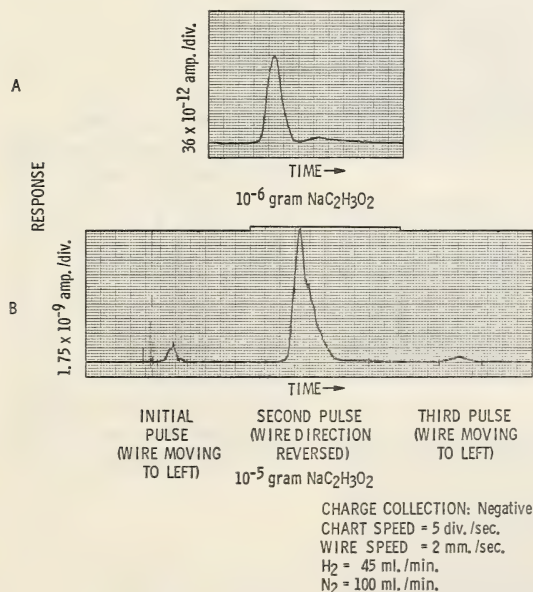
TABLE 3.—Solute acquisition test with a wire-through-drop technique

Concentration of albumin in water (wt %)	Response (mv)	Ratio: $\frac{\text{mv}}{\text{wt \%}}$
0.2	180	900
0.1	150	1500
0.05	85	1700
0.025	45	1800
Zero (pure water)	1	
Test conditions: Hydrogen flow = 50.5 ml/min		
Nitrogen flow = 100 ml/min		
Wire speed = 6.4 mm/sec		

analysis instrumentation, a rapid distribution plot of the results. If the cells are also removed from the drop by the wire in proportion to their population in the sample, a cell count could be obtained in conjunction with the carbon content distribution.

All the sample materials described above have been either hydrocarbons or proteins, and therefore the metal content has always been very low. The effect of a high metal content on the analyzer response was studied by using samples of sodium acetate dissolved in distilled water. Micro-liter droplets containing  $10^{-6}$  and  $10^{-5}$  g sodium acetate each were hung on the wire, dried over the oven, and then burned in the flame. A sodium salt was selected because of its known high volatility at wire operating temperatures and because it can readily form positive ions under the conditions used (14, 15). The collecting electrode was polarized at +300 volts to collect the negative charge current. Using the conditions for maximum sensitivity to gaseous hydrocarbons, the samples were introduced to the flame at a wire speed of 2 mm per second. Text-figure 7A shows the pulse recorded for a typical sample of  $10^{-6}$  g which amounts to  $3.8 \times 10^{-9}$  coulomb of charge. Following the major peak is a secondary pulse containing about 8 percent of the total charge. It has also been observed in samples whose metallic content is appreciable, *e.g.*, tap water residue, human perspiration, or sebum. Apparent sensitivities calculated from this and similar samples average about 0.04 coulomb per g carbon and indicate that materials other than carbon contributed to the ionization current during combustion.

Text-figure 7B shows the initial pulse recorded for a  $10^{-5}$  g sample of sodium acetate, and subsequent pulses obtained when the sample spot on the wire was (a) moved back into the flame shortly after leaving the



TEXT-FIGURE 7.—Chart recording of signals from discrete sodium acetate samples.

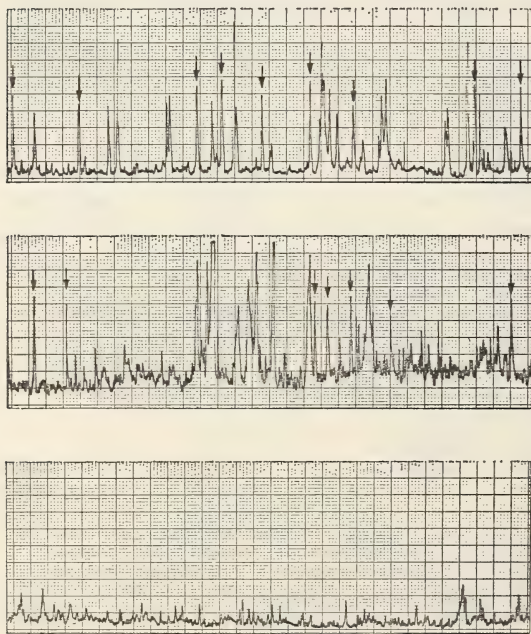
envelope, and (b) passed through the flame a third time in the original direction. The second pulse is about 18 times greater than the first, and is presumed due to thermionic emission by the sodium oxide remaining on the wire. The third pulse, about 0.6 the size of the first, is explained in the same manner.

It is readily apparent that results for samples having a high sodium content are not specific for carbon. Many other metals may also affect the negative charge current in a manner similar to that of sodium.

### POSITIVE ION COLLECTION

In the initial stages of this work, positive ion current was collected frequently instead of the electron current as a matter of general interest. It was soon recognized that, for solid samples, a much larger signal was obtained with positive collection.

An application of the use of the large positive ion current to improve the detection of particulate matter is shown in text-figure 8. Puff-ball spores (Stemen Laboratory, Oklahoma City, Oklahoma), about  $4\ \mu$  diameter, were collected onto the wire from an air dispersion by an electrostatic precipitator. Each particle had a calculated weight of  $3.7 \times 10^{-11}$  g. The carbon content of the spores was 46 percent, giving an estimated total carbon weight of  $1.7 \times 10^{-11}$  g per spore. This is obviously well below the limit of detectability using this equipment and negative charge collection; however, positive charge collection results in the large spike-like pulses shown in text-figure 8 for individual spore particles. That the samples



TEXT-FIGURE 8.—Chart recording of signals from individual puff-ball spores ( $4\ \mu$ ) with the use of positive ion collection. Each spore represents about  $1.7 \times 10^{-11}$  g carbon. *Upper:* Puff-ball spores (typical pulses at arrows) dispersed in filtered air. *Middle:* Puff-ball spores dispersed in laboratory air. *Lower:* Background signal from filtered air and wire noise.

were single spores was confirmed by microscopic examination of the wire immediately following its passage through the precipitator. The upper chart shows the pulses from the individual spores (typical pulses indicated by arrows) collected from a dispersion in filtered air. The center chart shows the results when the spores were collected from a dispersion in typical laboratory air. The increased background noise is the result of dust particles collected on the wire with the puff-ball spores. The lower chart record is that of the wire background noise and particulate matter remaining in the filtered air flowing through the precipitator. Similar results were obtained by using paper mulberry pollen and ragweed pollen grains (Stemen Laboratory), and the analysis of pulse charges from many individual grains showed a charge distribution similar to the size distribution of the several types of grains in a qualitative sense. The noise shown on the base line of the lower chart record in text-figure 8 is typical for positive ion collection under the conditions of this experiment. If the polarity was reversed for negative charge collection, a smooth base line would be obtained for the same and even higher gain settings.

The production of positive and negative ions by heated surfaces is a well-documented phenomena. Smith (14), Barnes (15), and White (16) have investigated the production of positive ions from metals at red heat and have shown that they are emitted as singly charged atoms directly from the metal surface, rather than as a neutral atom ionized after leaving the hot body. Both positive and negative ions are emitted in air (17) from hot wires, such as platinum, platinum-rhodium, and nichrome, when heated above 500° C.

The presence of certain impurities on the wire increases enormously the positive ion emission current obtainable over that observed with a "clean" wire (16). Thus positive ions could be produced in a conventional detector by an overly hot flame ionization detector jet for a jet-positive chamber polarity, and could be emitted from an overheated collector electrode (18) in the case of jet-negative chamber polarity, and appear as noise in the output signal in either instance. For positive collection, therefore, the presence of a wire in the flame provides a mechanism by which a large, nonspecific ion current is added to, and in most cases overwhelms, the current produced by the carbon in wire-borne samples. This larger current can be used to advantage, however, as a method for detecting the presence of materials whose carbon content is below the limit of detectability of other more specific methods. Further, since certain elements, such as the alkali metals, will form positive ions under the conditions described here without the simultaneous presence and combustion of organic material (16, 17), the detection of inorganic particulates should be possible using this technique, providing the sample contains at least one of these elements.

## REFERENCES

- (1) McWILLIAM, I. G., and DEWAR, R. A.: Flame ionization detector for gas chromatography. *Nature* (London) 181: 760, 1958.

- (2) JANAK, J.: Identification of the structure of non-volatile organic substances by gas chromatography of pyrolytic products. *Nature (London)* 185: 684-686, 1960.
- (3) KEULEMANS, A. I. M., and PERRY, S. G.: Identification of hydrocarbons by thermal cracking. *In Gas Chromatography 1962* (van Swaay, M., ed.). Washington and London, Butterworths, 1962, pp 356-367.
- (4) KARMEN, A., WALKER, T., and BOWMAN, R. L.: A scientific method for quantitative microdetermination of lipids. *J Lipid Res* 4: 103-106, 1963.
- (5) JAMES, A. T., RAVENHILL, J. R., and SCOTT, R. P. W.: A new method for the automatic detection of zones eluted from the liquid chromatogram. *Chem and Ind*, 18 (May 2), 1964, pp 746-748.
- (6) HAAHTI, E., and NIKKARI, T.: Continuous detection of fractions in effluents of silicic acid chromatography. *Acta Chem Scand* 17(9): 2565-2568, 1963.
- (7) ANDERSON, N. G., and STEVENS, R. H.: The Joint National Institutes of Health-Atomic Energy Commission Zonal Centrifuge Development Program Semi-annual Report, ORNL-3502, January 1-June 30, 1963, pp 83-85.
- (8) ———: The Joint National Institutes of Health-Atomic Energy Commission Zonal Centrifuge Development Program Semiannual Report, ORNL-3656, July 1-December 31, 1963, pp 78-82.
- (9) STERNBERG, J. C., GALLAWAY, W. S., and JONES, D. T. L.: The mechanism of response of flame ionization detectors. *In Gas Chromatography 1962* (Brenner, N., Callen, J. E., and Weiss, M. D., eds.). New York, Academic Press Inc., 1962, pp 231-267.
- (10) DEWAR, R. A.: The flame ionization detector—a theoretical approach. *J Chromatogr* 6: 312-323, 1961.
- (11) McWILLIAM, I. G.: Linearity and response characteristics of the flame ionization detector. *J Chromatogr* 6: 110-117, 1961.
- (12) VAN DER CRAATS, F.: Discussion following an article by Desty, D. H., *et al.* *In Gas Chromatography 1960* (Scott, R. P. W., ed.). Washington and London, Butterworths, 1960, p 63.
- (13) PLESNER, P., RASMUSSEN, L., and ZEUTHEN, E.: *In Synchrony in Cell Division and Growth* (Zeuthen, E., ed.). New York, Interscience, 1964, p 547.
- (14) SMITH, L. P.: The emission of positive ions from tungsten and molybdenum. *Phys Rev* 35: 381-395, 1930.
- (15) BARNES, L. L.: The emission of positive ions from heated metals. *Phys Rev* 42: 487-491, 1932.
- (16) WHITE, W. C.: Positive-ion emission, a neglected phenomenon. *Proc I R E* 38: 852-858, 1950.
- (17) HESSEMER, R. A., JR.: Effects of smokes on atmospheric ionization. *J Franklin Inst* 257-258: 31-41, 1954.
- (18) SCHILD, F.: Discussion following an article by Scott, R. P. W., and Cumming, C. A. *In Gas Chromatography 1960* (Scott, R. P. W., ed.). Washington and London, Butterworths, 1960, p 134. *See also* comments by Heywood, A., in the same discussion.

**The following articles have appeared in the literature since this paper was written.**

- (1) LIEBERMAN, S.: Method of and apparatus for monitoring for flowing stream content. U.S. Patent 3,128,619. April 14, 1964.
- (2) KARMEN, A.: Specific detection of halogens and phosphorus by flame ionization. *Anal Chem* 36: 1416-1421, 1964.
- (3) GIUFFRIDA, L.: A flame ionization detector highly selective and sensitive to phosphorus—a sodium thermionic detector. *J Assoc Offic Agricul Chemists* 47(2): 293-300, 1964.
- (4) STOFFER, J. E., KERSTEN, T. E., and KRUEGER, P. M.: A new method for the detection of substances separated by liquid chromatographic systems. *Biochim Biophys Acta* 93: 191-193, 1964.

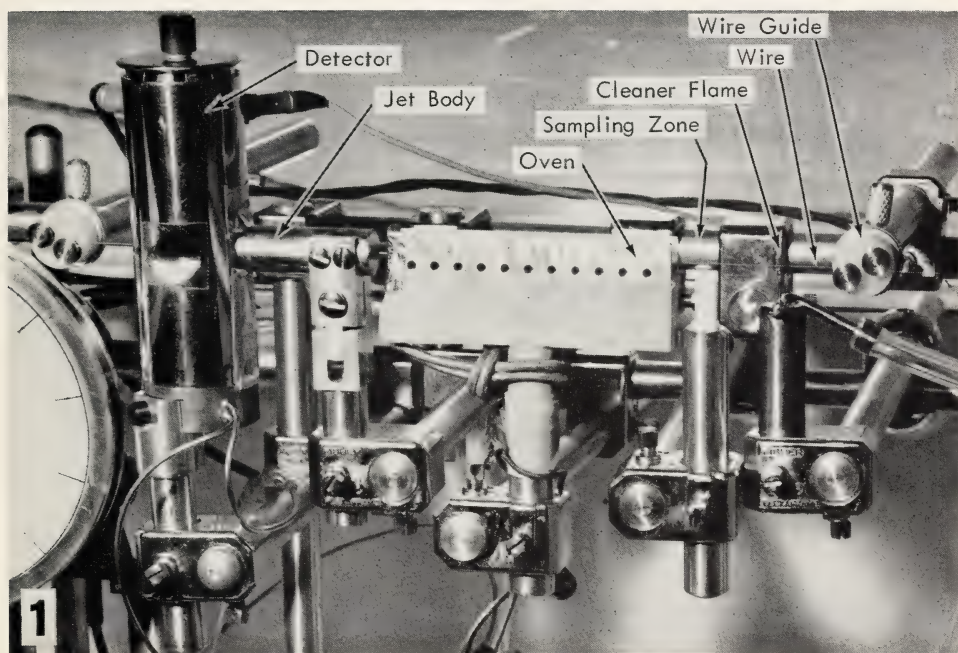


FIGURE 1.—Flame ionization analyzer for carbon determination in solid and liquid organic samples.



## Problems in Biocontainment<sup>1</sup>

N. CHO, H. P. BARRINGER, J. W. AMBURGEY, G. B. CLINE, N. G. ANDERSON, L. L. McCAULEY, R. H. STEVENS, and W. M. SWARTOUT, *Technical Division, Oak Ridge Gaseous Diffusion Plant,<sup>2</sup> and Biology Division, Oak Ridge National Laboratory,<sup>2</sup> Oak Ridge, Tennessee*

### SUMMARY

Rather large amounts of virus materials may be isolated by use of the rotor systems described in this volume. We have reduced the possibility of operator infection by redesigning an angle-head centrifuge rotor tube to prevent gross leakage of fluid, arranging to recover virus bands in disposable sterile syringes, and developing dialysis methods which minimize handling. Photographic means for locating bands are also described. For work with highly infectious agents, a completely contained laboratory has been built in which purification by continuous-flow centrifuga-

tion, rate-zonal centrifugation, and isopycnic banding may be carried out. The unit is completely sterilized with ethylene oxide, has an automatically programmed sterilization cycle, provides for steam sterilization of all wastes, and has an incinerator on the exhaust air line. If contained systems are to come into general use, research instrumentation and procedures must be redesigned so that experiments may be as easily done with containment as without it.—*Nat Cancer Inst Monogr* 21: 485-502, 1966.

WITHOUT THE development of new techniques for biocontainment, requiring elimination of all possible hazards associated with infectious agents would effectively stop a large fraction of research now in progress. This follows from the fact that only total containment can remove all conceivable means by which contamination of the environment could occur. For this reason the concept of grading the biocontainment requirements to the level of potential hazard has been adopted in most virology and microbiology laboratories. This concept has been reduced to a system of hazard classification by the Biohazards Committee of the Oak Ridge National Laboratory (1).

While no incidence level is considered acceptable for biological accidents, the rate reported without cessation of activities (*i.e.*, the level tacitly accepted) is quite high. Considering data available up until 1962, a total of 107 fatalities and 2,241 illnesses from laboratory-acquired

<sup>1</sup> This research performed under the Joint National Institutes of Health-Atomic Energy Commission Zonal Centrifuge Development Program which is supported by the National Cancer Institute, the National Institute of Allergy and Infectious Diseases, and the U.S. Atomic Energy Commission.

<sup>2</sup> Operated for the U.S. Atomic Energy Commission by the Nuclear Division of Union Carbide Corporation.

infections was recorded. This is considered to be only a modest fraction of the number that actually occurred (2).

The centrifuge systems described in this volume allow very large quantities of purified virus materials to be prepared. In addition, particles widely dispersed in tissues can be isolated in a high state of purity. Agents that are relatively innocuous or rarely infectious in very low concentrations may behave quite differently when introduced into animal or human recipients in concentrated or purified form.

Neither space, funds, nor human factors will allow all the biophysical and biochemical tools now used in virological and microbiological research laboratories to be enclosed in sealed chambers and manipulated through glove ports or by remote servomechanisms. In attempting to deal with this very difficult problem, we have directed our studies along three major lines.

First, efforts have been made to reduce (but not necessarily eliminate) hazards associated with existing procedures by relatively small changes. Second, complete containment units for existing separations and analytical systems, including zonal centrifuges, have been constructed to allow experimental studies to proceed. Third, the problem of redesigning procedures or equipment, specifically for convenient hazard-free operation, has been examined. The first line of endeavor seeks to decrease quickly hazards associated with existing procedures, the second allows new procedures and systems to be evaluated safely, and the third approaches the problem of contained research facilities that would be widely used, *i.e.*, systems allowing experiments to be performed more quickly and conveniently with containment than without it.

## IMPROVEMENT OF EXISTING METHODS

Attention has been directed initially to improvements in techniques that often involve physical contact between the operator and virus suspensions.

### Redesign of Angle-Head Centrifuge Tubes

Metal closures for high-speed centrifugation have been used with only slight modification for over 25 years. Contact with wet centrifuge tubes is probably the readiest source of gross contamination in a virological laboratory.

A series of polycarbonate<sup>3</sup> centrifuge tubes for the Spinco No. 30 rotor were machined to determine whether the plastic tubes and closures would withstand the centrifugal force at maximum rotor speed. No failures were observed. However, it was evident that machined tubes would be too expensive. Several alternate designs suitable for blow-molding were prepared and, in collaboration with a plastics fabrication firm,<sup>4</sup> one

<sup>3</sup>General Electric Company.

<sup>4</sup>Nalge Company, Rochester, N.Y.

basic design (fig. 1) was chosen for further study.<sup>5</sup> Two versions were fabricated and tested: Oak Ridge type 30 A has a  $\frac{1}{4}$ -inch diameter opening, while the Oak Ridge type 30 B has a  $\frac{1}{2}$ -inch diameter aperture. Type A can hold 27 ml when spun without the cap in place. If this or a smaller volume is used no fluid presses against the plastic tube cap (text-fig. 1). Leakage will occur only if the tube ruptures. The polypropylene caps are inexpensive and do not deform during centrifugation. Type A tubes are specifically designed for banding infectious agents by angle-head, density-gradient centrifugation (3) where the separated bands are withdrawn with a needle. For separations in which a pellet is to be recovered mechanically, type B tubes (capacity 25 ml if the suspension does not reach the cap during centrifugation) are preferable. The tubes can also be run empty or partly filled. No water is needed in the rotor holes if the tubes are fairly new. Both the tubes and closures may be steam-sterilized. For work with highly infectious agents, new tubes should be used, since failure in operation has been observed only in tubes that have been in service for some time. Recently, tubes of a similar design have been fabricated for the Spinco No. 40 rotor.

A thin cap, which may be cemented into position, has recently been developed that allows storage of sterile, sealed type A tubes at liquid nitrogen temperatures.

### Density Beads for Liquid Gradients

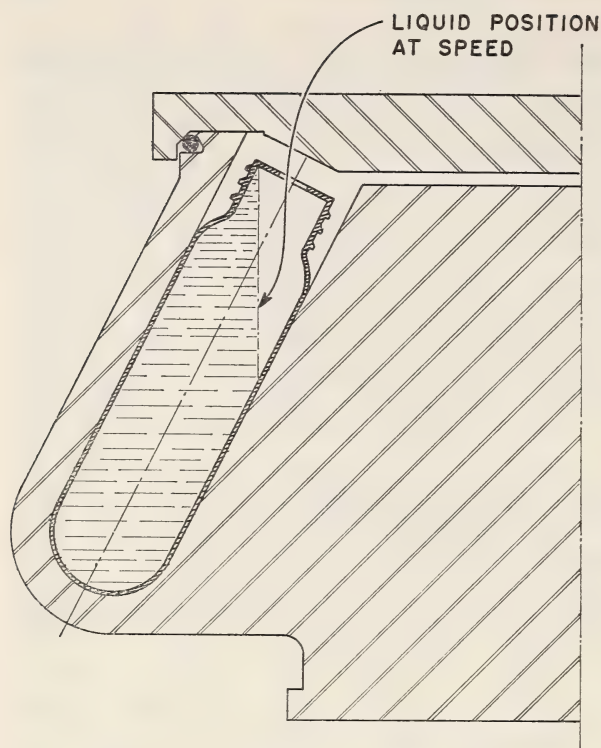
The physical density of fractions recovered from liquid gradients used in centrifuges is generally determined by measuring the refractive index. This is usually done manually, and ample opportunity for contact with the sample exists during preparation for measurement and when the optical surfaces are cleaned. It appeared desirable, therefore, to explore means for determining the buoyant density of observed bands in the centrifuge tubes. Plastic beads have been employed previously (4); however, a series of color-coded beads, whose densities covered the buoyant density range of the virus, have not been previously available.

During centrifugation, density-indicating beads are suspended in the gradient at their isopycnic positions as are viruses or other particles present in the sample. The use of the beads provides a simple means of estimating the density of the particles at their isopycnic positions without manipulation of the specimens.

The basic requirements to be met in developing density-indicating plastic beads are low cost and density homogeneity. Attempts to vary the density of a resin, such as polystyrene, by blending with a filler met with limited success because of inhomogeneity produced by incomplete mixing or entrapped air bubbles. The percentage of water uptake by the density beads should be low.

---

<sup>5</sup> These tubes are now available from International Equipment Company, Needham Heights, Mass., and the Spinco Division of Beckman Instruments, Inc., Palo Alto, Calif.



TEXT-FIGURE 1.—Position of fluid in type A tube during rotation. *Note* fluid does not touch the tube cap.

By use of commercially available resins,<sup>6</sup> beads of four different densities were prepared by a controlled process to obtain a porous-free starting material. The plastic was then extruded<sup>7</sup> in continuous strands, cooled, and chopped into short rods. The rods were then ball-milled<sup>8</sup> into  $\frac{1}{16}$ -inch diameter beads.

Density variations in each of 4 batches of beads were established by banding samples isopycnically in both shallow and steep density gradients. Sample populations ranging from 24 to 60 beads were used for each determination. Density distributions to within  $\pm 0.005$  g per  $\text{cm}^3$  were established from these data. The results are shown in table 1.

### Photography of Particle Bands in Density Gradients

Where sufficient virus material has been banded to be seen by scattered light, the location of plastic density indicator beads and virus particles may be determined photographically (fig. 2).

The design allows the box to be incorporated into a contained enclosure with only the camera and electrical components on the noncontained side. Methyl methacrylate light pipes conduct light to each tube. Twelve No. 30 rotor plastic tubes may be photographed at one time.

<sup>6</sup> Purchased from Eastman Kodak Co.

<sup>7</sup> Extruded by the Extron Corporation, Knoxville, Tenn.

<sup>8</sup> Milled by the United Plastic Company, Maywood, N.J.

TABLE 1.—Classification of density-indicating plastic beads

Plastic	Batch color	Range of densities (g/cm <sup>3</sup> )	Density distribution	
			Density ± 0.005 g/cm <sup>3</sup>	Percent of total sample
Polystyrene	Yellow	1. 065–1. 105	1. 070	3. 4
			1. 080	43. 3
			1. 090	43. 3
			1. 100	10. 0
			1. 275	100
Cellulose acetate	Green	1. 272–1. 278	1. 275	100
Polyvinylchloride (rigid)	Tan	1. 361–1. 369	1. 365	100
Polyvinylchloride (high temperature)	Gray	1. 518–1. 534	1. 520	10
			1. 530	90

### Recovery of Samples From Isopycnic Bands

The techniques for the recovery of gradients from plastic centrifuge tubes offer additional opportunities for exposure, especially where drops are collected through holes punched in the bottom of the tube. Where quantitative recovery of bands is not necessary, bands can be recovered by use of a motor-driven disposable plastic syringe (2.5 ml) and a disposable spinal needle (3.5 inches). These are mounted in the device shown in figure 3 and may be manually lowered to remove liquid from any level in the centrifuge tube. Variable illumination is provided from below. The syringe may be driven in either direction at the rate of 0.2 ml per minute.

### Combined Camera and Band Recovery Apparatus

We have also developed a compact system for photographing single tubes against a dark background. By use of Polaroid film, photographs may be obtained in short periods of time and used as a guide in removing samples with the recovery apparatus mounted in the camera.

### Dialysis of Samples

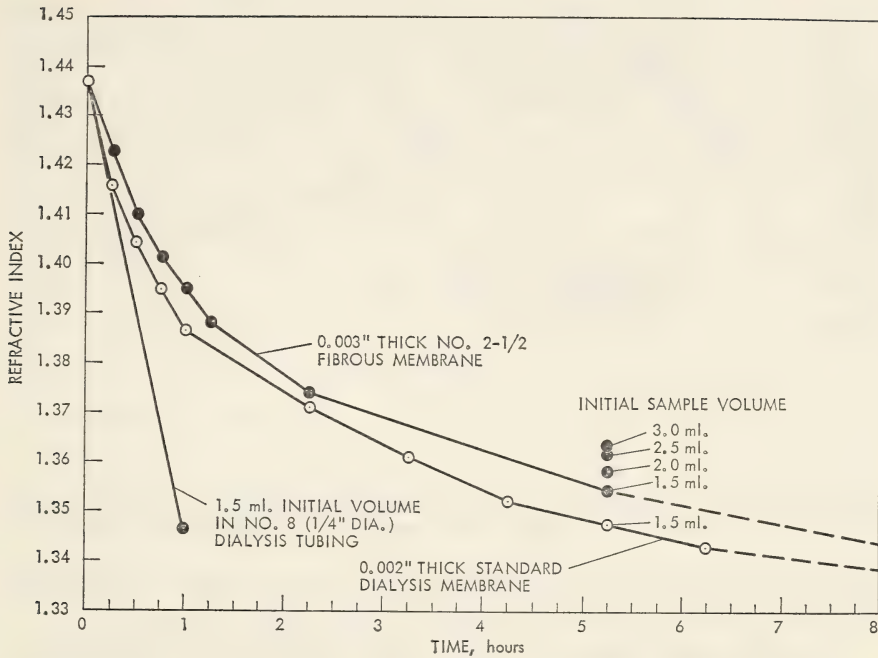
Dialysis of infectious or contaminated samples is an additional "wet" procedure with opportunity for infection. A variety of methods for the dialysis of samples removed with the band recovery apparatus have been examined. Of these, the two methods appearing to offer greatest promise are 1) a dialyzer board containing compartments for the simultaneous dialysis of up to twelve 3 ml fractions and 2) a plastic floater head, with serum cap and storage cover, used at one end of preclipped cellulose tubing for the pressure dialysis of individual pathogenic fractions up to 5 ml volume. The dialyzer board (fig. 4) consists of a 12-hole plastic base into which the fractions are collected or placed prior to dialysis, a sheet of fibrous cellulose dialysis membrane, and a clamped-on cover plate to seal the membrane around the lip of each 3/4-inch diameter hole. After assembly, the board is placed in a circulating water bath and inverted to rest on

the 4 plastic legs. In this position, the fraction is supported by the membrane and desalting proceeds as the fresh water is circulated underneath each dialysis "window." After the dialysis is completed, the board is removed from the bath and placed in the filling position. The dialyzates can then be removed with a syringe by piercing each window with a needle. The bottoms of the holes are coned to permit removal of all material. The experimental model is of a nonautoclavable plastic (methacrylate). If the method comes into general use, a sterilizable material will be used.

The membrane, cut from flattened cellulose tubing,<sup>9</sup> is similar to standard dialysis tubing, except that a fibrous cellulose web is embedded in the tubing for strength. The web is only exposed on one side of the membrane sheet, and the "rough side" is turned away from the base containing the fractions during assembly to assure a satisfactory seal. This type of membrane is used solely because of its increased tensile strength, and is necessary for safety since the osmotic pressure developed within the fraction compartments is frequently sufficient to rupture conventional membranes when concentrated solutions are dialyzed, *e.g.*, 5 M potassium citrate. The relatively small membrane area exposed to the solution in this method results in a considerably longer dialysis period than experienced with 1/4-inch diameter tubing for a given fraction volume; however, this may be desirable in certain cases, such as in the dialysis of fractions containing a myxovirus, since too rapid changes in salt concentration may result in inactivation. Text-figure 2 is a graph of the dialysis times required for 1.5 ml of 5 M potassium citrate with the use of both 1/4-inch (No. 8 size) standard dialysis tubing in the conventional manner and the dialysis board with sheet membranes of both standard and fibrous materials. Note that the tubing contents reached a refractive index of 1.348 in 1 hour and that the board fractions reached the same point in 5.25 and 7 hours for the standard and fibrous membranes, respectively. The difference in the latter two time periods is attributed to differences in initial membrane thicknesses and excessive bulging and stretching of the standard sheet, with a resultant increase in its pore size. The thickness measurement of the fibrous membrane includes the fiber-mat contribution, the effective dialyzing layer thickness is therefore unknown, but somewhat less than the total value. The three single points plotted vertically along the 5.25-hour ordinate represent the refractive indexes attained after this time in the dialysis of other 2, 2.5, and 3 ml samples with the use of a fibrous membrane in the same board. Standard membrane can be used to reduce the dialysis time required for these larger volumes if the initial salt concentration of the fraction is considerably less than 5 M. It cannot be safely used with over 1.5 ml of 5 M potassium citrate solutions because of the pressure developed within the fraction compartment.

The design of the dialyzing board simplifies the handling problems associated with the processing of up to 12 fractions in a glove box, since

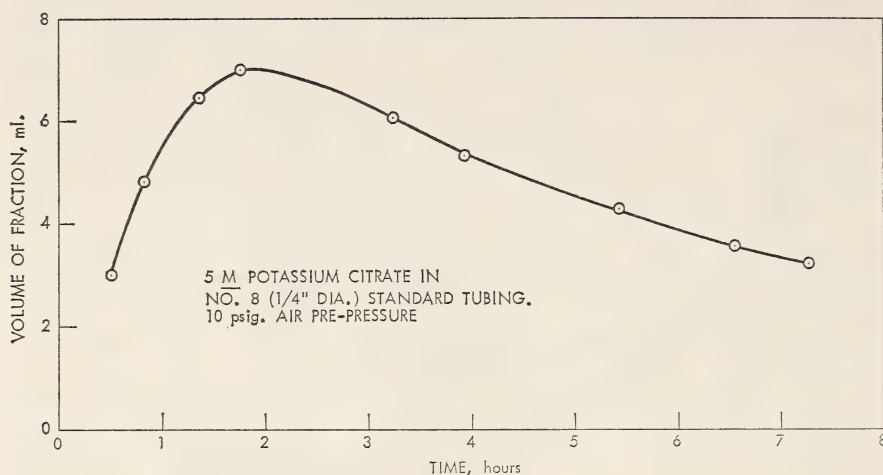
<sup>9</sup> Food Products Division, Union Carbide Corporation, Chicago, Ill., Fibrous Cellulose Casing, No. 2½, 3.8 inches flat width, 3.45 mils nominal thickness.



TEXT-FIGURE 2.—Dialysis times required for 1.5 ml fractions of 5 M potassium citrate to reach a refractive index of 1.348 in  $\frac{1}{4}$ -inch dialysis tubing. Standard and fibrous membranes with the 12-fraction dialysis board were used.

its rigid parts and the large cellulose sheet are considerably easier to handle with rubber gloves than wet dialysis tubing.

The floating plastic head (figs. 5 and 6) simplifies handling, containment, and storage in the dialysis of individual fractions whose volumes are up to about two thirds the volume of the attached tubing. A hollow float, having a serum cap septum access on the upper end and an O-ring to clamp the standard  $\frac{1}{4}$ -inch diameter dialysis tubing on the lower end, is intended for prior assembly and gas sterilization in the dry state. When needed, the assembly can be floated in a deep container of water to remove the glycerin from the tubing (if required), and the sample can then be introduced through the septum. Additional air can also be injected into the float through the septum to prepressurize the system and reduce the sample volume after the dialysis by forcing some of the water back through the tubing membrane. The results of the dialysis of a 3 ml fraction of 5 M potassium citrate, prepressurized to 10 psig, is shown in text-figure 3. In this case, the air volume contained in the head and tubing was about 12 ml at the start of the run. (A smaller head volume of 5 ml is planned, which should reduce the postdialysis time required to reach the original volume by reducing the air cushion above the liquid and thus raising the air pressure during the run.) The results illustrate the value of a pressurized floater head that has sufficient volume to allow expansion of the



TEXT-FIGURE 3.—Change in volume with time during the dialysis of a 3 ml fraction of 5 M potassium citrate under an initial pressure of 10 psig in a floating dialysis head.

fluid volume during the early phase of dialysis, and which then provides sufficient pressure to return the sample to its original volume.

The tubing used below the floater heads has thus far been standard 1/4-inch diameter dialysis tubing preclipped at 24-inch intervals<sup>10</sup> by an aluminum wire crimp identical to that used commercially for closing large cellulose tubing. A pair of clips placed three fourths of an inch apart and spaced at 24-inch intervals provide two 12-inch-long, "pre-tied" dialysis tubes. The present O-ring seal for the tubing at the base of the float will hold without slippage of the wet tubing to about 13 psig with Buna-N rings. Other O-ring materials and seal designs are being evaluated to increase the holding power of the tubing seal to about 18 psig, since the burst pressure of the standard dialysis tubing is about 23 psig. An improved seal will allow a higher air pressure in the head and reduce the dialysis time required to return to the original fraction volume or less.

In addition to the advantages of preassembly and dry presterilization afforded by this design, the injection of liquid fractions into the tubing by a syringe provides better contamination control and allows a partial withdrawal of the dialyzate during the desalting period. Another advantage is that, after the dialysis is completed, the liquid can be drained back into the floater head, the tubing rolled up, and the cap (fig. 6) screwed on for sealing and safe storage of the fraction in a refrigerator.

### CONTAINMENT SYSTEMS FOR ZONAL CENTRIFUGATION

Virus isolation in the zonal centrifuge has required that the centrifuge and its accessory equipment be sterilized and operated in a sterile envi-

<sup>10</sup> Supplied on an experimental basis by the Food Products Division, Union Carbide Corporation, Chicago, Ill.

ronment. The centrifuge and analytical equipment have been housed in a leak-proof Plexiglas glove box that can be sterilized before use with an ethylene oxide-Freon gas mixture and flushed with filtered air. This containment system has been used for the large-scale isolation of respiratory syncytial virus and ECHO-28 virus from liter volumes of tissue culture fluid and for the separation of subunits of adenovirus types 3, 4, and 7 from intact virus and cell debris.

The containment system (fig. 7) is essentially a complete laboratory, housing not only a zonal ultracentrifuge but also supporting analytical equipment, such as an ultraviolet spectrophotometer, density-gradient engine, sample pumps, water coolant system, refrigerators, a low-speed and high-speed centrifuge, zone fractionator, a modified Westphal balance, glassware, and such assorted items as syringes, pipettes, tubing, and vials. This equipment is manipulated through arm-length rubber gloves. The entire glove box can be sterilized by ethylene oxide by an automatic control system. Filtered air is pumped through the glove box to carry aerosols through an incinerator where the air is burned at 700° F. Aerosols are also exposed to ultraviolet light within the glove box. The temperature and humidity can be controlled to make the box equivalent to a cold room. This is of particular value when samples must be concentrated by pressure dialysis or pressure filtration.

Access to the interior of the glove box is by a double-door, pass-through, combination steam-gas autoclave on one end or by a double-door exchange compartment on the opposite end. The autoclave is used to steam-sterilize glassware and other autoclavable items needed inside the box and to sterilize contaminated glassware and tubing after completion of a run. It is also used as a gas sterilizer to decontaminate nonautoclavable items, such as centrifuge rotors, before or after use. Virus stocks are passed into the glove box after being wiped with formalin or 70 percent alcohol and are again wiped or dipped immediately inside the glove box. Virus samples produced during the separation procedures are capped in sterile vials or in screw-top test tubes and passed to the outside after being wiped or dipped in formalin.

Spilled materials in the glove box, dialysates, wash solutions, and waste from the steam sterilizer are dumped through valved ports in the floor of the glove box to a drain sterilizer where wastes are autoclaved before being run into the sewage lines.

This system has found ready application in continuous-flow centrifugation or in isopycnic centrifugation. Several runs on the same virus can be made without resterilizing the entire glove box each time. However, the rotor and accessory items are washed and gas is sterilized in the small autoclave before being reused. In experimental studies, up to 50 liters or more per week may be processed.

Corrosion of standard laboratory equipment, centrifuge equipment, drive systems, and electronic components after repeated exposure to ethylene oxide is being studied. For installations where the hazards are low but where containment is indicated, metal-supported plastic

enclosures that are attached to the vacuum chamber of a zonal centrifuge have been developed (fig. 8). These are sterilized by ethylene oxide, are provided with an air incinerator on the exhaust line, and are operated under negative pressure.

## DEVELOPMENT OF INTEGRATED, CONTAINED LABORATORY SYSTEMS

Increased study of infectious agents will require more widespread use of contained systems. Large units, such as those described in the preceding section, will probably not find widespread application in virology laboratories throughout the country. However, the isolation of larger and larger quantities of infectious viral agents of more different types in an increasing number of laboratories is certain to take place. For contained systems to be economically available, standardization must occur. However, if designs are frozen which have not been sufficiently well developed to be generally acceptable, they will not be used during actual experimental studies. We conclude that a series of experimental systems must be designed and evaluated in practice in several different laboratories. Only those designs which find general acceptance and meet established minimum requirements should reach the stage of commercial production.

It is unlikely that research and development in the field of biocontainment can be successfully carried out except as part of a continuing research program in biophysical separation techniques with maximum participation by the research community. This is especially true if containment procedures are to be formally adopted and their use required.

The chief uses of large-scale virus preparations are in vaccine production and for structural and chemical analysis. The first step, therefore, in the development of integrated, contained systems would appear to be the design of a fairly compact system including a zonal or continuous-flow centrifuge with mechanisms for sterilizing the rotor, chamber, lower drive seals, upper shaft seals, and an upper chamber including space for the fluid line seals, samples, and sample collection vessels. A small rate of air flow should be provided for and effluent air and vacuum pump exhaust should be incinerated. Such a unit need not be large, and costs can be reduced by making extensive use of existing components. The redesign of other laboratory procedures and analytical devices into systems that may easily be used in containment probably will require prolonged study and evaluation.

In the present study, emphasis has been placed on procedures associated with centrifugation. For the development of integrated, contained laboratory systems, other factors should be considered—initial isolation procedures, tissue culture production of infectious agents, and methods of biological assay.

## REFERENCES

- (1) ALLEN, R. C., BOLTON, N. E., LINCOLN, T. A., and UPTON, A. C.: Containment criteria for laboratories handling infectious agents. U.S. Atomic Energy Commission Report ORNL-TM-1162, Oak Ridge National Laboratory, 1965.
- (2) SULKIN, S. E.: Laboratory-acquired infections. *Bact Rev* 25: 203-209, 1961.
- (3) FISHER, W. D., CLINE, G. B., and ANDERSON, N. G.: Density gradient centrifugation in angle-head rotors. *Anal Biochem* 9: 477-482, 1964.
- (4) GOLDING, N. S.: Procedure for the Golding plastic bead test for solids-not-fat in milk. Extension Circular No. 340, Institute of Agricultural Sciences, Washington State University, Pullman, Washington, 1964.



## PLATES





FIGURE 1.—Plastic ultracentrifuge tubes. Type A (small opening for virus isolation) shown on *right*, type B (large opening) shown on *left*.

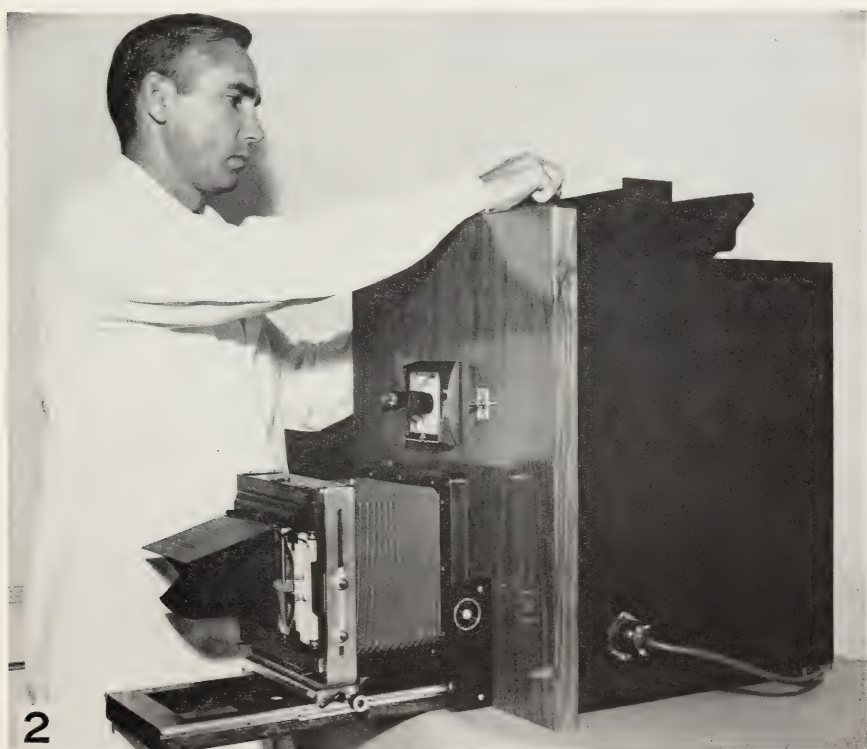


FIGURE 2.—Camera for photographing isopycnicly banded particles in 12 angle-head centrifuge tubes by scattered light.

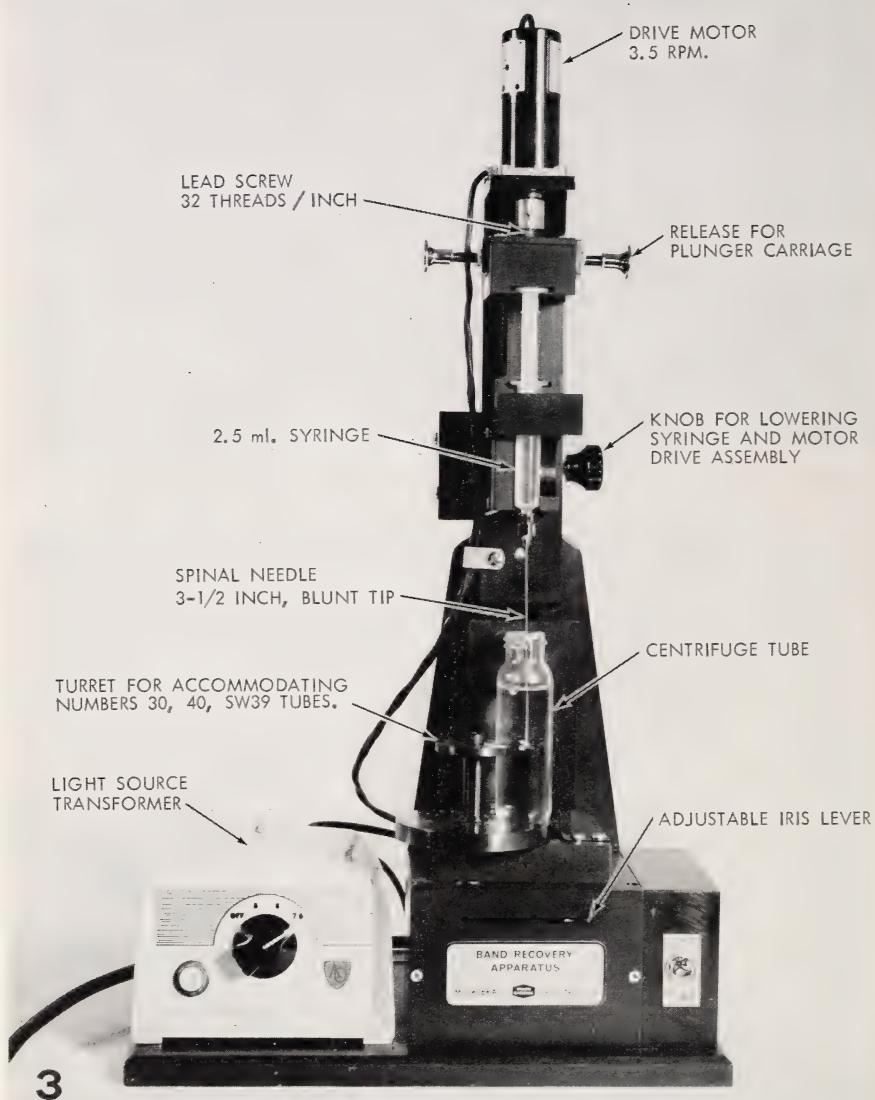


FIGURE 3.—Apparatus for recovering isopycnicly banded particles from centrifuge tubes.

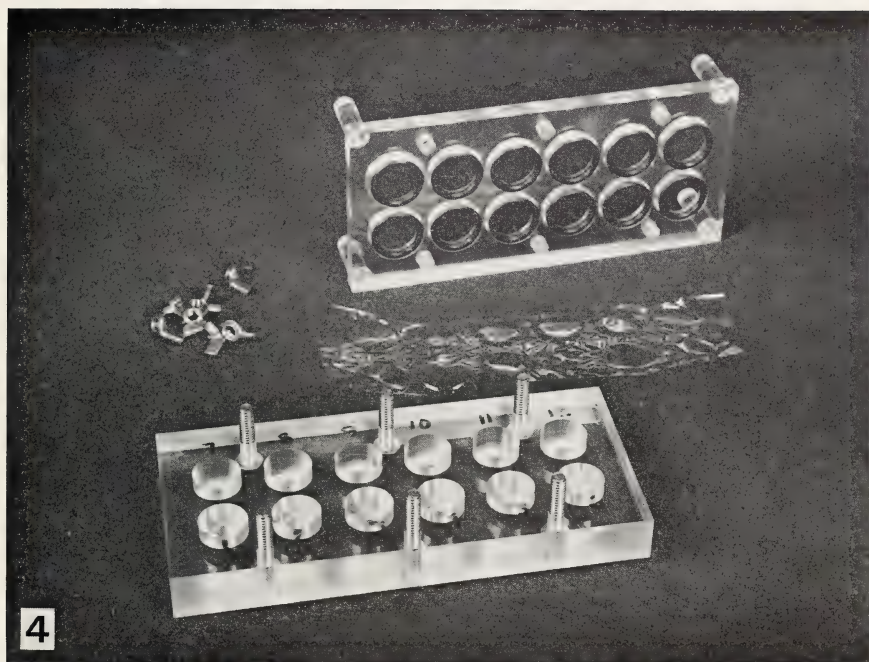


FIGURE 4.—Board for the aseptic dialysis of twelve 3 ml samples. The O-rings in the *upper section* seal the cellulose membrane sheet around the lip of each hole in the *lower section* when the 2 sections are clamped together.



FIGURE 5.—Plastic floater head for use with preclipped dialysis tubing for the dialysis, containment, and storage of pathogenic fractions. The assembly may be gas-sterilized and stored dry before being filled through the cap septum.

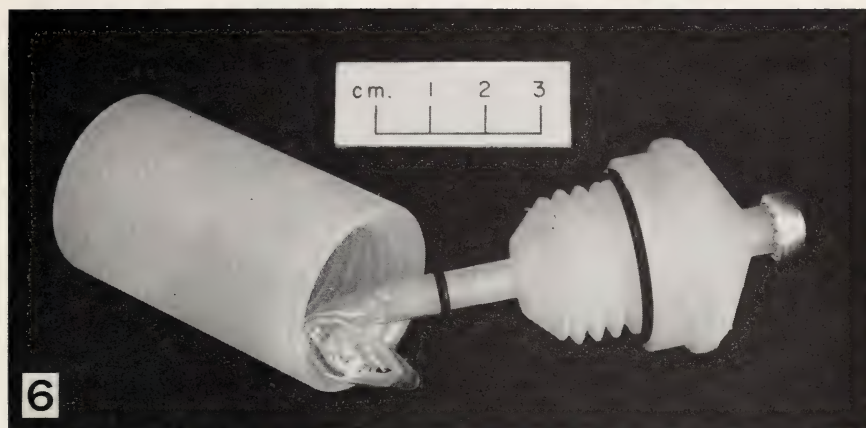


FIGURE 6.—Plastic dialysis floater head showing method of sealing the dialysis tubing and the use of a self-sealing cover for storing fractions after all liquid has been drained from the tubing into the hollow-head section.

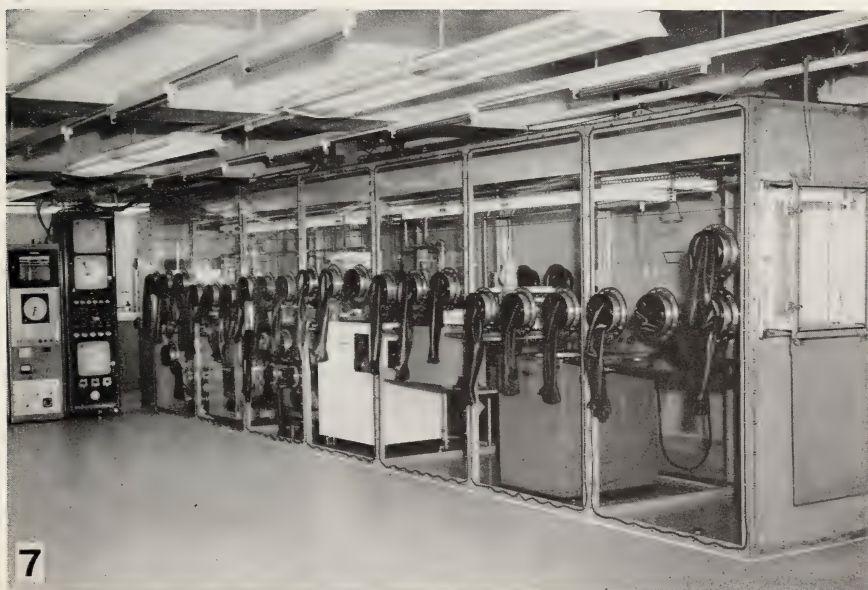


FIGURE 7.—Controls and complete containment system used for virus isolation. A combination steam and gas autoclave opens into the far end of the glove box. Centrifuge controls and automatic system for the glove-box sterilization cycle are shown at *left*. Air incinerators for decontaminating exhaust air are not shown.

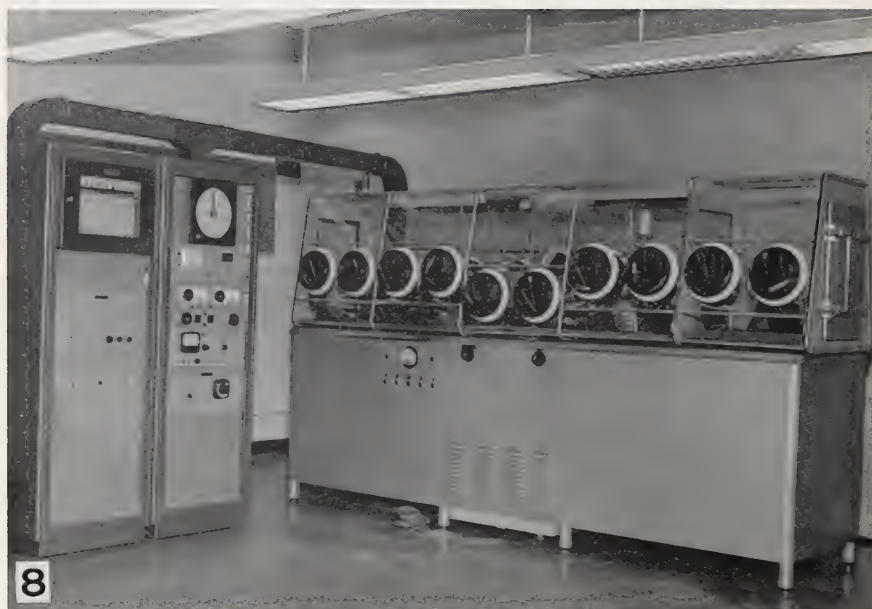


FIGURE 8.—Containment system for zonal centrifuge (installed at plant of Charles Pfizer and Co., Maywood, N.J.).

# NAME INDEX (AUTHOR,AU REFERENCE,R)

## -A-

ALM, R.S., 460R  
 ALMEIDA, J.D., 389, 392R  
 ALSBERG, C.L., 286, 295R,  
 296R  
 AMBLER, C.M., 54, 73R, 79,  
 80, 110R  
 AMBURGEY, J.W., JR., 4, 23,  
 32R, 137, 146, 151, 153R,  
 169, 170R, 199AU, 200,  
 212R, 262, 269R, 485AU  
 AMES, B.N., 13, 30R, 152,  
 154R, 175, 176, 178,  
 187R, 220, 239R, 364,  
 368R  
 ANDERSON, H.J., 335, 343R  
 ANDERSON, N.G., 1AU, 9AU,  
 13-15, 17-21, 23, 24, 26,  
 28, 30, 30R-32R, 33, 34,  
 46, 47, 73R, 78, 110R,  
 113AU, 113, 114-118, 121,  
 124R, 125R, 137AU,  
 137-139, 144-146, 151,  
 153, 153R, 154R, 165,  
 165AU, 166-169, 170R,  
 175, 176, 178, 179, 187,  
 187R, 188R, 191AU, 193,  
 195, 195R, 196R, 199,  
 199AU, 200, 207, 210,  
 211, 211R, 212R, 219,  
 239R, 241, 247R, 253,  
 253AU, 255, 257, 258,  
 262-264, 266R, 267R,  
 269R, 285, 285AU, 286,  
 287, 296R, 304, 305, 309,  
 310, 311R, 317, 317AU,  
 318, 320R, 333AU, 334,  
 343, 343R, 344R, 345,  
 346, 347, 350, 353R,  
 354R, 361, 363, 364,  
 368R, 375, 375AU, 376,  
 383, 383R, 384R, 389,  
 389AU, 390, 391, 392R,  
 397, 402R, 403, 404,  
 409R, 415AU, 431, 431AU,  
 432, 436, 438R, 439,  
 441-443, 445R, 446R, 447,  
 459R, 460R, 470, 482R,  
 485AU, 487, 495R  
 ANDERSON, T.F., 256, 268R  
 ANDERSSON-CEDERGREN, E., 346,  
 347, 353R  
 ANGUS, H.J.F., 448, 460R  
 ARGESINGER, J., 320, 320R  
 ARION, W.J., 329, 330R

ARNOLD, R.N., 86, 110R  
 ARNSTEIN, H.R.V., 255, 267R  
 ASPBERG, K., 448, 460R  
 AZZONE, G.F., 346, 347, 353R

## -B-

BABELAY, E.F., 4, 19, 20,  
 31R, 46, 73R, 113AU, 114,  
 116, 125R, 137, 137AU,  
 138, 153, 153R, 166, 167,  
 169, 170R, 175, 176, 178,  
 187R, 193, 195R, 199,  
 207, 211R, 287, 296R,  
 305, 311R, 317, 320R,  
 334, 343R, 346, 347,  
 353R, 361, 363, 368R,  
 376, 384R, 397, 402R,  
 403, 409R  
 BACHRACH, H.L., 256, 256R,  
 267R  
 BAKER, R.S., 153, 154R, 195,  
 196R, 199, 211R, 257,  
 269R, 375AU  
 BALL, F.L., 4, 4R  
 BALLANTYNE, A.J., 254, 266R  
 BARANY, M., 346, 350, 353R  
 BARBER, A.A., 4, 17, 20, 26,  
 31R, 153, 154R, 241,  
 247R, 253, 253AU, 255,  
 263, 267R, 269R, 285AU,  
 286, 287, 296R, 303AU,  
 304, 305, 309, 310, 311R,  
 333, 333AU, 342, 343,  
 343R, 344R, 345, 391,  
 392R, 436, 438R  
 BARBER, E.J., 4, 178, 180,  
 188R, 219AU  
 BARBER, M.L., 4, 24, 32R,  
 345AU, 348, 352, 353R,  
 431, 432, 436, 438R, 441,  
 442, 443, 445R, 447, 460R  
 BARKER, S.B., 286, 294, 296R  
 BARNES, L.L., 479, 482R  
 BARRINGER, H.P., 4, 19, 20,  
 23, 31R, 32R, 46, 73R,  
 77AU, 113AU, 114, 116,  
 125R, 137AU, 138, 144,  
 146, 151, 153, 153R,  
 154R, 165AU, 166, 167,  
 169, 170R, 175, 176, 178,  
 187R, 191AU, 193, 195,  
 195R, 196R, 199AU, 200,  
 207, 211R, 212R, 257,  
 262, 264, 269R, 287,  
 296R, 305, 311R, 317,

- 320R, 334, 343R, 346,  
 347, 353R, 361, 363,  
 368R, 375AU, 376, 383,  
 384R, 397, 402R, 403,  
 409R, 485AU  
 BARROWS, C.H., 255, 267R  
 BARTKUS, M.J., 4, 19, 20,  
 31R, 46, 73R, 137AU, 166,  
 169, 170R, 176, 178,  
 187R, 193, 195R, 199,  
 207, 211R, 397, 402R  
 BARTLETT, T.W., 4, 303AU,  
 345, 389AU, 390, 392R  
 BASSALI, W.A., 99, 111R  
 BEAMS, JESSE, 5  
 BEARD, J.W., 257, 268R, 389,  
 392R  
 BEAUFAY, H., 13, 28, 30R,  
 113, 125R, 175, 176,  
 187R, 219, 221, 222, 225,  
 239R, 255, 267R  
 BEHRENS, M., 16, 31R  
 BELL, D.J., 255, 267R, 286,  
 296R  
 BENEDETTI, E., 324, 329, 330R  
 BENTLEY, R., 448, 460R  
 BENYESH-MELNICK, M., 257,  
 269R, 389, 392R  
 BERMAN, A.S., 4, 14, 23, 30R,  
 32R, 41AU, 138, 153R,  
 191, 193, 195R, 199AU,  
 210, 211R  
 BERNHARD, W., 254, 266R  
 BERNHEIM, F., 335, 343R  
 BERTHET, J., 13, 28, 30R,  
 113, 125R, 175, 176,  
 187R, 219, 221, 222, 225,  
 239R, 255, 267R  
 BERTINI, F., 303, 310R  
 BERWICK, L., 256, 268R  
 BEYERLE, K., 88, 111R  
 BIEZENO, C.B., 86, 110R  
 BIOT, M.A., 93, 111R  
 BISHOP, B.S., 4, 144, 152,  
 153R, 175AU, 364, 368R  
 BLASS, G.A., 83, 110R  
 BLOCK, R.J., 448, 458, 460R  
 BLOOM, W.L., 286, 293, 294,  
 296R  
 BOCK, R.M., 342, 344R  
 BOESKEN, J., 448, 460R  
 BOFFA, G.A., 403, 407, 409R  
 BOGGS, L.A., 448, 460R  
 BOLTON, N.E., 485, 495R  
 BOS, C.J., 324, 329, 330R  
 BOURNE, E.J., 448, 460R  
 BOWMAN, K.O., 4  
 BOWMAN, R.L., 469, 482R  
 BOYLAND, D.A., 166, 170R  
 BRAKKE, M.K., 12, 13, 14,  
 30R, 57, 73R, 113, 124R,  
 219, 220, 239R  
 BRANDES, D., 303, 310R  
 BRAUNSTEINER, H., 389, 392R  
 BRAY, G.A., 364, 368R  
 BREEDIS, C., 256, 268R  
 BREESE, S.S., JR., 256, 257,  
 267R, 268R  
 BRENNER, S., 259, 269R, 287,  
 296R, 305, 311R  
 BRIGGS, F.N., 351, 354R  
 BRIGGS, N.G., 346, 353R  
 BRITTEN, R.J., 175, 187R  
 BRODSKAYA, N.I., 286, 296R  
 BROWN, D.M., 255, 267R  
 BROWN, K.B., 243, 247R  
 BROWNELL, L.E., 361, 368R  
 BRYAN, W.R., 4  
 BRYCE, W.A.J., 255, 267R  
 BUCHANAN, P.J., 305, 309,  
 311R  
 BUEDING, E., 286, 293, 296R  
 BUETOW, D.E., 303, 305, 309,  
 310R, 311R  
 BURGER, C.L., 4, 20, 21, 32R,  
 46, 73R, 176, 200, 212R,  
 287, 296R, 334, 343R,  
 353R, 361, 368R, 383R,  
 389, 390, 392R  
 BURGI, E., 255, 267R  
 BURNS, V.W., 445, 446R
- C-
- CAMERON, I.L., 4, 317, 317AU,  
 320R, 361AU, 363, 367,  
 368R, 441, 441AU  
 CANDLER, E.L., JR., 4, 17,  
 31R, 153, 154R, 241,  
 247R, 253AU, 286, 287,  
 296R, 305, 309, 311R,  
 343, 344R, 436, 438R  
 CANNING, R.E., 4, 19, 20, 21,  
 31R, 32R, 113AU, 121,  
 125R, 137, 138, 153,  
 153R, 154R, 167, 170R,  
 175, 187R, 199, 211R,  
 255, 266R, 317AU, 318,  
 320R, 345AU, 346, 347,  
 353R, 403AU  
 CARLOS, S., 139, 153R  
 CARSTEN, M.E., 352, 354R  
 CARTER, J.A., 4, 241AU  
 CECIL, R., 255, 267R  
 CHANOCK, R.M., 4  
 CHARNEY, J., 383, 384R

CHATTON, E., 320, 320R  
 CHAUVEAU, J., 324, 327, 330R  
 CHENG, P.-Y., 255, 267R  
 CHENIAE, G.M., 448, 460R  
 CHO, N., 4, 19, 31R, 113AU,  
 137, 138, 146, 151, 153R,  
 167, 170R, 175, 187R,  
 199, 211R, 262, 269R,  
 317, 320R, 346, 347,  
 353R, 485AU  
 CLARK, A.E., 303, 304, 308,  
 309, 310, 310R  
 CLINE, G.B., 4, 23, 29, 32R,  
 78, 110R, 116, 125R, 137,  
 146, 151, 153, 153R,  
 154R, 195, 196R, 199AU,  
 210, 211R, 257, 262,  
 269R, 287, 296R, 305,  
 311R, 361AU, 375, 375AU,  
 485AU, 487, 495R  
 COATES, HELEN, 4  
 COHEN, J.A., 256, 268R  
 COHN, W.E., 448, 460R  
 CORI, G.T., 285, 295R  
 COX, D.J., 255, 267R  
 COX, J., 286, 295R  
 COX, R.A., 255, 267R  
 CRAMER, M., 305, 311R  
 CRAWFORD, E.M., 256, 268R  
 CRAWFORD, L.V., 256, 268R  
 CREDE, C.E., 85, 88, 91,  
 110R, 111R  
 CRIDDLE, R.S., 342, 344R  
 CROUSE, D.J., 243, 247R  
 CUENDET, L.S., 448, 460R  
 CULPEPPER, H.D., 4

## -D-

DAHLE, L.K., 341, 342, 343R  
 DALLNER, G., 262, 269R, 327,  
 330R, 342, 343R  
 DALTON, A.J., 389, 392R  
 DANFORTH, W.F., 304, 311R  
 DARLINGTON, R.W., 256, 267R  
 DARMS, F.J., 97, 111R  
 DAVERN, C.I., 255, 267R  
 DE DUVE, C., 13, 28, 30R,  
 113, 125R, 175, 176,  
 187R, 219, 221, 222, 225,  
 239R, 255, 267R  
 DE VILLAFRANCA, G.W., 352,  
 354R  
 DERDULL, J.D., 103, 111R  
 DEUTSCH, H.F., 404, 407, 409R  
 DEWAR, R.A., 469, 470, 481R,  
 482R  
 DMUCHOWSKI, L., 254, 265,

266R, 269R, 389, 392R  
 DOEBBLER, G.F., 416, 422,  
 423R  
 DOOLITTLE, A.K., 224, 232,  
 239R  
 DORFMAN, B.Z., 442, 445, 446R  
 DOTY, P., 255, 267R, 397,  
 401R  
 DOORMASHKIN, R.R., 257, 268R  
 DREYER, D.A., 254, 266R  
 DRITT, W.S., 4, 20, 32R,  
 165AU  
 DROCHMANS, P., 287, 293,  
 296R, 391, 392R  
 DUBOIS, M., 287, 296R, 305,  
 311R, 448, 460R  
 DUBUISSON, M., 352, 354R  
 DUNHAM, C.L., 4  
 DURAND, D.P., 256, 268R  
 DURSO, D.F., 447, 460R

## -E-

EBASHI, S., 346, 351, 353R  
 EDELMAN, G.M., 403, 409R  
 EDSALL, J.T., 176, 187R  
 EIGNER, J., 256, 268R  
 EL-AASER, A.A., 17, 31R,  
 323AU, 324, 330R  
 ELLIOTT, A.M., 361, 368R  
 ELROD, L.H., 4, 317AU  
 EMMELOT, P., 324, 329, 330R  
 ENGELHARDT, W.A., 345, 352R  
 EPSTEIN, M.A., 256, 268R  
 ERNSTER, L., 324, 325, 330R  
 ESSNER, E., 329, 330R  
 EVANS, E.C., 4  
 EYRING, H., 232, 239R

## -F-

FALZONE, J.A., 255, 267R  
 FARR, A.L., 176, 353R, 383R,  
 262, 269R, 343R, 347  
 FARRANT, J.L., 391, 392R  
 FAULKNER, P., 256, 268R  
 FELLINGER, K., 389, 392R  
 FERNBACH, D.J., 389, 392R  
 FINE, J.M., 403, 407, 409R  
 FINK, J., 334, 343R  
 FISHER, W.D., 4, 19-22, 29,  
 31R, 32R, 46, 73R, 78,  
 110R, 114-116, 125R,  
 137AU, 138, 153, 153R,  
 154R, 166, 169, 170R,  
 176, 178, 187R, 193,  
 195R, 199, 207, 211R,  
 262, 269R, 287, 296R,

- 305, 311R, 334, 343R,  
361, 363, 368R, 376,  
384R, 397, 402R, 403AU,  
409R, 441AU, 487, 495R  
FLODIN, P., 448, 460R  
FORD, L., 334, 343R  
FRAENKEL-CONRAT, H., 397,  
401R  
FRANKLIN, E.C., 403, 409R  
FRENCH, D., 448, 460R  
FUCCILLO, DOMENIC, 5  
FUCHS, F., 352, 354R  
FUJITA, H., 41, 73R
- G-
- GALLAWAY, W.S., 470, 473,  
475, 482R  
GARNER, W., 286, 295R  
GASPAR, Z.N., 286, 293, 296R  
GAWLIK, S.R., 303, 310R  
GEBICKI, J.M., 334, 342, 343R  
GEHENIO, P.M., 415, 416,  
422R, 423R  
GEISTER, R., 265, 269R  
GELLERT, M.F., 349, 353R  
GERGELY, J., 346, 351, 352,  
354R  
GERIN, J.L., 4, 153, 154R  
GIBBS, S.P., 304, 310, 310R  
GIERER, A., 255, 267R  
GILLES, K.A., 287, 296R, 305,  
311R, 448, 460R  
GIUFFRIDA, L., 482R  
GLASSTONE, S., 232, 239R  
GOLDEN, P.E., 221, 230, 231,  
237, 239R  
GOLDER, R.H., 404, 409R  
GOLDFISCHER, S., 329, 330R  
GOLDING, N.S., 487, 495R  
GOMATOS, P.J., 256, 268R  
GOODMAN, H.M., 368, 369R  
GRABAR, P., 404, 409R  
GRAMMEL, R., 86, 110R  
GRAY, C.E., 389, 392R  
GREEN, D.E., 342, 344R  
GREEN, J.G., 4, 24, 32R,  
415AU, 431AU, 432, 436,  
438R, 441-443, 445R,  
447AU, 459R, 460R  
GREEN, M., 256, 267R  
GREENWOOD, C.T., 255, 267R,  
285, 295R  
GREY, A., 83, 110R  
GREY, C.E., 254, 265, 266R,  
269R  
GREY, T.C., 346, 353R  
GRIZZARD, TOM, 4, 403
- GROSS, J.A., 361, 368R  
GUERRA, F., 334, 343R  
GUGGOLZ, J., 404, 409R  
GUTFREUND, H., 255, 267R
- H-
- HAAHTI, E., 470, 482R  
HAGDAHL, L., 14, 30R, 57, 73R  
HALE, A.J., 255, 267R  
HALLEN, A., 448, 460R  
HALL, B.D., 397, 401R  
HAM, A.W., 389, 392R  
HAMILTON, J.K., 287, 296R,  
305, 311R, 448, 460R  
HAMILTON, P.B., 431, 438R  
HAMMOND, L.D., 221, 222, 225,  
239R  
HANSON, R.W., 286, 294, 296R  
HARDING, MARGIE, 5  
HARDY, R.C., 221, 230, 231,  
237, 239R  
HARRIS, C.M., 85, 88, 91,  
110R, 111R  
HARRIS, W.W., 4, 17, 20, 26,  
31R, 153, 154R, 241,  
247R, 253AU, 255, 263,  
267R, 285AU, 286, 287,  
296R, 304, 305, 309, 310,  
311R, 343, 344R, 345,  
389AU, 390, 391, 392R,  
436, 438R  
HARVEY, E.B., 15, 30R  
HARVEY, E.N., 15, 30R  
HASHIMOTO, Y., 345, 352R  
HASSELBACH, W., 346, 351,  
352, 353R, 354R  
HASSELBACK, R.C., 389, 392R  
HASTINGS, J.R.B., 397AU, 401R  
HATCH, D.K., 91, 111R  
HAUSEN, P., 256, 268R  
HAVENS, M.L., 153, 154R, 195,  
196R, 199, 211R, 257,  
269R, 375AU  
HAYFLICH, L., 391, 392R  
HELFERRICH, F., 432, 438R  
HERSHEY, A.D., 255, 267R  
HESSEMER, R.A., JR., 481,  
482R  
HILL, E.G., 341, 342, 343R  
HILL, P.R., 81, 110R  
HOCHGRAF, H.L., 354R  
HODGMAN, C.D., 230, 231, 239R  
HOFFSTEN, P.E., 334, 342,  
343R  
HOGEBOOM, G.H., 113, 124R  
HOLLAENDER, A., 4  
HOLLAND, J.J., 256, 268R

HOLLINGSWORTH, B.R., 255,  
267R  
HOLLOWAY, E.J., 415  
HOLMAN, R.T., 341, 342, 343R  
HOLPER, JACOB, 4  
HOLT, S.J., 256, 268R  
HOLTZER, A., 349, 353R, 354R  
HORNE, R.W., 259, 269R, 287,  
296R, 305, 311R  
HORNER, D.C., 243, 247R  
HOUGH, L., 448, 460R  
HOWATSON, A.F., 256, 268R  
HOYER, B.H., 256, 268R  
HUBER, PAUL, 4  
HUEBNER, ROBERT, 4  
HUMMELER, K., 391, 392R  
HUNTER, F.E., JR., 334, 342,  
343R

## -I-

INGRAHAM, L., 255, 267R

## -J-

JACOB, J., 352, 354R  
JACQUOT-ARMAND, Y., 403, 407,  
409R  
JAISLE, F., 346, 350, 353R  
JAMES, A.T., 470, 482R  
JAMIESON, G.R., 4  
JANAK, J., 469, 482R  
JESSE, R.H., JR., 254, 266R  
JOHNSON, P., 407, 409R  
JOHNSON, R., 349, 351, 353R  
JOKLIK, W.K., 257, 269R  
JONES, D.T.L., 470, 473, 475,  
482R  
JONES, I.G., 255, 267R  
JONES, J.K.N., 448, 460R

## -K-

KAFIG, E., 416, 422R.  
KAMAT, V.B., 324, 327, 329,  
330R  
KARMAN, T.J., 93, 111R  
KARMEN, A., 469, 482R  
KARRER, H.E., 286, 295R  
KATZ, A.M., 352, 354R  
KATZEN, H.M., 286, 294, 295R  
KAY, E.R.M., 255, 267R  
KELLEY, J.P., 222, 239R  
KELLEY, R.E., 86, 110R  
KERSTEN, T.E., 482R  
KEULEMANS, A.I.M., 469, 482R  
KHYM, J.X., 448, 460R  
KIRBY-SMITH, J.S., 4

KIRBY, K.S., 397AU, 401R  
KIRKLAND, R.J.A., 342, 344R  
KLIPFEL, F.J., 176, 187R,  
255, 267R  
KLUCIS, E., 17, 31R, 323,  
323AU, 397AU  
KNIGHT, G.B., 222, 239R  
KNISELEY, R.M., 389AU, 390,  
392R  
KOEHLER, L.H., 458, 461R  
KOHLE, H., 352, 354R  
KOHLE, K., 256, 267R  
KOTIN, P., 4  
KOVACS, E., 256, 268R  
KREGER, D.R., 303, 310R  
KRISMAN, C.R., 287, 296R  
KRUEGER, P.M., 482R  
KU, K-Y, 324, 330R  
KUFF, E.L., 113, 124R  
KUNIN, R., 448, 456, 461R  
KUNKEL, H.G., 403, 407, 409R

## -L-

LADD, SISTER F.C., 24, 32R,  
431, 432, 436, 438R,  
441-443, 445R, 447, 460R  
LAIDLER, K.J., 232, 239R  
LANDOLT, R., 349, 351, 353R  
LANGFORD, P., 254, 266R  
LARSON, C.E., 4  
LAZAROW, A., 286, 293, 295R,  
296R  
LEDERBERG, S., 363, 368R  
LEEDALE, G.F., 304, 310, 310R  
LEHNINGER, A.L., 28, 32R  
LEIBO, STANLEY, 260, 260R  
LELOIR, L.F., 287, 296R  
LERNER, K.D., 14, 30R, 57,  
73R  
LETT, J.T., 17, 31R, 323AU  
LEVEDAHL, B.H., 303AU  
LEVITT, J., 256, 268R  
LEWIS, G.T., 286, 293, 294,  
296R  
LIEBERMAN, S., 482R  
LINCOLN, T.A., 485, 495R  
LINDERSTROM-LANG, K., 15, 30R  
LINDNER, G.M., 4  
LIPMANN, F., 346, 351, 353R  
LIVERMAN, J.L., 4  
LORAND, L., 153, 154R, 350,  
354R  
LOVEJOY, C., 469  
LOWE, C.W., 286, 295R  
LOWEY, S., 349, 353R, 354R  
LOWRY, O.H., 176, 262, 269R,  
334, 343R, 347, 353R,

383R  
 LUCK, D.J.L., 294, 296R  
 LUYET, B.J., 415, 416, 422R,  
 423R  
 LWOFF, A., 320, 320R  
 LYTTLETON, J.W., 361, 368R

## -M-

MA, T.S., 404, 409R  
 MAC COMB, W.S., 254, 266R  
 MACHLOWITZ, R., 383, 384R  
 MADSEN, T., 256, 268R  
 MAKINOSE, M., 346, 351, 353R  
 MALKOFF, D.B., 303, 310R  
 MANNERS, D.J., 255, 267R,  
 285, 294, 295R, 310, 311R  
 MANNEY, T.R., 441, 442, 442R  
 MARMUR, J., 255, 267R  
 MARSH, B.B., 345, 346, 353R  
 MARTIN, E.F., JR., 4  
 MARTIN, E.M., 256, 268R  
 MARTIN, R.G., 13, 30R, 152,  
 154R, 175, 176, 178,  
 187R, 220, 239R, 364,  
 368R  
 MARUYAMA, K., 352, 354R  
 MARZULLO, G., 304, 311R  
 MASICA, W.J., 103, 111R  
 MAUNDER, L., 86, 110R  
 MAYOR, H.D., 256, 268R  
 MAZIA, D., 363, 368R  
 MAZUR, PETER, 4, 415AU, 416,  
 417, 419, 421, 422R, 423R  
 MC CAULEY, L.L., 4, 137, 146,  
 151, 153R, 262, 269R,  
 389AU, 485AU  
 MC CREADY, R.M., 404, 409R  
 MC DOUGALL, E.I., 407, 409R  
 MC LAREN, L.C., 256, 268R  
 MC WILLIAM, I.G., 469, 473,  
 481R, 482R  
 MEEUSE, B.J.D., 303, 304,  
 310, 310R  
 MELNICK, J.L., 256, 268R  
 MENZ, L., 416, 423R  
 MERYMAN, H.T., 416, 422R,  
 423R  
 MESELSON, M., 15, 30R, 241,  
 247R, 255, 267R  
 MEYER, F., 255, 267R  
 MICHAELSON, I.A., 342, 344R  
 MIKUTA, E.T., 13, 30R, 176,  
 187R  
 MILES, J.W., 88, 103, 110R,  
 111R  
 MILLER, A.A., 224, 233, 234,  
 237, 239R

MILLER, C.H., 350, 354R  
 MILLER, G.L., 404, 409R  
 MILLER, O.L., JR., 361AU  
 MIRSKY, A.E., 16, 31R  
 MISRA, B.N., 233, 239R  
 MITCHELL, E.Z., 389, 392R  
 MOLONEY, J.B., 389, 392R  
 MOMMAERTS, W.F.H.M., 349,  
 350, 352, 353R, 354R  
 MONTGOMERY, R., 287, 296R  
 MOOR, H., 415, 416, 422, 422R  
 MOORE, S., 404, 409R, 431,  
 438R, 447, 459R  
 MORALES, M.F., 349, 353R  
 MORDOH, J., 287, 296R  
 MORRIS, L., 431, 438R  
 MORTON, J.I., 404, 407, 409R  
 MOSS, F.M., 176, 187R  
 MOULE, Y., 324, 327, 330R  
 MUENCH, H., 176, 383R  
 MUFSON, M., 4  
 MUHLETHALER, K., 415, 416,  
 422, 422R  
 MUSCATELLO, U., 345, 346,  
 347, 353R  
 MYERS, J., 305, 311R

## -N-

NAGAI, T., 346, 351, 353R  
 NANNINGA, L.B., 347, 353R  
 NAORA, H., 16, 31R  
 NASS, M.M.K., 352, 354R  
 NAUDE, W. DUT., 256, 268R  
 NEWLIN, T.E., 153, 154R, 195,  
 196R, 199, 211R, 257,  
 269R, 375AU  
 NIKKARI, T., 470, 482R  
 NISHIMURA, C., 257, 269R  
 NOGGLE, G.R., 448, 460R  
 NOLL, H., 397, 401R  
 NORDLIE, R.C., 329, 330R  
 NOVIKOFF, A.B., 329, 330R  
 NUNLEY, C.E., 4, 19, 20, 23,  
 24, 31R, 32R, 46, 73R,  
 108AU, 113AU, 137AU, 138,  
 153, 153R, 154R, 165AU,  
 166, 167, 169, 170R, 175,  
 176, 178, 187R, 191AU,  
 193, 195, 195R, 196R,  
 199AU, 207, 211R, 257,  
 264, 269R, 317, 320R,  
 346, 347, 353R, 375AU,  
 383, 384R, 397, 402R,  
 431AU

## -O-

ODELL, C.N., 96, 111R  
 OGSTON, A.G., 255, 267R  
 ORRELL, S.A., JR., 286, 293,  
 296R  
 OSAWA, S., 16, 31R  
 OTTOLENGHI, A., 334, 343R  
 OURA, H., 397, 401R  
 OVERMAN, J.R., 257, 268R  
 OWENS, H.S., 404, 409R

## -P-

PADILLA, G.M., 4, 153, 154R,  
 310, 311R, 317AU, 320,  
 320R, 361AU, 391, 392R  
 PAKESCH, F., 389, 392R  
 PALADE, G., 324, 325, 330R  
 PAPPAS, W.S., 4, 241AU  
 PARISH, J.H., 397AU  
 PARKER, C.J., JR., 346, 353R  
 PARR, C.W., 448, 458, 460R  
 PARRISH, R.G., 349, 353R  
 PAUL, H.L., 258, 269R  
 PEDERSEN, K.O., 9, 30R, 41,  
 73R, 78, 85, 110R, 176,  
 187R  
 PERRY, S.G., 469, 482R  
 PERRY, S.V., 345, 346, 352R,  
 353R  
 PETERS, D., 265, 269R  
 PETRASH, D.A., 103, 111R  
 PETREE, L.G., 286, 296R  
 PHILLIPS, O.M., 103, 111R  
 PICKELS, E.G., 139, 153R  
 PIEZ, K.A., 431, 438R  
 PINKUS, O., 85, 110R  
 PLANTEROSE, D.N., 257, 269R  
 PLESNER, P., 361, 364, 368R,  
 478, 482R  
 PLUNKETT, R., 90, 111R  
 POLGLASE, V.J., 255, 267R  
 POLLARD, E.C., 295, 296R  
 POLSON, A., 256, 268R  
 PORTER, G.H. III, 389, 392R  
 PORTER, R.R., 403, 409R  
 PORTZEHL, H., 346, 353R  
 PRAGER, S., 58  
 PRESCOTT, D.M., 367, 368R,  
 369R  
 PRICE, C.A., 4, 20, 21, 32R  
 PRINGSHEIM, E.G., 304, 310,  
 310R

## -R-

RANDALL, C.C., 256, 267R  
 RANDALL, R.J., 176, 262,  
 269R, 343R, 347, 353R,

383R  
 RANKIN, C.T., JR., 4, 17, 19,  
 20, 31R, 46, 73R, 113AU,  
 137AU, 138, 153, 153R,  
 154R, 166, 167, 169,  
 170R, 175, 176, 178,  
 187R, 193, 195R, 199,  
 207, 211R, 241, 247R,  
 253AU, 286, 287, 296R,  
 305, 309, 311R, 317,  
 320R, 333AU, 343, 344R,  
 346, 347, 353R, 397,  
 402R, 436, 438R  
 RAPATZ, G.L., 416, 423R  
 RASMUSSEN, L., 478, 482R  
 RAVENHILL, J.R., 470, 482R  
 REBERS, P.A., 287, 296R, 305,  
 311R, 448, 460R  
 REBHUN, L.I., 415, 422R  
 REDA, I.M., 256, 268R  
 REED, L.J., 176, 383R  
 REID, E., 17, 31R, 323AU,  
 324, 327, 329, 330R  
 REIMER, C.B., 4, 153, 154R,  
 195, 196R, 199, 211R,  
 257, 269R, 375AU, 377,  
 384R  
 RICH, A., 368, 369R  
 RINFRET, A.P., 416, 422, 423R  
 RINGO, D.L., 303, 309, 310,  
 310R  
 ROARK, R.J., 103, 111R  
 ROBERTS, R.B., 175, 187R  
 ROLSTON, J.A., 95, 111R  
 ROSANDER, H., 469  
 ROSEBROUGH, N.J., 176, 262,  
 269R, 343R, 347, 353R,  
 383R  
 ROSEN, W.D., 303, 310R  
 ROSENBLOOM, J., 187R  
 ROTHEN, A., 255, 267R  
 ROTT, R., 256, 268R  
 ROUILLER, C., 324, 327, 330R  
 ROUTH, E.J., 81, 82, 110R  
 RUBIN, H., 258, 269R  
 RUMKE, PH., 324, 329, 330R  
 RUTENBERG, E.L., 4, 389AU  
 RUTENBERG, MRS. AARON, 403  
 RYLEY, J.F., 310, 311R

## -S-

SAGIN, J.F., 383, 384R  
 SAHYUN, M., 286, 295R  
 SALZMAN, N.P., 257, 269R  
 SAMUELSON, O., 448, 460R  
 SASLAW, L.D., 335, 343R  
 SCANLON, M., 265, 269R

- SCHACHMAN, H.K., 404, 409R  
 SCHAECHTER, M., 361, 368R  
 SCHAFFER, W., 256, 268R  
 SCHERBAUM, D.H., 368, 369R  
 SCHILD, F., 481, 482R  
 SCHILDKRAUT, C.L., 255, 267R  
 SCHLESSINGER, D., 255, 267R  
 SCHMIDT, J.J., 415  
 SCHNEEBELI, J., 324, 327, 330R  
 SCHNEIDER, A., 334, 343R  
 SCHNITZER, E., 81, 110R  
 SCHRAM, E., 153, 154R  
 SCHUEL, H., 4, 19, 31R, 153, 154R, 179, 188R, 350, 354R  
 SCHUEL, R., 153, 154R, 350, 354R  
 SCHUMAKER, V.N., 187R, 255, 267R  
 SCHUMPERT, M.Z., 286, 293, 294, 296R  
 SCHUTZ, B., 334, 343R  
 SCHWARTZ, H.S., 286, 294, 296R  
 SCOTT, A., 334, 342, 343R  
 SCOTT, R.P.W., 470, 482R  
 SEAMAN, G.R., 318, 320R  
 SEARLE, F., 448, 460R  
 SEIDEL, J.C., 351, 354R  
 SERAYDARIAN, M.W., 352, 354R  
 SHAPIRO, O.W., 335, 343R  
 SHARP, D.G., 257, 268R  
 SHEN, T.-M., 286, 293, 294, 296R  
 SHOUP, C.S., 4  
 SIEBERT, G., 324, 330R  
 SIEGESMUND, K.A., 303, 310R  
 SIEKEVITZ, P., 324, 325, 330R  
 SILVERIA, V., 404, 409R  
 SINGER, B., 397, 401R  
 SINSHEIMER, R.L., 256, 268R  
 SMART, E.H., 81, 110R  
 SMITH, E., 334, 343R  
 SMITH, E.L., 255, 267R  
 SMITH, F., 287, 296R, 305, 311R, 448, 460R  
 SMITH, JACQUELINE, 17, 31R, 323AU  
 SMITH, K.O., 257, 269R, 389, 392R  
 SMITH, L.P., 479, 482R  
 SNYDER, C.F., 221, 222, 225, 230, 231, 237, 239R  
 SOMOGYI, M., 286, 295R  
 SPACKMAN, D.H., 404, 409R, 431, 438R, 447, 459R  
 SPICER, D.S., 383, 384R  
 SPIKNER, J.E., 458, 461R  
 STAEHELIN, T., 397, 401R  
 STAHL, F.W., 15, 30R, 241, 247R  
 STALLMAN, R.C., 139, 153R  
 STAPLES, R.C., 448, 458, 460R  
 STEIN, W.H., 404, 409R, 431, 438R, 447, 459R  
 STENBACK, W.A., 256, 268R  
 STERN, H., 16, 31R  
 STERNBERG, J.C., 470, 473, 475, 482R  
 STERNLICHT, B., 85, 110R  
 STETTEN, D., JR., 285, 286, 294, 295R  
 STETTEN, M.R., 285, 286, 294, 295R  
 STEVENS, R.H., 4, 24, 25, 32R, 137, 146, 151, 153R, 262, 269R, 469AU, 470, 482R, 485AU  
 STEVENSON, R.E., 4  
 STEWARTSON, K., 103, 111R  
 STONE, B.A., 303, 304, 308, 309, 310, 310R  
 STOUFFER, J.E., 482R  
 STOUTHAMER, A.H., 256, 268R  
 SUDDATH, J.H., 81, 110R  
 SULKIN, S.E., 486, 495R  
 SVED, S., 256, 268R  
 SVEDBERG, T., 9, 30R, 41, 73R, 78, 85, 110R, 176, 187R  
 SVENSSON, H., 14, 30R, 57, 73R  
 SWANSON, H.D., 28, 32R  
 SWARTOUT, J.A., 4  
 SWARTOUT, W.M., 137, 146, 151, 153R, 262, 269R, 485AU  
 SWEELEY, C.C., 448, 460R  
 SWENSON, B., 448, 460R  
 SWINDELLS, J.F., 221, 230, 231, 237, 239R  
 SYAMANANDA, R., 448, 458, 460R  
 SYKES, J.A., 254, 265, 266R, 269R  
 SYVERTON, J.T., 256, 268R  
 SZENT-GYORGYI, A., 345, 352R
- T-
- TAKAHASHI, K., 345, 352R  
 TAMM, I., 256, 268R  
 TAPPEL, A.L., 334, 342, 343R  
 TATA, J.R., 294, 296R  
 THIERS, R.E., 342, 343R

THOMA, J.A., 448, 460R  
 THOMSON, J.F., 13, 30R, 176,  
 187R, 255, 267R  
 TIMOSHENKO, S., 86, 90, 93,  
 99, 103, 110R, 111R  
 TIPTON, S.R., 19, 31R, 153,  
 154R, 179, 188R  
 TISDALE, H.D., 342, 344R  
 TISELIUS, A., 5  
 TISSIERES, A., 255, 267R  
 TOMASSINI, N., 391, 392R  
 TONOMURA, Y., 345, 352R  
 TOPLIN, IRVING, 4  
 TOWNE, J.C., 458, 461R  
 TRAUTMAN, RODES, 5, 25, 179,  
 256, 256R, 257, 257R,  
 267R, 268R  
 TROESCH, B.A., 88, 103, 110R,  
 111R  
 TSUGITA, A., 397, 401R  
 TURNER, M.K., 324, 330R  
 TYTELL, A., 383, 384R

## -U-

UEDA, K., 303, 310R  
 UNGAR, E.E., 91, 111R  
 UPTON, A.C., 485, 495R

## -V-

VALENTINE, R.C., 256, 268R  
 VALLEE, B.L., 342, 343R  
 VAN DER CRAATS, F., 476, 482R  
 VAN DER SLUYS, I., 256, 268R  
 VAN DREAL, P.A., 361AU, 441  
 VANSTRUM, P.R., 4  
 VARSHNI, Y.P., 233, 239R  
 VASSILIOU, B., 448, 456, 461R  
 VINOGRAD, J., 15, 30R, 241,  
 247R  
 VON DER DECKEN, A., 353R  
 VON HIPPLE, P.H., 349, 353R

## -W-

WADMAN, W.H., 448, 460R  
 WALKER, T., 469, 482R  
 WALLACH, D.F.H., 324, 327,  
 329, 330R  
 WALLENIIUS, L.O., 448, 460R  
 WANG, C-T, 324, 330R  
 WARAVDEKAR, V.S., 335, 343R  
 WARNER, J.R., 369R

WATERS, D.A., 4, 89AU  
 WATSON, D.H., 201, 212R  
 WATSON, J.D., 255, 267R  
 WATSON, J.L., 271, 271R  
 WEAVER, B., 243, 247R  
 WEAVER, C.E., 4  
 WEBER, A., 352, 354R  
 WEBER, C.W., 4, 241AU  
 WEIGEL, H., 448, 460R  
 WEINBERG, A.M., 4  
 WEINSTEIN, J., 334, 342, 343R  
 WELLS, W.W., 448, 460R  
 WETTSTEIN, F.O., 397, 401R  
 WHISTLER, R.L., 447, 460R  
 WHITE, W.C., 481, 482R  
 WHITEHEAD, ALFRED NORTH, 1  
 WHITSON, G.L., 4, 317AU, 320,  
 320R  
 WHITTAKER, E.T., 81, 110R  
 WHITTAKER, V.P., 342, 344R  
 WILBUR, K.M., 28, 32R, 333,  
 335, 343R  
 WILCOX, W.J., JR., 4  
 WILDY, P., 201, 212R  
 WILLIAMS, C.A., 404, 409R  
 WILLIAMS, E.G., 352, 354R  
 WILLIAMS, N.E., 320, 320R  
 WILLS, E.D., 342, 343R  
 WINOCOUR, E., 256, 268R  
 WOOD, P.B., 222, 227, 230,  
 233, 234, 239R  
 WORK, T.S., 256, 268R  
 WRIGHT, H.B., 448, 460R  
 WRIGHT, R.R., 4, 241AU

## -Y-

YIENGST, M.J., 255, 267R  
 YOUNG, D.H., 86, 110R  
 YOUNG, F.G., 286, 296R  
 YOUNG, L., 265, 269R

## -Z-

ZALKIN, H., 334, 342, 343R  
 ZALTA, J.P., 255, 267R  
 ZEUTHEN, E., 478, 482R  
 ZIEHLKE, K.T., 4, 20, 32R,  
 165AU  
 ZILL, L.P., 448, 460R  
 ZUAZAGA, C., 404, 409R  
 ZUBROD, GORDON, 4  
 ZYDOWO, M., 346, 353R



# SUBJECT INDEX (FIGURE,F TABLE,T)

-A-

A AND B SERIES, PUBLIC AVAILABILITY OF DRAWINGS OF, 30  
A ROTOR, LOW-SPEED, 115-136  
A ROTOR, OPERATION OF, 127F  
A SEAL,, 120F, 132F  
A SERIES GRADIENT MONITORING, 121  
A THROUGH D SERIES ROTORS, DESCRIPTION OF, 29  
ABSOLUTE DENSITY OF SUCROSE SOLUTIONS, 221T  
ACTIN, SOLUBILITY CHANGES IN, 345  
ACTIVATION ENERGY COEFFICIENTS, 225T, 236T, 236F  
ACTOMYOSIN AND CONTRACTILE PROTEIN, 359F  
ACTOMYOSIN EXTRACTION, 345  
ADENOSINE TRIPHOSPHATASE ACTIVITY, 346-348T  
ADENOVIRUS 2, 204T, 205F, 216F  
AEROSOL FORMATION, SPRAYER FOR, 428F  
AEROSOLS, 23  
AEROSPACE MATERIALS FOR ROTOR, 95  
A-I THROUGH A-XII ROTORS, EVOLUTION OF, 18-19  
A-II, 34F  
A-III, 35F  
A-IV, 36F  
A-IX, 118-121, 118F, 131F  
A-IX PUMPS, 119, 120  
A-IX, FAILURE AT LOW SPEED, 135F  
A-IX, MITOCHONDRIA AND NUCLEI IN, 121  
A-IX-B, RUNOUT OF, 119F  
A-V, 114-116, 115F  
A-V, SEPTA IN, 114, 123  
A-VI, 116-118, 129F, 130F  
A-VI SEALS, 117  
A-XII, 122-124, 133F  
A-XII, ACTOMYOSIN SEPARATION IN, 347  
A-XII, BANDING OF MUSCLE IN, 355F  
A-XII, COMMERCIAL AVAILABILITY OF, 19  
A-XII, FOR TETRAHYMENA STRUCTURES, 317-321  
A-XIV, RUNOUT OF WATER-FILLED, 109  
A-XIV, WAVES IN, 107F  
AMPASE IN B-IV FRACTIONATED CYTOMEMBRANES, 325-329  
ANALYTICAL ROTOR, DESIGN OF, 78, 79F  
ANALYTICAL ULTRACENTRIFUGATION, 13  
ANALYZER, FLAME IONIZATION, 469-483, 483F  
ANGLE-HEAD CENTRIFUGE TUBE REDESIGN, 486, 487, 488F, 497F  
ANGLE-HEAD ROTOR, DESIGN OF, 78, 79F  
ANTIBODIES, PLASMA, 408  
ANTIGENS IN VACCINES, 23  
ANTOINE EQUATION AND VISCOSITY, 219, 224T, 232, 234  
ARBACIA PUNCTULATA, 30  
ARRHENIUS EQUATION AND VISCOSITY, 219, 232  
ASTASIA CELLS, 303  
ATPASE IN B-IV FRACTIONATED CYTOMEMBRANES, 325-329  
AUTOMATED SYSTEMS FOR ENZYMES AND PROTEIN, 20  
AUTOMATED ANALYTICAL SYSTEMS, 24  
AUTOMATED CARBOHYDRATE ANALYZER, 447-467, 449F, 463F  
AXIS, MOMENT-OF-INERTIA, 83

## -B-

- B SERIES ROTOR, 51, 155F
- B SERIES ROTOR INSTRUMENTATION, 159F, 164F
- BAMP, FOR CESIUM EXTRACTION, 243-245
- BAND CAPACITY ESTIMATE, WITH 30-S RIBOSOMES, 71, 72
- BAND CAPACITY THEORY, 63-67
- BAND CAPACITY VS. TIME DURING MIGRATION, 63
- BAND CAPACITY VS. WIDTH DURING CENTRIFUGATION, 66F
- BAND CAPACITY, EFFECT OF DIFFUSION ON, 69
- BAND CAPACITY, IN TIME-DEPENDENT GRADIENT, 73F
- BAND CHANGES, 66, 67
- BAND INSTABILITY, 62
- BAND STABILITY, EFFECT OF SOLUTE DIFFUSION ON, 67
- BAND STABILITY, TIME DEPENDENCE OF, 57, 61
- BANDING AND CONTINUOUS FLOW, 199-212
- BANDING DENSITY, FOR VIRUS AND CELL COMPONENTS, 256F
- BANDING DENSITY AND BINDING SITE, 16
- BANDING OF ESCHERICHIA COLI, 276F
- BANDING OF EUGLENA FRACTIONS, 313F
- BANDING OF LIVER HOMOGENATE, 297F
- BANDING OF T3 PHAGE, 275F
- BANDING, ISOPYCNIC, 262-263
- BATCH CENTRIFUGATION, 47, 48, 50, 56
- BATCH METHOD FOR VIRUS ISOLATION, 76F
- BATCH SEPARATION, CENTRIFUGATION TIME, 56
- BATCH VS. SEMIBATCH CENTRIFUGATION, 51F
- BEARINGS, DAMPER, 91-92, 139, 141F, 158F
- BEARINGS, DN VALUES OF, 85
- BEARINGS, FOR ELIMINATING WHIRL, 85
- BIOCONTAINMENT, PROBLEMS IN, 485-502
- BIOHAZARDS COMMITTEE, 485
- BITTNER VIRUS, 265
- B-I THROUGH B-XI ROTORS, EVOLUTION OF, 19, 20, 23, 24
- B-I, INSTABILITY OF, 19
- B-II, 37F, 47
- B-II VS. B-IV, 142, 142F, 143F, 143F
- B-II, BATCH TECHNIQUE FOR VIRUSES IN, 75F
- B-II, OSCILLOGRAM OF, 157
- B-II, PRECESSION OF, 140, 156F
- B-IV, 137-164, 160-163F
- B-IV, ASSEMBLY, 146, 147
- B-IV, AVAILABILITY OF, 19
- B-IV, BATCH TECHNIQUE FOR VIRUSES IN, 75F
- B-IV, BIOLOGICAL MATERIALS IN, 153
- B-IV, CLEANING AND STERILIZING, 151, 152
- B-IV CONTAINMENT, 146
- B-IV CORE, 141-144
- B-IV, DESIGN PROBLEMS, 138
- B-IV, EUGLENA FRACTIONS IN, 313F
- B-IV, GRADIENT AND SAMPLE INTO, 147-150, 148F, 149F
- B-IV, GRADIENT PUMP, 150, 151
- B-IV, GRADIENT RECOVERY FROM, 150
- B-IV INSTRUMENTATION, 145, 146
- B-IV, ISOLATION OF MACROGLOBULIN IN, 403-412, 405F, 408F
- B-IV, LIPID PEROXIDATION IN FRACTIONS BY, 334-344, 336F
- B-IV, LIVE POLIO VIRUS IN, 375-388
- B-IV, LIVER MICROSOMES IN, 323-332

B-IV, MOTIONS AND FREQUENCIES OF, 87F  
B-IV, OPERATION, 38F, 39F, 146-152  
B-IV ROTOR LENGTH, 144, 144F  
B-IV SEALS, 138, 139, 140F  
B-IV, SEDIMENTATION RATES IN, 152, 152F, 153  
B-IV, TETRAHYMENA LYSATE IN, 365F  
B-IV VS. B-II, 142, 142F, 143F  
B-IV AND B-V, REMOTE OPERATION OF, 385F  
B-IX, 199-212, 202F, 208T, 209F, 210F, 213F  
B-V, 47  
B-V, CONTINUOUS-FLOW, 191-198, 192F, 197F  
B-V, DISINFECTION OF, 198F  
B-V, LIVE POLIO VIRUS IN, 375-388  
B-V, OPERATION OF, 192, 192F  
B-V, ROTATING SEAL OF, 193, 194, 194F  
B-V, ZONE RECOVERY, 195  
B-VIII, 199-212, 202F, 207T  
B-VIII AND B-IX, ISOPYCNIC BANDING IN, 199-212  
B-VIII UNLOADING SPEEDS, 207  
B-VIII, FLOW PATH IN, 206F  
B-VIII, INLET PRESSURE IN, 205F  
B-X, 165-174, 166F, 172F, 173F  
B-X AND B-XI, MAXIMUM SPEEDS, 168T  
B-XI, 165-174, 174F  
B-XIV, 170  
B-XV, 170  
BLOOD, NITROGEN FREEZING OF, 430F  
BOUNDARY LAYER DIFFUSER, IN CHO ANALYZER, 458, 459F,  
466-467F  
BRAIN MICROSOME FRACTION, 342  
BRAIN PARTICLES, SEPARATION OF, 272F  
BROMGRASS MOSAIC VIRUS, IN B-IV, 153  
BUOYANT DENSITY SEPARATION, 15, 16, 23, 263-264

-C-

C SERIES ROTOR INSTRUMENTATION, 159F  
CELL COMPONENTS, S FOR, 256  
CALCIUM ACTIVATION OF ACTOMYOSIN, 352  
CALCULATIONS OF CENTRIFUGATION TIMES OR FLOW RATES, 56  
CAMERA, FOR ISOPYCNIC BANDS, 497F  
CAPACITY OF BAND IN ZONAL CENTRIFUGATION, 56  
CARBOHYDRATE ANALYZER, AUTOMATED, 447-467, 449F, 463F  
CARBOHYDRATE AND GLYCOGEN IN LIVER, 293  
CARBOHYDRATE IN RAT LIVER, 288-290F  
CARBOHYDRATE, FLUOROMETRIC, 458  
CARBOHYDRATE, IN EUGLAENA, 306F  
CARBON, INSTRUMENT FOR DETERMINATION OF, 469-483  
CELL COMPONENTS, S FOR, 255, 256F, 257  
CELL FRACTIONS, IN B-IV, 153  
CELL FREEZING AND THAWING, 415, 416  
CENTRIFUGAL FIELD, EFFECT OF, 43  
CENTRIFUGAL WAVES IN FLUIDS, 103-105, 107F  
CENTRIFUGATION IN CONSTANT DENSITY MEDIUM, 46-56  
CENTRIFUGATION TIME, EQUATIONS FOR, 56  
CENTRIFUGATION, CONTINUOUS, 51  
CENTRIFUGATION, THEORY OF, 41-76  
CESIUM CHLORIDE USE IN ROTOR DESIGN, 94, 97F

CESIUM CHLORIDE, ANALYSIS AFTER RECOVERY, 243T  
CESIUM CHLORIDE, REDUCING ABSORBANCY OF, 241-249  
CESIUM FOR DENSITY GRADIENT SOLUTIONS, 241-249  
CESIUM, AFTER EXTRACTION, 244, 245T  
CESIUM, EXTRACTION WITH BAMBP, 243-245  
CESIUM, PERMISSIBLE CATION IMPURITIES, 241  
CESIUM, PERMISSIBLE ELEMENTAL IMPURITIES, 241  
CESIUM, RECOVERY SYSTEM FOR, 244F, 246F, 249F  
CHROMATOGRAPHY OF SUGARS, 447, 448, 456  
CHROMATOGRAPHY, HIGH-PRESSURE, 431-440  
CHROMATOGRAPHY OF YEAST, 441, 443, 444T  
CLADOPHORA RUPESTRIS, 309  
CLARIFIER ROTOR; DESIGN OF, 79F, 80  
COLORIMETRY OF SUGARS, 458-459  
COLUMN CHROMATOGRAPHY, HIGH-PRESSURE, 431-440, 433F, 435F, 439F, 440F  
COLUMNS FOR CHO ANALYZER, 450, 450F, 451, 464F  
CONSTANT DENSITY MEDIUM, CENTRIFUGATION IN, 46-56  
CONTAINMENT FOR ZONAL CENTRIFUGATION, 492-495, 501-502F  
CONTAINMENT OF VIRUS, 485-502  
CONTAINMENT, FOR B-IV, 146  
CONTINUITY EQUATION, 58  
CONTINUOUS DENSITY GRADIENT, 21  
CONTINUOUS FLOW CENTRIFUGATION, 22-23, 51, 190-216  
CONTINUOUS FLOW CENTRIFUGATION OF VIRUS, 378-380  
CONTINUOUS FLOW VS. BATCH AND SEMIBATCH, 56  
CONTINUOUS FLOW WITH BANDING, 199-212  
CONTINUOUS FLOW, WITH B-IV, 139  
CONTINUOUS FLOW, B-VIII AND B-IX, 199-212  
CONTINUOUS-FLOW ROTOR, DESIGN OF DISK TYPE, 79-80, 79F  
CONTRACTILE PROTEIN AND ACTOMYOSIN, 359F  
CONTRACTILE PROTEIN, ENZYME ACTIVITY OF, 348T  
CONTRACTILE PROTEIN, EXTRACTION OF, 345-359  
CONVECTIVE DISTURBANCES, 12, 14  
CORE OF B-IV, 141-144  
CORIOLIS FORCES AND EFFECTS, 41-46  
CORROSION STUDIES, IN B-X AND B-XI, 169  
COUNTERCURRENT SEPARATIONS, 24  
CRITICAL FREQUENCY OF ROTOR, 89  
CRITICAL SPEED OF ROTOR, 89-91  
CROSS CONTAMINATION, 10

-D-

DAMPER BEARINGS, 77, 91-92  
DAMPER BEARING, IN B-IV, 139, 141F, 158F  
DAMPERS, VIBRATION, 91  
DECONTAMINATION FAILURE, 375  
DEFLECTION EQUATIONS, 77  
DENSITY GRADIENT IN TUBES, DISADVANTAGES OF, 13  
DENSITIES, BUOYANT OR BANDING, 11, 24  
DENSITY AND PRESSURE, 238, 239  
DENSITY AND VISCOSITY OF SUCROSE, 219-239  
DENSITY BEADS FOR GRADIENTS, 487, 488, 489T  
DENSITY CALCULATION, ACCURACY OF, 223  
DENSITY CONSTANTS, 222T, 223T  
DENSITY DISTRIBUTION, CONCENTRATION EFFECTS ON, 58  
DENSITY EQUATIONS, DEVIATION OF, 230F

DENSITY GRADIENT CENTRIFUGE, 18F  
DENSITY GRADIENT, ARBITRARY, 57  
DENSITY GRADIENT, CESIUM, 241-249  
DENSITY GRADIENT, CONTINUOUS, IN HOLLOW ROTORS, 47  
DENSITY GRADIENT, FACTORS IN PARTICLE SETTLEMENT, 56, 57  
DENSITY GRADIENT, IDEAL, 220  
DENSITY GRADIENT, TYPES AND CAPACITIES OF, 14, 15  
DENSITY INVERSION, 58, 60, 62F  
DENSITY, ABSOLUTE, OF SUCROSE SOLUTIONS, 221T  
DESIGN GRAPHS, 97F, 98F  
DESIGN OF ZONAL CENTRIFUGES, 77-111  
DESIGN, ROTOR, PROBLEMS IN, 107-108  
DETECTOR, FLAME IONIZATION, 470  
DIALYSIS, APPARATUS FOR ASEPTIC, 499-501F  
DIALYSIS, CONTAINED METHOD FOR, 489-492, 491F, 492F  
DIFFERENTIAL CENTRIFUGATION, 10, 11  
DIFFERENTIAL CENTRIFUGATION OF MICROSOMES, 335, 337T  
DIFFUSION COEFFICIENT FOR SUCROSE, 69  
DIFFUSION EQUATION, SOLUTION OF, 68-69  
DIFFUSION OF SOLUTE VS. SEDIMENTATION VELOCITY, 67  
DIFFUSION OF SOLUTE, EFFECT ON BAND STABILITY, 67-73  
DIFFUSION, EFFECT OF SUCROSE GRADIENT, 69F  
DIFFUSION, EFFECT ON BAND CAPACITY, 69  
DIFFUSION, IN CHROMATOGRAPHY, 432  
DISINFECTION OF B-V, 198F  
DISK TYPE ROTOR, DESIGN OF, 79-80, 79F  
DISTURBANCES TO ORIENTATION, 83  
DIVALENT CATIONS, BINDING BY NUCLEI, 28  
DN VALUES OF BEARINGS, 85  
DROSOPHILA MELANOGASTER RNA, 397  
DRY BOX, FOR VIRUS CONTAINMENT, 377, 385F  
DYNAMICALLY LOADED ROTOR, 114

-E-

ELECTRON MICROSCOPE, LIMIT OF, 271F  
ELIPSOIDS OF INERTIA, 82F  
ELUTION, ACCELERATED, 438F  
ELUTION, PLATE HEIGHT IN, 432  
END CAP STRESS, 99-103  
END CAPS, LOADED WITH PARABOLIC PRESSURE, 77  
ENZYME ACTIVITIES IN MICROSOMAL SUBFRACTIONS, 17  
ENZYME ACTIVITY OF CONTRACTILE PROTEIN, 348T  
ENZYMES AND SOLUBLE COMPONENTS, PARTITION OF, 16  
ENZYMES IN LIVER, 323  
EQUIVALENT SEDIMENTATION COEFFICIENT, 179  
ESCHERICHIA COLI RIBOSOME SUBUNITS, IN B-IV, 153  
ESCHERICHIA COLI RNA, 397  
ESCHERICHIA COLI, BANDING OF, 276F  
ETHYLENE OXIDE, VIRUS TITER AFTER, 382T  
EUGLENA CARBOHYDRATE, 306F  
EUGLENA FRACTIONS, 306F, 308T, 313F  
EUGLENA GRACILIS VAR. BACILLARUS SML-1, 303  
EUGLENA PARAMYLON, 303-316, 314F  
EUGLENA POLYSACCHARIDE, 309  
EXTRACTION OF CESIUM WITH BAMBP, 243-245  
EXTRACTION OF CONTRACTILE PROTEINS, 345-359

## -F-

FILAMENT-WOUND VESSELS, 95-100  
FINITE PARTICLE BAND, EFFECT OF MIGRATION OF, 57  
F-ACTIN, 351  
F-I, FOR FREEZING AND THAWING CELLS, 417-419  
F-IF, 425F  
F-II, 426F  
FLAME IONIZATION ANALYZER, 24, 469-483, 483F  
FLEXIBLE SHAFTS, ROTOR WITH, 86, 91-92  
FLEXURAL CRITICALS, 83  
FLEXURAL VIBRATIONAL OF FREELY SUSPENDED ROTOR, 77  
FLOTATION-RATE ZONAL (SF-ZONAL) CENTRIFUGATION, 13  
FLOW FUNCTION FOR CONTINUOUS-FLOW CENTRIFUGE, 54  
FLOW PATH IN B-VIII, 206F  
FLOW RATES, EQUATIONS FOR, 56  
FORCES ACTING ON PARTICLE, 25, 27, 42-43  
FRACTIONS, RADII OF, 176-179, 177F  
FREEZING OF BLOOD, 430F  
FREEZING OF CELLS, METHOD FOR, 427F  
FREEZING OF WATER IN NITROGEN, 429F  
FREEZING, ULTRARAPID, CENTRIFUGAL, 415-430  
FREQUENCIES AND MOTIONS OF B-IV, 87F

## -G-

G-6-PASE IN B-IV FRACTIONATED CYTOMEMBRANES, 325-329  
G-ACTIN, 352  
GLOBULINS AND HISTONES, SEQUENTIAL REMOVAL OF, 24  
GLOBULIN, PLASMA, ISOLATION OF, 403  
GLYCOGEN AND CARBOHYDRATE IN LIVER, 293  
GLYCOGEN IN CESIUM CHLORIDE, 292F  
GLYCOGEN IN SUCROSE GRADIENT, 291  
GLYCOGEN, AFTER CENTRIFUGATION, 298-299F  
GLYCOGEN, ISOLATION OF NATIVE, 17  
GLYCOGEN, LIVER, 26  
GLYCOGEN, METHODS OF SEPARATION, 286-288  
GLYCOGEN, S\* OF, 291, 292F  
GLYCOGEN, STAINED, 300-302F  
GLYCOGEN, TETRAHYMENA, IN B-IV, 153  
GRADIENT DENSITY,  $\rho$ , 15  
GRADIENT MATERIALS, STUDIES ON, 218-249  
GRADIENT MONITORING, A SERIES, 121  
GRADIENT PUMP FOR A-IX, 119  
GRADIENT RESOLUBILIZATION, 24  
GRADIENT, RECOVERY FROM B-VIII, 204T, 204F

## -H-

HAZARD CLASSIFICATION, 485  
HEPATOMA, RIBOSOMAL RNA FROM, 399  
HIGH-PRESSURE COLUMNS, 24  
HOLLOW LARGE-VOLUME ROTORS, 9, 18  
HOLLOW-BOWL ROTOR, 50, 113  
HUMAN PLASMA, UNUSUAL PARTICLES IN, 389-394  
HYBRID ROTOR, 77  
HYDROCARBON DETERMINATION, 475F, 476F, 477T, 479F

## -I-

IMPRISONED GRADIENT, 23  
INFECTIOUS UNIT, (IU), 258  
INFLOWING GRADIENT, DISADVANTAGES OF, 20  
INFLUENZA, TOTAL MASS, 201  
INSTABILITY, LIQUID, 87  
INSTABILITY, MECHANICAL, 77  
INSTRUMENTATION, B-IV, 145, 146  
INTEGRITY, FLUID-TIGHT, 77  
INTERMEDIATE-SPEED 'B' SERIES ROTORS, 9, 19  
ISODENSITY CURVES, 21, 22  
ISOLATION OF PARAMYLON FROM EUGLENA, 303-316  
ISOLATION OF TETRAHYMENA STRUCTURES, 317-321, 321F  
ISOPYCNIC AND RATE SEPARATION OF VIRUS, 253-283  
ISOPYCNIC BANDING, 9, 262-263  
ISOPYCNIC BANDING DENSITY, 16, 47  
ISOPYCNIC BANDING, IN B-VIII AND B-IX, 199-212, 214F, 215F  
ISOPYCNIC BANDS, APPARATUS FOR, 498  
ISOPYCNIC BANDS, RECOVERY OF, 489  
ISOPYCNIC CONDITIONS FOR MICROSOMES, 325-327  
ISOPYCNIC-ZONAL CENTRIFUGATION, 11, 15-17  
ISOPYCNIC-ZONAL (RHO-ZONAL) CENTRIFUGATION, 15-17, 15F

## -K-

KINETOSOME FRACTION IN TETRAHYMENA, 319F

## -L-

LEAST-SQUARES FIT OF NONLINEAR CURVES, 222  
LEUKEMIA, PARTICLES IN, 389-394, 393F  
LIMIT OF ELECTRON MICROSCOPE, 271F  
LIPID PEROXIDATION IN TISSUE, 333-344  
LIPID PEROXIDATION, MEASUREMENT OF, 335  
LIPID PEROXIDATION, COMPARISON OF, 337T, 338  
LIVER CARBOHYDRATE, 288-290F  
LIVER FRACTIONS IN B-IV, 331-332F  
LIVER GLYCOGEN, 285  
LIVER HOMOGENATE, BANDING OF, 297F  
LIVER MICROSOMES, IN B-IV, 323-332  
LIVER PARTICLES, SEPARATION OF, 274F  
LIVER PARTICULATES, FRACTIONATION OF, 33F  
LIVER, AFTER CENTRIFUGATION IN B-IV, 325-327, 326F  
LOOSE MOUNTINGS, 91  
LOW-SPEED 'A' SERIES ROTORS, 9  
LYMPHOSARCOMA, PARTICLES IN, 389-394, 393F, 394F

## -M-

MACROGLOBULIN, AMINO ACIDS IN, 407T  
MACROGLOBULIN, DIFFUSION ANALYSIS, 406F  
MACROGLOBULIN, ELECTROPHORETIC PATTERNS OF, 411F  
MACROGLOBULIN, IMMUNOELECTROPHORETIC PATTERNS OF, 412F  
MACROGLOBULIN, ISOLATION IN B-IV, 153, 403-412, 405F, 408F  
MACROGLOBULIN, MOBILITY VS. PH, 406F  
MACROGLOBULIN, PHYSICOCHEMICAL PROPERTIES OF, 407T  
MACROGLOBULIN, PLASMA, 29

MACROGLOBULIN VS. PROTEIN, 406F  
MAGNESIUM INHIBITION OF ACTOMYOSIN, 352  
MAGNESIUM IONS, EFFECT ON LIVER IN B-IV, 327-328, 328F  
MASS TRANSPORT, EQUATIONS FOR, 187  
MEMBRANE FRAGMENTS IN LIVER, 323, 324  
MEMBRANE PROFILES, 343  
MESSENGER RNA, 367  
MICROSOMES OF BRAIN, 342  
MICROSOMES, DIFFERENTIAL CENTRIFUGATION OF, 335, 337T  
MICROSOMES, IN B-IV, 153  
MICROSOMES, LIVER, IN B-IV, 323-332  
MIGRATION VELOCITY WITHOUT DIFFUSION, EQUATIONS FOR, 58-60  
MITOCHONDRIA AND NUCLEI, IN A-IX, 121, 134F  
MITOCHONDRIA, IN B-IV, 153  
MITOCHONDRIA, ISOPYCNIC SEPARATION, 335  
MITOCHONDRIA, MICROsome-FREE, 334  
MITOCHONDRIA, SEDIMENTATION OF, 28, 337F  
MOLECULAR SEPARATIONS, 396-412  
MOLONEY VIRUS, 204T  
MOLONEY VIRUS, IN B-IV, 153  
MOMENT-OF-INERTIA AXIS, 83  
MOMENT OF INERTIA, RATIO OF, 83  
MOMENTAL ELLIPSOID CONFIGURATIONS, 77  
MORPHOGENESIS OF CILIATES, KINETOSOME IN, 320  
MOTIONS AND FREQUENCIES OF B-IV, 87F  
MOTION, STEADY-STATE AND TRANSIENT, 80  
MOUNTINGS, LOOSE, 91  
MUSCLE RELAXING ACTIVITY, IN B-IV, 153  
MUSCLE SUBFRACTIONS, 356-358F  
MYOFIBRILS, CONTRACTILE PROTEINS FROM, 345-359  
MYOSIN EXTRACTION, 345  
MYOSIN, NONSPECIFIC BINDING OF, 345

## -N-

NAVIER-STOKES EQUATIONS, 51  
NEUROSPORA MEDIUM, ANALYSIS OF, 457F  
NUCLEI AND MITOCHONDRIA, IN A-IX, 121  
NUCLEIC ACID BANDING, 26, 29  
NUCLEI, FROM RAT LIVER, 28, 153  
NUCLEI, SEDIMENTATION RATE OF, 29  
NUCLEOSIDES, BY CHROMATOGRAPHY, 431-440, 436F  
NUCLEOTIDE ANALYZER, 441-446  
NUCLEOTIDES, BY CHROMATOGRAPHY, 431-440  
NUCLEOTIDES, SEPARATION FROM YEAST, 441-446, 445T

## -O-

OBSERVATION OF SEPARATIONS, 113, 121  
ONCOGENIC VIRUS, SEARCH FOR, 265  
ORAL STRUCTURES IN TETRAHYMENA, 319F, 321F  
OSMOTIC PROPERTIES, 13, 28

## -P-

PARAMYLON, COMPONENTS OF, 308, 309  
PARAMYLON, INDUCED CHANGES, BY KOH, 315-316F  
PARAMYLON, ISOLATION FROM EUGLENA, 303-316, 314F

PARTIAL SPECIFIC VOLUME, 16  
PARTICLE DENSITY, REDISTRIBUTION BY, 11  
PARTICLE ACCELERATION, 43  
PARTICLE BAND PHOTOGRAPHY, 488, 489  
PARTICLE BOUNDARIES, 11  
PARTICLE DENSITY, DIFFERENCES IN, 56  
PARTICLE IMMOBILIZATION DURING CHEMICAL DISSECTION, 23, 24  
PARTICLE RADIUS, EFFECT ON RATE SEPARATIONS, 17  
PARTICLES, MAXIMUM MASS IN BAND (BAND CAPACITY), 67  
PARTICLE, PHYSICALLY DEFINED (PP), 258  
PATHOGENIC VIRUS PARTICLES FROM LARGE VOLUMES, 23  
PERMEABILITY, 13  
PEROXIDATION, RELATION TO LIPID AND PROTEIN, 333-344, 336F, 339-341F  
PHAGE, T2 AND T3, IN B-IV, 153  
PHAGE, T2 AND T3, RECOVERY OF, 277F, 278F  
PHAGE, T3, BANDING OF, 275F  
PHAGE, T3, PURIFICATION AND RECOVERY OF, 264-265, 279F-281F  
PHOTOGRAPHY OF PARTICLE BANDS, 488  
PH, IN DENSITY GRADIENT, 220  
PICKELS FACE SEAL, 108  
POLHODE, 82F  
POLIO VIRUS, IN B-IV AND B-V, 153, 375-388  
POLIO VIRUS, INABILITY TO DECONTAMINATE, 383  
POLIO, TOTAL MASS, 201  
POLLEN, CARBON IN, 481  
POLYSACCHARIDES, AUTOMATED ANALYSIS OF, 447  
POLYSOMES FROM TETRAHYMENA, 361-371  
POLYSOMES, FOUND IN VIRUS FRACTION, 388F  
POLYSOMES, IN B-IV, 153  
POSITION EFFECT OF BAND, 67  
PRECESSION (ROTOR WHIRL), 83  
PRECIPITATION AND ISOPYCNIC BANDING, 24  
PRESSURE DISTRIBUTION, 104-106  
PRESSURE IN B-VIII AND B-IX, 205F, 206-208, 208F  
PRESSURE VS. VISCOSITY AND DENSITY, 238, 239  
PROGRAMING OF CARBOHYDRATE ANALYZER, 455F  
PROTEIN AND LIPID PEROXIDATION, IN B-IV, 336F, 339-341F  
PROTEIN BANDING, 26, 29  
PROTEIN DISTRIBUTION IN GRADIENTS, 261, 262  
PROTEIN SYNTHESIS, IN TETRAHYMENA, 320, 368  
PROTEIN, 'DIVISION,' IN TETRAHYMENA, 319F, 320, 321F  
PROTEIN, CONTRACTILE, 345  
PROTEIN, RATE SEPARATIONS OF, 29  
PUMPS, FOR A-IX, 119, 120  
PYRIMIDINES IN TETRAHYMENA, 361-371

-R-

RADIOACTIVE LABELING OF TETRAHYMENA, 363  
RAGWEED POLLEN IN A-V, 116, 123, 128F  
RAGWEED POLLEN IN A-XII, 124F  
RALEIGH-RITZ ANALYSIS, 89  
RANA PIPIENS, ACTOMYOSIN FROM, 346  
RAT RED CELLS, IN A-V, 116  
RATE AND ISOPYCNIC SEPARATION OF VIRUS, 253-283  
RATE-ZONAL (RHO-ZONAL) CENTRIFUGATION, 11, 12-15, 12F  
RAUSCHER VIRUS, IN B-IV, 153

ZONAL CENTRIFUGE

- REAGENT PUMPING MODULE IN CHO ANALYZER, 465F  
RECOVERY OF CSCL FROM WASTE SOLUTIONS, 241-249  
RECOVERY OF GRADIENTS DURING ROTATION, 113, 114  
RECOVERY OF T2 AND T3 PHAGE, 278F-281F  
RECOVERY SYSTEM FOR CESIUM, 244F, 246F, 249F  
RELAXING FACTOR SYSTEM IN ACTOMYOSIN EXTRACTION, 345, 350, 351  
REMOTE HANDLING OF VIRUS, 486  
REMOTE OPERATION, OF B-IV AND B-V, 385F  
REMOVABLE SEALS, OF B-X AND B-XI, 167, 171F  
REMOVABLE-SEAL ROTOR, 20, 22, 165-174  
REORIENTING GRADIENT (REOGRAD) ROTORS, 9, 20-22, 21F, 114  
RESONANT WHIP (SEE WHIRLS), 85  
RESPIRATORY SYNCYTIAL VIRUS, 153, 204T  
RFS IN RIGOR MORTIS, 355F  
RIBOSOMAL RNA, SEPARATION OF, 153, 397-402  
RIBOSOME BAND, EFFECT OF DIFFUSION, 69F  
RIBOSOME BAND, SEDIMENTATION OF 30-S, 69F, 71  
RIGID BODY, CRITICAL MOTION, 86  
RIGID-BODY ROTOR WHIRL FREQUENCY, 77  
RNA HYDROLYSATE, BY CHROMATOGRAPHY, 437F  
RNA IN B-IV FRACTIONATED CYTOMEMBRANES, 325-329  
RNA-DNA SEPARATIONS, 24  
RNA, DROSOPHILA, SEPARATION OF, 397, 398, 400F  
RNA, E. COLI, SEPARATION OF, 397, 400F, 401F  
RNA, FROM HEPATOMA, 399  
RNA, MESSENGER, 367  
RNA, RAT LIVER, SEPARATION OF, 398F, 399F  
RNA, RIBOSOMAL, SEPARATION OF, 397-402  
ROTATING SEAL, OF B-V, 193, 194, 194F  
ROTATIONAL STABILITY, 77, 83, 84F  
ROTOR CONFIGURATIONS, 80-83  
ROTOR CONFIGURATIONS, MOMENT OF INERTIA RATIO, 81, 82F  
ROTOR CONFIGURATIONS, STABILITY REQUIREMENTS OF, 81  
ROTOR CRITICAL SPEED, 89-91  
ROTOR DESIGN DATA, 94  
ROTOR DESIGN, PROBLEMS IN, 107-108  
ROTOR LENGTH, B-IV, 144, 144F  
ROTOR LENGTH, EFFECTIVE, 52, 53  
ROTOR MATERIAL, SELECTION OF, 94, 95T  
ROTOR RUNOUT, 80  
ROTOR UNBALANCE, 88  
ROTOR WHIRL (PRECESSION), 83  
ROTOR WITH REMOVABLE SEALS, 165-174  
ROTORS FOR BIOLOGICAL SYSTEMS, 78-80, 79F  
ROTOR, ANALYTICAL, DESIGN OF, 78, 79F  
ROTOR, ANGLE-HEAD, DESIGN OF, 78, 79F  
ROTOR, AS A FREE BEAM, 89  
ROTOR, CONTINUOUS-FLOW, DESIGN OF DISK TYPE, 79-80, 79F  
ROTOR, CRITICAL FREQUENCY OF, 89  
ROTOR, DESIGN OF VARIOUS TYPES, 79F  
ROTOR, DISK TYPE, DESIGN OF, 79-80, 79F  
ROTOR, DYNAMICALLY LOADED, 114  
ROTOR, HELICALLY WRAPPED, 100-102  
ROTOR, HOLLOW-BOWL, 113  
ROTOR, HYBRID, 77  
ROTOR, REORIENTING GRADIENT, 114  
ROTOR, SWINGING BUCKET, DESIGN OF, 79, 79F

ROTOR, TUBULAR CLARIFIER, DESIGN OF, 79F, 80  
ROTOR, WRAPPED, 95  
ROTOR, ZONAL, DESIGN OF, 79F, 80

-S-

S - RHO ZONAL METHODS, 16  
S20,W, IN SUCROSE GRADIENTS, 176  
SACCHAROMYCES CEREVISIAE, 417, 442  
SAFETY PRECAUTIONS, IN VIRUS WORK, 376  
SCALE OF CENTRIFUGES, 9  
SCANNER, PHOTOELECTRIC, FOR A SERIES, 124, 123, 136F  
SEAL COOLING, IN B-IV, 139  
SEALS, FLUID LINE, 108-110  
SEAL, FOR A-VI, 117, 120F  
SEAL, FOR B-IV, 138, 139, 140F  
SEAL, IN B-VIII AND B-IX, 202  
SEAL, PICKELS FACE, 108  
SEAL, ROTOR WITH REMOVABLE, 165-174  
SECTOR-SHAPED COMPARTMENTS, 14  
SEDIMENTATION COEFFICIENT, 13, 17  
SEDIMENTATION COEFFICIENT, EQUIVALENT, S\*, 29, 179  
SEDIMENTATION COEFFICIENT, S\*, COMPUTING, 175-188  
SEDIMENTATION COEFFICIENT PROGRAM, 179-187  
SEDIMENTATION COEFFICIENT, EQUATIONS FOR, 220  
SEDIMENTATION COEFFICIENT VS. FLOW RATE, 55F  
SEDIMENTATION EQUATION, HYDRODYNAMIC DERIVATION OF, 42-43  
SEDIMENTATION OF VIRUS IN B-IV, 381F  
SEDIMENTATION OF VIRUSES, BATCH TECHNIQUE FOR, 75F  
SEDIMENTATION RATE, 9, 11, 12, 24, 56  
SEDIMENTATION RATE OF SPHERICAL PARTICLE, 16  
SEDIMENTATION RATES OF SUBCELLULAR PARTICLES, RANGE OF, 17  
SEDIMENTATION VELOCITY, EQUATION FOR, 45  
SEDIMENTATION VELOCITY VS. SOLUTE DIFFUSION, 67  
SELECTION OF ROTOR CONFIGURATIONS, 83  
SELF-BALANCING, 20, 77, 83  
SEMIBATCH CENTRIFUGATION, 47, 49, 50, 56, 76F  
SEMIBATCH VS. BATCH CENTRIFUGATION, 51F  
SEPARATION OF BRAIN PARTICLES, 272F  
SEPARATION OF LIVER PARTICLES, 274F  
SEPARATION OF RIBOSOMAL RNA, 397-402  
SEPARATION OF SPLEEN PARTICLES, 273F  
SEPARATION OF SUBCELLULAR PARTICLES, 252-370  
SEPARATION OF T2 FROM T3 PHAGE, 277F  
SEPARATION OF TISSUE COMPONENTS, 260-265  
SEPARATION OF VIRUS BY RATE AND ISOPYCNIC METHODS, 253-283  
SEPTA IN A-V, 114, 123  
SEPTA, IN B-VIII, 201  
SEPTA, TAPERED, OF B-XI, 166F  
SEQUENTIAL GRADIENT PARTICLE DISSECTION, 24  
SERUM ALBUMIN, CARBON IN, 473, 474F, 478T  
SERUM ALBUMIN, IN A-V, 116  
SHAFT BENDING AND FATIGUE, 88  
SHAFT FLEXURAL CRITICALS, 88  
SHAFT SEALS, 77  
SHARPS PROCEDURE, MODIFIED, 377  
SHEARING FORCES, 14, 21  
S-RHO IN B-VIII AND B-IX, 211

ZONAL CENTRIFUGE

S-RHO PLOT, 17  
S-RHO SEPARATION OF VIRUS, 253-283  
S-RHO, SEPARATION OF GLYCOGEN BY, 285-302  
S-RHO, OF POLIO VIRUS, 375  
S-RHO, SEPARATION OF PARAMYLON BY, 303  
SPLEEN PARTICLES, SEPARATION OF, 273F  
SPORES, PUFF BALL, CARBON IN, 480F  
S\*, COMPUTER OUTPUT PLOT, 186F  
S\*, DEFINITIONS OF, 179  
S\*, IN LIPID PEROXIDATION, 338, 342  
S\*, IN SUCROSE, CALCULATION OF, 219-239  
S\*, OF GLYCOGEN, 291, 292F  
S\*, OF TETRAHYMENA RIBOSOMES, 366  
S\*, PROGRAM FOR, 179-187  
STABILITY OF ROTORS, 80, 81, 84F  
STABILITY, ROTATIONAL, 77, 83  
STEADY-STATE MOTION, 80  
STOKES RESISTANCE, 42  
STRESS EQUATIONS, 77  
STRESS IN ROTOR, 92-95  
STRESS, END CAP, 104F, 99-103  
STRESS, OPTIMUM WORKING, 96T, 97F  
SUBCELLULAR PARTICLES, FUNDAMENTALS OF SEPARATION, 25-29  
SUBCELLULAR PARTICLE SEPARATION, 252-370  
SUCROSE SOLUTIONS AND TEMPERATURE, 227, 228, 228F, 229T, 230  
SUCROSE SOLUTIONS, DENSITY OF, 221T, 227F  
SUCROSE WEIGHT FRACTION, 69  
SUCROSE, DENSITY AND VISCOSITY, 219-239  
SUCROSE, DIFFUSION COEFFICIENT FOR, 69  
SUGARS, AUTOMATED ANALYSIS OF, 24, 447, 449F  
SURVIVAL OF FROZEN CELLS, 421T, 419, 420-422, 421F  
SVEDBERG ULTRACENTRIFUGE, 9  
SVEDBERG UNIT, 17, 175, 55F, 56  
SVENSSON STABILITY CRITERION, MATHEMATICAL EXTENSION OF,  
63-67  
SWINGING BUCKET ROTOR, DESIGN OF, 79, 79F  
SWINGING-BUCKET ROTOR, 12, 13, 18  
SWIRLING, PREVENTION OF, 22  
S, FOR CELL COMPONENTS AND VIRUS, 255, 256, 256F, 257  
SYNAPTOSOMES, 342

-T-

T2 AND T3 PHAGE, IN B-IV, 153  
TAYLOR SERIES, APPLIED TO DENSITY VARIATION, 65  
TEMPERATURE CONTROL, IN B-X AND B-XI, 169  
TETRAHYMENA 'DIVISION PROTEINS', 320  
TETRAHYMENA GLYCOGEN, IN B-IV, 153  
TETRAHYMENA POLYSACCHARIDE, 309  
TETRAHYMENA PYRIFORMIS, 317, 361  
TETRAHYMENA, CARBON IN, 476F  
TETRAHYMENA, ISOLATION OF POLYSOMES FROM, 361-371  
TETRAHYMENA, LYSATE OF, IN B-IV, 365F, 370-371F  
TETRAHYMENA, MODIFIED MEDIUM FOR, 362  
TETRAHYMENA, ORAL STRUCTURES, 317-321, 321F  
TETRAHYMENA, POLYSOMES FROM, 361-371  
TETRAHYMENA, SYNCHRONIZED, 320  
THAWING OF CELLS, 415

THIN BAND APPROXIMATION, 64, 66  
THYMUS NUCLEI, CALF, IN A-V, 116  
TISSUE COMPONENTS, SEPARATION OF, 260-265  
TOBACCO MOSAIC VIRUS, IN B-IV, 153  
TRANSIENT MOTION, 80  
TRANSIENT TIME CONSTANT, 45  
TRANSIENT TIMES, 41-46  
TUBULAR CENTRIFUGE, 54  
TUBULAR CLARIFIER ROTOR, DESIGN OF, 79F, 80  
TUMOR, UNIDENTIFIED PARTICLES IN, 265, 283F

## -U-

UDPASE IN B-IV FRACTIONATED CYTOMEMBRANES, 325-329  
UNUSUAL PARTICLES IN HUMAN PLASMA, 389-394, 393F, 394F  
UV ABSORBANCE VS. FRACTIONS, 177F

## -V-

VACCINE PREPARATION, 23, 200  
VELOCITY, MAXIMUM INSIDE, 98T, 98F  
VERTICAL SEPTA, FUNCTION OF, 22  
VESICLES, 25, 27  
VIBRATION DAMPERS, 91  
VIBRATION IN B-II, 140, 156F  
VIBRATIONS, MODES OF, 87F, 91  
VIBRATION, FLEXURAL, OF FREELY SUSPENDED ROTOR, 77  
VIBRATION, EXTERNAL, 84  
VIBRATION, RIGID-BODY, 83, 85  
VIROGRAM, DEFINITION OF, 258  
VIRUS BANDING, REQUIREMENTS OF, 201  
VIRUS CONCENTRATION, IN B-SERIES ROTORS, 200  
VIRUS DETECTION BY ELECTRON MICROSCOPY, 259  
VIRUS ISOLATION BY CENTRIFUGAL METHODS, 374-394  
VIRUS ISOLATION ROTOR, 191-198  
VIRUS SPILL TESTS, 378  
VIRUS SUSPENSION, REMOVAL OF FRACTION OF, 47  
VIRUS TITER AFTER ETHYLENE OXIDE, 382T  
VIRUS WINDOW CONCEPT, 254-257, 256F  
VIRUSES, LIPID-CONTAINING, FROM CYTOPLASMIC FRAGMENTS, 11  
VIRUS-LIKE PARTICLES, 17, 389  
VIRUS, BANDING DENSITY, 256F  
VIRUS, BITTNER, 265  
VIRUS, BROMGRASS MOSAIC, IN B-IV, 153  
VIRUS, DETECTION IN GRADIENTS, 259  
VIRUS, MOLONEY, 204T  
VIRUS, ONCOGENIC, SEARCH FOR, 265  
VIRUS, OPTIMUM DETECTION OF, 257, 258  
VIRUS, POLIO, IN B-V, 153, 378F, 380T, 386F, 387F  
VIRUS, POLIO, INABILITY TO DECONTAMINATE, 383  
VIRUS, RATE AND ISOPYCNIC SEPARATION OF, 253-283  
VIRUS, RAUSCHER AND MOLONEY, IN B-IV, 153  
VIRUS, RESPIRATORY SYNCYTIAL, 153, 204T  
VIRUS, SAFE HANDLING, 485-502  
VIRUS, SEDIMENTATION COEFFICIENTS FOR, 255, 256, 256F, 257  
VIRUS, SEDIMENTATION OF, WITH BATCH TECHNIQUE, 75F  
VIRUS, SEPARATION FROM HOMOGENATES, 17  
VIRUS, TOBACCO MOSAIC, IN B-IV, 153

VIRUS, TOTAL MASS EQUATION, 201  
VIRUS, USE OF STAINING OF, 259, 260  
VISCOSITY COEFFICIENTS, 225T  
VISCOSITY AND ANTOINE EQUATION, 219, 232, 234  
VISCOSITY AND ARRHENIUS EQUATION, 219, 232  
VISCOSITY AND DENSITY OF SUCROSE, 219-239  
VISCOSITY AND PRESSURE, 238, 239  
VISCOSITY CALCULATION, ACCURACY OF, 223  
VISCOSITY EQUATIONS, ADAPTED NBS, 230  
VISCOSITY VALUES, DEVIATION OF, 237F, 238F

-W-

WALL EFFECTS, 14  
WALL THICKNESS, OPTIMUM, 96T, 97F  
WATER, NITROGEN FREEZING OF, 429F  
WAVE DISTURBANCE, CENTRIFUGAL, 77  
WAVES, CENTRIFUGAL, IN FLUIDS, 103-105, 107F  
WHIRL, 80, 85, 88F  
WHIRL FREQUENCY, EQUATION FOR, 86  
WHIRL, BEARING, 83, 85  
WHIRL, ROTOR (PRECESSION), 83  
WINDOW, VIRUS, 254-257, 256F  
WOODS NLLS PROGRAM, 222, 227, 233, 234

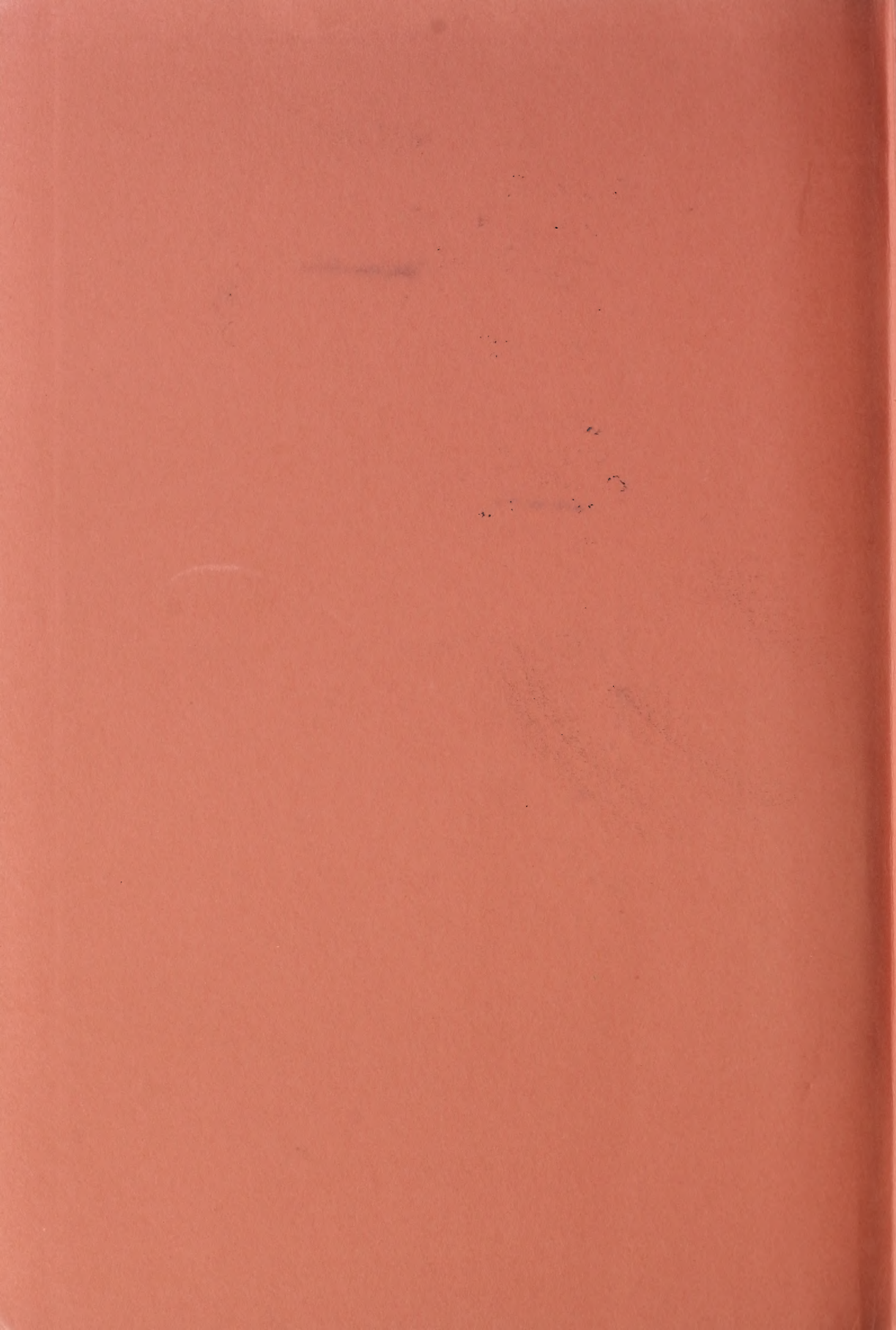
-Y-

YEAST CHROMATOGRAPHY, 441, 443F, 444T  
YEAST NUCLEOTIDE POOL, 445T  
YEAST NUCLEOTIDES, SEPARATION OF, 441-446  
YEAST, FREEZING AND THAWING OF, 419F

-Z-

ZONAL CENTRIFUGATION OF SUBCELLULAR PARTICLES, 252-370  
ZONAL CENTRIFUGATION, BANDING CAPACITY IN, 56-73  
ZONAL CENTRIFUGES, DESIGN OF, 77-111, 79F, 80  
ZONAL CENTRIFUGES, PRINCIPLES OF, 11-17  
ZONAL CENTRIFUGES, PARTICLE SEPARATIONS IN, 9-39  
ZONAL CENTRIFUGES, SUMMARY OF DEVELOPMENT, 18-20  
ZONE CAPACITY, THEORETICAL, 57  
ZONE DEFORMATION, 21F  
ZONE POSITION VS. UV ABSORBANCY, 177F  
ZONE RECOVERY, IN B-V, 195







<http://nihlibrary.nih.gov>

---

10 Center Drive  
Bethesda, MD 20892-1150  
301-496-1080

10/9



**U.S. DEPARTMENT OF HEALTH, EDUCATION, AND WELFARE**  
**Public Health Service**